World Journal of Gastroenterology®

Volume 13 Number 9
March 7, 2007

National Journal Award
2005

The WJG Press

The WJG Press, Apartment 1066 Yishou Garden, 58 North Langxinzhuang Road, PO Box 2345, Beijing 100023, China
Telephone: +86-10-85381892
Fax: +86-10-85381893
E-mail: wjg@wjgnet.com
http: //www.wjgnet.com

ISSN 1007-9327 CN 14-1219/R Local Post Offices Code No. 82-261

World Journal of Gastroenterology www.wjgnet.com Volume 13 Number 9 Mar 07 2007

ISSN 1007-9327
CN 14-1219/R

World Journal of Gastroenterology®

Indexed and Abstracted in:

Current Contents®/Clinical Medicine, Science Citation Index Expanded (also known as SciSearch®) and Journal Citation Reports/Science Edition, *Index Medicus*, MEDLINE and PubMed, Chemical Abstracts, EMBASE/Excerpta Medica, Abstracts Journals, *Nature Clinical Practice Gastroenterology and Hepatology*, CAB Abstracts and Global Health.
ISI JCR 2003-2000 IF: 3.318, 2.532, 1.445 and 0.993.

Volume 13 Number 9
March 7, 2007

World J Gastroenterol
2007 March 7; 13(9): 1313-1476
Online Submissions
www.wjgnet.com/wjg/index.jsp
www.wjgnet.com
Printed on Acid-free Paper

A Weekly Journal of Gastroenterology and Hepatology

National Journal Award
2005

World Journal of Gastroenterology®

Volume 13 Number 9
March 7, 2007

The WJG Press

Contents

World Journal of Gastroenterology
Volume 13 **Number** 9 **March** 7, 2007

Contents

World Journal of Gastroenterology
Volume 13 **Number** 9 **March** 7, 2007

Contents

Responsible E-Editor for this issue: Wen-Hua Ma

Responsible S-Editor for this issue: Jing Wang

World Journal of Gastroenterology (*World J Gastroenterol , WJG*), a leading international journal in gastroenterology and hepatology, has an established reputation for publishing first class research on esophageal cancer, gastric cancer, liver cancer, viral hepatitis, colorectal cancer, and *H pylori* infection, providing a forum for both clinicians and scientists, and has been indexed and abstracted in Current Contents®/Clinical Medicine, Science Citation Index Expanded (also known as SciSearch®) and Journal Citation Reports/Science Edition, *Index Medicus*, MEDLINE and PubMed, Chemical Abstracts, EMBASE/Excerpta Medica, Abstracts Journals, *Nature Clinical Practice Gastroenterology and Hepatology*, CAB Abstracts and Global Health. ISI JCR 2003-2000 IF: 3.318, 2.532, 1.445 and 0.993. *WJG* is a weekly journal published by The WJG Press. The publication date is on 7th, 14th, 21st, and 28th every month. The *WJG* is supported by The National Natural Science Foundation of China, No. 30224801 and No.30424812, which was founded with a name of *China National Journal of New Gastroenterology* on October 1,1995, and renamed as *WJG* on January 25, 1998.

PUBLISHED BY
The WJG Press

PRINTED BY
Printed in Beijing on acid-free paper by Beijing Kexin Printing House

Print ISSN 1007-9327
CN 14-1219/R

EDITORIAL OFFICE
World Journal of Gastroenterology,
The WJG Press, Apartment 1066 Yishou Garden, 58 North Langxinzhuang Road, PO Box 2345, Beijing 100023, China
Telephone: +86-10-85381892
Fax: +86-10-85381893
E-mail: wjg@wjgnet.com
http://www.wjgnet.com

SUBSCRIPTION AND AUTHOR REPRINTS
Jing Wang
The WJG Press, Apartment 1066 Yishou Garden, 58 North Langxinzhuang Road, PO Box 2345, Beijing 100023, China
Telephone: +86-10-85381892
Fax: +86-10-85381893
E-mail: j.wang@wjgnet.com
http://www.wjgnet.com

SUBSCRIPTION INFORMATION
Institutional Price 2007: USD 1500.00
Personal Price 2007: USD 700.00

INSTRUCTIONS TO AUTHORS
Full instructions are available online at http://www.wjgnet.com/wjg/help/instructions.jsp. If you do not have web access please contact the editorial office.

PO Box 2345, Beijing 100023, China
www.wjgnet.com
wjg@wjgnet.com

World J Gastroenterol 2007 March 7; 13(9): 1313-1332
World Journal of Gastroenterology ISSN 1007-9327

EDITORIAL

Neuropathophysiology of functional gastrointestinal disorders

Jackie D Wood

Jackie D Wood, Department of Physiology and Cell Biology, and Internal Medicine, The Ohio State University, College of Medicine, Columbus, Ohio 43210-1218, United States
Correspondence to: Jackie D Wood, Professor, Department of Physiology and Cell Biology, and Internal Medicine, The Ohio State University, College of Medicine, 304 Hamilton Hall, 1645 Neil Avenue, Columbus, Ohio 43210-1218, United States. wood.13@osu.edu
Telephone: +1-614-2925449 Fax: +1-614-2924888
Received: 2006-08-11 Accepted: 2007-02-05

Abstract

The investigative evidence and emerging concepts in neurogastroenterology implicate dysfunctions at the levels of the enteric and central nervous systems as underlying causes of the prominent symptoms of many of the functional gastrointestinal disorders. Neurogastroenterological research aims for improved understanding of the physiology and pathophysiology of the digestive subsystems from which the arrays of functional symptoms emerge. The key subsystems for defecation-related symptoms and visceral hypersensitivity are the intestinal secretory glands, the musculature and the nervous system that controls and integrates their activity. Abdominal pain and discomfort arising from these systems adds the dimension of sensory neurophysiology. This review details current concepts for the underlying pathophysiology in terms of the physiology of intestinal secretion, motility, nervous control, sensing function, immuno-neural communication and the brain-gut axis.

Key words: Neurogastroenterology; Visceral pain; Diarrhea; Irritable bowel syndrome; Constipation; Stress; Enteritis; Enteric nervous system; Neuroimmune communication; Mast cells

Wood JD. Neuropathophysiology of functional gastrointestinal disorders. *World J Gastroenterol* 2007; 13(9): 1313-1332

http://www.wjgnet.com/1007-9327/13/1313.asp

INTRODUCTION

Functional gastrointestinal disorders are those in which no abnormal metabolic or physical processes, which can account for the symptoms, can be identified[1]. The irritable bowel syndrome (IBS) is an example of a significant functional disorder, which affects 10-20 percent of the population worldwide[2-6]. Predominant symptoms of IBS are abnormal defecation associated with abdominal pain, both of which may be exacerbated by psychogenic stress[7]. The abnormal defecation in IBS is predominately diarrhea or constipation. A subgroup of IBS patients alternates from one to the other over time. In the absence of abdominal pain, persistent diarrheal states or states of constipation may also fall into the category of a functional disorder. Urgency to stool and incontinence for fecal liquid are often coincident with the diarrheal state. Patients with constipation-predominant IBS, and oftentimes functional constipation, often report bloating, straining and sensations of incomplete fecal evacuation. Significant subpopulations of IBS patients and functional dyspeptic patients are hypersensitive to distension of the recto-sigmoid region of the large bowel and the hypersensitivity can extend to other regions of the digestive tract (e.g. esophagus)[7,8].

The basic gastrointestinal physiology in this review deals with the normal and disordered physiology of the systems out of which the symptoms of IBS and functional diarrhea or constipation emerge. Knowledge of this kind is necessary for understanding the pathophysiology, which underlies the symptoms, and for rational therapeutic strategies. The subsystems involved in the defecation-related symptoms are the intestinal secretory glands, the musculature and the nervous system that controls their activity. Abdominal pain and discomfort, which arise from these systems, falls into the domain of sensory neurophysiology. This review will explore the pathophysiology in terms of current concepts of the physiology of intestinal secretion, motility, nervous control and sensing functions.

THE BRAIN-IN-THE-GUT

Gastrointestinal behavior reflects the integrated functioning of the musculature, mucosal epithelium and blood-lymphatic vasculature. The enteric division of the autonomic nervous system (i.e. brain-in-the-gut) organizes and coordinates the activity of the three effector systems to generate functionally effective patterns of behavior that are adaptive for differing digestive states. The enteric nervous system (ENS) is a local minibrain that contains a library of programs for the necessary patterns of intestinal behavior. Mixing in the digestive state, the migrating motor complex in the interdigestive state and emetic patterns of small intestinal motor behavior and haustral formation in the large intestine are examples of outputs from four of the neural programs in the ENS library. During emesis, the

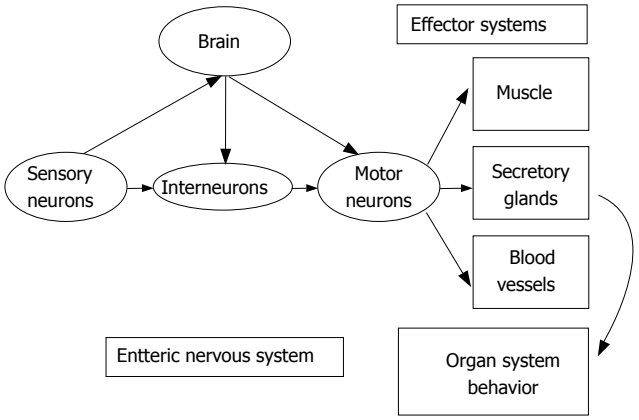

Figure 1 The heuristic model for the enteric nervous system is the same as for the central nervous system. Sensory neurons, interneurons and motor neurons are synaptically interconnected to form the neural networks of the ENS. Like the central nervous system, sensory neurons, interneurons and motor neurons are connected by chemical synapses for directional flow of information from sensory neurons to interneuronal integrative networks to motor neurons to effector systems. The ENS organizes and coordinates the activity of each effector system into meaningful behavior of the whole organ. Bidirectional communication occurs between the ENS and the central nervous system.

program output includes reversal of peristaltic propulsion in the upper jejunum and duodenum to rapidly propel the contents toward the open pylorus and relaxed gastric antrum and corpus.

Structure, function and neurochemistry of the ganglia of the enteric nervous system are unlike other autonomic ganglia. Neurons in the ganglia of the ENS are interconnected by chemical synapses to form an independent nervous system with mechanisms for integration and processing of information like those in the brain and spinal cord. Instead of housing neural control entirely within the central nervous system (CNS), a minibrain has evolved within the walls of the digestive tract placed in close proximity to the effector systems that must be controlled and regulated along several meters of bowel.

The ENS has as many neurons as the spinal cord. The large number of neurons, required for program control of digestive functions, would overly expand the CNS if housed there. Rather than crowding the neural control circuits exclusively within the skull or vertebral column and transmitting nerve impulses over long transmission lines to the gut, vertebrate animals have evolved with most of the neural networks, required for automatic feedback control, spatially distributed along the digestive tract close to the effector systems that must be controlled and integrated for whole organ function.

Like the CNS, the ENS has interneurons and motor neurons that are interconnected by chemical synapses into functional neural networks (Figure 1). Moreover, like the CNS, the ENS networks receive synaptic input from sensory neurons. The sensory neurons, most of which have their cell bodies in spinal dorsal root or nodose ganglia and their terminations in the intestinal wall and spinal cord, express receptor regions specialized for detecting and coding information on changes in thermal, chemical or mechanical stimulus energy within the environment of the receptor region. The receptor regions transform changes in stimulus energy into signals coded by action potentials that subsequently are transmitted along sensory nerve fibers to be received and processed in both the ENS and CNS.

Interneurons are connected by synapses into networks that process sensory information and determine the behavior of motor neurons. Multiple connections among many interneurons use the same mechanisms of chemical neurotransmission as the CNS to form "logic" circuits that decipher inputs from sensory neurons. Some of the circuits are reflex circuits that organize reflex responses to sensory inputs and others are integrative circuits that contain the programs for motor behavioral patterns, such as the migrating motor complex, haustral formation in the colon and postprandial mixing movements in the small intestine. Motor neurons are the final common output pathways for transmission of control signals from the interneuronal networks to the effector systems.

Enteric motor neurons

Motor neurons in the ENS are excitatory or inhibitory motor neurons (Figure 1). The excitatory motor neurons release neurotransmitters, which evoke contraction of the musculature and secretion from mucosal glands. Acetylcholine and substance *P* are the main excitatory neurotransmitters released at neuromuscular junctions to stimulate muscle contraction. Acetylcholine, vasoactive intestinal polypeptide and ATP are excitatory neurotransmitters responsible for evoking secretion from the intestinal glands.

Enteric inhibitory motor neurons release neurotransmitters at neuromuscular junctions where they act to suppress contractile activity of the musculature. Vasoactive intestinal polypeptide, nitric oxide and ATP are among the neurotransmitters implicated as inhibitory neurotransmitters at neuromuscular junctions in the digestive tract.

Inhibitory motor neurons

Enteric inhibitory motor neurons have central importance in consideration of ENS neuropathy because their loss is manifest as profound pathologic changes in contractile behavior of the intestinal musculature. The pathologic changes in motor behavior associated with degeneration of inhibitory motor neurons reflect the specialized physiology of the musculature. The gastrointestinal musculature is a self-excitable electrical syncytium consisting of interstitial cells of Cajal (ICCs) that function as pacemakers for the gastric musculature and the intestinal circular muscle coat. The term "electrical syncytium" infers that action potentials and pacemaker potentials spread by way of gap junctions from smooth muscle fiber to muscle fiber in three dimensions. The action potentials trigger contractions as they spread through the bulk of the musculature. The ICCs are a non-neural pacemaker system of electrical slow waves that are electrically coupled to the musculature and account for the self-excitable characteristics of the muscle[9-13]. The electrical slow waves, in this construct, are an extrinsic factor to which the circular muscle responds. Consideration of these

functional aspects of the musculature raises the question of why the circular muscle fails to respond with action potentials and contractions to each and every pacemaker cycle and why action potentials and contractions do not spread in the syncytium throughout the entire length of intestine whenever they occur at any point along the bowel. The answer is that the circular muscle in a segment of bowel can only respond to invading electrical slow waves from ICCs when the inhibitory motor neurons in the ENS of that segment are inactivated by input from the control circuits formed by interneurons (Figure 1). Likewise, action potentials and associated contractions can propagate only into regions of musculature where the inhibitory motor neurons are inactivated. Therefore, activity of inhibitory motor neurons determines when the omnipresent slow waves initiate a contraction, as well as the distance and direction of propagation once the contraction has begun.

Some of the inhibitory motor neurons to the circular muscle fire continuously and continuously release inhibitory neurotransmitters at their junctions with the muscle. This results in ongoing inhibition of contractile activity. Action potentials and contractions of the muscle are permitted only when the active inhibitory neurons are inactivated by input from the interneuronal control circuitry[14,15]. The behavior of inhibitory motor neurons to smooth muscle sphincters (e.g. lower esophageal and internal anal sphincters) is opposite to that of the intestinal circular muscle coat. Inhibitory motor neurons to the sphincters are normally silent and are switched to firing mode with timing appropriate for coordinated opening of the sphincter with physiological events in adjacent regions. When inhibitory motor neurons fire, they release inhibitory neurotransmitters that relax ongoing muscle contraction in the sphincteric muscle and prevent excitation-contraction in the musculature on either side of the sphincter from spreading into and closing the sphincter.

In non-sphincteric circular muscle, the activity state of the inhibitory innervation determines the length of a contracting segment by controlling the distance of spread of action potentials within the three-dimensional electrical geometry of the smooth muscle syncytium. Contraction can occur in segments in which ongoing inhibition is inactivated while adjacent segments with continuing inhibitory input cannot contract. The boundaries of the contracted segment reflect the transition zone from inactive to active inhibitory motor neurons. The directional sequence in which the inhibitory motor neurons are inactivated establishes the direction of propagation of the contraction. Normally, inhibition is progressively inactivated in the aboral direction, resulting in contractile activity that propagates in the aboral direction. During emesis, the inhibitory motor neurons must be inactivated in a reverse sequence to account for small intestinal propulsion that travels toward the stomach. In general, any treatment or condition that ablates the intrinsic inhibitory neurons results in spastic contractile behavior of the intestinal circular muscle coat.

Several conditions associated with ablation of enteric inhibitory neurons are associated with conversion from a hypoactive contractile condition of the circular muscle to a hyperactive contractile state. Observations of this nature, usually made by manometric recording methods *in vivo*, reinforces the evidence that a subset of the pool of inhibitory motor neurons is tonically active, and that blockade or ablation of these neurons releases the circular muscle from the inhibitory influence[14-16]. The behavior of the muscle in these cases is tonic contracture and recurring disorganized phasic contractile activity that is non-propulsive.

Disinhibitory motor disease

The inhibitory neuromuscular relations in the intestine predict that spasticity and "achalasia" (i.e. failure to relax) will accompany any condition where inhibitory motor neurons are rendered inactive or destroyed. Without ENS inhibitory neural control, the self-excitable smooth muscle contracts continuously and behaves as an obstruction. This occurs because the muscle responds to each and every ICC-generated electrical slow wave with contractions that propagate in all directions without any control of amplitude or distance of propagation. Contractions spreading in the uncontrolled syncytium collide randomly resulting in chaotic-ineffective behavior in the affected intestinal segment in ways which are reminiscent of fibrillation in the myocardium.

Loss or malfunction of inhibitory motor neurons is the pathophysiological starting point for disinhibitory motor disease, which includes several forms of chronic intestinal pseudoobstruction and sphincteric achalasia. Neuropathic degeneration of the ENS includes loss of the pool of inhibitory motor neurons along with the interneuronal pool and is a progressive disease that in its early stages may be manifest as symptoms that could be interpreted as a functional gastrointestinal disorder (e.g. IBS).

Intestinal pseudoobstruction is a pathophysiological state with symptoms that resemble those of a mechanical obstruction to forward propulsion, but without the presence of a mechanical obstruction. Chronic intestinal pseudoobstruction can be myopathic or neuropathic. The neuropathic form of chronic intestinal pseudoobstruction is a form of disinhibitory motor disease linked with neuropathic degeneration in the ENS. Failure of propulsive motility in the affected length of bowel reflects loss of the neural microcircuits that program and control the repertoire of motility patterns required for the necessary functions of that region of bowel. Pseudoobstruction occurs mainly because contractile behavior of the circular muscle is hyperactive, but disorganized in the denervated regions[17,18]. Hyperactivity determined by manometric recording methods is a diagnostic sign of the neuropathic form of chronic small bowel pseudoobstruction. The hyperactive and disorganized contractile behavior reflects the absence of inhibitory nervous input to the muscles, which are autogenic when released from the braking action of the inhibitory motor neurons of the ENS. Chronic pseudoobstruction is therefore symptomatic of the advanced stage of a progressive enteric neuropathy. Retrospective review suggests that IBS-like symptoms in a subgroup of patients can be an expression of early stages of the neuropathy[19-21].

Degenerative non-inflammatory and inflammatory ENS neuropathies are two kinds of disinhibitory motor

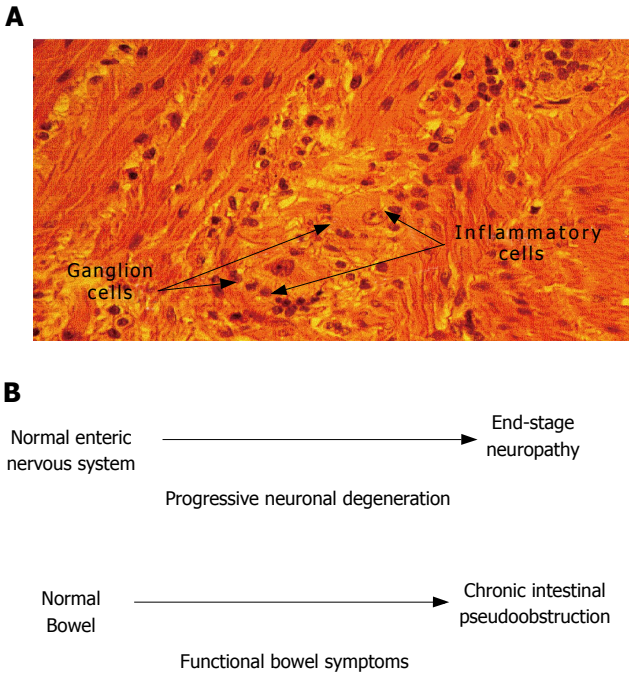

Figure 2 Enteric neuropathy underlies the pathophysiology in a subset of patients with functional gastrointestinal disorders. **A**: Idiopathic myenteric ganglionitis. Histology of the myenteric plexus in a full-thickness small intestinal biopsy taken during exploratory laparotomy for intestinal obstruction. A diagnosis of neuropathic pseudoobstruction was made on the basis of neuronal degeneration associated with an inflammatory infiltrate localized to the myenteric plexus. The patient had a multiple year history of complaints suggestive of IBS. Histological section and patient history courtesy of Dr. Claudio Fiocchi, The Cleveland Clinic, Cleveland, Ohio; **B**: Enteric neuronal degeneration and associated symptoms progress in parallel (e.g. symptoms of IBS). Most individuals start postnatal life with a normal ENS and normally functioning bowel. Neuronal degeneration mediated by autoimmune attack directed to the ENS (e.g. paraneoplastic syndrome, Chagas disease, idiopathic inflammatory neuropathy) can progress to a stage where ENS function is lost. Functional bowel symptoms appear and worsen as neurons are progressively lost from the ENS microcircuits required for integrated function of the whole organ. Chronic intestinal pseudoobstruction of the neuropathic form occurs when the loss of neurons progresses to a stage where the neuronal circuits for propulsive motility are no longer functional.

disorders that culminate in pseudoobstruction. Non-inflammatory neuropathies are classified as familial or sporadic[22]. In the former, the neuropathological findings include a marked reduction in the number of neurons in both myenteric and submucosal plexuses, and the presence of round, eosinophilic intranuclear inclusions in roughly 30% of the residual neurons. Histochemical and ultrastructural evaluations reveal the inclusions not to be viral particles, but rather proteinaceous material forming filaments that is are in some ways reminiscent of Alzheimer's disease in the brain[23,24]. Members of two families have been described with intestinal pseudoobstruction associated with the autosomal dominant form of ENS neuropathy[25,26]. The numbers of enteric neurons in these patients were decreased with no alterations found in the CNS or parts of the autonomic nervous system outside the gut.

Degenerative inflammatory ENS neuropathies are characterized by a dense inflammatory infiltrate confined to enteric ganglia. Paraneoplastic syndrome, Chagas disease and idiopathic degenerative disease are recognizable forms of pseudoobstruction related to inflammatory neuropathies.

Paraneoplastic syndrome is a form of pseudoobstruction where commonality of antigens between some forms of cancer cells (e.g. small-cell carcinoma of the lungs) and enteric neurons leads to autoimmune attack, which results in loss of neurons[27,28]. Most of the patients with symptoms of pseudoobstruction in combination with small-cell lung carcinoma express immunoglobulin-G autoantibodies that react with neurons in their ENS[29]. These antibodies react with molecules expressed on the nuclear membranes of neurons (e.g. Hu and Ri proteins) and with cytoplasmic Yo protein of Purkinje cells in the cerebellum[30,31]. Immunostaining with sera from paraneoplastic patients shows a characteristic pattern of staining in enteric neurons[30]. The detection of anti-enteric neuronal antibodies in the patient's serum establishes the specific diagnosis. The circulating antibodies damage the neurons by inducing apoptosis[32].

The association of enteric neuronal loss and symptoms of pseudo-obstruction in Chagas disease also reflects autoimmune attack on the neurons with accompanying symptoms that mimic the situation in sphincteric achalasia and paraneoplastic syndrome. *Trypanosoma cruzi*, the blood-borne parasite that causes Chagas disease, has antigenic epitopes similar to enteric neuronal antigens[33]. This antigenic commonality activates the immune system to assault the ENS coincident with its attack on the parasite.

Idiopathic inflammatory degenerative ENS neuropathy occurs unrelated to neoplasms, infectious conditions or other known diseases[32,34-38]. Patients have been described with early complaints of symptoms similar to IBS that progressively worsened and were later diagnosed as idiopathic degenerative inflammatory neuropathy based on full-thickness biopsies taken during exploratory laparotomy, which revealed chronic intestinal pseudoobstruction[20,35-38]. Each of these patients had inflammatory infiltrates localized to ganglia of the myenteric plexus. Sera from these patients contain antibodies against enteric neurons that are similar to those found in secondary inflammatory neuropathies (i.e. anti-Hu), but with different immunolabeling patterns characterized by prominent cytoplasmic rather than nuclear staining.

Recognition of the brain-like functions of the ENS leads to a conclusion that early neuropathic changes are expected to be manifest as symptoms that worsen with progressive neuronal loss. In diagnostic intestinal motility studies (e.g. manometry), degenerative loss of enteric neurons is reflected by hypermotility and spasticity[17] because inhibitory motor neurons are included in the missing neuronal population.

The observations in patients with autoimmune attack on the ENS suggest that early stages of an enteric neuropathy might be expressed as IBS-like symptoms. Early symptoms in these patients can be lower esophageal sphincter achalasia, which reflects loss of inhibitory innervation of the sphincter, and postprandial cramping abdominal pain and diarrhea. The disease in these individuals appears to progress from IBS-like symptoms to symptoms of chronic intestinal pseudoobstruction in parallel with progressive loss of neurons from their ENS (Figure 2).

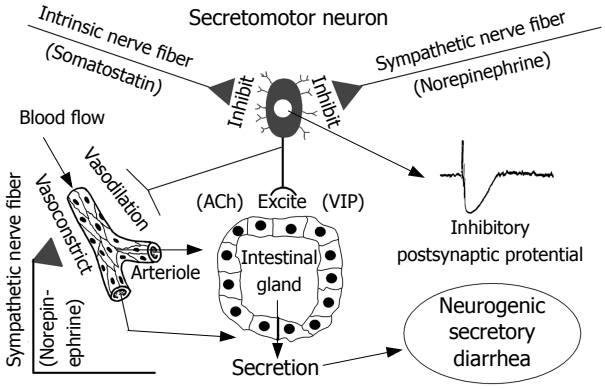

Figure 3 Intestinal secretory glands (i.e. crypts of Lieberkühn and Brunner's glands) are innervated by secretomotor neurons in the ENS. Neurotransmitters (e.g. ACh and VIP), which evoke secretion, are released at the neuro-epithelial junctions when secretomotor neurons fire. Axon collaterals to blood vessels simultaneously dilate submucosal vessels to increase blood flow in support of stimulated secretion. Noradrenergic input from the sympathetic nervous system and somatostatinergic input from intrinsic ENS neurons suppress firing of secretomotor neurons and thereby inhibit secretion. Factors that cause hyperactivity of secretomotor neurons enhance secretion and lead to neurogenic secretory diarrhea. In inflammatory states (e.g. ulcerative colitis and Crohn's disease) the release of inflammatory mediators elevates activity of secretomotor neurons leading to diarrhea. Certain pathogens and enterotoxins (e.g. cholera toxin and Clostridium difficille toxin A) activate secretomotor neurons to produce a diarrheal state. In food allergies, presence of sensitizing food antigens (e.g. shellfish, tree nuts) triggers mast cell degranulation and releases mediators such as histamine, serotonin and prostaglandins, all of which activate secretomotor neurons to evoke diarrhea. When secretomotor neurons are hypoactive, secretion is reduced, the liquidity of the intestinal contents is reduced and a state of constipation can follow. Activating opioid or somatostatinergic receptors (e.g. by opioid analgesics or octreotide) on secretomotor neurons inhibits their excitability and suppresses secretion.

NEUROGENIC SECRETION: DIARRHEA AND CONSTIPATION

Disordered defecation in IBS is related directly to the physiology of enteric secretomotor neurons. Secretomotor neurons are excitatory motor neurons in the submucosal plexus of the ENS, which innervate and stimulate secretion from the intestinal crypts of Lieberkühn, Brunner's glands and goblet cells (Figure 3).

Secretomotor neurons

Secretomotor neurons are uniaxonal with characteristic shapes described as Dogiel Type I and electrophysiological behavior like S-type enteric neurons[39-41]. When they fire, they release acetylcholine and vasoactive intestinal polypeptide at their junctions with the secretory epithelium. Collateral projections from the secretomotor axons innervate submucosal arterioles (Figure 3). Collateral innervation of the blood vessels links secretomotor activity in the glands to submucosal blood flow[42]. Active firing of secretomotor neurons releases acetylcholine simultaneously at neuroepithelial and neurovascular junctions. Acetylcholine acts at the blood vessels level to release nitric oxide from the endothelium, which in turn dilates the vessels and increases blood flow[42].

Secretomotor neurons have receptors that receive excitatory and inhibitory synaptic input from other neurons in the integrative circuitry of the ENS and from sympathetic postganglionic neurons (Figure 3)[43-45]. Secretomotor neuronal excitability is greatly influenced also by paracrine chemical messages from nonneural cell types in the mucosa and submucosa (e.g. enterochromaffin cells, mast cells and other kinds of immune/inflammatory cells). Activation of the excitatory receptors on secretomotor neurons stimulates the neurons to fire and release their transmitters at the junctions with the secretory glands and regional blood vessels. The overall result of secretomotor neuronal firing is stimulation of the secretion of H_2O, NaCl, bicarbonate and mucus from the intestinal glands into the intestinal lumen[46,47].

Inhibitory input to secretomotor neurons

Inhibitory inputs from other neurons hyperpolarize the membrane potential of secretomotor neurons and this decreases the probability of firing (Figure 3). The physiological effect of inhibiting secretomotor firing is suppression of mucosal secretion. Postganglionic neurons of the sympathetic nervous system are an important source of inhibitory input to the secretomotor neurons. Norepinephrine released from sympathetic nerve terminals in the submucosal plexus acts at alpha2 noradrenergic receptors to inhibit firing of the secretomotor neurons. Inhibition of secretomotor firing reduces the release of excitatory neurotransmitters at the junctions with the secretory epithelium. The end result is reduced secretion of water and electrolytes. Suppression of secretion in this manner is part of the mechanism involved in sympathetic nervous shut-down of gut function in homeostatic states where blood is shunted from the splanchnic to systemic circulation.

Neurogenic secretory diarrhea and neurogenic constipation

Knowledge of the neurobiology of submucosal secretomotor neurons is necessary for understanding the pathophysiology of secretory diarrhea, as well as constipation. In general, secretomotor hyperactivity is associated with neurogenic secretory diarrhea; hypoactivity is associated with decreased secretion and a constipated state. Suppression of secretomotor firing by antidiarrheal agents (e.g. opiates, clonidine and somatostatin analogs) is manifest as harder-drier stools. Stimulation by chemical mediators, such as vasoactive intestinal peptide (VIP), serotonin and histamine, is manifest as more liquid stools.

Watery diarrhea may be caused by several different pathophysiological events. For example, secretomotor neurons may be overly stimulated by circulating VIP released from VIPomas, excessive serotonin release from mucosal enterochromaffin cells or histamine release from inflammatory/immune cells in the mucosa/submucosa[48]. Release of histamine or other inflammatory mediators associated with diarrhea not only stimulates the firing of secretomotor neurons, but also simultaneously acts at presynaptic inhibitory receptors to suppress the release of norepinephrine from the postganglionic sympathetic axons that provide inhibitory input to secretomotor neurons[44,48]. Two pathological factors are therefore involved in the production of neurogenic secretory diarrhea. One is over

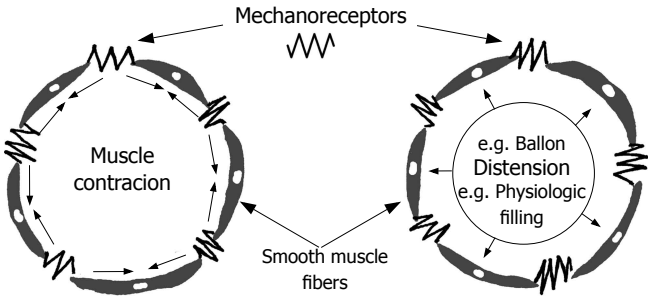

Figure 4 Mechanoreceptors are connected "in-series" with the long axes of the smooth muscle fibers that form the intestinal circular muscle layer. Either contraction of the muscle or distension of the intestinal wall "stretches" the receptors and evokes firing of impulses in the sensory afferent fibers connected to the receptor. Firing frequency of the receptor increases in direct relation to the amount of "stretch" or, in some receptors, the rate at which the length changes. Mechanosensory information generated in this manner is transmitted by spinal afferents to the spinal cord or vagal nerve afferents to the dorsal vagal motor complex in the brain stem.

stimulation of secretomotor neuronal firing and the other is presynaptic suppression of norepinephrine release from sympathetic postganglionic neurons. Presynaptic suppression of norepinephrine removes the sympathetic braking action from the neurons (Figure 3).

Excitatory Input to secretomotor neurons

Secretomotor neurons have excitatory receptors for several neurotransmitters, which include acetylcholine, VIP, substance *P* and serotonin[49]. One of the serotonergic receptors belongs to the 5-HT_3 receptor subtype[50].Efficacy of blockade of 5-HT_3 receptors by a 5-HT_3 antagonist in the treatment of diarrhea in the diarrhea-predominant population of women with IBS[51,52] suggests that hyperstimulation of secretomotor neurons by serotonin is a significant factor in this form of IBS. Observations that IBS symptoms of cramping abdominal pain, diarrhea and fecal urgency are commonly exacerbated in the postprandial state[7,53] and evidence for elevated postprandial release of serotonin[54,55] suggests that overactive release of serotonin from the enterochromaffin cell population might underlie the diarrheal symptoms of IBS. This is reinforced by suggestions of elevated numbers of serotonin-containing enterochromaffin cells and also mast cells in the mucosa of IBS patients[56-58].

ABDOMINAL PAIN AND DISCOMFORT

Primary causes of abdominal pain of digestive tract origin are distension and excessively strong muscular contractions. Stimuli, such as pinching and burning of the mucosa applied *via* fistulae, do not evoke pain. Hypersensitivity of the sensory mechanoreceptors for stretch (distension) and contractile force are implicated as pain factors in IBS. Hypersensitivity to distension is present in a substantial subset of IBS patients[59-62]. Filling of a balloon placed in the recto-sigmoid region evokes sensations of discomfort and pain at lower distending volumes for IBS patents than for normal subjects. Hypersensitivity of this nature to distension is not restricted to the distal bowel. Patients, who are diagnosed with functional dyspepsia, also experience more discomfort and pain at lower distending volumes in the stomach than normal subjects[63,64] and hypersensitivity to distension is present in the esophagus of patients with non-cardiac chest pain[65].

IBS patients experience the same kind of hypersensitivity to electrical stimulation applied to the lining of the recto-sigmoid region as they do during balloon distension in the recto-sigmoid[66]. This hypersensitivity to direct electrical stimulation of the intramural sensory innervation implicates abnormal sensory neurophysiology rather than mechanical factors (e.g. wall tension and compliance) as underlying the decreased sensory thresholds present in IBS patients. Identification of the sensory defect in IBS continues as an area of active investigation and is yet to be elucidated convincingly. The lower sensory threshold in IBS might reflect: (1) sensitization of intramural mechanoreceptors; (2) sensitization of neurotransmission at synapses in the spinal cord; (3) abnormal processing of the sensory information when it reaches the brain; (4) combinations of each of these possibilities.

Peripheral neuropathological factors

Mechanosensitive primary sensory afferents in the walls of the specialized organs of the digestive tract detect and signal contraction and distension of the musculature. The mechano-sensing structures at the afferent terminals behave as if they are attached "in-series" with the long axes of the smooth muscle fibers (Figure 4). This arrangement accounts for activation of the sensors by either muscle contraction or distension. The cell bodies of the neurons that give rise to intestinal afferents are located in vagal nodose ganglia and dorsal root spinal ganglia. Mechanosensitive information is transmitted along spinal afferents to the spinal cord by way of dorsal root ganglia and along vagal sensory afferents to the brain stem by way of the nodose ganglia and synaptic relays in the nucleus tractus solitarius.

Vagal and spinal afferent fibers are predominantly unmyelinated C-fibers or thinly myelinated A δ -fibers each of which transmits different modalities of sensory information at low conduction velocity. In general, vagal afferents transmit sensory information on the nature and composition of the luminal contents, the presence or absence of motility and on contractile tension in the musculature. Spinal afferents transmit mechanosensitive information and pathophysiological information related to potentially noxious mechanical or chemical stimuli arising through tissue injury, ischemia or inflammation. Sensations of pain and discomfort of digestive tract origin reflect transmission in spinal afferents and information processing in the spinal cord and brain. Sensory information transmitted by the vagus nerves appears not to reach the level of conscious sensation because patients with high spinal cord transections and intact vagal pathways experience little or no sensations of digestive tract origin. On the other hand, conscious perception of sensations from the digestive tract remains following a surgical vagotomy. This presumably reflects transmission over spinal afferents to the spinal cord and onward to conscious centers in the brain.

The barrage of mechanosensory information, which is

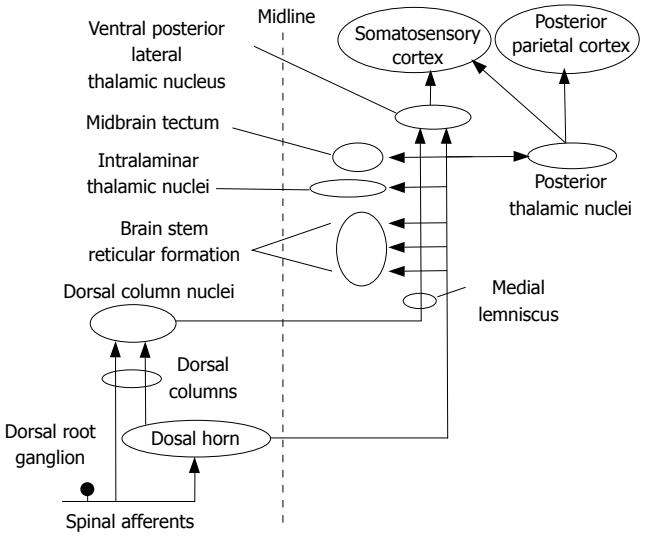

Figure 5 Visceral nociceptive information is transmitted along multiple ascending spinal pathways to multiple processing centers in the brain. Projection pathways in the dorsal spinal columns transmit information from tactile receptors in the skin and visceral pain from nociceptors in the bowel.

transmitted from the small and large intestine to the CNS is generated by three kinds of sensory afferents known as low-threshold, high-threshold and silent afferents[67]. Low-threshold afferents, which code small changes in wall tension, are thought to transmit the minute-to-minute information required for functional autonomic negative-feedback control during contractile events. High-threshold afferents require stronger changes in wall tension, which might be produced by distension of the lumen or strong contraction of the musculature, in order to be activated. The high-threshold afferents are postulated to be responsible for the range of sensations from mild to severe pain that are associated with excessive distension or exceptionally strong muscle contraction. Silent afferents cannot be activated by distension when the bowel is in its normal state. They take on pathophysiological significance by becoming active and highly sensitive to stimuli during inflammatory states[68,69].

Postinfectious IBS

A significant percentage of patients develop IBS-like symptoms following an acute bout of infectious enteritis[70-73]. Hypochondriasis and adverse life events during the infectious episode are reported to double the risk for development of postinfective IBS[70]. Nevertheless, the question of whether the association between acute infectious enteritis and IBS reflects low-level inflammation (e.g. microscopic enteritis) and chronic exposure of the neural and glial elements of the ENS to elevated levels of serotonin, histamine or other inflammatory mediators remains to be fully resolved.

Serotonin receptors on sensory afferents

Application of exogenous 5-HT evokes increased firing in extrinsic afferents and this is mediated by 5-HT_3 receptors that can be blocked by selective 5-HT_3 receptor antagonists (e.g. alosetron)[74,75]. Intramural terminals of both spinal and vagal sensory nerves express 5-HT_3 receptors. Reported efficacy of alosetron in the treatment of abdominal pain and discomfort in the diarrhea-predominant form of IBS in women suggests that these symptoms might reflect over-active endogenous release and elevated levels of 5-HT[51,76].

Persistence of 5-HT at its receptors, due to a defective serotonin transporter, is a second possibility for hyperstimulation of intramural serotoninergic receptors. Active uptake mediated by the serotonin transporter, which is expressed by enteric neurons and mucosal epithelial cells, restricts accumulation and action of 5-HT at its receptors following its release[77]. Down regulation of both transporter mRNA expression and expression of immunoreactivity for the serotonin transporter were reported to be present in mucosal biopsies taken from the large intestine of IBS patients[78]. Watery stools and enhanced propulsive motility occurred in mice with a deletion in the serotonin transporter gene and the mice were reported to sometimes alternated between diarrhea and constipation in a way reminiscent of the subset of IBS patients that are classified as "alternators"[79].

Receptors for inflammatory mediators on sensory afferents

Aside from the 5-HT_3, receptors for bradykinin, ATP, adenosine, prostaglandins, leukotrienes, histamine and mast cell proteases are expressed on spinal sensory nerve terminals[67,80]. Any one of these mast cell or ischemia-related mediators has potential for elevating the sensitivity of intestinal sensory nerves, especially in the disordered conditions of inflammation or ischemia. This suspicion is reinforced by findings that a reduced threshold for painful responses to balloon distension in the large bowel is associated with degranulation of mast cells in animal models. Treatment with mast cell stabilizing drugs prevents lowering of the pain threshold, which occurs during mucosal inflammation in the animal models[81], and suggests that mast cell stabilization might turn out to be an efficacious treatment in human IBS[82,83].

Central neuropathological factors

Much of the evidence suggests altered peripheral sensory transduction as the underlying factor for the exaggerated sensitivity to distension found in IBS patients[84]. In this scenario, mechanosensitive primary afferents in the gut wall become hypersensitive to mechanical stimuli and as a result transmit at elevated frequencies of firing that is interpreted in the CNS as nociceptive information. In an alternative scenario, normally functioning mechanoreceptors transmit accurate information, which is then misinterpreted in processing circuits in the spinal cord and/or brain to evoke conscious perceptions of disordered sensations from the gut.

Ascending sensory pathways in the spinal cord

Ascending spinal pathways involved in the transmission of nociceptive signals from the digestive tract are the spinothalamic, spinohypothalamic, spinosolitary, spinoreticular, and spinoparabrachial tracts (Figure 5). Visceral pain information is also transmitted to higher

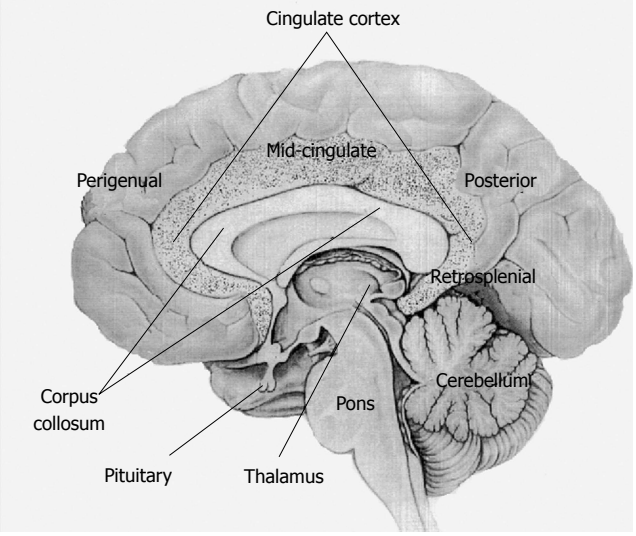

Figure 6 Conscious perception of visceral sensations emerge from the cingulate region of the cerebral cortex. Medial view of the brain showing organization of the cingulate cortex. Perigenual, midcingulate, posterior and retrosplenial are important structural and functional regions of the cingulate cortex with the following properties: (1) Perigenual anterior cingulate cortex surrounds the rostral portion of the cingulate cortex and is primarily involved in affect with a subsector devoted to visceromotor control *via* projections to the cranial parasympathetic and spinal sympathetic divisions of the autonomic nervous system. (2) Midcingulate cortex is involved in response selection and motivation and has a skeletomotor control subsector with neurons that project directly to the spinal cord. (3) Retrosplenial cingulate cortex is associated with memory recall. (4) Posterior cingulate cortex overlays the entire surface of the cingulate gyrus and has a caudomedial subsector that overlaps with the retrosplenial cingulate cortex. The retrosplenial cingulate cortex and posterior cingulate cortex are both involved in memory and activation of the caudomedial sector of the posterior cingulate cortex during memory of emotional events (e.g. emotional events associated with affect and gut function) provide an important framework for assessment of visceral function and disorder in brain imaging studies.

processing centers in the brain *via* pathways in the dorsal spinal columns[85,86-90]. Spinal afferents, which transmit nociceptive information, connect synaptically with second order neurons in the dorsal column nuclei (i.e. nucleus gracilis and nucleus cuneatus). Second order neurons in the spinal dorsal horn also provide input to the dorsal column nuclei (Figure 5). The pain signals are transmitted upward *via* the ipsilateral dorsal column nuclei to the contralateral ventroposterolateral nucleus of the thalamus[85,90-92]. Dorsal column transmission is now considered to be more important than the spinothalamic and spinoreticular tracts in visceral nociceptive transmission.

A midline myelotomy, which severs axons in the human dorsal columns, attenuates otherwise intractable visceral pain[87,90]. Stimulation of the dorsal columns in patients with severe IBS evokes an immediate increase in the intensity of their abdominal pain[93]. These observations in humans are consistent with experimental results in animals. Severing the axons of the dorsal columns in rats or monkeys reduces the neuronal responses to colorectal distension in the ventral posterolateral nucleus of the thalamus and of neurons in the dorsal column nuclei, particularly in the nucleus gracilis[86,88].

Sensory processing in the cerebral cortex

Methods of brain imaging offer another investigative modality for addressing questions related to abnormal processing of sensory information in the cerebral cortex of IBS patients[84,94-96]. Functional magnetic resonance imaging (fMRI) and positron emission tomography (PET) are now commonly used to study information processing in the higher brain centers that underlie an individual's experience of conscious sensations.

Results from imaging studies suggest that unlike somatic sensation, which has a main homuncular representation in the primary somatosensory cortex, visceral sensation is mainly represented in the secondary somatosensory cortex[96,97]. Differences in processing in these specialized regions might account for the vagueness of an individual's ability to localize visceral sensation in relation to somatic sensation. Beyond the sensory cortices, fMRI and PET images show representation of both somatic and visceral sensation to be similar in the limbic and paralimbic regions of the cortex (e.g. anterior insular, anterior and posterior cingulate, prefrontal and orbitofrontal cortices[94,95]. These areas are known to be involved in the individual's motivational and emotional mood states and in the cognitive components of visceral sensations.

Gender differences, reminiscent of those found in IBS, are seen in the cortical representation when a balloon is distended in the recto-sigmoid region in healthy subjects[98]. Activation in the sensory/motor and parieto-occipital areas does not differ between genders. On the other hand, more extensive activation appears in the anterior cingulate and prefrontal cortices in females than in males. The volume of evoked cortical activity in females is greater than in males for perception levels in the range from the urge to defecate to sensations of fullness, mild discomfort and pain. Significance of these gender differences is unclear; nevertheless, they are reminiscent of the greater perceptual responses reported in female patients with functional gastrointestinal disorders (e.g. IBS)[99].

In healthy subjects, painful sensations evoked by distension of a balloon in the recto-sigmoid region or the anticipation of a potentially painful distension are associated with increased blood flow in the anterior cingulate cortex (Figure 6). In IBS patients, activation of the anterior cingulate cortex was reported not to occur in response to painful distension or the anticipation of painful distension[94,100]. On the other hand, an fMRI study found that patients with IBS showed enhanced activation of the mid-cingulate cortex in response to rectal distension[101]. Selective activation of the pre-frontal cortex appeared to take place coincident with decreased activation of the anterior cingulate cortex in another study[94]. Attention is focused on the cingulate cortex because it is generally thought to be an integrative center for both emotional experience and specific representation for pain that might account for the linkage between pain and emotional state. This cortical region is formed around the rostrum of the corpus callosum and has projections into the motor regions of the cortex (Figure 6). The "affective" areas of the cingulate cortex have extensive connections with the amygdala and periaqueductal gray matter and with autonomic nuclei in the brain stem[102]. This connectivity integrates autonomic and endocrine functions and recall of

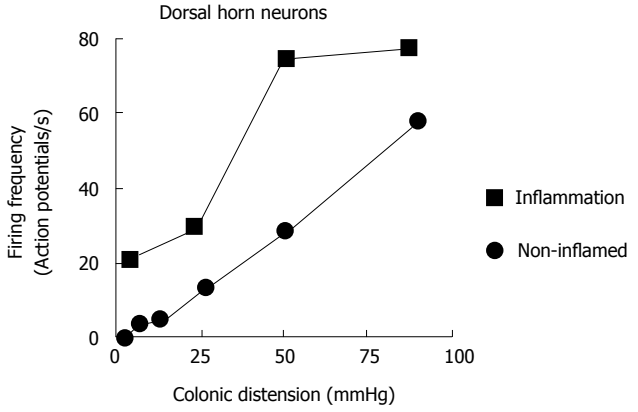

Figure 7 Firing frequency of neurons in the dorsal horns of the spinal cord in response to distension of the colon is increased during experimentally induced inflammation of the colon in rats. Increased sensitivity is reflected by a decreased firing threshold and increased gain (increased slope) of the relation of firing frequency to degree of distension. Data extracted from Cervero and Laird[177].

emotional experiences. Cognition is believed to reside in the caudal portion of the anterior cingulate cortex where the microcircuits are delegated to premotor functions and processing of nociceptive information.

The functional neuroanatomy of the cingulate cortex offers an explanation for the well documented association of psychosocial disturbances (e.g. negative life events) with more severe cases of IBS[99]. Rectal distension in persons with histories of severe sexual and/or physical abuse has been reported to selectively activate the perigenual region of the anterior cingulate cortex (Figure 6). One case report described a middle-aged female whose low pain threshold for rectal distension and diarrhea-predominant IBS improved after she was extricated from an abusive psycho-social situation. Brain imaging with fMRI in this individual showed activation of the mid-cingulate cortex during rectal distension prior to treatment and resolution of activation associated with improvement in the patient's psycho-social situation[103].

Sensory processing in the spinal cord

Nociceptive afferents, which do not project to dorsal column nuclei, terminate in the dorsal horn of the spinal cord. They form synapses with second order nociceptive neurons that are located mainly in laminae Ⅰ & Ⅱ. Most of the neurons in laminae Ⅰ & Ⅱ receive direct synaptic input from A-delta and nonmyelinated C-fibers. Large numbers of neurons in lamina Ⅰ respond exclusively to noxious stimulation and project the information to higher brain centers (Figure 5).

Central sensitization ("wind-up")

Elevated excitability in nociceptive dorsal horn neurons underlies spinally mediated hyperalgesia, which is termed central sensitization to distinguish it from sensitization that occurs at nociceptive terminals in the periphery. In conditions of severe tissue injury and persistent injury, nociceptive C fibers fire repetitively and the excitability of the second order neurons in the dorsal horn increases progressively in response to the elevated synaptic input. This effect is sometimes called "wind-up" and reflects the synaptic release of glutamate from the incoming C-fibers and activation of N-methyl-D-aspartate (NMDA)-type glutamate receptors expressed by the second order neurons. These long-lasting changes in the excitability of dorsal horn neurons are like a memory imprint of the nociceptive input. Accumulating evidence suggests that the spinal wind-up phenomenon may be operational and be an underlying factor in the intestinal hypersensitivity associated with IBS.

One piece of the suggestive evidence for wind-up hypersensitivity is the finding that second order neurons in the dorsal horn show induction of the early gene c-fos in response to noxious balloon distension of the colon in rats[104]. Changes in gene expression in this case are expected to underlie postsynaptic excitability changes in the second order nociceptive neurons. A related phenomenon occurs in the rat spinal cord where excitability of second order nociceptive neurons become sensitized to distension-evoked input following inflammation of the colon produced by application of acid to the mucosa (Figure 7). The same phenomenon is evident in dorsal column nuclei where firing of second order neurons to colo-rectal distension becomes sensitized following inflammation of the colon evoked by application of mustard oil to the mucosa[105]. These effects of inflammation are characterized by a decrease in threshold and an increase in firing rate of the neurons in the dorsal horn and dorsal column nuclei in response to distension of the large intestine. This is believed to reflect central sensitization secondary to peripheral sensitization and elevated firing of sensory nerve terminals in the inflamed intestinal wall.

In a study, which is reminiscent of the connection between sexual and physical abuse in early childhood and IBS in adult humans, Al-Chaer *et al*[106] reported that central sensitization may also be induced in animal models in the absence of inflammation. Neonatal rats in this study were subjected daily to noxious colo-rectal distension or intracolonic injection of mustard oil beginning 8 d postpartum and lasting for 21 d. When tested in adulthood, the rats that were "abused" as neonates were hypersensitive to colo-rectal distension as reflected by a lower threshold and elevated intensity of reflex responses indicative of abdominal pain. Single-unit electrophysiological recording from dorsal horn neurons in the lumbar and sacral regions of the spinal cord of the adult animals found significantly higher background firing frequencies in the animals that were "abused" as neonates and enhanced firing frequencies in response to colo-rectal distension when compared with non-abused controls. Histological examination found no evidence of an inflammatory state in the large intestine in either the adult "abused" animals or their controls in these studies.

Limited evidence for central sensitization to distension of the large bowel has been obtained for humans, who meet diagnostic criteria for IBS[61]. In IBS patients, repetitive inflation of a balloon in the sigmoid colon, to noxious levels of stimulation, alters the processing of afferent information entering the spinal cord from the rectum. Altered central processing appears to be present in IBS patients and not in normal subjects. The

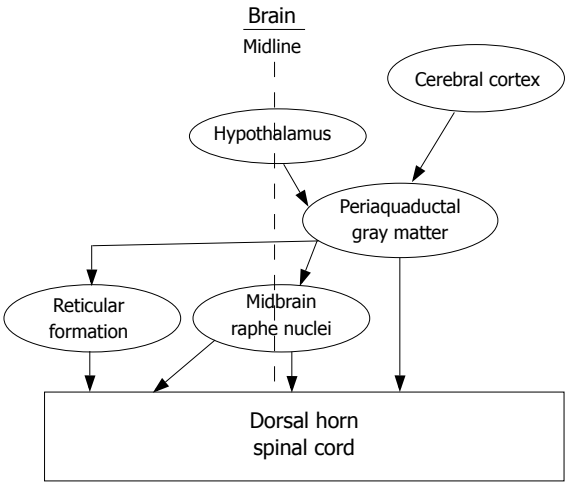

Figure 8 Multiple descending pathways from integrative centers in the brain project to the dorsal horn of the spinal cord where they release neurotransmitters that modulate the transmission of nociceptive signals after entry into the spinal cord.

altered central processing in human IBS is reflected by development of hyperalgesia in response to rectal distension and spontaneously developing hyperalgesia over an extended period of time in the recto-sigmoid region in the absence of any further application of the repetitive distension protocol.

Descending spinal modulatory pathways

Processing of incoming nociceptive signals in the spinal cord is subject to descending modulatory influences from supraspinal structures in the brain (e.g. periaqueductal gray, nucleus raphe magnus, nuclei reticularis gigantocellularis, and the ventrobasal complex of the thalamus) (Figure 8). The descending modulatory activity can be either inhibitory, facilitatory or both depending on the context of the visceral stimulus or the intensity of the descending neural activity. The descending pathways, which originate in the brainstem and higher centers, influence the processing of nociceptive signals from the bowel within the microcircuitry of the dorsal horn of the spinal cord. These descending pathways release serotonin and noradrenalin and to a lesser extent dopamine as neurotransmitters at their synapses in the spinal cord.

Descending modulation of visceral nociceptive processing at the spinal cord level is ongoing and includes both inhibitory and facilitative influences on synaptic transmission in the dorsal horn microcircuits. Experimental data, which correlate behavioral responses and neuronal electrical and synaptic behavior, suggest that activity in descending modulatory pathways influences neuronal activity at the spinal cord level and the behavior of individuals experiencing acute and persistent pain[107]. The descending modulation includes facilitative and inhibitory influences both of which can alter the sensing of pain of gut origin.

Electrical stimulation or chemical activation (i.e. intracerebral injection of neurotransmitters or blocking drugs) of several different supraspinal centers modulates the neuronal and behavioral responses to visceral stimuli. For example, nociceptive responses to intraperitoneal injection of hypertonic saline in rats are attenuated by electrical stimulation in the periaqueductal gray matter[108]. Chemically-induced activation of neuronal cell bodies in the rostro-ventral medulla also attenuates responses to visceral stimulation[109,110]. Electrical stimulation or microinjection of glutamate into the periaqueductal gray matter, nucleus raphe magnus or the nuclei reticularis gigantocellularis suppresses spinal dorsal horn neuronal responses to visceral afferent fiber stimulation and to noxious colo-rectal distention[111-113]. The descending inhibition from the rostro-ventral medulla travels along pathways in the dorsolateral spinal cord[114]. Electrical stimulation of the ventrobasal complex of the thalamus suppresses the responses of dorsal horn neurons to colorectal distension in normal rats[115].

Sensory visceral input to the dorsal horn is also subject to descending facilitative modulation. Descending facilitation might enhance conscious perception of the bowel in the absence of any noxious stimulation and could possibly explain the hypersensitivity often reported to be present in IBS. Several lines of evidence support the presence of tonic descending facilitative influences in animals. In cats, reversible blockade of descending pathways by cervical cooling suppresses the responses of a subset of visceral neurons to stimulation of the splanchnic nerves[116]. Zhuo and Gebhart[114] investigated the effects of electrical or chemical stimulation in the rostro-ventral medulla on reflex contractions of the abdominal musculature of the rat in response to noxious colo-rectal distension. Reflex contraction of the abdominal musculature in response to colorectal distension in this kind of study is regarded as a measurable perimeter for assessment of severity of visceral pain in this rat model. When applied at 22 different sites in the rostro-ventral medulla, electrical stimulation facilitated the reflex responses to noxious distension at low stimulus intensities of 5, 10, and 25 μA and suppressed the reflex responses at stimulus intensities greater than 50 μA. Electrical stimulation at all intensities tested (5-200 μA) in other sites in the rostro-ventral medulla only inhibited or only facilitated reflex responses to noxious colorectal distention. Microinjection of glutamate into the rostro-ventral medulla mimics the findings for electrical stimulation. Reversible spinal blockade by injection of lidocaine or irreversible transection of spinal funiculi revealed that descending facilitatory influences from the rostro-ventral medulla were transmitted in the ventrolateral/ventral funiculus and descending inhibitory influences were carried by the dorsolateral funiculi. Descending modulation, whether inhibitory or facilitative, is linked to a reflex response to noxious stimulation; neither electrical stimulation nor glutamate injection alters contractile behavior of the abdominal musculature in the absence of colorectal distension.

Intestinal motility and abdominal pain

Strong contractions of the intestinal circular muscle coat during intestinal power propulsion (Figure 9) underlie the sensation of cramping abdominal pain[21,117]. Power

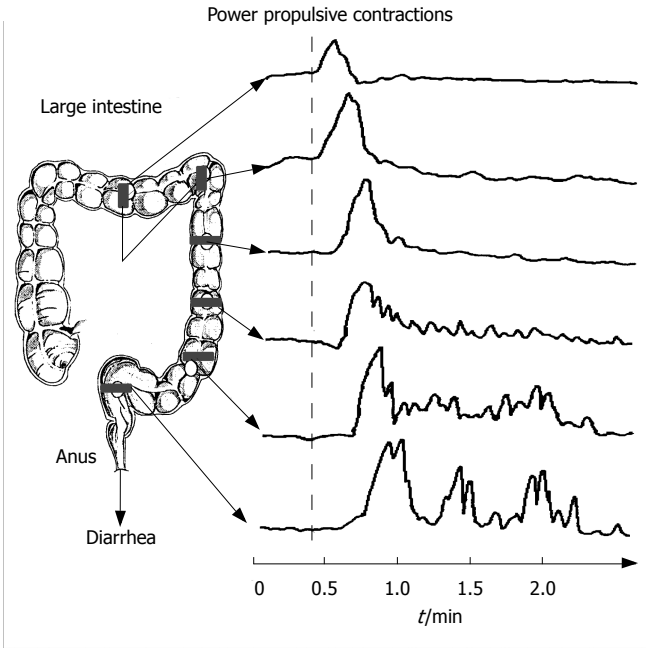

Figure 9 Power propulsion is a protective response to the presence of food allergens or other threatening agents in the intestinal lumen. It is an ENS programmed motility pattern that can be recorded with sensors (e.g. force transducers) as strong, long lasting contractions of the circular muscle that propagate rapidly for extended distances along the intestine. Power propulsion quickly strips the lumen clean as it travels along extended lengths of intestine. Abdominal cramping, urgency, diarrhea and threat of incontinence are associated with this motor program. Application of irritants to the mucosa, the introduction of luminal parasites, enterotoxins from pathogenic bacteria, allergic reactions and exposure to ionizing radiation each can trigger the propulsive motor program.

propulsion, which is one of the patterns of motility stored in the program library of the ENS, occurs more frequently in IBS patients than in normal subjects and the circular muscle contractions are significantly stronger than normal in IBS patients[53]. Postprandial power propulsion is more prevalent in the colon of IBS patients than in normal individuals and power propulsion in the colon is often associated with their diarrhea[48].

Power propulsion in the large intestine generally starts in the proximal colon and strips the lumen clean as it travels rapidly toward the recto-sigmoid region (Figure 9). In diarrheal states, large volumes of watery stool may be propelled quickly into the distal large bowel. Rapid distension of the recto-sigmoid region by the advancing luminal contents triggers the recto-anal reflex. Relaxation of the internal anal sphincter and conscious need for contraction of the external sphincter and puborectalis muscle occur at this time coincident with the sensation of urgency and concern about incontinence. The sensation of urgency is derived from mechanosensory information transmitted to the CNS along spinal afferents from the recto-sigmoid region and pelvic floor musculature.

The pain and discomfort in IBS patients during the powerful contractions of power propulsion may be explained in three ways, either separately or in combination. One explanation is for the exceptionally powerful circular muscle contractions to activate high-threshold mechanoreceptors that transmit the information centrally where it is processed and projected to consciousness as the perception of pain and discomfort. A second is for the mechanoreceptors to become sensitized in the IBS patients (e.g. by inflammatory mediators or other paracrine signals) and send erroneously coded information to processing centers in the spinal cord and brain. A third explanation is for accurately coded sensory information carried by spinal afferents to be mis-interpreted as it is decoded in the spinal cord and central processing centers of the brain.

PSYCHOGENIC STRESS

Psychological stress and negative life experiences are recognized as exacerbating psychosocial factors in IBS[5,99,100,103,118]. Stress often exacerbates symptoms of cramping abdominal pain, diarrhea and urgency in IBS patients. These stress-exacerbated symptoms in IBS are similar, if not identical, to the abdominal pain, diarrhea and urgency associated with enteric allergic responses, infectious enteritis, radiation-induced enteritis and noxious mucosal irritation (e.g. senna laxatives). Recent advances in the basic science of brain-to-gut and immune cells-to-ENS signaling have introduced fresh insight into mechanisms underlying the effects of psychological stress on the intestinal tract.

Neuro-immunophysiological paradigm for IBS-Like symptoms

The human enteric immune system is developed at birth and is colonized by populations of immune/inflammatory cells that will change continuously in response to luminal conditions and pathophysiological states throughout the individual's lifetime. The enteric immune system is positioned to provide security at one of the most contaminated borders between the interior of the body and the outside world. It deals continuously with dietary antigens, parasites, bacteria, viruses, and toxins as they appear in the warm-dark-moist-anaerobic environment of the intestinal lumen. The system is continuously challenged because physical and chemical barriers at the epithelial interface never exclude the large antigenic load in its entirety. Furthermore, stress in the form of threatening environmental conditions in animal models or handling of the gut during laparotomy in humans opens the barrier[119-121].

Immuno-neural crosstalk

Insight into how chemical communication between the mucosal immune system and the ENS takes place is derived from electrophysiological recording in enteric neurons in intestinal preparations from animal models after sensitization to foreign antigens[122-124]. Signals from enteric immune/inflammatory cells activate a neural program for defensive intestinal behavior in response to circumstances within the lumen that are threatening to the functional integrity of the whole animal. The signaling mechanism is chemical in nature (i.e. paracrine) and incorporates specialized sensing functions of intestinal mast cells for foreign antigens together with the capacity of the ENS for intelligent interpretation of antigen-evoked mast cell signals[16,48,125]. Immuno-neural integration starts with immune detection and progresses sequentially

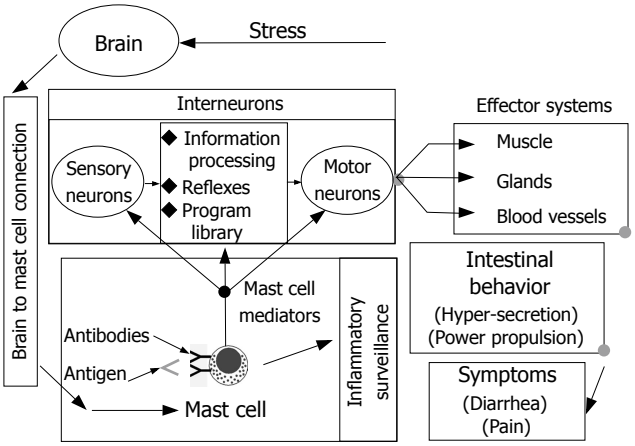

Figure 10 Heuristic model for brain-gut interaction in response to stress. The ENS is a minibrain located in close apposition to the gastrointestinal effectors it controls. Enteric mast cells are positioned to detect foreign antigens and signal their presence to the ENS. When, stimulated mast cells release several paracrine mediators simultaneously. Some of the mediators signal the ENS while others act as attractant factors for polymorphonuclear leukocytes responsible for acute inflammatory responses. The ENS responds to the mast cell signal by initiating a defensive program of coordinated secretion and propulsive motility that functions to rapidly expel the source of antigenic stimulation from the bowel. Symptoms of abdominal pain, fecal urgency and watery diarrhea result from operation of the defense program. Neural inputs to enteric mast cells from the brain stimulate simultaneous release of chemoattractant factors for inflammatory cells and chemical signals to the ENS with effects that mimic the symptoms of antigenic detection by the mast cells. Stress activates this brain-to-mast cell connection.

with signal transfer to the ENS, followed by neural interpretation and then by selection of a specific neural program of coordinated mucosal secretion and powerful motor propulsion (i.e. power propulsion, see Figure 9) that effectively clears the threat from the intestinal lumen. IBS-like symptoms of cramping lower abdominal pain, fecal urgency and watery diarrhea reflect operation of the immuno-neural defense program.

Sources of immuno-neural signals

Lymphoid and myeloid cells colonize the gastrointestinal tract in numbers that continuously fluctuate with changing luminal conditions and pathophysiological states[126]. Cell types including polymorphonuclear leukocytes, lymphocytes, macrophages, dendrocytes and mast cells are present in continuously varying numbers in the intestinal mucosa, lamina propria and smooth muscle and are potential sources of immuno-neural signals. Each of these cell types can be situated in close histoanatomical association with the neuronal elements of the ENS, vagal nerve fibers and spinal sensory nerves[56,58,127-130].

Signaling from the cells of the enteric immune/inflammatory system to the ENS establishes a first line of defense against foreign invasion at the vulnerable interface of a single epithelial cell barrier between the body and the outside environment. In inflammatory states, close histoanatomical proximity of elevated numbers of lymphocytes and polymorphonuclear leukocytes to enteric nerve elements suggests that inflammatory mediators released by these cells might access and influence the ENS. Electrophysiological studies in enteric neurons confirm that inflammatory mediators released in paracrine fashion alter electrical and synaptic behavior of enteric neurons[122-124].

Enteric mast cells

All kinds of immune/inflammatory cells are putative sources of paracrine signals to the ENS. Most is known, however, about signaling between enteric mast cells and the neural elements of the ENS. Enteric mast cells are packed with granules that are sites of storage for a broad mix of preformed chemical mediators. Antigens stimulate the mast cells to release the mediators, which then diffuse into the extracellular space inside the ENS. Enteric mast cells express high affinity receptors for IgE antibodies or other immunoglobulins on their surfaces. A deluge of multiple mediators is released from the mast cells when antibodies to a sensitizing antigen occupy the receptors and cross-linking occurs by interaction of the sensitizing antigen with the bound antibody (Figure 10).

Infections with nematode parasites stimulate proliferation of intestinal mast cells in animal models[127,131]. These nematode-infected models and food allergic models have been valuable for studies of mast cell involvement in enteric immuno-neural communication. In the sensitization models, a second exposure to antigen isolated from the infectious agent (e.g. intestinal nematode) or to a food antigen results in predictable protective integration of intestinal motor and secretory behavior[119,132-135]. Recognition of the antigen by antibodies bound to the sensitized mast cells triggers degranulation and release of the mast cell's mediators. Once released, the mediators become paracrine signals to the ENS, which responds by suspending operation of other programs in its library and running a defense program designed to eliminate the antigen from the lumen. Copious secretion and increased blood flow followed by orthograde power propulsion of the luminal contents are the behavioral components of the program. Abundant evidence supports a hypothesis that mast cells are equipped and strategically placed to recognize foreign agents that threaten whole body integrity and to signal the ENS to program a defensive response, which expels the threat. The immuno-neural defensive program in the lower half of the intestinal tract is reminiscent of the emetic program, which provides a similar defense for the upper gastrointestinal tract.

Mast cell function in immuno-neural communication is an immune counterpart of sensory detection and information coding in sensory neurophysiology. In sensory physiology, sensory neurons are genetically programed to express detection mechanisms for specific stimuli (e.g. touch, temperature or light), which remain fixed throughout the life of the individual. Mast cells, on the other hand, acquire specific detection capabilities through the flexibility of recognition functions inherent in synthesis of specific antibodies by the immune system. Detection specificity for foreign antigens is acquired and reinforced throughout life due to formation of new antibodies that bind to and occupy immunoglobulin receptors on mast cells. The output signals from mast cells, which are triggered by cross-linking of antigens with the attached antibodies, are chemical in nature and analogous to chemical output signals (i.e. neurotransmitters) from

sensory neurons to second order neurons in the brain and spinal cord. Both mast cells and sensory neurons ultimately code information on the sensed parameter by releasing a chemical message that is decoded by information processing circuits in the nervous system.

Mast cells and the brain-gut connection

Aside from their sensing function, enteric mast cells provide a connection node between the CNS and ENS. This is a brain-gut interaction in which central psychological status can be linked to irritable states of the digestive tract by way of mast cell degranulation and release of mediators. Mast cell degranulation evoked by psychological stress activates the ENS "defense program" to produce the same symptoms of diarrhea and abdominal distress as antigen-evoked degranulation. Evidence for a brain-mast cell connection appears in reports of Pavlovian conditioning of enteric mast cell degranulation[136]. Release of mast cell proteases into the systemic circulation and intestinal lumen is a marker for degranulation of enteric mucosal mast cells. Release of proteases into the circulation occurs as a conditioned response in laboratory animals to either light or auditory stimuli after pairing with antigenic sensitization[136]. In humans release of mast cell proteases into the lumen of the small intestine occurs as a conditioned response to stress[137], which like the animal studies, reflects a brain to enteric mast cell connection. Central nervous influence on mast cells in the upper gastrointestinal tract is suggested by close histological association between vagal afferents and enteric mast cells[130] and by elevated expression of histamine in intestinal mast cells in response to vagal nerve stimulation[128]. Electrical stimulation of spinal afferents in nerve trunks in the small intestinal mesentery likewise stimulates release of histamine from enteric mast cells, which is mediated by the action of substance *P* at the neurokinin-1 receptor subtype expressed by the mast cells[138].

Stimulation of neurons in the brain stem by intracerebroventricular injection of thyrotropin-releasing hormone (TRH) evokes degranulation of mast cells in the rat small intestine and adds to the evidence in support of a CNS to mast cell connection[139]. Intracerebroventricular injection of TRH in the rat brain evokes the same kinds of inflammation and erosions in the stomach as cold-restraint stress. In the large intestine, restraint stress exacerbates nociceptive responses to distension that are associated with increased release of histamine from mast cells[140]. Like the effects of central TRH on gastric mucosal pathology, intracerebroventricular injection of corticotropin releasing factor mimics large intestinal responses to stress. Injection of a corticotropin releasing factor receptor antagonist or pretreatment with mast cell stabilizing drugs suppresses stress-evoked responses in the lower gastrointestinal tract[141]. The brain-mast cell connection is significant because the gastrointestinal symptoms associated with mast cell degranulation are expected to be the same whether the mast cells are degranulated by antigen-antibody cross-linking in allergies or input from the brain during stress.

Mast cell degranulation releases mediators that sensitize "silent" nociceptors in the large intestine[67]. In animals, degranulation of enteric mast cells results in a reduced threshold for pain responses to intestinal distension and this is prevented by treatment with mast cell stabilizing drugs[81]. Receptors for mast cell mediators are expressed on the terminals of vagal and spinal sensory afferent neurons[142-144]. Actions of mast cell mediators to sensitize sensory nerves is reminiscent of the characteristic hypersensitivity to intestinal distension found in a subset of patients with IBS[60,61,64]. Colonic mucosal biopsies from patients with IBS reportedly contain elevated numbers of mast cells and this raises the question of whether the hypersensitivity to distension reflects sensitization of intramural endings of spinal mechanosensitive nerves by the release of mediators from these pools of mast cells[57,58].

Degranulating mast cells release mediators to signal the ENS that degranulation has taken place and at the same time attract immune/inflammatory cells into the intestinal wall from the mesenteric circulation. Placement of purified *Clostridium difficile* toxin-A into intestinal loops stimulates influx of acute inflammatory cells coincident with activation of the ENS "defense program". Activation of the defensive program becomes evident as copious mucosal secretion and power propulsion. Blockade of enteric nerves by tetrodotoxin, treatment with tachykinin NK-1 receptor antagonists or mast cell stabilizing drugs prevents the acute inflammatory response to the toxin[145-148]. Responses to *C. difficile* toxin-A do not occur in mast cell deficient mice[149].

Substance *P* is a recognized mediator in the chain of events leading to toxin-A-induced mast cell degranulation and release of chemoattractant factors for inflammatory cells from the circulation[150,151]. The neuropeptide is expressed by enteric neurons and spinal sensory afferent neurons. It is a putative neurotransmitter in the ENS and for intramural axonal reflexes mediated by spinal sensory afferents. Substance *P* is a secretagogue for histamine and cytokine release from mast cells[138,150,151]. The excitatory action of *C. difficile* toxin-A on enteric neurons is expected to releases neuronal substance *P*, which in turn acts to degranulate mast cells in the neighborhood where it is released.

Exposure of enteric myenteric and submucosal neurons to *C. difficile* toxin-A depolarizes the membrane potential and elevates excitability. This occurs coincident with presynaptic suppression of nicotinic fast excitatory synaptic transmission in both plexuses and with suppression of inhibitory noradrenergic neurotransmission to secretomotor neurons in the submucosal plexus[152]. Suppression of noradrenergic neurotransmission removes sympathetic braking action from secretomotor neurons and this facilitates stimulation of secretion (Figure 3). Together with toxin-A evoked excitation of secretomotor neurons, this is undoubtedly an underlying factor in the diarrhea associated with antibiotic-related overgrowth of *C. difficile* in the large intestine.

Mast cell signal substances

Several mast cell-derived mediators have neuropharmacological actions on electrical and synaptic behavior of neurons in the ENS. Some important mediators known

to act at their receptors on neural elements in the ENS are: (1) Histamine; (2) Interleukin-6; (3) Leukotrienes; (4) 5-hydroxytryptamine; (5) Platelet activating factor; (6) Mast cell proteases; (7) Adenosine; (8) Interleukin-1β; (9) Prostaglandins.

Histamine

Histamine is not synthesized by enteric neurons and is not considered to be a neurotransmitter in the ENS[153]. Mast cells and neutrophils are sources of histamine in the intestine. Knowledge of histaminergic actions on ENS neurons comes from results obtained from electrophysiological and immunohistochemical studies on single enteric neurons in animals. Application of histamine, to mimic release from mast cells and neutrophils, excites neurons in the small and large intestinal myenteric and submucosal plexuses of the guinea-pig[154,155]. Unlike the intestine, enteric neurons in the guinea-pig stomach do not express histamine receptors and do not respond to experimental applications of histamine[124].

Histamine has three significant actions on neural elements in the guinea-pig intestine. One action, which occurs at the level of neuronal cell bodies, is long-lasting excitation mediated by histamine H_2 receptors[154,155]. The second is at fast excitatory nicotinic synapses, where it acts at presynaptic inhibitory histamine H_3 receptors to suppress cholinergic synaptic transmission[45,156,157]. The third action is to prevent inhibition by the sympathetic innervation of the intestine of secretomotor-evoked mucosal secretion (Figure 3). Histamine acts at presynaptic histamine H_3 inhibitory receptors on sympathetic noradrenergic fibers to suppress sympathetic inhibitory input to submucosal secretomotor neurons and at H_3 presynaptic terminals of enteric somatostatinergic neurons that also provide inhibitory input to secretomotor neurons[45].

Mast cells in colonic mucosal biopsies from patients with diarrhea-predominant IBS release more histamine than normal subjects[58]. Elevated release and flooding of histamine onto the neural networks, which control the secretomotor innervation of the intestinal secretory glands in this subset of IBS patients, might enhance intestinal secretion leading to secretory diarrheal symptoms like those associated with infectious agents and food allergies. Histaminergic receptor antagonists have been used effectively in the past to treat watery diarrhea symptoms associated with mastocytosis and microscopic colitis[158]. The H_2 receptor antagonist cimetidine has been used effectively in the treatment of pediatric diarrhea and diarrhea associated with short-bowel syndrome in patients with Crohn's disease[159]. And finally, mast cell stabilizing drugs, which act to suppress histamine release, are efficacious in the treatment of diarrhea-predominant IBS[83].

Serotonin

5-Hydroxytryptamine is another preformed mediator that is known to be released during degranulation of enteric mast cells and mucosal enterochromaffin cells to form a neuromodulatory overlay on the ENS in animal models and humans. Two receptors mediate the excitatory actions of serotonin at the cell bodies of guinea-pig enteric neurons. One of the receptors, which was initially identified as a 5-HT_{1P} receptor, is a metabotropic receptor activation of which evokes long-lasting excitatory responses in enteric neurons[160-162]. What was initially reported as serotonergic slow synaptic excitation, mediated by the 5-HT_{1P} receptor, is now known to be blocked by a 5-HT_7 antagonist, SB 269970, and mimicked by application of a 5-HT_7 agonist, 5-carboxamidotryptamine[163]. Liu and Gershon[164] presented results, which suggested that the 5-HT_{1P} receptor is a dimer of a 5-HT_{1B} receptor and a dopamine D_2 receptor. Both receptors are expressed by enteric neurons.

The response to stimulation of the elusive 5-HT_{1P} receptors, like stimulation of histamine H_2 receptors, evokes long-lasting excitatory responses in the time range of minutes in ENS neurons. The second receptor, identified as a 5-HT_3 receptor, is an ionotropic receptor directly coupled to non-selective cation channels[165]. Binding of 5-HT to the 5-HT_3 receptor evokes "fast" depolarizing responses that quickly desensitize and occur in the millisecond time range like those evoked by nicotinic receptor stimulation. Expression of two kinds of serotonergic receptors with different mechanisms of postreceptor signal transduction differs from the situation for histamine where only a single metabotropic receptor subtype is expressed by the neuronal cell body.

Histamine and 5-HT both act at presynaptic inhibitory receptors on cholinergic axons to suppress fast neurotransmission at nicotinic synapses in the enteric neural networks[156,166]. Presynaptic inhibition by both neuromodulators is mediated by a different receptor subtype than the one that evokes excitatory responses in the neuronal cell bodies. Identification of the presynaptic inhibitory 5-HT receptor is equivocal; the evidence suggests that it might be a 5-HT_1 receptor[167,168]. In addition to presynaptic inhibitory action at enteric neuronal synapses, histamine and 5-HT each act presynaptically to suppress the release of norepinephrine from sympathetic postganglionic fibers in the ENS[45,169].

Serotonin and functional disorders

Infusion of 5-HT either intravenously or into the intestinal lumen evokes copious secretion of H_2O, electrolytes and mucus from the intestinal secretory glands[45,170]. The stimulatory action of 5-HT underlies its action as a diarrheagenic agent and its involvement in diarrheagenic syndromes in humans[171]. Efficacy of blockade of the 5-HT_3 serotonergic receptor subtype by the selective 5-HT_3 receptor antagonist, alosetron, in the treatment of diarrhea and abdominal pain in the diarrhea-predominant population of women with IBS[52,76] suggests that enhanced stimulation of neural elements in the ENS by 5-HT might be a pathophysiological factor in this form of IBS.

The IBS symptoms of cramping abdominal pain, diarrhea and fecal urgency are exacerbated in the postprandial state[6,7]. Elevated appearance of 5-HT in the hepatic portal circulation in the postprandial state reflects stimulated release from mucosal enterochromaffin cells[54]. The normal postprandial release of 5-HT is reported to be augmented in IBS patients[55] and this

contributes to the suspicion that overactive release of serotonin might be an underlying factor in the symptoms of IBS in diarrhea-predominant patients. This suspicion is reinforced by findings of elevated numbers of mast cells and enterochromaffin cells, both of which contain 5-HT, in colonic mucosal biopsies from IBS patients[57,58].

Reports that a significant proportion of IBS patients develop IBS-like symptoms following an acute bout of infectious enteritis are reminiscent of the basic research findings for the actions of inflammatory mediators, including histamine and serotonin, in the ENS. Gwee *et al*[70] reported that 23 percent of patients, who experienced an acute bout of gastroenteritis, progressed to IBS-like symptoms within 3 mo. Hypochondriasis and adverse life events are reported to double the risk for development of postinfective IBS and may account for the increased proportion of women who develop the syndrome[73]. Nevertheless, the question of whether the association between acute infectious enteritis and IBS reflects low-level inflammation (e.g. microscopic enteritis) and chronic exposure of the neural and glial elements of the ENS to elevated levels of serotonin, histamine or other inflammatory mediators remains to be fully resolved.

Exposure to 5-HT evokes increased firing in sensory nerves that leave the intestine and make synaptic connections in the spinal cord[74]. This excitatory action on intestinal sensory nerves is mediated by the 5-HT_3 receptor subtype and is blocked by selective 5-HT_3 receptor antagonists (e.g. alosetron)[75]. Intramural terminals of both spinal and vagal sensory nerves express 5-HT_3 receptors. Reported efficacy of the 5-HT_3 receptor blocking drug, alosetron, in the treatment of abdominal pain and discomfort in the diarrhea-predominant form of IBS in women[52,76] suggests that the pain and discomfort, like the diarrhea and fecal urgency, reflect disordered endogenous release of 5-HT and its action at the 5-HT_3 receptors present on sensory terminals in the intestinal wall.

Receptors on sensory nerve terminals

Aside from 5-HT_3 receptors, the sensory nerve terminals in the intestine express receptors for several other putative signal substances, including inflammatory mediators. Functional receptors for bradykinin, ATP, adenosine, prostaglandins, leukotrienes and mast cell proteases are expressed on spinal sensory nerve terminals[80]. Intramural pooling of any one of these mediators has potential for increasing the sensitivity of intestinal sensory nerves, especially in conditions of inflammation or ischemia.

Mediators, released by mast cells, are known to sensitize nociceptors in the large intestine[68]. Mast cell degranulation in animal models, results in a reduced threshold for pain responses to balloon distension in the large bowel. Treatment with mast cell stabilizing drugs prevents lowering of the pain threshold during mucosal inflammation in animal models[81]. The results obtained from animals leads to the unresolved question of whether the association between an acute bout of infectious enteritis and the follow-up IBS symptoms of abdominal pain and elevated sensitivity to distension reflects chronic sensitization of intestinal sensory nerves as they function in an environment with low-level inflammation.

Brain-to-mast cell connection: Implications for functional disorders

A brain-to-mast cell connection is currently the most plausible mechanism for explanation of the well-known relationship between stress and IBS-like bowel symptoms. Sympathetic nervous activation is not a plausible explanation! Activation of the sympathetic nervous system accounts for elevations of blood pressure and heart rate in the stressed individual, but cannot explain the symptoms of cramping lower abdominal, watery diarrhea and fecal urgency. Advances in understanding of the sympathetic interface with the ENS ruled-out sympathetic involvement because sympathetic activation inhibits secretomotor neurons and thereby suppresses the neurogenic secretion that is necessary for generation of loose stools (Figure 3)[172]. Sympathetic activation and the release of norepinephrine likewise suppress nicotinic synaptic transmission in the ENS and are, therefore, unlikely to initiate the powerful propulsive motility in the colon that accounts for cramping lower abdominal pain.

A brain-to-mast cell connection implies a mechanism that links central psycho-emotional status to irritable states of the digestive tract. The irritable state of the bowel (i.e. abdominal discomfort, cramping lower abdominal pain, diarrhea and urgency), known to result from degranulation of intestinal mast cells and release of signals to the ENS, is expected to occur irrespective of the mode of stimulation of the mast cells (Figure 10). Degranulation and release of mediators evoked by neural input to the mast cells will have the same effect of triggering a program of secretion and power propulsion as degranulation triggered by antigen detection. This most likely explains the similarity of bowel symptoms between those associated with noxious insults in the lumen and those associated with psychogenic stress in susceptible individuals.

The immuno-neurophysiological evidence reinforces the hypothesis that moment-to-moment behavior of the gut, whether normal or pathological, is determined primarily by integrative functions of the ENS. The enteric minibrain processes input signals derived from immune/inflammatory cells (e.g. mast cells), sensory receptors and the CNS. Enteric mast cells utilize the capacity of the immune system for detection of new antigens and long-term memory that permits recognition of the antigen if it ever reappears in the gut lumen. Should the antigen reappear, the mast cells signal its presence to the enteric minibrain. The minibrain interprets the mast cell signal as a threat and calls up from its program library secretory and propulsive motor behavior organized for quick and effective eradication of the threat. Operation of the program protects the integrity of the bowel and the individual, but at the expense of the side effects of abdominal distress and diarrhea. The same symptomatology is expected to result from activation of neural pathways that link psychological states in the brain to degranulation of mast cells in the gut. The immuno-neurophysiology in this respect is suggestive of mechanisms with susceptibility to malfunctions that could result in symptoms resembling diarrhea-predominant IBS.

A lingering issue for the enteric neuro-imunophysiological paradigm is the question of the functional significance of

the brain-mast cell connection. What were the selective pressures that led to evolution of central signaling to mast cells in the gut? A hypothesis emerges from the fact that the barrier between an extremely "dirty" luminal environment and the interior of the body is a single epithelial cell layer. Probability of a break in the barrier is higher during physical stress and the potential for trauma (e.g. "predacious attack, fright and flight"). Stress factors are known to increase the permeability of the barrier in animals[173]. The potential for threats to breach the mucosal barrier suggests a need for immune surveillance at a dangerous interface in the body. Increased immune surveillance would include an influx of acute inflammatory cells into the intestinal lamina propria and mucosa.

The brain has evolved to program homeostatic adjustments to environmental stressors and the emotional stress associated with negative life events. These adjustments include cardiovascular, hormonal and metabolic changes and probably the targeting of inflammatory cells into the gut from the systemic circulation. The only apparent mechanism available to the brain for selective targeting of inflammatory surveillance to the gut is to transmit nervous signals that degranulate enteric mast cells and release chemoattractant factors to "call-in" inflammatory cells from the circulating blood (Figure 10).

Studies of colitis in a non-human primate (cotton-top tamarin) implicate two co-existing factors as being necessary for the initiation and progression of inflammatory bowel disease (i.e. ulcerative colitis) in this model. One of the factors is environmental stress and the other is the large intestinal microflora[126,174,175]. Colitis was not found in cotton-top tamarins living in a natural "stress-free" environment and with the normal microflora present in the large intestine. Movement of colitis-free tamarins out of their natural environment and into a stressful environment leads to an acute inflammatory response in the large intestine only if the feces are present. Studies, in which the fecal stream was diverted from loops of large intestine, found that colonoscopic and histological features of colitis disappeared from the loops and progressed in the colon in the same animal. These changes occurred while the tamarins in the study remained in a colitis-inducing environment. Results of a preliminary study, in which putative neural input to colonic mast cells was suppressed by dosing cotton-top tamarins with a non-peptide neurokinin-1 receptor antagonist, showed suppression of the inflammatory response in cotton-top tamarins held in a colitis-inducing (i.e. stressful) environment[176,177].

ACKNOWLEDGMENT

The opinions and ideas expressed in this review are my own. Nevertheless, they are based on work and interactions in my laboratory with a progression of outstanding students and visiting scientists whose discoveries have helped shape current concepts of neurogastroenterology. The National Institutes of Health NIDDK Institute has supported work on enteric neurophysiology in my laboratory continuously since 1973. Some of the work in the past 5 years was supported by grants from the Norvartis Pharmaceuticals, Corp. and Sucampo Pharmaceuticals, Inc.

REFERENCES

1 **Drossman DA**. The functional gastrointestinal disorders and the Rome III process. *Gastroenterology* 2006; **130**: 1377-1390
2 **Pan GZ**. The epidemiology study of irritable bowel syndrome. *Zhonghua Yixue Zazhi* 2004; **84**: 267-268
3 **Pan G**, Lu S, Ke M, Han S, Guo H, Fang X. Epidemiologic study of the irritable bowel syndrome in Beijing: stratified randomized study by cluster sampling. *Chin Med J* (Engl) 2000; **113**: 35-39
4 **Gwee KA**, Wee S, Wong ML, Png DJ. The prevalence, symptom characteristics, and impact of irritable bowel syndrome in an asian urban community. *Am J Gastroenterol* 2004; **99**: 924-931
5 **Ringel Y**, Sperber AD, Drossman DA. Irritable bowel syndrome. *Annu Rev Med* 2001; **52**: 319-338
6 **Quigley EM**. Changing face of irritable bowel syndrome. *World J Gastroenterol* 2006; **12**: 1-5
7 **Thompson WG**, Longstreth GL, Drossman DA, Heaton K, Irvine EJ, Muller-lissner S. Functional bowel disorders and functional abdominal pain. In: Drossman DA, Corazziari E, Talley NJ, Thompson WG, Whitehead WE. The functional gastrointestinal disorders, 2nd ed. McLean VA: Degnon Associates, 2000: 351-432
8 **Bouin M**, Lupien F, Riberdy M, Boivin M, Plourde V, Poitras P. Intolerance to visceral distension in functional dyspepsia or irritable bowel syndrome: an organ specific defect or a pan intestinal dysregulation? *Neurogastroenterol Motil* 2004; **16**: 311-314
9 **Thomsen L**, Robinson TL, Lee JC, Farraway LA, Hughes MJ, Andrews DW, Huizinga JD. Interstitial cells of Cajal generate a rhythmic pacemaker current. *Nat Med* 1998; **4**: 848-851
10 **Ward SM**, Sanders KM. Physiology and pathophysiology of the interstitial cell of Cajal: from bench to bedside. I. Functional development and plasticity of interstitial cells of Cajal networks. *Am J Physiol Gastrointest Liver Physiol* 2001; **281**: G602-G611
11 **Huizinga JD**. Physiology and pathophysiology of the interstitial cell of Cajal: from bench to bedside. II. Gastric motility: lessons from mutant mice on slow waves and innervation. *Am J Physiol Gastrointest Liver Physiol* 2001; **281**: G1129-G1134
12 **Sanders KM**, Ordög T, Ward SM. Physiology and pathophysiology of the interstitial cells of Cajal: from bench to bedside. IV. Genetic and animal models of GI motility disorders caused by loss of interstitial cells of Cajal. *Am J Physiol Gastrointest Liver Physiol* 2002; **282**: G747-G756
13 **Sanders KM**, Koh SD, Ward SM. Organization and electrophysiology of interstitial cells of Cajal and smooth muscle cells. In: Johnson LR, Barrett KE, Ghishan FK, Merchant JL, Said HM, Wood JD, editors. Physiology of the Gastrointestinal Tract. 4th ed. San Diego: Academic Press, 2006: 533-576
14 **Wood JD**. Electrical activity from single neurons in Auerbach's plexus. *Am J Physiol* 1970; **219**: 159-169
15 **Wood JD**. Excitation of intestinal muscle by atropine, tetrodotoxin, and xylocaine. *Am J Physiol* 1972; **222**: 118-125
16 **Wood JD**. Integrative functions of the enteric nervous system. Johnson LR, Barrett KE, Ghishan FK, Merchant JL, Said HM, Wood JD, editors. Physiology of the Gastrointestinal Tract. 4th ed. San Diego: Academic Press, 2006: 665-683
17 **Stanghellini V**, Camilleri M, Malagelada JR. Chronic idiopathic intestinal pseudo-obstruction: clinical and intestinal manometric findings. *Gut* 1987; **28**: 5-12
18 **Wood JD**. Neuropathy in the brain-in-the-gut. *Eur J Gastroenterol Hepatol* 2000; **12**: 597-600
19 **De Giorgio R**, Stanghellini V, Barbara G, Corinaldesi R, De Ponti F, Tonini M, Bassotti G, Sternini C. Primary enteric neuropathies underlying gastrointestinal motor dysfunction. *Scand J Gastroenterol* 2000; **35**: 114-122

20 **Törnblom H**, Lindberg G, Nyberg B, Veress B. Full-thickness biopsy of the jejunum reveals inflammation and enteric neuropathy in irritable bowel syndrome. *Gastroenterology* 2002; **123**: 1972-1979
21 **Wood JD**, Alpers DH, Andrews PL. Fundamentals of neurogastroenterology. *Gut* 1999; **45** Suppl 2: II6-II16
22 **Camilleri M**, Phillips SF. Disorders of small intestinal motility. *Gastroenterol Clin North Am* 1989; **18**: 405-424
23 **Munoz-Garcia D**, Ludwin SK. Adult-onset neuronal intranuclear hyaline inclusion disease. *Neurology* 1986; **36**: 785-790
24 **Palo J**, Haltia M, Carpenter S, Karpati G, Mushynski W. Neurofilament subunit--related proteins in neuronal intranuclear inclusions. *Ann Neurol* 1984; **15**: 322-328
25 **Mayer EA**, Schuffler MD, Rotter JI, Hanna P, Mogard M. Familial visceral neuropathy with autosomal dominant transmission. *Gastroenterology* 1986; **91**: 1528-1535
26 **Roy AD**, Bharucha H, Nevin NC, Odling-Smee GW. Idiopathic intestinal pseudo-obstruction: a familial visceral neuropathy. *Clin Genet* 1980; **18**: 291-297
27 **Schuffler MD**, Baird HW, Fleming CR, Bell CE, Bouldin TW, Malagelada JR, McGill DB, LeBauer SM, Abrams M, Love J. Intestinal pseudo-obstruction as the presenting manifestation of small-cell carcinoma of the lung. A paraneoplastic neuropathy of the gastrointestinal tract. *Ann Intern Med* 1983; **98**: 129-134
28 **Lennon VA**, Sas DF, Busk MF, Scheithauer B, Malagelada JR, Camilleri M, Miller LJ. Enteric neuronal autoantibodies in pseudoobstruction with small-cell lung carcinoma. *Gastroenterology* 1991; **100**: 137-142
29 **Heidenreich F**, Schober R, Brinck U, Hartung HP. Multiple paraneoplastic syndromes in a patient with antibodies to neuronal nucleoproteins (anti-Hu). *J Neurol* 1995; **242**: 210-216
30 **Jean WC**, Dalmau J, Ho A, Posner JB. Analysis of the IgG subclass distribution and inflammatory infiltrates in patients with anti-Hu-associated paraneoplastic encephalomyelitis. *Neurology* 1994; **44**: 140-147
31 **Rosenblum MK**. Paraneoplasia and autoimmunologic injury of the nervous system: the anti-Hu syndrome. *Brain Pathol* 1993; **3**: 199-212
32 **De Giorgio R**, Bovara M, Barbara G, Canossa M, Sarnelli G, De Ponti F, Stanghellini V, Tonini M, Cappello S, Pagnotta E, Nobile-Orazio E, Corinaldesi R. Anti-HuD-induced neuronal apoptosis underlying paraneoplastic gut dysmotility. *Gastroenterology* 2003; **125**: 70-79
33 **Wood JN**, Hudson L, Jessell TM, Yamamoto M. A monoclonal antibody defining antigenic determinants on subpopulations of mammalian neurones and Trypanosoma cruzi parasites. *Nature* 1982; **296**: 34-38
34 **Krishnamurthy S**, Schuffler MD. Pathology of neuromuscular disorders of the small intestine and colon. *Gastroenterology* 1987; **93**: 610-639
35 **Smith VV**, Gregson N, Foggensteiner L, Neale G, Milla PJ. Acquired intestinal aganglionosis and circulating autoantibodies without neoplasia or other neural involvement. *Gastroenterology* 1997; **112**: 1366-1371
36 **De Giorgio R**, Guerrini S, Barbara G, Cremon C, Stanghellini V, Corinaldesi R. New insights into human enteric neuropathies. *Neurogastroenterol Motil* 2004; **16** Suppl 1: 143-147
37 **De Giorgio R**, Guerrini S, Barbara G, Stanghellini V, De Ponti F, Corinaldesi R, Moses PL, Sharkey KA, Mawe GM. Inflammatory neuropathies of the enteric nervous system. *Gastroenterology* 2004; **126**: 1872-1883
38 **De Giorgio R**, Barbara G, Stanghellini V, De Ponti F, Salvioli B, Tonini M, Velio P, Bassotti G, Corinaldesi R. Clinical and morphofunctional features of idiopathic myenteric ganglionitis underlying severe intestinal motor dysfunction: a study of three cases. *Am J Gastroenterol* 2002; **97**: 2454-2459
39 **Wood JD**. Application of classification schemes to the enteric nervous system. *J Auton Nerv Syst* 1994; **48**: 17-29
40 **Bornstein JC**, Furness JB, Kunze WA. Electrophysiological characterization of myenteric neurons: how do classification schemes relate? *J Auton Nerv Syst* 1994; **48**: 1-15
41 **Brookes SJH**, Costa M. Functional histoanatomy of the enteric nervous system. In: Johnson LR, Barrett KE, Ghishan FK, Merchant JL, Said HM, Wood JD, editors. Physiology of the Gastrointestinal Tract. 4th ed. San Diego: Academic Press, 2006: 577-602
42 **Andriantsitohaina R**, Surprenant A. Acetylcholine released from guinea-pig submucosal neurones dilates arterioles by releasing nitric oxide from endothelium. *J Physiol* 1992; **453**: 493-502
43 **North RA**, Surprenant A. Inhibitory synaptic potentials resulting from alpha 2-adrenoceptor activation in guinea-pig submucous plexus neurones. *J Physiol* 1985; **358**: 17-33
44 **Liu S**, Xia Y, Hu Hz, Ren J, Gao C, Wood JD. Histamine H3 receptor-mediated suppression of inhibitory synaptic transmission in the submucous plexus of guinea-pig small intestine. *Eur J Pharmacol* 2000; **397**: 49-54
45 **Hu HZ**, Gao N, Zhu MX, Liu S, Ren J, Gao C, Xia Y, Wood JD. Slow excitatory synaptic transmission mediated by P2Y1 receptors in the guinea-pig enteric nervous system. *J Physiol* 2003; **550**: 493-504
46 **Fang X**, Hu HZ, Gao N, Liu S, Wang GD, Wang XY, Xia Y, Wood JD. Neurogenic secretion mediated by the purinergic P2Y1 receptor in guinea-pig small intestine. *Eur J Pharmacol* 2006; **536**: 113-122
47 **Fie GJ**, Fang X, Wang XY, Wang GD, Liu S, Gao N, Hu HZ, Xia Y, Wood JD. Neurogenic Mucosal Bicarbonate Secretion Mediated by the Purinergic P2Y1 Receptor in Guinea-Pig Duodenum. *Gastroenterology* 2006; **130**: A380
48 **Wood JD**. Enteric neuroimmunophysiology and pathophysiology. *Gastroenterology* 2004; **127**: 635-657
49 **Cooke HJ**, Christofi FL. Enteric neural regulation of mucosal secretion. In: Johnson LR, Barrett KE, Ghishan FK, Merchant JL, Said HM, Wood JD, editors. Physiology of the Gastrointestinal Tract. 4th ed. San Diego: Academic Press, 2006: 737-762
50 **Frieling T**, Cooke HJ, Wood JD. Serotonin receptors on submucous neurons in guinea pig colon. *Am J Physiol* 1991; **261**: G1017-G1023
51 **Camilleri M**, Chey WY, Mayer EA, Northcutt AR, Heath A, Dukes GE, McSorley D, Mangel AM. A randomized controlled clinical trial of the serotonin type 3 receptor antagonist alosetron in women with diarrhea-predominant irritable bowel syndrome. *Arch Intern Med* 2001; **161**: 1733-1740
52 **Camilleri M**, Northcutt AR, Kong S, Dukes GE, McSorley D, Mangel AW. Efficacy and safety of alosetron in women with irritable bowel syndrome: a randomised, placebo-controlled trial. *Lancet* 2000; **355**: 1035-1040
53 **Chey WY**, Jin HO, Lee MH, Sun SW, Lee KY. Colonic motility abnormality in patients with irritable bowel syndrome exhibiting abdominal pain and diarrhea. *Am J Gastroenterol* 2001; **96**: 1499-1506
54 **Kellum JM**, Jaffe BM. Release of immunoreactive serotonin following acid perfusion of the duodenum. *Ann Surg* 1976; **184**: 633-636
55 **Bearcroft CP**, Perrett D, Farthing MJ. Postprandial plasma 5-hydroxytryptamine in diarrhoea predominant irritable bowel syndrome: a pilot study. *Gut* 1998; **42**: 42-46
56 **Park CH**, Joo YE, Choi SK, Rew JS, Kim SJ, Lee MC. Activated mast cells infiltrate in close proximity to enteric nerves in diarrhea-predominant irritable bowel syndrome. *J Korean Med Sci* 2003; **18**: 204-210
57 **O'Sullivan M**, Clayton N, Breslin NP, Harman I, Bountra C, McLaren A, O'Morain CA. Increased mast cells in the irritable bowel syndrome. *Neurogastroenterol Motil* 2000; **12**: 449-457
58 **Barbara G**, Stanghellini V, De Giorgio R, Cremon C, Cottrell GS, Santini D, Pasquinelli G, Morselli-Labate AM, Grady EF, Bunnett NW, Collins SM, Corinaldesi R. Activated mast cells in proximity to colonic nerves correlate with abdominal pain in irritable bowel syndrome. *Gastroenterology* 2004; **126**: 693-702
59 **Ritchie J**. Pain from distension of the pelvic colon by inflating a balloon in the irritable colon syndrome. *Gut* 1973; **14**: 125-132
60 **Whitehead WE**, Holtkotter B, Enck P, Hoelzl R, Holmes KD, Anthony J, Shabsin HS, Schuster MM. Tolerance

for rectosigmoid distention in irritable bowel syndrome. *Gastroenterology* 1990; **98**: 1187-1192
61 **Munakata J**, Naliboff B, Harraf F, Kodner A, Lembo T, Chang L, Silverman DH, Mayer EA. Repetitive sigmoid stimulation induces rectal hyperalgesia in patients with irritable bowel syndrome. *Gastroenterology* 1997; **112**: 55-63
62 **Chang L**, Munakata J, Mayer EA, Schmulson MJ, Johnson TD, Bernstein CN, Saba L, Naliboff B, Anton PA, Matin K. Perceptual responses in patients with inflammatory and functional bowel disease. *Gut* 2000; **47**: 497-505
63 **Camilleri M**, Coulie B, Tack JF. Visceral hypersensitivity: facts, speculations, and challenges. *Gut* 2001; **48**: 125-131
64 **Bouin M**, Lupien F, Riberdy-Poitras M, Poitras P. Tolerance to gastric distension in patients with functional dyspepsia: modulation by a cholinergic and nitrergic method. *Eur J Gastroenterol Hepatol* 2006; **18**: 63-68
65 **Richter JE**, Barish CF, Castell DO. Abnormal sensory perception in patients with esophageal chest pain. *Gastroenterology* 1986; **91**: 845-852
66 **Rössel P**, Drewes AM, Petersen P, Nielsen J, Arendt-Nielsen L. Pain produced by electric stimulation of the rectum in patients with irritable bowel syndrome: further evidence of visceral hyperalgesia. *Scand J Gastroenterol* 1999; **34**: 1001-1006
67 **Beyak MJ**, Bulmer DCE, Jiang W, Keating C, Rong W, Grundy D. Estrinsic sensory afferent nerves innervating the gastrointestinal tract. In: Johnson LR, Barrett KE, Ghishan FK, Merchant JL, Said HM, Wood JD, editors. Physiology of the Gastrointestinal Tract. 4th ed. San Diego: Academic Press, 2006: 685-725
68 **Ness TJ**, Gebhart GF. Acute inflammation differentially alters the activity of two classes of rat spinal visceral nociceptive neurons. *Neurosci Lett* 2000; **281**: 131-134
69 **Xu GY**, Huang LY, Zhao ZQ. Activation of silent mechanoreceptive cat C and Adelta sensory neurons and their substance P expression following peripheral inflammation. *J Physiol* 2000; **528** Pt 2: 339-348
70 **Gwee KA**, Leong YL, Graham C, McKendrick MW, Collins SM, Walters SJ, Underwood JE, Read NW. The role of psychological and biological factors in postinfective gut dysfunction. *Gut* 1999; **44**: 400-406
71 **Wang LH**, Fang XC, Pan GZ. Bacillary dysentery as a causative factor of irritable bowel syndrome and its pathogenesis. *Gut* 2004; **53**: 1096-1101
72 **Collins SM**, Barbara G. East meets West: infection, nerves, and mast cells in the irritable bowel syndrome. *Gut* 2004; **53**: 1068-1069
73 **Spiller RC**. Postinfectious irritable bowel syndrome. *Gastroenterology* 2003; **124**: 1662-1671
74 **Hillsley K**, Kirkup AJ, Grundy D. Direct and indirect actions of 5-hydroxytryptamine on the discharge of mesenteric afferent fibres innervating the rat jejunum. *J Physiol* 1998; **506**(Pt 2): 551-561
75 **Kozlowski CM**, Green A, Grundy D, Boissonade FM, Bountra C. The 5-HT(3) receptor antagonist alosetron inhibits the colorectal distention induced depressor response and spinal c-fos expression in the anaesthetised rat. *Gut* 2000; **46**: 474-480
76 **Camilleri M**, Mayer EA, Drossman DA, Heath A, Dukes GE, McSorley D, Kong S, Mangel AW, Northcutt AR. Improvement in pain and bowel function in female irritable bowel patients with alosetron, a 5-HT3 receptor antagonist. *Aliment Pharmacol Ther* 1999; **13**: 1149-1159
77 **Chen JX**, Pan H, Rothman TP, Wade PR, Gershon MD. Guinea pig 5-HT transporter: cloning, expression, distribution, and function in intestinal sensory reception. *Am J Physiol* 1998; **275**: G433-G448
78 **Coates MD**, Mahoney CR, Linden DR, Sampson JE, Chen J, Blaszyk H, Crowell MD, Sharkey KA, Gershon MD, Mawe GM, Moses PL. Molecular defects in mucosal serotonin content and decreased serotonin reuptake transporter in ulcerative colitis and irritable bowel syndrome. *Gastroenterology* 2004; **126**: 1657-1664
79 **Chen JJ**, Li Z, Pan H, Murphy DL, Tamir H, Koepsell H, Gershon MD. Maintenance of serotonin in the intestinal mucosa and ganglia of mice that lack the high-affinity serotonin transporter: Abnormal intestinal motility and the expression of cation transporters. *J Neurosci* 2001; **21**: 6348-6361
80 **Kirkup AJ**, Brunsden AM, Grundy D. Receptors and transmission in the brain-gut axis: potential for novel therapies. I. Receptors on visceral afferents. *Am J Physiol Gastrointest Liver Physiol* 2001; **280**: G787-G794
81 **Coelho AM**, Fioramonti J, Bueno L. Mast cell degranulation induces delayed rectal allodynia in rats: role of histamine and 5-HT. *Dig Dis Sci* 1998; **43**: 727-737
82 **Siddiqui AA**, Miner PB. The role of mast cells in common gastrointestinal diseases. *Curr Allergy Asthma Rep* 2004; **4**: 47-54
83 **Santos J**, Alonso C, Guilarte M, Vicario M, Malagelada JR. Targeting mast cells in the treatment of functional gastrointestinal disorders. *Curr Opin Pharmacol* 2006; **6**: 541-546
84 **Lawal A**, Kern M, Sidhu H, Hofmann C, Shaker R. Novel evidence for hypersensitivity of visceral sensory neural circuitry in irritable bowel syndrome patients. *Gastroenterology* 2006; **130**: 26-33
85 **Al-Chaer ED**, Lawand NB, Westlund KN, Willis WD. Visceral nociceptive input into the ventral posterolateral nucleus of the thalamus: a new function for the dorsal column pathway. *J Neurophysiol* 1996; **76**: 2661-2674
86 **Al-Chaer ED**, Lawand NB, Westlund KN, Willis WD. Pelvic visceral input into the nucleus gracilis is largely mediated by the postsynaptic dorsal column pathway. *J Neurophysiol* 1996; **76**: 2675-2690
87 **Al-Chaer ED**, Feng Y, Willis WD. A role for the dorsal column in nociceptive visceral input into the thalamus of primates. *J Neurophysiol* 1998; **79**: 3143-3150
88 **Willis WD**, Al-Chaer ED, Quast MJ, Westlund KN. A visceral pain pathway in the dorsal column of the spinal cord. *Proc Natl Acad Sci USA* 1999; **96**: 7675-7679
89 **Ness TJ**. Evidence for ascending visceral nociceptive information in the dorsal midline and lateral spinal cord. *Pain* 2000; **87**: 83-88
90 **Kim YS**, Kwon SJ. High thoracic midline dorsal column myelotomy for severe visceral pain due to advanced stomach cancer. *Neurosurgery* 2000; **46**: 85-90; discussion 90-92
91 **Al-Chaer ED**, Westlund KN, Willis WD. Nucleus gracilis: an integrator for visceral and somatic information. *J Neurophysiol* 1997; **78**: 521-527
92 **Malcolm A**, Phillips SF, Kellow JE, Cousins MJ. Direct clinical evidence for spinal hyperalgesia in a patient with irritable bowel syndrome. *Am J Gastroenterol* 2001; **96**: 2427-2431
93 **Silverman DH**, Munakata JA, Ennes H, Mandelkern MA, Hoh CK, Mayer EA. Regional cerebral activity in normal and pathological perception of visceral pain. *Gastroenterology* 1997; **112**: 64-72
94 **Mertz H**, Morgan V, Tanner G, Pickens D, Price R, Shyr Y, Kessler R. Regional cerebral activation in irritable bowel syndrome and control subjects with painful and nonpainful rectal distention. *Gastroenterology* 2000; **118**: 842-848
95 **Hobday DI**, Aziz Q, Thacker N, Hollander I, Jackson A, Thompson DG. A study of the cortical processing of ano-rectal sensation using functional MRI. *Brain* 2001; **124**: 361-368
96 **Ladabaum U**, Minoshima S, Hasler WL, Cross D, Chey WD, Owyang C. Gastric distention correlates with activation of multiple cortical and subcortical regions. *Gastroenterology* 2001; **120**: 369-376
97 **Kern MK**, Jaradeh S, Arndorfer RC, Jesmanowicz A, Hyde J, Shaker R. Gender differences in cortical representation of rectal distension in healthy humans. *Am J Physiol Gastrointest Liver Physiol* 2001; **281**: G1512-G1523
98 **Drossman DA**, Creed FH, Olden KW, Svedlund J, Toner BB, Whitehead WE. Psychosocial aspects of the functional gastrointestinal disorders. *Gut* 1999; **45** Suppl 2: II25-II30
99 **Ringel Y**, Drossman DA, Turkington TG, Bradshaw B, Hawk TC, Bangdiwala S, Coleman RE, Whitehead WE. Regional brain activation in response to rectal distension in patients with irritable bowel syndrome and the effect of a history of abuse. *Dig Dis Sci* 2003; **48**: 1774-1781

100 **Naliboff BD**, Derbyshire SW, Munakata J, Berman S, Mandelkern M, Chang L, Mayer EA. Cerebral activation in patients with irritable bowel syndrome and control subjects during rectosigmoid stimulation. *Psychosom Med* 2001; **63**: 365-375

101 **Devinsky O**, Morrell MJ, Vogt BA. Contributions of anterior cingulate cortex to behaviour. *Brain* 1995; **118** (Pt 1): 279-306

102 **Drossman DA**, Ringel Y, Vogt BA, Leserman J, Lin W, Smith JK, Whitehead W. Alterations of brain activity associated with resolution of emotional distress and pain in a case of severe irritable bowel syndrome. *Gastroenterology* 2003; **124**: 754-761

103 **Traub RJ**, Pechman P, Iadarola MJ, Gebhart GF. Fos-like proteins in the lumbosacral spinal cord following noxious and non-noxious colorectal distention in the rat. *Pain* 1992; **49**: 393-403

104 **Al-Chaer ED**, Westlund KN, Willis WD. Sensitization of postsynaptic dorsal column neuronal responses by colon inflammation. *Neuroreport* 1997; **8**: 3267-3273

105 **Al-Chaer ED**,Kawasaki M, Pasricha PJ. A new model of chronic visceral hypersensitivity in adult rats induced by colon irritation during postnatal development. *Gastroenterology* 2000; **119**: 1276-1285

106 **Dubner R**, Ren K. Endogenous mechanisms of sensory modulation. *Pain* 1999; **Suppl 6**: S45-S53

107 **Giesler GJ**, Liebeskind JC. Inhibition of visceral pain by electrical stimulation of the periaqueductal gray matter. *Pain* 1976; **2**: 43-48

108 **Coutinho SV**, Urban MO, Gebhart GF. Role of glutamate receptors and nitric oxide in the rostral ventromedial medulla in visceral hyperalgesia. *Pain* 1998; **78**: 59-69

109 **Urban MO**, Coutinho SV, Gebhart GF. Biphasic modulation of visceral nociception by neurotensin in rat rostral ventromedial medulla. *J Pharmacol Exp Ther* 1999; **290**: 207-213

110 **Ammons WS**, Blair RW, Foreman RD. Raphe magnus inhibition of primate T1-T4 spinothalamic cells with cardiopulmonary visceral input. *Pain* 1984; **20**: 247-260

111 **Cervero F**, Lumb BM, Tattersall JE. Supraspinal loops that mediate visceral inputs to thoracic spinal cord neurones in the cat: involvement of descending pathways from raphe and reticular formation. *Neurosci Lett* 1985; **56**: 189-194

112 **Ness TJ**, Gebhart GF. Quantitative comparison of inhibition of visceral and cutaneous spinal nociceptive transmission from the midbrain and medulla in the rat. *J Neurophysiol* 1987; **58**: 850-865

113 **Zhuo M**, Gebhart GF. Facilitation and attenuation of a visceral nociceptive reflex from the rostroventral medulla in the rat. *Gastroenterology* 2002; **122**: 1007-1019

114 **Saab CY**, Park YC, Al-Chaer ED. Thalamic modulation of visceral nociceptive processing in adult rats with neonatal colon irritation. *Brain Res* 2004; **1008**: 186-192

115 **Tattersall JE**, Cervero F, Lumb BM. Effects of reversible spinalization on the visceral input to viscerosomatic neurons in the lower thoracic spinal cord of the cat. *J Neurophysiol* 1986; **56**: 785-796

116 **Phillips SF**. Motility disorders of the colon. Textbook of gastroenterology. 2nd ed. Yamada T, editor. Philadelphia: J B Lippincott, 1995: 1856-1875

117 **Levy RL**, Olden KW, Naliboff BD, Bradley LA, Francisconi C, Drossman DA, Creed F. Psychosocial aspects of the functional gastrointestinal disorders. *Gastroenterology* 2006; **130**: 1447-1458

118 **Saunders PR**, Santos J, Hanssen NP, Yates D, Groot JA, Perdue MH. Physical and psychological stress in rats enhances colonic epithelial permeability via peripheral CRH. *Dig Dis Sci* 2002; **47**: 208-215

119 **Söderholm JD**, Yates DA, Gareau MG, Yang PC, MacQueen G, Perdue MH. Neonatal maternal separation predisposes adult rats to colonic barrier dysfunction in response to mild stress. *Am J Physiol Gastrointest Liver Physiol* 2002; **283**: G1257-G1263

120 **Türler A**, Moore BA, Pezzone MA, Overhaus M, Kalff JC, Bauer AJ. Colonic postoperative inflammatory ileus in the rat. *Ann Surg* 2002; **236**: 56-66

121 **Frieling T**, Cooke HJ, Wood JD. Neuroimmune communication in the submucous plexus of guinea pig colon after sensitization to milk antigen. *Am J Physiol* 1994; **267**: G1087-G1093

122 **Frieling T**, Palmer JM, Cooke HJ, Wood JD. Neuroimmune communication in the submucous plexus of guinea pig colon after infection with Trichinella spiralis. *Gastroenterology* 1994; **107**: 1602-1609

123 **Liu S**, Hu HZ, Gao N, Gao C, Wang G, Wang X, Peck OC, Kim G, Gao X, Xia Y, Wood JD. Neuroimmune interactions in guinea pig stomach and small intestine. *Am J Physiol Gastrointest Liver Physiol* 2003; **284**: G154-G164

124 **Perdue MH**, Marshall J, Masson S. Ion transport abnormalities in inflamed rat jejunum. Involvement of mast cells and nerves. *Gastroenterology* 1990; **98**: 561-567

125 **Wood JD**, Peck OC, Tefend KS, Rodriguez-M MA, Rodriguez-M JV, Hernández-C JI, Stonerook MJ, Sharma HM. Colitis and colon cancer in cotton-top tamarins (Saguinus oedipus oedipus) living wild in their natural habitat. *Dig Dis Sci* 1998; **43**: 1443-1453

126 **Stead RH**, Tomioka M, Quinonez G, Simon GT, Felten SY, Bienenstock J. Intestinal mucosal mast cells in normal and nematode-infected rat intestines are in intimate contact with peptidergic nerves. *Proc Natl Acad Sci USA* 1987; **84**: 2975-2979

127 **Gottwald TP**, Hewlett BR, Lhoták S, Stead RH. Electrical stimulation of the vagus nerve modulates the histamine content of mast cells in the rat jejunal mucosa. *Neuroreport* 1995; **7**: 313-317

128 **Befus D**. Reciprocity of mast cell-nervous system interactions. In: Tache Y, Wingate DL, Burks TF, editors. Innervation of the gut: pathophysiological implications. Boca Roton: CRC Press, 1994: 315-329

129 **Williams RM**, Berthoud HR, Stead RH. Vagal afferent nerve fibres contact mast cells in rat small intestinal mucosa. *Neuroimmunomodulation* 1997; **4**: 266-270

130 **Broaddus RR**, Castro GA. Mast cell-mediated colonic immune function and its inhibition by dietary aspirin in mice infected with Trichinella spiralis. *Int Arch Allergy Immunol* 1994; **105**: 135-142

131 **Wang YZ**, Palmer JM, Cooke HJ. Neuroimmune regulation of colonic secretion in guinea pigs. *Am J Physiol* 1991; **260**: G307-G314

132 **Baird AW**, Cuthbert AW. Neuronal involvement in type 1 hypersensitivity reactions in gut epithelia. *Br J Pharmacol* 1987; **92**: 647-655

133 **Harari Y**, Russell DA, Castro GA. Anaphylaxis-mediated epithelial Cl-secretion and parasite rejection in rat intestine. *J Immunol* 1987; **138**: 1250-1255

134 **McKay DM**, Perdue MH. Intestinal epithelial function: the case for immunophysiological regulation. Cells and mediators (1). *Dig Dis Sci* 1993; **38**: 1377-1387

135 **MacQueen G**, Marshall J, Perdue M, Siegel S, Bienenstock J. Pavlovian conditioning of rat mucosal mast cells to secrete rat mast cell protease II. *Science* 1989; **243**: 83-85

136 **Santos J**, Saperas E, Nogueiras C, Mourelle M, Antolín M, Cadahia A, Malagelada JR. Release of mast cell mediators into the jejunum by cold pain stress in humans. *Gastroenterology* 1998; **114**: 640-648

137 **Wang GD**, Wang XY, Liu S, Gao N, Fie GJ, Hu HZ, Xia Y, Wood JD. Extrinsic primary afferent neurons stimulate enteric mast cells to release histamine as a paracrine modulator in the enteric nervous system in the guinea-pig intestine. *Gastroenterology* 2006; **130**: A30

138 **Santos J**, Saperas E, Mourelle M, Antolín M, Malagelada JR. Regulation of intestinal mast cells and luminal protein release by cerebral thyrotropin-releasing hormone in rats. *Gastroenterology* 1996; **111**: 1465-1473

139 **Gué M**, Del Rio-Lacheze C, Eutamene H, Théodorou V, Fioramonti J, Buéno L. Stress-induced visceral hypersensitivity to rectal distension in rats: role of CRF and mast cells. *Neurogastroenterol Motil* 1997; **9**: 271-279

140 **Andrews PL**, Grundy D, Scratcherd T. Vagal afferent discharge from mechanoreceptors in different regions of the ferret stomach. *J Physiol* 1980; **298**: 513-524

141 **Haupt W**, Jiang W, Kreis ME, Grundy D. Prostaglandin EP

receptor subtypes have distinctive effects on jejunal afferent sensitivity in the rat. *Gastroenterology* 2000; **119**: 1580-1589
142 **Kirkup AJ**, Jiang W, Bunnett NW, Grundy D. Stimulation of proteinase-activated receptor 2 excites jejunal afferent nerves in anaesthetised rats. *J Physiol* 2003; **552**: 589-601
143 **Kreis ME**, Jiang W, Kirkup AJ, Grundy D. Cosensitivity of vagal mucosal afferents to histamine and 5-HT in the rat jejunum. *Am J Physiol Gastrointest Liver Physiol* 2002; **283**: G612-G617
144 **Pothoulakis C**, Karmeli F, Kelly CP, Eliakim R, Joshi MA, O'Keane CJ, Castagliuolo I, LaMont JT, Rachmilewitz D. Ketotifen inhibits Clostridium difficile toxin A-induced enteritis in rat ileum. *Gastroenterology* 1993; **105**: 701-707
145 **Castagliuolo I**, LaMont JT, Letourneau R, Kelly C, O'Keane JC, Jaffer A, Theoharides TC, Pothoulakis C. Neuronal involvement in the intestinal effects of Clostridium difficile toxin A and Vibrio cholerae enterotoxin in rat ileum. *Gastroenterology* 1994; **107**: 657-665
146 **Castagliuolo I**, Riegler M, Pasha A, Nikulasson S, Lu B, Gerard C, Gerard NP, Pothoulakis C. Neurokinin-1 (NK-1) receptor is required in Clostridium difficile-induced enteritis. *J Clin Invest* 1998; **101**: 1547-1550
147 **Pothoulakis C**, Castagliuolo I, LaMont JT, Jaffer A, O'Keane JC, Snider RM, Leeman SE. CP-96,345, a substance P antagonist, inhibits rat intestinal responses to Clostridium difficile toxin A but not cholera toxin. *Proc Natl Acad Sci USA* 1994; **91**: 947-951
148 **Wershil BK**, Castagliuolo I, Pothoulakis C. Direct evidence of mast cell involvement in Clostridium difficile toxin A-induced enteritis in mice. *Gastroenterology* 1998; **114**: 956-964
149 **Cocchiara R**, Albeggiani G, Azzolina A, Bongiovanni A, Lampiasi N, Di Blasi F, Geraci D. Effect of substance P on uterine mast cell cytokine release during the reproductive cycle. *J Neuroimmunol* 1995; **60**: 107-115
150 **Cocchiara R**, Albeggiani G, Lampiasi N, Bongiovanni A, Azzolina A, Geraci D. Histamine and tumor necrosis factor-alpha production from purified rat brain mast cells mediated by substance P. *Neuroreport* 1999; **10**: 575-578
151 **Xia Y**, Hu HZ, Liu S, Pothoulakis C, Wood JD. Clostridium difficile toxin A excites enteric neurones and suppresses sympathetic neurotransmission in the guinea pig. *Gut* 2000; **46**: 481-486
152 **Panula P**, Kaartinen M, Mäcklin M, Costa E. Histamine-containing peripheral neuronal and endocrine systems. *J Histochem Cytochem* 1985; **33**: 933-941
153 **Nemeth PR**, Ort CA, Wood JD. Intracellular study of effects of histamine on electrical behaviour of myenteric neurones in guinea-pig small intestine. *J Physiol* 1984; **355**: 411-425
154 **Frieling T**, Cooke HJ, Wood JD. Histamine receptors on submucous neurons in guinea pig colon. *Am J Physiol* 1993; **264**: G74-G80
155 **Tamura K**, Palmer JM, Wood JD. Presynaptic inhibition produced by histamine at nicotinic synapses in enteric ganglia. *Neuroscience* 1988; **25**: 171-179
156 **Wood JD**. Histamine, mast cells, and the enteric nervous system in the irritable bowel syndrome, enteritis, and food allergies. *Gut* 2006; **55**: 445-447
157 **Baum CA**, Bhatia P, Miner PB. Increased colonic mucosal mast cells associated with severe watery diarrhea and microscopic colitis. *Dig Dis Sci* 1989; **34**: 1462-1465
158 **Aly A**, Bárány F, Kollberg B, Monsén U, Wisén O, Johansson C. Effect of an H2-receptor blocking agent on diarrhoeas after extensive small bowel resection in Crohn's disease. *Acta Med Scand* 1980; **207**: 119-122
159 **Wood JD**, Mayer CJ. Slow synaptic excitation mediated by serotonin in Auerbach's plexus. *Nature* 1978; **276**: 836-837
160 **Wood JD**, Mayer CJ. Serotonergic activation of tonic-type enteric neurons in guinea pig small bowel. *J Neurophysiol* 1979; **42**: 582-593
161 **Mawe GM**, Branchek TA, Gershon MD. Peripheral neural serotonin receptors: identification and characterization with specific antagonists and agonists. *Proc Natl Acad Sci USA* 1986; **83**: 9799-9803
162 **Monro RL**, Bornstein JC, Bertrand PP. Slow excitatory post-synaptic potentials in myenteric AH neurons of the guinea-pig ileum are reduced by the 5-hydroxytryptamine7 receptor antagonist SB 269970. *Neuroscience* 2005; **134**: 975-986
163 **Liu MT**, Gershon MD. Slow excitatory ("5-HT1P"-like) responses of mouse myenteric neurons to 5-HT: Mediation by heterodimers of 5-HT1B/1D and Drd2 receptors. *Gastroenterology* 2005; **128** Suppl 2: A87
164 **Derkach V**, Surprenant A, North RA. 5-HT3 receptors are membrane ion channels. *Nature* 1989; **339**: 706-709
165 **North RA**, Henderson G, Katayama Y, Johnson SM. Electrophysiological evidence for presynaptic inhibition of acetylcholine release by 5-hydroxytryptamine in the enteric nervous system. *Neuroscience* 1980; **5**: 581-586
166 **Tack JF**, Janssens J, Vantrappen G, Wood JD. Actions of 5-hydroxytryptamine on myenteric neurons in guinea pig gastric antrum. *Am J Physiol* 1992; **263**: G838-G846
167 **Galligan JJ**, Surprenant A, Tonini M, North RA. Differential localization of 5-HT1 receptors on myenteric and submucosal neurons. *Am J Physiol* 1988; **255**: G603-G611
168 **Surprenant A**, Crist J. Electrophysiological characterization of functionally distinct 5-hydroxytryptamine receptors on guinea-pig submucous plexus. *Neuroscience* 1988; **24**: 283-295
169 **McFadden D**, Jaffe BM, Zinner MJ. Secretory effects of intravenous serotonin on the proximal jejunum of the awake dog. *Am J Surg* 1985; **149**: 60-64
170 **Jaffe BM**. Prostaglandins and serotonin: nonpeptide diarrheogenic hormones. *World J Surg* 1979; **3**: 565-578
171 **Wood JD**. Neurotransmission at the interface of sympathetic and enteric divisions of the autonomic nervous system. *Chin J Physiol* 1999; **42**: 201-210
172 **Söderholm JD**, Perdue MH. Stress and gastrointestinal tract. II. Stress and intestinal barrier function. *Am J Physiol Gastrointest Liver Physiol* 2001; **280**: G7-G13
173 **Stonerook MJ**, Weiss HS, Rodriguez MA, Rodríguez JV, Hernández JI, Peck OC, Wood JD. Temperature-metabolism relations in the cotton-top tamarin (Saguinus oedipus) model for ulcerative colitis. *J Med Primatol* 1994; **23**: 16-22
174 **Wood JD**, Peck OC, Tefend KS, Stonerook MJ, Caniano DA, Mutabagani KH, Lhoták S, Sharma HM. Evidence that colitis is initiated by environmental stress and sustained by fecal factors in the cotton-top tamarin (Saguinus oedipus). *Dig Dis Sci* 2000; **45**: 385-393
175 **Wood JD**, Peck OC, Sharma HS, Hernandez JI, Rodriquez JVR, Rodriquez MA, Stonerook MJ, Tefend KS, Gardeazabal J Nassar F. A non-peptide neurokinin 1 (NK-1) receptor antagonist suppresses initiation of acute inflammation in the colon of the cotton-top tamarin model for spontaneous colitis and colon cancer. *Gastroenterology* 1996; **110**: A1047
176 **Peck OC**, Wood JD. Brain-gut interactions in ulcerative colitis. *Gastroenterology* 2000; **118**: 807-808
177 **Cervero F**, Laird JMA. Irritable bowel disease: possible role of spinal mechanisms. In: Krammer HJ, Singer MV, editors. Neurogastroenterology from the basics to the clinics. Boston: Kluwer Academic Publishers, 2000: 664-673

S- Editor Liu Y **L- Editor** Alpini GD **E- Editor** Zhou T

PO Box 2345, Beijing 100023, China
www.wjgnet.com
wjg@wjgnet.com

World J Gastroenterol 2007 March 7; 13(9): 1333-1334
World Journal of Gastroenterology ISSN 1007-9327

Hans Gregersen, Professor, *Series Editor*

The GIOME: Concept and current role in gastrointestinal tract studies

The goal of the Physiome Project is to understand and describe the physiology and pathophysiology of the human organism. Multiscale mathematical and computer models are developed within this concept to help understand human health. From its beginning about 15 years ago, most of the focus has been in the cardiac field (the Cardiome project) but other areas are developing as well now.

Gastroenterology research has traditionally been based on experimental approaches rather than on mathematical modeling. However, in the past five to ten years several groups independently started to model the gastrointestinal tract and Gregersen introduced the term "GIOME" a couple of years ago (Gregersen H. The Giome Project. Neurogastroenterol Motility 2006; 18:401-402, www.giome.com). Thus, the Physiome based GIOME project is a very new concept in gastroenterology. The purpose is to facilitate modeling of physiological and pathophysiological processes in the gastrointestinal tract. It is a framework that allows experts from a variety of disciplines to work collaboratively to database and analyze observations and models. GIOME work so far has been on the mechanics and electromechanical properties at the tissue and organ level based on medical imaging and other highly advanced techniques. However, the long-term goal is to develop integrative models at all levels of gastrointestinal organization from the genes through regulatory pathways to the whole gastrointestinal tract function. Such models will have applications not only in research but also in teaching, training, development of medical devices and in clinical work. Models span from simple analytical computations to advanced multiscale models that need input and validation from highly skilled experimental work.

This special issue of *World Journal of Gastroenterology* contains a number of reviews and original papers related to the GIOME Project from the majority of the active groups in this field. The studies represent bioengineering models, primarily anatomical, functional and pathophysiological models, from most parts of the gastrointestinal tract. By publishing such a special issue we hope to increase the awareness of GIOME related research and to stimulate further research and collaboration in this area. The GIOME Project together with other European Physiome groups recently received funding from the European Union to develop a Strategy for the EuroPhysiome. It is the hope that this will facilitate further funding from the European Union and major funding agencies around the World to nurse this important effort.

PO Box 2345, Beijing 100023, China
www.wjgnet.com
wjg@wjgnet.com

World J Gastroenterol 2007 March 7; 13(9): 1335-1346
World Journal of Gastroenterology ISSN 1007-9327

TOPIC HIGHLIGHT

Hans Gregersen, Professor, *Series Editor*

Function of longitudinal *vs* circular muscle fibers in esophageal peristalsis, deduced with mathematical modeling

James G Brasseur, Mark A Nicosia, Anupam Pal, Larry S Miller

James G Brasseur, Department of Mechanical Engineering, Pennsylvania State University, University Park, PA 16802, United States
Mark A Nicosia, Department of Mechanical Engineering, Widener University, Chester, PA 19013, United States
Anupam Pal, Department of Biological Sciences & Bioengineering, Indian Institute of Technology Kanpur, UP, 208016, India
Larry S Miller, Department of Gastroenterology, Temple University Medical Center, Philadelphia, PA 19140, United States
Correspondence to: James G Brasseur, PhD, Professor of Mechanical Engineering, Bioengineering, and Mathematics, Department of Mechanical Engineering, 205 Reber Building, The Pennsylvania State University, University Park, PA 16802, United States. brasseur@psu.edu
Telephone: +1-814-8653159 Fax: +1-814-8658499
Received: 2007-01-11 Accepted: 2007-02-08

Abstract

We summarize from previous works the functions of circular vs. longitudinal muscle in esophageal peristaltic bolus transport using a mix of experimental data, the conservation laws of mechanics and mathematical modeling. Whereas circular muscle tone generates radial closure pressure to create a local peristaltic closure wave, longitudinal muscle tone has two functions, one physiological with mechanical implications, and one purely mechanical. Each of these functions independently reduces the tension of individual circular muscle fibers to maintain closure as a consequence of shortening of longitudinal muscle locally coordinated with increasing circular muscle tone. The physiological function is deduced by combining basic laws of mechanics with concurrent measurements of intraluminal pressure from manometry, and changes in cross sectional muscle area from endoluminal ultrasound from which local longitudinal shortening (LLS) can be accurately obtained. The purely mechanical function of LLS was discovered from mathematical modeling of peristaltic esophageal transport with the axial wall motion generated by LLS. Physiologically, LLS concentrates circular muscle fibers where closure pressure is highest. However, the mechanical function of LLS is to reduce the level of pressure required to maintain closure. The combined physiological and mechanical consequences of LLS are to reduce circular muscle fiber tension and power by as much as 1/10 what would be required for peristalsis without the longitudinal muscle layer, a tremendous benefit that may explain the existence of longitudinal muscle fiber in the gut. We also review what is understood of the role of longitudinal muscle in esophageal emptying, reflux and pathology.

Key words: Esophagus; Longitudinal muscle; Circular muscle; Longitudinal shortening; Peristalsis

Brasseur JG, Nicosia MA, Pal A, Miller LS. Function of longitudinal *vs* circular muscle fibers in esophageal peristalsis, deduced with mathematical modeling. *World J Gastroenterol* 2007; 13(9): 1335-1346

http://www.wjgnet.com/1007-9327/13/1335.asp

INTRODUCTION

Figure 1 is a schematic of the cross section of the esophagus. The muscularis propria is comprised of a layer of circularly aligned muscle fibers within, and a layer of longitudinally aligned muscle fibers without, surrounding mucosal layers of loosely connected tissue. The muscle mass of the circular and longitudinal muscle layers is nearly the same. In the resting state, the circumferentially averaged thickness of the muscularis has been measured by various researchers as 1.1-1.4 mm in the esophageal body, and 1.9-2.4 mm in the abdominal esophagus near the junction with the gastric cardia[1-6].

The function of the circular muscle layer of the esophageal muscularis propria is clear. Esophageal peristalsis (as well as segmental contraction in the intestines) requires luminal closure against the resisting forces within a viscous bolus, demanding the existence of circumferential, or "hoop" stresses to generate applied pressures at a level sufficient to squeeze the lumen closed[7]. "Peristalsis" implies that the circular muscle contraction travels as a wave along the esophageal lumen to create a traveling contraction wave and a moving point of luminal closure that forces the bolus fluid ahead, and ultimately into the stomach[7,8]. As indicated in Figure 2, peristalsis generates fluid pressure at the mucosal surface equal to the closure pressure from circular muscle hoop stress.

A similar plot can be created for luminal frictional shear stress[8]. Within the bolus fluid pressure must generally decrease in the direction of fluid motion to force the fluid forward against frictional resisting forces in this friction-dominated flow. The axial pressure gradient is very small in the distended part of the bolus, but becomes very sensitive to luminal radius as the fluid layer thins[7]. Near the moving point of closure, fluid pressure rises in response both to the radial closure force and to frictional stresses associated with the forcing of fluid from the point of closure[7,8]. Proximal to the bolus tail (Figure 2), the circular muscle squeezes against the mucosae, which are forced onto a thin layer of residual liquid that lubricates the interface between the mucosa and manometric catheter surface (and, in the absence of a catheter, fills pockets within the mucosal folds). Above the tail, pressure rises in direct response to the tonic component of hoop stress within the circular muscle layer[9].

However, the mass of the esophageal muscularis propria is split evenly between circular and longitudinal muscle fiber[1,2]. What, then, is the role of longitudinal muscle in the esophagus, and why is it there? This is the question that we, at least partially, address in this integrative summary of current understanding.

Consider in Figure 3 the classic data of Dodds *et al*[10] in which four metal markers were sewn into the wall of the lower esophagus of cats and tracked radiographically during swallows. They found that shortly after the initiation of the swallow, all markers except for the one at the hiatus shifted orally together, implying longitudinal shortening of the upper esophagus. Because only longitudinally aligned muscle fibers can generate the active tension necessary to shorten the upper esophagus, we conclude that longitudinal muscle in the upper esophagus has contracted locally during the initial period after a swallow. As the bolus tail passed a wall marker in the lower esophagus, the marker moved aborally, and the relative distance between pairs of markers surrounding the tail shortened, implying local shortening of longitudinal muscle fibers. The process continued as the bolus tail progressed distally, until it approached the hiatus, at which time the hiatal marker was pulled orally, an ampulla formed[11], and esophageal emptying began. Still the relative distance between adjacent markers surrounding the bolus tail decreased as the intrinsic lower sphincter was pulled into the thoracic cavity and then returned to its original position well after emptying was complete.

Basic features of the marker motions observed in the feline esophagus by Dodds *et al*[10] have also been observed more crudely in various studies in the human esophagus where 11 mm metal clips were attached to the mucosal surface and observed fluoroscopically during liquid swallows[12-15]. Pouderoux *et al*[14], in particular, using three clips in the distal esophagus, observed initial stretch followed by shortening during bolus transport, consistent with Figure 3.

We address here the questions: (1) how does longitudinal muscle contract locally in the human esophagus during peristalsis, (2) is the contraction coordinated in any way with peristaltic contraction of the circular muscle, (3) why does longitudinal muscle contract during esophageal peristalsis, and (4) are there benefits to longitudinal muscle contraction that are of sufficient importance to explain the existence of a longitudinal muscle layer comprising nearly half the total muscle mass? To answer these questions we integrate the literature with two studies which apply basic laws of mechanics, endoluminal ultrasound, and a mathematical model, to analyze local contraction of longitudinal muscle in the esophagus during peristaltic transport. We follow with a review of other studies relevant to esophageal longitudinal muscle function and close with a summary discussion and speculation on at least one reason why evolution has created a gut with a longitudinal muscle layer as massive as the circular muscle layer that clearly underlies gut function.

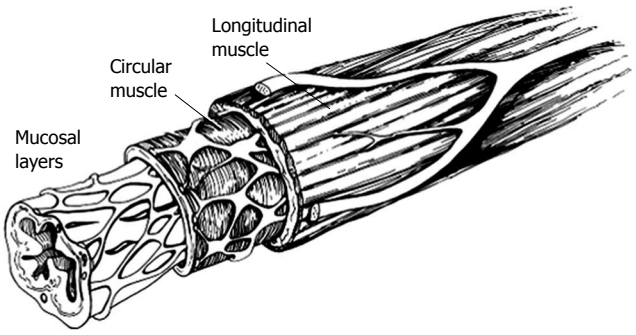

Figure 1 Schematic of esophageal cross section, showing the primary esophageal layers.

METHODS TO QUANTIFY LONGITUDINAL AND CIRCULAR MUSCLE CONTRACTION CONCURRENTLY

Application of manometry to measure circular muscle tone

Circumferential "hoop" stress in the esophageal wall is a summation of neurologically induced active stress (or "tone") in the circular muscle, a passive elastic contribution resulting purely from muscle distension, and a contribution that arises from external pressures on the muscle surfaces. Changes in hoop stress are directly reflected in changes in intraluminal "closure" pressure, so that manometric measurement of intraluminal pressure can be used in the study of the mechanics and physiology of circular muscle tone. This is especially the case near the bolus tail where passive contributions are negligible and pressure reflects directly the active stress component[9].

The relationship between intraluminal pressure and hoop stress is given by a Newton's law force balance across the esophageal wall, as illustrated in Figure 4. The following is an exact expression for a cylindrical esophagus with hoop stress entirely within the muscularis propria (Figure 4):

$$P_{closure} - P_{thorax} = (S_{hoop} + P_{thorax}) \frac{T_{muscle}}{R_{circ}} \quad (1)$$

$P_{closure}$ is the pressure at the mucosal-fluid interface

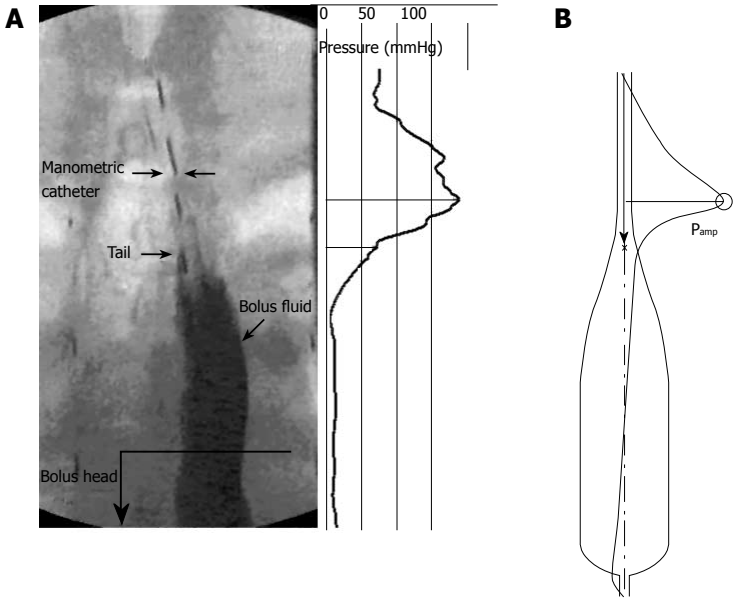

Figure 2 Frozen time image of peristaltic transport of a liquid bolus through the esophagus, with corresponding spatial variation in intraluminal pressure. **A**: Fluoroscopic image and pressure distribution (relative to atmospheric) concurrent with interpolated high-resolution manometry data; **B**: Bolus shape and overlayed pressure distribution from a mathematical model computer simulation.

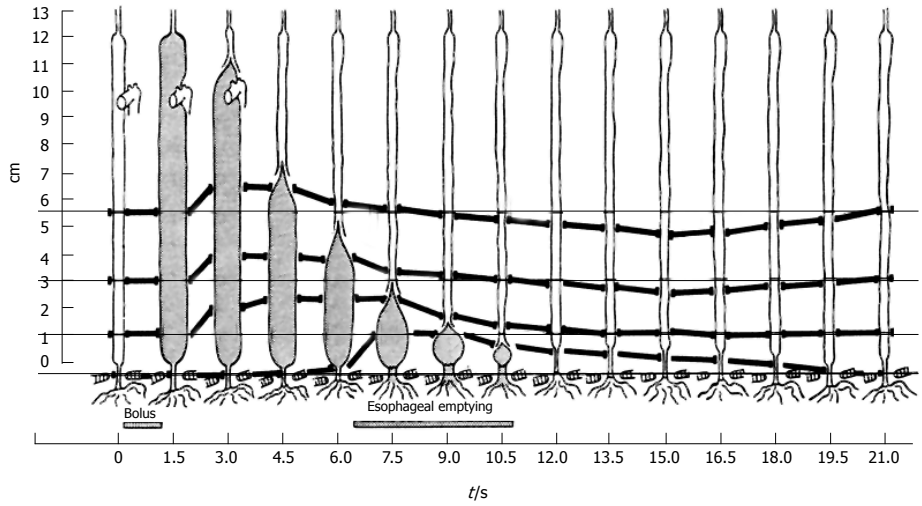

Figure 3 The classic experiment by Dodds *et al*[10] in which the motion of four material points in the muscle wall of the feline esophagus were recorded over time concurrently with bolus transport using fluoroscopy.

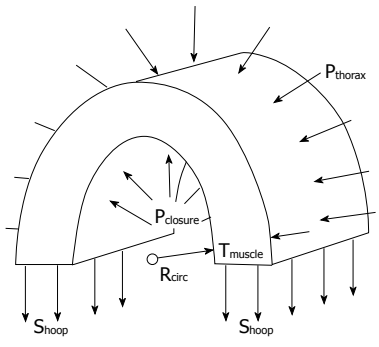

Figure 4 Schematic of the force balance across an axial segment of the muscularis propria of the esophageal wall, showing the relationship between closure pressure ($P_{closure}$) and average hoop stress (S_{hoop}) across the circular and longitudinal muscle layers.

required to maintain closure and S_{hoop} is the total average hoop stress (force per unit muscle area) across the muscle layers (muscularis propria), T_{muscle} is the total thickness of the muscle layers, R_{circ} is the radius to the inner surface of circular muscle, and P_{thorax} is the pressure in the thoracic cavity external to the esophageal lumen. Equation (1) is a good approximation for the real noncylindrical esophagus when the stress and thickness are interpreted as averages over both the thickness and circumference of the muscle layer, and therefore only dependent on the axial distance x along the lumen (Figure 2). (Note that the "Laplace law" is derived from equation (1) by assuming that T_{muscle} is very much smaller than R_{circ}. This is never the case, however, in a contracted gut segment[16]).

Equation (1) shows that relative intraluminal pressure ($P_{closure}$ - P_{thorax}) increases in direct proportion to hoop stress (S_{hoop}) in the fully contracted regions, so that the inner circular muscle radius R_{circ} is fixed, to the extent that the muscle thickness (T_{muscle}) does not change with change in hoop stress. Experimentally, therefore, we interpret manometrically measured changes in pressure as indicating changes in circular muscle tone. As will be discussed next, these measurements have been made together with quantifications in local shortening of longitudinal muscle fibers, with implications on the assumption of fixed muscle thickness during contracted esophageal segments.

Application of endoluminal ultrasound to measure local longitudinal muscle shortening

Whereas intraluminal pressure responds to circular muscle tone because of the force balance involving hoop stress

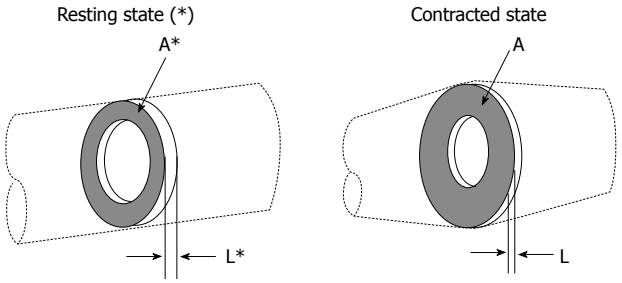

Figure 5 Application of the principle of mass conservation to quantify local longitudinal shortening from measurement of the change in cross sectional area from endoluminal ultrasound images, leading to L/L* = 1/(A/A*).

and intraluminal pressure, there is no corresponding balance between longitudinal stress and intraluminal pressure in a tubular esophagus. Manometry therefore provides no direct information on longitudinal muscle. The only way to measure longitudinal muscle stress directly is the implantation of strain gauges within the muscle wall. This has been done in an animal model[17], but cannot be done in humans. In humans the only approach currently available to measure longitudinal muscle contraction is indirect, through the measurement of relative changes in longitudinal wall displacement, as shown in Figure 3. Because muscle can only contract in response to neurological stimulation of muscle tone, the shortening of a localized axial segment implies one of two possible scenarios. In a previously unstimulated esophagus, local longitudinal shortening implies a local increase in active stress (tone) in the longitudinal muscle fibers within the shortened segment. In a longitudinally stimulated esophagus, local shortening of one axial segment produces stretching in adjacent segments; shortening of previously stretched segments, therefore, can arise from relaxation of a previously contracted adjacent segment. Local longitudinal shortening can therefore be used indirectly to indicate longitudinal muscle contraction when the history of longitudinal shortening is understood. To estimate longitudinal muscle stresses, would require a more complex integration of measurement with the laws of mechanics and modeling[9] than is possible from the simple force balance that produced equation (1).

In a number of studies, to measure longitudinal shortening of esophageal segments in humans, metal clips have been applied to the epithelial surface and their axial motions measured radiographically[12-15]. Whereas all of these studies are at lower spatial resolution and contain less detail than the Dodds *et al*[10] study in the cat (Figure 3), the results are consistent. Technical difficulties and lack of comfort during the endoscopic placement of clips has limited the application to 1-3 clips. Furthermore, the clips are large (11 mm), and the relative change in length between two clips typically spaced 3-5 cm is an average over the clip spacing, and has been shown to be a significant underestimate of more localized longitudinal shortening[1]. Finally, since clips mark the motion of the mucosal surface, which moves relative to the muscularis, there is inherent uncertainty in the interpretation of relative clip motion as inferring muscle shortening.

The practical limitations of clips can be avoided by combining a basic law of mechanics with the measurement of muscle cross section with endoluminal ultrasound (EUS) imaging of the esophageal muscle cross section. The principle is illustrated in Figure 5. Imagine a thin slice of the muscularis propria at some axial location, x, in the resting state (denoted by*), and the same slice containing the same muscle mass at some later time, for example during the passage of a contraction wave (no*). Muscle is a mixture of liquid and solid material within the mixture muscle fiber, collagen, etc., which are incompressible, meaning that the density (mass per unit volume) is always the same. Thus, since the mass of the slice in Figure 5 is the same before and after contraction, so is the volume (volume = mass/density). The volume of the slice is the cross sectional area times its thickness, so that L*A* = LA. The relative shortening of the slice is L/L*, which is therefore given by:

$$\frac{L}{L^*} = \frac{1}{A/A^*} \qquad (2)$$

A decrease in the longitudinal shortening parameter L/L^*, or equivalently an increase in A/A^*, quantify longitudinal muscle shortening localized to the axial position of the measurement.

To quantify local longitudinal shortening (LLS), one measures the cross-sectional areas of the muscle layer in the relaxed state (A^*) and during contraction (A) using endoluminal ultrasound (EUS) and image analysis methods. Nicosia *et al*[1], using the data of Miller *et al*[4], and Dai *et al*[2] used a custom assembly that combined high-frequency ultrasound with water-perfused manometry to collect esophageal segment cross-sectional images simultaneously with intraluminal pressure. A 20 MHz ultrasonographic transducer, placed within a 6 French catheter, rotated at 15-30 Hz to provide 360 degrees esophageal cross-sectional imaging with a 0.1 mm axial slice thickness and a typical penetration depth of 2 cm was used. Images were recorded on super VHS videotape at 30 frames/s. To quantify intraluminal pressure at the same location, a second, 3 French angiography catheter was glued to the EUS catheter and a small side-hole was made at the same level as the ultrasound transducer for perfused manometry. The two data sets were synchronized to within one video frame when recorded on a Kay Elemetrics swallowing workstation. The video images were digitized at 30 frames/s in single byte uncompressed tiff format and pressure was digitized at 250 Hz.

It should be noted that with EUS one measures local longitudinal shortening at a fixed axial location, similar to pressure measurement with manometry. Figure 3 shows that the muscle material moves axially relative to the point of measurement associated with longitudinal shortening in the axial segment surrounding the point of measurement.

Figure 6 is an example of cross sections of the esophagus as seen from EUS (A) in the resting state, (B) while the head of the bolus passes the EUS transducer, and (C) when the peak intraluminal pressure passes the transducer [ref. 1]. The black circle with white outline in the center of each image is the EUS transducer. In each image, the inner boundary of the circular muscle and the

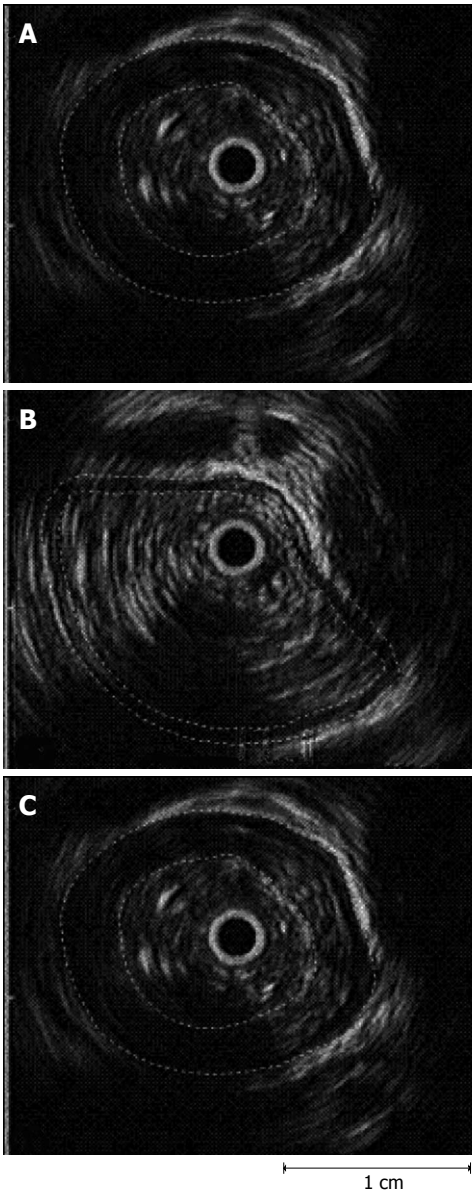

Figure 6 Example of the use of EUS with image analysis to determine the cross sectional area of the muscularis propria (**A**) in the resting state (*), (**B**) with distention at the bolus head, and (**C**) at peak contractile pressure.

outer boundary of the longitudinal muscle were outlined and the coordinates obtained using specially designed edge-detection software with a graphic user interface for interactive semi-automated edge detection[1]. In addition to extracting the muscle boundaries, the white band that identifies the interconnective tissue at the interface between the two muscle layers was quantified. (Because the boundary between the circular and longitudinal muscle layers was generally less visible than the inner and outer boundaries of the muscularis, the accuracy of the digitized coordinates of the interconnective tissue layer was correspondingly less accurate).

In each image a pie-shaped black area facing outward from the catheter towards the bottom of each image is produced as a result of the manometric catheter interfering with the acoustic wave. To objectively define the muscle edges through this black area, the missing data were estimated using cubic spline interpolation from the portions of the detected edges on each side of the missing segment (Figure 6). The edges were always superimposed on the image and the user adjusted segments incorrectly extracted by the automated image-analysis system. Consequently, the human time required to segment the hundreds of images needed was very high, limiting the number of images that could be quantified. In the end, Nicosia *et al*[1] segmented and quantified several hundred images over the entire swallowing sequence with four normal subjects.

From the digitized coordinate data of the three edges from each image the cross sectional areas of the total muscle area, as well as the individual circular and longitudinal muscle areas, were quantified. Given the difficulties in the accurate estimation of the interconnective tissue on many of the images, the accuracy of the quantification for the individual longitudinal and circular muscle areas was less than the accuracy of the entire muscle area. However, quantification of total muscle area, and therefore the LLS shortening parameters A/A^* and L/L^* with equation (2), are felt to be quite accurate. Furthermore, only this approach allows for direct quantification of the local longitudinal shortening of esophageal muscle layers.

Application of mathematical modeling to evaluate closure pressures

In Figure 2A we show interpolated high-resolution manometry data plotted axially along the lumen during peristaltic transport. Not surprisingly, the pressure is highest in the zone of complete occlusion, just proximal to the bolus tail. The measured pressure is, in reality, within a thin liquid film between the manometric catheter and mucosa. Equation (1) gives the relationship between the fluid pressure, muscle stress, and geometry. Thus, the stress required by the muscles to close the lumen above the bolus tail is the pressure within the bolus fluid in the closed lumen. This fluid pressure is determined by the details of bolus fluid motion in response to the motion of the mucosal surface that, in turn, moves the bolus fluid and generates pressure and resisting frictional forces at the fluid-epithelial interface. The motion of the mucosal surface originates in circular muscle contraction moving the mucosal surface radially (transverse to the lumen), and in longitudinal muscle contraction moving the surface axially (along the lumen).

We ask the following functionally important questions: If longitudinal muscle contracts locally, coordinated in some way with circular muscle contraction during peristalsis, does the resulting motion of the mucosal surface in any way alter the pressure force that maintains luminal closure ($P_{closure}$ in equation 1)? If so, is the alteration beneficial or detrimental to the efficacy of peristalsis? These questions cannot be answered experimentally, because it would be necessary to repeat the experiment with circular muscle contraction precisely the same in all experiments, but with the degree of longitudinal muscle contraction suppressed without altering circular muscle physiology. However, a physics-based mathematical model of peristaltic fluid transport can be applied to fill in certain gaps between experimentally measurable data to

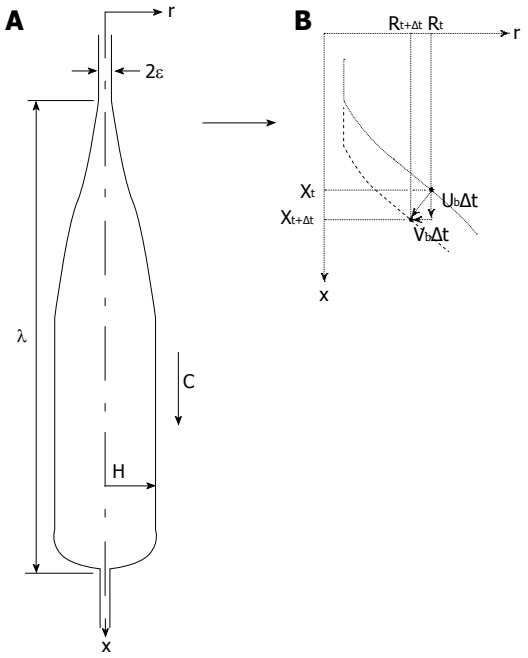

Figure 7 Schematic of essential elements in the mathematical model. **A**: Bolus shape with geometrical parameters. H is the bolus head radius, λ is bolus length, ε is the thickness of the lubrication layer in the contracted zone, and c is the peristaltic wave speed; **B**: Specification of mucosal surface velocity in the model. Ub and Vb are the axial and radial surface velocity components, respectively, of a material element of the mucosal surface.

address questions inaccessible to experiment. (By "physics-based, we mean modeling derived directly from the laws of physics which, in mathematical form, are predictive.) To answer the questions above we therefore integrate a mathematical model of bolus fluid motion with image and pressure data of esophageal bolus transport. In this section we describe this model in general terms without mathematical equations. Mathematical details can be found in Pal & Brasseur[18] and Li & Brasseur[8].

Figure 2B shows a prediction of intraluminal pressure for bolus transport with a bolus shape designed as representative of esophageal peristalsis. The modeled bolus geometry is an idealized version of the physiological bolus shape (Figure 2A) in order to capture the essential elements of esophageal bolus transport needed for the study. These essential elements are: (1) Accurate mathematical representation of Newton's second law of mechanics applied to liquid bolus motion, intrabolus pressure, and intrabolus frictional stress, driven by the motion of a lumen boundary surrounding the bolus liquid. A basic discussion of these physical effects in esophageal bolus transport is give in[7]; (2) Specification of a "tear-drop" bolus shape at specified peristaltic wave speed that is representative of the actual bolus during peristalsis. As discussed by Li & Brasseur[8], near the bolus tail there is a coupling between the bolus shape and the pressure that, through equation (1), reflects the manner in which circular muscle stress increases to a peak proximal to the bolus tail[9]. The basic nature of peristaltic muscle squeeze produces a "tear-drop" shaped bolus, as shown in fluoroscopic imaging of bolus transport (e.g., Figure 2A) and as modeled in Figure 2B; (3) The diameter of the modeled esophageal lumen in the fully contracted region proximal to the bolus tail is a direct reflection of the liquid layer that coats the manometric catheter as in Figure 2A, or lubricates the mucosal folds during transport. In the model, this occlusion diameter is an "effective" lubrication layer that, for given peristaltic wave speed, reflects the maximum squeeze of the circular muscle[7]. Peak muscle squeeze pressure is adjusted to match experiment by adjusting this occlusion diameter; (4) For the purposes of this study, the most important advantage of the mathematical model is the ability to fully specify the longitudinal motions of the lumen surface. We do this consistent with measured local shortening of longitudinal muscle and measured coordination with circular muscle contraction. However, we explore the consequences of local longitudinal shortening (LLS) with our unique ability, with the model, to systematically alter the contribution of LLS to contractile pressure, from no contribution to the measured physiological contribution, as well as to systematically explore the consequences of alignment and misalignment between longitudinal and circular muscle contraction. Through this unique property of a mathematical model, we are able to explain mechanical function of longitudinal muscle that is difficult to explain through experiment alone.

Figure 7 shows the basic elements and parameters of the mathematical model. The esophageal geometry is simplified to a straight axisymmetric deformable tube along which a bolus of fixed shape travels at wave speed c. Deviations from axisymmetry are unimportant to the effects of longitudinal muscle function that interest us here. The volume of the bolus, bolus length λ and radius H are specified consistent with fluoroscopic imaging of esophageal bolus transport. As discussed above, lubrication thickness, ε, is specified consistent with manometric measurement of peak closure pressure, P_{amp} (Figure 2).

To study the effects of local longitudinal shortening on closure pressure, the space-time motions of the surface of the mucosa are explicitly specified in the model calculation to be consistent with (1) no longitudinal shortening, (2) the EUS and clip measurements of LLS, and (3) systematic variations in level of LLS between no shortening and the measured levels of shortening. In addition we systematically vary the degree of coordination between local circular muscle contraction, and LLS. As illustrated in Figure 7B, in the model we ultimately specify the axial (U_b) and radial (V_b) velocities of each surface point along the axial coordinate (x) and time (t). The standard model of esophageal bolus transport does not include longitudinal shortening, so there is no axial motion in the model ($U_b = 0$). With longitudinal shortening, the axial velocity is made nonzero consistent both with the shape of the propagating bolus, and with measured LLS consistent with the EUS results of Nicosia *et al*[1], and the marker studies of Dodds *et al*[10], Pouderoux *et al*[14]. and Shi *et al*[15]. These will be discussed in the following section.

ANALYSIS OF ENDOLUMINAL ULTRASOUND WITH MARKER STUDIES

Figure 8 shows the essential result from the EUS analysis of Nicosia *et al*[1]. By making use of conservation of

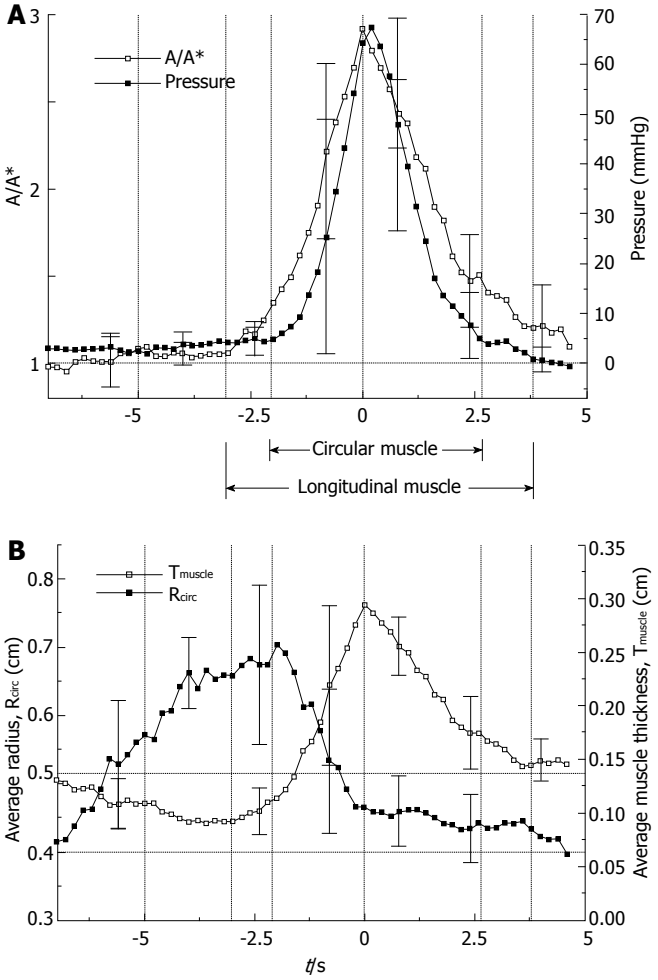

Figure 8 The primary result from Nicosia *et al*[1]. In (**A**) the inverse of local longitudinal shortening (A/A* = 1/(L/L*), see equation 2) is plotted together with circular muscle closure pressure (see equation 1) and in (**B**) the effective thickness of the muscularis propria is plotted together with effective lumen radius. All variables are plotted during the passage of a peristaltic wave with the transport of a 10 mL liquid bolus in the mid esophagus. Averages over four normal subjects were done referenced to the peak in LLS.

muscle mass, equation (2), the LLS parameter A/A* is plotted against time together with intraluminal pressure during the transport of 10 mL liquid boluses through the mid esophagus (Figure 8A). An increase in A/A^* implies a decrease L/L^*, a *local* shortening of the esophageal segment at the axial location of the ultrasound transducer. From equation (1) and the analysis in[9], we may interpret the variation in intraluminal closure pressure as a close approximation to the variation in circular muscle hoop stress, or tone. In Figure 8B are plotted the average muscle thickness, T_{muscle}, and the luminal radius to the circular muscle, R_{circ}, in the same time axis as Figure 8A. Ensemble averages were carried out over four normal subjects with the time reference as the peak in A/A^*, or maximum LLS.

The Nicosia *et al*[1] result (Figure 8) is important for several reasons. It tells us that during peristaltic transport of a bolus through the mid esophagus, longitudinal muscle contracts and shortens in a highly localized manner that is tightly coordinated with the contraction of the circular muscle. At a fixed axial location within the esophagus, longitudinal muscle contraction precedes circular muscle contraction, but longitudinal muscle maximally shortens coincident with maximum circular muscle contraction. Longitudinal muscle then relaxes, but more slowly than circular muscle. The Nicosia *et al*[1] result in the mid esophagus has recently been replicated by Mittal *et al*[19] at 5 and 10 cm above the LES. We can relate this result to the marker studies in the cat by Dodds *et al*[10] in Figure 3 where the time of maximal shortening of the three marked segments always occurred when the bolus tail was between the markers. Combined with the more precise result of Figure 8, we conclude that esophageal peristalsis may be described as overlapping peristaltic waves of circular and longitudinal muscle contraction that are spatially aligned so that peaks in longitudinal and circular muscle contraction occur nearly together as the two waves propagate concurrently along the esophageal lumen. The *in vivo*-modeling study by Nicosia & Brasseur[9] showed that the spatial pressure distribution surrounding the bolus tail in Figure 2 is a good approximation of hoop stress. If it were possible to plot local stress in longitudinal muscle on the same plot, Figure 8 suggests that the local longitudinal stress distribution would peak at the same place as hoop stress and pressure in Figure 2, but would be broader-LLS would envelope circular muscle contraction as the peristaltic waves propagate along the esophageal body.

Figure 8B indicates that as the bolus distends the esophagus, a thinning of the muscularis occurs with no change in the muscle cross sectional area, and therefore without LLS. The initiation of LLS coincides with transition from a thinning to a thickening muscle layer, while the initiation of circular muscle contraction coincides with the transition from a distending to a closing lumen. When the lumen is fully closed, change in muscle thickness implies change in muscle area, however the true marker of LLS is relative change in cross sectional muscle area rather than thickness.

Function of longitudinal muscle with esophageal emptying

Note in Figure 3 that the distal segment of the cat esophagus initially lengthens, then shortens longitudinally as the bolus tail (just distal to the point of peak circular/longitudinal muscle contraction) approaches. This initial lengthening has also been measured with clips in the distal human esophagus[14,15], but is not observed in the data of Figure 8 from the mid esophagus (nor in[19]). The initial lengthening appears to result from a pulling on the distal esophagus from above against an initially immobile LES, until the bolus tail enters the mid esophagus (Figure 3) and forms an ampulla, preceding the opening of the hiatus and esophageal emptying[11]. Ghosh *et al*[20] used a combination of concurrent manometry/fluoroscopy data and mathematical modeling of the process of hiatal opening and esophageal emptying to show that the circular muscle of the distal esophagus undergoes a rapid increase in tone that rapidly raises intrabolus pressure to force open the relaxed sphincter segment, and then maintains high pressure while bolus fluid is driven through the hiatus and into the stomach.

Ghosh *et al*[20] argued that longitudinal shortening plays a role in this process by pulling the intrinsic component of

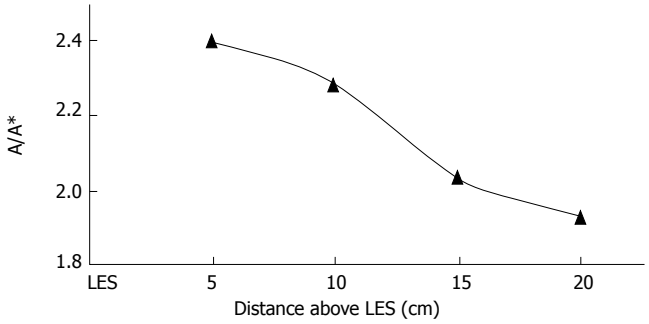

Figure 9 From Dai *et al*[2], local longitudinal shortening at peak intraluminal pressure during swallowing of 5 mL water bolus at different locations above the upper margin of lower esophageal sphincter high-pressure zone. Averages of 20 normal subjects.

the smooth muscle sphincter orad and over the surface of a forming ampulla, as suggested by the Dodds *et al*[10] data in Figure 3. Since sphincteric smooth muscle is designed to maintain tone in the resting contracted state, it is well suited to the generation of sustained tone over an ampulla, as needed during esophageal emptying. The hypothesis, therefore, is that the active suppression of LES tone ceases not when the LES returns to its resting state after esophageal emptying, but rather before emptying begins as the LES is pulled orad and placed over the ampulla surface by contraction of longitudinal muscle in the esophageal body. In this way, the LES contributes to the opening of the hiatus by increasing intrabolus pressure during ampulla formation, and to transsphincteric flow by the maintenance of high ampullary pressure. It would follow, then, that immobilizing the LES with fundoplication may explain the insufficient generation of muscle tone required to open the hiatus and drive esophageal emptying and, consequently, to fully empty the esophagus with a single peristaltic wave as has been consistently observed.

A question of mechanics now arises: how is it that the LES is not pulled orad until the peristaltic circular/longitudinal muscle waves enter the distal esophagus? Why does the LES initially remain at its resting position? Newton's second law states that the LES will move orad only if there is an orad force on the sphincteric segment of esophagus that overbalances a caudal force. Apparently, until the bolus tail passes into the distal-most esophagus, the upward pull of the esophageal body on the sphincteric segment is insufficient to overcome the caudal pull of the phreno-esophageal ligaments. However, as the peristaltic wave enters the lower esophagus, the balance of forces on the sphincteric segment must change. Given that the phreno-esophageal ligaments are purely elastic elements, and therefore cannot generate tone, it must be the case that the total upward force supplied by the longitudinal muscle must increase as the peristaltic circular/longitudinal wave approaches the hiatus and an ampulla forms. This conclusion is supported by Dai *et al*[2] who measured A/A^* at peak intraluminal pressure at different distances from the LES during swallowing of 5 mL boluses. Their result is shown in Figure 9; the level of local longitudinal shortening increases as the peristaltic wave passes into the lower esophagus, suggesting a corresponding increase in orad longitudinal stress on the gastro-esophageal segment. Longitudinal muscle, therefore, appears to play an important functional role in the process of hiatal opening and esophageal emptying.

However, there is another, more important, role for concurrent local longitudinal shortening and circular muscle peristaltic contraction waves, that we describe next.

AN EXPLANATION FOR LOCAL LONGITUDINAL SHORTENING: APPLICATION OF MATHEMATICAL MODELING AND MECHANICS

As discussed above in context with equation (1), the pressure required to maintain closure proximal to the bolus tail is generated by an integration of circular muscle hoop stress over the muscle thickness, which represents a summation of the forces of the individual circular muscle fibers on the cross section illustrated in Figure 4. It follows that if a longitudinal segment of the esophagus shortens, circular muscle fibers will be compressed within a narrower longitudinal segment and the number of fibers that contribute to hoop stress in that narrowed segment increases. Consequently, the total force available to maintain closure is larger for the same individual fiber force by the increase in number of fibers within the narrow segment. Conversely, for a given total closure force required to maintain the closure of a fixed longitudinal segment, local longitudinal shortening will reduce the force per circular muscle fiber by the increase in the number of circular muscle fibers recruited to create that given closure force.

Mechanical vs physiological consequence of local longitudinal shortening

Figure 8A shows a maximum local longitudinal shortening of $L/L^* = 1/(A/A^*) \approx 1/3$. This implies three times more circular muscle fibers available for generating closure pressure after LLS, which reduces the force required by each fiber by 1/3. This is a substantial savings in force, and correspondingly energy required to effect esophageal peristalsis. This increase in longitudinal density of muscle fibers might be described as a "physiological" explanation for the existence of a longitudinal muscle layer[1].

Another way to make the same argument is through the force balance, equation (1), and Figure 4. Above the bolus tail, the radius R_{circ} remains fixed. Up to now we have focused on the relationship between hoop stress (S_{hoop}) and closure pressure ($P_{closure}$) in equation 1. However, local longitudinal shortening increases the cross sectional muscle area $A \approx (2\pi R_{circ})T_{muscle}$, so that increasing the area by a factor of three (Figure 8A) with fixed R_{circ} also increases the thickness by roughly a factor of three. Thus, for the same closure pressure, $P_{closure}$, the hoop stress, and therefore average fiber force, can reduce by at least a factor of three.

However, equation (1) also produces the following question: Is the closure pressure $P_{closure}$ the same with local longitudinal shortening as without? That is, if evolution had

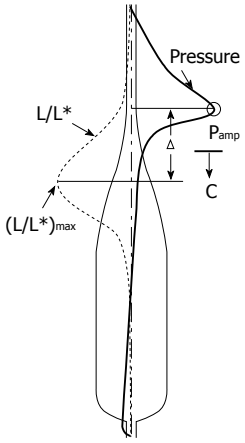

Figure 10 Schematic of the parameterization of local longitudinal shortening in the model. The shape of the shortening parameter L/L* is fixed while maximum LLS and offset between the longitudinal and circular muscle contraction waves are varied.

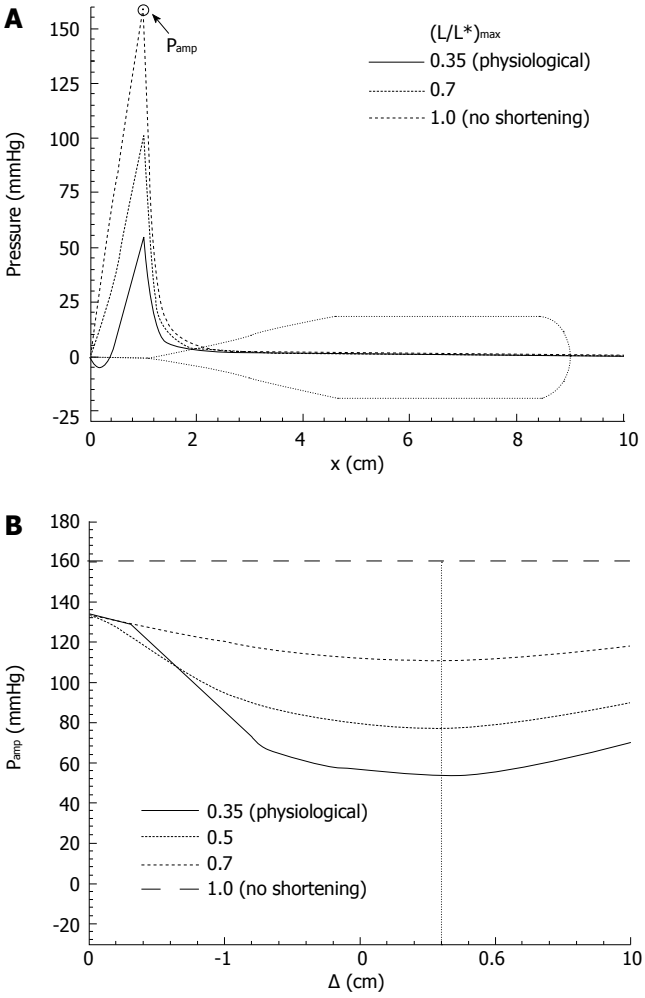

Figure 11 Primary result from Pal & Brasseur[18]. **A**: Mathematical model calculation of pressure during esophageal peristaltic transport with different levels of local longitudinal shortening, from the measured physiological level, to no shortening; **B**: Calculation of peak closure pressure as a function of separation △ between the circular muscle and longitudinal muscle contraction waves (Figure 10).

not created a longitudinal muscle layer, would the pressure required to maintain closure (left side of equation 1) be the same? The reason why the closure pressure might be different is that a traveling wave of LLS causes the mucosal surface to move axially (Figure 3). As the bolus tail approaches a material point on the mucosal surface, the material point moves orad; then, as the tail passes that material point, it reverses direction and moves caudal. Because there is a thin liquid film above the tail the pressure in the tail region is very sensitive to tail geometry[8], so that axial motions of the mucosal surface close to the tail have the potential to impact fluid pressure and frictional stresses there. It might be the case, for example, that the pressure near the tail required to maintain closure is higher as a result of the axial motions associated with LLS than without in which case, the gain in muscle fiber force from the compression of muscle fibers by physiological stimulation of longitudinal muscle would be offset by an increase in closure pressure. So, the answer to the question is important for the role of longitudinal muscle in esophageal peristalsis. However, these questions cannot be answered through *in vivo* experiment, so we employ the power of mathematical modeling to extend data measurable *in vivo* to data unavailable to physiological experiment.

The mechanical consequence of local longitudinal shortening

The basic mathematical model[18] from which closure pressure can be predicted was described in "MATERIALS AND METHODS" above and the basic parameters of bolus motion are shown in Figure 7. However, the axial motions of the lumen surface in the model were described only in general terms, in the absence of the local longitudinal shortening data from Figure 8. These data were used to specify and parameterize the boundary axial and radial velocities U_b and V_b of all material points on the modeled mucosal surface. LLS was modeled as a longitudinal muscle contraction wave that propagates together with the circular muscle contraction wave, as illustrated in Figure 10. The longitudinal muscle contraction wave was modeled as a longitudinal shortening wave with specified shape L/L^* *vs* axial coordinate x that moves with the specified luminal geometry at the same bolus speed c. The peak in LLS was displaced from peak intraluminal pressure by the specified amount Δ. The shape and width of L/L^* were determined from the data of Figure 8A, assuming a wave speed of 3 cm/s (typical for bolus transport through the mid esophagus). Peak LLS, $(L/L^*)_{max}$, was varied: from no shortening ($L/L^* = 1$, implying no axial motion of the mucosal surface, or $U_b = 0$), to the physiological value of shortening, $(L/L^*)_{max} = 0.35$), leading to surface motions similar to the upper markers in Figure 3. The displacement between the longitudinal and circular muscle contraction waves, Δ (Figure 10), was also systematically varied from 0 to ± 2 cm. The mathematical details are given in[18].

The primary result from Pal & Brasseur[18] is given in Figure 11. In Figure 11A closure pressure is plotted along the bolus axis for different levels of local longitudinal shortening, with the longitudinal and circular muscle contraction waves perfectly aligned ($\Delta = 0$). The lubrication layer thickness ε was fixed at a value where peak closure pressure in the absence of LLS was roughly 150 mmHg. We discover that a coordinated peristaltic wave of

local longitudinal shortening reduces peak closure pressure progressively, and very significantly, with increasing levels of LLS. At the physiological level of LLS measured by Nicosia *et al*[1], the level of pressure required to maintain closure is one third what would be required in the absence of a longitudinal muscle wave coordinated with the circular muscle peristaltic wave. This is a very substantial reduction in the pressure required to maintain the same level of luminal closure, and is a fully mechanical effect that arises from the changes in fluid stresses that arise from relatively subtle axial movements of the lumen surface induced by the LLS associated with longitudinal muscle peristalsis.

In Figure 11B we plot the effect of displacement between the peak LLS and circular muscle contraction waves on peak closure pressure, for different levels of LLS. Whereas the minimum is relatively broad, we find that the effect of LLS on reduction of closure pressure is maximal when the circular and longitudinal muscle contraction waves are aligned to within roughly 1 cm, or on a time axis within about 1/3 second, consistent with Figure 8A.

An explanation for the existence of longitudinal muscle

Using a combination of intraluminal ultrasound with image analysis, the laws of mechanics, and mathematical modeling, we have arrived at a convincing functional explanation for the existence of longitudinal muscle in the esophagus. Combined longitudinal-with-circular-muscle peristaltic contraction waves have two beneficial multiplicative consequences to the circular muscle tone and energy required for esophageal peristalsis. Firstly, local contraction of longitudinal muscle shortens the longitudinal dimension of axial segments and increases the concentration of circular muscle fibers at the location of maximal circular muscle squeeze by nearly a factor of 3, thus reducing the force required by each circular muscle fiber by nearly 1/3 as compared to the same esophagus without the longitudinal muscle layer. Secondly, the local axial motions of the mucosal surface induced by a peristaltic wave of local longitudinal shortening reduce the level of applied pressure required to locally close the lumen also by roughly a factor of three, a result of the local changes in fluid stresses within the lubrication layer. The net result is an overall reduction of fiber force by about 1/9, or roughly 10% what would have been required in the absence of the longitudinal muscle layer! To obtain this benefit, longitudinal muscle contraction envelopes circular muscle contraction.

Furthermore, given that the power required by individual muscle fibers to transport a bolus through the esophagus is proportional to the fiber force, the coordination of longitudinal and circular muscle peristaltic waves greatly reduces the energy requirements for circular muscle fibers. Because the reduction in fiber force is so high, even when the additional power requirements of longitudinal muscle are taken into account, the net savings in energy requirements are substantial. Indeed the combined physiological and mechanical benefits are so great that one might extrapolate this observation as a potential explanation for the existence of longitudinal muscle and local longitudinal muscle shortening throughout the GI tract, including the intestines and sphincters.

RELATED OBSERVATIONS

Having understood how to interpret EUS data in context with LLS, EUS research preceding the Nicosia *et al*[1] study can now be interpreted in context with the discussions above. Furthermore, three additional studies involving clips provide additional insight.

Miller *et al*[4] were the first to report measurements of muscle thickness concurrent with intraluminal pressure during esophageal bolus transport. They report results essentially equivalent to the thickness and pressure results in Figure 8, showing an increase and decrease in muscle thickness surrounding the pressure as in Figure 8. In a more recent study, Dai *et al*[21] showed that the time period of circular muscle contraction with bolus transport through the esophageal body, as inferred from the duration of the peristaltic pressure, is strongly correlated to the time period of longitudinal muscle contraction as inferred from LLS ($r = 0.92$), further confirming the integration of longitudinal and smooth muscle contraction in esophageal peristalsis.

In an interesting study of concurrent changes in pressure and muscle thickness above and below local balloon distension of the esophagus above the LES, Yamamoto *et al*[22] showed that a peripherally induced increase in circular muscle tone above local balloon distension is strongly correlated with a local increase in muscle thickness. Below the balloon distension neither pressure nor muscle thickness increased. Because these studies were carried out in the absence of a bolus, we may interpret the increase in thickness as an increase in muscle cross sectional area, and therefore the presence of local longitudinal shortening above the distension, but not below. We conclude that a strong correlation exists between circular and longitudinal muscle contraction associated with local discussion. Based on studies of primary peristalsis, it is reasonable to hypothesize that the correlation between circular and longitudinal muscle contraction is maintained after balloon deflation and the initiation of secondary peristalsis an association that was suggested in clip studies by Shi *et al*[15].

Pehlivanov *et al*[6] showed a significant correlation between maximum muscle thickness and pressure amplitude during esophageal bolus transport, which we now may interpret as a correlation between LLS and closure pressure as was shown explicitly by Nicosia *et al*[1]. These results support the physiological explanation of longitudinal muscle function discussed above, since a higher degree of LLS would imply a higher concentration of circular muscle fibers and, potentially, a higher closure pressure (equation 1, Figure 4). Pehlivanov *et al*[23] went on to show that this correlation weakens in patients with nutcracker esophagus and diffuse esophageal spasm, suggesting that pathology of circular and longitudinal muscle during bolus transport may be intertwined. Interestingly, Balaban *et al*[24] demonstrated a correlation in

thickening of the esophageal muscularis propria sustained for a minute and chest pain, in the absence of peristalsis and circular muscle contraction. In the absence of a bolus, an increase in muscle thickness implies an increase in muscle cross sectional area, so we may conclude that the recorded chest pain was associated with sustained shortening of esophageal longitudinal muscle.

Using mucosal clips in the distal esophagus, Kahrilas *et al*[13] showed that longitudinal shortening is impaired by hiatal hernia. This result is understandable in light of the balance between longitudinal muscle stress orad, and elastic stress within the phreno-esophageal ligaments caudal, as discussed above. The mucosal clip study by Shi *et al*[15] suggests that transient lower esophageal relaxation (tLESR) may be associated with longitudinal shortening of the distal esophagus, and therefore that gastro-esophageal reflux may be preceded by longitudinal muscle contraction and esophageal shortening. A recent study reported by Pandolfino *et al*[25], with far more subjects that combine two mucosal clips with high-resolution manometry, provides convincing evidence that this is the case. The physiology and function of local longitudinal shortening in reflux, and in distinguishing normal from pathological reflux, is not yet understood.

DISCUSSION: THE IMPORTANCE OF LONGITUDINAL MUSCLE

Research within the last several years has greatly increased our understanding of longitudinal muscle function in the esophagus. In particular, we now have a reasonable explanation for why evolution has lead to the creation of a longitudinal muscle layer. Peristalsis underlies esophageal function. From a mechanical perspective, peristalsis requires force and power. From a physiological perspective, the peristaltic forces originate in the generation of muscle fiber tone, regulated and controlled in space-time by central and enteric neuromuscular interactions. Underlying luminal transport in the esophagus, transport and mixing in the gut, and regulation of transport in the sphincters, is the controlled opening and closure of localized luminal segments by circularly aligned muscle fibers. Thus the efficiency of circular muscle function underlies the efficiency of gut function. We have observed (Figure 8) that at peak closure pressure, the circular muscle layer area and thickness in the esophagus are roughly three times larger than the resting state, implying that in the absence of the longitudinal muscle layer, the circular muscle should have to be three times thicker than evolution has produced. Thus, taking into account a longitudinal muscle layer with the same thickness as the circular muscle layer, and assuming the same number density of longitudinal and circular muscle fibers, the presence of a longitudinal muscle layer implies a 33% savings in the required number of muscle fibers.

However, the savings are much greater than simply a reduction by one third in the number of required muscle fibers. By producing a local wave of longitudinal muscle contraction coordinated with circular muscle contraction, the longitudinal muscle layer generates controlled axial motions of the mucosal surface that affect the frictional and pressure stresses within the fluid lubrication layer between the mucosa and catheter, or within the mucosal folds. The consequence of these changes is to reduce by two thirds the pressure force required to close the lumen and effect peristaltic transport, and therefore the tension force by each circular muscle fiber. The major reductions in circular muscle force also imply major reductions in power required to transport the bolus, and therefore the energy required by the circular muscle fibers during peristalsis. If one assumes that axial stresses induced by longitudinal muscle contraction are, at best, comparable to the hoop stresses during peristalsis, the additional power required by longitudinal muscle is of order or less than circular muscle, and a net savings of at least one third is again obtained. Thus, the presence of the longitudinal muscle layer both reduces substantially the number of muscle fibers required for peristaltic bolus transport and the energy required by the muscles involved in the transport process. The motivation for the existence of a longitudinal muscle layer is clear.

Whereas the mechanical consequences of longitudinal muscle function in esophageal peristalsis are somewhat clarified, there is very little that is understood about the neurophysiology that controls the coordination between longitudinal and circular muscle peristalsis, or about the function and physiology of longitudinal muscle not associated with peristalsis. Furthermore, whereas there have been some tantalizing hints about the role of longitudinal muscle in pathology, very little is known, much less understood, about longitudinal muscle pathology, its role in gut dysfunction, and its relationship to diseases of the gastro-intestinal tract.

REFERENCES

1 **Nicosia MA**, Brasseur JG, Liu JB, Miller LS. Local longitudinal muscle shortening of the human esophagus from high-frequency ultrasonography. *Am J Physiol Gastrointest Liver Physiol* 2001; **281**: G1022-G1033

2 **Dai Q**, Korimilli A, Thangada VK, Chung CY, Parkman H, Brasseur J, Miller LS. Muscle shortening along the normal esophagus during swallowing. *Dig Dis Sci* 2006; **51**: 105-109

3 **Ulerich R**, Dai Q, Miller LS, Brasseur JG. Detailed 3-D Anatomy of the Human Gastro-Esophageal Segment. *Gastroenterology* 2003; **124**: A259-A259

4 **Liu JB**, Miller LS, Goldberg BB, Feld RI, Alexander AA, Needleman L, Castell DO, Klenn PJ, Millward CL. Transnasal US of the esophagus: preliminary morphologic and function studies. *Radiology* 1992; **184**: 721-727

5 **Miller LS**, Liu JB, Colizzo FP, Ter H, Marzano J, Barbarevech C, Helwig K, Leung L, Goldberg BB, Hedwig K corrected to Helwig K. Correlation of high-frequency esophageal ultrasonography and manometry in the study of esophageal motility. *Gastroenterology* 1995; **109**: 832-837

6 **Pehlivanov N**, Liu J, Kassab GS, Puckett JL, Mittal RK. Relationship between esophageal muscle thickness and intraluminal pressure: an ultrasonographic study. *Am J Physiol Gastrointest Liver Physiol* 2001; **280**: G1093-G1098

7 **Brasseur JG**, Dodds WJ. Interpretation of intraluminal manometric measurements in terms of swallowing mechanics. *Dysphagia* 1991; **6**: 100-119

8 **Li M**, Brasseur JG. Nonsteady peristaltic transport in finite length tubes. *J Fluid Mech* 1993; **248**: 129-151

9 **Nicosia MA**, Brasseur JG. A mathematical model for estimating muscle tension in vivo during esophageal bolus transport. *J Theor Biol* 2002; **219**: 235-255

10 **Dodds WJ**, Stewart ET, Hodges D, Zboralske FF. Movement of the feline esophagus associated with respiration and peristalsis. An evaluation using tantalum markers. *J Clin Invest* 1973; **52**: 1-13

11 **Lin S**, Brasseur JG, Pouderoux P, Kahrilas PJ. The phrenic ampulla: distal esophagus or potential hiatal hernia? *Am J Physiol* 1995; **268**: G320-G327

12 **Edmundowicz SA**, Clouse RE. Shortening of the esophagus in response to swallowing. *Am J Physiol* 1991; **260**: G512-G516

13 **Kahrilas PJ**, Wu S, Lin S, Pouderoux P. Attenuation of esophageal shortening during peristalsis with hiatus hernia. *Gastroenterology* 1995; **109**: 1818-1825

14 **Pouderoux P**, Lin S, Kahrilas PJ. Timing, propagation, coordination, and effect of esophageal shortening during peristalsis. *Gastroenterology* 1997; **112**: 1147-1154

15 **Shi G**, Pandolfino JE, Joehl RJ, Brasseur JG, Kahrilas PJ. Distinct patterns of oesophageal shortening during primary peristalsis, secondary peristalsis and transient lower oesophageal sphincter relaxation. *Neurogastroenterol Motil* 2002; **14**: 505-512

16 **Thatte A**, Brasseur JG. The Misuse of the Laplace Law in Measurement of Gastro-Intestinal Wall Compliance. *(abstract) Bull Amer Phys Soc* 2005; **50**: 88

17 **Sugarbaker DJ**, Rattan S, Goyal RK. Mechanical and electrical activity of esophageal smooth muscle during peristalsis. *Am J Physiol* 1984; **246**: G145-G150

18 **Pal A**, Brasseur JG. The mechanical advantage of local longitudinal shortening on peristaltic transport. *J Biomech Eng* 2002; **124**: 94-100

19 **Mittal RK**, Padda B, Bhalla V, Bhargava V, Liu J. Synchrony between circular and longitudinal muscle contractions during peristalsis in normal subjects. *Am J Physiol Gastrointest Liver Physiol* 2006; **290**: G431-G438

20 **Ghosh SK**, Kahrilas PJ, Zaki T, Pandolfino JE, Joehl RJ, Brasseur JG. The mechanical basis of impaired esophageal emptying postfundoplication. *Am J Physiol Gastrointest Liver Physiol* 2005; **289**: G21-G35

21 **Dai Q**, Liu JB, Brasseur JG, Thangada VK, Thomas B, Parkman H, Miller LS. Volume (3-dimensional) space-time reconstruction of esophageal peristaltic contraction by using simultaneous US and manometry. *Gastrointest Endosc* 2003; **58**: 913-919

22 **Yamamoto Y**, Liu J, Smith TK, Mittal RK. Distension-related responses in circular and longitudinal muscle of the human esophagus: an ultrasonographic study. *Am J Physiol* 1998; **275**: G805-G811

23 **Pehlivanov N**, Liu J, Kassab GS, Beaumont C, Mittal RK. Relationship between esophageal muscle thickness and intraluminal pressure in patients with esophageal spasm. *Am J Physiol Gastrointest Liver Physiol* 2002; **282**: G1016-G1023

24 **Balaban DH**, Yamamoto Y, Liu J, Pehlivanov N, Wisniewski R, DeSilvey D, Mittal RK. Sustained esophageal contraction: a marker of esophageal chest pain identified by intraluminal ultrasonography. *Gastroenterology* 1999; **116**: 29-37

25 **Pandolfino JE**, Zhang QG, Ghosh SK, Han A, Boniquit C, Kahrilas PJ. Transient lower esophageal sphincter relaxations and reflux: mechanistic analysis using concurrent fluoroscopy and high-resolution manometry. *Gastroenterology* 2006; **131**: 1725-1733

S- Editor Liu Y **L- Editor** Alpini GD **E- Editor** Ma WH

PO Box 2345, Beijing 100023, China
www.wjgnet.com
wjg@wjgnet.com

World J Gastroenterol 2007 March 7; 13(9): 1347-1351
World Journal of Gastroenterology ISSN 1007-9327

TOPIC HIGHLIGHT

Hans Gregersen, Professor, *Series Editor*

The oesophageal zero-stress state and mucosal folding from a GIOME perspective

Donghua Liao, Jingbo Zhao, Jian Yang, Hans Gregersen

Donghua Liao, Jingbo Zhao, Jian Yang, Hans Gregersen, Centre of Excellence in Visceral Biomechanics and Pain, Aalborg Hospital, Aalborg DK-9100, Denmark
Hans Gregersen, Center of Sensory-Motor Interaction, Aalborg University, Aalborg DK-9220, Denmark
Hans Gregersen, Department of mechanical Engineering, ITT, Dublin, Ireland, and Haukeland University Hospital, Bergen, Norway
Correspondence to: Donghua Liao, Aalborg Hospital Science and Innovation Centre, Sdr. Skovvej 15, Aalborg DK-9000, Denmark. dl@rn.dk
Telephone: +45-99326907 Fax: +45-99326801
Received: 2006-12-09 Accepted: 2007-02-07

Abstract

The oesophagus is a cylindrical organ with a collapsed lumen and mucosal folds. The mucosal folding may serve to advance the function of the oesophagus, i.e. the folds have a major influence on the flow of air and bolus through the oesophagus. Experimental studies have demonstrated oesophageal mucosal folds in the no-load state. This indicates that mucosal buckling must be considered in the analysis of the mechanical reference state since the material stiffness drops dramatically after tissue collapse. Most previous work on the oesophageal zero-stress state and mucosal folding has been experimental. However, numerical analysis offers a promising alternative approach, with the additional ability to predict the mucosal buckling behaviour and to calculate the regional stress and strain in complex structures. A numerical model used for describing the mechanical behaviour of the mucosal-folded, three-layered, two-dimensional oesophageal model is reviewed. GIOME models can be used in the future to predict the tissue function physiologically and pathologically.

Key words: Oesophagus; Finite element analysis; Zero-stress state; Buckling

Liao D, Zhao J, Yang J, Gregersen H. The oesophageal zero-stress state and mucosal folding from a GIOME perspective. *World J Gastroenterol* 2007; 13(9): 1347-1351

http://www.wjgnet.com/1007-9327/13/1347.asp

EXPERIMENTAL AND MODELING APPROACHES TO THE ZERO-STRESS STATE AND MUCOSAL BUCKLING

New computational models for describing the gastrointestinal (GI) tract mechanical behaviour precisely are a GIOME approach for bioengineering tissue modelling. The zero-stress state provides a standardized reference state for describing the mechanical response to external loading[1-4]. A large number of studies have been published on the zero-stress state of the cardiovascular and GI systems. The zero-stress state in soft biological tissues can be obtained by an experiment where tissue rings are cut radically, opening up into sectors. The angle subtended by the open ring, referred to as the opening angle, is used as a measure of the residual stress present in the intact ring of the tissue[2]. However, recent studies on multi-layered organs such as blood vessels and the GI tract indicate that the zero-stress state differs between layers and that a stress jump exists between the layers[5-11]. Thus, the true stress-free configuration for a multi-layered model is at least a twice cut tissue ring; one circumferential cut for layer separation and one radial cut in each layer to generate a true stress-free state.

Longitudinal mucosal folds exist throughout the length of the oesophagus. It was originally believed that the folding was caused by the contraction of the muscle layer in an *in vivo* state[12]. However, the folds appear even at the no-load state[5]. Hence, additional tension caused by the compressed mucosa-submucosal layer exists in the muscle layer at the no-load state. Furthermore, the mucosal layer is not perfectly elastic, its circumferential length cannot decrease to zero, thus the tension in the muscle layer will collapse the mucosal layer[12]. Therefore, the buckling feature of the oesophagus must be accounted for in a reference state analysis since the material stiffness drops dramatically after tissue collapse.

In the airways it has been shown that the number of folds depends on the luminal radius, mucosal thickness and on the elasticity of the mucosal layer[13,14]. However, since only experimental work has been done on oesophageal mucosal folding, no detailed information exists on relations between the stress-strain and buckling of the oesophageal mucosa. A numerical model used for

Table 1 The average geometry data of the three-layered oesophagus

	Opening angle (TS) (degree)	Inner radius (TS) (mm)	Thickness (TS) (mm)	Inner radius (NS) (mm)	Interface radius (NS) (mm)
Muscle	47	1.28	0.37	0.95	
MMS	91	2.21	0.15	1.23	1.19
Epithelial	91	2.14	0.07	1.16	

MMS: Muscularis mucosae-Submucosa; TS: true zero-stress state; NS: no-load state.

buckling analysis in a three-layered (the epithelium, the muscularis mucosal-submucosal (MMS) and the muscle), two dimensional oesophageal model has been generated. Such bioengineering GIOME models can be used in the future to predict the tissue function both physiologically and pathologically.

NUMERICAL MODELING

Previous zero-stress state analysis has been based on data from rat, rabbit and guinea pig[1,5,6,9,10,15]. In yet unpublished studies, the zero-stress morphology data were obtained from five male 300 g Wistar rats. Geometric models for the oesophageal muscle and mucosal-submucosal layer were generated based on the morphology of the separated oesophagus at the zero-stress state[5,6,15]. The oesophageal passive mechanical properties were tested from the two other Wistar rats by using a tensile test machine[16,17].

Geometric models

Previous studies have shown that the muscle layer at the no-load state is stretched while the mucosal layer (the epithelial layer + the MMS layer) is compressed (Table 1)[5,6,9,18]. Tensile and radial stresses induced by muscle layer stretch existed at the interface between the muscle layer and the mucosal layer. The radial stress is the balance stress that acts on the mucosal layer to produce the folds. For simulating the three-layered, mucosal folded oesophageal wall, the analysis was divided into two steps. The first step was to simulate the separated muscle layer and mucosal layer from an opening sector to the closed rings. The configurations for the opening sectors and the closed ring are illustrated in Figure 1. The second step was to stretch the muscle layer according to the experimental morphological measurement and to compress the mucosal layer by using the pressure that acted on the interface between the muscle and the mucosal layer (the pressure was equal to the radial stretch stress at the inner surface of the muscle layer).

Mechanical properties

The mechanical properties of the muscle and mucosal-submucosal layers were obtained based on the un-axial tensile test and circumferential planar test on each layers. The tests were conducted in a tensile test machine consisting of an organ bath, motion table, force transducer and electronics[15,16]. The force and displacement curves were obtained simultaneously during the tensile test. Hence, the uni-axial stress-strain can be calculated.

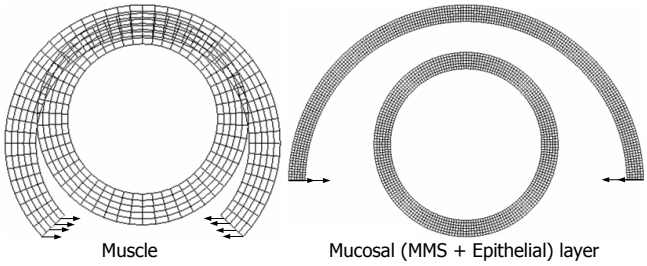

Figure 1 The configurations of the separated muscle (left) and the mucosal (right) layer at the zero-stress state (open sectors) and the no-load state (closed circular rings). The no-load state was obtained by forcing the opening sector to be closed using a pure bending deformation. The pure bending loads are indicted by arrows. The numerical model was conducted by using the ABAQUS software.

Stress-strain calculation

The stress and strain calculation for the circumferential uni-axial tensile test and planar test:

$$\text{Stretch ratio: } \lambda = (C/C_0) \quad (1)$$

$$\text{Lagrangian Stress } T = F/(W_{ring} \times h \times 2) \quad (2)$$

where C and C_0 are the length between the centre of the two rods before and during deformation, F is the recorded force. C, h, and W_{ring} refer to the circumference, thickness and width of the rings, respectively.

The circumferential stress-strain curves for both the muscle and mucosal layer show an exponential, large deformation pattern. Consequently, the muscle layer and the mucosal layer must be modelled as a hyperelastic material by using 2nd Ogden strain energy functions[19] (Figure 2A). To the best of our knowledge, data on the material properties do not exist on the separated MMS and epithelial layer. Thus, it was assumed that the stress-strain curve obtained from the separated mucosa-submucosal layer mainly determined the mechanical properties of the epithelial layer. The stress-strain curve of the MMS layer was assumed to have a similar pattern as the epithelial layer but it was about one order softer than the epithelial layer. Hence, for achieving the same stress level, the submucosal layer will be deformed about ten times more than the epithelial layer) (Figure 2B).

Boundary conditions

The boundary conditions for the first step are: The separated muscle and mucosal opening sectors were forced to be closed by using a pure bending deformation (Figure 1).

The boundary conditions for the second step were defined based on the morphological data in Table 1:

For the muscle layer

$$u_{r-muscle}|_{r=r_i} = 0.244mm$$

for the mucosal layer

$$\sigma_{r-mucosal}|_{r=r_o} = -\sigma_{r-muscle}|_{r=r_i}$$

u is displacement in the radial direction, σ_r is the radial stress and the substitute r_o and r_i are the inner surface of the muscle and the outer surface of the mucosal layer.

Buckling analysis and mesh independent test

The first step for the buckling analysis was to compute the buckling mode or shape by using a linearized buckling analysis. The preferred buckling mode according to the experimental images was introduced into the numerical model by using imperfections. A nonlinear static analysis

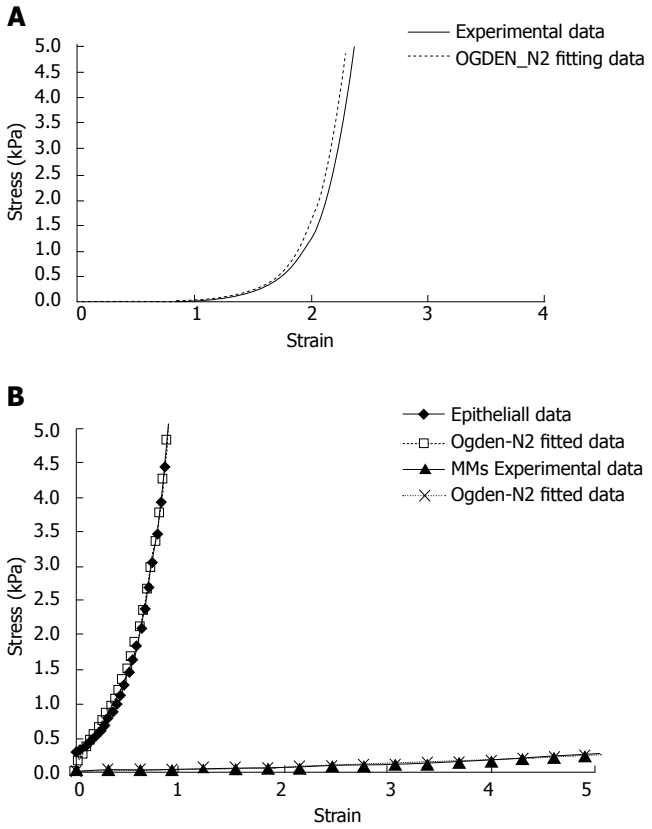

Figure 2 Circumferential experimental and curvefitted stress-strain curves for the muscle (**A**) and mucosal (**B**) layers. The curves were fitted by using the Ogden 2nd order strain energy function. The stress-strain curve of the epithelial layer was tested from the mucosal-submucosal layer while the stress strain curve of the MMS layer was assumed to have a similar pattern as the epithelial layer with the magnitude about one order softer than the epithelial layer. For the circumferential uni-axial test and the circumferential planar test the separated muscle and mucosal-submucosal rings were fixed in two L shape rods, one end of the L shape rod was connected to a cannula. The cannulas were connected to rods that could be moved at controlled velocities by a motor. One of the rods was attached to a force transducer. The distance between the rods was adjusted manually to the *in vitro* length of the strips (reference length). The force (F) was recorded online by a Labview program.

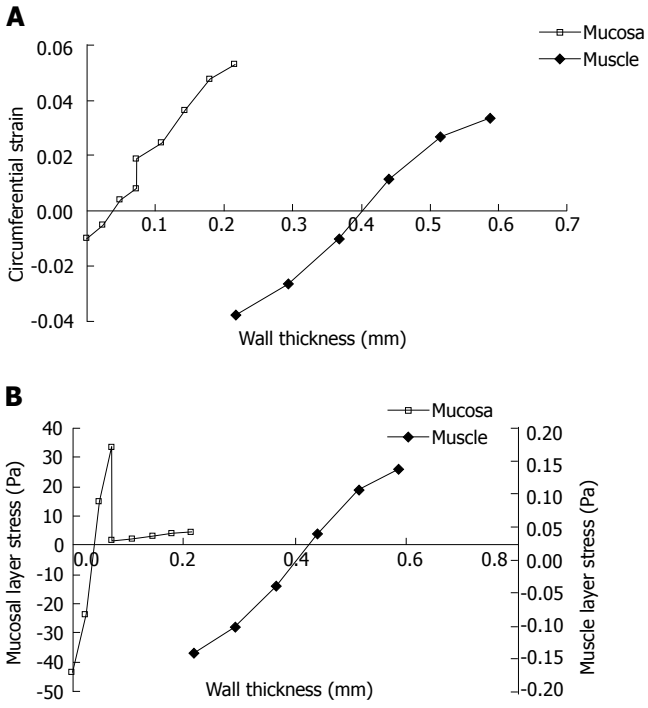

Figure 3 The circumferential strain (**A**) and stress (**B**) distribution throughout the muscle and mucosal (MMS + epithelial) layers after the separated muscle and mucosal layer sectors were closed. The strain and stress jump occurred at the interface between the epithelial and MMS layer.

was then applied to generate quantitative relationships between the external compression stress and the associated internal deformations and stress distributions for an imperfect structure.

The mesh independent test was processed on the double amount of the meshes each time for looking for the convergence. The mesh was considered independent when the displacement errors between the two analyses were less than 5%.

LAYERED BUCKLING MODELING

Circumferential stress and strain in the separated layers after bending

For the strain analysis, the numerical model presented similar result as the previous experimental studies, i.e. the inner wall was in compression and the outer wall was in tension for both the muscle and mucosal layer (Figure 3A). However, the strain distribution through the wall can be further advanced using the numerical model. The neutral surface (with zero strain) was located 50% and 18% from the inner side of the muscle and mucosal layer. The residual stress analysis in most of the previous zero-stress study was neglected due to the lack of the material properties. The numerical model shows the compressive and tensile stresses in the epithelial layer were significantly higher than that in the muscle layer, which is consistent with the stiffer tissue material in the epithelial layer (Figure 3B).

Residual stress and strain distribution at the no-load state

The muscle layer at the no-load state was fully stretched (Figure 4A). The radial stress at the interface between the inner muscle surface and the outer MMS surface was 0.26 Pa (Figure 4B). Buckling mode three and five were used for imperfection in the buckling analysis according to the experimental observation (Figure 5). The stress distributions after buckling are heterogeneous. The region with the lowest stress was found in the MMS region (blue colour in Figure 5) due to the softer stiffness. The highest stress region was located at the bending place in the epithelial layer (Figure 5).

SUMMARY AND PERSPECTIVES

Buckling in the oesophagus

Some materials are strong in tension but offer little resistance to deformation when uni-axially compressed. The large deformation in compression is called buckling. Buckling is a common phenomenon in organs. Tissue is in tension when the stretch ratio > 1 and in compression when the stretch ratio < 1. Tissue buckling occurs when the stretch ratio < 1[2]. The oesophagus uses buckling to

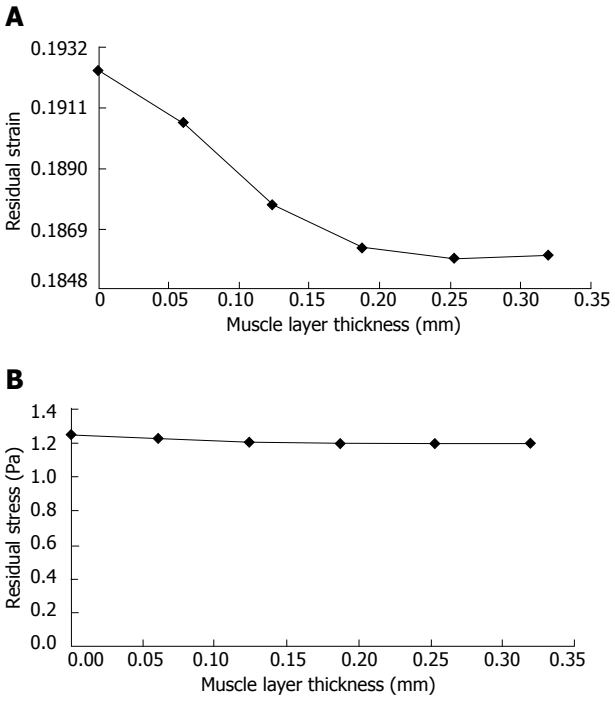

Figure 4 Circumferential residual strain (**A**) and residual Mises stress (**B**) distribution in the muscle layer at the no-load state. Strain was positive throughout the muscle wall.

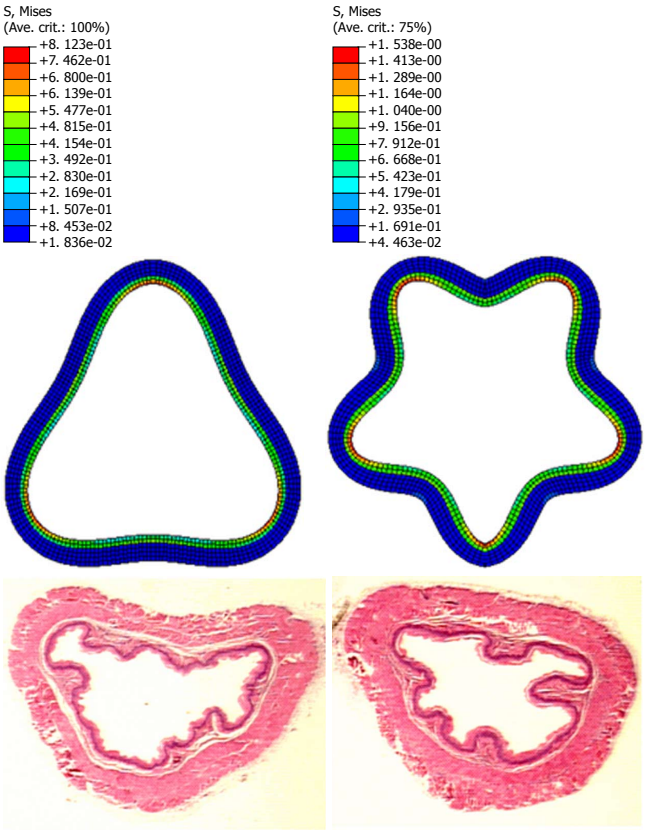

Figure 5 Residual stress of the mucosal layer in a three folds model (Top, left) and five folds model (Top, right). The morphological oesophageal images indicated that the folds numbers are between three (bottom, left) and five (bottom, right) at the no-load state.

advance its normal function. Without food in the lumen, a small tension in the circumferential muscle is sufficient to cause large buckling to the mucosa and submucosa. Qualitatively, the course of fold formation can be as follows: As the oesophagus contracts, no folds need to form until the radius of the hollow organ is reduced beyond the ability of the mucosal elasticity to take up the slack. Thereafter, the surface is thrown into folds as the increasingly redundant lining membrane adjusts to the diminishing circumference of the lumen. Finally, when the tone of the contracted organ reduces the area of the lumen to zero, the maximum number of folds will be present[12].

Advantage of the numerical model

Mucosal folds in previous multi-layered oesophageal models were either neglected[6]or simulated as the irregular boundary[5]. This paper points out that the wall stiffness of the inner layer dropped dramatically after the collapse. Thus, the buckling appeared under a very small critical buckling stress at the no-load state. This phenomenon is consistent with *in vitro* experiments showing that rabbit oesophageal mucosal folds disappear at the luminal pressure of 1 cm H_2O (unpublished data). It is thus suggested that the extended inner mucosal layer must be used as a reference state for tension or stress calculation during *in vivo* ultrasound studies, for example.

The stress level in the modelling study is significantly smaller than the previous layered oesophageal numerical studies[11]. One reason could be that a different stress-strain relationship was used. Another reason is that the buckling feature was neglected in the previous residual stress and strain analysis. Hence, the no-load state in the previous study was simplified. The residual stress and residual strain were calculated based on the configuration difference between the zero-stress state and the no-load state[1,2,4]. Thus, a precise description of the zero-stress state and the no-load state of the layered oesophagus is necessary for accurate estimation of the residual stress and residual strain.

Limitations of the current model

Since 2-D analysis was done the assumption of plain strain implies no deformation in the axial direction. The external loading in the model, simulating the effect of smooth muscle constriction, consisted entirely of radial and circumferential stresses since only the separated zero stress state and the no-load state was investigated. The *in vivo* axial stretch ratio of the oesophagus is about 150%. Consequently, it is expected that the muscle wall will be compressed even more and the number and the size of the folds may be different. An obvious simplification of the anatomy of the oesophagus was used in this model, i.e. that the buckles formed in a symmetric pattern. The non-circular oesophageal geometry is expected to influence the folding pattern (Figure 5, bottom).The mechanical properties of the MMS-epithelial layer were assumed from the measured mucosal-submucosal layer since no data exist.

Clinical perspective and future GIOME studies

The buckling behaviour has been studied previously on the upper GI tract and the airway system[11-14,20,21]. It has been

found that the folds size and number are related to the mucosal thickness and the material stiffness. Inflammation, edema, lymphoma, and Menitrier's disease all thicken the mucosa; they are all associated with a reduction in the number and an increase in the size of the folds[12]. Longitudinal folding exists along the inner surface of the oesophagus, and possibly occluding the internal lumen. This has a major influence on the flow through the lumen. The nature of this folding and the resistance to narrowing are functions of the composition, geometry and structural properties of the various oesophageal wall components. Hence, buckling analysis can be further used clinically for predicting the tissue remodelling physiologically and pathologically. This study shows that bioengineering models in the future of the GIOME can provide important new knowledge on tissue function.

REFERENCES

1 **Gregersen H**, Kassab GS, Fung YC. The zero-stress state of the gastrointestinal tract: biomechanical and functional implications. *Dig Dis Sci* 2000; **45**: 2271-2281
2 **Gregersen H**. Biomechanics of the Gastrointestinal Tract. London: Springer, 2002
3 **Chuong CJ**, Fung YC. On residual stresses in arteries. *J Biomech Eng* 1986; **108**: 189-192
4 **Fung YC**. Biomechanics: Mechanical Properties of Living Tissues. New York: Springer-Verlag, 1993
5 **Liao D**, Zhao J, Fan Y, Gregersen H. Two-layered quasi-3D finite element model of the oesophagus. *Med Eng Phys* 2004; **26**: 535-543
6 **Liao D**, Fan Y, Zeng Y, Gregersen H. Stress distribution in the layered wall of the rat oesophagus. *Med Eng Phys* 2003; **25**: 731-738
7 **Peterson SJ**, Okamoto RJ. Effect of residual stress and heterogeneity on circumferential stress in the arterial wall. *J Biomech Eng* 2000; **122**: 454-456
8 **Taber LA**, Humphrey JD. Stress-modulated growth, residual stress, and vascular heterogeneity. *J Biomech Eng* 2001; **123**: 528-535
9 **Gregersen H**, Lee TC, Chien S, Skalak R, Fung YC. Strain distribution in the layered wall of the esophagus. *J Biomech Eng* 1999; **121**: 442-448
10 **Lu X**, Gregersen H. Regional distribution of axial strain and circumferential residual strain in the layered rabbit oesophagus. *J Biomech* 2001; **34**: 225-233
11 **Yang W**, Fung TC, Chian KS, Chong CK. 3-D finite element model of the two-layered esophagus: The effects of residual strains and buckling of mucosa. In: Proceeding of the second IASTED International Conference. Spain: Benidorm, 2005: 194-199
12 **Stiennon A.O**. The Longitudinal Muscle in Esophageal Disease. Internet edition; 1996. Available from: http://www.inxpress. net/~oastiennon/webdoc2. htm
13 **Hrousis CA**, Wiggs BJ, Drazen JM, Parks DM, Kamm RD. Mucosal folding in biologic vessels. *J Biomech Eng* 2002; **124**: 334-341
14 **Wiggs BR**, Hrousis CA, Drazen JM, Kamm RD. On the mechanism of mucosal folding in normal and asthmatic airways. *J Appl Physiol (1985)* 1997; **83**: 1814-1821
15 **Fan Y**, Zhao J, Liao D, Gregersen H. The effect of digestion of collagen and elastin on histomorphometry and the zero-stress state in rat esophagus. *Dig Dis Sci* 2005; **50**: 1497-1505
16 **Yang J**, Liao D, Zhao J, Gregersen H. Shear modulus of elasticity of the esophagus. *Ann Biomed Eng* 2004; **32**: 1223-1230
17 **Yang J**, Zhao J, Zeng Y, Gregersen H. Biomechanical properties of the rat oesophagus in experimental type-1 diabetes. *Neurogastroenterol Motil* 2004; **16**: 195-203
18 **Gregersen H**, Kassab G. Biomechanics of the gastrointestinal tract. *Neurogastroenterol Motil* 1996; **8**: 277-297
19 **ABAQUS**: Analysis User's Manual. Volume III: *Materials* 2005
20 **Lambert RK**, Codd SL, Alley MR, Pack RJ. Physical determinants of bronchial mucosal folding. *J Appl Physiol (1985)* 1994; **77**: 1206-1216
21 **Lambert RK**, Paré PD, Okazawa M. Stiffness of peripheral airway folding membrane in rabbits. *J Appl Physiol (1985)* 2001; **90**: 2041-2047

S- Editor Liu Y **L- Editor** Alpini GD **E- Editor** Che YB

PO Box 2345, Beijing 100023, China
www.wjgnet.com
wjg@wjgnet.com

World J Gastroenterol 2007 March 7; 13(9): 1352-1359
World Journal of Gastroenterology ISSN 1007-9327

TOPIC HIGHLIGHT

Hans Gregersen, Professor, *Series Editor*

Finite element simulation of food transport through the esophageal body

Wei Yang, Tat Ching Fung, Kerm Sim Chian, Chuh Khiun Chong

Wei Yang, Tat Ching Fung, School of Civil and Environmental Engineering, Nanyang Technological University, Singapore
Kerm Sim Chian, School of Mechanical and Aerospace Engineering, Nanyang Technological University, Singapore
Chuh Khiun Chong, School of Chemical and Tissue Engineering, Nanyang Technological University, Singapore
Supported by the Agency for Science, Technology and Research and Nanyang Technological University, Singapore
Correspondence to: Wei Yang, School of Civil and Environmental Engineering, Nanyang Technological University, #07-135, Block 904, Jurong West Street 91, 640904, Singapore. pg05544456@ntu.edu.sg
Telephone: +65-6-7906324 Fax: +65-6-7912274
Received: 2006-12-09 Accepted: 2007-02-10

Abstract

The peristaltic transport of swallowed material in the esophagus is a neuro-muscular function involving the nerve control, bolus-structure interaction, and structure-mechanics relationship of the tissue. In this study, a finite element model (FEM) was developed to simulate food transport through the esophagus. The FEM consists of three components, i.e., tissue, food bolus and peristaltic wave, as well as the interactions between them. The transport process was simulated as three stages, i.e., the filling of fluid, contraction of circular muscle and traveling of peristaltic wave. It was found that the maximal passive intraluminal pressure due to bolus expansion was in the range of 0.8-10 kPa and it increased with bolus volume and fluid viscosity. It was found that the highest normal and shear stresses were at the inner surface of muscle layer. In addition, the peak pressure required for the fluid flow was predicted to be 1-15 kPa at the bolus tail. The diseases of systemic sclerosis or osteogenesis imperfecta, with the remodeled microstructures and mechanical properties, might induce the malfunction of esophageal transport. In conclusion, the current simulation was demonstrated to be able to capture the main characteristics in the intraluminal pressure and bolus geometry as measured experimentally. Therefore, the finite element model established in this study could be used to further explore the mechanism of esophageal transport in various clinical applications.

Key words: Food transport; Finite element simulation; Esophagus

Yang W, Fung TC, Chian KS, Chong CK. Finite element simulation of food transport through the esophageal body. *World J Gastroenterol* 2007; 13(9): 1352-1359

http://www.wjgnet.com/1007-9327/13/1352.asp

FUNCTIONALITY OF ESOPHAGUS

The transit of food the bolus through the esophageal body depends on the properties of the bolus as well as the positions of the thorax when the swallow occurs. If the food is fluid-like and a person stands upright, it only takes 2-3 s for the food to approach the lower esophageal sphincter (LES). In this case, the bolus moves mainly under the influence of gravity. When either or both the content of bolus and the position of the thorax reduce the effects of gravity, the peristaltic mechanism plays the most important role for the bolus transport. The muscle contraction is first inhibited to allow the bolus to distend and fill the esophageal lumen. This inhibition is followed by the active muscle contractions near the bolus tail to maintain the lumen closure and propel the bolus towards the stomach. The contraction wave travels at a speed of 1-4 cm/s and duration of 5-10 s is required for the bolus to reach the LES, when the muscle at LES stats to relax and LES opens. The LES remains open for 5-10 s during which the food content is emptied from the esophagus to the stomach. Thus, food transport is an interactive process between the esophageal tissue, food bolus and muscle activity.

It is well known that the stress distribution within the esophageal wall is important to understand the mechanics-function relationship of the esophagus. The stress distribution under the physiological state has been widely investigated in the literature[1,2]. However, the effect of food bolus on tissue structure has usually been represented by a luminal pressure imposed on the internal surface of the esophageal tube while the bolus and the interaction between the tissue and bolus have been ignored. On the other hand, in the study conducted by Li *et al*[3], a mathematical model was established to simulate the fluid (food bolus) flow within the esophageal lumen. By applying the lubrication theory[4], the intraluminal

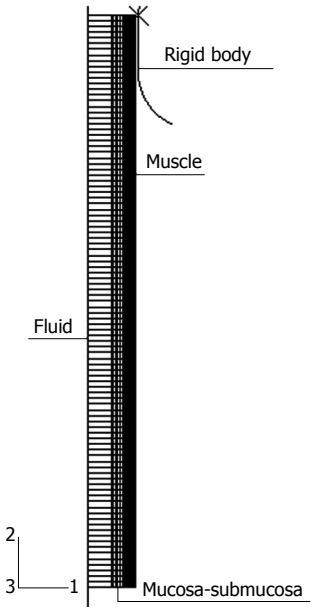

Figure 1 Geometrical model for the simulation of food transport process.

pressure was predicted from the bolus geometry. It was shown that the simulation was able to capture the main feature of the variation in intraluminal pressure. However, due to the high sensitivity of the pressure variation in the contraction zone to the variation in bolus geometry, accurately prescribed geometry must be supplied. In the current study, rather than specifying the bolus geometry, the shape of food bolus is determined from a simulated peristaltic transport process by adjusting the contraction wave, bolus viscosity and material parameters of the tissue in the physiological range. A finite element model consisting of three primary composites, i.e., tissue, bolus and muscle contraction, as well as the interactions between them is established. The simulation aims to explore the physiological features during the food transport process and to investigate the effects of the tissue properties, the fluid viscosity and volume, as well as the active contraction wave on the transport efficiency.

FINITE ELEMENT MODEL

The parameters used to characterize the active contraction and bolus properties were borrowed from a few studies on the human esophagus in the literature[3,5-8] while the geometry and material parameters were measured from the porcine esophagus. In our previous study[9], it was proved that the porcine esophagus has similarities with the human being's esophagus in terms of both axial length (25-30 cm for the pig 3-4 mo old *vs* 25 cm for an adult) and tensile strengths (circumferential and axial strengths are 1.2 and 3.7 MPa for the muscle and 1.6 and 8.7 MPa for the mucosa-submucosa[9] *vs* 1.4 and 2.2 MPa for the entire wall). Since detailed geometrical and mechanical parameters for the human's esophagus were not available for our simulation, those for the porcine esophagus were taken as the representative so that the effects of the variations in mechanical properties on the efficiency of food transport could be examined. By assuming the esophagus a straight, circular cylindrical tube, an axisymmetrical model was constructed as shown in Figure 1. A segment of 10 cm in length was modeled to represent the abdominal region of esophagus connecting to the lower esophageal sphincter (LES). The finite element model was developed with ABAQUS 6.5 and it consisted of the following three components.

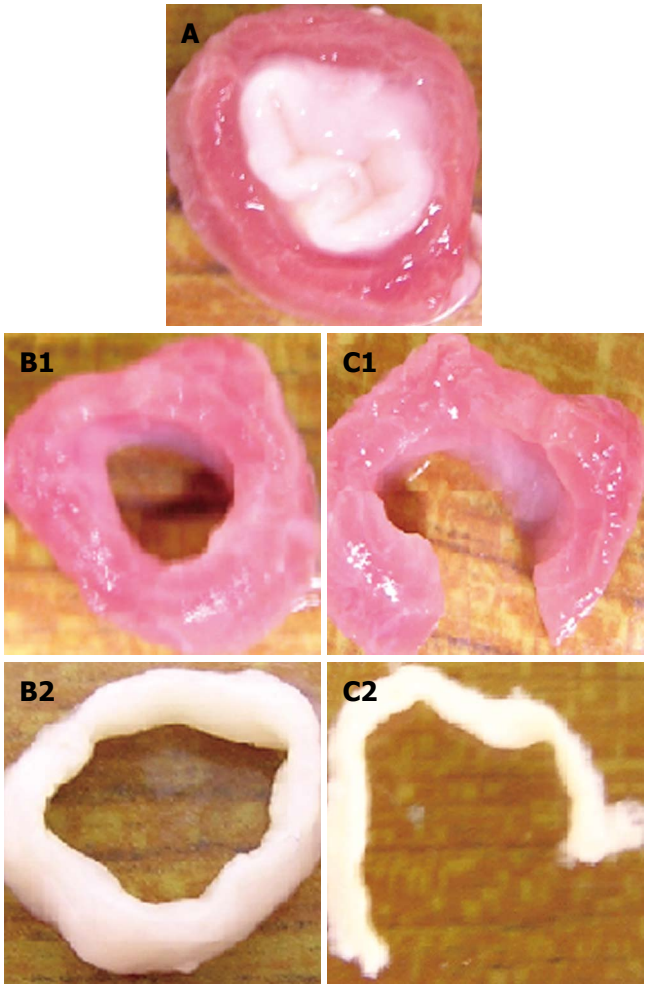

Figure 2 Procedure used to obtain the true zero-stress state and definition of three states: (**A**) Bonded no-load state; (**B**) separated no-load state; and (**C**) true zero-stress state.

Esophageal wall

The first component is the esophageal tissue, which is modeled with both the inner mucosa-submucosal layer and outer muscle layer. Following the procedure used by Liao *et al*[1], the true zero-stress state was obtained by a circumferential cut for layer separation followed by a radial cut in each layer (Figure 2). The geometrical parameters, including the inner and outer radii at both the no-load state and zero-stress state as well as the opening angles at the zero-stress state, were measured with the image processing software Micro Image 4.5 (OLYMPUS-SZX12). The geometrical model was established by using the parameters at the no-load state as given in Table 1.

It is known that the no-load state of the esophagus is not stress-free[10] and the residual stretches at the no-load

Table 1 Parameters of the tissue, fluid bolus and peristaltic wave used in the model

Tissue	Muscle					Mucosa-submucosa				
Geo.	Bonded no-load state		True zero-stress state			Bonded no-load state		True zero-stress state		
	r_i (mm)	r_0 (mm)	R_i (mm)	R_0 (mm)	θ (°)	r_i (mm)	r_0 (mm)	R_i (mm)	R_0 (mm)	θ (°)
	6.49	8.28	6.49	8.49	79.4	4.12	6.49	15.7	17.7	33.9
Mat.	μ_{el} (Pa)	κ_1 (Pa)	κ_2	α (°)	λ_0	μ_{el} (Pa)	κ_1 (Pa)	κ_2	α (°)	λ_0
	3752	23997	17.9	45	1.11	1010	9012	50.7	50.7	1.33
Fluid	μ = 0.2 Pa.s; ρ = 0.7 kg/m^3; C_v = 7.2E^5 Pa.s/kg									
Wave	v_r = 0.5 mm/s; v_t = 0.9 cm/s									

state referred to the zero-stress state are evaluated as[11]:

$$\lambda_r = \frac{\partial r}{\partial R} = \frac{\Theta\sqrt{R_o^2 - \pi\lambda_z\left(r_o^2 - r^2\right)/\Theta}}{\pi r \lambda_z} \quad (1)$$

$$\lambda_\theta = \frac{\pi r}{\Theta R} = \frac{\pi r}{\Theta\sqrt{R_o^2 - \pi\lambda_z\left(r_o^2 - r^2\right)/\Theta}} \quad (2)$$

where r_o and R_o are the outer radius at the no-load and zero-stress state; $\Theta = \pi - \theta$ and θ is the opening angle; λ_z is the axial stretch ratio and it is assumed to be the unit. For the esophagus, the inner mucosa is compressed and the outer muscle layer is extended at the no-load state. It has been demonstrated in a previous study[10] that the residual strain significantly influences the stress distribution. For a more accurate simulation, the residual strain was introduced with the following method. Firstly, the residual deformation gradient tensor F_r was defined as the initial value of a solution-dependent variable in the subroutine SDVINI. Secondly, in the user material code (UMA) the current deformation gradient tensor referred to the true zero-stress state $\boldsymbol{F}_c^Z$ calculated at the start of iteration by multiplying the deformation gradient tensor referred to the no-load state $\boldsymbol{F}_c^N$ with F_r. The stress tensor and stiffness tensor were also calculated based on $\boldsymbol{F}_c^Z$.

A structure-based constitutive model, which has been successfully applied for the esophageal tissue[9], was adopted in the simulation. With this model, the esophageal wall was modeled as an isotropic matrix of elastin reinforced with collagen fibers. Accordingly, the strain energy function ψ was decoupled into two components:

$$\psi = \psi_{iso} + \psi_{aniso} \quad (3)$$

The neo-Hookean model was employed to describe the elastin as given in Eq. (4).

$$\psi_{iso} = \frac{\mu_{el}}{2}(I_1 - 3) \quad (4)$$

where μ_{el} is a material constant equivalent to the shear modulus of elastin. It was assumed that the two families of collagen fibers were symmetrically arranged in θ - z plane and their orientations rendered the preferred direction of the tissue. An exponential function, as given in Eq. (5), was used to capture the nonlinear elasticity of the collagen fibers:

$$\psi_{aniso} = \begin{cases} 0, & \text{for } \sqrt{I_i} \le \lambda_0 \\ \frac{k_1\lambda_0^2}{2k_2}\sum_{i=4,6}\left\{\exp\left[k_2\left(\sqrt{I_i}/\lambda_0 - 1\right)\right] - k_2\left(\sqrt{I_i}/\lambda_0 - 1\right) - 1\right\} & \text{for } \sqrt{I_i} > \lambda_0 \end{cases} \quad (5)$$

where k_1 is a material constant with the same dimension as stress and k_2 is a dimensionless parameter related to the stiffening speed. I_4 and I_6 are the fourth and sixth invariants and can be expressed as:

$$I_4 = \lambda_\theta^2 cos^2\alpha + \lambda_z^2 sin^2\alpha \quad (6)$$

$$I_6 = \lambda_\theta^2 cos^2(-\alpha) + \lambda_z^2 sin^2(-\alpha) \quad (7)$$

where α denotes the angle of the collagen fibers away from θ direction. I_4 and I_6 actually represent the squares of stretch ratios in the directions of the associated families of collagen fibers. A dimensionless parameter λ_0 is introduced to scale the stretch ratio $\sqrt{I_i}$ so that the unfolding process of the collagen fiber can be accounted for. To characterize the distinct stiffness of each layer, two different groups of material parameters were given for the inner mucosa-submucosa and outer muscle layer. The parameters were determined from the inflation test with a regression method[10] and they were summarized in Table 1.

The tissue was meshed with a 4-node linear axisymmetric element (CAX4H) and it was discreted with 18 and 100 elements in the radial and axial directions, respectively. Geometrical nonlinearity was switched on for all the simulation steps.

Food bolus

The food bolus was simulated as 100 fluid cavities connected in sequence by the fluid link elements. An example of fluid and fluid link element is illustrated in Figure 3. Each of the cavities is composed of three hydrostatic fluid elements (FAX2) and they share one common node called cavity reference node (RF). The fluid volume is that enclosed by the cylinder which is formed by revolving the three line elements. The outer boundaries of the cavity (e.g., element 2) share the same nodes with the inner boundaries of the tissue element so that the deformation of the fluid-filled tissue and the pressure exerted by the contained fluid on the cavity boundary of the structure are coupled.

In each cavity, the hydrostatic pressure is the same everywhere. However, the pressure in each cavity could be different and the difference in pressure between two

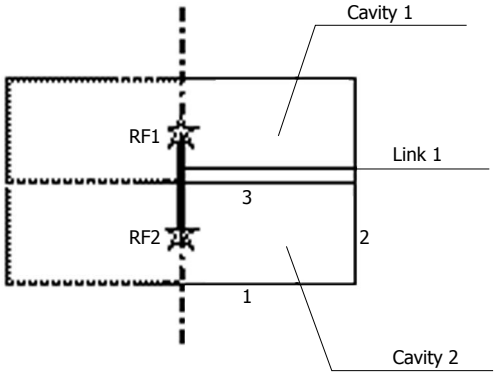

Figure 3 Example of the fluid element and fluid link element.

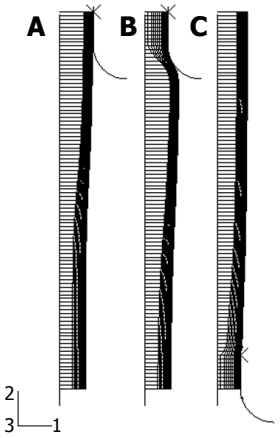

Figure 4 Bolus shape (**A**) before the muscle contraction (**B**) at the end of muscle contraction and (**C**) when the peristaltic wave reaches the LES.

adjacent cavities determines the flow rate through a fluid link element (FLINK) connecting the two RF nodes. There are 100 fluid link elements and the last one connects the RF node of the last cavity to an unconnected node representing the gastric pressure in the stomach. The relationship between the pressure difference (Δp) and the mass flow rate (q) is defined as the property of fluid link element as given in Eq. (8).

$$\Delta p = C_v q \tag{8}$$

where C_v denotes the viscous resistance coefficient. The effect of gravity has been ignored by assuming a supine position. For a local Poiseuille flow in a circular tube, C_v can be calculated as:

$$C_v = \frac{8\mu}{\pi\rho r_l^4} \tag{9}$$

where μ and ρ represent the fluid viscosity and density and they were given at 0.2 Pa.s and 0.7 kg/m^3 for a normal food content[3]. r_l is the luminal radius and it is equal to the inner radius of mucosa-submucosa at the bonded no-load state.

Peristaltic wave

At the start of a peristaltic wave, the circular muscle cells shorten themselves and generate the contraction force. The mechanism of muscle contraction is complicated involving both the nerve controls and intrinsic properties of muscle cells[12]. However, from the view of consequence, the peristaltic contraction acts as an external force on the tissue structure and travels downward at a certain speed. In the model, a rigid body was defined as shown in Figure 1. By applying an inward radial displacement, the rigid body was in contact with the tissue structure and exerted a pressure force on the outer surface of the tissue. As it has been reported that the contraction zone extends 1-2 cm in length for the normal case[8], a 1 cm straight line and a 1/4 arc with the radius of 1 cm was defined as an axisymmetrical rigid body (RAX2). The arc segment was used in order to prevent the numerical singularity induced by the sudden increase in contact force at the transition point between the attached and detached region. The longitudinal travel of the contraction wave was simulated by controlling the axial displacement of the rigid body. The contraction speed v_r and longitudinal traveling speed v_l were set at 0.5 mm/s (i.e., circular muscle shortened at 3.14 mm/s) and 0.9 cm/s, respectively[8].

SIMULATION

The objectives of simulation are, firstly, to investigate the main feature of the intraluminal pressure distribution and bolus shape at each stage of peristaltic transport; and secondly to study the effects of tissue properties, bolus properties, contraction and wave speed on the transport process.

Filling of fluid

When considering that the simulated segment of esophagus connects the stomach through a LES at the distal end, the initial configuration of tissue (Figure 1) is self-balanced and hence the fluid filled in the tissue structure does not exert any force on the tissue. At this moment the fluid volume (V), which is equal to the lumen volume of the esophageal tube, is 5 mL. We start the simulation by perfusing another 2.5 mL fluid at the speed of 2.5 mL/s through the most proximal cavity. The filling of fluid expands and deforms the tissue at the top and the tissue reacts and in turn restrains further deformation. So the circumferential tensile stress is generated within the deformed wall and the intraluminal pressure at the top cavity has to increase to balance the stress in the tissue. As a consequence of the increase in pressure at the top fluid cavity, pressure difference is induced between the top cavity and its adjacent lower cavity and fluid transport is initiated. After the filling of fluid, free redistribution of fluid within all the cavities is allowed in the following 3 s. This is to simulate the 'off' response of muscle cells, i.e., muscle contraction begins 2-3 s after being stimulated[13,14]. Figure 4A presents the bolus shape after the redistribution of fluid and immediately before the muscle contraction. In this step, the bolus shape and intraluminal pressure distribution are determined by the properties of both the tissue and fluid bolus. By plotting the bolus shape and intraluminal pressure distribution simultaneously, the relationship between them is explored. Particularly, the effects of bolus viscosity and tissue properties on the maximal luminal radius (r_{max}) and maximal intraluminal pressure (p_{max}) are evaluated by changing m from 0.2 to

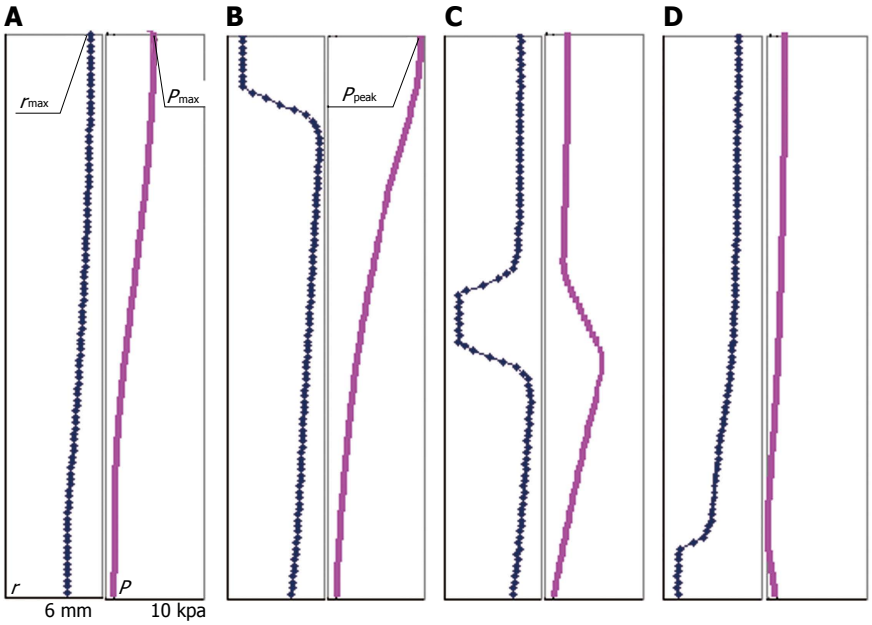

Figure 5 Bolus shape and intraluminal pressure distribution along the length (**A**) at the end of bolus filling and off response (before muscle contraction) (**B**) at the end of muscle contraction at the top 1 cm segment (**C**) when the peristaltic wave reaches the middle of the entire segment and (**D**) when the peristaltic wave reaches the end of segment (LES).

0.02 Pa.s, k_1 in the muscle layer from 23997 to 2399.7 Pa, and λ_0 in the mucosa-submucosal layer from 1.33 to 1.

Muscle contraction

In this step, the contact between the rigid body and the outer boundary of tissue is activated and the muscle contraction is simulated by specifying an inward radial velocity of the rigid body at 0.5 mm/s until the luminal radius decreases to about 0.5 mm. Since the cavity volume at the contraction zone (1 cm at the top) is forced to be reduced quickly, the intraluminal pressure in these cavities increases greatly which accelerates the downward flowing speed of the fluid. At the end of the muscle contraction, the main body of fluid bolus moves downward as shown in Figure 4B. In addition to the tissue and bolus properties, the intraluminal pressure distribution and bolus shape are also influenced by the contraction speed. The effect of the contraction speed on the peak pressure (p_{peak}) is assessed by changing v_r from 0.5 to 0.25 mm/s.

Transport of peristaltic wave

Due to the muscle contraction at the top region, the bolus content is pushed down to the lower region so that the muscle cells at the lower region are also stimulated and start to contract as well. So the contraction zone moves downwards at a certain speed as a peristaltic wave. This is simulated by specifying the axial velocity of the rigid body at 0.9 cm/s. With the downwards moving of peristaltic wave, the pressure at the bottom end increases and the LES opens. From this moment, the fluid in the esophageal lumen starts to flow into the stomach. The gastric pressure in the stomach is set at zero in this simulation. As shown in Figure 4C, some amount of food content has refluxed to the esophageal lumen when the peristaltic wave reaches the LES. This is because the continuous fluid flow is simulated and the fluid always flows from the higher-pressure region to the lower-pressure region. The secondary peristaltic wave or the next fluid bolus is supposed to further push the remaining bolus down and empty the food from the esophageal lumen. The fraction of bolus which has been cleared is evaluated as an index of the efficiency of peristaltic transport (*Eff.*). Our preliminary simulation showed that the transport efficiency was affected by the peristaltic wave speed. So the effect of the wave speed on the value of *Eff.* is investigated by changing v_l from 0.9 to 0.38 cm/s. The effects of bolus viscosity, tissue properties and contraction speed are also examined.

Simulation with bigger bolus

In order to observe the features of food transport with bigger bolus, the simulation described above is repeated with a bolus volume of 10 mL.

PARAMETERS OBTAINED FROM THE SIMULATION

Figure 5 presents the bolus shape and intraluminal pressure distribution along the esophageal length at four representative stages, i.e., at the end of bolus filling and off response (before muscle contraction); at the end of muscle contraction at the top 1 cm segment; when the peristaltic wave reaches the middle of the entire segment; and when the peristaltic wave approaches to the end of the segment (LES).

Maximal bolus radius and maximal intraluminal pressure

At every moment before muscle contraction, the pressure in fluid is balanced by the stress in tissue. As the pressure difference between the cavities induces the fluid flow, the bolus shape has to adjust its shape continuously with time to maintain the balance. At 3 s after the filling of food bolus, the luminal radius is the maximal at the top end (r_{max} = 5.3 mm) and smoothly decreases from the top to the bottom, as shown in Figure 5A. Correspondingly the maximal pressure p_{max} is 4.4 kPa at the top end, which is in the range of the measured pressure in a normal human

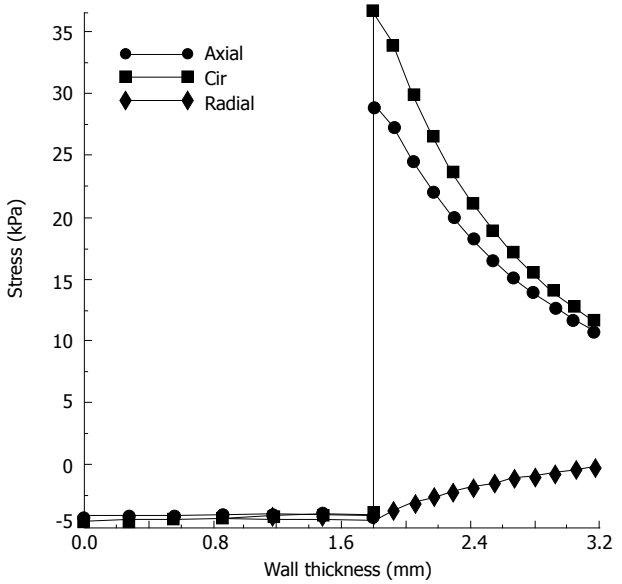

Figure 6 Stress distributions along the esophageal wall under the expansion of food bolus.

esophagus (Gregersen, 2003). It is found that all the stresses are significantly higher in the muscle layer than the mucosa-submucosal layer. The axial and circumferential stresses are the highest at the inner surface of muscle layer at the top end (29.0 and 36.5 kPa). Figure 6 presents the distribution of three normal stresses along the esophageal wall thickness. It shows that the muscle layer withstands most of the loading while the mucosa-submucosa layer just transmits the pressure. In addition to the normal stress, the shear stress also occurs due to the nonuniform bolus radius along the lumen length. The shear stress is the highest at the inner surface of muscle layer at 3.7 cm from the top end (238.6 Pa), where the greatest curvature of luminal radius occurs.

If a more fluid-like bolus is swallowed, the viscous resistance becomes smaller and the fluid flow is eased and accelerated. As given in Table 2, the maximal bolus radius and maximal intraluminal pressure are reduced by 15% and 83% respectively when the bolus viscosity decreases to 10% of the original viscosity. When the stiffness in the muscle layer decreases (k_1 decreases by 90%) the tissue is easier to be dilated (r_{max} increases by 19%) and the intraluminal pressure is reduced (p_{max} decreases by 46%). On the opposite, if the inner mucosa-submucosa layer becomes stiffer (by decreasing λ_0 from 1.33 to 1) the maximal bolus radius is greatly decreased by 173% and the maximal intraluminal pressure is increased by 46%. Therefore, it is indicated that both the bolus properties and tissue properties effects the bolus radius and intraluminal pressure significantly.

Peak pressure

At the end of muscle contraction, the bolus radius at the top 1 cm segment is reduced to 0.5 mm and a steep slope forms due to the rapid increase of radius in the distal 1 cm segment as shown in Figure 5B. The intraluminal pressure is the maximal at the top end (p_{peak} = 9.7 kPa), which is the pressure required for the fluid flow and is expected to be provided by the active muscle contraction. It is known that the stretch level of the circular muscle during the expansion of bolus affects the activity level of the muscle cells and hence the contraction force that they are able to generate (Cohen and Green, 1973). It is found that, for bolus with viscosity of 0.2 and 0.02 Pa.s, the circular muscle is stretched by 18% and 10% on average and the required peak pressures are 9.7 and 1.2 kPa respectively (Table 2). We assume that it represents the physiological condition for the normal esophagus, i.e., the muscle cells are able to generate the pressure which is required if and only if they are stretched to the corresponding levels indicated in the above two cases.

Table 2 Effects of bolus viscosity, tissue properties and contraction wave on the maximal bolus radius, maximal pressure, stretch of muscle, peak pressure and transport efficiency

Parameter	r_{max} (mm)	P_{max} (kPa)	λ_θ (muscle)	P_{peak} (kPa)	*Eff.* (%)
Control (V = 7.5 mL)	5.30	4.39	1.18	9.71	31.8
μ = 0.02 Pa.s	4.48	0.75	1.10	1.24	48.7
κ_1 = 2399.7 Pa	6.32	2.37	1.30	6.65	19.0
λ_0 = 1	4.27	12.0	1.08	14.1	73.6
v_r = 0.25 mm/s	5.30	4.39	1.18	6.25	33.9
v_l = 0.38 cm/s	5.30	4.39	1.18	9.71	38.0
Control (V = 10 mL)	5.91	9.58	1.25	14.4	43.9
μ = 0.02 Pa.s	4.62	1.17	1.11	1.32	61.5
κ_1 = 2399.7 Pa	7.12	7.28	1.39	9.73	22.4
λ_0 = 1	4.41	14.8	1.09	15.0	80.0
v_r = 0.25 mm/s	5.91	9.58	1.25	8.94	46.7
v_l = 0.38 cm/s	5.91	9.58	1.25	14.4	51.2

For the case of systemic sclerosis (SS) where the amount of collagen in mucosa increases and the tissue becomes stiffer (which is simulated by decreasing λ_0 from 1.33 to 1 for the mucosa-submucosal layer), the inflation of the esophageal wall reduces during the transit of food and accordingly the stretch of muscle also reduces (λ_θ = 1.08). In this case, the contraction force generated by the muscle should be less than 1.2 kPa based on the above assumption. However, the pressure needed for the fluid flow is shown to be 14.1 kPa (Table 2), which is even higher than can be generated when the muscle is stretched by 18%. So the simulation implies that, in the case of SS disease, the esophageal tissue has to remodel itself so that higher contraction force can be generated when the muscle is stretched to a relatively small level. The simulation also shows that if the contraction speed decreases by 50%, the intraluminal pressure required for the fluid flow decreases by 36% (Table 2). It implies that if the self-adjustment does not work, the transport process of the SS esophagus will become slower compared to the normal case.

Transport efficiency

Figure 7 presents the mass flow rate from the fluid cavity 5091 (1 cm away from the top) to the fluid cavity 5090, two of which the fluid link element 8091 connects, during the muscle contraction and the moving of peristaltic wave. It shows that the flow rate increases suddenly when the contraction starts, decreases slightly during the

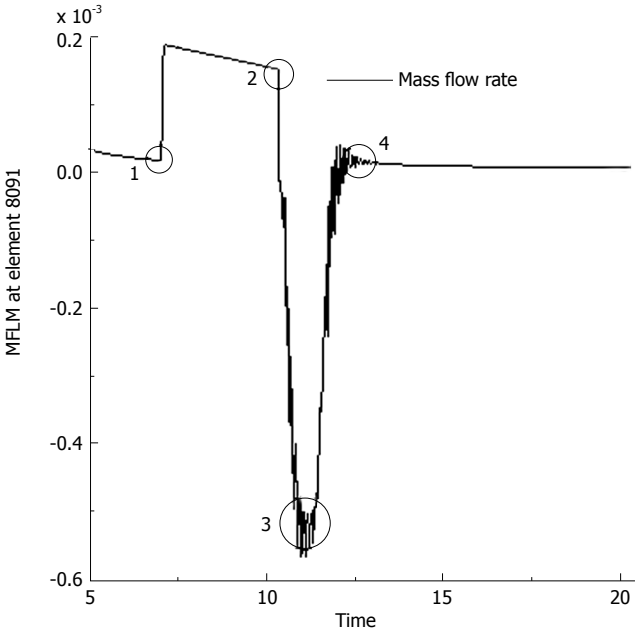

Figure 7 Mass flow rate at fluid link element 8091 (1 cm away from the top end connecting the fluid cavity 5091 and 5090) during the muscle contraction and wave transport. 1 represents the moment when the rigid body is in contact with the tissue structure (start of contraction); 2 the end of contraction at the top 1 cm segment; 3 when the contraction wave leaves the fluid cavity 5091 (1 s after contraction); 4 when the contraction wave is 1 cm away from cavity 5091 (2 s after contraction).

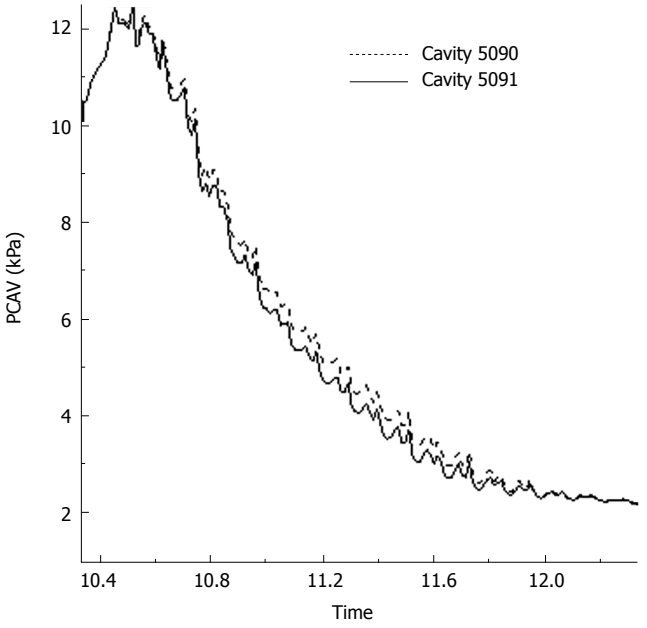

Figure 8 Intraluminal pressure at cavity 5090 and 5091 during the two seconds of fluid reflux.

process of contraction, and suddenly decreases at the end of contraction. During the first two seconds after the contraction, i.e., from the moment when the contraction wave leaves to the moment when it is 1 cm away from the cavity 5091, backward flow occurs. The reflux of fluid is due to the intraluminal pressure in the cavity 5090 is higher than that in cavity 5091 during this period, as shown in Figure 8. Even though the period of fluid reflux is short, it induces that the food content cannot be cleared up from the esophageal lumen to the stomach and some of them are retained in the esophagus as shown in Figure 5C and D. The transport efficiency is 31.8% for a bolus volume of 7.5 mL and viscosity of 0.2 Pa.s (Table 2). For fluid with lower viscosity (μ = 0.02 Pa.s), the transport efficiency increases by 53%. In the case of osteogenesis imperfecta (OI) where the collagen deficiency occurs (which is simulated by decreasing k_1 to 10% of the original value for the muscle layer), the transport efficiency is reduced by 44%. While for the SS esophagus where the tissue becomes stiffer, it increases by 93% instead. So it is indicated that the higher stiffness of tissue results in higher percentage of bolus content to be cleared up. However, for the SS esophagus, the muscle contraction force required for the fluid flow increases greatly which might exceed the magnitude that the muscle contraction can provide. In conclusion, both esophageal diseases might induce the malfunction of the esophagus. From Table 2, it can also be found that the decrease of either the contraction speed or the peristaltic wave speed can increase the transport efficiency to some extent. It implies that higher transport efficiency could be achieved at the cost of slowing down of transport speed.

Effects of bolus volume

The simulation with a bolus volume of 10 mL shows similar features as described above. In comparison, with a bigger bolus, the maximal luminal radius increases by 12% during the filling process. Due to the stiffening of tissue properties, the maximal intraluminal pressure increases by an even higher percentage (118%). The peak pressure and transport efficiency also increase by 48% and 38% respectively. It implies that the muscle contraction has to be strengthened in order to transmit a bigger bolus. The simulation indicates that the efficiency increases for a bigger bolus transport. However, it is under the condition of this, that the increased peak pressure can be provided by the active muscle contraction, as assumed during the simulation. In reality, there is a limit for the maximum muscle contraction force. Therefore, the conclusion that the transport efficiency increases with bolus size could only be true within the physiological range. The parametric studies show that the effects of bolus viscosity, tissue properties and contraction wave speed are also similar with those found for the transport of the a 7.5 mL bolus.

IMPLICATIONS OF THE SIMULATION

In this study, the fluid is simulated as the fluid cavities between which the fluid could transmit through a fluid link as a Poiseuille flow. The fluid and tissue structure are coupled to simulate the interaction between them. It is found that the maximal intraluminal pressure increases with bolus volume and fluid viscosity. This is consistent with the observations in an experimental study conducted by Ren *et al*[6]. The active muscle contraction is represented as an external force imposed through a rigid body. By specifying the displacement of the rigid body, the contraction speed and wave speed is controlled. With the parameters in the

physiological range, the peak pressure is predicted to be 1-15 kPa depending on bolus volume and viscosity. The predicted peak pressure agrees with the manometrically measured peak pressure very well[6]. It is also found that the peak pressure required for bolus transport could be reduced by slowing down the contraction speed. For the SS esophagus, the required peak pressure greatly increases, which might induce the failure and incomplete of bolus transport. The transport efficiency is found to be higher for the food bolus with lower viscosity and higher volume. For the IO disease, the esophageal wall is severely dilated and the transport efficiency greatly decreases. In order to regain the transport efficiency, the contraction speed or wave speed has to be reduced. In conclusion, both the IO or SS diseases might induce the malfunction of esophageal transport.

It is found that, during the filling of food bolus, both the normal and shear stresses are the highest at the inner surface of muscle layer. In contrast, the stresses in the mucosa-submucosa are very low. This is mainly because, at the bonded no-load state, the mucosa-submucosa is compressed substantially in order to accommodate the smaller space confined by the outer muscle layer. When the food bolus expands the esophageal lumen, the mucosa-submucosal layer unfolds itself first and hence it is exposed to a relatively lower circumferential strain. Therefore, the residual strain could be a protective mechanism to prevent the mucosa-submucosa tissue being over-stretched or over-stressed. It also indicates that the residual strain should be taken into account for an accurate evaluation of stress distribution along the esophageal wall.

In the current simulation, the lumen at the tail of the bolus is not occluded completely. This is due to the numerical difficulties encountered for further reducing of the lumen radius. In a previous study[3], a mathematical singularity in pressure also appeared in the limit of complete occlusion when the lubrication theory approximation was applied to simulate the esophageal transport. A very thin layer of bolus fluid, which was called the lubrication layer, was assumed to exist and extend through the simulated esophagus. It was demonstrated that the simulation could successfully capture the main feature of the pressure distribution under this assumption. In the current study, we adopted the same assumption and specified the lubrication radius at 0.5 mm throughout our simulation. In the physiological state, it is believed that the muscle contraction is able to seal the lumen at the bolus tail and there is less reflux for a normal transport process. Therefore, the transport efficiency is expected to be higher than that predicted in this simulation. However, the general trend in the transport efficiency due to the variations of physical parameter should still be valid and it could provide valuable information for future clinical studies.

REFERENCES

1 **Liao D**, Fan Y, Zeng Y, Gregersen H. Stress distribution in the layered wall of the rat oesophagus. *Med Eng Phys* 2003; **25**: 731-738

2 **Liao D**, Zhao J, Fan Y, Gregersen H. Two-layered quasi-3D finite element model of the oesophagus. *Med Eng Phys* 2004; **26**: 535-543

3 **Li M**, Brasseur JG, Dodds WJ. Analyses of normal and abnormal esophageal transport using computer simulations. *Am J Physiol* 1994; **266**: G525-G543

4 **Li M**, Brasseur JG. Non-steady peristaltic transport in finite-length tubes. *J Fluid Mech* 1993; **248**: 129-151

5 **Brasseur JG**, Dodds WJ. Interpretation of intraluminal manometric measurements in terms of swallowing mechanics. *Dysphagia* 1991; **6**: 100-119

6 **Ren J**, Massey BT, Dodds WJ, Kern MK, Brasseur JG, Shaker R, Harrington SS, Hogan WJ, Arndorfer RC. Determinants of intrabolus pressure during esophageal peristaltic bolus transport. *Am J Physiol* 1993; **264**: G407-G413

7 **Ren JL**, Dodds WJ, Martin CJ, Dantas RO, Mittal RK, Harrington SS, Kern MK, Brasseur JG. Effect of increased intra-abdominal pressure on peristalsis in feline esophagus. *Am J Physiol* 1991; **261**: G417-G425

8 **Pal A**, Brasseur JG. The mechanical advantage of local longitudinal shortening on peristaltic transport. *J Biomech Eng* 2002; **124**: 94-100

9 **Yang W**, Fung TC, Chian KS, Chong CK. Directional, regional, and layer variations of mechanical properties of esophageal tissue and its interpretation using a structure-based constitutive model. *J Biomech Eng* 2006; **128**: 409-418

10 **Yang W**, Fung TC, Chian KS, Chong CK. 3D Mechanical properties of the layered esophagus: experiment and constitutive model. *J Biomech Eng* 2006; **128**: 899-908

11 **Gregersen H**, Lee TC, Chien S, Skalak R, Fung YC. Strain distribution in the layered wall of the esophagus. *J Biomech Eng* 1999; **121**: 442-448

12 **Gregersen H**. Biomechanics of the Gastrointestinal Tract: New Perspectives in Motility Research and Diagnostics. London: Springer, 2003

13 **Cohen S**, Green F. The mechanics of esophageal muscle contraction. Evidence of an inotropic effect of gastrin. *J Clin Invest* 1973; **52**: 2029-2040

14 **Muinuddin A**, Paterson WG. Initiation of distension-induced descending peristaltic reflex in opossum esophagus: role of muscle contractility. *Am J Physiol Gastrointest Liver Physiol* 2001; **280**: G431-G438

S- Editor Liu Y **L- Editor** Alpini GD **E- Editor** Ma WH

PO Box 2345, Beijing 100023, China
www.wjgnet.com
wjg@wjgnet.com

World J Gastroenterol 2007 March 7; 13(9): 1360-1364
World Journal of Gastroenterology ISSN 1007-9327

TOPIC HIGHLIGHT

Hans Gregersen, Professor, *Series Editor*

Computation of flow through the oesophagogastric junction

Barry P McMahon, Karl D Odie, Kenneth W Moloney, Hans Gregersen

Barry P McMahon, Department of Medical Physics and Clinical Engineering, Adelaide and Meath Hospital Dublin, Incorporating the National Children's Hospital, Tallaght, Dublin 24, Ireland
Karl D Odie, Kenneth W Moloney, IMed Centre, Department of Mechanical Engineering, Institute of Technology Tallaght, Dublin 24, Ireland
Hans Gregersen, Center for Visceral Biomechanics and Pain, Aalborg Hospital, Aalborg DK-9100, Denmark
Hans Gregersen, IMed Centre, Institute of Technology, Tallaght, Dublin 24, Ireland
Supported by a Science Foundation Ireland through the ETS Walton Visiting Professor Programme and a grant from the Higher Education Authority in Ireland
Correspondence to: Dr. Barry P McMahon, Department of Medical Physics & Clinical Engineering, Adelaide & Meath Hospital, Tallaght, Dublin 24, Ireland. barry@mech-sense.com
Telephone: +353-1-4145898 Fax: +353-1-4142501
Received: 2006-12-29 Accepted: 2007-02-02

Abstract

Whilst methods exist to indirectly measure the effects of increased flow or gastro-oesophageal refluxing, they cannot quantitatively measure the amount of acid travelling back up into the oesophagus during reflux, nor can they indicate the flow rate through the oesophago-gastric junction (OGJ). Since OGJ dysfunction affects flow it seems most appropriate to describe the geometry of the OGJ and its effect on the flow.

A device known as the functional lumen imaging probe (FLIP) has been shown to reliably measure the geometry of and pressure changes in the OGJ. FLIP cannot directly measure flow but the data gathered from the probe can be used to model flow through the junction by using computational flow dynamics (CFD). CFD uses a set of equations known as the Navier-Stokes equations to predict flow patterns and is a technique widely used in engineering. These equations are complex and require appropriate assumptions to provide simplifications before useful data can be obtained. With the assumption that the cross-sectional areas obtained *via* FLIP are circular, the radii of these circles can be obtained. A cubic interpolation scheme can then be applied to give a high-resolution geometry for the OGJ.

In the case of modelling a reflux scenario, it can be seen that at the narrowest section a jet of fluid squirts into the oesophagus at a higher velocity than the fluid surrounding it. This jet has a maximum velocity of almost 2 ms^{-1} that occurs where the OGJ is at its narrowest. This simple prediction of acid 'squirting' into the oesophagus illustrates how the use of numerical methods can be used to develop a better understanding of the OGJ. This initial work using CFD shows some considerable promise for the future.

Key words: Computational flow dynamics model; Oesophagus

McMahon BP, Odie KD, Moloney KW, Gregersen H. Computation of flow through the oesophagogastric junction. *World J Gastroenterol* 2007; 13(9): 1360-1364

http://www.wjgnet.com/1007-9327/13/1360.asp

INTRODUCTION

The Giome is a subset of the Physiome project, which was originally proposed by Bassingthwaighte in 1995[1]. The Giome Project initiated by Gregersen represents a method for obtaining an integrated understanding of the human gastrointestinal (GI) tract based on bioengineering models[2]. To use this method to advance our understanding of the GI tract, it will be necessary to generate new computational models and capture data pertinent to these models. The output from the functional lumen imaging probe (FLIP) is potentially one of these sources of data for sphincteric regions in the GI tract.

In patients where compliance of the sphincter is not ideal, control of reflux is not optimal. Often oesophago-gastric junction (OGJ) dysfunction is the prime suspect in this phenomenon, which effects up to 44% of the population in the western world. It is logical to deduce that an increase in sphincter compliance will result in increased flow through the OGJ. Measuring flow directly in the oesophago-gastric junction *in vivo* would prove very difficult, especially because it must be accessed from the oral or nasal cavity. This review looks at another option for predicting flow parameters in the OGJ.

FLIP

Recently, a device known as the FLIP has been shown to reliably measure the geometry of and pressure changes in the OGJ by using a distensibility technique[3-6]. FLIP can measure the geometric data needed to model flow

through the junction. The concept of measuring flow by a distensibility technique is not new[7] but the acquisition and analysis of FLIP data seems much easier than with any other known technique. Thus, FLIP could provide a practical solution with the potential for clinical use in the future.

Data from FLIP provides a platform for carrying out numerical flow analysis, where the complexities of flow through the junction could be represented using a technique known as computational flow dynamics (CFD).

CHARACTERISTICS OF THE OGJ

At the OGJ, the oesophagus opens into the stomach. It is important that backflow of stomach secretions into the oesophagus is controlled at the OGJ opening only transiently to allow passage of the swallowed food into the stomach. The diaphragmatic hiatus, through which the oesophagus passes at the OGJ, has a role in this valvular mechanism[8].

Several structures are important in maintaining a barrier at the OGJ. The lower oesophageal sphincter (LOS) forms part of the OGJ structure. The intrinsic muscles of the distal oesophagus and the sling fibers of the proximal stomach make up the internal mechanism structures of the LOS. The muscles of the diaphragm that connect to the OGJ make up the crural diaphragm and this constitutes the external LOS mechanism structures. The tissue that connects the distal oesophagus to the crural diaphragm is known as the phreno-oesophageal ligament[9].

The OGJ can be distinguished from the body of the oesophagus by its behavior pattern. There is an increase in the tone of the circular muscle in this region. The sphincter relaxes in response to a swallow and this usually precedes the arrival of a contraction wave travelling down the oesophagus. This phase of relaxation is followed by a short-lasting elevation of pressure above resting values[10]. In recent years it has been known that the sphincter sometimes relaxes even when a swallow does not occur. These relaxations are known as transient lower oesophageal sphincter relaxations (tLOSRs)[11]. Pressures in the abdominal and thoracic cavities are involved in creating the barrier, as well as the exact intra-abdominal location of the junction. Time and posture are also important factors.

It is clear that the OGJ and the components that affect its function as a valvular region between the stomach and oesophagus have a complex interaction. In normal healthy individuals this region provides adequate protection from the effects of acid and non-acid liquids refluxing or back-flowing up into the oesophagus.

REFLUX IN GENERAL

Gastro-oesophageal reflux disease (GORD) symptoms are very common in the general population affecting up to 44% of the US population at least once a month and 20% of the population once a week[12-14]. It has been shown that patients suffering from GORD have a lower health related quality of life than patients with angina and mild heart failure[15]. There is solid evidence that incompetence or dysfunction of the OGJ is a primary determinant of GORD. Three mechanisms at the OGJ lead to an increased number of acid reflux events associated with GORD: tLOSRs, free reflux during periods of low LOS pressure and deglutitive relaxation of the LOS[11,16-18].

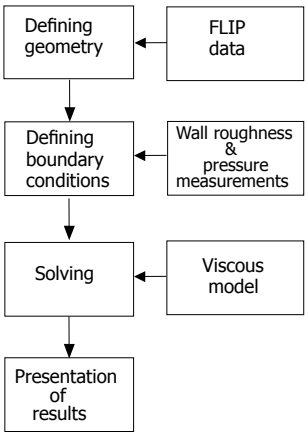

Figure 1 Flow diagram of CFD process.

Other methods exist to indirectly measure the effects of increase flow or refluxing. The most widely used of these are 24 h pH studies and intraluminal impedance. Studies of 24 h pH indicate the amount of time the oesophagus is exposed to an acidic environment in a 24 h period. However, they cannot quantitatively measure the amount of acid travelling back up into the oesophagus nor can they indicate the flow rate. Intraluminal impedance on the other hand demonstrates the presence of liquids, solids and gases in different longitudinal segments of the oesophagus, hence giving flow patterns related to refluxing but still without precise data on flow.

WHY PREDICT FLOW IN THE OGJ?

By using data gathered with FLIP, it is possible to predict the flow patterns that occur during a reflux event. By analysing the predicted flow patterns, a variety of information can be obtained, such as shear stresses along walls, which may contribute to the tissue damaging potential of acid. With a better understanding of the flows that develop in the area of the oesophago-gastric junction, knowledge of its function will be improved. To model the type of flow behaviour observed in the OGJ, a set of equations known as the Navier-Stokes equations is required (See appendix I). These equations are complex and therefore require computational numerical analysis to obtain useful data. By making appropriate assumptions, however, simplifications to the equations are made.

METHODS AND ASSUMPTIONS

CFD simulation is a process that has been used successfully in the engineering industry, particularly aerospace, for many years. CFD analysis has become advanced enough that it is no longer considered as simply an evaluation tool. It is increasingly being used in the design process of everything from aircraft to racing cars. In recent years, the technology has been applied to the flow within arteries and the respiratory system of the human body. For this application, the way a CFD simulation is preformed can be broken down into 4 basic steps, as shown in Figure 1.

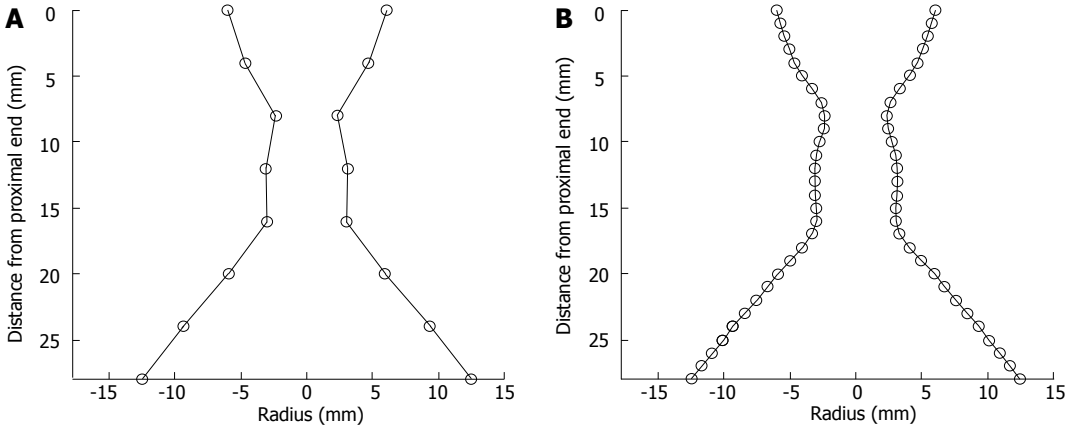

Figure 2 **A**: OGJ geometry as extracted from FLIP. **B**: Interpolated OGJ geometry.

Defining geometry

The data gathered by a FLIP probe provides, at the current stage of development, eight cross-sectional areas. By making the assumption that these cross-sectional areas are circular, then the radii of these circles can be obtained. By utilising these radii as X co-ordinates and the distances of the electrode pairs from the ends of the probe as Y co-ordinates, it is possible to construct a 2D representation of the geometry of the OGJ, as shown in Figure 2A.

The data gathered from FLIP probes is currently limited in that it can only gather information at eight points with a 4 mm separation. However, by using a cubic interpolation scheme, a higher resolution image of the OGJ can be obtained (Figure 2B).

The final step in defining the geometry of the problem is to provide a mesh or grid (Figure 3) over which the CFD solver can perform its calculations. To do this, the geometric data above is imported into a modelling program where the parameters of the mesh, such as cell shape and resolution, are set before being created over the geometry. Generally speaking, higher resolutions result in more accurate results but require greater computational time. Similarly, a carefully designed grid will yield better results but will require more man-hours.

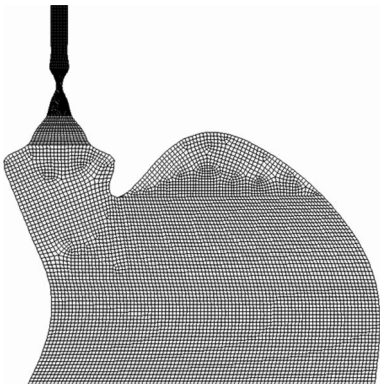

Figure 3 Example of a CFD mesh.

Defining boundary conditions

The second stage in performing a CFD analysis is to define the boundary conditions along each edge/wall of the geometry and to define the operating fluid. For the sample illustrated in this work, this results in a total of 5 definitions (2 walls, 2 edges and the fluid).

For the purposes of a simple CFD simulation, the assumption is made that the flow field consists of a single fluid, and that this fluid fills the field entirely. The physical parameters, such as density and viscosity of this fluid, must be set. For the general case it can be assumed that the operating fluid is liquid water. This has very similar viscosity and density characteristics to the saline used in the FLIP probe from where the data was acquired.

The walls present a unique problem for this CFD simulation. It is known from basic flow dynamics that boundary layers, which are areas of slower moving fluid, form along these walls. The behaviour of these layers has a large effect on the overall flow dynamics and can cause turbulent flows in regions of fast moving fluid. In order to properly simulate these walls it is necessary to define a roughness length. Since the FLIP probe cannot provide this information, a value of 120 nm for the oral mucosa was assumed[19].

The proximal edge is an imaginary wall that defines the top of the area where the data is collected. The flow of the fluid is not stopped by this wall, but its presence allows the flow behaviour along this edge of the problem to be defined. The most important parameter to be defined along this wall is the hydrostatic pressure. If this hydrostatic pressure is higher than that at the distal edge, it will drive fluid down through the junction. Conversely, if this pressure is lower it will allow fluid to flow upwards from the stomach.

The FLIP probe measures two manometric pressures. These measurements are used to identify the position of the OGJ, but the proximal pressure measurement can also be used to estimate the pressure along the proximal edge of the problem.

The distal edge is similar in most respects to the proximal edge but is located along the bottom of the problem. The second pressure measurement on the FLIP probe is located within the balloon and during the placement of the probe within the OGJ it is temporarily dropped to a position below the junction and into the stomach. As the gastric pressure does not vary greatly during an examination, the balloon pressure at this point can be used to define the pressure along the distal edge of the problem.

Practical assumptions

In order to be sure that the result obtained is an accurate representation, the flow at the exit of the system must be fully developed. In the case of the OGJ, this is generally facilitated by extending the problem upwards into the oesophagus and downwards into the stomach. By doing this, the OGJ becomes the central core of the problem and hence any problems that may be encountered due to the proximity of the proximal and distal edges are removed. An example of such geometry is shown in Figure 2B, where the oesophagus is assumed to have a resting diameter equal to the uppermost diameter recorded by the FLIP probe and the geometry of the cardia and stomach are estimated from illustrations. It is necessary to acknowledge these changes when estimating the pressures on the data recorded by the FLIP probe.

Following the above method and using the grid illustrated in Figure 3, a preliminary CFD simulation was performed. The conditions for this simulation were as follows (all pressures relative to atmospheric): (1) Pressure at lower limit of stomach, 10 cmH_2O; (2) Pressure in the oesophagus, 0 cmH_2O; (3) Roughness length of walls, 120 nm (estimated from data on oral mucosa); (4) Operating fluid, water.

Solving

Before calculations can begin it is necessary to define a few more parameters, which are the solution type and the viscous model to be used.

For the rudimentary simulation shown here, the flow does not change with time and hence a steady state solver was used. Whilst this does not reflect the true complexity of the situation, it provides a decent estimation that can be used to develop an understanding in preparation for more complex problems. For a dynamic problem, it is possible to simulate the motion of the OGJ walls. In these cases, where the geometry is allowed to move with successive time steps and thus provides a more representative model, an unsteady solver will be used in the future.

The way in which the thickness, or viscosity, of the fluid is modelled in a CFD simulation is *via* a viscous model. Each model makes different simplifications to the governing equations of fluid flow, and has an effect on the number of equations that must be solved over the cells defined by the mesh. It is therefore important to select a model that is appropriate to the problem. For a smooth, simplistic flow a laminar model can be chosen, which provides a fast calculation. For flows that feature turbulent areas, a more complex viscous model is required. In these cases there are a variety of models available from the faster κ-ε solver to the more accurate Reynolds Stress solver. A balance between speed and accuracy must be struck when selecting the solver to be used.

After these parameters have been set, the calculation can be started. This is a complex process, known as iteration, where calculations must be performed over each cell in the mesh and then repeated using the results from one calculation to start the next. When the difference between a given result and the one before it is small enough, it is taken as an acceptable estimation and is called convergence. At this point the calculations are complete and the results can be presented.

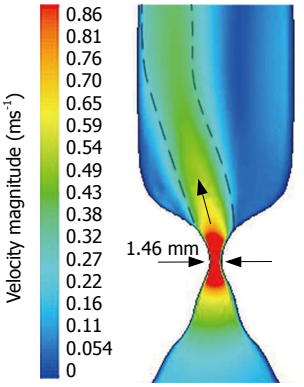

Figure 4 Velocity Magnitude (m/s) through the OGJ and into the oesophagus (limited to 0.9 m/s).

Presentation of results

The CFD solver provides information on a variety of parameters describing the flow, such as hydrodynamic and hydrostatic pressures as well as flow velocities and vectors of the operating fluid. These results can be plotted on contour plots (Figure 4) to provide a picture of how these parameters vary through the flow field allowing an understanding of the flow itself.

RESULTS

Figure 4 illustrates a contour plot of velocity magnitude. In this situation, the stomach pressure is higher than the pressure in the oesophagus. This causes the flow to move upwards, which represents the situation that occurs in reflux. It can be observed in this plot that as the flow moves upwards towards the oesophagus, its velocity increases whilst the cross-sectional area decreases as predicted by the continuity equation. The velocity of the flow then reaches a maximum of almost 2 m/s at the narrowest section of the OGJ, which has a diameter of 1.46 mm.

DISCUSSION AND PERSPECTIVES

This initial work using a CDF analysis of the OGJ shows some promise for the future. For the case shown above, it can be seen that at the narrowest section, a jet of fluid emerges at a higher velocity than the fluid surrounding it. This jet, illustrated by a green to light blue colouring in Figure 4, does not travel vertically and is seen to brush against the left side of the oesophagus. The cause of this deflection from vertical is the bend between the cardia and the stomach. This illustrates how the geometry surrounding the OGJ must be considered for an accurate analysis. The prediction of this jet of fluid corresponds with anecdotal evidence of acid 'squirting' into the oesophagus as the OGJ relaxes during tLOSRs and illustrates how the use of numerical methods can be used to further understanding of the OGJ operation.

The presented model is of a 2D nature, which provides only a general picture of the flow in the OGJ. In the future, the possibilities of CFD analysis will allow a fully 3D model to be constructed, including dynamic changes in the geometry of the OGJ and surrounding

geometry, which is more representative of reality. With these improvements, the numerical analyses will produce better results and greater knowledge of the nature and complexity of flow through the OGJ.

APPENDIX I

The Navier-Stokes Equations are the series of equations that describe the relationship between the pressure and viscous forces acting on a fluid particle and its acceleration.

$$\rho\frac{Du}{Dt}=\rho g_x-\frac{\partial p}{\partial x}+\frac{\partial}{\partial x}\left[\mu\left(2\frac{\partial u}{\partial x}-\frac{2}{3}\nabla\cdot\vec{V}\right)\right]+\frac{\partial}{\partial y}\left[\mu\left(\frac{\partial u}{\partial y}+\frac{\partial v}{\partial x}\right)\right]+\frac{\partial}{\partial z}\left[\mu\left(\frac{\partial w}{\partial x}+\frac{\partial u}{\partial z}\right)\right]$$

The X-Component of the Navier-Stokes Equations

Since these are differential equations, only the most basic of fluid flows can be solved via hand methods. This means that the solution to these equations must be sought via numerical methods in a field known as Computational Fluid Dynamics. When attempting to solve the Navier-Stokes equations for a fluid flow, it is generally necessary to discretise a problem into a grid or mesh. By doing this, it is possible to define a complex problem as a collection of simpler computations that can be solved simultaneously to obtain a solution. In reality, the solution obtained via this method will contain imbalances (or residuals) between the different cells of the mesh. By repeating these calculations, and using the results from the previous calculation as a starting point each time, these residuals can be reduced until they can be considered negligible.

REFERENCES

1 **Bassingthwaighte JB**. Toward modeling the human physionome. *Adv Exp Med Biol* 1995; **382**: 331-339
2 **Gregersen H**. The Giome project. *Neurogastroenterol Motil* 2006; **18**: 401-402
3 **McMahon BP**, Frøkjaer JB, Kunwald P, Liao D, Funch-Jensen P, Drewes AM, Gregersen H. The functional lumen imaging probe (FLIP) for evaluation of the esophagogastric junction. *Am J Physiol Gastrointest Liver Physiol* 2007; **292**: G377-G384
4 **McMahon BP**, Drewes AM, Gregersen H. Functional oesophago-gastric junction imaging. *World J Gastroenterol* 2006; **12**: 2818-2824
5 **McMahon BP**, Frøkjaer JB, Liao D, Kunwald P, Drewes AM, Gregersen H. A new technique for evaluating sphincter function in visceral organs: application of the functional lumen imaging probe (FLIP) for the evaluation of the oesophago-gastric junction. *Physiol Meas* 2005; **26**: 823-836
6 **McMahon BP**, Frøkjaer JB, Drewes AM, Gregersen H. A new measurement of oesophago-gastric junction competence. *Neurogastroenterol Motil* 2004; **16**: 543-546
7 **Pandolfino JE**, Shi G, Curry J, Joehl RJ, Brasseur JG, Kahrilas PJ. Esophagogastric junction distensibility: a factor contributing to sphincter incompetence. *Am J Physiol Gastrointest Liver Physiol* 2002; **282**: G1052-G1058
8 **Boyle JT**, Altschuler SM, Nixon TE, Tuchman DN, Pack AI, Cohen S. Role of the diaphragm in the genesis of lower esophageal sphincter pressure in the cat. *Gastroenterology* 1985; **88**: 723-730
9 **Mittal RK**, Balaban DH. The esophagogastric junction. *N Engl J Med* 1997; **336**: 924-932
10 **Mann CV**, Greenwood RK, Ellis FH Jr. The esophagogastric junction. *Surg Gynecol Obstet* 1964; **118**: 853-862
11 **Mittal RK**, Holloway RH, Penagini R, Blackshaw LA, Dent J. Transient lower esophageal sphincter relaxation. *Gastroenterology* 1995; **109**: 601-610
12 **Locke GR**, Talley NJ, Fett SL, Zinsmeister AR, Melton LJ. Prevalence and clinical spectrum of gastroesophageal reflux: a population-based study in Olmsted County, Minnesota. *Gastroenterology* 1997; **112**: 1448-1456
13 **Gallup**. Heartburn Across America. Princeton. NJ: Gallup Organisation; 1988
14 **Gallup**. Heartburn Across America. Princeton. NJ: Gallup Organisation; 2000
15 **Dimenäs E**. Methodological aspects of evaluation of Quality of Life in upper gastrointestinal diseases. *Scand J Gastroenterol Suppl* 1993; **199**: 18-21
16 **Dent J**, Dodds WJ, Friedman RH, Sekiguchi T, Hogan WJ, Arndorfer RC, Petrie DJ. Mechanism of gastroesophageal reflux in recumbent asymptomatic human subjects. *J Clin Invest* 1980; **65**: 256-267
17 **Dodds WJ**, Dent J, Hogan WJ, Helm JF, Hauser R, Patel GK, Egide MS. Mechanisms of gastroesophageal reflux in patients with reflux esophagitis. *N Engl J Med* 1982; **307**: 1547-1552
18 **Barham CP**, Gotley DC, Mills A, Alderson D. Precipitating causes of acid reflux episodes in ambulant patients with gastro-oesophageal reflux disease. *Gut* 1995; **36**: 505-510
19 **Ravnholt G**, Kaaber S. Surface roughness of oral mucosa and its reproduction in dental materials. *J Dent* 1994; **22**: 169-174

S- Editor Liu Y **L- Editor** Lutze M **E- Editor** Lu W

PO Box 2345, Beijing 100023, China
www.wjgnet.com
wjg@wjgnet.com

World J Gastroenterol 2007 March 7; 13(9): 1365-1371
World Journal of Gastroenterology ISSN 1007-9327

TOPIC HIGHLIGHT

Hans Gregersen, Professor, *Series Editor*

Mechanics of flow and mixing at antroduodenal junction

Seth Dillard, Sreedevi Krishnan, HS Udaykumar

Seth Dillard, Sreedevi Krishnan, HS Udaykumar, Department of Mechanical Engineering, University of Iowa, United States
Correspondence to: HS Udaykumar, Associate Professor, Mechanical Engineering, University of Iowa, 2408 Seamans Center, Iowa City, IA 52242, United States. ush@engineering.uiowa.edu
Telephone: +1-319-3840832 Fax: +1-319-3355669
Received: 2006-12-09 Accepted: 2007-02-08

Abstract

The morphology of tissue structures composing the pyloric orifice is thought to play a role in effectively mixing aqueous gastric effluent with duodenal secretions. To understand the physical mechanisms leading to efficient digestion requires computational models that allow for analyses of the contributions of individual structural components. Thus, we have simulated 2-D channel flows through representative models of the duodenum with moving boundary capabilities in order to quantitatively assess the importance of notable features. A well-tested flow solver was used to computationally isolate and compare geometric and kinematic parameters that lead to various characteristics of fluid motion at the antroduodenal junction. Scalar variance measurement was incorporated to quantify the mixing effectiveness of each component. It was found that the asymmetric geometry of the pyloric orifice in concert with intermittent gastric outflow and luminal constriction is likely to enhance homogenization of gastric effluent with duodenal secretions.

Key words: Computational fluid dynamics; Mixing; Homogenization

Dillard S, Krishnan S, Udaykumar HS. Mechanics of flow and mixing at antrodoudenal junction. *World J Gastroenterol* 2007; 13(9): 1365-1371

http://www.wjgnet.com/1007-9327/13/1365.asp

INTRODUCTION

The gastric outlet to the small intestine or antroduodenal junction is thought to influence the effectiveness of mixing and subsequent absorption of nutrients in the gastrointestinal tract[1-3]. Following ingestion of meals, the stomach secretes gastric juice containing protein-denaturing hydrochloric acid and pepsinogen, and effectively grinds the mixture with a series of strong muscular contractions to produce a slurry of small solid particles and gastric juice known as chyme. Peristaltic contractions in the sinus of the stomach then serve to transport chyme distally into the small intestine, where further enzymatic catalysis, transport, and digestion continue[1-4]. The objective of this study is to determine what role, if any, the morphology of the antroduodenal junction (Figure 1) plays in affecting transport and dynamic mixing of nutrients in the proximal duodenum. For this purpose we computed the flow of gastric effluent *in silico*, modeling a set of experiments that were conducted on the cat gut *in vitro*[5].

The pylorus is comprised of a collection of tissue structures that connect the antrum to the duodenum. Its luminal diameter is controlled by a sphincter muscle complex that sets the resistance to bulk gastric effluent by regulating the tone of the pyloric orifice. During gastric digestion, the proximal and distal pyloric muscle loops occlude the pyloric lumen, preventing premature discharge of unprocessed material to the duodenum. Once the stomach has completed its task of breaking down large solid agglomerates into smaller particles, the pylorus relaxes and peristaltic contractions in the antrum begin to force chyme distally. At this point, antral contraction waves approach the pyloric orifice and, along with the sphincter complex and mucosal folds, cause steady constriction of the pyloric lumen. Chyme continues to be forcibly transported through this lumen until it is fully occluded, a process thought to potentiate an effluent jet into the superior duodenum[1-3]. To date, it seems that no specific attention has been paid to how the geometry and contractile activity of the pylorus might impact gastric outflow and mixing in the first part of the duodenum, although mixing of chyme with duodenal contents (in particular pancreaticobiliary secretions) is essential for digestion and absorption to proceed[3]. The purpose of this study is to examine, through computer modeling and simulation, the mechanics of flow and mixing in the antroduodenal junction.

COMPUTATIONAL MODELING OF TRANSPORT AND MIXING IN ANTRODUODENAL REGION

Laboratory *in vivo* and *in vitro* experiments provide a great

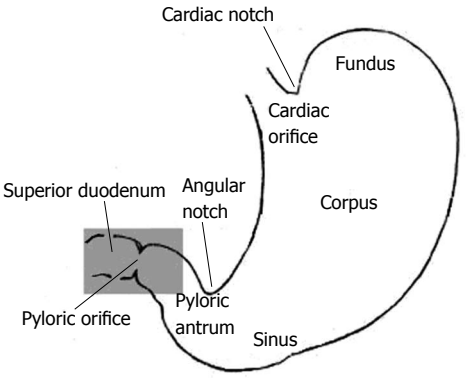

Figure 1 The region of interest (highlighted in grey) includes gastric outlet, or antrum, pylorus, and superior duodenum.

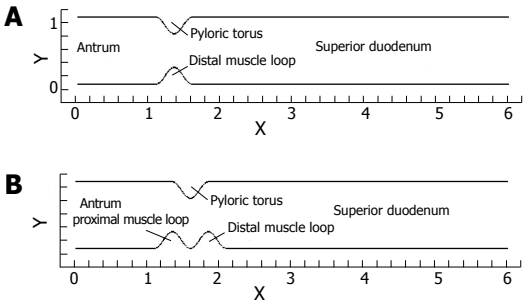

Figure 2 Two representative channel domains used in flow calculations: (**A**) relaxed pylorus; (**B**) "notched" configuration resulting from tonicity of pyloric torus and both muscle loops.

deal of information regarding the function of various components of the GI tract. However, better understanding the mechanics requires development of quantitative models that allow precise and isolated effects of these components to be more thoroughly investigated. Such models must include the essential physical mechanisms pertinent to the physiology of the overall system. Clearly, inclusion of all the known mechanisms acting in the GI tract leads to a highly complex dynamical system. While a 3-dimensional transient model of the entire system would best reproduce actual physical behavior, there is much physical insight to be revealed in simple models that allow for examination of specific features over a range of flow and geometric parameters. This approach is being taken presently, with emphasis on morphology and dynamic properties of the pylorus.

In these preliminary calculations we examined the basic aspects of fluid mechanics across the gastric outlet in simplified models of its geometry. Several cases were constructed and analyzed in order to assess the importance of individual aspects of anatomical structure and kinematics. Flow calculations were performed in a series of channel-like domains (Figure 2) representing the distal antrum and superior duodenum, separated by various configurations of the pylorus. The particular aspects being evaluated are: (1) How does the pulsatile nature of gastric outflow affect the dynamics of nutrient transport and mixing? (2) What are the geometric features of the antro-duodenal junction that enhance or suppress transport/mixing in that region? (3) To what extent does wall motion in concert with pulsatile gastric outflow (aspect 1) through different geometric configurations (aspect 2) lead to enhanced transport and mixing?

To examine the aspects 1-3 listed above, flow fields were computed in the following configurations.

(A) steady flow through a relaxed (symmetric) pylorus; (B) pulsatile flow through a relaxed pylorus; (C) pulsatile flow through a closing pylorus; (D) pulsatile flow through a static pylorus, with asymmetry produced by tonicity of the proximal and distal pyloric muscle loops along with the pyloric torus; (E) pulsatile flow through a similarly asymmetrical, but closing pylorus; and (F) In addition, some of these cases varied in a range of gastric outflow rates or effluent viscosities alternately to determine the effect of the pylorus on homogenization of the chyme of different consistencies, more precisely different viscosities.

Computational methods for solving equations of flow around moving boundaries in the manner chosen here have been thoroughly validated in several papers[6-9].

Following fluid mechanical conventions, the governing equations are "non-dimensionalized" or normalized, by dividing dimensional quantities based on their corresponding representative scales in order to reveal parametric relationships to govern the physical behavior. In our cases, length L^* is normalized by the characteristic unit length of the focal region (i.e. nominal diameter of the duodenum), velocity V* by the maximum inflow velocity in the gastric pulse V_{max}, and time t^* by L/V_{max}. This normalization leads to an important non-dimensional quantity known as the Reynolds number, $Re = (LV)/\nu$, where ν is the kinematic viscosity of the fluid. Physically, when the Reynolds number is very small, viscous effects dominate over fluid inertia. The Reynolds number for all cases in this investigation varied from Re = 1 (low) to Re = 333 (moderate), the upper-bound value obtained from duodenal dimensions and flow rates of normal saline was introduced into the cat gut *in vitro*[5]. In moderate Reynolds number flows (Re = 100 to Re = 1000), the presence of relatively strong laminar vortical fluid patterns is expected. It is widely recognized by fluid mechanicians that such vortical patterns can lead to intense fluid mixing, particularly if they possess temporal and spatial variations[10-12].

The flow field equations solved in our level set models include the standard Navier-Stokes (continuity and momentum) equations (Eqs. 1 and 2), where $\vec{u}^*$ is a non-

$$\vec{\nabla} \cdot \vec{u}^* = 0 \quad (1)$$

$$\frac{\partial \vec{u}^*}{\partial t^*} + \vec{u}^* \cdot \vec{\nabla} \vec{u}^* = -\vec{\nabla} p^* + \frac{1}{\mathrm{Re}} \nabla^2 \vec{u}^* \quad (2)$$

dimensional fluid velocity vector with u^*, ν^* (x- and y-velocity) components in 2D.

Based on the available data and non-dimensional techniques described above, the channel height in the antral and duodenal regions was set at 1.0 unit length, with the overall channel length from the inlet to the exit of 6.0 units. The 2D computational domain for all cases was discretized into square Eulerian grid elements measuring 0.05, 0.025, or 0.0125 units length per side depending on

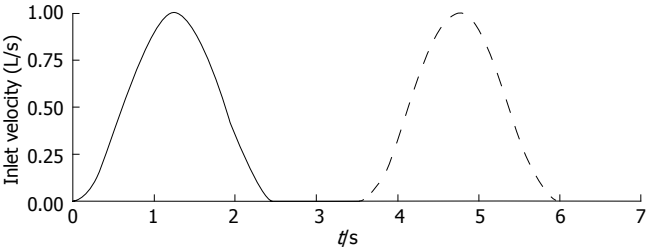

Figure 3 Temporal variation of inlet velocity.

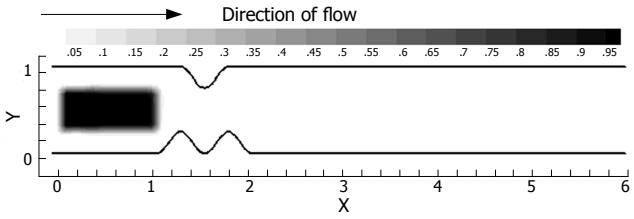

Figure 4 The scalar species block was initialized identically for each case evaluated.

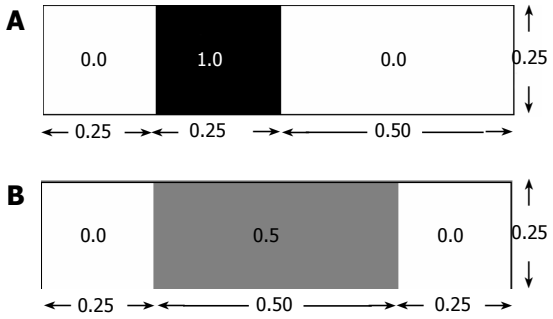

Figure 5 Illustrative example of scalar variance calculation: (**A**) initial and (**B**) final states, each with a mean concentration of 0.25.

the level of mesh refinement demanded by localized fluid motion to obtain a suitable solution[13].

For each model involving temporal variation of fluid velocity in digestive systems, a pulsatile inlet velocity condition was imposed to represent rudimentary flow characteristics generated by periodic antral contractions (Figure 3). Nondimensional inlet velocity V^* varied in a sinusoidal manner between 0.0 and 1.0, and the frequency of oscillation was set to $f = 0.4$ per time unit so that one pulse would have a total duration of 2.5 time units (corresponding to *in vitro* experimental data on cats[5].) To complete the cycle, each pulse was separated by a quiescent period ($V^* = 0.0$) of 1.0 time unit, giving a total cycle duration of $t^* = 3.5$. The quiescent phase was principally designed to represent the refractory period during which pyloric relaxation and return to an open position occur, but it was retained in all cases, with or without dynamic wall events, to make the results more directly comparable.

In addition to the standard flow variables (velocities and pressure), a conserved species of transport equation was implemented to measure the spatial gastric effluent homogenization with duodenal contents. Mixing effectiveness was quantified in each case by calculating the scalar variance[14] of an evolving species (marked fluid region) that was initialized as a block measuring 1.0 unit in length and 0.5 unit in height, with a concentration of 1.0 (Figure 4). The species was given a negligible diffusivity of $D^* = 0.0001$, being vertically centered around the domain's longitudinal axis with the front (right) side of the block giving the same horizontal coordinates as the distal terminus of the antrum. These scalar species blocks were

$$\frac{\partial}{\partial t}\int_{\forall}\phi d\forall + \oint \phi(\vec{u}\cdot\vec{n})dS = \frac{1}{Pe}\oint \vec{\nabla}\phi\cdot\vec{n}dS \qquad (3)$$

evolved in ϕ ıch of the flow fields by solving the transport equation[11]:

In Eq. 3, represents scalar species concentration, $Pe = (U_0L)/D$ is the Peclet number (the ratio of convective to diffusive transport in the fluid continuum), and U_0 represents the characteristic bulk fluid velocity (ranging from 0.0 to V_{max}). Clearly, a small diffusivity coefficient results in very little diffusive transport, implying that the scalar species simply advects along fluid streamlines.

$$\mathrm{var}(\phi) \equiv \langle \phi^2 \rangle = \int_{\forall}(\phi - \bar{\phi})^2 d\forall \qquad (4)$$

The sc∀r species variance calculated for each case is defined by

In E$\bar{\phi}$ 4, is the volume of the computational domain and is the volume averaged concentration of the initial

$$\bar{\phi} = \frac{\int_{\forall}\phi d\forall}{\int_{\forall} d\forall} \qquad (5)$$

species block, i.e.

In our 2-D computations, "volume" is the area. The concept of scalar variance is clarified by considering a rectangular domain of species concentration zero (no species present), and initialized with a scalar species block of concentration 1.0, or 100% $\bar{\phi}$ Figure 5A.)

$$\bar{\phi} = \frac{0.0\times(0.75\times0.25)+1.0\times(0.25\times0.25)}{(0.75\times0.25)+(0.25\times0.25)} = \frac{1}{4}$$

The mean

$$\langle \phi^2 \rangle = (0.0-0.25)^2\times(0.75\times0.25)+(1.0-0.25)^2\times(0.25\times0.25) = \frac{3}{64}$$

concentration of the field in this state is:which gives a variance of

In a field that has become twice as "well mixed" (Figure

$$\langle \phi^2 \rangle = (0.0-0.25)^2\times(0.5\times0.25)+(0.5-0.25)^2\times(0.5\times0.25) = \frac{1}{64}$$

5B), the variance decreases with the increased level of species homogenization:

In this way, the variance approaches zero as perfect mixing is nearly achieved.

COMPUTATIONAL RESULTS

Steady flow across gastric outlet through a relaxed pylorus

Volumetrically, a large portion of gastric emptying aqueous

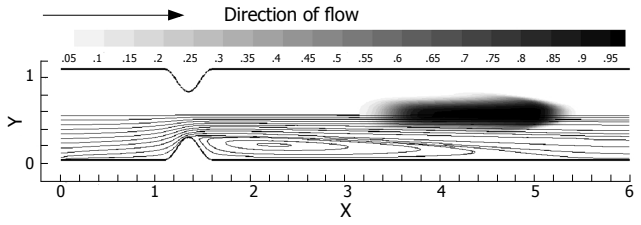

Figure 6 Passage of a passive scalar marker through a relaxed pylorus under steady flow conditions, with inlet velocity set to V* = 1.0 and Re = 333. In this image, 2.0 time units have passed, with the marked fluid exhibiting vertical compression toward and horizontal stretching along the symmetry axis in the weak jet created by the pyloric constriction. Aside from an increase in surface area due to longitudinal stretching, no mixing is seen in this case.

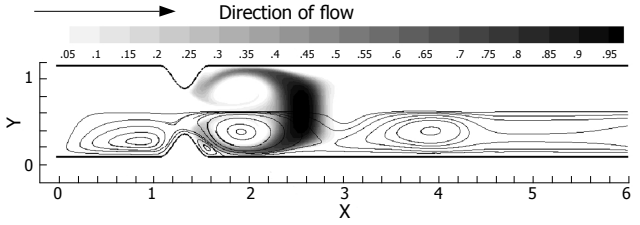

Figure 7 Scalar species distribution following the active phase of one inlet pulse (t = 2.5 time units, Re = 333), illustrating vortical stretching and resultant increase in interfacial area between regions of concentration 1.0 and 0.0.

material is believed to occur across an initially relaxed pylorus[1-4]. In a relaxed state, the torus and distal muscle loop of the human pylorus form a lumen of about 1 cm in diameter between the antrum and duodenum, whose diameters are several times larger[3]. To isolate the effect of such a localized channel narrowing on flow, steady flow behavior (at Re = 333) was computed through the channel (Figure 2A). This calculation was designed to establish a baseline for comparison with forthcoming cases exhibiting pulsatility. The flow is from left to right, i.e. the antrum (inlet) lies to the left of the pylorus and the duodenum to the right. A constant velocity of $V^* = 1.0$ was imposed at the channel inlet, with the resultant flow of 10.0 time units to propagate through the domain in order to achieve steady-state conditions. After this initial period, the scalar species marker was introduced as described previously and allowed to pass through the channel domain to the exit (Figure 6).

As anticipated from this steady flow case, the flow field consists of a pair of recirculation zones distal to the pylorus (Figure 7) and only one is shown with streamlines due to symmetry. While the marker fluid is distorted, it is essentially unmixed as it passes into the superior duodenum. This is primarily due to the lack of dynamic vortical activity in the flow. Vorticity is limited to the separating region distal to the pylorus, and segregated from the rest of the flow by a separatrix[10,16,17]. The separatrix thus blocks the passage of bulk advecting fluid into the recirculation zone, and vice versa, the ability to effectively mix different regions of fluid is severely limited unless some mechanism for disrupting the manifold (i.e. the separatrix) between the recirculating zone and the core flow is put into action. This is provided by pulsatility (intermittent gastric outflow) as shown below.

Pulsatile flow across gastric outlet through a relaxed pylorus

Pulsatile inflow conditions were imposed next (Figure 3) on a channel that was identical to the one evaluated in the steady flow. Pulsatility in the flow has apparently increased the mixing a great deal over the steady flow solution, and in a relatively small spatial region (Figure 7). Streamlines illustrate a pattern of dynamic vortex behavior absent in the previous case. In the pulsatile flow, jet development through the pylorus is coincident with vortex growth and strengthening in the distal recirculation zones; the marked fluid is entrained by vortices as they gain momentum and push the separatrix further into the jet region. As the inlet flow decelerates, mean flow through the channel decelerates as well. This leads to "shedding" of the vortices, i.e. the vortices detach from the wall distal to the pylorus and carry away downstream, and a new pair of vortices forms at the next flow pulse, leading to a periodic vortical flow field in the superior duodenum. Vortex formation and shedding from the divergent distal aspect of the pylorus provide a key mechanism for drawing the scalar species into the sheet; the separatrix between regions of large-scale advection and recirculation has been disrupted during the deceleration phase of the cycle, allowing the marked species to become entrained in the vortical flow.

Pulsatile flow across gastric outlet through a closing pylorus

Transport of gastric effluent induced by periodic antral contractions occurs in concert with the closure of pyloric orifice, and fluid is forced through a narrowing lumen. To isolate the contributions made by this narrowing to the mixing process, a model was constructed identically to that described in the previous section, but with the inclusion of pyloric closure. In this model, temporal motion of the solid boundary defining the pyloric geometry varied quasi-sinusoidally, e.g. the pylorus was in its fully open position at the beginning of a pulse cycle, and closed by the time the inlet velocity returned to zero at the end of the active part of the cycle. Temporally sinusoidal reopening of the pylorus was set to take place during the 1.0 time unit refractory period marking the end of the cycle.

Immediately, one can see the enhanced mixing achieved by closure of the pyloric lumen in concert with flow pulsatility (Figure 8). The jet flow affected by the narrowing lumen gives locally advecting fluid a great deal of axial momentum, while the recirculation zones grow concurrently with the increasing obstruction. This effectively leads to large regions of vorticity, which act to stretch marked fluid along the domain's axis in addition to rolling it into sheets within each vortex. Prominent secondary vortices are also observed in this case, possessing a rotational sense opposite to the primary vortices. This leads to further stretching and folding of the scalar field.

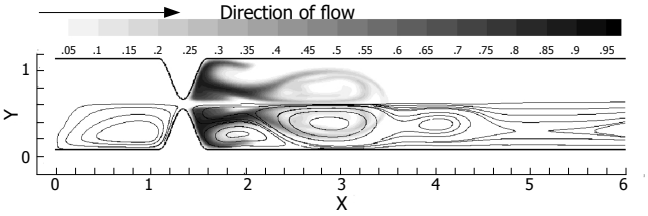

Figure 8 Scalar species passage through a narrowing pylorus (Re = 333): t = 2.5 time units; the pyloric lumen is occluded and inlet velocity has returned to 0.0. The thin, high velocity jet affected by the narrow lumen has led to rapid growth of a strong vortex pair, which sheds and propagates downstream as the bulk flow is halted.

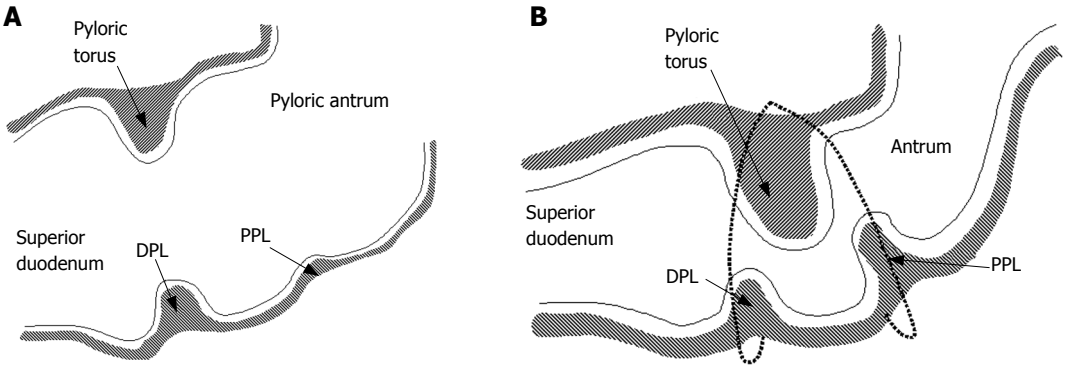

Figure 9 **A**: Relaxed pylorus; **B**: 2-D asymmetry is produced by tonicity of both pyloric muscle loops in the contracted state.

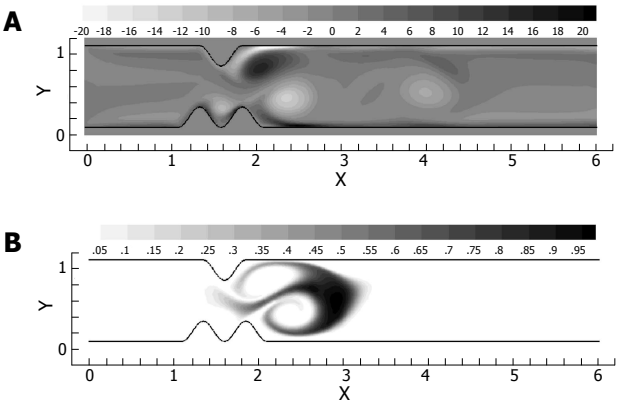

Figure 10 Vorticity (**A**) and scalar field (**B**) after 2.5 time units at Re = 333. Inlet velocity has returned to 0.0 and vortices have shed from divergent surfaces distal to the lumen.

Pulsatile flow across gastric outlet through a static asymmetric pylorus

In the previous three sections, three ingredients were examined that concertedly lead to increases in the degree of fluid mixing in a channel flow, namely, some sorts of partial obstruction leading to convergence and subsequent divergence of the flow, pulsatility, and wall motion. So far, however, we have only covered highly simplified, symmetric geometries to make this point. In reality, with increased tonicity, the positioning of the proximal and distal pyloric muscle loops lead to a "notched" pyloric configuration when viewed in two-dimensional longitudinal sections (Figure 9). In the next case, we seek to capture the effect of this geometric feature of the pylorus on flow into the proximal duodenum. Figure 10 illustrates the static asymmetric pylorus increasing mixture of the scalar field over its symmetric counterpart. As fluid is accelerated through the pylorus, the resultant efflux is directed away from the centerline due to geometric asymmetry. As the jet evolves downstream and diverges further from the axial midline, it collides with the upper wall of the channel and is subsequently deflected away toward the lower wall. This results in a meandering pathway of bulk advection, demarcated by vortices which are staggered in the channel and free to occupy the whole channel width rather than being mirrored symmetrically. The resulting path of the fluid jet (advected scalar) is highly contorted, leading to longer residence time, i.e.,streamlines within the domain are much longer and take more time to traverse, and stretching of fluid elements, and therefore to enhanced mixing.

Pulsatile flow across gastric outlet through a closing asymmetric pylorus

Asymmetry is seen to be a significant contributor to mixing effectiveness. Next, all of the mechanisms (pulsatility, asymmetry, pyloric closure) were involved by examining the effect of closure of an asymmetric pylorus.

Immediately evident is the fact that the mechanisms of pulsatility, asymmetry and pyloric closure concertedly lead to significant enhancement of mixing. Figure 11 shows that after a single gastric pulse, the scalar marker species has become much more homogenized. It is noteworthy that this homogenization not only occurs rapidly, but takes place within a small spatial region as well; scaling with the human GI system, the level of mixing seen in this case would occur within a 4-5 cm segment of the proximal duodenum[3], even neglecting the presence of prominent geometric features such as the duodenal cap and mucosal folds in the channel.

Mixing effectiveness attributed to geometric and dynamic properties

To quantify scalar mixing, the commonly employed scalar variance measures were obtained during each flow calculation. For each of the cases above, normalized scalar variance (computed using Eq. 4) was plotted for one complete pulse cycle to directly compare the mixing

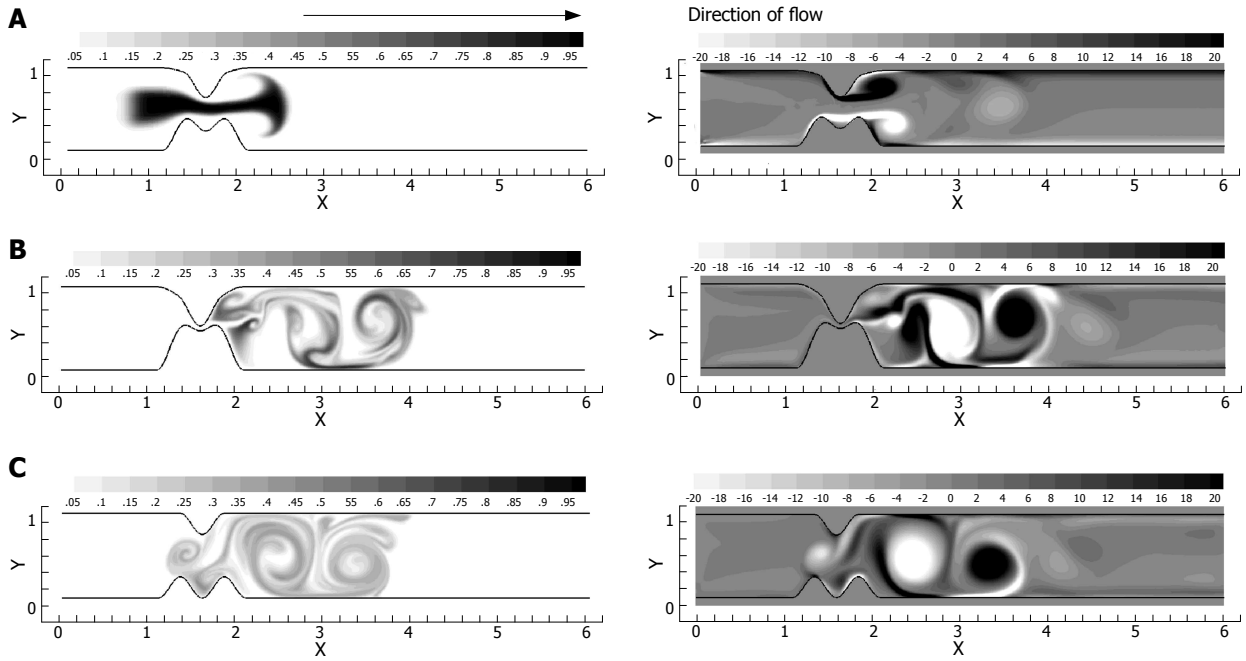

Figure 11 A temporal progression of scalar species (left) and vorticity (right) during one complete inlet pulse cycle (3.5 time units) through the closing asymmetric pylorus: **A**: t = 1.25 time units, with the vortical jet becoming apparent as inlet velocity is maximized and luminal narrowing occurs; **B**: t = 2.5 time units. The lumen is fully closed, and the inlet velocity has returned to 0.0; **C**: t = 3.5 time units. The pylorus has returned to its original open state during the 1.0 time unit refractory period. Strong, stable regions of vorticity remain, entraining weaker unstable vortices and further stretching the species.

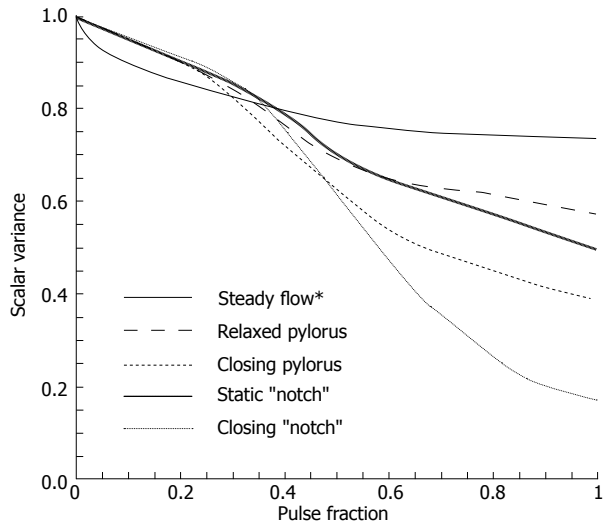

Figure 12 Scalar variance plots of each case through one complete pulse cycle; Re = 333.

effectiveness of each flow. In Figure 12, the scalar variance measurement of the 5 cases is plotted. Dynamic behavior of the pylorus, combined with pulsatility, clearly results in effective mixing. Imperfections in the form of channel asymmetry enhance this phenomenon even more; the physical structure of the pylorus appears to have a significant effect in mixing patterns, at least in the Reynolds number (i.e. the fluid viscosity) regime corresponding to saline in the cat gut examined *in vitro*[5].

Mixing effectiveness attributed to Reynolds number

Chyme viscosity can vary considerably based upon a meal's solid fraction[1-3,5], with more viscous solutions yielding lower Reynolds numbers. Thus, the Reynolds number varied over several orders of magnitude to study the effects of viscosity in our model (Figure 13). For brevity, results are limited to Re variations in the fifth and final case involving a closing and asymmetric pylorus.

As seen from the scalar variance plot in Figure 14, the flows with Reynolds numbers of order 1 and order 10 lack the momentum necessary to overcome viscous stresses in the fluid and generate vorticity, leaving the initial scalar species blocks largely intact as they progress through the channel. Advection begins to dominate as chyme viscosity decreases, resulting in a large degree of fluid stretching, vortex formation and hence, mixing. Scalar variance plots help quantify this shift in behavior, and leave one to conclude that pyloric structure may not play a large role in the homogenization of dense meals without adequate dilution.

CONCLUSIONS

The lumen of the gastroduodenal junction has a complex geometry which changes with the contractile activity of gastroduodenal musculature in response to the pH, osmolarity, caloric density and mechanical properties of the luminal contents[1-3]. Here we focused on the contribution likely to be made by several specific anatomical parameters (like the notching of pyloric lumen produced by its muscle loops), and by some specific functional parameters (steady versus intermittent gastric outflow). We also compared the results between aqueous and more viscous luminal contents. Our results indicate that intermittent gastric outflow in combination with the complex geometry and motion of the pyloric lumen is likely to enhance duodenal

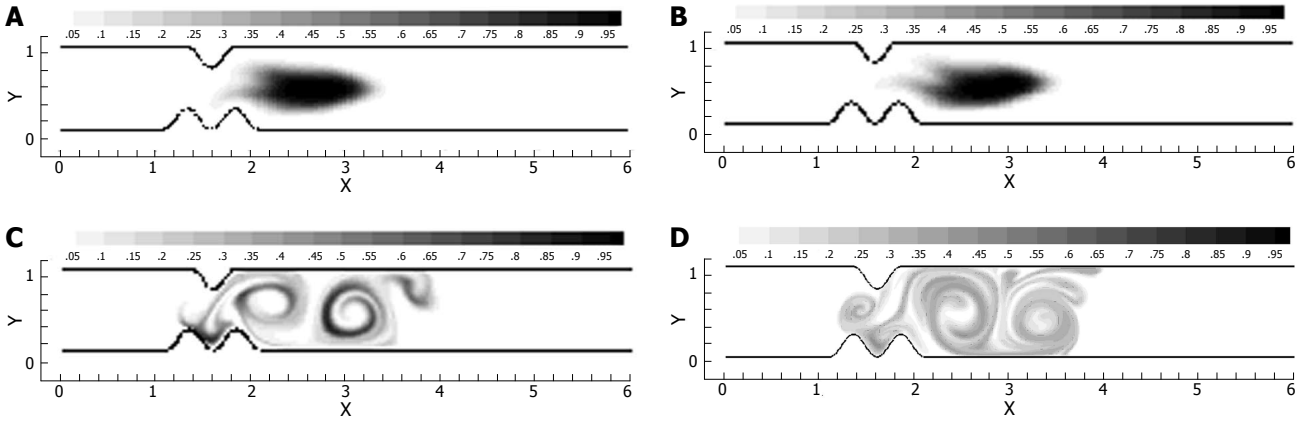

Figure 13 Scalar species plots following one pulse cycle through a closing, asymmetric pylorus at four different Reynolds numbers: **A**: Re = 1; **B**: Re = 10; **C**: Re = 100; **D**: Re = 333.

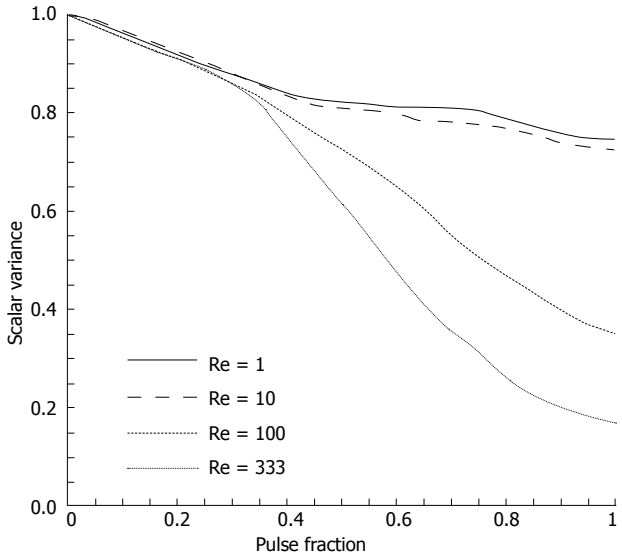

Figure 14 Scalar variance of asymmetric pylorus model at four different Reynolds numbers.

mixing of aqueous fluids, facilitating rapid chemical digestion and subsequent absorption of nutrients in the duodenum. More viscous meals may remain unmixed and will necessarily involve contractions of the duodenum to provide any significant homogenization.

ACKNOWLEDGEMENTS

The authors wish to acknowledge support from the Veterans Administration, and the valuable insight provided by Dr. Konrad Schulze at VAMC and UIHC, Iowa City, which enabled the conduct of this work.

REFERENCES

1 **Ramkumar D**, Schulze KS. The pylorus. *Neurogastroenterol Motil* 2005; **17** Suppl 1: 22-30
2 **Schulze-Delrieu K**, Ehrlein HJ, Blum AL. Mechanics of the pylorus. In: Gastric and gastroduodenal motility. New York: Praeger Publishers, 1984: 87-102
3 **Schulze K**. Imaging and modelling of digestion in the stomach and the duodenum. *Neurogastroenterol Motil* 2006; **18**: 172-183
4 **Malbert CH**, Ruckebusch Y. Passage of chyme and contractile patterns at the antro-duodenal junction in the dog. In: Gastro-pyloro-duodenal coordination. Hampshire: Wrightson Biomedical Publishing Ltd, 1990: 197-208
5 **Schulze-Delrieu K**, Brown CK. Emptying of saline meals by the cat stomach as a function of pyloric resistance. *Am J Physiol* 1985; **249**: G725-G732
6 **Gibou F**, Fedkiw R, Caflisch R, Osher S. A level set approach for the numerical simulation of dendritic growth. *J Sci Comp* 2003; **19**: 183-199
7 **Liu H**, Krishnan S, Marella S, Udaykumar HS. Sharp interface Cartesian grid method II: A technique for simulating droplet interactions with surfaces of arbitrary shape. *J Comp Physics* 2005; **210**: 32-54
8 **Marella S**, Krishnan S, Liu H, Udaykumar HS. Sharp interface Cartesian grid method I: An easily implemented technique for 3D moving boundary computations. *J Comp Physics* 2005; **210**: 1-31
9 **Yang Y**, Udaykumar HS. Sharp interface Cartesian grid method III: Solidification of pure materials and binary solutions. *J Comp Physics* 2005; **210**: 55-74
10 **Horner M**, Metcalfe G, Wiggins S, Ottino JM. Transport enhancement mechanisms in open cavities. *J Fluid Mech* 2002; **452**: 199-229
11 **Howes T**, Shardlow PJ. Simulation of mixing in unsteady flow through a periodically obstructed channel. *Chem Eng Sci* 1997; **52**: 1215-1225
12 **Ottino JM**. The kinematics of mixing: stretching, chaos, and transport. New York: Cambridge University Press, 1989: 64-95
13 **Krishnan S**, Marella S, Udaykumar HS. Sharp interface Cartesian grid method IV: Local mesh refinement. *J Comp Physics*, in press
14 **Mackley MR**, Veves Saraiva RMC. The quantitative description of fluid mixing using Lagrangian and concentration-based numerical approaches. *Chem Eng Sci* 1999; **54**: 159-170
15 **Jeffrey B**, Udaykumar HS, Schulze KS. Flow fields generated by peristaltic reflex in isolated guinea pig ileum: impact of contraction depth and shoulders. *Am J Physiol Gastrointest Liver Physiol* 2003; **285**: G907-G918
16 **Baker GL**, Gollub JP. Chaotic dynamics. 2nd ed. New York: Cambridge University Press, 1996: 59-62
17 **Drazin PG**. Nonlinear Systems. New York: Cambridge University Press, 1992: 26-27

S- Editor Liu Y **L- Editor** Ma JY **E- Editor** Zhou T

PO Box 2345, Beijing 100023, China
www.wjgnet.com
wjg@wjgnet.com

World J Gastroenterol 2007 March 7; 13(9): 1372-1377
World Journal of Gastroenterology ISSN 1007-9327

TOPIC HIGHLIGHT

Hans Gregersen, Professor, *Series Editor*

Using computed tomography scans to develop an *ex-vivo* gastric model

Jerome A Henry, Gerard O'Sullivan, Abhay S Pandit

Jerome A Henry, Abhay S Pandit, Network of Excellence for Functional Biomaterials, National University of Ireland, Galway. Ireland
Gerard O'Sullivan, Section of Interventional Radiology, Department of Radiology, University College Hospital Galway, Ireland
Supported by the Irish Research Council for Science Engineering and Technology and by the National Development Plan
Correspondence to: Abhay Pandit, Professor, Department of Mechanical and Biomedical Engineering, National University of Ireland, Galway, Ireland. abhay.pandit@nuigalway.ie
Telephone: +353-91-492758 Fax: +353-91-563991
Received: 2006-12-09 Accepted: 2007-01-05

Abstract

The objective of this research was to use abdominal computed tomography (CT) scans to non-invasively quantify anthropometrical data of the human stomach and to concomitantly create an anatomically correct and distensible *ex-vivo* gastric model. Thirty-three abdominal CT scans of human subjects were obtained and were imported into reconstruction software to generate 3D models of the stomachs. Anthropometrical data such as gastric wall thickness, gastric surface area and gastric volume were subsequently quantified. A representative 3D computer model was exported into a selective laser sintering (SLS) rapid prototyping machine to create an anatomically correct solid gastric model. Subsequently, a replica wax template of the SLS model was created. A negative mould was offset around the wax template such that the offset distance was equivalent to that of the gastric wall thickness. A silicone with similar mechanical properties to the human stomach was poured into the offset. The lost wax manufacturing technique was employed to create a hollow distensible stomach model. 3D computer gastric models were generated from the CT scans. A hollow distensible silicone *ex-vivo* gastric model with similar compliance to that of the human stomach was created. The anthropometrical data indicated that there is no significant relationship between BMI and gastric surface area or gastric volume. There were inter- and intra-group differences between groups with respect to gastric wall thickness. This study demonstrates that abdominal CT scans can be used to both non-invasively determine gastric anthropometrical data as well as create realistic *ex-vivo* stomach models.

Key words: Gastric anthropometrical data; Rapid prototyping; *Ex-vivo* gastric model; Computed tomography

Henry JA, O'Sullivan G, Pandit AS. Using computed tomography scans to develop an *ex-vivo* gastric model. *World J Gastroenterol* 2007; 13(9): 1372-1377

http://www.wjgnet.com/1007-9327/13/1372.asp

INTRODUCTION

Computed tomography (CT) is a non-invasive radiological examination tool which is capable of producing superior diagnostic images of soft tissue organs, such as the stomach, compared to other radiographic procedures[1-4]. Diagnostic imaging techniques have been used to extract anthropometrical data of the human stomach such as gastric wall thickness, surface area and volume[1,5,6]. Researchers investigating obesity have considered whether obese persons have a significantly larger gastric volume than non-obese persons[6].

Whilst employing diagnostic imaging scans for quantitative analysis, it is also possible to transform diagnostic scans into computer aided design models. Magnetic resonance angiography (MRA) scans have been used to create *ex-vivo* compliant tissue models[7]. MRA scans were exported into computer software and later manipulated through rapid prototyping techniques to create solid models, which were subsequently used to develop hollow arterial models.

Rapid prototyping (RP) is a fabrication method which enables accurate and economic reproduction of devices or models without the need for tooling[8]. Files from computer aided design software may be exported to a variety of RP processes such as 3D printing, stereolithography and selective laser sintering to produce solid prototypes. These prototypes may in turn be used to cast hollow models using moulding techniques.

The lost wax process is a mould fabrication method for creating thin-walled objects[9]. Using solid rapid-prototyped objects as a template, it is possible to produce high detail hollow objects after offsetting the template with a low melting point material such as wax.

The objectives of this study were: (1) to demonstrate

that abdominal CT scans could be used to consistently quantify anthropometric parameters of the human stomach, specifically gastric wall thickness, surface area and volume of non-obese and obese patients and (2) develop an anatomically correct, distensible *ex-vivo* stomach model using abdominal CT scans.

ANALYSIS OF ANTHROPOMETRICAL DATA

Statistical analysis

Data are expressed as mean ± SD. Statistical analysis was performed using Minitab® (v. 13, Minitab, Inc. PA, USA). Statistical comparisons were made by analysis of variance (ANOVA). Tukey's honestly square difference was used for *post-hoc* analyses to determine statistical difference between groups. A p-value of < 0.05 was considered to be statistically significant. Regression analysis compared BMI against gastric surface area and volume.

Subject classification

The abdominal CT scans of 33 patients were obtained (Siemens Somatom Emotion 6™ Power CT scanner, Siemens Medical Systems, Germany) from Merlin Park Imaging Centre, Merlin Park Hospital, Galway, after an approval from the Ethics Committee of the National University of Ireland, Galway. Patients mass and height were recorded and the patient's body mass index (BMI) was determined according to the World Health Organisation (WHO) definition.

BMI is calculated by dividing a persons mass (kilograms) by the square of their height (m^2). Group I ($n = 19$) contained those with a BMI between 17.58-24.9 kg/m^2, considered underweight-normal by the WHO, while Group Ⅱ ($n = 14$) comprised those with a BMI between 25.0-39.66 kg/m^2, deemed clinically overweight-obese by the WHO.

The mean BMI of Group I was 21.83kg/m^2 while the mean BMI of Group Ⅱ was 29.27 kg/m^2. Grubb's test to identify outliers was applied to the raw data before statistical analysis. No patient in either Group I or Group Ⅱ was identified as outliers. Both categories were statistically different ($P < 0.05$) to each other with respect to their mass and BMI, as shown in Table 1.

Table 1 Height, mass and BMI measurements of patients

	BMI 17.58-24.9 kg/m^2 $n = 19$	BMI 25.0-39.66 kg/m^2 $n = 14$
Height (m)	1.69 ± 0.10	1.69 ± 0.10
Mass (kg)	62.50 ± 10.25[a]	83.61 ± 11.34[a]
BMI (kg/m^2)	21.83 ± 2.16[c]	29.27 ± 3.79[c]

All values mean ± SD. [a,c]$P < 0.05$.

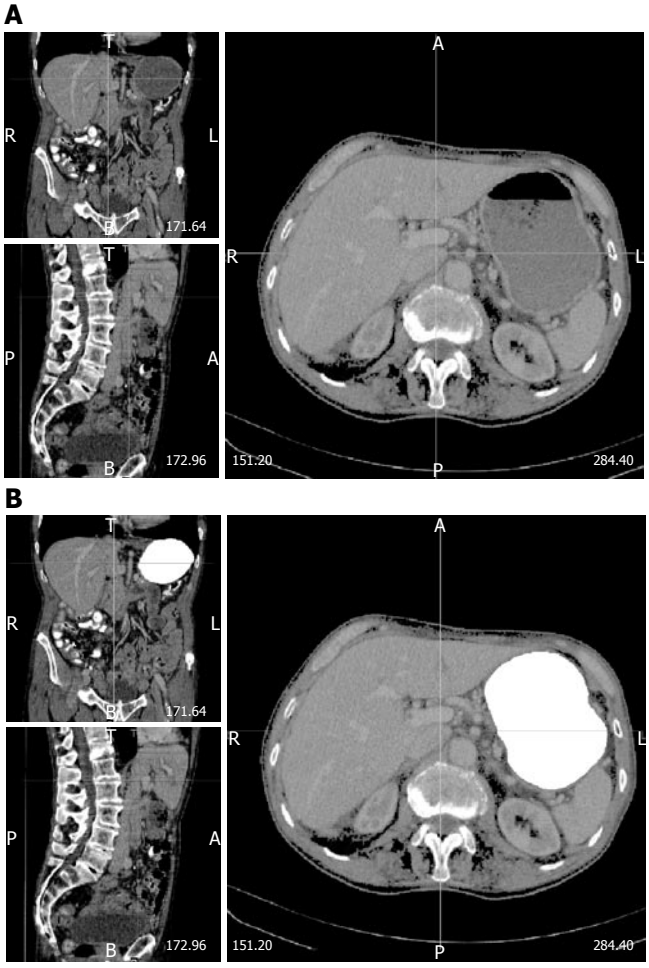

Figure 1 A: Typical imported CT image; B: mask applied to highlight stomach.

Manipulation of CT scans

The CT scans were individually imported into a 3D reconstruction software package (MIMICS™, Materialise, UK), as per Figure 1A. Upon being imported into the 3D reconstruction software package, the anterior, posterior and lateral orientations of the patient were defined. The transaxial plane images were used for all patients as the stomach was discriminately defined in this plane. The grey-scale of the scans was adjusted to differentiate the stomach from adjacent organs such as the spleen and liver. The threshold level was set by drawing a profile line across a cross-section of the stomach. The threshold levels were established by adjusting the HounsField units, which accentuated the stomach on all the CT scans with a mask, as shown in Figure 1B. An editing tool was utilised to remove any superfluous thresholding that may have been picked up by adjacent organs. Smoothing algorithms were used to remove any undesirable edge effects due to pixilation and to optimise the geometries of the anatomically correct stomachs.

Having edited the CT slices to isolate the stomach, the slices were grouped together to form a 3D image of the stomach. The 3D stomach images were saved in ".stl" format and exported to a rapid prototype machine.

Gastric volume and gastric surface area

Upon manipulating the CT slices to isolate the stomach, the slices were grouped together to form a 3D image of the stomach. The 3D images were attained by choosing the region growing function. Gastric volumes and gastric surface areas were determined from the 3D images. The gastric surface area and gastric volume 3D images

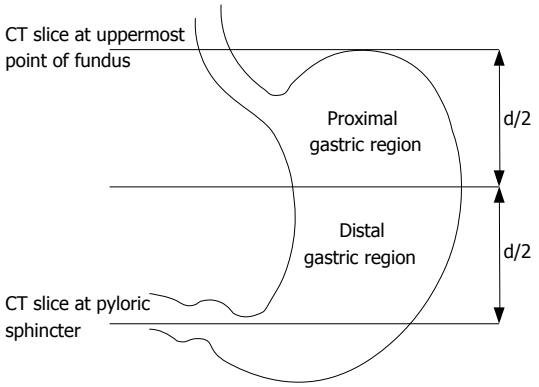

Figure 2 Schematic diagram indicating how the proximal and distal gastric regions were defined.

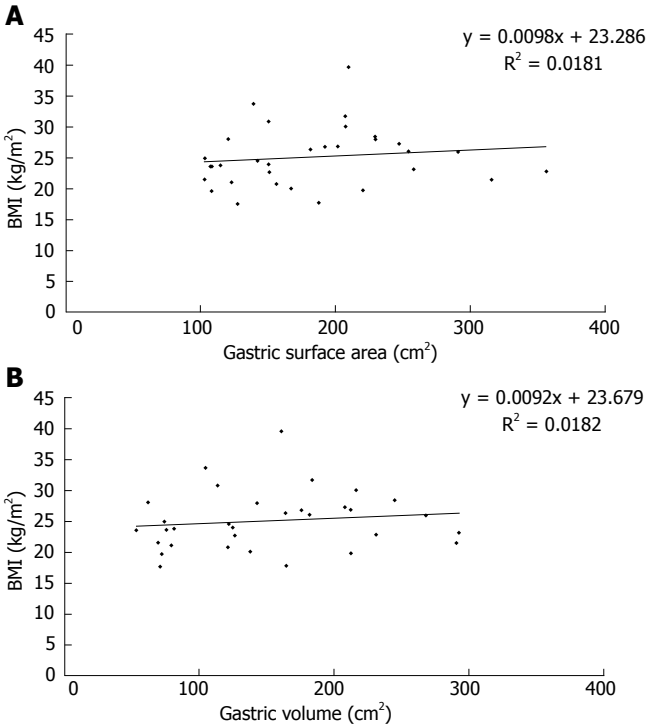

Figure 3 Graphs of regression of BMI on (A) gastric surface area and (B) gastric volume, indicating no linear relationship between these parameters.

were further divided into proximal and distal sections to investigate whether there were significant differences between these sections. Half-way between the uppermost point on the fundus and the pyloric sphincter defined the proximal and distal stomach, as shown in Figure 2.

There were no significant differences between Group I and Group II when comparing their gastric surface areas or volumes, as shown in Table 2. Gender had no influence on gastric volume or surface area. There were no significant differences between the groups with respect to proximal and distal gastric surface area and gastric volume data (Table 3). The regression graphs of BMI against gastric surface area and volume are shown in Figure 3A and B respectively. The low regression coefficient values in Figure 4 indicate that there is no linear relationship when comparing BMI to gastric surface area or volume.

Table 2 Anthropometrical data from CT scans compared to those reported in literature

	Group I $n = 19$	Group II $n = 14$	Kuiken *et al*[13]	Kim *et al*[6] Obese	Kim *et al*[6] Non-obese
GV (cm^3)	143 ± 97	190 ± 88	182 ± 11	217 ± 40	208 ± 38
GSA (cm^2)	154 ± 65	191 ± 6			
Pearson's coefficient, *r*	0.98	0.98			

All values expressed as mean ± SD. GV: Gastric volume. GSA: Gastric surface area.

Table 3 Proximal and distal gastric volume and gastric surface area data from CT scans

BMI (kg/m^2)	Proximal GV (cm^3)	Distal GV (cm^3)	Proximal GSA (cm^2)	Distal GSA (cm^2)
17.58-24.90 kg/m^2	78 ± 54	91 ± 36	84 ± 36	76 ± 37
25.00-39.66 kg/m^2	67 ± 52	87 ± 26	96 ± 31	94 ± 18

All values expressed as mean ± SD. GV: Gastric volume. GSA: Gastric surface area.

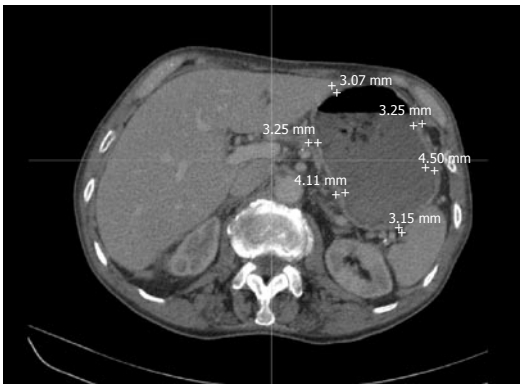

Figure 4 Typical gastric wall thickness measurements on transverse plane CT scan using electronic callipers.

Gastric wall thickness

The tranverse slices were examined from the oesophagus to the pyloric sphincter. Due to the positioning of the patients on the CT scanner bed and the discrepancy in slice thickness (range 2.5-4.5 mm) between patients, there was variability between patients as to where the stomach became evident and when the stomach was no longer detectable in the CT scans. Using the electronic callipers on the 3D imaging reconstruction software, six representative gastric wall thickness measurements were taken on each slice, as in Figure 4. The location of each thickness was such that there were three anterior and posterior measurements, with equidistance between the points.

It was also investigated whether or not there was a difference between the anterior and posterior, and

Table 4 Mean gastric wall thickness from CT scans

BMI (kg/m^2)	Gastric Wall Thickness (mm)
17.58-24.90 kg/m^2	3.61 ± 0.51
25.00-39.66 kg/m^2	3.37 ± 0.41
Gossios *et al*[3]	3.2
Scatarige *et al*[4]	3
Huh *et al*[14]	3.92 ± 0.16

All values expressed as mean ± SD. Values from literature are given as a comparison.

Table 5 Mean anterior and posterior gastric wall thickness data from CT scans

BMI (kg/m^2)	Anterior (mm)	Posterior (mm)	Proximal (mm)	Distal (mm)
17.58-24.9 kg/m^2	3.54 ± 0.77	3.37 ± 0.66	3.55 ± 0.73	3.64 ± 0.74
25.0-39.66 kg/m^2	3.61 ± 0.72	3.53 ± 0.69	3.42 ± 0.72	3.42 ± 0.68
Pickhardt *et al*[1]	5.00 ± 1.90	5.20 ± 1.70		

All values expressed as mean ± SD. Values from literature are given as a comparison.

Figure 5 Anatomically correct hollow distensible silicone stomach after wax removal.

proximal and distal stomach with respect to gastric wall thickness. The anterior and posterior gastric regions were defined by drawing a horizontal line through the midpoint of the stomach on each CT slice. The proximal and distal gastric regions were defined as described previously.

Mean gastric wall thickness values varied between 2.35 and 5.43 mm. Table 4 indicates that there was no statistical difference in gastric wall thickness between Group I and Group Ⅱ. Analysis of the mean anterior and posterior gastric wall thicknesses revealed that location does not significantly influence gastric wall thickness, as per Table 5.

DEVELOPMENT OF *EX-VIVO* GASTRIC MODEL

Model rapid prototyping

A 3D computer model file was recreated in a selective laser sintering machine (DTM Sinterstation^{TM} 2500 plus, 3D Systems Corp, USA). Powdered nylon was layered in 0.1 mm increments to produce a solid stomach model, which was then used to create a mould for the hollow stomach model. Solid stomach models were developed from the 3D computer models using the SLS machine. This solid model was used as a template to create the anatomically correct hollow distensible stomach model.

Selection of distensible polymer

The next phase involved selecting a suitable polymer that possessed the same mechanical and distensibility properties as that of the stomach. Egorov *et al*[10] have previously determined the mechanical properties of the human stomach: modulus of elasticity about 0.4 MPa, elongation to break about 225%, ultimate tensile strength about 0.9 MPa. A silicone (Elastosil M4400^{TM}, Wacker-Chemie GmbH, Germany) was identified as a polymer with similar distensibility to the human stomach.

Fabrication of hollow model

A replica model of the rapid prototyped stomach was created using wax. The wax model was then offset using nylon reinforced modelling clay, which afforded a varying thickness similar to that of the stomach wall. The clay-covered model was secured in a retort stand *via* the rod. Subsequently, a two-part negative mould (plaster of Paris) of the clay model was created. Positioning guides were marked on and around the mould so as to later ensure accurate repositioning of the mould around the wax stomach.

Once set, the mould halves were opened and the modelling clay was removed, with the wax model still secured in the retort stand. A thin wax-coating (Shellac) was applied to the mould inner surfaces to aide removal of the silicone stomach afterwards. Using the pre-marked positioning indicators, the mould was repositioned around the wax model and sealed. Air holes were drilled into the mould at the oesophageal end and offset to the cardiac notch to allow any trapped air to escape. These locations were chosen as they were the two natural high points on the mould.

Silicone was poured in at the oesophageal end of the mould to fill the gap previously occupied by the modelling clay. The air-hole near the cardiac notch was plugged once silicone poured out of this hole. When the silicone came out of the air-hole at the oesophageal end the pouring process was deemed complete and the silicone was left to set for 24h. Thereafter, the silicone and wax stomach were placed in an oven at 80℃ for 3 h to melt the wax out. The lost-wax process proved successful in fabricating an anatomically correct distensible stomach model, as in Figure 5. The exterior surface was smooth with an opening at the oesophageal end.

Validation of hollow model

A non-destructive pressure-volume method was used to determine gastric compliance in the *ex-vivo* model. Gregerson *et al*[11] reported pressure-volume measurements of the human antrum by incrementally inflating an intra-gastric bag, while Distrutti and associates determined gastric compliance using a barostat[12].

For this study, a tube connected through a peristaltic pump (Watson-Marlow 323S, Watson-Marlow, UK) and a tube connected to a digital pressure gauge (ZSE30, SMC, Ireland) were inserted into the oesophageal end of the

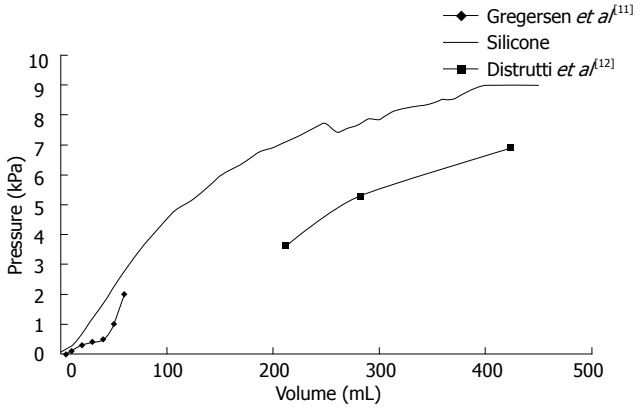

Figure 6 Pressure volume curves of silicone stomach compared to human stomach values reported by Gregersen et al[11] and Distrutti et al[12].

gastric model, which was then hermetically sealed. The peristaltic pump was programmed to inflate the gastric model using 10 mL increments of fluid, with a 1min interval between steps, up to 200 mL. Any resulting change in pressure after each volume increment was noted. This procedure was repeated twelve times on the same stomach, from which pressure-volume curves were derived.

The mean pressure-volume curve for the silicone stomach was plotted against literature values, as shown in Figure 6. Gregersen *et al*[11] reported on gastric compliance after low volumes (< 100 mL) of fluid were introduced into the stomach while Distrutti and colleagues reported on gastric compliance after introducing higher volumes of fluid (ca. 200-400 mL)[12]. It is evident from Figure 6 that the curves from literature have three distinctive curve slopes, reflecting the three muscle layers (longitudinal, circular and oblique) that surround the human stomach. The compliance curve for the silicone stomach has similar slopes to both literature values at low and high pressures. Furthermore, it is evident that the silicone stomach curve also has three different slopes, thus replicating the three gastric muscle layers.

CONCLUSION

The aim of this study was to demonstrate that it is possible to utilise abdominal CT scans to create an anatomically correct, distensible *ex-vivo* gastric model. An image reconstruction software package was used to create 3D gastric models from abdominal CT scans. These computer models were later exported to a rapid prototyping machine to produce solid, anatomically correct stomach models. The rapid prototyped models were used to develop plaster of Paris moulds. Using the lost wax process, an anatomically correct, hollow *ex-vivo* gastric model with similar compliance to that of the human stomach was developed.

Analysis of the anthropometrical data showed statistical differences between the groups when comparing their mass and BMI. However, the data in this study correlates with the fact that the WHO range values which define the BMI categories never overlap. Examination of the gastric surface area and volume data indicated no statistically significant difference between the two groups. Comparison of the proximal and distal gastric regions showed no significant difference in their surface area and volume. This finding suggests that both proximal and distal regions behave similarly when accommodating food. The gastric volume values in this study correlates with previous studies that also quantified gastric volume through non-invasive methods (Table 2)[6,13]. However we are unable to compare the distal and proximal gastric volumes in this study with the reported values as Kim *et al*[6] defined the proximal and distal regions differently, while Kuiken and colleagues did not specify the BMI of their patients[13]. Low regression coefficient values of BMI compared to gastric volume and surface area indicate that BMI is not an indicator of gastric surface area or gastric volume, or vice-versa

There were both intra- and inter-group differences with respect to the gastric wall thickness. The inter-group variability was due to a number of reasons such as that some of the stomachs were fully distended whilst others were not, and there may have been gastric wall pseudothickening as a result of oblique sectioning by the CT scanner. Such a phenomenon has been previously reported by Pickhardt and Asher[1]. In this study, there was a wide range for the gastric wall thickness, between 2.35 and 5.43 mm, with the majority of gastric wall thickness measurements being between 3 and 4 mm. Previous examinations of gastric wall thickness have indicated a gastric wall thickness between 2.80 and 5 mm for fully distended stomachs, hence validating our findings[3,4,14]. Pickhardt and Asher reported values greater than 12mm for the gastric antrum wall thickness[1]. However, no such large values were found in this study.

The use of CT scans to determine the volume and surface area of the stomach hasn't been reported thus far. Previous attempts to quantify gastric volume and surface area have relied on invasive methods such as intragastric barostat balloon[15,16], whilst non-invasive techniques have used single photon emission computed tomography (SPECT)[17], MRI[5] and endoscopic ultrasound[14]. However the aforementioned methods are not without their limitations such as poor image resolution, erroneous gastric volume measurements and difficulty in reproducibility[13,16-19]. Hence, the utilisation of CT scans would make an ideal method for non-invasive measurement of gastric accommodation.

Magnetic resonance angiography (MRA) scans and the lost core technique were used to accurately create an anthropomorphic model of the human carotid artery[7]. Thus far, there have been no reports of generating an *ex-vivo* gastric model using CT scans. Therefore, the described techniques in this study could be used to develop anatomically correct *ex-vivo* models of other systems or organs such as the respiratory system and heart. The *ex-vivo* gastric model in this study was validated by the similar compliance at both low and high pressures to the human data reported in literature[11,12,20].

Hence, it may concluded that it is possible to manipulate abdominal CT scans to obtain anatomically correct 3D

models of the stomach, from which anthropometrical data can be obtained.

ACKNOWLEDGMENTS

Ms. Susan Harty and Ms Sharon Clegg, Clinical Specialist Radiographers, Merlin Park Imaging Centre, Galway for their help attaining the CT scans. Dr. Stefan Lohfeld, National Centre for Biomedical Engineering Science, National University of Ireland, Galway for his help with the selective laser sintering machine. Mr. Raymond Quinn, Castlebar for his help with the moulding process.

REFERENCES

1 **Pickhardt PJ**, Asher DB. Wall thickening of the gastric antrum as a normal finding: multidetector CT with cadaveric comparison. *AJR Am J Roentgenol* 2003; **181**: 973-979
2 **Komaki S**. Normal or benign gastric wall thickening demonstrated by computed tomography. *J Comput Assist Tomogr* 1982; **6**: 1103-1107
3 **Gossios KJ**, Tsianos EV, Demou LL, Tatsis CK, Papakostas VP, Masalas CN, Merkouropoulos MC, Kontogiannis DS. Use of water or air as oral contrast media for computed tomographic study of the gastric wall: comparison of the two techniques. *Gastrointest Radiol* 1991; **16**: 293-297
4 **Scatarige JC**, DiSantis DJ. CT of the stomach and duodenum. *Radiol Clin North Am* 1989; **27**: 687-706
5 **Schwizer W**, Steingötter A, Fox M, Zur T, Thumshirn M, Bösiger P, Fried M. Non-invasive measurement of gastric accommodation in humans. *Gut* 2002; **51** Suppl 1: i59-i62
6 **Kim DY**, Camilleri M, Murray JA, Stephens DA, Levine JA, Burton DD. Is there a role for gastric accommodation and satiety in asymptomatic obese people? *Obes Res* 2001; **9**: 655-661
7 **O'Flynn PM**, Roche ET, Pandit AS. Generating an ex vivo vascular model. *ASAIO J* 2005; **51**: 426-433
8 **Ryan G**, Pandit A, Apatsidis DP. Fabrication methods of porous metals for use in orthopaedic applications. *Biomaterials* 2006; **27**: 2651-2670
9 **Johnson T**, van Noort R, Stokes CW. Surface analysis of porcelain fused to metal systems. *Dent Mater* 2006; **22**: 330-337
10 **Egorov VI**, Schastlivtsev IV, Prut EV, Baranov AO, Turusov RA. Mechanical properties of the human gastrointestinal tract. *J Biomech* 2002; **35**: 1417-1425
11 **Gregersen H**, Gilja OH, Hausken T, Heimdal A, Gao C, Matre K, Ødegaard S, Berstad A. Mechanical properties in the human gastric antrum using B-mode ultrasonography and antral distension. *Am J Physiol Gastrointest Liver Physiol* 2002; **283**: G368-G375
12 **Distrutti E**, Azpiroz F, Soldevilla A, Malagelada JR. Gastric wall tension determines perception of gastric distention. *Gastroenterology* 1999; **116**: 1035-1042
13 **Kuiken SD**, Samsom M, Camilleri M, Mullan BP, Burton DD, Kost LJ, Hardyman TJ, Brinkmann BH, O'Connor MK. Development of a test to measure gastric accommodation in humans. *Am J Physiol* 1999; **277**: G1217-G1221
14 **Huh CH**, Bhutani MS, Farfán EB, Bolch WE. Individual variations in mucosa and total wall thickness in the stomach and rectum assessed *via* endoscopic ultrasound. *Physiol Meas* 2003; **24**: N15-N22
15 **Sarnelli G**, Vos R, Cuomo R, Janssens J, Tack J. Reproducibility of gastric barostat studies in healthy controls and in dyspeptic patients. *Am J Gastroenterol* 2001; **96**: 1047-1053
16 **Mundt MW**, Hausken T, Samsom M. Effect of intragastric barostat bag on proximal and distal gastric accommodation in response to liquid meal. *Am J Physiol Gastrointest Liver Physiol* 2002; **283**: G681-G686
17 **Bouras EP**, Delgado-Aros S, Camilleri M, Castillo EJ, Burton DD, Thomforde GM, Chial HJ. SPECT imaging of the stomach: comparison with barostat, and effects of sex, age, body mass index, and fundoplication. Single photon emission computed tomography. *Gut* 2002; **51**: 781-786
18 **De Schepper HU**, Cremonini F, Chitkara D, Camilleri M. Assessment of gastric accommodation: overview and evaluation of current methods. *Neurogastroenterol Motil* 2004; **16**: 275-285
19 **Gilja OH**, Lunding J, Hausken T, Gregersen H. Gastric accommodation assessed by ultrasonography. *World J Gastroenterol* 2006; **12**: 2825-2829
20 **Lee KJ**, Vos R, Janssens J, Tack J. Differences in the sensorimotor response to distension between the proximal and distal stomach in humans. *Gut* 2004; **53**: 938-943

S- Editor Liu Y **L- Editor** MC Govern **E- Editor** Che YB

PO Box 2345, Beijing 100023, China
www.wjgnet.com
wjg@wjgnet.com

World J Gastroenterol 2007 March 7; 13(9): 1378-1383
World Journal of Gastroenterology ISSN 1007-9327

TOPIC HIGHLIGHT

Hans Gregersen, Professor, *Series Editor*

Anatomically realistic multiscale models of normal and abnormal gastrointestinal electrical activity

Leo K Cheng, Rie Komuro, Travis M Austin, Martin L Buist, Andrew J Pullan

Leo K Cheng, Rie Komuro, Travis M Austin, Andrew J Pullan, Bioengineering Institute, The University of Auckland, Private Bag 92019, Auckland 1142, New Zealand
Martin L Buist, Division of Bioengineering, National University of Singapore, Singapore
Andrew J Pullan, Department of Engineering Science, The University of Auckland
Supported in part by NIH grant R01 DK64775
Co-correspondence to: Andrew J Pullan
Correspondence to: Leo K Cheng, Bioengineering Institute, The University of Auckland, Private Bag 92019, Auckland 1142, New Zealand. l.cheng@auckland.ac.nz
Telephone: +64-9-3737599-83013 Fax: +64-9-3677157
Received: 2006-12-09 Accepted: 2007-01-10

Abstract

One of the major aims of the International Union of Physiological Sciences (IUPS) Physiome Project is to develop multiscale mathematical and computer models that can be used to help understand human health. We present here a small facet of this broad plan that applies to the gastrointestinal system. Specifically, we present an anatomically and physiologically based modelling framework that is capable of simulating normal and pathological electrical activity within the stomach and small intestine. The continuum models used within this framework have been created using anatomical information derived from common medical imaging modalities and data from the Visible Human Project. These models explicitly incorporate the various smooth muscle layers and networks of interstitial cells of Cajal (ICC) that are known to exist within the walls of the stomach and small bowel. Electrical activity within individual ICCs and smooth muscle cells is simulated using a previously published simplified representation of the cell level electrical activity. This simulated cell level activity is incorporated into a bidomain representation of the tissue, allowing electrical activity of the entire stomach or intestine to be simulated in the anatomically derived models. This electrical modelling framework successfully replicates many of the qualitative features of the slow wave activity within the stomach and intestine and has also been used to investigate activity associated with functional uncoupling of the stomach.

Key words: Model; Bidomain; Simulation; Interstitial cells of Cajal; Physiome; GIOME

Cheng LK, Komuro R, Austin TM, Buist ML, Pullan AJ. Anatomically realistic multiscale models of normal and abnormal gastrointestinal electrical activity. *World J Gastroenterol* 2007; 13(9): 1378-1383

http://www.wjgnet.com/1007-9327/13/1378.asp

INTRODUCTION

The concept of a "Physiome Project" was presented in a report from the Commission on Bioengineering in Physiology to the International Union of Physiological Sciences (IUPS) Council at the 32nd World Congress in Glasgow in 1993. In 2001, this project was designated as a major focus of the IUPS for the next decade. The long term goal of this project is to understand and describe the human organism, its physiology and its pathophysiology. One of the major aims of the overall Physiome concept is to develop multiscale mathematical and computer models that can be used to help understand human health. Since the beginning, momentum has continued in the Physiome project, with much effort focused on the heart and associated Cardiome project. In contrast, the gastrointestinal Physiome project (the GIOME) is still in its infancy. However, GIOME related activities are beginning to appear at several research centres, as highlighted in this issue.

In this paper we present an integrated biophysically based modelling framework for the gastrointestinal system, which is being used to examine electrical activity within the stomach and small bowel. Much of this work parallels work carried out in the Cardiome project, although there are clear anatomical and physiological deviations.

In the human stomach, there is rhythmic electrical activity with a normal frequency of approximately 3 cycles/min (cpm; termed "slow wave activity"). Similar electrical activity exists within the human small intestine although the frequency varies between 8 and 12 cpm, depending on the distance from the pylorus. It is now widely accepted that slow wave activity is a spontaneous event that arises in the interstitial cells of Cajal (ICCs), and is then conducted to the surrounding smooth muscle. Once the electrical activity reaches the smooth muscle, a further excitable event may occur. This event, recently

termed an action potential and historically referred to as "spiking behaviour" or "electrical response activity", is responsible for the major contraction of smooth muscle.

Our understanding of gastrointestinal electrical activity is still in its infancy when compared to that of other muscles, most notably the heart. In the cardiac area, for instance, there exist several anatomically realistic and biophysically detailed multiscale modelling studies[1]. In contrast, only in the last few years have modelling studies of gastric slow waves been performed using anatomically based models[2-4]. Before 2002, most gastrointestinal models were designed to capture the general behaviour of the slow wave in simplified geometries, such as simplified conoid or ellipsoid geometry[5-8]. Anatomically-based models have now been used to investigate normal slow wave rhythm, functional uncoupling, and associated electromagnetic activity. Besides geometric models based on the Visual Human Project, geometric models have also been derived from computed tomography (CT) images, allowing an investigation of patient-specific geometries and their effects on the simulated results. For all of these geometric models, a continuum level description of electrical behaviour that is based on the work of Aliev[9] has been employed.

Presented below is a brief description of our anatomically and physiologically based multiscale models of the human stomach and small intestine. Following this, we present some of the results obtained to date using these models. Initially, normal slow wave activity was simulated and, as far as possible, compared and contrasted to what is currently known about slow wave activity. The models have also been used to investigate abnormal activity such as functional uncoupling. These simulations illustrate the versatility of the modelling framework being developed.

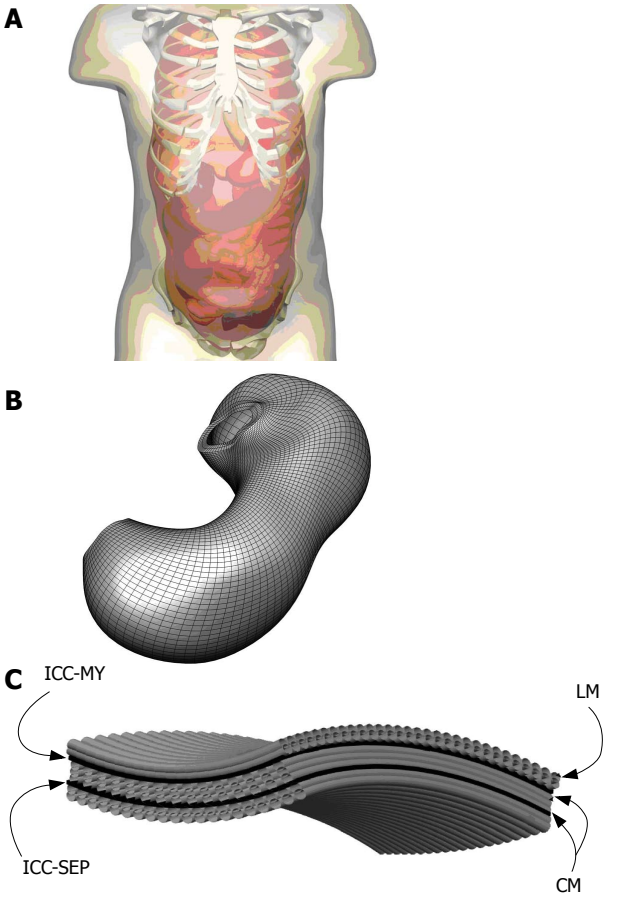

Figure 1 Shown above in (**A**) is the skin surface enclosing the esophageous, stomach, small and large intestines and a portion of the skeletal system where the components of the digestive system were created from digitized images from the visible man project. Shown in (**B**) is an enlarged view of the stomach with a high resolution mesh created over the finite elements that define the stomach geometry and (**C**) is an enlarged view of layers and muscle fibers on that stomach. Specifically modelled are the longitudinal (LM) and circular muscle (CM) layers separated by the ICC-MY (myenteric) and ICC-SEP (septa) layers.

ANATOMICALLY REALISTIC MODELS

An initial model of the human gastrointestinal system has been created from photographic slices from the Visible Human data set[10]. Details of the model development were described in Pullan *et al*[1]. In brief, the components of the gastrointestinal system were digitized from the images, creating over 60 000 data points. From these digitized points, surface and volume meshes of the stomach and intestine were fitted to sub-millimetre accuracy. An illustration of this model is given in Figure 1, together with an enlarged view of the components of the gastric model. Specifically represented are the longitudinal and circular smooth muscle layers (LM and CM respectively), with appropriate fibre orientations, separated by the layers of ICCs, which are the myenteric layer (ICC-MY) and the septa layer (ICC-SEP).

Further geometric models have been developed using CT images acquired from normal human subjects and porcine Magnetic Resonance Images (MRI) (Figure 2). To improve the contrast in the CT images, the human subjects ingested 16 ounces of oral contrast (containing 10 g hypaque sodium powder, Amersham Health) over a period of 90 min prior to the abdominal spiral CT scan. For the animal MRI scans, axial, coronal and saggital T2-weighted images were obtained. As with the models constructed from the Visible Human data set, the images were manually digitized and then geometric models were fitted to these data. Shown in Figure 3 are four different examples of human stomach models that have been created from CT images. This figure illustrates the large variability in stomach location and size among different subjects.

CONTINUUM BASED MODELLING

A continuum modelling approach was used to simulate the electrical activity of the stomach and intestine. The bidomain model, widely used in simulations of cardiac electrical activity[11,12], was used to represent the transmembrane and extracellular potentials in the active tissues of the stomach and intestine. These equations are summarised in Equations 1 and 2:

$$\nabla \cdot (\sigma_i \nabla V_m) + \nabla \cdot (\sigma_i \nabla \varphi_e) = A_m \left(C_m \frac{\partial V_m}{\partial t} + I_{ion} \right) \quad (1)$$

$$\nabla \cdot ((\sigma_i + \sigma_e) \nabla \varphi_e) = -\nabla (\sigma_i \nabla V_m) \quad (2)$$

where the i and e subscripts represent properties of the intracellular and extracellular domains respectively. The σ terms are tissue conductivities (which in general will

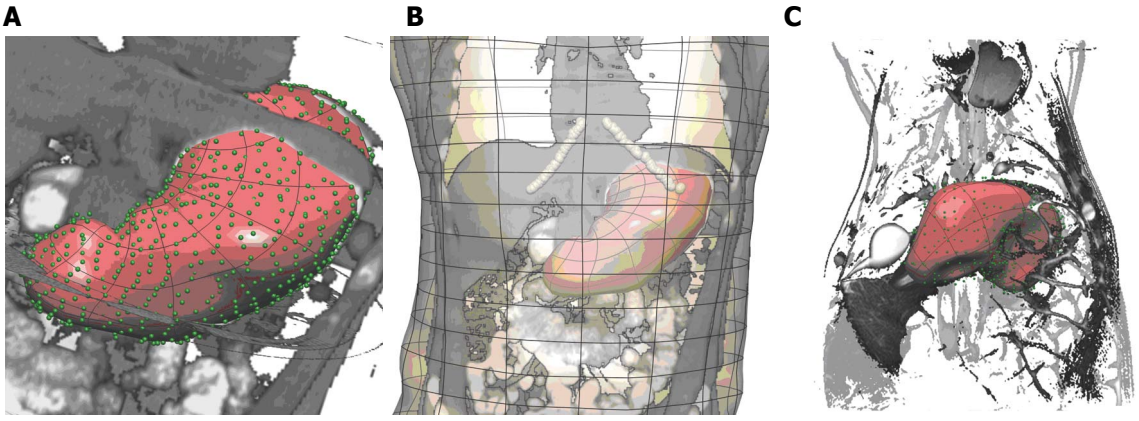

Figure 2 Gastric geometric models of a normal human (A and B) and pig (C). **A**: Enlarged view of human stomach surface with green points showing the digitized points of the stomach, overlaid with a CT image; **B**: the fitted stomach and skin surfaces with a CT image overlaid. The costal margin is outlined by the white interconnected points. **C**: Anterior view of a pig stomach created from MR images. Shown are the digitised points corresponding to the stomach (green points), the stomach surface (transparent surface) as well as a coronal MR image from which the model was created.

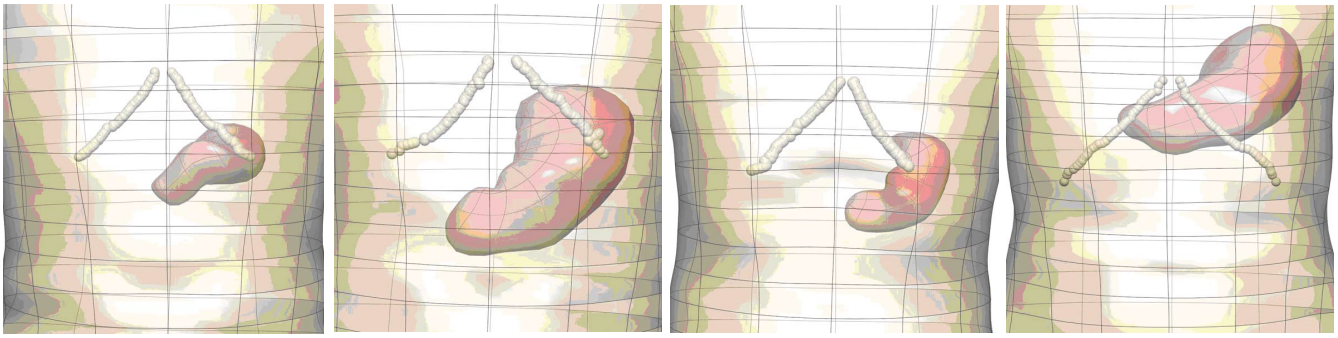

Figure 3 Anterior views of models of stomachs created from CT images acquired from 4 different human volunteers, illustrating some of the high degree of anatomical variability. Shown are the stomach (red surfaces), skin (transparent surface) and the costal margin (white interconnected points).

be tensors), the φ terms are potentials, the V_m term is the transmembrane potential (the potential difference across the cell membrane), A_m is the surface to volume ratio of the membrane and C_m is the membrane capacitance. Individual cellular models are able to plug directly into these equations through the I_{ion} term in the first equation. At a fine scale, each cellular model is able to incorporate complex subcellular processes.

Using this geometric model, these equations are solved using either the finite element based finite difference method or the structured finite element method[12]. An illustration of a high resolution mesh that has been defined over the stomach geometry is shown in Figure 1B. A modified Fitzhugh-Nagumo (FHN) model[9,13] was used to model the electrical activity of the muscle cells and ICCs, since this currently appears to be the most advanced model that explicitly differentiates between the different cell types (ICCs and smooth muscle). The cellular equations are based on a normalised transmembrane potential, u, that varies from 0 to 1 and a single recovery variable, v. These equations are:

$$\frac{du}{dt} = ku(u-a)(1-u) - v \quad (3)$$

$$\frac{dv}{dt} = \varepsilon(\gamma(u-\beta) - v) \quad (4)$$

where k is the maximum membrane conductance, a is the normalized threshold potential, ε controls the excitability of the system, γ is the recovery rate constant and β is used to shift the cellular equilibrium from an excitatory to an oscillatory state. The smooth muscle and ICC layers were coupled through a scaled potential gradient with a diffusion coefficient of 0.03.

Outside the active tissues of the gastrointestinal tract, a generalized Laplace's equation describes the current flows within the passive tissue regions,

$$\nabla \cdot (\sigma_o \nabla \varphi_o) = 0 \quad (5)$$

Here the o subscripts denote quantities outside the active region. The extracellular domain described by Equation 2 above is directly coupled to the external passive regions (governed by Equation 5) through continuity of potentials and currents. Using this equation set, the resultant electrical activity within, on and surrounding the active tissues of the stomach and small bowel can be determined from the (continuum) cellular level activity.

SIMULATIONS OF GASTRIC ELECTRICAL ACTIVITY

Normal slow wave activity

Normal slow wave activity in the stomach and intestine has previously been simulated using the Visible Human

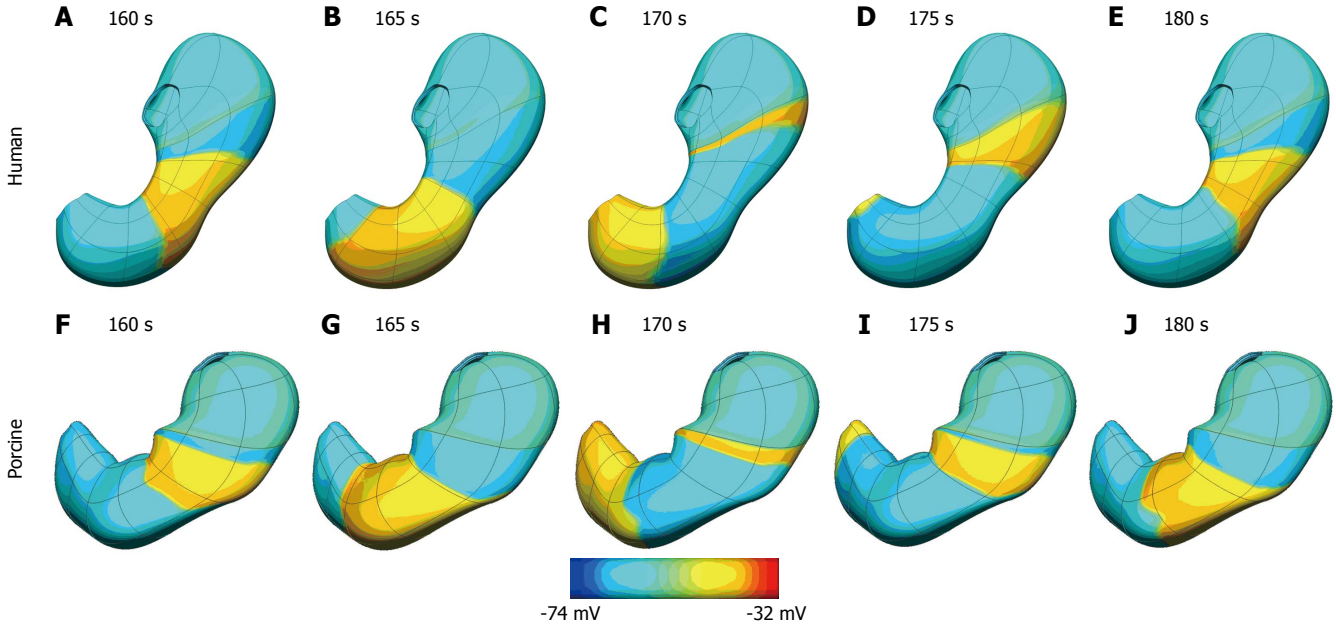

Figure 4 Simulation results at five second intervals showing gastric slow wave activity wave in a human (**A-E**) and porcine (**F-J**) stomach. The human stomach has a dominant frequency of 3.0 cpm while the porcine model has a dominant frequency of 3.7 cpm. Shown above is the transmembrane potential distribution on the outer surface of the stomach coloured by the scale bar below the images.

Table 1 Summary of simulated gastric model parameters compared to published values that have been determined experimentally

Source	[14]	[15]	[16]	[17]	Model
Species	Hound dogs	Mongrel dogs	Human	Mongrel dogs	Human
Frequency (cpm)	4-6	1.58-1.88	2.68-3.28	N/A	3
Duration (s)	N/A	6.8-8.5	N/A	Submucosal cells: 4.4-5.6 Myenteric cells: 6.1-6.5	7.9
Propagation velocity (mm/s)	N/A	Circular muscle: 16.6-19.2	Corpus: 2.2 Antrum: 6.8	Circular muscle (fibre): 15.5-29.9 Circular muscle (cross fibre): 5.8-16.6	Antrum: LM: 16.9 CM1: 12.5 CM2: 10.7

Note the results from Horiguchi *et al*[16] are indirect measurements while the other sources are direct tissue measurements and results from Xu *et al*[15] correspond to isolated tissue strips. In the model results, LM is the outer longitudinal muscle layer, CM1 is the middle circular muscle layer and CM2 is the inner circular muscle layer.

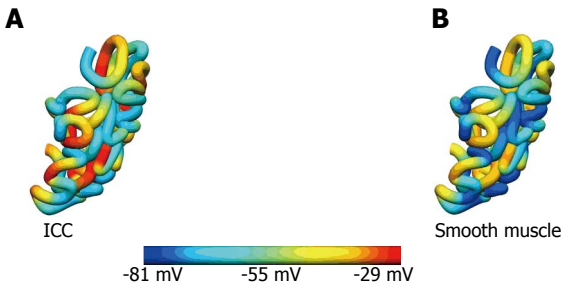

Figure 5 Slow wave intestinal activity. Shown are the transmembrane potentials from the (**A**) ICC and (**B**) smooth muscle layers at a particular time instance.

model[3,4,14]. The gastric computational model had a total of 432 nodes, 320 elements and 566 656 grid points with average spatial resolutions (distance between grid points) of 1.06 mm (circumferentially), 0.84 mm [longitudinally] and 0.33 mm (transmurally). The intestinal model had an average spatial resolution of 0.95 mm down the entire length. These length scales were small enough to provide close to a converged solution to the governing equations while remaining computationally feasible to solve. The parameters in the cellular equations (Equation 3 and 4) were chosen to match published serosal recordings. Illustrative examples of normal gastric and intestinal slow wave activity are given in Figures 4A-E and 5 respectively.

From these simulations, conduction velocities and other parameters were computed and compared to experimental observations. A summary of these comparisons for the stomach is given in Table 1, and for the intestine in Table 2.

Normal gastric activity has also been simulated on the porcine stomach model (shown previously in Figure 2C). In this case the model has a dominant frequency of 3.7

Table 2 Summary of simulated intestinal model parameters compared to published values that have been determined experimentally

	Experimental data (Canine)			Model		
	Frequency (cpm)	Conduction velocity (cm/s)	Wavelength (cm)	Frequency (cpm)	Conduction velocity (cm/s)	Wavelength (cm)
Duodenum	17.4	10.0	36.4	17.4	10.30	34.0
Jejunum	16.0	7.11	25.0	15.4	6.50	26.6
Ileum	12.2	1.22	3.7	9.9	1.65	8.2

Experimental data from Bauer *et al*[18].

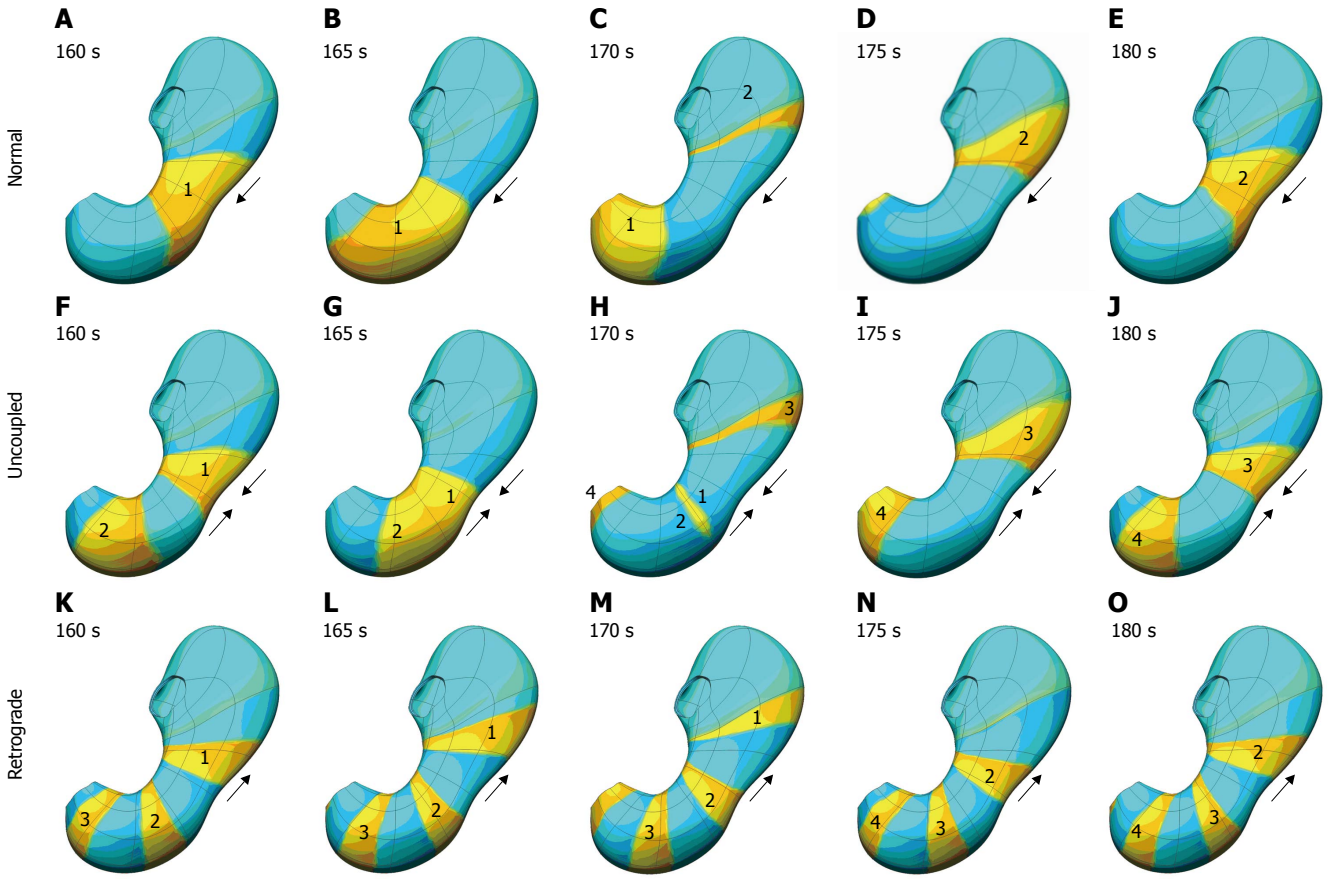

Figure 6 Top row (**A-E**) shows normal slow wave activity at 5 second interval. In this case the antrum is entrained by the slow wave activity originating in the corpus, is shown. In the second row (**F-J**), the corpus and antrum maintain the same frequency of slow wave activity, but in this situation, the antrum is not being entrained by the activity of the corpus. The bottom row (**K-O**) illustrates what happens when the intrinsic frequency of the antrum exceeds that of the corpus, resulting in some retrograde slow wave behaviour.

cpm, which is within the expected experiment range of 3-4.5 cpm. This activity is shown graphically in Figure 4F-J.

Functionally uncoupled activity

In a normal stomach, slow waves originate from dominant pacemakers along the greater curvature in the mid-corpus and spread aborally through the antrum to the pyloric sphincter. The pacemaker region in the corpus is dominant in the stomach because it generates slow waves at the highest frequency. With a breakdown in the ICC network, as can occur for instance in diabetes[20], regions of ICC-MY within the gastric network can become uncoupled from the dominant pacemaker, and the synchronised spread of electrical activity from corpus to pylorus is disrupted. In such a situation, ICC-MY within the antral region may become local pacemakers, and electrical slow waves may be generated in ectopic sites. An increase in the intrinsic frequency of antral pacemakers can lead to functional uncoupling and ectopic pacemaking. This can result in collisions between slow waves propagating from ectopic sites and the normal pacemaker site, disrupting gastric peristalsis and delaying gastric emptying (gastroparesis).

To simulate this phenomenon, the excitability parameter, ε, was defined to be spatially varying. Under normal conditions, the ICC excitability was at a maximum in the proximal corpus on the greater curvature, decreasing slightly circumferentially and more prominently longitudinally[3,21]. By altering the ICC excitability profile, functionally uncoupled activity was generated. Figure 6 shows some of the different types of functionally uncoupled behaviour that can arise. Figure 6A-E shows normal slow wave activity in which the antrum is entrained

by the slow wave activity originating in the corpus. In Figure 6F-J, the corpus and antrum maintain the same frequency of slow wave activity, but in this situation the antrum is not being entrained by the activity of the corpus. Figure 6K-O illustrates what happens when the intrinsic frequency of the antrum exceeds that of the corpus, resulting in retrograde slow wave behaviour.

CONCLUSION

We have presented an extensible anatomically and biophysically based modelling framework that can be used to investigate the electrical activity of the stomach and small intestine. While still in its infancy, the electrical modelling framework has successfully replicated many of the features of the slow wave activity within the stomach and intestine. It has also being used to investigate activity associated with functional uncoupling of the stomach. We are currently exploring wider applicability of the method so that it can be used, for example, in investigating the response to electrical stimuli that are used within gastric electrical stimulation[22,23].

There is much work that still needs to be done, including further validation and refinement of the existing model. In terms of validation, there are a number of avenues that can be explored to aid in this endeavour. These include directly comparing simulated extracellular potentials against high-resolution *in vivo* measurements of extracellular potentials in the stomach and intestine walls. Experiments of this nature have recently been performed by Ver Donck *et al*[24]. Additionally, electrical activity within the organs and the magnetic activity arising from this can be computed at and above the body surface and compared to non-invasive EGG and MGG recordings such as those obtained by Bradshaw *et al*[25]. We are currently working with various experimental groups to acquire such electrical and magnetic data so that we can continue to enhance and extend our model.

ACKNOWLEDGMENTS

The authors would also like to greatly acknowledge the input of Anita Lin and Rita Yassi in some of the earlier modelling work, the assistance of Phillip Williams, L Alan Bradshaw and William O Richards from Vanderbilt University and Jiande Chen from the University of Texas Medical Branch.

REFERENCES

1 **Pullan AJ**, Buist ML, Cheng LK. Mathematically Modelling the Electrical Activity of the Heart: From Cell to Body Surface and Back Again. New Jersey: World Scientific, 2005
2 **Pullan A**, Cheng L, Yassi R, Buist M. Modelling gastrointestinal bioelectric activity. *Prog Biophys Mol Biol* 2004; **85**: 523-550
3 **Buist ML**, Cheng LK, Yassi R, Bradshaw LA, Richards WO, Pullan AJ. An anatomical model of the gastric system for producing bioelectric and biomagnetic fields. *Physiol Meas* 2004; **25**: 849-861
4 **Lin AS**, Buist ML, Cheng LK, Smith NP, Pullan AJ. Computational simulations of the human magneto- and electroenterogram. *Ann Biomed Eng* 2006; **34**: 1322-1331
5 **Liang J**, Chen JD. What can be measured from surface electrogastrography. Computer simulations. *Dig Dis Sci* 1997; **42**: 1331-1343
6 **Mirizzi N**, Stella R, Scafoglieri U. Model to simulate the gastric electrical control and response activity on the stomach wall and on the abdominal surface. *Med Biol Eng Comput* 1986; **24**: 157-163
7 **Mintchev MP**, Bowes KL. Computer simulation of the effect of changing abdominal thickness on the electrogastrogram. *Med Eng Phys* 1998; **20**: 177-181
8 **Irimia A**, Bradshaw LA. Ellipsoidal electrogastrographic forward modelling. *Phys Med Biol* 2005; **5**0: 4429-4444
9 **Aliev RR**, Richards W, Wikswo JP. A simple nonlinear model of electrical activity in the intestine. *J Theor Biol* 2000; **204**: 21-28
10 **Spitzer V**, Ackerman MJ, Scherzinger AL, Whitlock D. The visible human male: a technical report. *J Am Med Inform Assoc* 1996; **3**: 118-130
11 **Plonsey R**, Barr RC. Mathematical modeling of electrical activity of the heart. *J Electrocardiol* 1987; **20**: 219-226
12 **Buist M**, Sands G, Hunter P, Pullan A. A deformable finite element derived finite difference method for cardiac activation problems. *Ann Biomed Eng* 2003; **31**: 577-588
13 **Fitzhugh R**. Impulses and Physiological States in Theoretical Models of Nerve Membrane. *Biophys J* 1961; **1**: 445-466
14 **Lin AS**, Buist ML, Smith NP, Pullan AJ. Modelling slow wave activity in the small intestine. *J Theor Biol* 2006; **242**: 356-362
15 **Xu X**, Wang Z, Hayes J, Chen JD. Is there a one-to-one correlation between gastric emptying of liquids and gastric myoelectrical or motor activity in dogs? *Dig Dis Sci* 2002; **47**: 365-372
16 **Horiguchi K**, Semple GS, Sanders KM, Ward SM. Distribution of pacemaker function through the tunica muscularis of the canine gastric antrum. *J Physiol* 2001; **537**: 237-250
17 **Familoni BO**, Abell TL, Bowes KL. A model of gastric electrical activity in health and disease. *IEEE Trans Biomed Eng* 1995; **42**: 647-657
18 **Bauer AJ**, Publicover NG, Sanders KM. Origin and spread of slow waves in canine gastric antral circular muscle. *Am J Physiol* 1985; **249**: G800-G806
19 **Lammers WJ**, Ver Donck L, Schuurkes JA, Stephen B. Peripheral pacemakers and patterns of slow wave propagation in the canine small intestine *in vivo*. *Can J Physiol Pharmacol* 2005; **83**: 1031-1043
20 **Ordög T**, Takayama I, Cheung WK, Ward SM, Sanders KM. Remodeling of networks of interstitial cells of Cajal in a murine model of diabetic gastroparesis. *Diabetes* 2000; **49**: 1731-1739
21 **Buist ML**, Cheng LK, Sanders KM, Pullan AJ. Multiscale modelling of human gastric electric activity: can the electrogastrogram detect functional electrical uncoupling? *Exp Physiol* 2006; **91**: 383-390
22 **Cigaina V**. Gastric pacing as therapy for morbid obesity: preliminary results. *Obes Surg* 2002; **12** Suppl 1: 12S-16S
23 **D'Argent J**. Gastric electrical stimulation as therapy of morbid obesity: preliminary results from the French study. *Obes Surg* 2002; **12** Suppl 1: 21S-25S
24 **Ver Donck L**, Lammers WJ, Moreaux B, Smets D, Voeten J, Vekemans J, Schuurkes JA, Coulie B. Mapping slow waves and spikes in chronically instrumented conscious dogs: implantation techniques and recordings. *Med Biol Eng Comput* 2006; **44**: 170-178
25 **Bradshaw LA**, Irimia A, Sims JA, Gallucci MR, Palmer RL, Richards WO. Biomagnetic characterization of spatiotemporal parameters of the gastric slow wave. *Neurogastroenterol Motil* 2006; **18**: 619-631

S- Editor Liu Y **L- Editor** Lutze M **E- Editor** Che YB

PO Box 2345, Beijing 100023, China
www.wjgnet.com
wjg@wjgnet.com

World J Gastroenterol 2007 March 7; 13(9): 1384-1392
World Journal of Gastroenterology ISSN 1007-9327

TOPIC HIGHLIGHTS

Hans Gregersen, Professor, *Series Editor*

On the mechanical behavior of the human biliary system

Xiaoyu Luo, Wenguang Li, Nigel Bird, Swee Boon Chin, NA Hill, Alan G Johnson

Xiaoyu Luo, NA Hill, Department of Mathematics, University of Glasgow, Glasgow, G12 8QW, United Kingdom
Wenguang Li, Swee Boon Chin, Department of Mechanical Engineering, University of Sheffield, Sheffield, S1 3JD, United Kingdom
Nigel Bird, Alan G Johnson, Academic Surgical Unit, Royal Hallamshire Hospital, Sheffield, S10 2JF, United Kingdom
Correspondence to: Dr. Xiaoyu Luo, Department of Mathematics, University of Glasgow, Glasgow, G12 8QW, United Kingdom. x.y.luo@maths.gla.ac.uk
Telephone: +44-141-3304746 Fax: +44-141-3304111
Received: 2006-12-11 Accepted: 2007-02-06

Abstract

This paper reviews the progress made in understanding the mechanical behaviour of the biliary system. Gallstones and diseases of the biliary tract affect more than 10% of the adult population. The complications of gallstones, i.e. acute pancreatitis and obstructive jandice, can be lethal, and patients with acalculous gallbladder pain often pose diagnostic difficulties and undergo repeated ultrasound scans and oral cholecystograms. Moreover, surgery to remove the gallbladder in these patients, in an attempt to relieve the symptoms, gives variable results. Extensive research has been carried out to understand the physiological and pathological functions of the biliary system, but the mechanism of the pathogenesis of gallstones and pain production still remain poorly understood. It is believed that the mechanical factors play an essential role in the mechanisms of the gallstone formation and biliary diseases. However, despite the extensive literature in clinical studies, only limited work has been carried out to study the biliary system from the mechanical point of view. In this paper, we discuss the state of art knowledge of the fluid dynamics of bile flow in the biliary tract, the solid mechanics of the gallbladder and bile ducts, recent mathematical and numerical modelling of the system, and finally the future challenges in the area.

Key words: Fluid dynamics; Gallstone; Bile flow; Cystic duct; Gallbladder; Soft tissue mechanics; Acalculous biliary pain; Stress; Mechanical factors

Luo X, Li W, Bird N, Chin SB, Hill NA, Johnson AG. On the mechanical behaviour of human biliary systems. *World J Gastroenterol* 2007; 13(9): 1384-1392

http://www.wjgnet.com/1007-9327/13/1384.asp

INTRODUCTION

The human biliary system consists of the gallbladder, the cystic duct, common bile duct and the sphincter of Oddi. The gallbladder is a thin-walled, pear-shaped sac and generally measures 7-10 cm in length and about 3 cm in width. This muscular sac is located in a fossa in the posterior of the right lobe of the liver. The average storage capacity of a gallbladder is about 20-30 mL. Bile, the liquid that flows in the biliary system, is composed of three major components: cholesterol, bile salts, and bilirubin. When the gallbladder is not functioning properly, the components of the bile are supersaturated leading to the formation of solid crystals, called gallstones.

Archaeologists have found human gallstones originating from the 17th century B C in Mycenae, Greece which suggests that mankind has been suffering from this disease for at least 4000 years[1]. Cholecystectomy is the most commonly performed abdominal operation in the West, with some 60 000 operations performed in England and Wales every year[2] at a cost to the National Health Service (NHS) of approximately £60 million[3]. However, not all the operations provided an effective cure; in 50% of acalculous diseases, patients complained about the recurrence of the symptoms[4]. Therefore, understanding the mechanisms of gallstone diseases is essential for better diagnosis and treatments of these diseases.

The earliest attempts to understand gallstone formation focused on phenomena occurring within the gallbladder. Cholesterol gallstone formation depends upon two conditions: (1) cholesterol crystal nucleation; (2) cholesterol crystal growth. The necessary physical-chemical factor for crystal nucleation or growth is cholesterol super-saturation in bile[5-8]. Bile stasis may cause cholesterol super-saturation and allow the formation of cholesterol stones[9]. Additional studies have shown that hyper-secretion of gallbladder mucus is also an important factor in gallstone formation by accelerating cholesterol nucleation[10-12]. It has also been found that increased glycoproteins in bile precede cholesterol saturation and crystallization[13].

The gallbladder is able to react to the stimulus of eating by contracting and discharging bile into the duodenum.

Currently the gallbladder is regarded as a 'slow pump', where emptying or refilling is concerned; its volume change is related to the pressure inside the gallbladder and its compliance[14-16]. This relationship is often assumed to be linear[14], but more recently it has been described as a 'bellows' plus pump, in which emptying and refilling alternates[9,17]. Cholecystokinin (CCK), a chemical stimulus, not only causes the gallbladder to contract but also allows the cystic duct[18] and sometimes the common bile duct[19] to contract. Thus, an injection of CCK is often used to study gallbladder motor function *in vivo*.

Poor gallbladder motor function can lead to abnormal gallbladder emptying and is believed to contribute to bile stasis and hence gallstone formation. Many studies have shown that gallbladder emptying is abnormal in patients with gallstones[20-31]. In addition, it has been observed that cystic duct flow resistance is increased before gallstone formation[32,33].

All these studies suggest that the mechanics of the bile duct and flow within it play an important role in bile stasis and gallstone formation. From a mechanical point of view, the biliary system can be considered to be a pump-pipe system, where the gallbladder provides the driving pressure, and the flow rate of the bile going through the ducts depends on the resistance as well as the pressure drop between the gallbladder and the downstream end of the common bile duct. In this sense, gallbladder motor function is closely related to the pressure drop, flow rate and the flow resistance in the biliary system. For a given pressure drop, if the flow resistance of the system is higher, then a smaller volume of bile will be driven out of the gallbladder during emptying. Thus the principal areas of interest are mechanical details, such as flow rate, pressure drop and resistance of the biliary system which are related to the geometry of the gallbladder and the ducts. Bile flow in the biliary system is governed not only by the fluid dynamics but also by the solid mechanics, since it is the interaction between the bile flow and soft tissue deformation which determines the characteristics of the system. In addition, it is important to identify which geometric parameters, material properties, or external stimuli have the most significant influence on the system behaviour. It is the purpose of this paper to review the current studies of the mechanical aspects of the biliary system, and their relationship with gallbladder diseases, in particular, gallstones.

THE ROLE OF BILE FLUID DYNAMICS

Bile rheology

Bile rheology, the study of bile viscosity, is of interest in any consideration of the mechanics of bile flow, since it contributes directly to the flow resistance in the biliary tract. Experimental measurements showed that the density of gallbladder bile is very close to that of water, i.e. 1000 kg/m^3, at room temperature[34]. However, the viscosity of bile is very different to that of water (which is constant at approximately 1 mPa.s) and it can change significantly in pathological situations.

Bouchier *et al*[35] reported that the dynamic viscosity of gallbladder bile is higher than that of hepatic bile and that viscosity is increased in pathological states[36]. Doty[37] suggested that this was due to the presence of mucus in gallbladders with stones. Jungst *et al*[38] also showed that the viscosity of bile was markedly higher in patients with cholesterol (5.0 mPa.s) and mixed stones (3.5 mPa.s) compared to that of hepatic bile (0.92 mPa.s). He also found a positive correlation between mucin and viscosity in gallbladder bile but not in hepatic bile.

Tera[39] found experimentally that normal gallbladder bile formed layers when left to stand. The dynamic viscosity of the top thinnest layer is 2.0 mPa.s, but that of the thickest layer is 2.2 mPa.s after allowing 2 h for sedimentation to take place[39]. Gottschalk and Lochner[40] measured postoperative bile viscosity, sampled by T-tube drainage of 29 patients with a modified horizontal capillary viscometer, from the day of operation to the 9th post-operative day and confirmed that the viscosity changes with time and the bile behaves like a visco-elastic Maxwell fluid (viscous-elastic fluid). Non-Newtonian shear-thinning behaviour was also observed using a Contraves Low Shear viscometer: the bile dynamic viscosity decreased from 5 mPa.s at a shear rate of 0.1 s^{-1} to 1.5 mPa.s at 2.0 s^{-1}[40]. Coene *et al*[41] reported that the bile viscosity of patients with gallstones varied as a function of shear rate, and that the bile dynamic viscosity decreased from 2.5 mPa. s at a shear rate of 0.1s^{-1} to 1.5 mPa.s at 100s^{-1}. These observations seem to indicate that the bile in gallbladder with gallstones has shear-thinning non-Newtonian behaviour at low shear rate. Ooi[34] measured the dynamic viscosity in fresh bile samples from 59 patients undergoing cholecystectomy and found the dynamic viscosity of gallbladder bile to be between 1.77-8.0 mPa.s for shear rates between 0.5 s^{-1}-75 s^{-1}[34]. He discovered that the bile in 20 subjects behaved like a Newtonian fluid, while in 22 subjects it showed shear-thinning at a low shear rate and then shear-thickening at a higher shear rate. In 8 subjects there was shear-thickening, but in 4 other subjects with mucus shear-thinning was observed. In general, the Newtonian bile seemed to be associated with normal subjects. Increased viscosity of gallbladder bile has been considered an important factor in the pathogenesis of gallstone disease[38].

It is clear that the bile viscosity can be subject-dependent even in normal physiological cases. In pathological cases, it can also vary between Newtonian, weakly non-Newtonian and strongly non-Newtonian behaviours. However, for healthy subjects, it may be reasonable to assume that bile is a Newtonian fluid. Indeed, this assumption has been widely used in modelling of cystic ducts[34,42-44].

Geometry of biliary duct and flow resistance

During gallbladder refilling and emptying in response to hormonal and neural stimuli[45], the bile flow passes through the cystic duct which connects the gallbladder and common bile duct, see Figure 1. Observations on the cystic duct anatomy have shown that the duct typically presents a combination of two types of structure: (1) in which the duct lumen wall may present the valve of Heister[46,47]; (2) the duct has a smooth lumen which

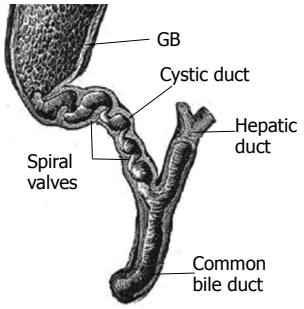

Figure 1 The geometry of the biliary tract, where the valves of Heister in the cystic duct are shown.

describes various geometries such as spiral, winding, kinks or spiral incorporating an M-shape loop *etc*[34,48]. Different cystic duct structures can significantly affect the pressure drop required to drive the same flow of bile through the system. Structure type (1), for example, offers much more flow resistance compared to type (2).

The relation between the cystic duct geometry and cholelithiasis has been investigated *in vivo*. Based on 250 patients with cholelithiasis and 250 healthy controls, Deenitchin *et al*[49] discovered that patients with gallstones have significantly longer and more narrow cystic ducts (of mean length 48 mm and diameter 4 mm) than those without stones (of mean length 28 mm and diameter 7 mm). The results suggest that flow resistance is affected by the cystic duct geometry, and may be associated with cholelithiasis.

Rodkiewicz *et al*[42], on examining the pressure drop across the biliary system of a dog, found that flow rate of bile, Q, in the biliary system tree (including the sphincter of Oddi) was related to the pressure drop, Δp, by a power law, i.e. $\Delta p^n \propto Q$, not the Poiseuille law commonly used for flow in a rigid straight tube which is $\Delta p \propto Q$. The power index n was in the range of 1.47-2.05. On the other hand, they found that the Poiseuille law was approximately valid when the bile flowed along a long, circular, smooth and rigid tube[42], which suggested that dog's bile is more or less a Newtonian fluid.

The key to a more accurate estimation of detailed flow resistance is the reconstruction of the biliary tract for each patient. 2D real-time ultrasonography and HIDA scintigraphy techniques have long been applied in gallbladder volume measurement and diagnosis of cholecystitis[50-52]. However, these can only give limited information on the 3D biliary tract. A 3D real-time ultrasonography technique is now being developed and has been applied to the measurement of gallbladder shape and volume[53]. The 3D spiral/helical computed tomography (CT) has also been involved in diagnosis of cholecystitis, since it not only shows the 3D images of the gallbladder but also of the whole biliary tract[54-60]. These techniques may in the future facilitate the development of specific models for measuring flow resistance.

Sphincter of Oddi

The sphincter of Oddi is located at the termination of the common bile duct and pancreatic duct. The human sphincter of Oddi segment is 6-15 mm in length and has a muscular structure. The physiological functions of sphincter of Oddi include: (1) regulating bile flow into the duodenum; (2) diverting hepatic bile into the gallbladder and (3) preventing reflux of duodenal contents from the duodenum into the biliary tree[61,62]. When CCK is released, it causes the gallbladder to contract and the sphincter of Oddi to relax allowing bile to empty. Coordination of gallbladder and sphincter of Oddi function may also be influenced by nerve bundles which connect the gallbladder and the sphincter of Oddi *via* the cystic duct[63,64]. The effect of enteric hormones on sphincter of Oddi motor function was determined by recording intraluminal pressure[65]. It was found that the human sphincter of Oddi demonstrated unique phasic contractions, which would have an important role in regulating biliary and pancreatic duct emptying[65]. Several studies on the opossum sphincter of Oddi showed that it regulates bile like a peristaltic pump at low common bile duct pressure and as a resistor at higher common bile duct pressures[66-68]. Funch-Jensen *et al*[69] observed that the CCK injection inhibited the activity of the sphincter of Oddi of dogs, thus as bile flow increased, the gallbladder pressure remained unchanged. Funch-Jensen[62] further argued that the peristaltic pump activity of the human sphincter of Oddi was probably less important since CCK inhibited the phasic wave of the sphincter.

The basal pressure of human sphincter of Oddi is affected by gallstone disease. Cicala *et al*[70] investigated motor activity of the sphincter in 155 patients, and found that gallstones are frequently associated with increased basal pressure, which might obstruct bile flow causing gallbladder stasis. The early work on pressure drop and flow resistance across dog biliary duct illustrated that the resistance of sphincter of Oddi is at least about 3 times higher than that of the cystic duct[71]. These results suggest the mechanical role for the sphincter of Oddi in the system can be significant. In fact, this may contribute to the reasons that the computational prediction of pressure drop in the cystic duct resistance is much lower than the clinically observed opening pressure during emptying[34].

THE ROLE OF SOLID MECHANICS

Mechanical properties of gallbladder muscles

The gallbladder contracts under the control of nervous and hormonal stimuli during the emptying process[64]. Contraction of the muscle fibre mesh generates a vector of force directed toward the centre of the gallbladder lumen. To model the muscle changes due to the contraction, a relationship which describes the muscle responses of a system to external forces is required. This important relationship is known as the constitutive relation, which allows us to predict the stress distribution within the muscle. Most of the current mechanical studies on gallbladder muscles have concentrated on the constitutive relations either in the form of the gallbladder volume-pressure relationship, or the length-tension relationship of a muscle strip.

The pressure-volume relation

The relationship between the volume change ΔV and the differential pressure Δp in the gallbladder can be

expressed as $\Delta V = C\Delta p$ (1), where C is the compliance of the gallbladder, which can be determined from *in vitro* or *in vivo* experiments.

The pressure-volume response of opossum was studied by Ryan and Cohen[14] under basal conditions and after a continuous intravenous infusion of gastrin I , secretin, and CCK. It was found that without stimulation, the gallbladder was capable of accommodating a volume increase with only slight changes in pressure whereas CCK significantly increased the pressure in the gallbladder. They found that the gallbladder compliance was about 0.77 mL/mmHg under basal conditions, but decreased to 0.38, and 0.34 mL/mmHg as CCK stimulation increased from 0.025 to 2.5 μg/kg.h. Schoetz *et al*[15] measured the dynamic pressure-volume relation of adult female baboons. Their results showed a hysteresis loop in the pressure-volume relation which was exacerbated by CCK stimulation. This suggests that the gallbladder muscle may behave as a visco-elastic material. However, the mean values they measured, with and without stimuli, were very close to that of Ryan and Cohen[14]. Middelfart *et al*[16] measured the pressure-volume relationship of the gallbladders in 11 patients with gallstones, in which the gallbladders were injected with saline *via* a McGaham catheter. It was found that the compliance varied from 0.17 to 4.0 mL/mmHg, and was highly subject dependent, with a mean value of about 2.66 mL/mmHg.

The length-tension relation

Since the gallbladder consists of a layer of smooth muscle, it is subject to both active and passive tensions during emptying. The active tension is generated by hormonal stimuli, and the passive tension is caused by stretch of the muscle. The constitutive equation between the active force and length variation in the gallbladder has been studied in strips of gallbladder using uni-axial experiments. Although the response of the smooth muscle to the hormone should vary with time, currently all studies assumed that the length-tension relation in gallbladder is time-independent.

Mack and Todd[72] studied 50 strips from 25 human gallbladders obtained at operation. They found that the human gallbladder muscle was capable of maintained tone *in vitro* and that peak tension could be achieved within 3-5 min following hormonal stimulation. Unfortunately, they did not measure the quantitative relation between length and tension, therefore no constitutive equation for these studies could be established.

Washabau *et al*[73] used gallbladder muscle strips from mature female guinea pigs to measure the isometric stress stimulated with either 10-8 to 10-4M acetyl choline or 10-80 mmol/L KCl stimulations. The passive tension increased with the length ratio L/L_0 (where L is the deformed length, and L_0 is the initial length). The active tension was found to achieve its maximal value at L_0, and declined afterward, although the total tension (active + passive) rose with L/L_0. Bird *et al*[74] measured the tension of muscle strips from human gallbladder removed at cholecystectomy. They found no differences for samples taken from the longitudinal, circular and oblique planes. However, the samples taken from the gallbladder body region contracted more forcefully than those from the gallbladder neck region. Strips from the body region were also more sensitive to muscarinic stimulation. They did not measure the length-tension relation. Ahmed *et al*[75] compared the response of strips from patients with acalculous biliary pain to those of normal gallbladders following CCK-8 and carbachol stimulation. They found no difference in the CCK responses in these two groups; but again, the group also did not measure the length-tension relation.

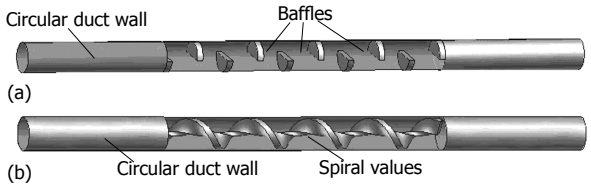

Figure 2 Two types of the cystic duct models used by Ooi *et al*[43] (modified from Figure 2 in the Journal of Biomechanics, vol 37, page 1913-1922) .

The mechanical properties of bile duct

There are no experimental data available for mechanical properties of human biliary ducts at the present time. Most of the measurements on biliary ducts were conducted on animals. Jian and Wang[76] measured 16 bile duct systems in healthy adult dogs and found that in normal physiological condition the bile duct experiences an almost uniform circumferential and longitudinal stress. However, in diseased cases the stresses are non-uniform, and much larger at the inside wall than at the outside wall. They also found that the elastic modulus (a material property which represents the ratio of stress to strain in an elastic body) decreases from the common bile duct to the common hepatic duct and is lowest in the hepatic duct. The elastic modulus of the cystic duct is comparable to that of the hepatic duct. Duch *et al*[77] examined 11 pig hepatic and the common bile ducts. They found that the cross-sectional areas in the common bile duct are significantly higher than those of the hepatic duct under a pressure range of 0-8 kPa. In a second study, the structural and mechanical changes were quantified in the common bile duct at different time intervals following experimental acute obstruction[78]. In this study, the duct was ligated near the duodenum in pigs, and studied after 3 h, 12 h, 2 d, 8 d and 32 d. It was found that the circumferential stress-strain relation changed with time.

NUMERICAL AND MATHEMATICAL MODELLING

Ooi *et al*[34] studied the effect of the cystic duct geometry on the flow resistance using both two-, and three dimensional cystic duct models. In their numerical study, the cystic duct was modelled as a straight pipe with two types of baffles of different numbers and height (Figure 2). The bile was assumed to be Newtonian, and its viscosity varied between 1-4 mPa.s. The results were then compared with more realistic two-dimensional models based on patient's biliary system images (Figure3). It was found that both the baffle height and number of baffles can

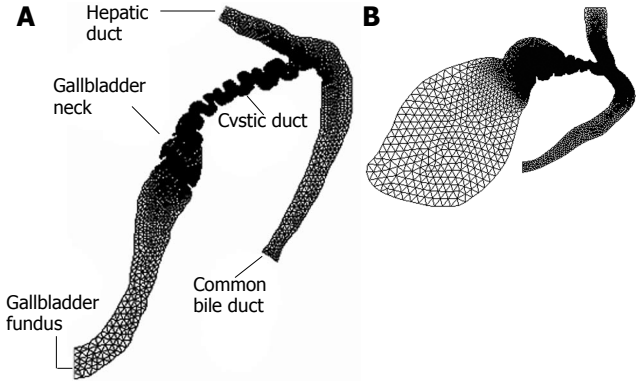

Figure 3 Computational models built from two patients' biliary system images used by Ooi *et al*[43] (modified from Journal of Biomechanics, vol. 37, page 1913-1922, Figure 2). Patient **A** is reported to have gallstones, and patient **B** is the normal control.

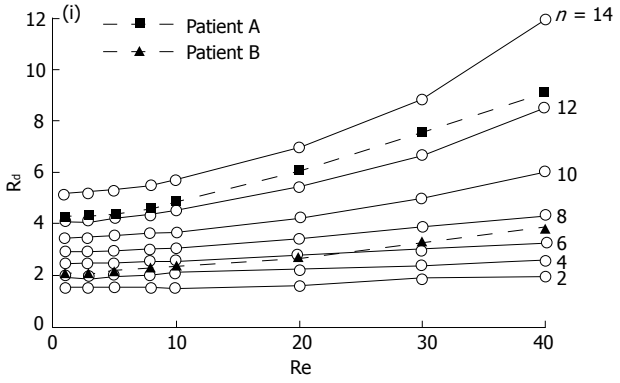

Figure 4 The resistance, Rd, plotted with the Reynolds number, Re (which is defined as the ratio of inertia over viscous forces, and is proportional to the flow rate for a given duct and bile). *n* is the number of the baffles in the duct[43] (modified from Journal of Biomechanics, vol. 37, page 1913-1922, Figure 6).

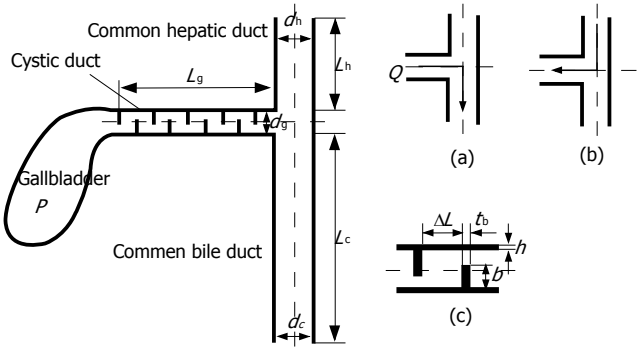

Figure 5 One-dimensional model of human billiary system and bile flow directions in the (a) emptying and (b) refill phases, (c) details of baffles at one section of the cystic duct[44]. *p* is the pressure inside the gallbladder, and Q is the flow rate of bile fluid. (Modified from figure 2 to be published in ASME Journal of Biomechanical Engineering).

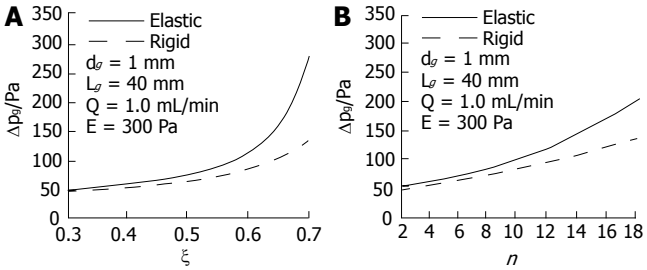

Figure 6 Pressure loss variations with baffle height ratio (**A**) and baffle number (**B**) for both rigid and elastic models[44]. (Modified from figure 8 to be published in ASME Journal of Biomechanical Engineering).

significantly affect the flow resistance. In fact, the flow resistance responds to these geometric effects much more than to an increased bile viscosity. Under the same flow conditions, the resistance from the scanned model based on a diseased gallbladder was found to be larger than that of a healthy one (Figure 4).

In an attempt to validate the numerical results by Ooi *et al*[43], Al-Altabi *et al*[79-81] performed a series of experimental studies on the flow patterns in a tube with uniform baffles as shown in Figure 2A. In these experiments, the Reynolds number was more than 50, which is much higher than that in the human biliary system (which is usually less than 10). Therefore, only qualitative comparisons between the experiments and the numerical modelling of could be made. However, in the higher Reynolds number range, good quantitative agreement between the numerical results from these duct models and the experimental measurements were obtained by Al-Altabi *et al*[80,81]. In addition, they discovered that the flow in the duct with baffles presented complicated mixing layers and possibly turbulent flows when the Reynolds number was higher. Based on these findings, a one-dimensional model was put forward to predict the pressure drop for a turbulent flow in the duct model with baffles[81]. However, it remains to be shown that these results are of any relevance to biliary flow which operates at a much lower Reynolds number range.

In all these studies, the cystic duct was studied in isolation, and the duct wall was assumed to be rigid. A further development by Li *et al*[44] studied one-dimensional rigid and elastic wall models for the biliary system, including the cystic duct, and the T-junction of the common bile duct and hepatic duct (Figure 5). Cystic ducts with baffles were modelled using the concept of equivalent diameter and length, and can be either rigid or elastic. Both emptying and refilling phases were considered. Using this model, the effects of the geometry, elasticity of cystic duct wall, bile flow rate and viscosity on the pressure drop, were studied in detail. It was found that many factors, including the elastic modulus and bile viscosity, can affect the pressure drop. However, the geometric changes in the cystic duct were still dominant. Among the geometric factors, the baffle height, b, was found to have more significant effect than the number of baffles, because it caused a greater change in the equivalent diameter and length. The pressure drop also increased with a decrease in the Young's modulus of the cystic duct during emptying, as a more compliant duct tended to collapse at the downstream end, thus narrowing the equivalent diameter further (Figure 6). However, it was also found that a more compliant gallbladder duct gave rise to an area of expansion near the gallbladder neck thus increasing the equivalent diameter, which reduced the

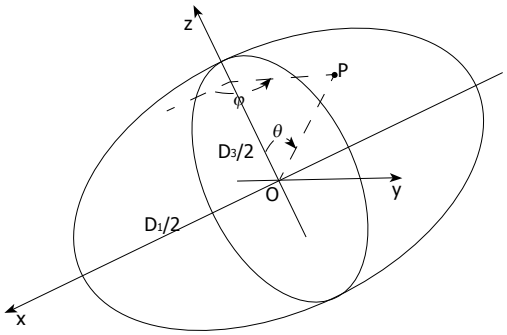

Figure 7 Gallbladder body shape during emptying is assumed to be ellipsoidal with major and minor axis lengths D_1, D_2 and D_3 ($D_1 > D_2 \geqslant D_3$); the gallbladder is subjected to a uniform internal pressure. The stress due to the pressure at any point P has three components, σ_θ (meridian), σ_φ (latitude) and $\tau_{\theta\varphi}$ (in surface)[85].

pressure drop required to drive the bile during emptying. In Li *et al*'s[44] model, it was found that when the elastic modulus of the cystic duct was more than 700 Pa, the wall deformation became negligible, and a rigid-walled model gave a good estimate of the pressure drop in the system. However, it was noted that the pressure drop in the cystic duct models predicted by both Ooi *et al*[34,44] and Li *et al*, as well as that from the *in vitro* measurements of Al-Atabi *et al*[79,80], was much smaller than the clinical observations of the opening pressure during emptying. The reason for this is, at least in part, that the function of the Sphincter of Oddi was not included, and also because the real nature of the bile, the complicated cystic duct geometry, the soft tissue deformation, and their interactions were not fully taken into account.

CORRELATION OF MECHANICAL FACTORS TO BILIARY PAIN

Acalculous biliary pain or functional biliary pain is defined as steady pain located in the epigastrium and right upper quadrant in the absence of gallstones or when other structural abnormalities exists in the biliary tract[82]. However, surgery for this condition is often conducted without any guarantee of relieving the symptoms, so a reliable pain prediction model is needed. Previous attempts to provide an accurate predictor for relief of gallbladder symptoms have not been successful with only about 50% of patients obtaining symptomatic relief following surgery[83]. Moreover some patients without stones appear to have typical gallbladder pain, but only half of them gain relief of their pain if the gallbladder is removed. It would therefore be useful to have a way of determining whether the pain is actually arising in the gallbladder, because similar symptoms can be produced by adjacent organs, such as the stomach, duodenum and pancreas, even without obvious disease.

Impaired motor function of gallbladder and sphincter of Oddi have long been suspected as a major factor contributing to gallbladder pain. The presumed mechanism for the pain is obstruction leading to distension and inflammation. The obstruction might result from a lack of co-ordination between the gallbladder and either the

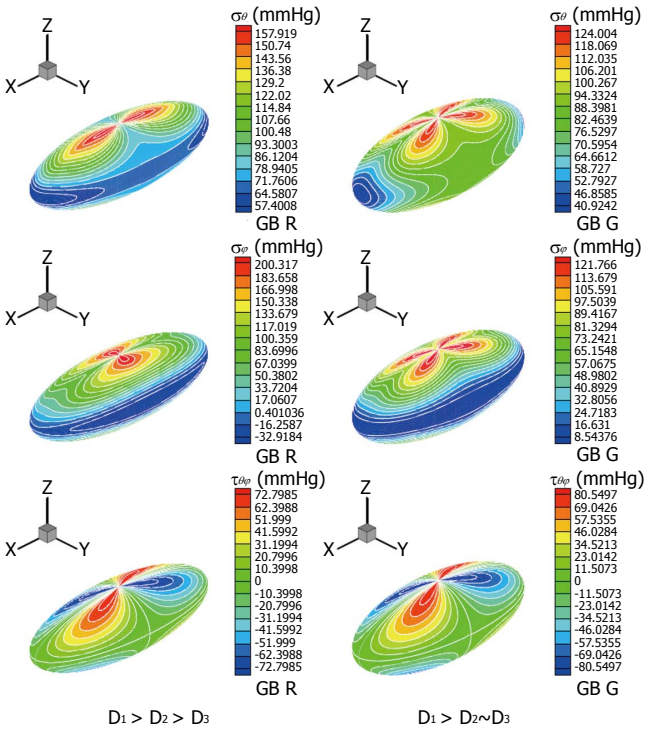

Figure 8 Li *et al*[85] calculated the stress distributions for two different subjects: R (left) and G (right). The top frame is the principal meridian stress, σ_θ, the middle frame is the principal latitude stress, σ_φ, and the bottom one is the in-plane shear stress $\tau_{\theta\varphi}$. It is seen that the location and the maximum stresses change as the ratio of the lengths of the three axes change.

cystic duct or the sphincter of Oddi due to increased flow resistance or tone[84]. In other words, pain may be produced by contraction against resistance or stretch of the gallbladder wall. When the gallbladder is inflamed, artificial distension produces typical pain[62].

Preliminary work has been carried out to identify the correlation between possible mechanical factors to biliary pain[85]. Li *et al*[44,86] developed a mathematical model for the human biliary system during the emptying phase, based on a clinical test in which gallbladder volume changes are measured in response to a standard stimulus and a recorded pain profile. In their model the gallbladder was assumed to be a thin-walled ellipsoid under uniform pressure (Figure 7), where the three axis lengths can be estimated from the *in vivo* volume measurements. Using this information, together with the constitutive equation (1), choosing the compliance C to be 2.731 mL/mmHg[87], they predicted the flow resistance, *R*, in the biliary ducts using a Windkessel model[88]:

$$C\frac{dP}{dt} + \frac{P - P_d}{R} = 0 \quad (1)$$

where P_d is the pressure at the downstream end of the tract. The detailed stress distributions in the gallbladder wall during emptying for different gallbladder geometries were also calculated analytically (Figure 8). This model was then applied to clinical data from CCK provocation tests from 25 patients. It was found that the pressure change in the gallbladder, the gallbladder ejection fraction and the shape change are all contributing to, but not solely responsible for the pain. However, the maximum stress in the gallbladder, σ_{max}, is singled out to be the only factor

closely correlated with gallbladder pain. In fact, using the simple criterion that the maximum stress $\sigma_{max} > 200$ mmHg, 76% of the model predictions for pain agreed with the clinical results[44]. However further research is required to confirm the stress-pain relationship, and to validate and improve the model.

FUTURE CHALLENGES

Patient-specific prediction of flow resistance

Current studies show that geometry changes in the biliary system play the dominant role in controlling bile flow and pressure drop. Further modelling work on 3D models of the biliary system is clearly required to help identify the key geometrical parameters.

In addition, if any prediction of flow resistance is to be used in clinical diagnosis, the model clearly needs to be patient-specific. The key to predicting patient specific flow features relies on obtaining the realistic geometry of the biliary system. This will involve three-dimensional geometrical reconstructions of the biliary system during emptying. Therefore, techniques for the reconstructions based on non-invasive clinical measurements need to be developed.

Bile rheology

It has been found that the bile can demonstrate non-Newtonian behaviour at low shear rates, but its relation with gallstone formation is not understood. Experiments on bile's viscosity can be contradictory and it seems that the bile property is not only subject dependent, but also pathologically dependent. In other words, it changes with the status of bile concentration and with tiny stones (crystals) forming, and the collective behaviour is controlled by the resulting two-phase flow. More experimental and modelling work are required to understand the bile rheology before we can estimate the flow details more accurately; this is especially true if the measurement to be patient specific.

The constitutive equations for the gallbladder (and biliary tract) are still to be established even for a healthy subject. Currently, only limited information on the volume-pressure relation of the gallbladder and the length-tension relation for single muscle strips, are available. More experimental work is required to identify the mechanical properties both for healthy and diseased gallbladders. The lack of data on the mechanical properties makes it impossible to build a quantitatively reliable mathematical or numerical model to deal with the contraction and emptying activity of the human gallbladder. The biliary system also presents active contraction under chemical stimulations such as CCK. For instance, the gallbladder, the sphincter of Oddi, and even the cystic duct are reported to have this activity[89]. Needless to say, studying the active smooth muscle behaviour and its response to chemical stimulations during physiological and pathological gallbladder emptying poses an exciting challenge at the next level, both for experimentalists and biomechanics modellers.

Fluid-structure interactions

Fluid-structure interactions add to the complications when attempting to describe the behaviour of the biliary system. To date, only limited work has been carried out on the fluid structure interactions. Ooi *et al*[90] simulated the bile flow in a simple two-dimensional elastic cystic duct model, and the nature of the fluid-structure interactions was only crudely modelled in a one-dimensional model[44]. No work on the fluid-structure interactions in a three-dimensional model has been reported. However, it is the fluid-structure interactions in the biliary system that provide the crucial link between chemical stimuli and mechanical response in the biliary systems, since these chemical stimuli changes the tissue structure, hence the geometry and the elastic modulus, which in turn change the flow resistance and stresses in the system.

Prediction of the biliary pain

To date, only preliminary work has been carried out on the link between biliary pain and levels of stress within the system[44,86]. More work is required to confirm a positive correlation between the stress and bililary pain. Although the study by Li *et al*[86] considered both the active and the passive stresses, the active stress was not obtained from modelling of the smooth muscle mechanics; rather, it assumed a same generic form for all subjects. In practice, this will vary between individuals and in pathological situations.

DISCUSSION

The fluid dynamics in the human biliary system depend on the gallbladder motor function, biliary tract geometry, the smooth muscle activity, bile rheology and their interactions. These mechanical factors play important roles in the normal functions of the biliary systems and may help us to understand the nature and origin of 'gallbladder pain'. There hasve been extensive clinical and experimental work both on human and animal biliary systems, however, only few modelling and numerical studies have been carried out to study the system from the mechanical point of view. This paper has reviewed the current progress in understanding the mechanical aspects of the biliary system, and covered the areas in bile fluid dynamics, bile rheology, gallbladder and duct tissue mechanics, mathematical and numerical modelling, and the correlations between the mechanical stresses and the gallbladder. The preliminary work reported here represents a significant step forward towards understanding the origins of gallbladder pain and gallstone disease.

REFERENCES

1 **Sandor J**, Sandor A, Zaborszky A, Megyaszai S, Benedek G, Szeberin Z. Why laparoscopic cholecystectomy today? *Surg Today* 1996; **26**: 556-560
2 **Lam CM**, Murray FE, Cuschieri A. Increased cholecystectomy rate after the introduction of laparoscopic cholecystectomy in Scotland. *Gut* 1996; **38**: 282-284
3 **Calvert NW**, Troy GP, Johnson AG. Laparoscopic cholecystectomy: a good buy? A cost comparison with small-incision (mini) cholecystectomy. *Eur J Surg* 2000; **166**: 782-786
4 **Smythe A**, Majeed AW, Fitzhenry M, Johnson AG. A requiem for the cholecystokinin provocation test? Gut 1998; 43: 571-574

5 **Brenneman DE**, Connor WE, Forker EL, DenBesten L. The formation of abnormal bile and cholesterol gallstones from dietary cholesterol in the prairie dog. *J Clin Invest* 1972; **51**: 1495-1503
6 **Holzbach RT**, Marsh M, Olszewski M, Holan K. Cholesterol solubility in bile. Evidence that supersaturated bile is frequent in healthy man. *J Clin Invest* 1973; **52**: 1467-1479
7 **Holzbach RT**. Effects of gallbladder function on human bile: compositional and structural changes. *Hepatology* 1984; **4**: 57S-60S
8 **Holzbach RT**. Factors influencing cholesterol nucleation in bile. *Hepatology* 1984; **4**: 173S-176S
9 **Jazrawi RP**, Pazzi P, Petroni ML, Ahmed HA, Northfield TC. Role of the gallbladder in the pathogenesis of gallstone disease. In: Northfield TC, Ahmed HA, Jazrawi RP. Bile Acid in Hepatology Disease. Boston: Kuwer Academic Publishers, 2000: 182-191
10 **Doty JE**, Pitt HA, Kuchenbecker SL, DenBesten L. Impaired gallbladder emptying before gallstone formation in the prairie dog. *Gastroenterology* 1983; **85**: 168-174
11 **Levy PF**, Smith BF, LaMont JT. Human gallbladder mucin accelerates nucleation of cholesterol in artificial bile. *Gastroenterology* 1984; **87**: 270-275
12 **LaMont JT**, Smith BF, Moore JR. Role of gallbladder mucin in pathophysiology of gallstones. *Hepatology* 1984; **4**: 51S-56S
13 **Zak RA**, Frenkiel PG, Marks JW, Bonorris GG, Allen A, Schoenfield LJ. Cyclic nucleotides and glycoproteins during formation of cholesterol gallstones in prairie dogs. *Gastroenterology* 1984; **87**: 263-269
14 **Ryan J**, Cohen S. Gallbladder pressure-volume response to gastrointestinal hormones. *Am J Physiol* 1976; **230**: 1461-1465
15 **Schoetz DJ**, LaMorte WW, Wise WE, Birkett DH, Williams LF. Mechanical properties of primate gallbladder: description by a dynamic method. *Am J Physiol* 1981; **241**: G376-G381
16 **Middelfart HV**, Jensen P, Højgaard L, Funch-Jensen P. Pain patterns after distension of the gallbladder in patients with acute cholecystitis. *Scand J Gastroenterol* 1998; **33**: 982-987
17 **Lanzini A**, Northfield TC. Gallbladder motor function in man. In: Bile Acid in Hepatology Disease. Northfield TC, Ahmed HA, Jazrawi RP. Boston: Kuwer Academic Publishers, 1998: 83-96
18 **Courtney DF**, Clanachan AS, Scott GW. Cholecystokinin constricts the canine cystic duct. *Gastroenterology* 1983; **85**: 1154-1159
19 **Severi C**, Grider JR, Makhlouf GM. Functional gradients in muscle cells isolated from gallbladder, cystic duct, and common bile duct. *Am J Physiol* 1988; **255**: G647-G652
20 **Shaffer EA**, McOrmond P, Duggan H. Quantitative cholescintigraphy: assessment of gallbladder filling and emptying and duodenogastric reflux. *Gastroenterology* 1980; **79**: 899-906
21 **Thompson JC**, Fried GM, Ogden WD, Fagan CJ, Inoue K, Wiener I, Watson LC. Correlation between release of cholecystokinin and contraction of the gallbladder in patients with gallstones. *Ann Surg* 1982; **195**: 670-676
22 **Fisher RS**, Stelzer F, Rock E, Malmud LS. Abnormal gallbladder emptying in patients with gallstones. *Dig Dis Sci* 1982; **27**: 1019-1024
23 **Forgacs IC**, Maisey MN, Murphy GM, Dowling RH. Influence of gallstones and ursodeoxycholic acid therapy on gallbladder emptying. *Gastroenterology* 1984; **87**: 299-307
24 **Pomeranz IS**, Shaffer EA. Abnormal gallbladder emptying in a subgroup of patients with gallstones. *Gastroenterology* 1985; **88**: 787-791
25 **Portincasa P**, Di Ciaula A, Baldassarre G, Palmieri V, Gentile A, Cimmino A, Palasciano G. Gallbladder motor function in gallstone patients: sonographic and in vitro studies on the role of gallstones, smooth muscle function and gallbladder wall inflammation. *J Hepatol* 1994; **21**: 430-440
26 **Portincasa P**, Di Ciaula A, Palmieri V, Velardi A, VanBerge-Henegouwen GP, Palasciano G. Impaired gallbladder and gastric motility and pathological gastro-oesophageal reflux in gallstone patients. *Eur J Clin Invest* 1997; **27**: 653-661
27 **Sylwestrowicz TA**, Shaffer EA. Gallbladder function during gallstone dissolution. Effect of bile acid therapy in patients with gallstones. *Gastroenterology* 1988; **95**: 740-748
28 **van Erpecum KJ**, van Berge Henegouwen GP, Stolk MF, Hopman WP, Jansen JB, Lamers CB. Fasting gallbladder volume, postprandial emptying and cholecystokinin release in gallstone patients and normal subjects. *J Hepatol* 1992; **14**: 194-202
29 **Spengler U**, Sackmann M, Sauerbruch T, Holl J, Paumgartner G. Gallbladder motility before and after extracorporeal shock-wave lithotripsy. *Gastroenterology* 1989; **96**: 860-863
30 **Masclee AA**, Jansen JB, Driessen WM, Geuskens LM, Lamers CB. Plasma cholecystokinin and gallbladder responses to intraduodenal fat in gallstone patients. *Dig Dis Sci* 1989; **34**: 353-359
31 **Festi D**, Frabboni R, Bazzoli F, Sangermano A, Ronchi M, Rossi L, Parini P, Orsini M, Primerano AM, Mazzella G. Gallbladder motility in cholesterol gallstone disease. Effect of ursodeoxycholic acid administration and gallstone dissolution. *Gastroenterology* 1990; **99**: 1779-1785
32 **Pitt HA**, Roslyn JJ, Kuchenbecker SL, Doty JE, Denbesten L. The role of cystic duct resistance in the pathogenesis of cholesterol gallstones. *J Surg Res* 1981; **30**: 508-514
33 **Pitt HA**, Doty JE, DenBesten L, Kuchenbecker SL. Stasis before gallstone formation: altered gallbladder compliance or cystic duct resistance? *Am J Surg* 1982; **143**: 144-149
34 **Ooi RC**. The flow of bile in human cystic duct. PhD Thesis. UK: Department of Mechanical Engineering, University of Sheffield; 2004
35 **Bouchier IA**, Cooperband SR, el-Kodsi BM. Mucous substances and viscosity of normal and pathological human bile. *Gastroenterology* 1965; **49**: 343-353
36 **Cowie AG**, Sutor DJ. Viscosity and osmolality of abnormal biles. *Digestion* 1975; **13**: 312-315
37 **Doty JE**, Pitt HA, Kuchenbecker SL, Porter-Fink V, DenBesten LW. Role of gallbladder mucus in the pathogenesis of cholesterol gallstones. *Am J Surg* 1983; **145**: 54-61
38 **Jüngst D**, Niemeyer A, Müller I, Zündt B, Meyer G, Wilhelmi M, del Pozo R. Mucin and phospholipids determine viscosity of gallbladder bile in patients with gallstones. *World J Gastroenterol* 2001; **7**: 203-207
39 **Tera H**. Sedimentation of bile constituents. *Ann Surg* 1963; **157**: 468-472
40 **Gottschalk M**, Lochner A. Behavior of postoperative viscosity of bile fluid from T-drainage. A contribution to cholelithogenesis. *Gastroenterol J* 1990; **50**: 65-67
41 **Coene PP**, Groen AK, Davids PH, Hardeman M, Tytgat GN, Huibregtse K. Bile viscosity in patients with biliary drainage. Effect of co-trimoxazole and N-acetylcysteine and role in stent clogging. *Scand J Gastroenterol* 1994; **29**: 757-763
42 **Rodkiewicz CM**, Otto WJ, Scott GW. Empirical relationships for the flow of bile. *J Biomech* 1979; **12**: 411-413
43 **Ooi RC**, Luo XY, Chin SB, Johnson AG, Bird NC. The flow of bile in the human cystic duct. *J Biomech* 2004; **37**: 1913-1922
44 **Li WG**, Luo XY, Johnson AG, Hill NA, Bird NC, Chin SB. One-Dimensional models of the human biliary system. *ASME J Biomechanic Engineering* 2007; in press
45 **Dasgupta D**, Stringer MD. Cystic duct and Heister's "valves". *Clin Anat* 2005; **18**: 81-87
46 **Johnston CG**, Brown CE. Studies of gall-bladder function. American Physiological Society, 1932: 477-485
47 **Lichtenstein ME**, Ivy AC. The function of the "Valve" of Heister. *Surgery* 1937; **1**: 38-52
48 **Bird NC**, Ooi RC, Luo XY, Chin SB, Johnson AG. Investigation of the functional three-dimensional anatomy of the human cystic duct: a single helix? *Clin Anat* 2006; **19**: 528-534
49 **Deenitchin GP**, Yoshida J, Chijiiwa K, Tanaka M. Complex cystic duct is associated with cholelithiasis. *HPB Surg* 1998; **11**: 33-37
50 **Everson GT**, Braverman DZ, Johnson ML, Kern F. A critical evaluation of real-time ultrasonography for the study of gallbladder volume and contraction. *Gastroenterology* 1980; **79**:

40-46
51 **Dodds WJ**, Groh WJ, Darweesh RM, Lawson TL, Kishk SM, Kern MK. Sonographic measurement of gallbladder volume. *AJR Am J Roentgenol* 1985; **145**: 1009-1011
52 **Gill PT**, Dillon E, Leahy AL, Reeder A, Peel AL. Ultrasonography, HIDA scintigraphy or both in the diagnosis of acute cholecystitis? *Br J Surg* 1985; **72**: 267-268
53 **Rohling RN**, Gee AH, Berman L. Automatic registration of 3-D ultrasound images. *Ultrasound Med Biol* 1998; **24**: 841-854
54 **Kwon AH**, Uetsuji S, Yamada O, Inoue T, Kamiyama Y, Boku T. Three-dimensional reconstruction of the biliary tract using spiral computed tomography. *Br J Surg* 1995; **82**: 260-263
55 **Polkowski M**, Palucki J, Regula J, Tilszer A, Butruk E. Helical computed tomographic cholangiography versus endosonography for suspected bile duct stones: a prospective blinded study in non-jaundiced patients. *Gut* 1999; **45**: 744-749
56 **Caoili EM**, Paulson EK, Heyneman LE, Branch MS, Eubanks WS, Nelson RC. Helical CT cholangiography with three-dimensional volume rendering using an oral biliary contrast agent: feasibility of a novel technique. *AJR Am J Roentgenol* 2000; **174**: 487-492
57 **Chopra S**, Chintapalli KN, Ramakrishna K, Rhim H, Dodd GD. Helical CT cholangiography with oral cholecystographic contrast material. *Radiology* 2000; **214**: 596-601
58 **Hirao K**, Miyazaki A, Fujimoto T, Isomoto I, Hayashi K. Evaluation of aberrant bile ducts before laparoscopic cholecystectomy: helical CT cholangiography versus MR cholangiography. *AJR Am J Roentgenol* 2000; **175**: 713-720
59 **Ichii H**, Takada M, Kashiwagi R, Sakane M, Tabata F, Ku Y, Fujimori T, Kuroda Y. Three-dimensional reconstruction of biliary tract using spiral computed tomography for laparoscopic cholecystectomy. *World J Surg* 2002; **26**: 608-611
60 **Persson A**, Dahlström N, Smedby O, Brismar TB. Volume rendering of three-dimensional drip infusion CT cholangiography in patients with suspected obstructive biliary disease: a retrospective study. *Br J Radiol* 2005; **78**: 1078-1085
61 **Dodds WJ**, Hogan WJ, Green JE, Motility of the biliary system. In: Schultz SG. Handbook of Physiology: the gastrointestinal system, Vol. 1, Section 6, Part 2(28). Bethesda: American Physiological Society, 1989: 1055-1101
62 **Funch-Jensen P**, Ebbehøj N. Sphincter of Oddi motility. *Scand J Gastroenterol Suppl* 1996; **216**: 46-51
63 **Luman W**, Williams AJ, Pryde A, Smith GD, Nixon SJ, Heading RC, Palmer KR. Influence of cholecystectomy on sphincter of Oddi motility. *Gut* 1997; **41**: 371-374
64 **Mawe GM**. Nerves and Hormones Interact to Control Gallbladder Function. *News Physiol Sci* 1998; **13**: 84-90
65 **Geenen JE**, Hogan WJ, Dodds WJ, Stewart ET, Arndorfer RC. Intraluminal pressure recording from the human sphincter of Oddi. *Gastroenterology* 1980; **78**: 317-324
66 **Toouli J**, Dodds WJ, Honda R, Sarna S, Hogan WJ, Komarowski RA, Linehan JH, Arndorfer RC. Motor function of the opossum sphincter of Oddi. *J Clin Invest* 1983; **71**: 208-220
67 **Calabuig R**, Ulrich-Baker MG, Moody FG, Weems WA. The propulsive behavior of the opossum sphincter of Oddi. *Am J Physiol* 1990; **258**: G138-G142
68 **Grivell MB**, Woods CM, Grivell AR, Neild TO, Craig AG, Toouli J, Saccone GT. The possum sphincter of Oddi pumps or resists flow depending on common bile duct pressure: a multilumen manometry study. *J Physiol* 2004; **558**: 611-622
69 **Funch-Jensen P**, Stødkilde-Jørgensen H, Kraglund K, Løvgreen NA. Biliary manometry in dogs. Influence of selective electrostimulation of the right and left vagus nerves. *Digestion* 1981; **22**: 89-93
70 **Cicala M**, Habib FI, Fiocca F, Pallotta N, Corazziari E. Increased sphincter of Oddi basal pressure in patients affected by gall stone disease: a role for biliary stasis and colicky pain? *Gut* 2001; **48**: 414-417
71 **Otto WJ**, Scott GW, Rodkiewicz CM. A comparison of resistances to flow through the cystic duct and the sphincter of Oddi. *J Surg Res* 1979; **27**: 68-72
72 **Mack AJ**, Todd JK. A study of human gall bladder muscle in vitro. *Gut* 1968; **9**: 546-549
73 **Washabau RJ**, Wang MB, Dorst CL, Ryan JP. Effect of muscle length on isometric stress and myosin light chain phosphorylation in gallbladder smooth muscle. *Am J Physiol* 1991; **260**: G920-G924
74 **Bird NC**, Wegstapel H, Chess-Williams R, Johnson AG. In vitro contractility of stimulated and non-stimulated human gallbladder muscle. *Neurogastroenterol Motil* 1996; **8**: 63-68
75 **Ahmed R**, Bird NC, Chess-Williams R, Thomas WE, Johnson AG. In vitro responses of gallbladder muscle from patients with acalculous biliary pain. *Digestion* 2000; **61**: 140-144
76 **Jian C**, Wang G. Biomechanical study of the bile duct system outside the liver. *Biomed Mater Eng* 1991; **1**: 105-113
77 **Duch BU**, Petersen JA, Gregersen H. Luminal cross-sectional area and tension-strain relation of the porcine bile duct. *Neurogastroenterol Motil* 1998; **10**: 203-209
78 **Duch BU**, Andersen HL, Smith J, Kassab GS, Gregersen H. Structural and mechanical remodelling of the common bile duct after obstruction. *Neurogastroenterol Motil* 2002; **14**: 111-122
79 **Al-Atabi M**, Chin SB, Luo XY. Flow structure in circular tubes with segmental baffles. *J Flow Vis Image Proc* 2005; **3**: 301-311
80 **Al-Atabi M**, Chin SB, Luo XY. Visualization Experiment of Flow Structures inside Two-Dimensional Human Biliary System Models. *J Mech Med Biol* 2006; **6**: 249-260
81 **Al-Atabi M**, Sulaiman Al-Zuhair, Chin SB and Luo XY. Pressure drop in laminar and turbulent flows in circular pipe with baffles-An experimental and analytic study. *Inter J Fluid Mech Res* 2006; **33**: 303-319
82 **Shaffer E**. Acalculous biliary pain: new concepts for an old entity. *Dig Liver Dis* 2003; **35** Suppl 3: S20-S25
83 **Smythe A**, Ahmed R, Fitzhenry M, Johnson AG, Majeed AW. Bethanechol provocation testing does not predict symptom relief after cholecystectomy for acalculous biliary pain. *Dig Liver Dis* 2004; **36**: 682-686
84 **Corazziari E**, Shaffer EA, Hogan WJ, Sherman S, Toouli J. Functional disorders of the biliary tract and pancreas. *Gut* 1999; **45** Suppl 2: II48-II54
85 **Liao D**, Duch BU, Stødkilde-Jørgensen H, Zeng YJ, Gregersen H, Kassab GS. Tension and stress calculations in a 3-D Fourier model of gall bladder geometry obtained from MR images. *Ann Biomed Eng* 2004; **32**: 744-755
86 **Li WG**, The mechanical behaviour of human biliary system, PhD thesis, England: University of Sheffield, 2007
87 **Ness TJ**, Gebhart GF. Visceral pain: a review of experimental studies. *Pain* 1990; **41**: 167-234
88 **Fung YC**, Biomechanics, mechanical properties of living tissues. 2nd ed. New York: Springer, 1984
89 **Scott GW**, Otto WJ. Resistance and sphincter-like properties of the cystic duct. *Surg Gynecol Obstet* 1979; **149**: 177-182
90 **Ooi RC**, Luo XY, Chin SB, Johnson AG, Bird NC. Fluid-structure-interaction (FSI) simulation of the human cystic duct. Florida: Summer Bioengineering Conference; 2003 Jun 25-29

S- Editor Liu Y **L-Editor** Alpini GD **E- Editor** Chin GJ

PO Box 2345, Beijing 100023, China
www.wjgnet.com
wjg@wjgnet.com

World J Gastroenterol 2007 March 7; 13(9): 1393-1398
World Journal of Gastroenterology ISSN 1007-9327

TOPIC HIGHLIGHT

Hans Gregersen, Professor, *Series Editor*

A framework for the modeling of gut blood flow regulation and postprandial hyperaemia

Adam David Jeays, Patricia Veronica Lawford, Richard Gillott, Paul A Spencer, Karna Dev Bardhan, David Rodney Hose

Adam David Jeays, Patricia Veronica Lawford, David Rodney Hose, Medical Physics, University of Sheffield, United Kingdom
Richard Gillott, Paul A Spencer, Karna Dev Bardhan, Rotherham General Hospital, United Kingdom
Supported by the Bardhan Research and Educational Trust
Correspondence to: Adam David Jeays, Medical Physics, I Floor, Royal Hallamshire Hospital, Glossop Rd, Sheffield, S10 2JF, United Kingdom. a.jeays@sheffield.ac.uk
Telephone: +44-114-2712234 Fax: +44-114-2713403
Received: 2006-12-09 Accepted: 2007-01-17

Abstract

After a meal the activity of the gut increases markedly as digestion takes place. Associated with this increase in activity is an increase in blood flow, which has been shown to be dependent on factors such as caloric content and constitution of the meal. Much qualitative work has been carried out regarding mechanisms for the presence of food in a section of gut producing increased blood flow to that section, but there are still many aspects of this process that are not fully understood. In this paper we briefly review current knowledge on several relevant areas relating to gut blood flow, focusing on quantitative data where available and highlighting areas where further research is needed. We then present new data on the effect of feeding on flow in the superior mesenteric artery. Finally, we describe a framework for combining this data to produce a single model describing the mechanisms involved in postprandial hyperaemia. For a section of the model, where appropriate data are available, preliminary results are presented.

Key words: Modeling; Small intestine; Superior mesenteric artery; Blood flow

Jeays AD, Lawford PV, Gillott R, Spencer PA, Bardhan KD, Hose DR. A framework for the modelling of gut blood flow regulation and postprandial hyperaemia. *World J Gastroenterol* 2007; 13(9): 1393-1398

http://www.wjgnet.com/1007-9327/13/1393.asp

INTRODUCTION

This study was motivated by our previous work on blood flow in the superior mesenteric artery (SMA). When we explored the literature on the vasculature downstream of the SMA in order to develop appropriate boundary conditions for our work on computational fluid dynamic modeling[1], we found little quantitative information on the smaller vessels of the mesentery. These vessels control the distribution of blood to the small intestine and as such are of great importance in understanding gut physiology and problems such as gut hypoperfusion following surgery[2].

This paper reviews current knowledge on blood flow regulation in the gut vasculature, presents new data on flow in the SMA and develops a framework for its integration with a structural model of the gut vasculature (to be published separately).

Following a meal, food arrives in the stomach, mixes with gastric juices to become chyme, and is slowly emptied into the small intestine. This rate of emptying is largely governed by the stomach and is dependent on the chemical and physical properties of the food. The chyme is digested as it travels through the small intestine and this propagating metabolic front is met by an increase in blood flow through the capillaries supplying the gut wall, which can be seen at a macroscopic level as an increase in flow through the superior mesenteric artery.

Except for the proximal part of the duodenum, the small intestine is wholly vascularised by vessels arising from the superior mesenteric artery, which originates from the aorta at the level of the L1 vertebra[3]. The vessels run through a convoluted sheet of tissue called the mesentery and then branch and anastomose (forming arcades) before reaching the vascular bed of the gut wall.

The direction of blood to the appropriate part of the gut is achieved by changes in vascular smooth muscle (VSM) tone, with the basal state being partial tone, thus allowing for both dilatation and contraction of the vessel wall. As well as affecting the diameter of the vessel lumen and hence its resistance to flow, VSM tone also mediates vessel wall stiffness[4].

There are two mechanisms likely to be of key importance in the control of gut blood flow following feeding. These are the response of vessels to food stimulus and the myogenic response.

The aim of modeling this system is to bring together the knowledge and understanding available in each of the specialist fields alluded to above, and to combine the information to allow greater appreciation of the organ as a whole. By definition, the model will not represent every facet of the system being studied, nor should it. Instead, the aim of the model is to capture the key factors that play an important part in determining gut blood flow and allow 'what if' questions to be asked. In order to be predictive and to allow a wide range of questions to be posed, the model must be flexible.

GASTRIC EMPTYING AND CHYME PROGRESSION

Gastric emptying rates show substantial inter- and intra-subject variability and are dependent on meal nutrient content and physical properties. Emptying of digestible solids is generally characterized by a lag phase followed by a period during which the emptying rate is approximately constant. Animal studies suggest that the rate-limiting factor leading to this constant rate of gastric emptying is trituration (grinding up of solid food). In contrast, isotonic liquid meals need no trituration and hence exhibit a different pattern of gastric emptying, emptying more quickly and following an exponential relationship[5]. Nutrient-containing liquids lie between these two extremes with the rate of emptying rising quickly to 1.5-3 kCal/min[5,6]. The presence of solid and liquid foods in the same meal leads to modification of the emptying profiles of both foods[5].

A model where nutrient content is detected locally within the gut and to some extent influences blood flow requires information on the progression of chyme through the small intestine. Standard scintigraphic methods for investigating small bowel transit times give little direct data on the rate of transit of food through the small intestine due to the gut's convoluted nature and the poor resolution of gamma cameras. Instead, short intestinal transit times are often inferred from gastric emptying and colonic filling[7,8]. A spectrum of transit times is often presented, reflecting the fact that different parts of the chyme progress through the gut at different rates (although solid and liquid markers have been shown to progress along the bowel at similar rates[7]). Motion of chyme through the small intestine is governed by irregular pressure waves moving along the gut[9] and it has been suggested that transit is fast initially, acting to spread chyme through the gut, and then slows as digestion takes place[10]. However, quantitative data is limited.

In a scintigraphic study of six subjects, Malagelada *et al*[7] reported median pylorus to caecum transit times in the range of 95 to 245 min. For 8 of 12 tests (considering progression of solid and liquid meals in each subject) a normal distribution was considered by the authors to be a good model for the transit time spectrum. No significant difference in mean transit times was observed after solid and liquid meals. The full-width half maximums (FWHM) of the normal distributions were in the range 33-261 min with mean FWHMs of 169 min (liquid) and 63 min (solid). Whilst there was no difference in mean transit rates, the liquid meal tended to become more spread out during its passage through the small intestine.

Table 1 Average coefficients of apparent digestibility for the nutrients in different food groups and for nutrients in a mixed diet

Food Group	Protein	Fat	Carbohydrates
Total foods[1]	92	95	97

[1]Weighted by consumption statistics based on a survey of 185 dietaries.

$$Apparent\ digestibil\ ity = \frac{E_{FOOD} - E_{FAECES}}{E_{FOOD}} \times 100 \quad (1)$$

Assuming that digestion is exclusively confined to the small intestine, small intestinal efficiency will be equal to the 'apparent digestibility' of the foodstuff, as given by equation 1 above[11].

Where E_{FOOD} and E_{FAECES} are the caloric contents of the food and faeces respectively. At the beginning of the twentieth century, Atwater published several papers[12-14] on the available energy in various foodstuffs, finding the E values in equation 1; his key results are reproduced in Table 1.

DETECTION OF CHYME CONSTITUENTS IN THE SMALL INTESTINE

From the 1970s, Chou *et al*[15-17] have performed work on characterizing the response of the gut to various luminal contents. In descending order, the most potent inducers of increased blood flow to the gut are: lipids and fats (in combination with bile salts), glucose and other carbohydrates, proteins, peptides, amino acids. Chou *et al*[15] also experimented with the solid and fluid phases of the chyme and they found that the compounds responsible for postprandial hyperaemia exist in the hydrolytic products of food digestion.

The basic control mechanisms relating the arrival of chyme in an intestinal segment to an increase in local blood flow are not fully understood. Chou and Coatney[16] suggested five categories of potential influences on local postprandial hyperaemia. The understanding of these various effects has recently been reviewed by Matheson *et al*[18]. The five categories are: (1) Direct effects of absorbed nutrients: Intra-arterial injection of some nutrients (micellar solutions containing bile and oleic acid, capoic acid or taurocholate) has an effect on jejunal blood flow, while most amino acids and carbohydrates do not. Carbon dioxide and hydrogen ions present in the gut can diffuse into the blood supply and also have an effect; (2) Enteric nervous system effects and reflexes: It has been shown that extrinsic sympathetic and parasympathetic innervation is not required for post-prandial hyperaemia; however, the role of other (non-adrenergic, non-cholinergic) neurons cannot be ruled out; (3) Gastrointestinal hormones and peptides: While many of these can have vasoactive effects, levels measured experimentally have always been too low to produce vaso-

dilatation; (4) Local non-metabolic vasoactive mediators; (5) Local metabolic vasoactive mediators.

As well as the factors mentioned above, the myogenic response may be of key importance. The myogenic response is an increase in vascular tone associated with an increase in transmural pressure, or a decrease in vascular tone associated with a decrease in transmural pressure. This has been reviewed from a biological perspective by Schubert and Mulvany[19] and by Davis and Hill[20]. The *in vivo* myogenic response is not well understood. Most experiments to date have been performed in vitro and often give conflicting results.

The myogenic response is seen primarily in small arteries and arterioles and varies between arterial beds. It is widely held to be dependent mainly on the reaction of vascular smooth muscle to changes in vessel wall tension (hoop stress). Osol *et al*[21] showed that in rats the response is weaker in small mesenteric vessels than in cerebral vessels that are equivalent. No similar studies have been carried out in human mesenteric vessels.

Whilst work continues in each of these areas the dominant mechanism controlling postprandial hyperaemia in humans has not yet been isolated.

MECHANICAL PROPERTIES OF MESENTERIC BLOOD VESSELS

In order to build the model, the mechanical and vasoactive properties that govern the resistance to blood flow in the mesenteric vessels must be characterized. These important parameters may be considered as two sets; those that change with VSM tone, and those that can be considered constant.

The key parameters that vary with vascular tone are vessel diameter and stiffness. Ideally, from a modeling perspective, these would be well-documented in terms of basal values and deviations from these values associated with each of the mechanisms described above. However, this is not the case. The complex, layered structure of the vessel wall combined with the difficulties associated with *in vivo* measurement, mean that the mechanical behavior of human arteries has yet to be characterized thoroughly[22].

The constant properties are the branching patterns and lengths of the mesenteric vessels. Whilst some contrast-enhanced x-ray images exist[23] from which a model of a segment of gut could be derived, no one has yet numerically recorded the branching patterns of an entire human mesentery.

AN MRI STUDY OF FLOW IN THE SUPERIOR MESENTERIC ARTERY

Due to the invasive nature of most flow measurement techniques and poor spatial resolution of non-invasive techniques; accurate measurement of flow in the smaller arteries of the mesentery and gut is at present impossible in normal human subjects. Studies have however been carried out measuring flow in the parent vessel (the SMA)[24,25]. Such data can be used to validate models of the downstream vasculature. We added to this knowledge by using a flow-measuring phase contrast sequence on a 1.5T clinical MRI scanner to quantify the effect of a 600 kCal Scandishake® (registered trademark of Axcan Pharma) test meal on blood flow in the SMA. Twenty-one anatomical and flow images were acquired representing an average cardiac cycle over the 5 min acquisition time. For details of phase contrast MRI, the reader is referred to Edelman *et al*[26].

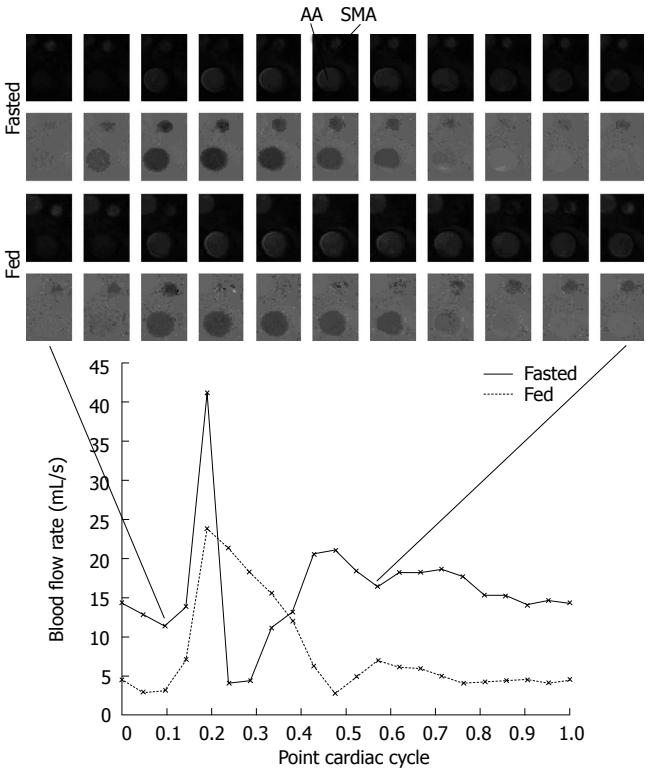

Figure 1 Fasted (top) and fed (bottom) cine phase-contrast magnitude (upper) and phase (lower) images of the SMA and abdominal aorta with associated graph of fasted and postprandial flow profiles, showing signal loss through peak systole in the fed case.

Eighteen healthy volunteers (11 male, 7 female, average age 36) fasted from midnight on the day of the scan and a base-line scan was taken between 9 and 10 am to give a measure of resting SMA flow. Each was then fed a 600 kCal Scandishake test meal containing 11.7 g of protein, 69.5 g of carbohydrates including 35.8 g of sugars, and 30.4 g of fat including 14.8 g of saturates. A second scan was taken 30 min postprandial (identified as the time of peak SMA blood flow in a previous ultrasound study[27]).

For the postprandial scan, in 15 of the 18 subjects the phase contrast signal was lost around peak systole as previously observed in some[24] but not all[25] previous similar experiments. In contrast to other authors[24], we believe that this is not due to a change in the shape of the flow waveform, but signal loss was due to disturbed flow causing intravoxel dephasing through the systolic period. Figure 1 shows postprandial PCMRA magnitude and phase images for one subject. The absence of the SMA at peak systole in both the magnitude and phase images supports the disturbed flow hypothesis.

In 2 of the 15 subjects, the same signal loss was also witnessed before feeding. For these reason we consider

Table 2 Results of PCMRA flow experiments

Parameter		Mean	SD	Range
Heart rate (BPM)	Fasted	62.1	8.5	45-76
	Postprandial	69.3	9.9	50-90
	Change[1]	11.9%	16.5%	0%-33%
Mean SMA diastolic flow (mL/s)	Fasted	4.3	3.3	0.6-14.5
	Postprandial	11.9	4.8	3.0-18.7
	Change[1]	177%	45.5%	881%-18.6%
Total SMA diastolic flow (mL/heart beat)	Fasted	4.1	2.8	0.6-11.9
	Postprandial	10.4	4.4	2.7-17.7
	Change[1]	154%	57.1%	798%-20.8%

[1]Percentage change normalized against fasted value.

only the diastolic portion of the cardiac cycle. At 30 min post-prandial, mean diastolic flow was 2.8 times that of the fasted value (Table 2).

AN INTEGRATED MODEL

We propose an integrated model of the small intestine and the mesenteric arteries with arteries modeled as a branching tree structure and the gut as a series of connected segments. The arterial model is a digital implementation[28] of Westerhof's branching tree model first published in 1969[29], with each artery having specified properties in terms of segment length, internal radius, wall thickness and wall stiffness. One key function of the intestinal model is to modulate the radius and stiffness of each vessel in accordance with food intake and other parameters. A suggested framework for this control is shown in Figure 2.

Due to the absence of quantitative human data in many areas, the model framework is designed to work logically within the limits of physiologically realistic values for the various inputs and to capture the key understood processes without recourse to the detailed underlying biology. For example, no caloric input, along with expected systolic pressure, will ensure that vessel stiffness and diameter remain at their basal levels, while saturation elements within the model reflect the fact that there are limits on the range of effect of the myogenic and calorie dependent response.

Data relating to sensitivity of vessels to caloric load, pressure difference associated with maximal myogenic response, and the effect of smooth muscle, is particularly difficult to obtain. For this reason, we now show results for the digestion part of the model alone (top left of figure 2 down to signal '*i*'), based on the consumption of a 600 kCal milkshake as used in our MRI study. Gastric emptying-rate data, a small intestinal transit time spectrum and a calorie absorption profile are the inputs to this part of the model. The model assumes a single food traveling along the gut with the three inputs inferred from the composition of the food being modeled.

The osmolarity of the milkshake was 880 mOsm/L putting it firmly in the "nutrient-containing liquid" category (normal osmolarity of blood 300 mOsm/L),

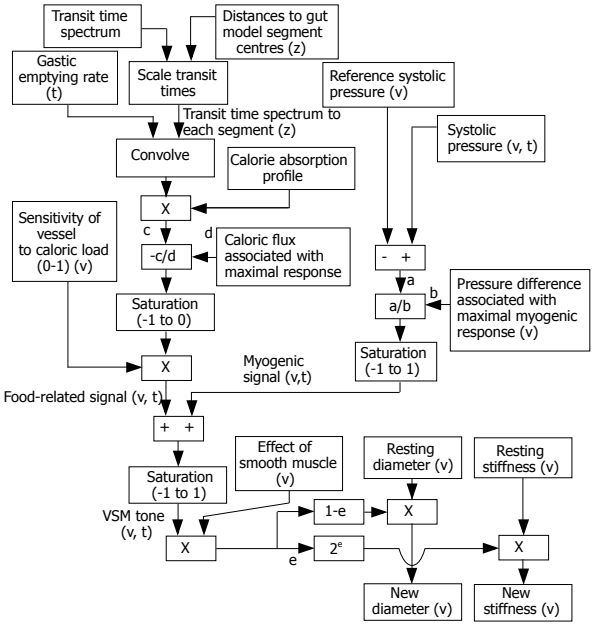

Figure 2 Suggested framework for control of gut blood flow. "(v)"denotes dependence of a parameter on the vessel in question, "(z)" on gut segment of interest, and "(t)" on time.

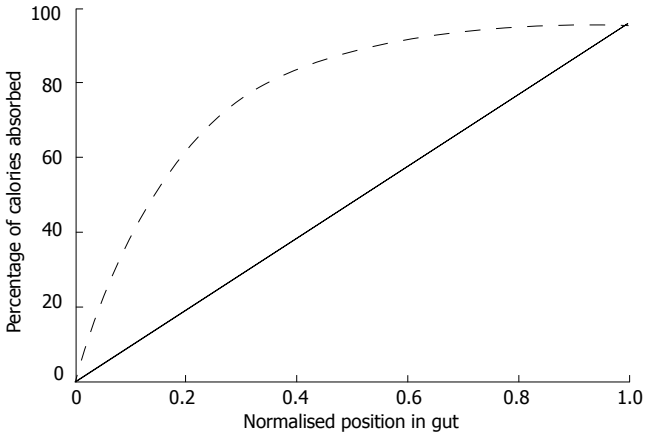

Figure 3 Linear (solid line) and exponential (dashed line) calorie absorption profiles.

therefore a gastric emptying rate of 3 kCal/minute was assumed.

The intestinal transit model consisted of a normally distributed transit time spectrum with mean transit time of 172 min and FWHM 169 min. It was assumed that each particle of chyme traveled along the gut at a constant rate.

The calorie absorption profile relates the percentage of calories that have been absorbed from the food at a given distance along the gut. Applying the nutritional data above to table one and weighting by caloric load, we calculate a coefficient of apparent digestibility for the milkshake of 96%. This becomes the final value in the calorie absorption profile. We consider two calorie absorption profiles; one is a linear profile assuming that caloric absorption is spread evenly along the gut, the other an exponentially-governed profile assuming that just over half of the calories are absorbed in the proximal 20% of the gut. Both profiles are shown in Figure 3.

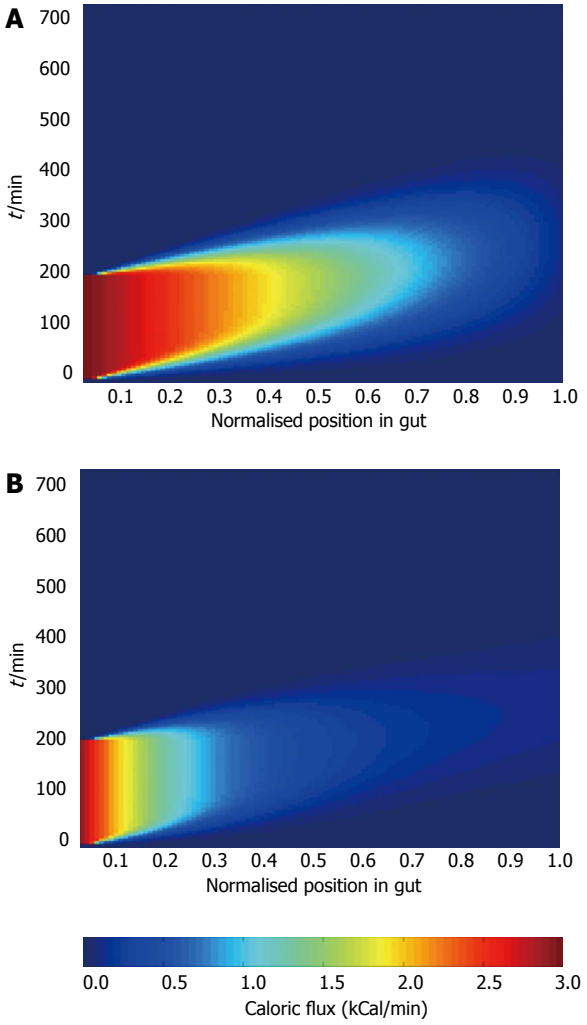

Figure 4 Pseudocolour plots showing caloric load against time and position in the gut for given gastric emptying and transit spectrum data with 96% gastric efficiency, based on linear (**A**) and asymptotic (**B**) absorption profiles.

Combining the three inputs in the manner defined in Figure 2 allows us to generate a surface showing caloric flux past each point in the gut with time. Surface plots for the two absorption profiles are shown in Figure 4.

The analysis illustrates the dependence of the pattern of caloric flux on the absorption profile, which is likely to result in altered arterial demand. This highlights the need for good quality data to drive the model, and demonstrates the ability of the model to show the effect of changes of individual inputs on the wider system.

CONCLUSIONS

This paper introduces the potential utility of modeling techniques to aid understanding of the complex interactions within the gut and its supporting vasculature.

We have reviewed the available data on diverse subjects that play an important role in the regulation of gut blood flow and postprandial hyperaemia, developed a modeling framework for the simulation of these processes, and presented preliminary results from the part of the model where the required data is available. We have also presented new data on blood flow in the SMA following feeding.

The development of this type of model brings together concepts and data from diverse fields and aids understanding of the physiology at organ and system levels.

REFERENCES

1 **Jeays AD**, Lawford PV, Gillott R, Spencer P, Barber DC, Bardhan KD, Hose DR. Characterisation of the haemodynamics of the superior mesenteric artery. *J Biomech* 2007; 40: 1916-1926
2 **Wakeling HG**, McFall MR, Jenkins CS, Woods WG, Miles WF, Barclay GR, Fleming SC. Intraoperative oesophageal Doppler guided fluid management shortens postoperative hospital stay after major bowel surgery. *Br J Anaesth* 2005; **95**: 634-642
3 **Gray H**. Gray's Anatomy. 38th ed. Philadelphia: Churchill Livingston, 1995
4 **Safar ME**, Levy BI, Struijker-Boudier H. Current perspectives on arterial stiffness and pulse pressure in hypertension and cardiovascular diseases. *Circulation* 2003; **107**: 2864-2869
5 **Horowitz M**, Dent J, Fraser R, Sun W, Hebbard G. Role and integration of mechanisms controlling gastric emptying. *Dig Dis Sci* 1994; **39**: 7S-13S
6 **Brener W**, Hendrix TR, McHugh PR. Regulation of the gastric emptying of glucose. *Gastroenterology* 1983; **85**: 76-82
7 **Malagelada JR**, Robertson JS, Brown ML, Remington M, Duenes JA, Thomforde GM, Carryer PW. Intestinal transit of solid and liquid components of a meal in health. *Gastroenterology* 1984; **87**: 1255-1263
8 **Camilleri M**, Colemont LJ, Phillips SF, Brown ML, Thomforde GM, Chapman N, Zinsmeister AR. Human gastric emptying and colonic filling of solids characterized by a new method. *Am J Physiol* 1989; **257**: G284-G290
9 **Husebye E**. The patterns of small bowel motility: physiology and implications in organic disease and functional disorders. *Neurogastroenterol Motil* 1999; **11**: 141-161
10 **Johansson C**, Ekelund K. Relation between body weight and the gastric and intestinal handling of an oral caloric load. *Gut* 1976; **17**: 456-462
11 **Merrill AL**, Bernice KW. Energy Value of Foods: basis and derivation (Agriculture Handbook No. 74). Washington: US government printing office, 1973
12 **Atwater WO**, Bryant AP. The availability and fuel values of food materials. Conn Agric Exp Stn. 12th ed. Middletown, CT: Storrs Agricultural Experiment Station Storrs, 1900: 73
13 **Atwater WO**, Bryant AP. The availability and fuel values of food materials. Conn Agric Exp Stn. 12th ed. Middletown, CT: Storrs Agricultural Experiment Station Storrs, 1900: 69
14 **Atwater WO**. The demands of the body for nourishment and dietary standards. In: Annual Report of the Storrs Agricultural Experiment Station. Middletown, CT: Storrs Agricultural Experiment Station, 1903: 123–146
15 **Chou CC**, Kvietys P, Post J, Sit SP. Constituents of chyme responsible for postprandial intestinal hyperemia. *Am J Physiol* 1978; **235**: H677-H682
16 **Chou CC**, Coatney RW. Nutrient-induced changes in intestinal blood flow in the dog. *Br Vet J* 1994; **150**: 423-437
17 **Chou CC**, Hsieh CP, Yu YM, Kvietys P, Yu LC, Pittman R, Dabney JM. Localization of mesenteric hyperemia during digestion in dogs. *Am J Physiol* 1976; **230**: 583-589
18 **Matheson PJ**, Wilson MA, Garrison RN. Regulation of intestinal blood flow. *J Surg Res* 2000; **93**: 182-196
19 **Schubert R**, Mulvany MJ. The myogenic response: established facts and attractive hypotheses. *Clin Sci* (Lond) 1999; **96**: 313-326
20 **Davis MJ**, Hill MA. Signaling mechanisms underlying the vascular myogenic response. *Physiol Rev* 1999; **79**: 387-423
21 **Osol G**, Laher I, Cipolla M. Protein kinase C modulates basal myogenic tone in resistance arteries from the cerebral circulation. *Circ Res* 1991; **68**: 359-367
22 **Schulze-Bauer CA**, Holzapfel GA. Determination of

constitutive equations for human arteries from clinical data. *J Biomech* 2003; **36**: 165-169

23 **Bergeron L**, Tang M, Morris SF. A review of vascular injection techniques for the study of perforator flaps. *Plast Reconstr Surg* 2006; **117**: 2050-2057

24 **Chan FP**, Li KCP, Nayak KS, Hilfiker PR, Pauly JM. Efficient Characterization of Mesenteric Blood Flow Using Color-Flow Real-Time Interactive MRI. Philadelphia: Proceedings ISMRM Seventh Scientific Session, 1999: 1638

25 **Masui T**, Isoda H, Mochizuki T, Takahashi M, Kaneko M, Shirakawa T, Ota A. Effects of meal intake on the flow velocity in the superior mesenteric artery: evaluation with 2D phase mapping MRI. *J Comput Assist Tomogr* 1994; **18**: 590-595

26 **Edelman RR**, Hesselink JR, Zlatkin MB. Clinical Magnetic Resonance Imaging. 2nd ed. Philadelphia: W.B.Sauders Company, 1996

27 **Spencer PA**, Pramanik A, Chaudhuri A, Hill E, Berry C, Pryce WI, Willemse PJA, Bardhan KD. Small Intestinal Blood Flow in Man: The Effects of Age and Caloric Loading. *Gut* 2000; **46** (suppl II): A67

28 **Jones DM**, Hose DR, Lawford PV, Hill DLG, Razavi RS, Barber DC. Creation of patient-specific CFD models by morphing a previously-meshed reference geometry using image registration. In: Rueckert D, Hajnal J, Yang GZ, editors. Medical Image Understanding and Analysis 2004: Proceedings of the eighth annual conference; September 23-24; London: England, 2004: 173-176

29 **Westerhof N**, Bosman F, De Vries CJ, Noordergraaf A. Analog studies of the human systemic arterial tree. *J Biomech* 1969; **2**: 121-143

S- Editor Liu Y **L- Editor** Lutze M **E- Editor** Lu W

PO Box 2345, Beijing 100023, China
www.wjgnet.com
wjg@wjgnet.com

World J Gastroenterol 2007 March 7; 13(9): 1399-1407
World Journal of Gastroenterology ISSN 1007-9327

TOPIC HIGHLIGHT

Hans Gregersen, Professor, *Series Editor*

Towards a multiscale model of colorectal cancer

Ingeborg MM van Leeuwen, Carina M Edwards, Mohammad Ilyas, Helen M Byrne

Ingeborg MM van Leeuwen, Helen M Byrne, Centre for Mathematical Medicine and Biology, School of Mathematical Sciences, University of Nottingham, Nottingham NG7 2RD, United Kingdom
Carina M Edwards, Centre for Mathematical Biology, Oxford Centre for Industrial and Applied Mathematics, Mathematical Institute, University of Oxford, Oxford OX1 3LB, United Kingdom
Mohammad Ilyas, Division of Pathology, School of Molecular Medical Sciences, Queen's Medical Centre, University of Nottingham, Nottingham NG7 2UH, United Kingdom
Supported by the EPSRC, No. GR/S72023/01
Correspondence to: Helen M Byrne, Professor, Centre for Mathematical Medicine and Biology, School of Mathematical Sciences, University of Nottingham, Nottingham NG7 2RD, United Kingdom. helen.byrne@nottingham.ac.uk
Telephone: +44-115-9513852 Fax: +44-115-9513837
Received: 2006-12-09 Accepted: 2007-01-11

Abstract

Colorectal cancer (CRC) is one of the best characterised cancers, with extensive data documenting the sequential gene mutations that underlie its development. Complementary datasets are also being generated describing changes in protein and RNA expression, tumour biology and clinical outcome. Both the quantity and the variety of information are inexorably increasing and there is now an accompanying need to integrate these highly disparate datasets. In this article we aim to explain why we believe that mathematical modelling represents a natural tool or language with which to integrate these data and, in so doing, to provide insight into CRC.

Key words: Intestinal epithelium; Crypt fission; APC mutations; Mathematical modelling; Stem cell niche; Wnt signalling

van Leeuwen IMM, Edwards CM, Ilyas M, Byrne HM. Towards a multiscale model of colorectal cancer. *World J Gastroenterol* 2007; 13(9): 1399-1407

http://www.wjgnet.com/1007-9327/13/1399.asp

INTRODUCTION

Colorectal cancers (CRCs) originate from the rapidly renewing epithelium that covers the luminal surface of the bowel and lines the colonic crypts (Figure 1). At the bottom of these crypts, stem cells proliferate continuously producing amplifying transit cells that divide rapidly several times before differentiating into the various cell types that constitute the epithelium (e.g. absorptive columnar cells, mucinous Goblet cells, and neuroendocrine cells). The production of new cells is synchronised with migration of the epithelium upwards along the crypt axis. Upon reaching the orifice, cells undergo apoptosis and are shed into the lumen. Under normal conditions, these cellular processes are tightly regulated by biochemical and biomechanical signals (e.g. Wnt factors, cell-cell contacts and growth factors)[1,2]. CRC arises when genetic alterations, for example in the Wnt pathway, disrupt normal crypt dynamics. Proliferating cells are then no longer confined to the crypt's base and the associated proliferative excess generates biomechanical stress on the crypt structure, which may deform in order to accommodate the newborn cells. The dysplastic cell population will expand further by invading neighbouring crypts and/or inducing crypt fission, leading to the formation of an adenoma[3,4].

Cancers of the colon and rectum are the third most frequent malignancies in the United Kingdom, being responsible for 16148 deaths in 2004[5]. Most CRCs occur sporadically, with only 5% attributable to hereditary syndromes[6], such as familial adenomatous polyposis (FAP). The first detailed genetic model for the development of CRC was published in 1990[7], with adenomatous polyposis coli (*APC*), *K-ras*, *DCC* and *p*53 as candidate cancer genes that undergo mutation in an ordered sequence. Due to its high socio-economic impact, CRC is studied extensively world-wide. While some of the mechanisms of CRC development have now been revealed, as more biochemical, genetic, histological and clinical information is made available, new layers of complexity are becoming apparent. We believe that CRC research has now reached a stage at which theoretical thinking and mathematical modeling have become essential to integrate and make sense of the biological information being generated and, more importantly, to generate new biological hypotheses that can then be tested in the laboratory. Among the benefits of modeling are: (1) mathematical models act as *in silico* tools with which to carry out and iterate virtual experiments that might be dismissed by experimentalists for being unethical, expensive, time consuming, or simply impossible; (2) modeling necessitates the statement of explicit hypotheses, a process which often enhances comprehension of the biological system; and (3) simulations can reveal hidden patterns and/or counter-intuitive mechanisms in complex systems. The use of mathematical modeling to tackle

complex biological problems is becoming increasingly popular within the life sciences[8,9]. Hence, cancer modeling is a rapidly growing field within applied mathematics (critical reviews[10,11]) and, in particular, a number of models have been developed specifically to study issues associated with the normal gut and CRC (reviewed in Van Leeuwen *et al*[12]). Epidemiological models, for instance, have sought to describe CRC incidence in human populations[13,14]. Notably, such models have provided insight into the multistage nature of carcinogenesis and the importance of clonal expansion. Furthermore, discrete models characterising the position and behaviour of individual cells within an intestinal crypt have been formulated to advance our understanding of the mechanisms of cell migration and differentiation[15-17], while stochastic models have been used to investigate the accumulation of genetic (or epigenetic) alterations in epithelial cells[18-21].

Most theoretical studies of CRC, including those exemplified above, were designed to investigate specific biological questions and, consequently, they typically focus on a single time and length scale. In reality, the dynamics of normal tissue, colorectal carcinogenesis and cancer progression involves the integration of a large number of processes occurring over different levels of organisation; ranging from the fast enzymatic reactions taking place inside individual cells to the relatively slow dynamics of tumour growth and metastasis (Figure 2). In order to understand the ways in which subcellular events influence macroscopic tumour progression, it is necessary to develop models that incorporate multiple time and length scales. Such multiscale models are also needed to account for feedback within the system; for example, hypoxic cues, mechanical stress, immunological response and chemotherapeutic interventions all act on the macro- and cell-scales but have a profound influence on subcellular dynamics[22,23]. A natural consequence of this coupling across scales is that models cannot be built from the bottom-up by coarse-graining proteomic data, even if this were computationally feasible[24,25]. We propose that a multilevel approach be adopted, with (sub)models assembled at different scales before being coupled together so that more complex emergent behaviour can be explained.

The potential use of multiscale modeling to tackle complex biological problems is best exemplified by the sophisticated computational models of the heart developed by Noble and co-workers[26,27] where the simulation of normal and abnormal physiology, from the molecular level to the whole-organ, is well established. Only recently have these efforts been mirrored by similar projects focused on solid tumour growth. For example, Swanson and co-workers[28] have developed three-dimensional models that describe the spread of gliomas through the brain. While the mathematical model that they use is highly idealised (Fisher's equation describes how the tumour cells migrate and proliferate), they have gone to considerable efforts to replicate the detailed anatomical structure of the brain and to calibrate their models against MRI scans. In particular, the random motility and proliferation rates of tumour cells are assumed to differ between grey and white matter. Their models show excellent agreement with clinical data and are being used to predict the response of patients to different treatment protocols. The limitations of the models described in Swanson *et al*[28] are that they do not explicitly account for nutrient supply to the expanding tumour mass and they neglect the multiscale nature of solid tumour growth. Several multiscale models of tumour growth that attempt to resolve these issues have been developed recently[22,29-31]. For example, Alarcón and co-workers have formulated a hybrid cellular automaton of vascular tumour growth that links submodels that describe processes occurring at the subcellular, cellular and tissue scales[22]. In more detail, progress through the cell cycle and the production of angiogenic factors are incorporated at the subcellular level and competition for resources are considered at the cellular level. The transport of nutrients and angiogenic factors, blood flow and vascular adaptation are included at the tissue scale. Coupling between the different submodels occurs in several ways. For example, oxygen levels, which are determined at the macroscale, influence subcellular processes such as progress through the cell cycle and the production of angiogenic factors. Equally, subcellular production of angiogenic factors modulates vascular adaptation at the tissue scale. Model simulations reveal that the tumour's growth dynamics and, in particular, its morphology, are heavily influenced by the way in which the haematocrit distribution in the vasculature is modeled. For example, if it is heterogeneously distributed, then the tumour's growth is highly irregular, being confined to well-oxygenated regions. By contrast, if the haematocrit is uniformly distributed then the tumour expands radially outwards as a compact mass.

Most existing multiscale models of solid tumour growth are generic in nature, in the sense that they are not specialised to a particular tissue or a specific type of cancer. We believe that it is now timely to develop mathematical models of this type to describe CRC. We aim in this article to explain the potentially valuable role of multiscale modeling in advancing our understanding CRC. We start by describing briefly some areas where modeling has generated insight into CRC (for a more exhaustive review, see Van Leeuwen *et al*[12]). These include signalling pathways, CRC initiation and crypt buckling. We conclude by explaining how we intend to integrate such models within a multiscale framework and, in so doing, enable experimentalists to explore, in a controlled *in silico* environment, the ways in which phenomena occurring on different space and time scales interact (Figure 2).

BIOCHEMICAL NETWORKS IN CRC

APC inactivation is believed to be an early, initiating event in CRC. Genetic alterations in the APC gene have been found in about 85% of all CRC cases and germline mutations are responsible for FAP[6,7]. Although APC is a multifunctional protein, it is generally accepted that APC's tumour suppressor potential relies upon its ability to inhibit Wnt signalling[32]. This is best illustrated by the fact that activation of Wnt signalling by other means obviates the need for APC inactivation. Wnt signalling is essential for maintaining the stem-cell niche at the base of

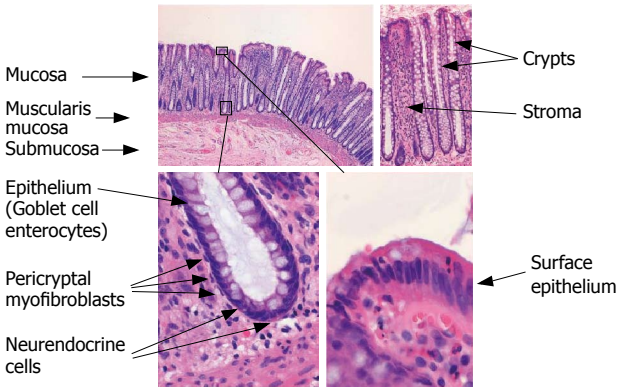

Figure 1 Normal colonic mucosa. The normal colonic mucosa consists of crypts (lined with epithelium) embedded within a connective tissue stroma. The mucosa rests on a layer of smooth muscle, called the muscularis mucosae, below, which is a loose connective tissue layer, called the submucosa. The epithelium consists of a number of different cell types including goblet cells (containing mucin), enterocytes and neuroendocrine cells (which secrete hormones). The crypts are enveloped by a sheath of myofibroblasts that are separated from the epithelium by basement membrane. The stroma contains a number of different cell types including macrophages, fibroblasts and lymphoid cells. The crypt is a dynamic structure that turns over every 3-6 d. The base of the crypts contains the stem cells that are thought to give rise to transit amplifying cells. The cells migrate up the crypt and undergo differentiation along the way. The goblet cells secrete mucin into the crypt and intestinal lumen and the surface epithelium usually contains few goblet cells. Upon reaching the surface, the cells undergo apoptosis and are shed into the lumen. The migration along the crypt by the epithelial cells is accompanied by a similar migration of myofibroblasts. The microenvironment is thought to change along the crypt axis and this is thought to give environmental cues for induction of maturation and inhibition of proliferation.

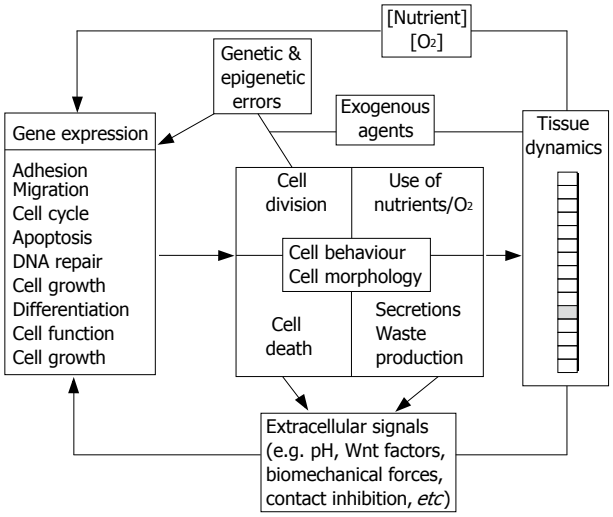

Figure 2 Prototype multiscale model of the gut. Subcellular, cellular and tissue elements are represented in black, grey and white boxes, respectively. The schematic shows possible interactions and feed-back loops coupling the different levels of organisation and illustrates the complexity of the biological system. An additional challenge in building such multiscale models is coupling phenomena that act on very short time scales (e.g. the diffusion of metabolites and signalling molecules in the extracellular medium) with processes that occur on longer time scales (e.g. tumour growth).

the crypt[33] and it has been proposed that, under normal physiological conditions, spatial gradients in extracellular factors acting on Wnt signalling, regulate cell proliferation, migration, differentiation and apoptosis along the vertical crypt axis[34]. This maintains the integrity of the normal crypt and allows renewal of the intestinal epithelium to occur in an ordered and controlled fashion. Inappropriate activation of Wnt signalling, however, results in loss of this normal control, leading to tumour development. The importance of Wnt signalling in carcinogenesis means that a model of this subcellular biochemical network should play an integral role in the development of any multiscale model of CRC.

Since the biochemical details and biological implications of the Wnt pathway have been reviewed elsewhere[32,35], here we summarise the key points. In the absence of an external Wnt stimulus, a destruction complex (including APC and axin) keeps cytoplasmic and nuclear levels of β-catenin low, thus allowing the repressor Groucho to bind preferentially to TCF/LEF transcription factors, thereby preventing the expression of Wnt target genes. In contrast, when extracellular Wnt factors bind to specific cell-surface receptors, a cascade of protein activation/inactivation events is triggered, leading eventually to the inhibition and destabilisation of the β-catenin destruction complex. Consequently, β-catenin protein accumulates in the cytoplasm and travels to the nucleus, whereby displacing Groucho from TCF/LEF proteins, it can induce the expression of target genes. Lee *et al*[36] have formulated a mathematical model of the Wnt pathway that describes normal protein turnover, step-wise assembly/dissociation of the destruction complex, binding and phosphorylation of β-catenin by the destruction complex, and assembly/dissociation of the transcription complex formed by β-catenin and TCF. The model provides quantitative expressions for dynamic changes in the level of 15 molecular components, based on parameter values either measured or estimated from experiments with *Xenopus* extracts. The combination of theoretical and experimental results revealed the importance of a novel regulatory loop involving APC-dependent degradation of axin. Hence, when this feedback mechanism is active, β-catenin levels are relatively resistant to reductions in active APC.

While Lee and co-workers[36] focused on the role of β-catenin in signalling, Van Leeuwen *et al*[37] have recently developed an alternative model of the Wnt pathway that accounts for its dual role in signalling and cadherin-mediated cell-cell adhesion. Instead of restricting their analysis to a limited set of parameter values, they used mathematical methods to gain insight into the general properties of the model system. In Figure 3, we exemplify this approach with a simple network involving only three components, i.e. A, B and AB. The reader can reduce the level of abstraction by considering the often presumed hypothesis that E-cadherin (A) can sequester β-catenin (B) from signalling. Both proteins are subject to normal protein turnover and to reversible binding to form a complex AB. The time-dependent change in the concentration of each molecular component is determined by its production and elimination rates. However, once enough time has elapsed, the compounds will reach a steady-state and no further changes in concentration will occur. For the given system, the final levels can easily be deduced from the kinetic equations. The final concentration of B, for example, is given by the ratio of its synthesis and degradation rates and does not, therefore, depend on any parameters associated

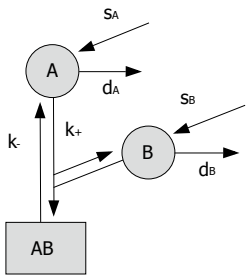

Figure 3 Example of a simple kinetic model. The proteins A and B undergo normal protein turnover (s = synthesis rates, d = degradation rates) and associate to form a protein complex, AB (k_+ = assembly rate, k_- = dissociation rate). The behaviour of the system is captured by the following system of ordinary differential equations:

$d[A]/dt = s_A - k_+[A][B] + k_-[AB] - d_A[A]$;

$d[B]/dt = s_B - k_+[A][B] + k_-[AB] - d_B[B]$;

$d[AB]/dt = k_+[A][B] - k_-[AB]$;

with initial conditions $[A](0) = A_0$, $[B](0) = B_0$ and $[AB](0) = 0$. It can be shown that, eventually, the components stabilise at levels given by: $[A] = s_A/d_A$; $[B] = s_B/d_B$, and $[AB] = s_A s_B/(d_A d_B K)$, with $K = k_-/k_+$ the dissociation constant.

with either A or the initial concentrations. This implies that the long-term, equilibrium level of cytoplasmic β-catenin is independent of E-cadherin and, consequently, changes in E-cadherin expression can only transiently affect the cytoplasmic β-catenin level. This example illustrates the potential value of adopting a theoretical approach; even in the absence of detailed parameter values, it is possible to extract meaningful conclusions and to generate new (experimentally-testable) hypotheses.

The approach of Van Leeuwen *et al*[37] made it possible to compare two potential mechanisms of interaction between signalling, transcription and cell-cell adhesion. According to the first hypothesis (H.1), E-cadherin and TCF simply compete for β-catenin. Alternatively, under H.2, the Wnt signal induces the production of a 'closed' molecular form of β-catenin that binds preferentially to TCF. This might occur, for instance, *via* the activation of a kinase that phosphorylates β-catenin at Tyr-142. As might be expected, in both cases the model predicted an increase in the level of transcription complexes in response to Wnt. Surprisingly, however, the final equilibrium level of β-catenin-TCF complexes was independent of whether H.1 or H.2 was active and, consequently, it is not possible to discriminate between the two alternatives based on target gene expression alone. Under H.1, the model always predicted an increase in cell-cell adhesion in response to Wnt, whereas under H.2 this was not always the case: under H.2, the degree of cell-cell adhesion at equilibrium decreased as the rate of β-catenin Tyr-phosphorylation increased.

Van Leeuwen *et al*[37] also used their model to investigate the impact of two genetic alterations commonly observed in CRC; i.e. aberrant inactivation of APC and mutations that render β-catenin resistant to APC-mediated degradation. Simulations showed that in wild-type cells and single mutants, the level of transcription complexes depends on the strength of the Wnt gradient; by contrast, double mutants achieve the same (high) level of target gene expression and this value does not depend on the strength of the Wnt stimulus. As a consequence, the proportion of functional APC needed to maintain a normal phenotype increases with increasing extracellular Wnt levels. This result illustrates that the environment can have a substantial impact on malignant transformation and tumour phenotype.

STOCHASTIC MODELS FOR CRYPT DYNAMICS AND CRC-INITIATION

According to Knudson's classic model for inactivation of tumour suppressors, two mutations (one in each copy of the gene) are required to completely abrogate APC's anti-cancer activity. Given the extensive period of time required for a cancer to develop, stem cells have been widely regarded as the most likely targets for these mutations due to their apparent immortality. Komarova and Wang[18] used mathematical modeling to investigate whether neoplastic change could, instead, take place in the semi-differentiated, transit cell population. For this purpose, they considered an idealised crypt containing a single stem cell and investigated three complementary scenarios: (SS) both hits happen in stem cell; (ST) the first hit occurs in the stem cell and the second in a transit cell; and (TT) the first hit is in a transit cell and the second in one of its progeny. Scenarios SS and ST share an intermediate state in which the crypt is monoclonal, being filled with single APC mutants ($APC^{+/-}$ cells). Challenging *a priori* intuition, the model revealed that the probability that the first double mutant appeared in the stem cell pool was negligible. The authors thus concluded that at least one of the hits occurs in the migrating, transit population and remarked that "a possible role of differentiated cells in cancer initiation cannot be discarded simply based on the fact that they are short-lived[18]."

In Komarova and Wang[18], the 'immortal' stem cell always divided asymmetrically, renewing itself and producing a transit cell. Their model can therefore easily be extended for crypts with multiple immortal stem cells, as such crypts can be seen as multiple single-stem cell crypts. Alternatively, Yatabe *et al*[21] considered 'mortal' stem cells that underwent asymmetric division, symmetric division (giving two stem cells), or cell death, with certain probabilities. To gain insight into the number and patterns of division of human stem cells, they monitored *in silico* the accumulation of random methylation changes in individual crypts. By comparing the predicted intra- and inter-crypt variability with experimental data on the methylation content of specific CpG islands, they concluded that "the complex epigenetic patterns were more consistent with a crypt niche model wherein multiple stem cells were present and replaced through periodic symmetric divisions[21]". An important consequence is the concept of niche succession, which is, after a random waiting time, the crypt will be filled with the progeny from a single stem cell. More recently, it has been suggested that these 'lineage bottlenecks' enhance malignant transformation, because the progeny of an $APC^{+/-}$ stem cell could take over the stem-cell pool, thereby increasing the number of candidates for the second hit. Van Leeuwen *et al*[12] performed a series of stochastic simulations to test this hypothesis. Their model was built upon the following basic assumptions: (1) stem cells divide synchronously; (2) for any given generation, two random sets of m stem cells divide symmetrically and die/differentiate, respectively; (3) newborn cells acquire an *APC* mutation with a certain probability. For a crypt with 64 stem cells, simulations were iterated for values of m between 0 and 16. As expected,

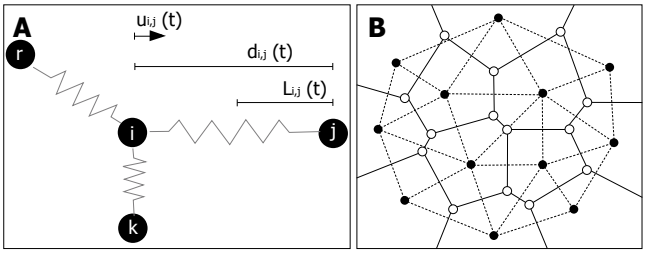

Figure 4 Schematics illustrating the lattice-free approach developed by Meineke *et al*[16]. (**A**) *In silico* cells attached by springs. According to Hooke's law, the restoring force due to each spring is proportional to its net extension and acts in the opposite direction. The total force acting on a cell i is equal to the sum of all forces applied by neighbouring cells j: $F_i(t) = \mu \Sigma u_{ij}(t) (d_{ij}(t) - L_{ij}(t))$, with μ the spring constant, L_{ij} the equilibrium length of the spring between i and j, d_{ij} the distance between i and j, and u_{ij} the unit vector from i to j. The new position of cell i after a small time interval Δt is given by: $r_i(t + \Delta t) = r_i(t) + F_i(t) \Delta t/\eta$, with η a damping constant. (**B**) *In silico* 2D tissue, showing cell centres (black nodes) and the associated Voronoi tesselation (solid lines). The related Delauney triangulation (dashed lines) is obtained by connecting all neighbouring nodes and defines the network of springs.

the average niche succession time decreased as the number of symmetric divisions per generation increased. The average time to a first double mutant, however, appeared to increase with *m*. In particular, crypts with immortal stem cells only (i.e. $m = 0$), on average, developed cancer earlier than crypts with mortal stem cells (i.e. $m > 0$). As expressed by the authors, "the stem cell lineage bearing a single APC mutation has more chance of becoming extinct during the next niche succession cycle than of benefiting from the advantages of fixation in the crypt". It is therefore proposed that symmetric stem cell division and niche succession protect stem cells against malignant transformation[12].

Lobachevsky and Radford[38] have recently proposed a different view of the crypt's architecture in that their *in silico* stem cells cannot divide indefinitely. This assumption was motivated by experimental evidence supporting the occurrence of significant telomere-shortening in stem cells. The authors classified stem cells into two pools; i.e. deep, slowly proliferating stem cells that produce rapidly dividing proximate stem cells. The former always divide asymmetrically whereas the latter either divide symmetrically or die, as necessary, to maintain the homeostasis and integrity of the crypt. Furthermore, the probability of symmetric division or death depends on the cell's age. Comparison of model predictions with experimental data suggested a replicative lifespan for stem cells of about 50-150 divisions, which differs markedly from the 5000 divisions estimated by other modellers. The new model was also able to reproduce the observed time-dependent appearance of partially and monoclonally mutant crypts in mice following treatment with ethyl nitrosourea.

SPATIALLY-STRUCTURED MODELS OF CRYPT-DYNAMICS

None of the models discussed thus far incorporate spatial effects. For example, the models for Wnt signalling view cells as 'well-stirred buckets' and, thus, consider only time-dependent changes in protein levels[36]. Equally, the carcinogenesis models record the accumulation of genetic or epigenetic alterations in a population of cells, without considering the relative positions of individual cells within an individual crypt[12,18,21]. Given that external cues to such subcellular phenomena are often spatially distributed (c.f. variations in extracellular Wnt levels along the crypt axis), it is natural to include spatial effects in order to describe accurately the dynamics of normal and pathological crypts. Several computational models of normal crypt dynamics that account for spatial effects have been proposed. In these models the cylindrical crypt is usually cut open and rolled out to give a two-dimensional surface, which is computationally easier to simulate. For example, Loeffler and co-workers[15,17] have built a series of models in which cells are constrained to move within a rectangular grid. During their simulations, they monitored the progress of individual cells through the cell cycle. This enabled them to compare their results with tritiated thymidine labelling data showing how the proportion of proliferating cells changes with spatial position and over time. The model was used to compare eight alternative hypotheses concerning the positioning of newly-formed daughter cells. Of these, only two of the hypotheses were consistent with the experimental data. The first placed the daughter cell at the site of the oldest neighbour, whereas the second combined random insertion with inevitable final differentiation at a certain position along the crypt axis[15].

A major weakness of the 2D-grid approaches is that insertion of each newborn cell displaces a whole column of cells upwards, breaking many cell-cell contacts. This is biologically unrealistic, as epithelial cells are known to form tight cell-cell junctions. Meineke *et al*[16] resolved this problem by developing a lattice-free model in which cell movement was governed by the net effect of the repulsive and attractive forces acting on each cell, these forces being modeled by a network of springs connecting the centre of neighbouring cells (Figure 4A). An advantage of this approach is that the insertion of newborn cells causes local rearrangements only. To display the geometry, the nodes from the network of springs were used to generate a Voronoi tessellation (Figure 4B). The resulting model was then used to simulate the dynamics of a healthy crypt and shown to reproduce the experimentally observed polygonal shape of epithelial cells and the spatial distribution of proliferating cells. Although the model by Meineke *et al*[16] resolved the major weakness of the 2D-grid models, both types of model have several limitations in common. For instance, no biological mechanism regulates the removal of cells from the upper edge of the crypt and the model does not account for cell death occurring in cells other than fully differentiated cells. Furthermore, cell size is independent of growth processes, the time since the cell' s last division and extracellular conditions. Finally, the proliferative capacity is an intrinsic property of each cell and the progression of individual cells through the cell cycle is fixed at the time of their birth, with the duration of each phase being independent of any biochemical or biomechanical control (e.g. Wnt signals and cell-

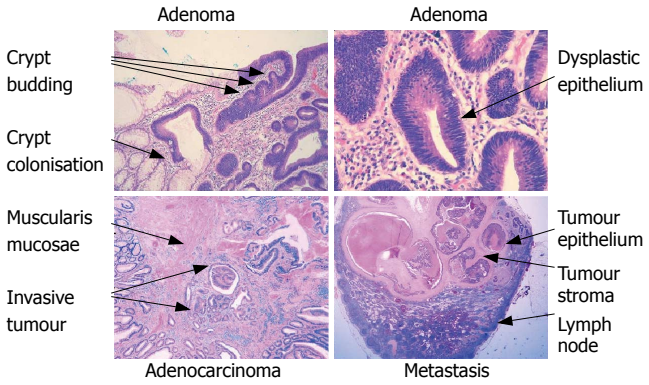

Figure 5 The stages of tumour development. Colorectal cancers develop through a variety of stages. Disruption of Wnt signalling (usually through *APC* mutation) will cause adenoma formation. This is manifest as dysplasia of the epithelial cells (characterised by enlargement of the epithelial nuclei, loss of mucin and deeply staining nuclei). Adenomas can grow by crypt branching and colonisation of other crypts but, importantly, remain bounded by the basement membrane. The branching of the crypts causes adenomas to develop a very complex architecture and, as more mutations accrue, the architecture becomes more complex and the cells become more severely dysplastic. Eventually the tumour cells will break through the basement membrane and invade into the stroma and this represents the transition from and adenoma into a carcinoma. Once within the stroma, the tumour cells can grow, infiltrate more deeply into the bowel wall and also can invade into lymphatic and vascular structures to allow metastasis to distant sites, such as lymph nodes. It is noteworthy that metastatic deposits also contain stroma showing the importance of the relationship between the tumour epithelium and the tumour stroma.

cell contacts). Integrating biologically realistic models of such subcellular processes and biochemical network dynamics with extracellular cues will be challenging and computationally intensive, with the approach depending on the correct coupling of the constituent submodels.

Smallwood and colleagues[39] have used an agent-based framework to develop an alternative, lattice-free model that describes the expansion of a population of epithelial cells cultured *in vitro* on a monolayer. Individual cells are represented as three-dimensional, rigid spheres that can proliferate, migrate, differentiate or die. The model also accounts for cell-cell and cell-substrate interactions. At every time step, a set of simple predefined rules determines the behaviour of each cell, based on its position, internal parameters and the composition of the local, extracellular environment. Under the assumption that calcium enhances cell-cell adhesion, the resulting computational model showed substantial differences in monolayer growth in the presence of low and physiological calcium concentrations, which nicely mimicked the results from equivalent *in vitro* studies with normal human urothelial cells. Agent-based models could, in principle, be modified to describe the intestinal epithelium and, in particular, be used to study the impact of changes in cadherin-mediated (Ca^{++}-dependent) cell-cell adhesion on the dynamics of the crypt.

MODELS FOR CRYPT BUDDING AND FISSION

The genetic changes that underlie colorectal carcinogenesis usually manifest themselves at a tissue level through the formation of an adenoma, which may subsequently develop into a malignant tumour (Figure 5). This progression is known as the adenoma-carcinoma sequence[7]. Two competing theories have been postulated to explain how such adenomas form. According to the *top-down* hypothesis, dysplastic cells in the superficial portions of the crypt spread laterally, invading healthy crypts from the 'top-down'. According to Shih *et al*[4], dysplastic cells are found to reside on the luminal surface either because the initial APC mutant has migrated to the surface, or because genetic precursors of the dysplastic cells reside in the intercryptal zones; the possibility of a second genetic hit in the migrating population, as suggested by Komarova and Wang[18] and discussed above, could also explain the appearance of a dysplastic luminal epithelial layer. The alternative mechanism for adenoma formation is known as the *bottom-up* hypothesis[3]. Here adenoma formation always starts with a monocryptal lesion, which then expands by crypt fission and/or by colonisation of neighbouring crypts.

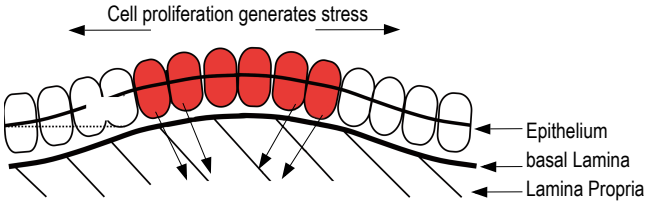

Figure 6 Schematic of the biomechanical model developed in Edwards and Chapman[44]. Proliferation in the epithelium generates stress within the layer through cellular attachment to the underlying basal lamina. For certain choices of the model parameters, the stress that is generated causes the layer to buckle, inducing a displacement *y* and initiating crypt budding and fission.

Adenomatous crypts are typically elongated and deformed, exhibiting multiple branching events, although still lined by a single layer of epithelial cells[40-42] (Figure 5). In order to explain how crypt fission may occur, Drasdo and Loeffler[43] developed an agent-based model in which a vertical cross-section through a crypt was treated as a U-shaped chain of growing, deformable cells that interact elastically with each other. The authors show that decreasing the cell cycle time and reducing the Young modulus of the cells can cause the crypt to buckle and undergo crypt fission. These results are consistent with experimental observations, which suggest that an increase in cell proliferation accompanied by a reduction in cell-cell adhesion (both perhaps associated with a mutation in *APC*) may lead to crypt fission.

More recently Edwards and Chapman[44] have developed a biomechanical model of crypt budding and fission in which the epithelial cells are treated as a continuous tissue layer that is attached to a rigid basal lamina (Figure 6). The model input parameters quantify cell proliferation, adhesion, movement and apoptosis, which are dependent on lower-scale effects. Using a combination of numerical and analytical techniques, Edwards and Chapman were able to identify parameter regimes in which a flat (rolled-out) crypt would buckle. This instability was indicative of crypt fission. For example, they determined the extent to which the proportion of proliferating cells can be increased before the layer buckles. Also, in

qualitative agreement with Drasdo and Loeffler[43], they found that decreasing the cell cycle time could destabilise the layer. As Edwards and Chapman treat the epithelial cells as a continuous sheet rather than as individual entries, it may prove easier to extend their model to simulate more realistic three-dimensional geometries and larger tissue regions, possibly containing multiple crypts.

DISCUSSION

In this article we have reviewed a range of mathematical models of CRC that provide insight into different aspects of its development. These include stochastic models designed to investigate where in the crypt the second APC hit associated with CRC initiation is most likely to occur[18], detailed models of Wnt signalling to enhance our understanding of the mechanisms of action of this pathway[36,37] and continuous models to explore the causes of crypt buckling and fission[43,44]. While useful, models that focus on a single time and length scale provide limited insight into crypt dynamics and CRC.

Advances in biotechnology mean that it is now possible to generate vast amounts of different types of experimental data. For example, high-throughput gene and protein expression data can be obtained from microarrays[45-47] and more detailed information from microdissection and tagging specific genes with green fluorescent protein (GFP)[19,48]. Multiscale mathematical models that account for subcellular, cellular and tissue scale phenomena represent a natural framework for integrating and exploiting these different datasets. As part of a UK government funded project in *Integrative Biology*[49], we are using grid technology and high performance computing to perform multiscale simulations of cardiovascular disease[25,27] and cancer[12,37,44,50]. The protype multiscale model of a colonic crypt that we are developing uses a lattice-free model to describe epithelial cell movement and will incorporate subcellular, biochemical phenomena, such as the Wnt signalling pathway and detailed models of the cell cycle[51]. For example, using our Wnt signalling model[37], it is possible to determine β-catenin levels in the nucleus (and hence involved in gene expression) and the number of molecules forming adhesion complexes, and how these values change with the extracellular Wnt stimulus. By incorporating this information into our multiscale model, we will investigate the way in which Wnt signalling co-ordinates cell movement, proliferation and differentiation along the crypt axis. Additionally, with knowledge of how single and double mutations in the genes coding for APC and β-catenin affect the Wnt signalling pathway, we may use our model to simulate the spread of mutant cells and establish whether their ability to colonise a crypt depends on the spatial location at which the mutation originates. This will provide a comparison of the top-down and bottom-up theories of adenoma formation. By further extending our model to account for the attachment of epithelial cells to the underlying tissue stroma, it will be possible to see how increases in cell proliferation associated with CRC and changes in cell-stroma adhesion contribute to crypt fission. Finally, by upscaling or homogenising our cell-level models, we aim to derive tissue scale models similar in form to that of Edwards and Chapman[44]. In addition to permitting the simulation of large tissue regions (and hence the colonisation of neighbouring crypts by malignant cells), this will enable us to relate tissue level parameters, associated with, for example, cell proliferation and adhesion to experimentally measurable quantities, such as nuclear β-catenin levels and extracellular concentrations of Wnt factors.

Mathematical modeling and computational methods are not only powerful tools for enhancing our understanding of how tumours originate and grow; they may also be used to improve cancer diagnosis and treatment. Hence, modern imaging techniques make it possible to detect and stage the primary tumour and to identify the presence of early metastases, thereby facilitating patient management decisions[52]. Furthermore, a number of mathematical models have been developed to investigate tumour invasion[53,54] and metastasis[55,56]. Such models could, in principle, be adapted to evaluate the aggressiveness of colorectal neoplasms. Finally, we anticipate that *in silico* studies will be exploited to predict a patient's prognosis following cancer therapy and/or surgery[23,52,57].

In summary, we believe that mathematical modeling has an important role to play in advancing our understanding of CRC. In addition to being used to test biological hypotheses (concerning, for example, adenoma formation), well-validated models have the potential for generating new theories (regarding, for example, the ways in which phenomena at different spatial and temporal scales interact) that will themselves stimulate further experimental work. In the longer term, and perhaps most importantly, realistic simulation tools of crypt turnover should assist in the development of new drugs and the optimisation of existing therapies for treating CRC.

ACKNOWLEDGMENTS

The authors gratefully acknowledge financial support from the EPSRC through the Integrative Biology project (IvL, CME) and through an Advanced Research Fellowship (HMB). The authors also thank Professors Philip Maini and John King for helpful discussions.

REFERENCES

1 **Booth C**, Brady G, Potten CS. Crowd control in the crypt. *Nat Med* 2002; **8**: 1360-1361
2 **Leedham SJ**, Brittan M, McDonald SA, Wright NA. Intestinal stem cells. *J Cell Mol Med* 2005; **9**: 11-24
3 **Preston SL**, Wong WM, Chan AO, Poulsom R, Jeffery R, Goodlad RA, Mandir N, Elia G, Novelli M, Bodmer WF, Tomlinson IP, Wright NA. Bottom-up histogenesis of colorectal adenomas: origin in the monocryptal adenoma and initial expansion by crypt fission. *Cancer Res* 2003; **63**: 3819-3825
4 **Shih IM**, Wang TL, Traverso G, Romans K, Hamilton SR, Ben-Sasson S, Kinzler KW, Vogelstein B. Top-down morphogenesis of colorectal tumors. *Proc Natl Acad Sci USA* 2001; **98**: 2640-2645
5 **Cancer Research UK Statistics**. Available from: http://info.cancerresearchuk.org/cancerstats/
6 **de la Chapelle A**. Genetic predisposition to colorectal cancer. *Nat Rev Cancer* 2004; **4**: 769-780

7 **Fearon ER**, Vogelstein B. A genetic model for colorectal tumorigenesis. *Cell* 1990; **61**: 759-767
8 **Di Ventura B**, Lemerle C, Michalodimitrakis K, Serrano L. From in vivo to in silico biology and back. *Nature* 2006; **443**: 527-533
9 **Mogilner A**, Wollman R, Marshall WF. Quantitative modeling in cell biology: what is it good for? *Dev Cell* 2006; **11**: 279-287
10 **Araujo RP**, McElwain DL. A history of the study of solid tumour growth: the contribution of mathematical modelling. *Bull Math Bio*l 2004; **66**: 1039-1091
11 **Mantzaris NV**, Webb S, Othmer HG. Mathematical modeling of tumor-induced angiogenesis. *J Math Biol* 2004; **49**: 111-187
12 **van Leeuwen IM**, Byrne HM, Jensen OE, King JR. Crypt dynamics and colorectal cancer: advances in mathematical modelling. *Cell Prolif* 2006; **39**: 157-181
13 **Luebeck EG**, Moolgavkar SH. Multistage carcinogenesis and the incidence of colorectal cancer. *Proc Natl Acad Sci USA* 2002; **99**: 15095-15100
14 **Moolgavkar SH**, Luebeck EG. Multistage carcinogenesis: population-based model for colon cancer. *J Natl Cancer Inst* 1992; **84**: 610-618
15 **Loeffler M**, Stein R, Wichmann HE, Potten CS, Kaur P, Chwalinski S. Intestinal cell proliferation. I. A comprehensive model of steady-state proliferation in the crypt. *Cell Tissue Kinet* 1986; **19**: 627-645
16 **Meineke FA**, Potten CS, Loeffler M. Cell migration and organization in the intestinal crypt using a lattice-free model. *Cell Prolif* 2001; **34**: 253-266
17 **Paulus U**, Loeffler M, Zeidler J, Owen G, Potten CS. The differentiation and lineage development of goblet cells in the murine small intestinal crypt: experimental and modelling studies. *J Cell Sci* 1993; **106** (Pt 2): 473-483
18 **Komarova NL**, Wang L. Initiation of colorectal cancer: where do the two hits hit? *Cell Cycle* 2004; **3**: 1558-1565
19 **Taylor RW**, Barron MJ, Borthwick GM, Gospel A, Chinnery PF, Samuels DC, Taylor GA, Plusa SM, Needham SJ, Greaves LC, Kirkwood TB, Turnbull DM. Mitochondrial DNA mutations in human colonic crypt stem cells. *J Clin Invest* 2003; **112**: 1351-1360
20 **Tomlinson IP**, Bodmer WF. Failure of programmed cell death and differentiation as causes of tumors: some simple mathematical models. *Proc Natl Acad Sci USA* 1995; **92**: 11130-11134
21 **Yatabe Y**, Tavaré S, Shibata D. Investigating stem cells in human colon by using methylation patterns. *Proc Natl Acad Sci USA* 2001; **98**: 10839-10844
22 **Alarcón T**, Byrne HM, Maini PK. Towards whole-organ modelling of tumour growth. *Prog Biophys Mol Biol* 2004; **85**: 451-472
23 **Ribba B**, Colin T, Schnell S. A multiscale mathematical model of cancer, and its use in analyzing irradiation therapies. *Theor Biol Med Model* 2006; **3**: 7
24 **Noble D**. The rise of computational biology. *Nat Rev Mol Cell Biol* 2002; **3**: 459-463
25 **Noble D**. Systems biology and the heart. *Biosystems* 2006; **83**: 75-80
26 **Crampin EJ**, Halstead M, Hunter P, Nielsen P, Noble D, Smith N, Tawhai M. Computational physiology and the Physiome Project. *Exp Physiol* 2004; **89**: 21-26
27 **Noble D**. Modeling the heart--from genes to cells to the whole organ. *Science* 2002; **295**: 1678-1682
28 **Swanson KR**, Alvord EC, Murray JD. A quantitative model for differential motility of gliomas in grey and white matter. *Cell Prolif* 2000; **33**: 317-329
29 **Anderson AR**. A hybrid mathematical model of solid tumour invasion: the importance of cell adhesion. *Math Med Biol* 2005; **22**: 163-186
30 **Gevertz JL**, Torquato S. Modeling the effects of vasculature evolution on early brain tumor growth. *J Theor Biol* 2006; **243**: 517-531
31 **McDougall SR**, Anderson AR, Chaplain MA, Sherratt JA. Mathematical modelling of flow through vascular networks: implications for tumour-induced angiogenesis and chemotherapy strategies. *Bull Math Biol* 2002; **64**: 673-702
32 **Ilyas M**. Wnt signalling and the mechanistic basis of tumour development. *J Pathol* 2005; **205**: 130-144
33 **Korinek V**, Barker N, Moerer P, van Donselaar E, Huls G, Peters PJ, Clevers H. Depletion of epithelial stem-cell compartments in the small intestine of mice lacking Tcf-4. *Nat Genet* 1998; **19**: 379-383
34 **Gaspar C**, Fodde R. APC dosage effects in tumorigenesis and stem cell differentiation. *Int J Dev Biol* 2004; **48**: 377-386
35 **Giles RH**, van Es JH, Clevers H. Caught up in a Wnt storm: Wnt signaling in cancer. *Biochim Biophys Acta* 2003; **1653**: 1-24
36 **Lee E**, Salic A, Krüger R, Heinrich R, Kirschner MW. The roles of APC and Axin derived from experimental and theoretical analysis of the Wnt pathway. *PLoS Biol* 2003; **1**: E10
37 **van Leeuwen IM**, Byrne HM, Jensen OE, King JR. Elucidating the interactions between the adhesive and transcriptional functions of β-catenin in normal and cancerous cells. *J Theor Biol* 2007; **247**: 77-102
38 **Lobachevsky PN**, Radford IR. Intestinal crypt properties fit a model that incorporates replicative ageing and deep and proximate stem cells. *Cell Prolif* 2006; **39**: 379-402
39 **Walker DC**, Southgate J, Hill G, Holcombe M, Hose DR, Wood SM, Mac Neil S, Smallwood RH. The epitheliome: agent-based modelling of the social behaviour of cells. *Biosystems* 2004; **76**: 89-100
40 **Araki K**, Ogata T, Kobayashi M, Yatani R. A morphological study on the histogenesis of human colorectal hyperplastic polyps. *Gastroenterology* 1995; **109**: 1468-1474
41 **Brittan M**, Wright NA. Stem cell in gastrointestinal structure and neoplastic development. *Gut* 2004; **53**: 899-910
42 **Wong WM**, Mandir N, Goodlad RA, Wong BC, Garcia SB, Lam SK, Wright NA. Histogenesis of human colorectal adenomas and hyperplastic polyps: the role of cell proliferation and crypt fission. *Gut* 2002; **50**: 212-217
43 **Drasdo D**, Loeffler M. Individual-based models to growth and folding in one-layered tissues: intestinal crypts and early development. *Nonlinear Analysis* 2001; **47**: 245-256
44 **Edwards CM**, Chapman SJ. Biomechanical modelling of colorectal crypt budding and fission. *Bull Math Biol* 2007; **69**: 1927-1942
45 **Mariadason JM**, Nicholas C, L'Italien KE, Zhuang M, Smartt HJ, Heerdt BG, Yang W, Corner GA, Wilson AJ, Klampfer L, Arango D, Augenlicht LH. Gene expression profiling of intestinal epithelial cell maturation along the crypt-villus axis. *Gastroenterology* 2005; **128**: 1081-1088
46 **Segal E,** Friedman N, Kaminski N, Regev A, Koller D. From signatures to models: understanding cancer using microarrays. *Nat Genet* 2005; **37** Suppl: S38-S45
47 **Tinker AV**, Boussioutas A, Bowtell DD. The challenges of gene expression microarrays for the study of human cancer. *Cancer Cell* 2006; 9: 333-339
48 **Greaves LC**, Preston SL, Tadrous PJ, Taylor RW, Barron MJ, Oukrif D, Leedham SJ, Deheragoda M, Sasieni P, Novelli MR, Jankowski JA, Turnbull DM, Wright NA, McDonald SA. Mitochondrial DNA mutations are established in human colonic stem cells, and mutated clones expand by crypt fission. *Proc Natl Acad Sci USA* 2006; **103**: 714-719
49 **Gavaghan DJ**, Simpson AC, Lloyd S, Mac Randal DF, Boyd DR. Towards a Grid infrastructure to support integrative approaches to biological research. *Philos Trans A Math Phys Eng Sci* 2005; **363**: 1829-1841
50 **Byrne HM**, Owen MR, Alarcón T, Murphy J, Maini PK. Modelling the response of vascular tumours to chemotherapy: a multiscale approach. *Math Models Meth Appl Sci* 2006; **16**: 1219-1241
51 **Tyson JJ**, Novak B. Regulation of the eukaryotic cell cycle: molecular antagonism, hysteresis, and irreversible transitions. *J Theor Biol* 2001; **210**: 249-263
52 **Pitt-Francis J**, Chen D, Slaymaker M, Simpson A, Brady M, Van Leeuwen I, Reddington F, Quirke P, Brown G, Gavaghan

D. Multimodal imaging techniques for the extraction of detailed geometrical and physiological information for use in multi-scale models of colorectal cancer and treatment of individual patients. *Comp Math Method Med* 2006; **7**: 177-188

53 **Smallbone K**, Gavaghan DJ, Gatenby RA, Maini PK. The role of acidity in solid tumour growth and invasion. *J Theor Biol* 2005; **235**: 476-484

54 **Turner S**, Sherratt JA. Intercellular adhesion and cancer invasion: a discrete simulation using the extended Potts model. *J Theor Biol* 2002; **216**: 85-100

55 **Hanin L**, Rose J, Zaider M. A stochastic model for the sizes of detectable metastases. *J Theor Biol* 2006; **243**: 407-417

56 **Michor F**, Nowak MA, Iwasa Y. Stochastic dynamics of metastasis formation. *J Theor Biol* 2006; **240**: 521-530

57 **Gaffney EA**. The application of mathematical modelling to aspects of adjuvant chemotherapy scheduling. *J Math Biol* 2004; **48**: 375-422

S- Editor Liu Y **L- Editor** Lutze M **E- Editor** Che YB

PO Box 2345, Beijing 100023, China
www.wjgnet.com
wjg@wjgnet.com

World J Gastroenterol 2007 March 7; 13(9): 1408-1421
World Journal of Gastroenterology ISSN 1007-9327

TOPIC HIGHLIGHTS

Hans Gregersen, Professor, *Series Editor*

Advanced imaging and visualization in gastrointestinal disorders

Odd Helge Gilja, Jan G Hatlebakk, Svein Ødegaard, Arnold Berstad, Ivan Viola, Christopher Giertsen, Trygve Hausken, Hans Gregersen

Odd Helge Gilja, Svein Ødegaard, Trygve Hausken, National Centre for Ultrasound in Gastroenterology, Department of Medicine, Haukeland University Hospital, Norway
Odd Helge Gilja, Jan G Hatlebakk, Svein Ødegaard, Arnold Berstad, Trygve Hausken, Hans Gregersen, Institute of Medicine, 3Institute of Informatics University of Bergen, Bergen, Norway
Ivan Viola, Institute of Informatics, University of Bergen, Bergen, Norway
Christopher Giertsen, Christian Michelsen Research AS, Bergen, Norway
Hans Gregersen, Center for Visceral Biomechanics and Pain, Aalborg Hospital and Center for Sensory-motor Interaction, Aalborg University, Denmark
Correspondence to: Odd Helge Gilja, NSGU, Department of Medicine, Haukeland University Hospital, Bergen N-5021, Norway. odd.gilja@uib.no
Telephone: +47-55975000 Fax: +47-55972950
Received: 2006-12-11 Accepted: 2007-01-10

Abstract

Advanced medical imaging and visualization has a strong impact on research and clinical decision making in gastroenterology. The aim of this paper is to show how imaging and visualization can disclose structural and functional abnormalities of the gastrointestinal (GI) tract. Imaging methods such as ultrasonography, magnetic resonance imaging (MRI), endoscopy, endosonography, and elastography will be outlined and visualization with Virtual Reality and haptic methods. Ultrasonography is a versatile method that can be used to evaluate antral contractility, gastric emptying, transpyloric flow, gastric configuration, intragastric distribution of meals, gastric accommodation and strain measurement of the gastric wall. Advanced methods for endoscopic ultrasound, three-dimensional (3D) ultrasound, and tissue Doppler (Strain Rate Imaging) provide detailed information of the GI tract. Food hypersensitivity reactions including gastrointestinal reactions due to food allergy can be visualized by ultrasonography and MRI. Development of multi-parametric and multi-modal imaging may increase diagnostic benefits and facilitate fusion of diagnostic and therapeutic imaging in the future.

Key words: Ultrasonography; Medical imaging; Functional imaging; Elasticity

Gilja OH, Hatlebakk JG, Ødegaard S, Berstad A, Viola I, Giertsen C, Hausken T, Gregersen H. Advanced imaging and visualization in gastrointestinal disorders. *World J Gastroenterol* 2007; 13(9): 1408-1421

http://www.wjgnet.com/1007-9327/13/1408.asp

INTRODUCTION

Medical imaging has a strong impact on clinical decision making and its significance and utility seems increasing. In the field of gastroenterology, new imaging methods like double-balloon and capsule enteroscopy are recent additions to the more traditional methods. In contrast to X-ray, Computed tomography (CT), magnetic resonance imaging (MRI), single photon emission computed tomography (SPECT) and positronen emissions-tomographen (PET) scanning, ultrasonography is a clinical method that can easily be applied even bedside using mobile, hand-carried scanners[1]. Despite its favourable cost, availability, flexibility, and user friendliness, ultrasonography stands out as the imaging method with highest temporal and spatial resolution. In addition, its real-time and functional imaging capacity makes it well suited for soft tissue modelling. Ultrasonography can provide physiological, pathopfysiological and biomechanical information to the clinician and constitutes an important tool in the diagnosis and follow up of large populations of patients.

The gastrointestinal tract is a very long system of organs that poses a particular challenge to medical imaging. In this paper, we aim at outlining how advanced imaging and visualization, particularly ultrasonography is able to disclose structural and functional information of the GI tract.

FUNCTIONAL ULTRASONOGRAPHY

Functional ultrasonography (f-US) is ultrasound imaging of organ function, in contrast to conventional imaging of anatomic structures. Using f-US, information on motility, biomechanics, flow, perfusion, organ filling and emptying can be obtained non-invasively.

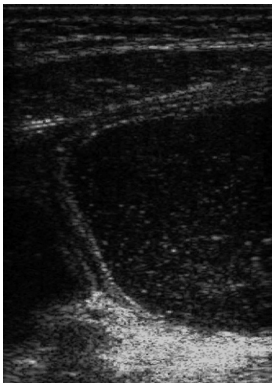

Figure 1 Ultrasonogram of the fluid-filled gastric antrum showing the different wall layers and a propagating contraction wave that occludes the lumen.

Contractile activity

Ultrasonography can provide both qualitative and quantitative information about motility, both in a fasting state and after meal ingestion. Gastric contractions and propagation of waves can be visualized and monitored by ultrasound[2-7]. Both frequency and amplitude are easily measured; the latter defined as the maximal reduction of antral area induced by a contraction, as a fraction of the relaxed area. High resolution ultrasound using frequencies in the range 7-15 MHz enables detailed studies of gastric wall layer involvement during peristalsis (Figure 1). Ultrasound is more sensitive than manometry in detecting antral contractions and in particular the detection of non-occlusive contractions[8].

Acute mental stress induced by a video game in which the subjects were driving a simulated car trying to avoid collisions on a highway, reduced postprandial antral motility during the stress period in healthy volunteers, but not in patients with functional dyspepsia[9]. Stress mainly reduced the amplitudes of antral contractions and cisapride had no effect on these stress-induced responses.

Gastric emptying

Ultrasonography has been widely used to assess gastric emptying rates[10-16] and good correlation to radionuclide estimates of emptying rates have been detected[12,17,18]. However, ultrasound is best suited for emptying of liquid meals. Scintigraphy, with appropriate labelling of the test meal components and appropriate corrections applied, is still considered the gold standard for measurement of gastric emptying. However, its application is limited by the need to restrict exposure to ionising radiation. In depth description of ultrasound estimation of gastric emptying and findings in functional dyspepsia have been reported elsewhere[19].

Gastroduodenal flow

The movements of gastroduodenal contents and velocity curves of transpyloric flow can be synchronously visualized by duplex ultrasound, a combination of Doppler measurement and B-mode image[20,21]. It has been shown, using duplex scanning, that a short gush of duodenogastric reflux normally precedes the peristaltic closure of the pylorus. An antral contraction can be defined as an indentation of the gastric wall greater than one antral wall thickness observed to propagate in space and time, as long as the indentation is not due to respiration, pulsation transmitted from the aorta or heart, or to movements of adjacent intestine. First gastric emptying is defined as the first occurrence of gastric emptying after drinking the "test" soup. An episode of gastric emptying is defined as flow across the pylorus with a mean velocity of more than 10 cm/s lasting for greater than one second. Occluding peristaltic-related transpyloric emptying is defined as gastric emptying associated with contractile activity in which the ultrasound image demonstrates an occlusion of the stomach wall. Non-occluding peristaltic-related emptying is defined as transpyloric emptying of gastric contents associated with contractile activity of the gastric wall which does not occlude the lumen. During maximal contractions transpyloric flow can be seen passing back and forth through the open pylorus. Non-peristaltic-related transpyloric emptying can be defined as transpyloric emptying of gastric contents, without contractions detected on ultrasound or manometry. Using this Doppler method, timing of postprandial dyspeptic symptoms and transpyloric passage of gastric contents can be studied with great temporal and spatial resolution[22], including after pharmacological intervention[23].

Gastric emptying of a low calorific liquid meal follows sequences of emptying-reflux-emptying pulses. About half of the sequences are peristaltic related, but both non-occluding, peristaltic related and non-peristaltic related emptying sequences occur. Non-peristaltic related flow sequences have often more alternating emptying-reflux episodes than those associated with peristalsis, and the duration of non-peristaltic related emptying and reflux pulses are longer. The pressure gradients for all types of emptying are low and the pressure gradients during non-peristaltic related emptying are significantly lower than during peristaltic related emptying.

Flow can only occur in the presence of an open pylorus. Transpyloric flow can be classified into flow associated with a local increase in the pressure gradient between antrum and duodenum (Pa-Pd) due to antral propagating pressure waves, and flow associated with a common cavity pressure difference between the distal antrum and the proximal duodenum as was observed during non-peristaltic related flow. The second type of flow is independent of peristalsis and is likely to be caused by changes in gastric tone, or by pressure changes outside the stomach such as aortic pulsation and inspiration.

Hausken and co-workers also developed a non-invasive method for evaluating transpyloric flow and duodenogastric reflux stroke volumes using a three-dimensional guided digital color doppler imaging model[24]. They studied healthy subjects both during ingestion of a soup meal and 10 min postprandially. Cross-sectional color doppler digital images of duodenogastric reflux episodes were acquired with a 5-3 MHz phased array transducer. The 3D position and orientation data were acquired using a magnetic sensing system. They found high intra- and inter individual variations of the stroke volumes of transpyloric flow episodes during the initial gastric emptying. The duodenogastric reflux episodes lasted on average 2.4 s with a volume of on average of 8.3 mL. This method minimized geometric assumptions and angular ambiguity.

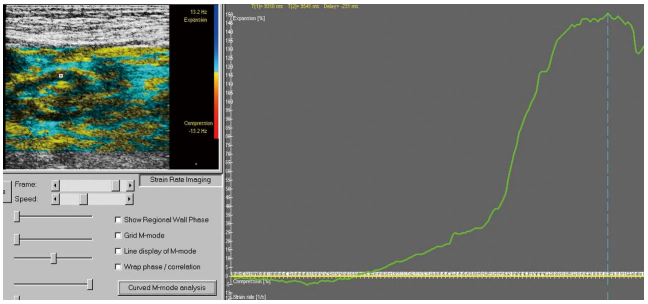

Figure 2 These graphics outline the relative radial strain of the circular muscle layer of the antral wall. The exact sampling point in the gastric wall is denoted with a red marker in the color Doppler ultrasonogram of the left panel. In the right panel, the positive strain curve with a maximum of 150% radial elongation of the muscle layer is demonstrated.

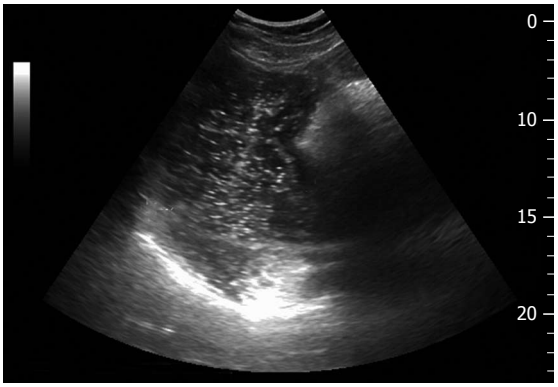

Figure 3 An oblique frontal section applied for ultrasound scanning of the proximal stomach. The top margin of the fundus is shown as a white line in the bottom of the image. A proximal gastric diameter is outlined in the frontal section by tracing normally to the longitudinal axis of the proximal stomach, thus indicating the size of the proximal stomach.

Strain rate imaging

Tissue Doppler imaging (TDI) enables mapping of local tissue velocities, thus increasing the physiological information about moving walls[25,26]. However, the point velocity of tissue does not differentiate between actively contracting and passively following tissue. Therefore, a Doppler method based on strain rate imaging (SRI) and estimation of relative strain was developed to enable this differentiation. In general terms, strain means tissue deformation as a function of applied force (stress)[27]. The temporal derivative of strain, i.e. the strain rate, is a measure of the rate of deformation.

Doppler SRI was evaluated *in vitro* using a silicone strip phantom mimicking slowly moving tissue[28]. A test apparatus was developed that enabled controlled strain experiments with variable strain and strain rate to be performed. We found low intra- and interobserver variation. For the SRI method to give accurate estimates of strain, the strain sample size should be in the region of 2 mm and averaging over several ultrasound (US) beams increased the accuracy further.

In another study, we evaluated the accuracy of SRI in measuring strain in the porcine antral wall *in vitro*[29]. An experimental set-up enabled controlled distension of a porcine stomach in a saline reservoir. SRI gave accurate measurement of radial strain of the antral wall, but seemed to be less accurate for measurement of circumferential strain in this *in vitro* set-up.

Estimation of relative strain of the muscle layer of the gastric wall by Doppler ultrasonography is feasible (Figure 2) and enabled detailed mapping of local strain distribution[30,31]. SRI is capable of distinguishing contractile activity of the longitudinal and circular muscle layers, even though the two layers cannot be separated visually in the 2D images. During balloon distension of the antrum, we found a significant inverse correlation between pressure and SRI measurement (r = -0.87). Ongoing studies are evaluating whether SRI can be applied to evaluate the relation between symptoms and biomechanical factors in dyspepsia.

Ultrasonography to evaluate gastric accommodation

A sonographic method for assessment of proximal gastric size was developed to estimate accommodation of meals[32]. The transducer was positioned in the epigastrium by the left subcostal margin and tilted cranially while the subject was sitting in a chair, leaning slightly backwards. Two standardised sonographic image sections were chosen to monitor the size of the proximal stomach. First, a sagittal section with the left renal pelvis in a longitudinal projection, using the left lobe of the liver and the tail of the pancreas as internal landmarks, was recorded. Then, the transducer was rotated 90° clockwise to obtain an oblique frontal section where the top margin of the fundus is clearly visible (Figure 3). Utilising this technique the existence of an impaired proximal gastric accommodation to a meal in patients with functional dyspepsia was observed[33]. Impaired proximal stomach accommodation was in fact a much more prevalent finding than a wide gastric antrum. Because nitric oxide (NO) is a key neurotransmitter in the reflex regulating adaptive relaxation, it was tempting to administer glyceryl trinitrate, an exogenous donor of NO, to patients with functional dyspepsia to examine if it would improve gastric accommodation and symptoms in response to a meal. In a double blind placebo-controlled cross-over study, Gilja *et al*[34]demonstrated that glyceryl trinitrate caused a concomitant improvement of proximal gastric accommodation and epigastric pain, nausea and total symptom scores in response to a meat soup meal.

This 2D method has also been used to study gastric accommodation in diabetes mellitus[35], in patients with reflux oesophagitis[36], in liver cirrhosis[37], and in children with recurrent abdominal pain[38]. The method has also been applied to study pharmacological intervention[39] and the effect of a barostat bag in the stomach[40]. In contrast to the barostat, ultrasonography is a non-invasive and widely available method for the study of accommodation of the proximal stomach.

3D ULTRASONOGRAPHY

A method for volume estimation of the stomach based on mechanical tilting acquisition of 3D ultrasonography was developed[41]. Using a motor device, the transducer

was tilted through an angle of 90°, capturing sequential 2D-frames before the data set was transferred to a graphic workstation for final 3D processing. This 3D ultrasound system demonstrated excellent accuracy *in vitro* both on phantoms[42] and on animal organs. Furthermore when validated *in vivo* against magnetic resonance imaging (MRI) this 3D system was in good agreement with the MRI and produced results with high precision[43]. This system has also been used to study diseases of the liver[44], and to evaluate patients with functional dyspepsia[45-47]. However, this 3D investigation could only acquire a 90° fan-like data set from a pre-determined, fixed position of the transducer. Accordingly, a mechanical acquisition system like this could only capture small volumes of data and not cover completely a large organ like the stomach or liver.

To enable scanning of the fluid-filled stomach, a commercially available magnetometer-based position and orientation measurement (POM) device was interfaced to the scanner. This system for magnetic scanhead tracking (Bird, Ascencion Technology Inc. Vermont, USA) was validated both with respect to its precision in locating specific points in space[48] and to its accuracy in volume estimation[28,49]. For the first time, total gastric volumes and intragastric distribution of meals could be studied by ultrasonography[50]. Sagittal sections of the stomach were recorded throughout its entire length, starting in the proximal part where the transducer was positioned by the left subcostal margin and tilted cranially to image the most superior part of the stomach. After stepwise scanning of the proximal stomach angling from left to right, the transducer was moved and held to insonicate normally to the skin surface. Then the distal stomach was scanned stepwise moving distally to the gastroduodenal junction.

We validated this 3D ultrasonographic method *in vivo* in healthy controls[51]. A barostat bag was positioned in the proximal stomach of 6 healthy subjects who underwent scanning with the Bird® magnetic system. This 3D ultrasound system correlated very well to infused volumes and showed very good agreement with true volumes, and in addition there was low inter-observer variation. Patients with reflux esophagitis exhibited an abnormally large volume of the proximal stomach soon after a liquid meal, concomitant with the perception of fullness. The abnormal distention of the proximal stomach may represent a pathogenic mechanism in reflux oesophagitis.

In functional dyspepsia, poor accommodation of the proximal stomach to a meal has been found in many studies[33,52-54]. Drinking capacity is often reduced in these patients and drink tests may therefore have a diagnostic potential. A simple drink test in combination with 3D ultrasonography was applied in a test using Toro meat soup, Nutridrink, and water[55]. The meals were ingested at a rate of 100 mL/min until maximal drinking capacity was reached. Intragastric volume at maximal drinking capacity was determined using 3-dimensional ultrasonography. Optimal discrimination between patients and controls was obtained by the combination of symptoms and intragastric volume (S/V) using meat soup as the test meal. In another study, an analytical method was developed to describe the three-dimensional geometry of the gastric antrum, the gastric fundus and the whole stomach based on 3D ultrasound acquisitions[56]. The Fourier series method was used to simulate the organ surface geometry. The principal curvatures spatial distributions were non-homogeneous in the gastric antrum, gastric fundus and the stomach due to their complex geometry.

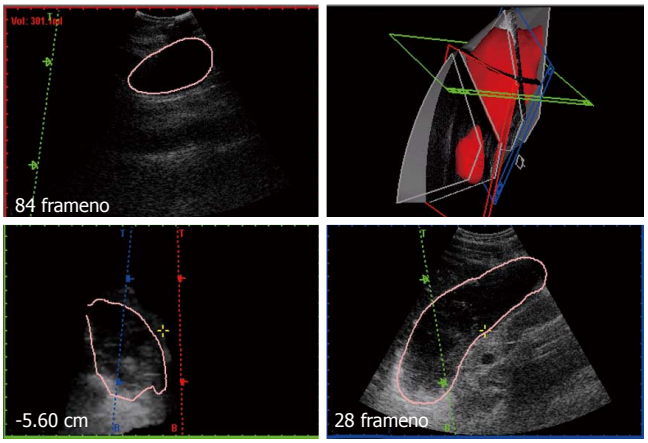

Figure 4 A 3D reconstruction of the total stomach volume (red) in the upper left panel. The acquisition is based on magnetic scanhead tracking. Three orthogonal orientation planes are shown in red, green and blue. The upper left panel is a volume reconstruction window where manual outlining of the structures are made.

Data processing and display requires specialized computer software to handle the ultrasound images. We have, in collaboration with Christian Michelsen Research (Bergen, Norway) and Vingmed Sound (Horten, Norway), developed a software package called EchoPac3D® to help with this process[57,58]. EchoPac3D enables the import of image data that are acquired both with mechanical devices and magnetic position sensors as well as with endosonographic acquisitions. Manual segmentation or semiautomatic rendering of structures in the 3D data set makes accurate volume estimation and reconstruction of organs or pathologic tissue achievable. A display of the EchoPac3D software is shown in Figure 4. The 3D ultrasound system used in our lab is outlined more in depth in a previous review[59].

FUNCTIONAL IMAGING OF THE ESOPHAGUS

Esophageal function in swallowing and competence in gastro-oesophageal reflux has traditionally been assessed with manometry, or alternatively barium radiography. Standard manometry with relatively few (3-8) channels measures the pressures generated in the distal and proximal sphincters and in the body of the esophagus. With high-resolution manometry and computer-generated graphics, a much more detailed and complex picture is composed from 16-24 pressure signals evenly spaced along the catheter, allowing for detailed analysis of the physiology of peristalsis and sphincter function. High-resolution manometry has recently been used to study the physiology of peristalsis and the pathophysiology of gastro-oesophageal reflux in patients with reversible hiatal hernias[60].

Manometry has important limitations in studies of oesophageal motor function. Firstly it does not measure bolus transport. Furthermore it measures exclusively

contractions of the inner circular muscle layer of the oesophageal wall, and only if and at the time when a contraction obliterates the lumen around the catheter. These limitations can be overcome with high-frequency intraluminal ultrasonography (HFIUS), with which one can measure the thickness and contractile activity of the muscularis propria, and also to some extent that of each separate muscle layer. It has been demonstrated that it is possible to detect hypertrophy of the muscularis in hypercontractile disorders of the esophagus such as achalasia, diffuse oesophageal spasm and nutcracker esophagus[61]. Contractile activity of the longitudinal muscle layer is thought to contribute stiffness and support to the peristaltic wave generated in the inner circular muscle layer. Isolated sustained contractions of the longitudinal layer are seen as increased muscle thickness, and have been shown to coincide with sensations of chest pain in patients with idiopathic chest pain[62]. Furthermore, in patients with heartburn, symptom episodes were preceded by similar contractions, whether associated with acid reflux occurred or not. Asynchrony between contractions of the muscle layers are also likely to contribute to symptoms[63]. The miniaturization of HFIUS probes allows them to be combined with manometry and laser Doppler flowmetry into multi-modal catheters for studying the biomechanical parameters and genesis of pain in healthy subjects and patients with idiopathic chest pain[64].

Radiographic studies with barium contrast have traditionally been used to screen for motility disorders of the esophagus and when properly performed, can be extremely useful. These techniques have occasionally been combined with manometry to quantify parameters of sphincter function. Scintigraphic studies only assess bolus transport. Bolus transport has also recently been studied with multichannel intraluminal impedance (MII), which measures lumen dilatation at the time of passage of a food bolus, enabling one to classify food passage as complete or incomplete. MII can also be combined with manometry. Multiple impedance channels as well as manometry are also incorporated into the functional lumen imaging probe (FLIP) for studying the distensibility and opening characteristics of the oesophago-gastric junction[65]. The limitation of impedancemetry is that it only measures the geometry of the lumen and not the wall of an organ and therefore yields limited biomechanical data. However, in contrast to any other medical imaging technology, FLIP is capable of providing quasi-3D lumen geometry in real time.

Recently, endoscopy of the oesophageal mucosa has been supplemented by the promising new method of confocal laser endoscopy, which allows a detailed study of mucosal layers. The characteristics of dysplasia and minor changes of inflammation have been evaluated in preliminary studies, indicating that the method may become an important guidance for detecting early cancers in the metaplastic or squamous oesophageal mucosa[66].

DYNAMIC ENDOSONOGRAPHY OF THE GI TRACT

Endosonography (ES) is performed with intraluminal ultrasound transducers which can be inserted blindly into hollow organs or under endoscopic guidance (EUS). ES is usually performed as B-mode imaging but other modalities can also be applied (M-mode, Doppler, elastography). EUS makes visualisation of the mucosal surface of the GI tract as well as the individual wall layers, adjacent organs and other structures possible. Real-time ES probes allow imaging of GI motility and biomechanics and when a probe is used to apply pressure directly to the tissue, information about tissue stiffness can also be obtained[19].

Instrumentation

The small diameter of ES-miniprobes allows these probes to be inserted through the biopsy channel of conventional endoscopes or a suitable catheter. Currently available miniprobes operate with ultrasound frequencies between 12 and 30 MHz. Dedicated echoendoscopes combine endoscopy with integrated radial or curvilinear array ultrasound transducers with frequencies between 5 and 30 MHz. New echoendoscopes can be connected to modern ultrasound machines with advanced software making it possible to use different ultrasound modalities (B-mode, M-mode, Doppler, sonoelastography, strain rate imaging, 3D-imaging, contrast-enhanced ultrasound).

Endosonographic assessment of GI biomechanics

Biomechanical functions of the GI tract and neighbouring organs have in recent years been increasingly studied with real time endosonography. Both active properties such as peristaltic contractions (motility) and active and passive forces and deformation (biomechanics) of the tissue can be visualized with this technique[67]. ES- miniprobes combine the advantages of high ultrasound frequencies with small transducers thus being a technique which can be combined with other methods, especially with manometry. Echoendoscopes are suitable for examination both of the GI wall and for studying extraintestinal organs and structures because they use lower ultrasound frequencies and have larger ultrasound transducers.

The GI tract and wall layers

The normal GI wall is imaged by ES as a layered structure consisting of several layers (5-9 layers) but most often a 5-layer structure is seen[68]. Many disorders and diseases may have an influence on GI wall morphology, motility and other biomechanical functions which can be examined using ES. The transducer can also be used as a diagnostic tool to "palpate" the GI wall, thus giving additional information about changes in GI wall thickness, layers and echogenicity[69].

Esophagus

Endosonographic changes of the esophageal wall, especially the proper muscle layer, have been found to correlate with the increase in luminal pressure by manometry. Hoff *et al*[64] have described a multimodal device which can be inserted into esophageus combining bag distension, manometry, high frequency intraluminal ultrasound, laser Doppler flowmetry and symptom registration. Preliminary experience indicates that these modalties can be used in combination without significant

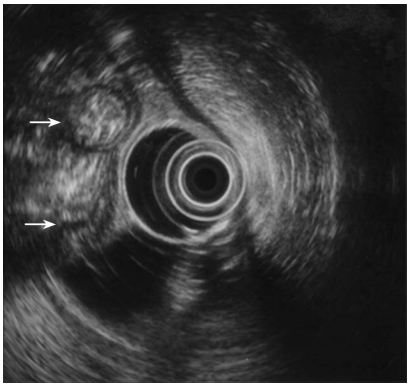

Figure 5 Small bowel loops (arrows) imaged from the stomach with an echoendoscope. Liquid within the gastric lumen gives an excellent acoustic window.

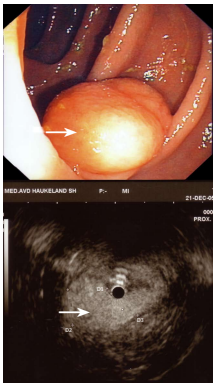

Figure 6 Endoscopic image of a tumour in the colon (arrow, top). An ultrasound miniprobe is used to "palpate" the relatively soft echo-rich tumour (arrow) which is a lipoma.

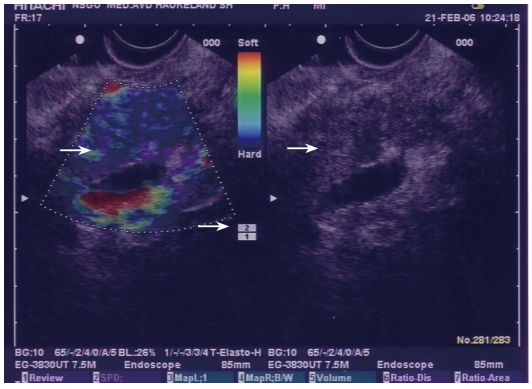

Figure 7 ES-elastography (colour coded, left) in chronic pancreatitis displaying hard (blue) and softer (green) areas (left, large arrow). Corresponding B-image (right, arrow). Transducer pressure is indicated by a scale (small arrow).

and detrimental technical influence on each other. In a study by Taniguchi *et al*[70], the esophagus was investigated with M-mode ES and manometry. Swallowing events were found to produce simultaneous increases in intraluminal pressure and esophageal wall thickness. Furthermore, patients with achalasia and nutcracker esophagus have been examined with both ES and manometry showing high correlation between wall changes and manometric findings. Patients with sclerodermia may also demonstrate abnormal ES findings in the esophageal wall due to smooth muscle atrophy and variable fibrosis and collagen parameters. In patients with reflux esophagitis, ES often demonstrates inflammatory changes affecting all, or individual, wall layers in the distal part of the esophagus as well as demonstrating abnormalities in peri-esophageal tissue and lymph nodes. These morphologic changes may thus affect esophageal motility and thereby also influence acid clearance.

Stomach, duodenum and extraintestinal organs

In wide and curved organs ES can be technically challenging but ES is a well documented method for examination of the stomach, duodenal wall, retroperitoneum, pancreas, vessels, common bile duct and part of the liver. The stomach and duodenum represent good acoustic windows for transmural imaging and for transducer palpation of extraluminal organs (Figure 5). Thus, dynamic changes of the pancreatic duct in suspected chronic pancreatitis can be examined by ES after drug administration (Secretin) or by compressing the organ with the transducer. A device which combines endosonographic real-time imaging with intraluminal volume-controlled bag distensions has also been developed for use in large lumens. Detailed images of GI wall layers corresponding to the area of bag pressure can be obtained using this technique.

Rectum, colon and small intestine

Rectum and the large bowel may be examined with dedicated echoendoscopes and rectal probes. However, transcolonoscopic ES using miniprobes is a practical method for imaging the colon and rectum wall (Figure 6). The small intestine can now be examined by capsule endoscopy or with enteroscopes. Capsule endoscopy is performed with a small device which is swallowed by the patient and endoscopic imaging of the entire small intestine is possible. ES/EUS of the small intestine may in the future be accomplished if a miniature ultrasound device is integrated in the capsule or in an enteroscope. The interpretation of wall layers, biomechanics and motility of the small intestine and large bowel is as for the upper GI tract.

Elastography

The stiffness of the GI wall and the individual wall layers can be evaluated by compressing the tissue with the ES transducer. Sonoelastography (SE) and SRI are new ultrasound methods which can give information about tissue hardness and contractility[31,71,72]. The underlying principle of SE is that the deformation of tissue by a mechanical excitation is a function of its mechanical properties. For gastrointestinal purposes, the intraluminal pressure may be used as the excitation force. Imaging of ultrasound tissue elasticity has thus gained considerable interest as a method to differentiate normal from abnormal tissue. Cancer and inflammation may be otherwise influenced by transducer pressure than normal tissue and SE. Color codes seems to be a helpful technique to separate pancreatic cancer from chronic pancreatitis (Figure 7).

Strain rate imaging provides quantitative information on velocities within a tissue. By color-coded tissue velocity imaging, velocity data from the whole field of view are available simultaneously. This allows extraction of parameters through spatial and temporal processing of

the velocity data. Trans-esophageal probes primarily used in echocardiography can also be inserted into the stomach thus having potential for SRI of esophageal and gastric motor function.

3D ES images can be obtained using images acquired by both echoendoscopes and miniprobes. 3D-ES may be applied for improved recognition of the GI anatomy and pathological lesions. Mostly, a pullback device has been used to obtain parallel 2D images which are reconstructed to a 3D-image[73]. However, the recent development of 3D real time transducers and advanced software programs opens the way for three-dimensional motility and otherwise dynamic studies of the GI tract.

FOOD HYPERSENSITIVITY AND IMAGING

Intolerance to food is prevalent in the general population. In Western countries, the frequency of perceived food hypersensitivity is as high as around 25%. However, only 2% of the population have food allergy as medically defined. It is therefore important, and often a challenge, to prove whether the ingestion of suspected food items really causes symptoms, and by which mechanism. Hypersensitivity is defined as objectively reproducible symptoms or signs, initiated by exposure to a defined stimulus at a dose tolerated by normal subjects. The term "food allergy", should be restricted to reactions mediated by classical immune mechanisms. It is divided into IgE-mediated food allergy (type- I), mixed IgE and non-IgE-mediated, and non-IgE-mediated food allergy. Non-IgE-mediated food allergy (type Ⅲ or Ⅳ) involves cell-mediated immunologic reactions, immune complex formation or complement deposition. Non-IgE-mediated allergic reactions are therefore subdivided into those in which the reaction is initiated predominantly by mechanisms associated with allergen-specific antibodies other than IgE, and those in which a cellular response is predominant.

Subjective food hypersensitivity

Subjective food hypersensitivity is poorly defined. In practice, the diagnosis is based on self-reported symptoms and absence of indications of allergic and non-allergic hypersensitivity mechanisms or organic disease that can explain the symptoms. Many patients with organic or functional gastrointestinal disorders claim that they are intolerant to various kinds of food. For instance, in a recent study from our department, 75% of the patients with *H pylori* positive dyspepsia claimed intolerance for one or more food items. Eradication of the bacterium reduced the prevalence of food intolerance significantly, but 51% of the patients still reported food intolerance[74]. Likewise, patients with irritable bowel syndrome (IBS) commonly report various kinds of food hypersensitivity[75,76].

A typical food allergic reaction

In an allergic rat, intestinal provocation with an allergen elicits mucosal swelling and leakage of plasma into the lumen lasting a couple of hours before the mucosa returns to normal[77]. The mucosal hyperaemia and exudation of plasma is regarded as a non-injurious defence mechanism. In man, the intestinal response to food allergens is less well characterised, but the consequences appear to be much the same[78]. Massive luminal influx of fluid might be the cause of the symptoms, which usually are acute, short-lasting abdominal cramps, nausea and diarrhoea. A major problem in such IgE-mediated reactions is that all traces of an allergic reaction might have disappeared at the time of consultation. A positive skin prick test and abnormal levels of total or specific IgE indicate allergic predisposition, but do not prove that the complaints of the patients are in any way related to allergy. Therefore, a provocation test is often mandatory.

Double-blind placebo-controlled food challenge

The best method for diagnosing food allergy is still not known. For many years, double-blind placebo-controlled food challenge was considered the "gold standard". Because the procedure is extremely labour-intensive and time-consuming, and the assessment based on subjective symptoms such as abdominal discomfort and bloating, which makes the results more equivocal than generally thought, the method has become disputed. In practice, the diagnosis relies on history, documentation of IgE-sensitisation by skin prick tests or serology, registration of food intake, elimination diets and open provocation tests. Double-blind placebo-controlled food challenge is seldom performed. Other cumbersome methods such as endoscopic food allergen injection[79], jejunal perfusion and recording of the intestinal mucosal response by endosonography[80] have been tried, but further evidence is required before these methods may be applicable in clinical routines.

Response to intestinal provocation monitored by endosonography

The duodenal mucosa was challenged with allergen extracts *via* a nasoduodenal tube in 20 patients with self-reported adverse reactions to food. Seven of the patients had food allergy according to history, specific IgE and skin prick tests, whereas the remaining 13 patients were said to have food intolerance.

The tube was positioned with its tip in the descending part of the duodenum by first introducing a stylet during gastroduodenoscopy and thereafter pushing the tube in position over the stylet. The correct position of the tube was checked by fluoroscopy. Endosonography was performed by pushing a 20 MHz miniature ultrasound probe (Fujinon Sonoprobe System, SP 701, Omiya City, Japan) through the tube and installing a suspension of the suspected food item into the duodenum through the tube after temporarily withdrawing the ultrasound probe. Apparently, the mucosal responses were potentiated if the mucosal barrier was weakened by installing 10 mL of 48% alcohol either simultaneously of just prior to food challenge. Alcohol alone had no effect. The thickness of mucosa, submucosa and muscularis propria was measured directly on ultrasonographic sections frozen on the screen every 3 min before and after allergen challenge. Clinical symptoms were recorded at same intervals. After

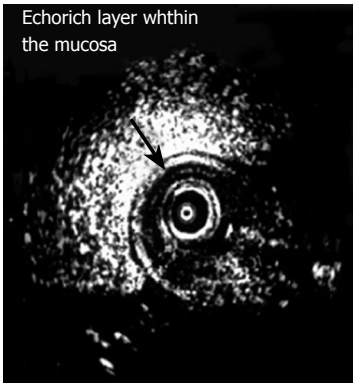

Figure 8 Endosonographic changes i.e. any resolvable wall thickening of the duodenum, contraction or new echogenic layer) were observed in many patients with food hypersensitivity. Increased mucosal thickness associated with a new echogenic layer was seen in two patients[82].

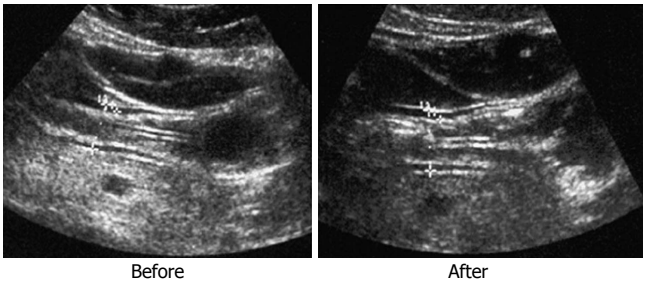

Figure 9 The sonographic features; wall thickness and diameter of the duodenal bulb and jejunum, peristalsis activity, and luminal fluid were recorded before and during allergen challenge by external ultrasound. The ultrasonographic view of the duodenal bulb shows wall thickening and increased diameter in response to provocation[83].

completing the ultrasonographic recordings, intestinal lavage was performed by infusing 2 L of an isotonic solution of polyethylene glycol into the duodenum. The first clear fluid passed per rectum and all urine voided for 5 h were sampled for analysis.

Endosonographic changes (i.e. any resolvable wall thickening, contraction or new echogenic layer) were observed in 15 of the 20 patients (75%). Increased mucosal thickness in response to provocation was recorded in 11 patients, but not more often or pronounced in allergic than in intolerant patients. Interestingly, increased mucosal thickness associated with a new echogenic layer was seen in two patients and a sustained duodenal contraction associated with pain lasting 15-20 min in another two (Figure 8). Intestinal permeability and inflammatory mediators (calprotectin) were not significantly different in the two groups.

Response to intestinal provocation monitored by transabdominal ultrasound

The feasibility of using external transabdominal ultrasound to monitor the response of the proximal intestine to direct luminal provocation was examined in 32 patients with chronic abdominal complaints, self-attributed to food hypersensitivity/allergy[81]. *Via* a nasoduodenal tube, the duodenal mucosa was challenged with the suspected food item dissolved in 10 mL water or saline. Gastrointestinal symptoms were scored on a visual analogue scale. The sonographic features (wall thickness and diameter of the duodenal bulb and jejunum, peristalsis activity, and luminal fluid) were recorded before and during one hour after challenge by external ultrasound. Sonographic changes after challenge were observed in 14 (44%) of the 32 patients (Figure 9). A positive sonographic response (increased wall thickness, diameter, peristalsis and/or luminal fluid) was significantly related to positive skin prick test ($P = 0.008$) and positive double-blind placebo-controlled food challenge ($P = 0.03$). A significant correlation was found between provocation-induced symptoms and intestinal wall thickness, both in the duodenal bulb ($r = 0.50$, $P = 0.004$) and in the jejunum ($r = 0.42$, $P = 0.02$). Intra- and interobserver variation of the tracing procedure revealed low values.

Sonography appeared to be the most sensitive test applied. It was positive in 14 patients, while the skin prick test was positive in 10 and the double-blind placebo-controlled food challenge in four. However, the specificity of the new test is not yet known. We conclude that responses of the proximal small intestines to direct provocation (swelling of the wall and exudation of fluid into the lumen) could be visualised by transabdominal ultrasound, and that this new provocation test may become helpful in the evaluation of patients with food hypersensitivity. However, we acknowledge that further validation studies are required.

Food hypersensitivity reactions visualised by ultrasonography and magnetic resonance imaging

Particularly in the absence of systemic food-specific IgE, a firm diagnosis of food allergy is difficult. Using ultrasonography and MRI we were able to visualise the intestinal response in one such case[82]. A 24-year-old female presented with self-reported food hypersensitivity, particularly related to intake of egg. Nausea and diarrhoea were predominant symptoms. Double-blind placebo-controlled food challenge with raw egg was positive, but all other conventional tests of food hypersensitivity, including skin prick test, total and food specific IgE in serum, were negative. A thorough investigation programme could not reveal any organic disease. We extended the evaluation to include two new provocation tests namely monitoring intestinal wall thickness and the amount of luminal liquid by external abdominal ultrasound and MRI.

Both ultrasound and MRI investigations indicated intestinal wall thickening and influx of large amounts of fluid into the proximal small intestines within 10 min after duodenal challenge with egg. The response was associated with abdominal pain and bloating. We conclude that the response to provocation was typical of an immediate allergic reaction. Our results indicate that local food-induced hypersensitivity reactions can occur in the gut in the absence of systemic indications of IgE-mediated allergy. Abdominal ultrasonography and MRI might become valuable tools for documenting such responses.

Visualization of stress-induced responses

It has long been known that there are close anatomical and functional connections between the enteric nervous system and the mucosal mast cells. Electron microscopic examinations show that the two structures are in direct

contact[83]. Using intestinal intubation and multilumen tubes allowing intestinal perfusion studies in man, Santos *et al*[78] demonstrated release of histamine and tryptase from mucosal mast cells in response to stress. The stress model applied was repeated insertion of the left hand in ice water. In addition to mast cell mediator release, the response was characterised by oedema and marked increase in flow of liquid into the lumen (a well-known consequence of histamine-induced mucosal hyperaemia). Hence, the intestinal response to stress includes several features typical of the response provoked by allergens both in animals[79] and man[84]. No wonder, therefore, that differentiating between allergy- and stress-induced intestinal problems in patients can be extremely difficult.

Food hypersensitivity reactions including gastrointestinal reactions due to food allergy can be visualized by several modalities. From a practical clinical point of view, visualization by ultrasound and MRI appear particularly promising.

INTRALUMINAL MULTIMODAL IMAGING DEVICES

Within the past five years there has been a considerable interest in the development of multimodal probes for studying visceral pain mechanics and physiology. Drewes, Gregersen and coworkers have, through a series of studies published from 2001 onwards, developed multimodal stimulation probes and protocols using mechanical, thermal, chemical and electrical stimuli with the purpose of differentiating pain mechanisms. For example mechanical stimuli are believed to stimulate receptors primarily in the muscle layers whereas chemical stimuli are sensed by mucosal receptors. Furthermore, electrical stimulation is believed to bypass the receptors and to stimulate the nerves directly. Using an advanced setup the stimuli can be combined in many ways. In order to study whether distension-induced pain is due to the mechanical stretch of to tissue ischemia induced by the distension, Hoff and coworkers developed a multimodal imaging device combining bag distension, manometry, high frequency intraluminal ultrasound, laser Doppler flowmetry and symptom registration. Successful development of these modalities will have important implications on our understanding of functional pain in the viscera and the development has now passed through several stages and prototypes were bench-tested before trials were done in pigs and subsequently in human subjects.

The probe consists of a 6 mm OD multi-lumen bag catheter with a radial 20-MHz miniature ultrasound probe with a diameter of 2.6 mm (UM-3R, Olympus Corp, Tokyo, Japan) and a laser Doppler flow sensor (Perimed, Sweden) placed inside the bag. Furthermore, the catheter contained channels for filling and emptying the bag and for pressure measurements. The laser Doppler provides a qualititative measure of perfusion in the mucosa (approximately 1 mm into the mucosa) and the combined measurement of pressure and geometry data using ultrasonography allow the computation of mechanical stress (force per area) and strain (a measure of deformation). Hence, by running various advanced distension protocols it is possible to differentiate pain mechanisms.

In a typical study the device is inserted through the mouth into the stomach and retracted to the esophagus, with the tip of the bag placed approximately 8 cm proximal to the upper border of the LES, as determined with manometry and ultrasound. A total of six distensions are performed at a bag infusion rate of 15 mL/min. The inflations are reversed when moderate pain is reported by the subject under study. The first distensions serve to precondition the tissue mechanically. The fifth distension is started 1 min after an intravenous injection of 20 mg butylscopolaminebromide (Buscopan®, Boehringer Ingelheim, Germany). Buscopan serves to inhibit muscle contraction and thus provides a "cleaner" experimental situation.

Studies done until now in the human esophagus have shown that the multimodal imaging device is safe to use and provides accurate and reproducible data. Furthermore, the ultrasound and laser Doppler signals do not interfere with each other. Distensions increase the bag pressure and lumen cross-sectional area and decrease the wall thickness. Hence, increase in circumferential wall stress and strain occurs. Furthermore, the Laser Doppler signal decreases invariably during bag distensions but artifacts, likely due to motions, may interfere with the Doppler signal. Contractions characterized by high amplitudes and long duration are often associated with a decrease in mucosal perfusion whereas less strong contractions do not seem to interfere with tissue perfusion. There are unpublished data that contradict this hypothesis that distension-induced pain is ischemia-related. However, such data does not exclude that functional visceral pain is ischemic, and indeed there may be dual mechanisms involved in visceral pain. Studies are ongoing to shed light on this issue.

ADVANCED VISUALIZATION

Advanced screening technologies in medicine drive needs for image processing research and visualization research. Image processing deals with issues such as filtering, feature enhancement, tissue segmentation, and tissue classification. Visualization is usually performed after image processing, and deals with the problem of transforming data into a graphic representation that can aid in understanding the meaning of the data.

Many medical screening technologies produce slices of data, which may be aligned to form 3D data. Visualization has become particularly important when 3D acquisitions are available and the inspection of the two-dimensional slices does not justify the particular goal of the medical procedure. In such cases, 3D visualization provides added value in terms of more holistic understanding of the data. Typical examples here are pre-operative surgical planning or virtual training of medical students.

Medical data is becoming more and more complex. The resolution of the imaging modalities increases resulting in an enormous number of cross-sectional 'slices' where manual slice-by-slice inspection is just not possible. Furthermore, new co-registration techniques produce multimodal data sets, i.e. combinations of CT, MRI, PET,

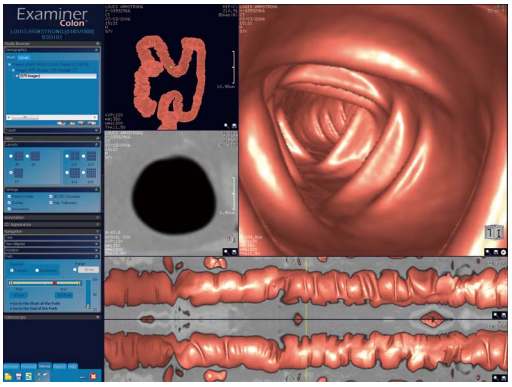

Figure 10 Example of a colonoscopy layout in a 3D medical workstation 3Dnet Examiner (Copyright Biotronics3D Ltd, Used by permission).

and US (ultrasound). In many cases the data are also acquired over time. This complexity creates a new area for advanced visualization research, where different data types can be combined and presented in new ways.

In the following text we will discuss advanced visualization techniques that assist medical scenarios dealing with lesions in the gastrointestinal tract. We review techniques already integrated into daily clinical routine or currently under development. Following this we give an outlook of possible research directions for visualization of the gastrointestinal tract.

Virtual endoscopy

The visualization technique probably having the highest impact on the diagnostic procedure in gastrointestinal medicine is the virtual endoscopy[85]. It is mostly applied to diagnosis of early stage cancer in the colon and aims to overcome problems associated with original optical endoscopy. The original procedure is uncomfortable for the patient, provides limited views, does not give access to areas behind colon collapses, and introduces potential risk of lesions due to the endoscope. Virtual endoscopy is realized as a 'flythrough' visualization of the patient' s body acquired from CT or MRI scanning. The clinician can freely navigate the camera in the scanned data to select arbitrary views. The position of the 'light' can be also freely manipulated. The spatial location of the camera in the volume is depicted in overview, which is linked to the detail view that shows the actual endoscopic view. This guarantees that the user does not loose orientation in the three-dimensional data.

Virtual colonoscopy is one specific type of virtual endoscopy applied to the data acquired from the patient' s colon. The goal is to identify polyps on the colon wall, i.e. indications of early stage colon cancer or the identification of pre-malignant lesions. The pipeline for virtual colonoscopy diagnosis starts with acquiring data (usually using CT modality) of cleaned colon that is pumped-up with air. The colon structures are then rapidly segmented, and various analysis tools are applied. For example, in order to allow easy interaction a default camera path is located on the pre-computed centerline of the colon. Additionally, some recent work has concentrated on shape analysis of underlying data for automatic polyp detection[86]. This allows the clinician to focus on the most important region, and to reduce the overall time of the diagnosis. The colon data can be shown using surface rendering in order to clearly identify the polyps or by using volume rendering to show structures behind the colon walls[85]. The surface can be rendered directly using first-hit raycasting or a polygonal model of the colon walls can be generated using the marching cubes algorithm[87], which are then rendered using standard graphics hardware. In cases where the clinician is interested in structures behind the colon walls, the direct volume rendering technique using semi-transparent colon walls can be selected. This enables clinicians to examine tissues close to the colon such as a tumor located adjacent to the colon. An example of a commercial medical workstation featuring virtual colonoscopy is shown in Figure 10.

Virtual colonoscopy and virtual endoscopy in general has its limitations, and optical endoscopy will never be fully replaced. The quality of the endoscopic visualization highly depends on the quality of acquired data and the chosen segmentation technique. The flaws of the data acquisition and segmentation cannot be usually fixed during rendering. In contrast to the optical endoscopy, the visualization is done for the diagnostic purposes only, so the in-situ analyses (e.g. biopsy probes) are not possible. The main strengths of virtual endoscopy are clear understanding of the spatial location and the non-invasive character of the procedure.

Colon unfolding

A different visualization for inspection and diagnosis of colon lesions is colon unfolding[88]. The data set is acquired in the same way as in the case of virtual colonoscopy. Colon unfolding is, in contrast to previously mentioned optical and virtual endoscopy, still a research area in development and not used in daily clinical use. The goal of colon unfolding is to eliminate all the problems associated with the manipulation in the three-dimensional space. The approach performs unfolding of a cylindrical structure to a plane. Unfolding the tubular structure provides an instant overview of the entire organ. The topological change from a cylindrical structure to a planar structure has the potential to significantly speed-up in the diagnostic procedure and decision making. This is very important in order to reduce the overall costs of the process.

The reasons why this technique is still not routinely used in the clinical setting are the artefacts associated with the topological change to a planar structure that require some advanced re-sampling strategies. Typical artifacts of the re-sampling step are double appearance of the same polyp in the re-sampled plane or missing a polyp due to under sampling. Another problem may be missing a polyp that is located at the 'cut' of the cylinder. Careful treatment of the re-sampling step may, however, make this unfolding a very powerful and popular feature among clinicians. A comparison between a real dissected colon containing polyps and colon unfolding of the CT scan obtained from the same patient can be observed in Figure 11.

Virtual elastography

Elastography is a new ultrasound screening modality

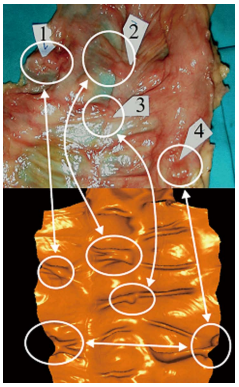

Figure 11 Comparison between real colon dissection and the resulting visualization of colon unfolding technique (Copyright Anna Vilanova, Used by permission).

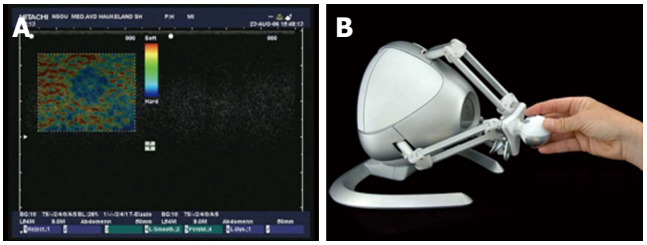

Figure 12 Screenshot of current two-dimensional ultrasound elastography visualization (**A**) and the Novint Falcon 3D haptic controller (**B**).

where the strain of the tissue is measured[89]. Figure 12A shows one slice of elastography data visualized by means of standard techniques provided by the hardware vendor. In this figure blue corresponds to hard tissue, while red corresponds to soft tissue. Elastography is very well suited for being combined with new volume rendering techniques and new haptics (force-feedback) interaction devices into a solution that may be termed "Virtual Elastography". Here the idea is that the strain of the tissue can often characterize a presence of a tumor as neoplastic tissue is usually much harder than surrounding tissue. In such cases, 3D acquisitions followed by volume rendering techniques can be used to show strain of the entire three-dimensional structure. Advanced volume rendering techniques, such as importance-driven volume rendering[90], can be used to automatically emphasize features of interest. This can be done by mapping the tissue strain to the importance function. This will result in a clear view of the three-dimensional shape of the entire suspicious region characterized by high strain values. The clinician will get information about the entire stiff structure instead of information only about the cross-section. Two-dimensional cross-sections are currently the only visualization technique supported by ultrasound hardware vendors. Three-dimensional acquisitions will also allow for three-dimensional measurements of the volume of the stiff region, which may influence the selection of appropriate medical treatment.

In addition to the advanced visualization strategies using the importance-driven concept, the virtual elastography solution may include smart interaction hardware such as haptic devices (Figure 12B). Such devices are used to give the user the sense of touch by applying forces, vibrations or other motions to the user. The usage of haptic devices for medicine has, for example, been studied for remote surgery or training of palpatory diagnosis[91]. Using the elastography data as input for the haptic device can very effectivelly convey the stiffness information to the clinician by means of haptic cues. Virtual elastography will in this case introduce a completely new interaction to medicine, i.e. the ability to 'touch' and 'palpate' a patient's internal organs.

Navigation 3D maps

Clinicians often refer to the lack of information about the exact position and orientation of the imaging device as a limitation or difficulty, e.g. in the practical use of endosonography. The large Bird sensor has been used for many clinical applications including external GI ultrasonography[50,92]. New virtual reality tracking technologies, such as the microBIRD (Ascension Technology Corporation, Vermont, USA), can be used to overcome this problem even in invasive procedures[93,94]. This device measures position and orientation in real time, and is designed for use in catheters. The diameter of the sensor is only 1.3 mm.

Miniature tracking devices are thus enablers for a broad range of new medical applications. Within endoscopy, it is very likely to see a development towards solutions we may call "Navigation 3D Maps". Here the idea is to firstly perform screening of the patient prior to the endoscopic procedure, e.g. by using CT, MRI or PET. Then the endoscopic intervention is performed by including a miniature tracking device in the setup. By combining the screening data and the endoscopic data it will be possible to visualize the internal structures of the patient together with endoscopic ultrasound data.

Several technical issues need to be addressed before we can expect to see Navigation 4D Maps in clinical use. For example, during endoscopy of the upper GI tract, the structures can move a considerable amount due to digestion, heart beating, and breathing. This problem can be addressed in several ways depending on the medical procedure. In some cases it may be possible to perform simultaneous acquisitions of map data and endoscopic data, while in other cases it may be possible to correct for movements in the map data. Such corrections can be based upon acquisitions of cyclic movements, or be based upon real-time data from the endoscope. In addition it is a great challenge to explore and evaluate which visualization techniques that are best suited for each of the broad range of medical problems being addressed.

CONCLUSION

There are many imaging modalities and visualization methods that can be used to diagnose and follow-up patients with diseases of the Gi tract. CT, MRI, SPECT, PET, X-ray, ultrasonography, endoscopy, roentgenological and radionuclide methods have different strengths and weaknesses and must be tailored to the specific task demanded. Regarding temporal and spatial resolution, SPECT and PET are at the lower end of, and ultrasonography is at the high end of, the resolution spectrum. Regarding functional imaging capacity,

X-ray and CT are at the lower end, whereas PET and ultrasonography are at the higher end of the spectrum.

The introduction of 3D ultrasonographic imaging in the field of gastroenterology seems to improve standardization of data acquisition and analysis. Moreover, acquisition time during an unpleasant procedure for the patient can be reduced. 3D imaging also make ultrasonography less operator dependant and facilitates easier interpretation of ultrasonographic images. A successful development of modern endosonographic devices can be achieved on the basis of a fruitful collaboration between medicine, technology and soft-ware producers. Different modalities can be merged into new multimodal devices making it possible to measure multiple parameters in one procedure. This also paves the way for fusion of diagnostic and therapeutic imaging enabling patients to have a one-session procedure.

REFERENCES

1 **Gilja OH**, Hausken T, Ødegaard S, Wendelbo Ø, Thierley M. Mobile ultrasonography in a medical department. *Tidsskr Nor Laegeforen* 2003; 123: 2713-2714
2 **Bateman DN**, Leeman S, Metreweli C, Willson K. A non-invasive technique for gastric motility measurement. *Br J Radiol* 1977; **50**: 526-527
3 Holt S, McDicken WN, Anderson T, Stewart IC, Heading RC. Dynamic imaging of the stomach by real-time ultrasound--a method for the study of gastric motility. *Gut* 1980; **21**: 597-601
4 **Hausken T**, Berstad A. Wide gastric antrum in patients with non-ulcer dyspepsia. Effect of cisapride. *Scand J Gastroenterol* 1992; **27**: 427-432
5 **Hausken T**, Odegaard S, Berstad A. Antroduodenal motility studied by real-time ultrasonography. Effect of enprostil. *Gastroenterology* 1991; **100**: 59-63
6 **Ahluwalia NK**, Thompson DG, Mamtora H, Troncon L, Hindle J, Hollis S. Evaluation of human postprandial antral motor function using ultrasound. *Am J Physiol* 1994; **266**: G517-G522
7 **Wedmann B**, Adamek RJ, Wegener M. Ultrasound detection of gastric antrum motility--evaluating a simple semiquantitative method. *Ultraschall Med* 1995; **16**: 124-126
8 **Hveem K**, Sun WM, Hebbard G, Horowitz M, Dent J. Insights into stomach mechanics from concurrent gastric ultrasound and manometry. *Gastroenterology* 1995; **107**: 1236
9 **Hveem K**, Svebak S, Hausken T, Berstad A. Effect of mental stress and cisapride on autonomic nerve functions in functional dyspepsia. *Scand J Gastroenterol* 1998; **33**: 123-127
10 **Bateman DN**, Whittingham TA. Measurement of gastric emptying by real-time ultrasound. *Gut* 1982; **23**: 524-527
11 **Bolondi L**, Bortolotti M, Santi V, Calletti T, Gaiani S, Labò G. Measurement of gastric emptying time by real-time ultrasonography. *Gastroenterology* 1985; **89**: 752-759
12 **Holt S**, Cervantes J, Wilkinson AA, Wallace JH. Measurement of gastric emptying rate in humans by real-time ultrasound. *Gastroenterology* 1986; **90**: 918-923
13 **Duan LP**, Zheng ZT, Li YN. A study of gastric emptying in non-ulcer dyspepsia using a new ultrasonographic method. *Scand J Gastroenterol* 1993; **28**: 355-360
14 **Ricci R**, Bontempo I, Corazziari E, La Bella A, Torsoli A. Real time ultrasonography of the gastric antrum. *Gut* 1993; **34**: 173-176
15 **Desaga JF**, Hixt U. Sonographic determination of gastric emptying. *Ultraschall Med* 1987; **8**: 138-141
16 **Gerards C**, Tromm A, May B. Optimizing antrum planimetry for ultrasound determination of gastric emptying using emptying function reference lines. *Ultraschall Med* 1998; **19**: 83-86
17 **Marzio L**, Giacobbe A, Conoscitore P, Facciorusso D, Frusciante V, Modoni S. Evaluation of the use of ultrasonography in the study of liquid gastric emptying. *Am J Gastroenterol* 1989; **84**: 496-500
18 **Tympner F**, Feldmeier J, Rösch W. Study of the correlation of sonographic and scintigraphic results in measuring stomach emptying. *Ultraschall Med* 1986; **7**: 264-267
19 **Odegaard S**, Gilja OH, Gregersen H. Basic and new aspects of gastrointestinal ultrasonography. 1st ed. Singapore: World Scientific , 2005: 1-502
20 **King PM**, Adam RD, Pryde A, McDicken WN, Heading RC. Relationships of human antroduodenal motility and transpyloric fluid movement: non-invasive observations with real-time ultrasound. *Gut* 1984; **25**: 1384-1391
21 **Hausken T**, Odegaard S, Matre K, Berstad A. Antroduodenal motility and movements of luminal contents studied by duplex sonography. *Gastroenterology* 1992; **102**: 1583-1590
22 **Hausken T**, Gilja OH, Undeland KA, Berstad A. Timing of postprandial dyspeptic symptoms and transpyloric passage of gastric contents. *Scand J Gastroenterol* 1998; **33**: 822-827
23 **Hausken T**, Gilja OH, Odegaard S, Berstad A. Flow across the human pylorus soon after ingestion of food, studied with duplex sonography. Effect of glyceryl trinitrate. *Scand J Gastroenterol* 1998; **33**: 484-490
24 **Hausken T**, Li XN, Goldman B, Leotta D, Ødegaard S, Martin RW. Quantification of gastric emptying and duodenogastric reflux stroke volumes using three-dimensional guided digital color Doppler imaging. *Eur J Ultrasound* 2001; **13**: 205-213
25 **Uematsu M**, Nakatani S, Yamagishi M, Matsuda H, Miyatake K. Usefulness of myocardial velocity gradient derived from two-dimensional tissue Doppler imaging as an indicator of regional myocardial contraction independent of translational motion assessed in atrial septal defect. *Am J Cardiol* 1997; **79**: 237-241
26 **Grubb NR**, Fleming A, Sutherland GR, Fox KA. Skeletal muscle contraction in healthy volunteers: assessment with Doppler tissue imaging. *Radiology* 1995; **194**: 837-842
27 **Gregersen H**, Barlow J, Thompson D. Development of a computer-controlled tensiometer for real-time measurements of tension in tubular organs. *Neurogastroenterol Motil* 1999; **11**: 109-118
28 **Matre K**, Stokke EM, Martens D, Gilja OH. In vitro volume estimation of kidneys using three-dimensional ultrasonography and a position sensor. *Eur J Ultrasound* 1999; **10**: 65-73
29 **Ahmed AB**, Gilja OH, Gregersen H, Ødegaard S, Matre K. In vitro strain measurement in the porcine antrum using ultrasound doppler strain rate imaging. *Ultrasound Med Biol* 2006; 32: 513-522
30 **Gilja OH**, Heimdal A, Hausken T, Gregersen H, Matre K, Berstad A, Ødegaard S. Strain during gastric contractions can be measured using Doppler ultrasonography. *Ultrasound Med Biol* 2002; **28**: 1457-1465
31 **Heimdal A**, Gilja OH. Strain Rate Imaging - A new tool for studying the GI tract. In: Odegaard S, Gilja OH, Gregersen H, editors. Basic and new aspects of gastrointestinal ultrasonography. Singapore: World Scientific, 2005: 243-263
32 **Gilja OH**, Hausken T, Odegaard S, Berstad A. Monitoring postprandial size of the proximal stomach by ultrasonography. *J Ultrasound Med* 1995; **14**: 81-89
33 **Gilja OH**, Hausken T, Wilhelmsen I, Berstad A. Impaired accommodation of proximal stomach to a meal in functional dyspepsia. *Dig Dis Sci* 1996; **41**: 689-696
34 **Gilja OH**, Hausken T, Bang CJ, Berstad A. Effect of glyceryl trinitrate on gastric accommodation and symptoms in functional dyspepsia. *Dig Dis Sci* 1997; **42**: 2124-2131
35 **Undeland KA**, Hausken T, Gilja OH, Aanderud S, Berstad A. Gastric meal accommodation studied by ultrasound in diabetes. Relation to vagal tone. *Scand J Gastroenterol* 1998; **33**: 236-241
36 **Tefera S**, Gilja OH, Hatlebakk JG, Berstad A. Gastric accommodation studied by ultrasonography in patients with reflux esophagitis. *Dig Dis Sci* 2001; **46**: 618-625
37 **Izbéki F**, Kiss I, Wittmann T, Várkonyi TT, Légrády P,

Lonovics J. Impaired accommodation of proximal stomach in patients with alcoholic liver cirrhosis. *Scand J Gastroenterol* 2002; **37**: 1403-1410

38 **Olafsdottir E**, Gilja OH, Aslaksen A, Berstad A, Fluge G. Impaired accommodation of the proximal stomach in children with recurrent abdominal pain. *J Pediatr Gastroenterol Nutr* 2000; **30**: 157-163

39 **Vingerhagen S**, Hausken T, Gilja OH, Berstad A. Influence of a 5HT1 receptor agonist on gastric accommodation and initial transpyloric flow in healthy subjects. *Neurogastroenterol Motil* 2000; **12**: 95-101

40 **Mundt MW**, Hausken T, Samsom M. Effect of intragastric barostat bag on proximal and distal gastric accommodation in response to liquid meal. *Am J Physiol Gastrointest Liver Physiol* 2002; **283**: G681-G686

41 **Gilja OH**, Thune N, Matre K, Hausken T, Odegaard S, Berstad A. In vitro evaluation of three-dimensional ultrasonography in volume estimation of abdominal organs. *Ultrasound Med Biol* 1994; **20**: 157-165

42 **Thune N**, Hausken T, Gilja OH, Matre K. A practical method for estimating enclosed volumes using 3D ultrasound. *Eur J Ultrasound* 1996; **3**: 83-92

43 **Gilja OH**, Smievoll AI, Thune N, Matre K, Hausken T, Odegaard S, Berstad A. In vivo comparison of 3D ultrasonography and magnetic resonance imaging in volume estimation of human kidneys. *Ultrasound Med Biol* 1995; **21**: 25-32

44 **Hokland J**, Hausken T. An interactive volume rendering method applied to ultrasonography of abdominal structures. *IEEE Ultrason Symp Proc* 1994; **3**: 1567-1571

45 **Hausken T**, Thune N, Matre K, Gilja OH, Odegaard S, Berstad A. Volume estimation of the gastric antrum and the gallbladder in patients with non-ulcer dyspepsia and erosive prepyloric changes, using three-dimensional ultrasonography. *Neurogastroenterol Mot* 1994; **6**: 263-270

46 **Gilja OH**, Hausken T, Odegaard S, Berstad A. Three-dimensional ultrasonography of the gastric antrum in patients with functional dyspepsia. *Scand J Gastroenterol* 1996; **31**: 847-855

47 **Berstad A**, Hausken T, Gilja OH, Thune N, Matre K, Odegaard S. Volume measurements of gastric antrum by 3-D ultrasonography and flow measurements through the pylorus by duplex technique. *Dig Dis Sci* 1994; **39**: 97S-100S

48 **Detmer PR**, Bashein G, Hodges T, Beach KW, Filer EP, Burns DH, Strandness DE. 3D ultrasonic image feature localization based on magnetic scanhead tracking: in vitro calibration and validation. *Ultrasound Med Biol* 1994; **20**: 923-936

49 **Hodges TC**, Detmer PR, Burns DH, Beach KW, Strandness DE. Ultrasonic three-dimensional reconstruction: in vitro and in vivo volume and area measurement. *Ultrasound Med Biol* 1994; 20: 719-729

50 **Gilja OH**, Detmer PR, Jong JM, Leotta DF, Li XN, Beach KW, Martin R, Strandness DE. Intragastric distribution and gastric emptying assessed by three-dimensional ultrasonography. *Gastroenterology* 1997; **113**: 38-49

51 **Tefera S**, Gilja OH, Olafsdottir E, Hausken T, Hatlebakk JG, Berstad A. Intragastric maldistribution of a liquid meal in patients with reflux oesophagitis assessed by three dimensional ultrasonography. *Gut* 2002; **50**: 153-158

52 **Tack J**, Piessevaux H, Coulie B, Caenepeel P, Janssens J. Role of impaired gastric accommodation to a meal in functional dyspepsia. *Gastroenterology* 1998; **115**: 1346-1352

53 **Ahluwalia NK**, Thompson DG, Barlow J, Troncon LE, Hollis S. Relaxation responses of the human proximal stomach to distension during fasting and after food. *Am J Physiol* 1994; **267**: G166-G172

54 **Berstad A**, Hauksen T, Gilja OH, Hveem K, Undeland KA, Wilhelmsen I, Haug TT. Gastric accommodation in functional dyspepsia. *Scand J Gastroenterol* 1997; **32**: 193-197

55 **Hjelland IE**, Ofstad AP, Narvestad JK, Berstad A, Hausken T. Drink tests in functional dyspepsia: which drink is best? *Scand J Gastroenterol* 2004; **39**: 933-937

56 **Liao D**, Gregersen H, Hausken T, Gilja OH, Mundt M, Kassab G. Analysis of surface geometry of the human stomach using real-time 3-D ultrasonography in vivo. *Neurogastroenterol Motil* 2004; **16**: 315-324

57 **Martens D**, Hausken T, Gilja OH, Steen EN, Alker HJ. 3D processing of ultrasound images using a novel echopac-3D software. *Ultrasound Med Biol* 1997; **23**: 136

58 **Martens D**, Gilja OH. The EchoPAC-3D software for 3D image analysis. In: Odegaard S, Gilja OH, Gregersen H, editors. Basic and new aspects of gastrointestinal ultrasonography. Singapore: World Scientific, 2004: 305-329

59 **Gilja OH**, Hausken T, Berstad A, Odegaard S. Measurements of organ volume by ultrasonography. *Proc Inst Mech Eng H* 1999; **213**: 247-259

60 **Bredenoord AJ**, Weusten BL, Timmer R, Smout AJ. Intermittent spatial separation of diaphragm and lower esophageal sphincter favors acidic and weakly acidic reflux. *Gastroenterology* 2006; **130**: 334-340

61 **Mittal RK**, Liu J, Puckett JL, Bhalla V, Bhargava V, Tipnis N, Kassab G. Sensory and motor function of the esophagus: lessons from ultrasound imaging. *Gastroenterology* 2005; **128**: 487-497

62 **Pehlivanov N**, Liu J, Mittal RK. Sustained esophageal contraction: a motor correlate of heartburn symptom. *Am J Physiol Gastrointest Liver Physiol* 2001; **281**: G743-G751

63 **Jung HY**, Puckett JL, Bhalla V, Rojas-Feria M, Bhargava V, Liu J, Mittal RK. Asynchrony between the circular and the longitudinal muscle contraction in patients with nutcracker esophagus. *Gastroenterology* 2005; **128**: 1179-1186

64 **Hoff DA**, Gregersen H, Odegaard S, Nesje LB, Oevreboe K, Hausken T, Gilja OH, Matre K, Hatlebakk JG. A multimodal laser Doppler and endosonographic distension device for studying mechanosensation and mucosal blood flow in the oesophagus. *Neurogastroenterol Motil* 2006; **18**: 243-248

65 **McMahon BP**, Frøkjaer JB, Kunwald P, Liao D, Funch-Jensen P, Drewes AM, Gregersen H. The functional lumen imaging probe (FLIP) for evaluation of the esophagogastric junction. *Am J Physiol Gastrointest Liver Physiol* 2007; **292**: G377-G384

66 **Goetz M**, Hoffman A, Galle PR, Neurath MF, Kiesslich R. Confocal laser endoscopy: new approach to the early diagnosis of tumors of the esophagus and stomach. *Future Oncol* 2006; **2**: 469-476

67 **Odegaard S**, Nesje LB, Hoff DA, Gilja OH, Gregersen H. Morphology and motor function of the gastrointestinal tract examined with endosonography. *World J Gastroenterol* 2006; **12**: 2858-2863

68 **Kimmey MB**, Martin RW, Haggitt RC, Wang KY, Franklin DW, Silverstein FE. Histologic correlates of gastrointestinal ultrasound images. *Gastroenterology* 1989; **96**: 433-441

69 **Odegaard S**, Kimmey MB, Martin RW, Yee HC, Cheung AH, Silverstein FE. The effects of applied pressure on the thickness, layers, and echogenicity of gastrointestinal wall ultrasound images. *Gastrointest Endosc* 1992; **38**: 351-356

70 **Taniguchi DK**, Martin RW, Trowers EA, Silverstein FE. Simultaneous M-mode echoesophagram and manometry in the sheep esophagus. *Gastrointest Endosc* 1995; **41**: 582-586

71 **Ophir J**, Alam SK, Garra B, Kallel F, Konofagou E, Krouskop T, Varghese T. Elastography: ultrasonic estimation and imaging of the elastic properties of tissues. *Proc Inst Mech Eng H* 1999; **213**: 203-233

72 **Giovannini M**, Hookey LC, Bories E, Pesenti C, Monges G, Delpero JR. Endoscopic ultrasound elastography: the first step towards virtual biopsy? Preliminary results in 49 patients. *Endoscopy* 2006; **38**: 344-348

73 **Molin S**, Nesje LB, Gilja OH, Hausken T, Martens D, Odegaard S. 3D-endosonography in gastroenterology: methodology and clinical applications. *Eur J Ultrasound* 1999; **10**: 171-177

74 **Olafsson S**, Berstad A. Changes in food tolerance and lifestyle after eradication of Helicobacter pylori. *Scand J Gastroenterol* 2003; **38**: 268-276

75 **Isolauri E**, Rautava S, Kalliomäki M. Food allergy in irritable bowel syndrome: new facts and old fallacies. *Gut* 2004; **53**: 1391-1393

76 **Simrén M**, Månsson A, Langkilde AM, Svedlund J, Abrahamsson H, Bengtsson U, Björnsson ES. Food-related gastrointestinal symptoms in the irritable bowel syndrome. *Digestion* 2001; **63**: 108-115

77 **Persson CG**, Gustafsson B, Erjefält JS, Sundler F. Mucosal exudation of plasma is a noninjurious intestinal defense mechanism. *Allergy* 1993; **48**: 581-586

78 **Santos J**, Saperas E, Nogueiras C, Mourelle M, Antolín M, Cadahia A, Malagelada JR. Release of mast cell mediators into the jejunum by cold pain stress in humans. *Gastroenterology* 1998; **114**: 640-648

79 **Bischoff SC**, Mayer J, Wedemeyer J, Meier PN, Zeck-Kapp G, Wedi B, Kapp A, Cetin Y, Gebel M, Manns MP. Colonoscopic allergen provocation (COLAP): a new diagnostic approach for gastrointestinal food allergy. *Gut* 1997; **40**: 745-753

80 **Arslan G**, Ødegaard S, Elsayed S, Florvaag E, Berstad A. Food allergy and intolerance: response to intestinal provocation monitored by endosonography. *Eur J Ultrasound* 2002; **15**: 29-36

81 **Arslan G**, Gilja OH, Lind R, Florvaag E, Berstad A. Response to intestinal provocation monitored by transabdominal ultrasound in patients with food hypersensitivity. *Scand J Gastroenterol* 2005; **40**: 386-394

82 **Arslan G**, Lillestøl K, Mulahasanovic A, Florvaag E, Berstad A. Food hypersensitivity reactions visualised by ultrasonography and magnetic resonance imaging in a patient lacking systemic food-specific IgE. *Digestion* 2006; **73**: 111-115

83 **Bienenstock J**, MacQueen G, Sestini P, Marshall JS, Stead RH, Perdue MH. Mast cell/nerve interactions in vitro and in vivo. *Am Rev Respir Dis* 1991; **143**: S55-S58

84 **Santos J**, Bayarri C, Saperas E, Nogueiras C, Antolín M, Mourelle M, Cadahia A, Malagelada JR. Characterisation of immune mediator release during the immediate response to segmental mucosal challenge in the jejunum of patients with food allergy. *Gut* 1999; **45**: 553-558

85 **Bartz D**. Virtual endoscopy in research and clinical practice. *Computer Graphics Forum* 2005; **24**: 111-126

86 **Yoshida H**, Näppi J. Three-dimensional computer-aided diagnosis scheme for detection of colonic polyps. *IEEE Trans Med Imaging* 2001; **20**: 1261-1274

87 **Lorensen**, B. and Cline, H. Marching cubes: A High Resolution 3D Surface Construction Algorithm. Proceedings of Acm siggraph. Ref Type: Conference Proceeding, 1987: 163-169

88 **Vilanova A**, Bartoli I, Wegenkittl R, Konig M, Groller ME. Nonlinear Virtual Colon Unfolding. Proceedings of IEEE Visualization; 2001 October. USA: Diego, 2001: 91-98

89 **Ophir J**, Garra B, Kallel F, Konofagou E, Krouskop T, Righetti R, Varghese T. Elastographic imaging. *Ultrasound Med Biol* 2000; **26** Suppl 1: S23-S29

90 **Viola I**, Kanitsar A, Gröller ME. Importance-driven feature enhancement in volume visualization. *IEEE Trans Vis Comput Graph* 2005; **11**: 408-418

91 **Holland KL**, Williams RL, Conatser Jr RR, Howell JN, Cade DL. Implementation and Evaluation of a Virtual Haptic Back. *J Virtual Reality Society* 2004; **7**: 94-102

92 **Gilja OH**, Hausken T, Olafsson S, Matre K, Odegaard S. In vitro evaluation of three-dimensional ultrasonography based on magnetic scanhead tracking. *Ultrasound Med Biol* 1998; **24**: 1161-1167

93 **Leotta DF**, Detmer PR, Gilja OH, Jong JM,Martin RW,Primozich JF. Three-dimensional ultrasound imaging using multiple magnetic tracking systems and miniature magnetic sensors. *Proc IEEE Int Ultrasonics Symp Seattle WA USA* 1995; 1415-1418

94 **Molin SO**, Liedman B, Lundell L, Martens D, Gilja OH, Hausken T, Nesje LB, Odegaard S. Peformance of a miniature magnetic postion sensor for 3D-EUS imaging. *EUS 2000 Program* 2000; **17**: 133

S-Editor Liu Y **L-Editor** Mcgovern D **E- Editor** Chin GJ

PO Box 2345, Beijing 100023, China
www.wjgnet.com
wjg@wjgnet.com

World J Gastroenterol 2007 March 7; 13(9): 1422-1426
World Journal of Gastroenterology ISSN 1007-9327

CLINICAL RESEARCH

Long-term outcome and prognostic factors of patients with hilar cholangiocarcinoma

Andreas Weber, Sonja Landrock, Jochen Schneider, Manfred Stangl, Bruno Neu, Peter Born, Meinhard Classen, Thomas Rösch, Roland M Schmid, Christian Prinz

Andreas Weber, Sonja Landrock, Jochen Schneider, Bruno Neu, Peter Born, Meinhard Classen, Roland M Schmid, Christian Prinz, Department of Internal Medicine Ⅱ, Technical University of Munich, Germany
Manfred Stangl, Department of Surgery, Technical University of Munich, Germany
Thomas Rösch, Department of Internal Medicine, Rudolf Virchow Klinikum Charite, Berlin, Germany
Correspondence to: Christian Prinz, Professor, Ⅱ Medizinische Klinik, Klinikum rechts der Isar der Technischen Universität München, Ismaningerstr. 22, 81675 München, Germany. christian.prinz@lrz.tum.de
Telephone: +49-89-41405973 Fax: +49-89-41407366
Received: 2006-10-21 Accepted: 2007-02-12

Abstract

AIM: To evaluate the long-term outcome and prognostic factors of patients with hilar cholangiocarinoma.

METHODS: Ninety-six consecutive patients underwent treatment for malignant hilar bile duct tumors during 1995–2005. Of the 96 patients, 20 were initially treated with surgery (n = 2 R0 / n = 18 R1). In non-operated patients, data analysis was performed retrospectively.

RESULTS: Among the 96 patients, 76 were treated with endoscopic transpapillary (ERC, n = 45) and/or percutaneous transhepatic biliary drainage (PTBD, n = 31). The mean survival time of these 76 patients undergoing palliative endoscopic and/or percutaneous drainage was 359 ± 296 d. The mean survival time of patients with initial bilirubin levels > 10 mg/dL was significantly lower (P < 0.001) than patients with bilirubin levels < 10 mg/dL. The mean survival time of patients with Bismuth stage Ⅱ (n = 8), Ⅲ (n = 28) and Ⅳ (n = 40) was 496 ± 300 d, 441 ± 385 d and 274 ± 218 d, respectively. Thus, patients with advanced Bismuth stage showed a reduced mean survival time, but the difference was not significant. The type of biliary drainage had no significant beneficial effect on the mean survival time (ERC *vs* PTBD, P = 0.806).

CONCLUSION: Initial bilirubin level is a significant prognostic factor for survival of patients. In contrast, age, tumor stage according to the Bismuth-Corlette classification, and types of intervention are not significant prognostic parameters for survival. Palliative treatment with endoscopic or percutaneous biliary drainage is still suboptimal, new diagnostic and therapeutic tools need to be evaluated.

Key words: Klatskin tumor; Cholangiocarcinoma; Bilirubin; Prognostic factors; Endoscopic therapy; Operative therapy; Survival; Bismuth stage

Weber A, Landrock S, Schneider J, Stangl M, Neu B, Born P, Classen M, Rösch T, Schmid RM, Prinz C. Long-term outcome and prognostic factors of patients with hilar cholangiocarcinoma. *World J Gastroenterol* 2007; 13(9): 1422-1426

http://www.wjgnet.com/1007-9327/13/1422.asp

INTRODUCTION

Hilar cholangiocarinomas (Klatskin-tumors) are classified into 4 stages according to the Bismuth classification: stage Ⅰ or Ⅱ for tumors expanding up the hilus, type Ⅲ A/B infiltrating the right or left hepatic duct, and stage Ⅳ with infiltration of both hepatic ducts and subsegments[1]. Epidemiological data reveal an increasing mortality of primary intrahepatic cholangiocarcinoma. Because of the late presentation of symptoms, tumors are usually diagnosed in their later stages, and thus most therapy concepts cannot be curative[2, 3]. The prognosis of patients with hilar cholangiocarcinoma is poor, and the survival rate reported so far describes a very limited life expectancy < 3 mo if no treatment is offered. Although radical hilar tumor is a formidable challenge for surgeons, endoscopic transpapillary and/or percutaneous transhepatic biliary drainage offers the best survival[4, 5].

Possible treatment strategies for best supportive care include endoscopic retrograde cholangiography (ERC) with transpapillary stent therapy or percutaneous transhepatic biliary drainage (PTBD)[6-8]. Effective endoscopic stent placement provides adequate relief of symptoms associated with biliary obstruction and leads to increased overall survival[9,10]. Systemic chemotherapy, another palliative therapy concept, is marginally effective and dose-limited because of toxic side effects[11]. Unfortunately, the efficacy of percutaneous radiation, brachytherapy or radiochemotherapy is limited[12,13].

In the present study, the clinical outcome of patients

with hilar cholangiocarinoma was investigated with regard to possible prognostic factors such as Bismuth stage, bilirubin levels, age, and types of endoscopic intervention. Special attention was given to endoscopic transpapillary versus percutaneous transhepatic biliary drainage.

MATERIALS AND METHODS

Data selection

Long-term follow-up of patients with hilar cholangiocarcinoma undergoing endoscopic and/or surgical therapy was performed by retrospective analysis. The study included 96 unselected consecutive patients (56 males and 40 females with a mean age of 67 years) undergoing treatment for hilar cholangiocarinoma from 1995 to 2005 in the Department of Gastroenterology and Surgery at the Technical University Munich. Data acquisition was based on hospital records. Furthermore, follow-up data were obtained by telephone contact with relatives of the patients or referring physicians. In order to evaluate the life expectancy of patients with cholangiocarcinoma, follow-up analysis was done from the time when the patient received his or her first treatment until death. Baseline characteristics were age, gender, bilirubin levels, alkaline phosphatase, γ-GT, leucocytes, and type of therapeutic procedures including endoscopic transpapillary drainage, percutaneous transhepatic drainage and surgery.

Bismuth classification and diagnostic procedures

The biliary stricture location was classified in relation to the confluence of hepatic ducts as described by Bismuth-Corlette[1]. Bismuth stage was assessed by endoscopic retrograde cholangiography, endoscopic retrograde cholangioscopy, percutaneous transhepatic cholangiography and/or percutaneous transhepatic cholangioscopy. In addition, selected patients underwent computertomography (CT-scan), magnetic resonance imaging (MRI), or magnetic resonance cholangiopancreatic ography (MRCP). The final diagnosis was made by surgical specimens, autopsy, percutaneous ultrasound-guided fine needle biopsy, endoscopic ultrasound guided-fine needle biopsy, endoscopic transpapillary forceps biopsy/brush cytology, percutaneous transhepatic cholangioscopic guided biopsy, and clinical course.

Treatment strategies

The type of therapeutic procedures depended on tumor expansion and clinical conditions of patients. If the tumor was resectable, surgery was the first choice of treatment for patients in good clinical conditions. In all patients the possibility of a curative therapy concept with tumor resection was evaluated. In patients with non-resectable tumors or bad clinical conditions, palliative procedure using endoscopic transpapillary and/or percutaneous transhepatic biliary drainage was performed. R1-resected patients received also endoscopic and/or percutaneous drainage as a second-line treatment.

Endoscopic transpapillary drainage

ERC was done by a standard videoduodenoscope Olympus TFJ 160-R (Olympus, Hamburg, Germany). The first ERC comprised an endoscopic sphincterotomy (EPT) using an Olympus papillotom (Olympus, Hamburg, Germany) introduced over a Terumo guide wire. Under radiographic guidance using contrast fluid bile duct strictures were localized. Subsequently, one or more plastic endoprotheses were placed above the stricture to obtain biliary drainage. The caliber of stents varied between 7 F and 12 F. Elective stent changes were conducted at a time interval of 3 mo unless the clinical situation of patients required an earlier intervention.

Table 1 Characteristics, physical and laboratory parameters of patients at admission

	Resection	No resection	Standart values	Scale unit
Number of patients	20	76	-	-
Age (yr)	62 ± 8.4	68 ± 8.3	-	-
Bismuth Ⅱ	2	8	-	-
Bismuth Ⅲ	7	28	-	-
Bismuth Ⅳ	11	40	-	-
Bilirubin	5.4 ± 5.28	10.87 ± 7.11	< 1.2	mg/dL
Alkaline phosphatase	561 ± 278	610 ± 275	40–120	U/L
γ-GT	401 ± 225	365 ± 237	< 66	U/L
Leucocytes	8.95 ± 2.64	9.21 ± 2.79	4-9	G/L

Percutaneous transhepatic biliary drainage

In patients with percutaneous transhepatic drainage the biliary system was punctured with a steel needle, and a nitinol-coated guide wire (35") was introduced into the bile duct after contrast visualization of the biliary system. Dilation of the bile duct stricture was carried out using 8 F, 10 F, and 12 F bougies. After a first attempt, a 10 F pigtail catheter was introduced. In a second attempt, bile duct dilatation was continued to allow the placement of a 12 F, 14 F or 16 F Yamakawa drainage. The Yamakawa drainage was changed at a time interval of 3 mo.

Statistical analysis

Survival curves in relation to bilirubin, Bismuth stage and type of endoscopic procedures (ERC versus PTBD) were estimated by the Kaplan-Meier curves and comparisons were made by using the log rank test. $P < 0.05$ was considered statistically significant.

RESULTS

Characteristics of patients

A total of 96 consecutive patients underwent treatment for malignant hilar bile duct tumors during 1995-2005. The characteristics of patients entered into this study included mean age of 67 ± 8.6 years, 9.73 ± 7.1 mg/dL bilirubin, 599 ± 277 U/L alkaline phosphatase L, 373 ± 235 U/L γ-GT, and 9.17 ± 2.75 G/L leucocytes. Of the 96 patients at the time of their initial diagnosis, 10 were diagnosed as Bismuth stage Ⅱ, 35 as Bismuth stage Ⅲ, and 51 as Bismuth stage Ⅳ. Patients with Bismuth stage Ⅰ were not identified by endoscopic and percutanoeus procedures. The characteristics of resected and non-resected patients are given in Table 1. A characteristic radiological

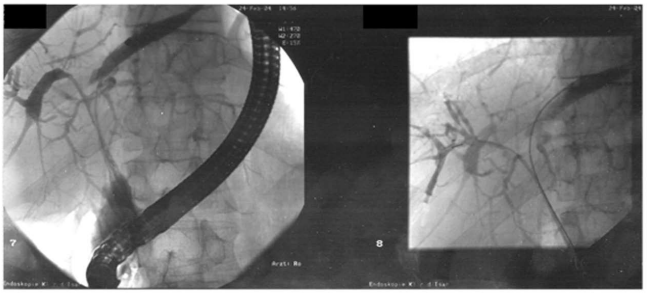

Figure 1 ERC/X-ray contrast of the bile duct system in a 57-year old patient with hilar cholangiocarcinoma (Bismuth Ⅳ).

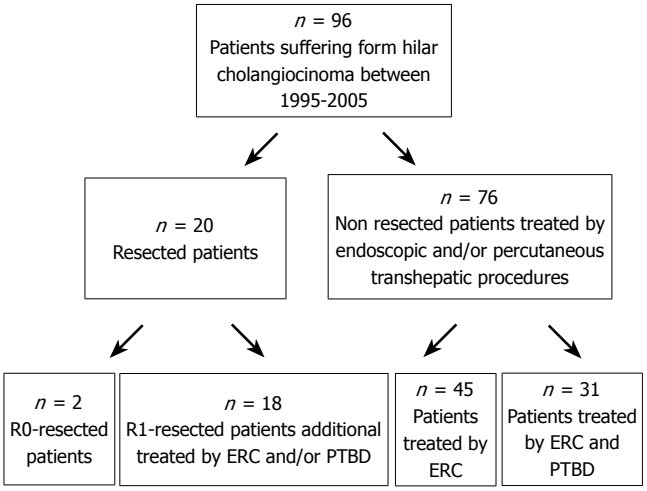

Figure 2 Algorithm of treatment strategies.

examination *via* ERC is shown in Figure 1. The patients presented with jaundice (bilirubin > 10 mg/dL) and almost complete obstruction of the left and right hepatic duct.

Treatment strategies

Of the 96 patients 20 were initially treated with surgery. Two of these 20 patients had R0-resection with complete tumor removal, 18 had R1-resection. All the 18 R1-resected patients had recurrent biliary obstruction, thus requiring subsquent endoscopic (ERC) and/or PTBD. Seventy-six out the 96 patients underwent only endoscopic transpapillary (n = 45) and/or percutaneous transhepatic biliary drainage (n = 31). Figure 2 shows the algorithm of treatment strategies in the resected and endoscopic group. The overall mean survival was 359 ± 296 d in the endoscopic group, 656 ± 299 d in the R0-resected group, and 1114 ± 924 d in the R1-resected group. Due to the small number of resected patients and unbalanced baseline characteristics, a direct comparison of survival time between the endoscopic and resected groups was not carried out.

Dependence on initial Bismuth stage for mean survival of non-resected patients

We investigated the correlation of mean survival time and Bismuth stage at the time of initial diagnosis in 76 patients with non-respectable hilar cholangiocarcinoma. The mean survival time of patients with Bismuth stage Ⅱ (n = 8), Ⅲ (n = 28) and Ⅳ (n = 40) was 496 ± 300 d, 441 ± 385 d and 274 ± 218 d, respectively. The Kaplan-Meier estimate for survival depending on Bismuth stage is shown in Figure 3A. The mean survival time of patients with Bismuth stage Ⅱ was not significantly higher than that of patients with Bismuth stage Ⅲ (P = 0.707) or Bismuth Ⅳ (P = 0.169). Patients with Bismuth stage Ⅲ also did not

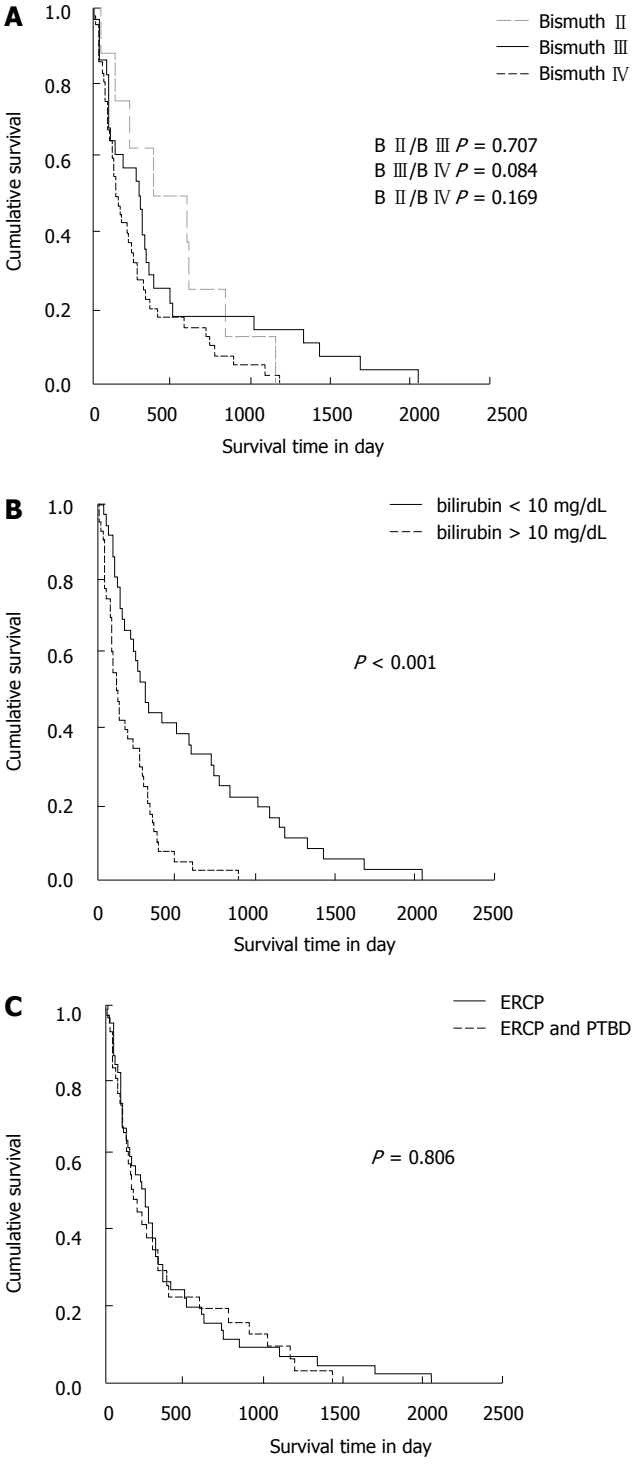

Figure 3 Kaplan-Meier estimate for survival depending on Bismuth stage at the time of initial diagnosis in 76 (**A**) initial serum bilirubin levels (**B**), and endoscopic procedure (ERC *vs* ERC/PTBD) (**C**) in 76 non resected patients.

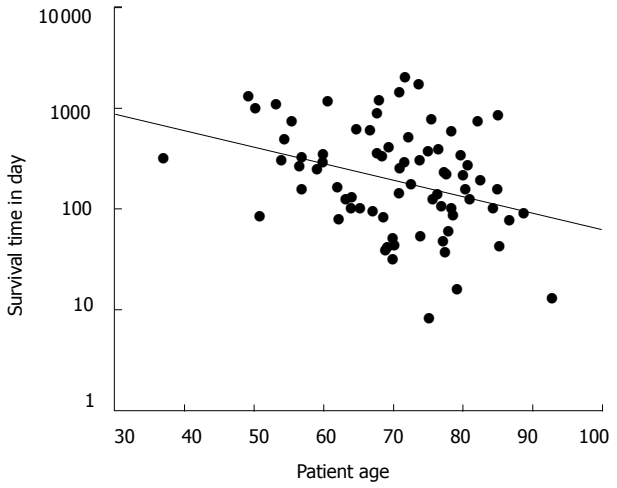

Figure 4 Mean survival depending on patients age in the non resected group (n = 76).

have a significantly longer survival time than patients with Bismuth stage Ⅳ (P = 0.084).

Dependence on initial bilirubin levels for mean survival of non-resected patients

The Kaplan-Meier estimate for mean survival depending on serum bilirubin levels at the time of primary diagnosis is shown in Figure 3B. The mean survival time of patients with bilirubin levels < 10 mg/dL (n = 36) was 541 ± 420 d, the mean survival of patients with bilirubin levels > 10 mg/dL (n = 40) was 195 ± 141 d. Thus, in the non-resected group, the mean survival time of patients with initial bilirubin levels > 10 mg/dL was significantly lower (P < 0.001) than that of patients with initial bilirubin levels < 10 mg/dL.

Dependence on endoscopic procedure for mean survival of non-resected patients

The type of endoscopic procedures had no significant beneficial effect on the mean survival of non-resected patient (Figure 3C). Forty-five patients only treated with endoscopic transpapillary drainage (ERC) had a mean survival time of 381 ± 286 d, and 31 patients who were additionally treated with PTBD had a mean survival time of 368 ± 312 d (P = 0.806).

Dependence on age for mean survival of non-resected patients

Concerning the age of non-resected patients at the time of primary diagnosis, the mean survival rate appeared to decline with increasing age. The regression line in the scatter plot (Figure 4) showed that life expectancy measured in days was reduced to about 50% between the age of 50 and 80 years at the time of primary diagnosis.

DISCUSSION

Cholangiocarcinoma is the second most common primary hepatic cancer. Although its overall incidence is low, it is on the rise globally[14]. Risk factors for development of cholangiocarcinoma are liver cirrhosis, primary sclerosing cholangitis (PSC), chronic choledocholithiasis, liver cirrhosis, bile duct adenoma, and other rare diseases such as biliary papillomatosis, Caroli's disease, choledochal cyst and parasitic biliary infestation and chronic typhoid carrier state[15,16]. However, in the majority of patients with cholangiocarcinoma etiology is unknown. In our cohort only a minority showed risk factors including liver cirrhosis or primary sclerosing cholangitis. Consequently, it remains to be determined what other causes of tumor development play a role in this disease, specially the role of bacterial colonisation, e.g. Helicobacter species that have been previously associated with cholangiocarcinoma formation.

Most commonly, cholestasis occurs in later stages when the bile duct is obstructed in the subhilar or hilar regions. Surgical resection is a mainstay of treatment with curative intent. However, previous reports indicate that not all patients are able to undergo a surgical treatment and thus, palliative options can be offered in a lot of cases[17-19]. In line with these results, in the current retrospective analysis tumour resection was performed only in 20/96 patients. To some extent, surgical procedures have been restricted since R0-resection is hard to achieve and preoperative diagnostic procedure cannot accurately predict stages of tumor extent and infiltration. In our study R0-resection could be achieved in only 2/20 patients. Eighteen of these 20 patients had no complete tumor removal and underwent additional endoscopic and/or percutaneous transhepatic procedures. Of the 96 non-respectable patients, 76 underwent endoscopic and/or percutaneous treatment as the first-line therapy. It has to be mentioned that the decision for surgery was biased in our study since younger patients with lower bilirubin levels were chosen. Nevertheless, our study supported the resection of the tumours even more aggressively, which is consistent with other reports[20,21].

The current study focussed on the long-term outcome of 76 patients with non-resected cholangiocarinoma. Palliative treatment strategies including ERC and PTBD, routinely performed in our hospital, had only few complications and were safe and effective measures to improve excretion of bile fluid. No difference was found in the effectiveness between ERC and PTBD. However, previous reports indicate that PTBD may be superior to ERC[9].

Most important, we found that bilirubin levels at initial diagnosis were a significant prognostic parameter. Kaplan-Meier analysis revealed that bilirubin levels seemed to correlate with the survival time. So far, no other reports have shown this association as clear as in the current study, and thus, this factor needs to be taken into account when initial diagnose is made.

Other groups performed photodynamic therapy (PDT) for bile duct cancer and have achieved survival time of 98 d in the control group treated with endoscopic stenting, and 493 d in the group additionally treated with PDT[22]. Zoepf *et al*[23] showed that patients not treated with PDT could survive 7 mo, and those treated with PDT could survive 21 mo. In the current study the mean survival

time of patients undergoing palliative endoscopic and/or percutaneous drainage was 359 d. Ortner *et al*[22] showed that the control group has a significant shorter survival time, which is comparable to our results. This may be explained by the lack of adequate bilirubin drop after endoscopic procedures in the control group.

In conclusion, bilirubin level is a significant prognostic factor for the survival of patients. Endoscopic and/or percutaneous biliary drainge represents the mainstream of palliative treatment for patients with non-resectable hilar cholangiocarcinoma. Although newer treatment modalities such as PDT can improve the expectancy of life, the overall survival is still unsatisfactory. Thus, additional diagnostic and therapeutic strategies should be evaluated.

REFERENCES

1 **Bismuth H**, Castaing D, Traynor O. Resection or palliation: priority of surgery in the treatment of hilar cancer. *World J Surg* 1988; **12**: 39-47
2 **de Groen PC**, Gores GJ, LaRusso NF, Gunderson LL, Nagorney DM. Biliary tract cancers. *N Engl J Med* 1999; **341**: 1368-1378
3 **Ahrendt SA**, Nakeeb A, Pitt HA. Cholangiocarcinoma. *Clin Liver Dis* 2001; **5**: 191-218
4 **Isa T**, Kusano T, Shimoji H, Takeshima Y, Muto Y, Furukawa M. Predictive factors for long-term survival in patients with intrahepatic cholangiocarcinoma. *Am J Surg* 2001; **181**: 507-511
5 **Hanazaki K**, Kajikawa S, Shimozawa N, Shimada K, Hiraguri M, Koide N, Adachi W, Amano J. Prognostic factors of intrahepatic cholangiocarcinoma after hepatic resection: univariate and multivariate analysis. *Hepatogastroenterology* 2002; **49**: 311-316
6 **Bismuth H**, Nakache R, Diamond T. Management strategies in resection for hilar cholangiocarcinoma. *Ann Surg* 1992; **215**: 31-38
7 **Reed DN**, Vitale GC, Martin R, Bas H, Wieman TJ, Larson GM, Edwards M, McMasters K. Bile duct carcinoma: trends in treatment in the nineties. *Am Surg* 2000; **66**: 711-714; discussion 714-715
8 **Chamberlain RS**, Blumgart LH. Hilar cholangiocarcinoma: a review and commentary. *Ann Surg Oncol* 2000; **7**: 55-66
9 **Born P**, Rösch T, Brühl K, Sandschin W, Weigert N, Ott R, Frimberger E, Allescher HD, Hoffmann W, Neuhaus H, Classen M. Long-term outcome in patients with advanced hilar bile duct tumors undergoing palliative endoscopic or percutaneous drainage. *Z Gastroenterol* 2000; **38**: 483-489
10 **Liu CL**, Lo CM, Lai EC, Fan ST. Endoscopic retrograde cholangiopancreatography and endoscopic endoprosthesis insertion in patients with Klatskin tumors. *Arch Surg* 1998; **133**: 293-296
11 **Hejna M**, Pruckmayer M, Raderer M. The role of chemotherapy and radiation in the management of biliary cancer: a review of the literature. *Eur J Cancer* 1998; **34**: 977-986
12 **McMasters KM**, Tuttle TM, Leach SD, Rich T, Cleary KR, Evans DB, Curley SA. Neoadjuvant chemoradiation for extrahepatic cholangiocarcinoma. *Am J Surg* 1997; **174**: 605-608; discussion 608-609
13 **Bowling TE**, Galbraith SM, Hatfield AR, Solano J, Spittle MF. A retrospective comparison of endoscopic stenting alone with stenting and radiotherapy in non-resectable cholangiocarcinoma. *Gut* 1996; **39**: 852-855
14 **Patel T**. Increasing incidence and mortality of primary intrahepatic cholangiocarcinoma in the United States. *Hepatology* 2001; **33**: 1353-1357
15 **Chapman RW**. Risk factors for biliary tract carcinogenesis. *Ann Oncol* 1999; **10** Suppl 4: 308-311
16 **Acalovschi M**. Cholangiocarcinoma: risk factors, diagnosis and management. *Rom J Intern Med* 2004; **42**: 41-58
17 **Chu KM**, Lai EC, Al-Hadeedi S, Arcilla CE, Lo CM, Liu CL, Fan ST, Wong J. Intrahepatic cholangiocarcinoma. *World J Surg* 1997; **21**: 301-305; discussion 305-306
18 **Lang H**, Sotiropoulos GC, Frühauf NR, Dömland M, Paul A, Kind EM, Malagó M, Broelsch CE. Extended hepatectomy for intrahepatic cholangiocellular carcinoma (ICC): when is it worthwhile? Single center experience with 27 resections in 50 patients over a 5-year period. *Ann Surg* 2005; **241**: 134-143
19 **Witzigmann H**, Berr F, Ringel U, Caca K, Uhlmann D, Schoppmeyer K, Tannapfel A, Wittekind C, Mossner J, Hauss J, Wiedmann M. Surgical and palliative management and outcome in 184 patients with hilar cholangiocarcinoma: palliative photodynamic therapy plus stenting is comparable to r1/r2 resection. *Ann Surg* 2006; **244**: 230-239
20 **Zervos EE**, Pearson H, Durkin AJ, Thometz D, Rosemurgy P, Kelley S, Rosemurgy AS. In-continuity hepatic resection for advanced hilar cholangiocarcinoma. *Am J Surg* 2004; **188**: 584-588
21 **Lygidakis NJ**, Sgourakis GJ, Dedemadi GV, Vlachos L, Safioleas M. Long-term results following resectional surgery for Klatskin tumors. A twenty-year personal experience. *Hepatogastroenterology* 2001; **48**: 95-101
22 **Ortner ME**, Caca K, Berr F, Liebetruth J, Mansmann U, Huster D, Voderholzer W, Schachschal G, Mössner J, Lochs H. Successful photodynamic therapy for nonresectable cholangiocarcinoma: a randomized prospective study. *Gastroenterology* 2003; **125**: 1355-1363
23 **Zoepf T**, Jakobs R, Arnold JC, Apel D, Riemann JF. Palliation of nonresectable bile duct cancer: improved survival after photodynamic therapy. *Am J Gastroenterol* 2005; **100**: 2426-2430

S- Editor Liu Y **L- Editor** Wang XL **E- Editor** Zhou T

PO Box 2345, Beijing 100023, China
www.wjgnet.com
wjg@wjgnet.com

World J Gastroenterol 2007 March 7; 13(9): 1427-1430
World Journal of Gastroenterology ISSN 1007-9327

RAPID COMMUNICATION

Cadaveric liver transplantation for non-acetaminophen fulminant hepatic failure: A 20-year experience

Olivier Detry, Arnaud De Roover, Carla Coimbra, Jean Delwaide, Marie-France Hans, Marie Hélène Delbouille, Joseé Monard, Jean Joris, Pierre Damas, Jacques Belaïche, Michel Meurisse, Pierre Honoré

Olivier Detry, Arnaud De Roover, Carla Coimbra, Marie-France Hans, Marie Hélène Delbouille, Joseé Monard, Michel Meurisse, Pierre Honoré, Department of Liver Surgery and Transplantation, University of Liège, CHU Sart Tilman B35, Liège B4000, Belgium
Jean Delwaide, Jacques Belaïche, Department of Hepato-gastroenterology, University of Liège, CHU Sart Tilman B35, Liège B4000, Belgium
Jean Joris, Pierre Damas, Department of Anaesthesia and Intensive Care, University of Liège, CHU Sart Tilman B35, Liège B4000, Belgium
Correspondence to: Dr. Olivier Detry, MD, PhD, Department of Abdominal Surgery and Transplantation, CHU Sart Tilman B35, Liège B4000, Belgium. oli.detry@chu.ulg.ac.be
Telephone: +32-4-3667645 Fax: +32-4-3777069
Received: 2006-12-21 Accepted: 2007-02-09

Abstract

AIM: To investigate the long-term results of liver transplantation (LT) for non-acetaminophen fulminant hepatic failure (FHF).

METHODS: Over a 20-year period, 29 FHF patients underwent cadaveric whole LT. Most frequent causes of FHF were hepatitis B virus and drug-related (not acetaminophen) liver failure. All surviving patients were regularly controlled at the out-patient clinic and none was lost to follow-up. Mean follow-up was 101 mo.

RESULTS: One month, one-, five- and ten-year patient survival was 79%, 72%, 68% and 68%, respectively. One month, one-, five- and ten-year graft survival was 69%, 65%, 51% and 38%, respectively. Six patients needed early (< 2 mo) retransplantation, four for primary non-function, one for early acute refractory rejection because of ABO blood group incompatibility, and one for a malignant tumor found in the donor. Two patients with hepatitis B FHF developed cerebral lesions peri-transplantion: One developed irreversible and extensive brain damage leading to death, and one suffered from deep deficits leading to continuous medical care in a specialized institution.

CONCLUSION: Long-term outcome of patients transplanted for non-acetaminophen FHF may be excellent. As the quality of life of these patients is also particularly good, LT for FHF is clearly justified, despite lower graft survival compared with LT for other liver diseases.

Key words: Liver transplantation; Liver failure; Surgery; Hepatitis B; Liver support

Detry O, Roover AD, Coimbra C, Delwaide J, Hans MF, Delbouille MH, Monard J, Joris J, Damas P, Belaïche J, Meurisse M, Honoré P. Cadaveric liver transplantation for non-acetaminophen fulminant hepatic failure: A 20-year experience. *World J Gastroenterol* 2007; 13(9): 1427-1430

http://www.wjgnet.com/1007-9327/13/1427.asp

INTRODUCTION

Fulminant hepatic failure (FHF) is a rare but a dreadful disease affecting mostly young patients. FHF is mainly managed based on symptoms and the identification of the FHF causes requiring specific treatment and supportive care, as FHF patients have chances of recovery[1]. The main causes of death of FHF patients are intracranial hypertension leading to brain stem death, and sepsis with multiple organ failure (MOF)[2]. Many liver support systems have been tried, but the ideal and efficient artificial liver has still to be designed and its efficacy to be proven[3]. In the sickest cases, when established predicting factors of death are reached, liver transplantation (LT) has been established as the standard treatment for FHF patients[4]. However, the results of LT for FHF may be disappointing, especially compared with the results of LT for chronic liver diseases since FHF patients often suffer from risk factors for graft failure or high morbidity or/and mortality[5].

In the United States of America (USA) and in the United Kingdom (UK), FHF is very frequently caused by acetaminophen intoxication[6-9]. However this etiology is far less frequent in other Western countries. The aim of this study is to report the 20-year experience and the results of LT for non-acetaminophen FHF of the liver transplantation program of the University of Liège, Belgium, a transplantation center working within the Eurotransplant allocation system. As many variables changed during such a long period of time, the authors

focused this report on the outcome of FHF patients who underwent LT.

MATERIALS AND METHODS

The liver transplantation program of the University of Liège started in 1986[10]. From 1986 to December 2005, 345 cases of LT were performed, mostly in adult patients, including 7 adult-to-adult living-related LT[11]. Among this series, 58 patients were listed for Hyper Urgent (HU) LT, meaning patients with FHF, or patients requiring urgent retransplantation for primary non-function (PNF) or vascular thrombosis after LT. Thirty-two patients were registered for FHF. All these patients were suffering from FHF as defined by the occurrence of encephalopathy within 8 wk after jaundice development in patients without previous histories of liver disease[12]. All reached the established criteria for bad prognosis as established by the Clichy' s group (non-acetaminophen FHF group) or the King's College (acetaminophen FHF group)[13,14]. Three patients who suffered from acetaminophen FHF and who met the King's College criteria for bad prognosis, recovered under medical therapy and intravenous N-acetylcysteine therapy. They were removed for subsequent analysis.

All patients were hospitalized in the intensive care unit and underwent standard medical therapy[1]. None but one patient received liver support with the Molecular Adsorbents Recirculating System (MARS). Patients in encephalopathy stage Ⅲ were intubated for airway protection, if necessary. Continuous veno-venous hemofiltration was used for renal support. No patient underwent intracranial pressure monitoring.

All patients were registered for HU cadaveric LT in the Eurotransplant allocation system. Until 1992, transplantation of an ABO non-compatible liver graft was authorized for recipient life-saving purpose. As results of the non-compatible LT were not satisfactory in terms of graft survival, ABO compatible LT was required after 1992. All patients were transplanted with cadaveric whole liver. Orthotopic whole LT with veno-venous bypass was performed as the standard LT procedure from 1986 to 1994. After 1995 the standard surgical procedure for LT was the Belghiti's technique, i.e. a piggy-back LT with temporary surgical porto-caval shunt, without use of veno-venous bypass and with large cavo-caval side-to-side anastomosis as venous reconstruction[15,16]. During this 20-year period, many other variables changed in the management of patients with FHF and of LT recipients. Immunosuppressive protocols in triple therapy regimens included cyclosporine/tacrolimus, Imuran/Cellcept and steroids. Steroids were progressively weaned, and most patients were under calcineurin inhibitor monotherapy at one-year follow-up. Patients transplanted for hepatitis B virus (HBV) FHF received life-long immunoprophylaxis with intravenous anti-HBs antibodies (10 000 UI every 3-4 mo, aiming at a minimum blood level > 100 mUI/mL).

All surviving patients were regularly controlled at the out-patient clinic and none was lost to follow-up. Mean follow-up was 101 mo (range: 5-204 mo). Statistical analysis was undertaken using patient and graft survival as endpoints. Survival was calculated using the method of Kaplan-Meier.

Table 1 Causes of fulminant hepatic failure in this series

Causes	No.
Viral infection	12 (HBV: 11, HAV: 1)
Drug induced	5
Miscellaneous	7
Budd-Chiari	1
Wilson	2
Ischemic	2
Alcohol	1
Autoimmune	1
Undetermined	5

HBV: Hepatitis B virus; HAV: Hepatitis A virus.

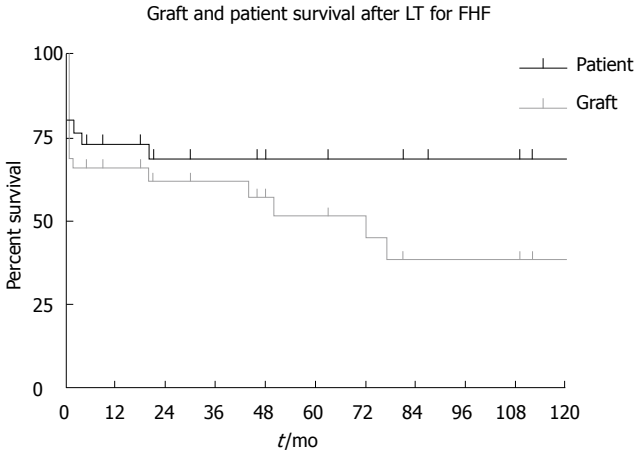

Figure 1 Patient and graft survivals after liver transplantation for fulminant hepatic failure according to the Kaplan-Meier method.

RESULTS

Twenty-nine patients (nine males, twenty females; mean age 39 years, range: 14-66 years) who developed non-acetaminophen FHF, were listed for cadaveric LT and underwent transplantation. The etiology of FHF is presented in Table 1. Most frequent causes of FHF in this group were hepatitis B virus (HBV) and drug-related. Three patients were in encephalopathy stage Ⅱ, 10 in stage Ⅲ and 16 in stage Ⅳ, at time of LT listing. Mean factor V level was 16% (range: 5%-31%). Mean waiting time between listing for HU LT and availability of a liver graft was 23 h (range: 4-49 h). Twenty patients were mechanically ventilated at time of listing and until LT. Nineteen developed acute renal failure and needed hemofiltration. Mean cadaveric donor age was 40 years (range: 14-57 years). Mean total graft ischemia was 417 min (range: 245-750 min). One month, one-, five- and ten-year survival was 79%, 72%, 68% and 68%, respectively (Figure 1). All patients who survived the first two years were alive at follow-up. Causes of early death (< 2 mo) were MOF, PNF (1 case) and peri-operative brain death (1 case). The only patient who died after 2 mo was not compliant to medical therapy after transplantation,

suffered from chronic allograft rejection but was denied for re-transplantation (died at 18 mo of follow-up).

Six patients needed early (< 2 mo) re-LT, 4 for PNF, 1 for early acute refractory rejection because of ABO blood group incompatibility, and 1 for a malignant tumor found in the donor[17]. Three patients needed late (> 2 mo) re-tranplantation due to chronic rejection or chronic graft dysfunction due to ABO blood group incompatibility in two cases and to non-compliance in one case. One patient needed a third transplantation because of chronic cholangitis on the second graft. One month, one-, five- and ten-year graft survival was 69%, 65%, 51% and 38%, respectively (Figure 1).

In the group of long-term survivors, two young females later enjoyed a total of three normal pregnancies. Among the patients transplanted for HBV FHF, one developed HBV graft reinfection treated first by lamivudine, and afterwards adefovir when the virus became resistant to lamivudine. This patient is well at follow-up, with graft fibrosis at biopsy. Two patients with HBV FHF, developed cerebral lesions during the peri-transplantation period: one developed irreversible and extensive brain damage leading to death, and one suffered from deep deficits leading to the continuous medical care in a specialized institution.

DISCUSSION

FHF is nowadays a well-admitted indication for urgent liver transplantation if the King's College or Clichy' s criteria are met. According to the European Liver Transplant Registry (www.eltr.org), 9% of the LT performed in Europe are performed for FHF. In our experience at the University of Liège, FHF represents 8.5% of the indications of LT. If acetaminophen intoxication is one of the main indications in the USA and UK, this etiology is rare in other Western countries. In the authors' experience, only three patients were listed for LT because of liver failure due to acetaminophen overdose in a 20-year period, and these three patients recovered on medical therapy including intravenous N-acetylcysteine, while listed for urgent LT. It is therefore important to assess the results of LT in patients with liver failure due to other causes, to confirm long-term survival despite a very unstable medical condition at the time of listing and at the time of transplantation. This is the case, as 68% of the patients transplanted for FHF were alive at the 10-year follow-up.

In our experience, HBV infection represents the main cause of FHF leading to LT (38%). In the 1990' s, systematic vaccination against HBV was initiated in Belgium. This policy reduced the frequency of HBV FHF in the native population, but recent immigrants still face HBV-related FHF. Drug-related FHF represents the second identified cause of FHF in this series (17%), and in five other cases we were not able to define the causative factor, as it was frequently reported in other series[18].

In our series the patients who underwent LT for FHF enjoyed excellent long-term survival, 68% of them were alive and well at 10-year follow-up. These results compare favorably to other series of the literature[4,13,18-21]. Moreover, as our experienced showed, if the patients survived the peri-operative period, they would have a good hope of survival with a low risk of late death. They also enjoy a very good quality of life with a low risk of liver disease recurrence or chronic rejection if they are compliant to the medical treatment. However, these good results in terms of graft survival are obtained at the price of a high rate of re-transplantation, as graft survival rate was 38% at 10 years.

The main cause of death in our series was MOF. This is certainly linked to medical status of these instable patients who often suffered from kidney and respiratory failure at the time of transplantation. This is also related to the high rate of PNF and the urgency for LT in this indication. This series also showed the efficiency of the Eurotransplant organization in providing rapidly a cadaveric liver graft for these urgent patients. In the early period of this experience, transplantation of an ABO uncompatible graft was allowed as a life-saving bridge to a later compatible graft. However, this policy was not prolonged because it consumes two grafts at a time of organ shortage. However, the change of policy did not have a significant impact on the waiting time of these urgent patients, and to our view, there is no need for a living-related liver program for FHF in resident patients within the Eurotransplant area. In recent series of the literature, creatinine levels, body mass index, recipient age and history of life support have been established as significant risk factors for post-LT death in FHF patients[5,18].

At least two patients of this series developed neurological lesions during the peri-transplantation period. This is certainly due to intracranial hypertension, a frequent complication of FHF, promoted by brain edema and increased blood flow[2]. We demonstrated that during LT for FHF the dissection and reperfusion phases are particularly at risk of intracranial hypertension[22]. On the contrary, the anhepatic phase, even if prolonged, may be associated with good neurologic outcome[23]. The development of neurological lesions during the peri-transplantation period has also been reported in larger series[18,24].

In conclusion, this series confirmed that long-term outcome of patients transplanted for non-acetaminophen FHF may be excellent. As the quality of life of these patients is also particularly good, these results proved that LT for FHF is clearly justified, despite a lower graft survival compared to LT for other liver diseases.

REFERENCES

1 **Detry O**, Honoré P, Meurisse M, Jacquet N. Management of fulminant hepatic failure. *Acta Chir Belg* 1998; **98**: 235-240
2 **Detry O**, De Roover A, Honore P, Meurisse M. Brain edema and intracranial hypertension in fulminant hepatic failure: pathophysiology and management. *World J Gastroenterol* 2006; **12**: 7405-7412
3 **Arkadopoulos N**, Detry O, Rozga J, Demetriou AA. Liver assist systems: state of the art. *Int J Artif Organs* 1998; **21**: 781-787
4 **Bismuth H**, Samuel D, Gugenheim J, Castaing D, Bernuau J, Rueff B, Benhamou JP. Emergency liver transplantation for fulminant hepatitis. *Ann Intern Med* 1987; **107**: 337-341
5 **Barshes NR**, Lee TC, Balkrishnan R, Karpen SJ, Carter BA, Goss JA. Risk stratification of adult patients undergoing orthotopic liver transplantation for fulminant hepatic failure.

Transplantation 2006; **81**: 195-201
6 **Larson AM**, Polson J, Fontana RJ, Davern TJ, Lalani E, Hynan LS, Reisch JS, Schiødt FV, Ostapowicz G, Shakil AO, Lee WM. Acetaminophen-induced acute liver failure: results of a United States multicenter, prospective study. *Hepatology* 2005; **42**: 1364-1372
7 **Ostapowicz G**, Fontana RJ, Schiødt FV, Larson A, Davern TJ, Han SH, McCashland TM, Shakil AO, Hay JE, Hynan L, Crippin JS, Blei AT, Samuel G, Reisch J, Lee WM. Results of a prospective study of acute liver failure at 17 tertiary care centers in the United States. *Ann Intern Med* 2002; **137**: 947-954
8 **Schiodt FV**, Atillasoy E, Shakil AO, Schiff ER, Caldwell C, Kowdley KV, Stribling R, Crippin JS, Flamm S, Somberg KA, Rosen H, McCashland TM, Hay JE, Lee WM. Etiology and outcome for 295 patients with acute liver failure in the United States. *Liver Transpl Surg* 1999; **5**: 29-34
9 **Bernal W**, Wendon J, Rela M, Heaton N, Williams R. Use and outcome of liver transplantation in acetaminophen-induced acute liver failure. *Hepatology* 1998; **27**: 1050-1055
10 **Lejeune G**, Limet R, Meurisse M, Honoré P, Defraigne JO, Detry O, De Roover A. History of solid organ transplantation at the University of Liège. *Acta Chir Belg* 2003; **103**: 32-36
11 **Detry O**, De Roover A, Delwaide J, Coimbra C, Kaba A, Joris J, Damas P, Meurisse M, Honoré P. Living related liver transplantation in adults: first year experience at the University of Liège. *Acta Chir Belg* 2004; **104**: 166-171
12 **Trey C**, Davidson CS. The management of fulminant hepatic failure. *Prog Liver Dis* 1970; **3**: 282-298
13 **Bernuau J**, Goudeau A, Poynard T, Dubois F, Lesage G, Yvonnet B, Degott C, Bezeaud A, Rueff B, Benhamou JP. Multivariate analysis of prognostic factors in fulminant hepatitis B. *Hepatology* 1986; **6**: 648-651
14 **O'Grady JG**, Alexander GJ, Hayllar KM, Williams R. Early indicators of prognosis in fulminant hepatic failure. *Gastroenterology* 1989; **97**: 439-445
15 **Belghiti J**, Noun R, Sauvanet A. Temporary portocaval anastomosis with preservation of caval flow during orthotopic liver transplantation. *Am J Surg 1995*; **169**: 277-279
16 **Belghiti J**, Noun R, Sauvanet A, Durand F, Aschehoug J, Erlinger S, Benhamou JP, Bernuau J. Transplantation for fulminant and subfulminant hepatic failure with preservation of portal and caval flow. *Br J Surg* 1995; **82**: 986-989
17 **Detry O**, Honoré P, Jacquet N, Meurisse M. Management of recipients of hepatic allografts harvested from donors with malignancy diagnosed shortly after transplantation. *Clin Transplant* 1998; **12**: 579-581
18 **Farmer DG**, Anselmo DM, Ghobrial RM, Yersiz H, McDiarmid SV, Cao C, Weaver M, Figueroa J, Khan K, Vargas J, Saab S, Han S, Durazo F, Goldstein L, Holt C, Busuttil RW. Liver transplantation for fulminant hepatic failure: experience with more than 200 patients over a 17-year period. *Ann Surg* 2003; **237**: 666-675; discussion 675-676
19 **Bismuth H**, Samuel D, Castaing D, Williams R, Pereira SP. Liver transplantation in Europe for patients with acute liver failure. *Semin Liver Dis* 1996; **16**: 415-425
20 **Ascher NL**, Lake JR, Emond JC, Roberts JP. Liver transplantation for fulminant hepatic failure. *Arch Surg* 1993; **128**: 677-682
21 **McCashland TM**, Shaw BW, Tape E. The American experience with transplantation for acute liver failure. *Semin Liver Dis* 1996; **16**: 427-433
22 **Detry O**, Arkadopoulos N, Ting P, Kahaku E, Margulies J, Arnaout W, Colquhoun SD, Rozga J, Demetriou AA. Intracranial pressure during liver transplantation for fulminant hepatic failure. *Transplantation* 1999; **67**: 767-770
23 **Detry O**, De Roover A, Delwaide J, Hans MF, Canivet JL, Meurisse M, Honoré P. 60 h of anhepatic state without neurologic deficit. *Transpl Int* 2006; **19**: 769
24 **Bismuth H**, Samuel D, Castaing D, Adam R, Saliba F, Johann M, Azoulay D, Ducot B, Chiche L. Orthotopic liver transplantation in fulminant and subfulminant hepatitis. The Paul Brousse experience. *Ann Surg* 1995; **222**: 109-119

S- Editor Liu Y **L- Editor** Ma JY **E- Editor** Zhou T

PO Box 2345, Beijing 100023, China
www.wjgnet.com
wjg@wjgnet.com

World J Gastroenterol 2007 March 7; 13(9): 1431-1434
World Journal of Gastroenterology ISSN 1007-9327

RAPID COMMUNICATION

Surgical approaches of resectable synchronous colorectal liver metastases: Timing considerations

Ioannis Vassiliou, Nick Arkadopoulos, Theodosios Theodosopoulos, Georgios Fragulidis, Athanasios Marinis, Agathi Kondi-Paphiti, Lazaros Samanides, Andreas Polydorou, Constantinos Gennatas, Dionysios Voros, Vassilios Smyrniotis

Ioannis Vassiliou, Nick Arkadopoulos, Theodosios Theodosopoulos, Georgios Fragulidis, Athanasios Marinis, Lazaros Samanides, Andreas Polydorou, Dionysios Voros, Vassilios Smyrniotis, 2nd Department of Surgery, Aretaieion Hospital, University of Athens, School of Medicine, Athens, Greece
Agathi Kondi-Paphiti, Department of Pathology, Aretaieion Hospital, University of Athens, School of Medicine, Athens, Greece
Constantinos Gennatas, Department of Oncology, Aretaieion Hospital, University of Athens, School of Medicine, Athens, Greece
Correspondence to: Ioannis Vassiliou MD, 2nd Department of Surgery, Aretaieion Hospital, University of Athens, School of Medicine, FACS, 29 El. Venizelou str., GR-154 51 Athens, Greece. ianvass@otenet.gr
Telephone: +30-210-7759546 Fax: +30-210-7759546
Received: 2006-10-26 Accepted: 2006-12-15

Abstract

AIM: To compare the safety and efficacy of simultaneous versus two stage resection of primary colorectal tumors and liver metastases.

METHODS: From January 1996 to May 2004, 103 colorectal tumor patients presented with synchronous liver metastases. Twenty five underwent simultaneous colorectal and liver surgery and 78 underwent liver surgery 1-3 mo after primary colorectal tumor resection. Data were retrospectively analyzed to assess and compare the morbidity and mortality between the surgical strategies. The two groups were comparable regarding the age and sex distribution, the types of liver resection and stage of primary tumors, as well as the number and size of liver metastases.

RESULTS: In two-stage procedures more transfusions were required (4 ± 1.5 *vs* 2 ± 1.8, pRBCs, $P < 0.05$). Chest infection was increased after the two-stage approach (26% *vs* 17%, $P < 0.05$). The two-stage procedure was also associated with longer hospitalization (20 ± 8 *vs* 12 ± 6 d, $P < 0.05$). Five year survival in both groups was similar (28% *vs* 31%). No hospital mortality occurred in our series.

CONCLUSION: Synchronous colorectal liver metastases can be safely treated simultaneously with the primary tumor. Liver resection should be prioritized over colon resection. It is advisable that complex liver resections with marginal liver residual volume should be dealt with at a later stage.

Key words: Synchronous colorectal liver metastases; Colon resections; Liver resections

Vassiliou I, Arkadopoulos N, Theodosopoulos T, Fragulidis G, Marinis A, Kondi-Paphiti A, Samanides L, Polydorou A, Gennatas C, Voros D, Smyrniotis V. Surgical approaches of resectable synchronous colorectal liver metastases: Timing considerations. *World J Gastroenterol* 2007; 13(9): 1431-1434

http://www.wjgnet.com/1007-9327/13/1431.asp

INTRODUCTION

Colorectal metastases to the liver either synchronous or metachronous can be excised resulting in a 5-year survival of 25%-40%[1-6], provided that the extrahepatic disease has been controlled and the remaining liver harbors no cancer. Even re-resections of liver metastases are rewarded with a 5 year-survival of 20%-30% and should be carried out in selected patients[6-9]. Many aspects of surgical strategies for the management of colorectal liver metastases have been extensively analyzed[10-15] and patient selection has been elucidated[1,3,7,15-17]. However, the question of when is the most favorable time to operate on synchronous liver metastases in relation to the primary colorectal tumor remains a controversial and debatable issue[10,12,14,16,18]. Several authors assume that combined liver and colon resection has higher morbidity and mortality rates[9,19,20] and favor a staged approach resecting the liver metastases 2 to 3 mo after treating the primary tumors.

However, recent advances in anesthesiology and surgical techniques prompted some surgeons to resect simultaneously colon lesions and liver metastases with mortality rates varying from 0% to 24%[10,12,14,18,21]. The conclusion is that in selected patients, one-stage approach is comparable to the two-stage procedure in mortality, morbidity and long-term survival[3,10,12,14,18].

Our retrospective study aimed to determine whether the one-stage surgical strategy for synchronous colorectal

liver metastases grants an optimal outcome to the patients compared to the two-stage procedure.

MATERIALS AND METHODS

From January 1996 to May 2004 one hundred and three patients with resectable synchronous colorectal liver metastases underwent surgical treatment. Both endoscopies and biopsies confirmed the diagnosis of the primary tumors. The resectability of the liver metastases was assessed by ultrasonography (US), computed tomography (CT), magnetic resonance imaging (MRI) and intraoperative ultrasonography (IUS), only in cases where there was no extrahepatic tumor spreading and the number of lesions was $\leqslant 3$. The decision for the type of surgical treatment was based on whether both liver lesions could be managed through one subcostal or midline incision. When trisegmentectomy or biliary reconstruction was anticipated the two-stage procedure was adopted.

Based on the timing of surgical excision of the liver secondaries, the patients were assigned to two groups. The one-stage group ($n = 25$) underwent simultaneous colorectal and liver surgery and the two-stage group ($n = 78$) underwent liver surgery 1 to 3 mo after excision of the primary lesion. The patients suitable for combined colorectal and liver surgery were operated through either a bilateral subcostal ($n = 19$, 75%) or a midline ($n = 6$, 25%) incision. Two patients (8%) had bilobar metastases. Patients of the two-stage group ($n = 78$) were operated *via* a midline incision for the control of the primary tumors and 1 to 3 mo later *via* a bilateral subcostal incision for the resection of liver metastases. The bilateral subcostal incision provided adequate surgical field suitable for any liver resection and was a safe approach for primary tumors located in the cecum to the descending colon. In contrast, the midline incision offered an access to the whole colorectal tract but only to the left hepatic lobe and segments V and VI of the right lobe. Twelve patients (16%) had bilobar resectable liver diseases. Patient characteristics, histological features, location of the primary lesions and the liver metastases are illustrated in Table 1.

The Pringle maneuver[22] was used in minor liver resections, while in major hepatic resections additional occlusion of the hepatic veins was opted. Liver transection was conducted by the clamp crushing technique with Kelly clamp or by the sharp liver transection technique. Details of the liver transection have been described elsewhere[10,23].

The factors analyzed to compare the two surgical strategies were: intraoperative blood loss, transfusion requirements to keep hematocrit above 29%, postoperative complications, hospital stay, 30-day mortality rate and cumulative survival. Oncological validity of each procedure was assessed by the narrowest tumor-free margin determined by painting the cut surface of the resected specimen with Sinic ink.

Statistical analysis

Statistical analyses of the data were performed with chi-square test for qualitative variables and Student's *t*-test for quantitative variables. Cumulative long-term survival was calculated by the Kaplan-Meier method and differences were analyzed by the log rank test. $P < 0.05$ was significant.

Table 1 Epidemiological and pathological data of patients with synchronous colorectal metastases to the liver, operated on in one stage (Group A) and two stages (Group B) *n* (%)

Characteristics	Group A ($n = 25$)	Group B ($n = 78$)	*P*
Gender			NS
Male	15 (58)	47 (61)	
Female	10 (42)	31 (39)	
Age (yr, mean ± SD)	63 ± 12	61 ± 14	NS
Tumor differentiation			NS
Well	6 (21)	17 (21)	
Moderate	9 (37)	28 (36)	
Poor	10 (42)	24 (32)	
Astler-Coller staging[27]			NS
B2	5 (21)	8 (11)	
C1	11 (42)	37 (47)	
C2	9 (37)	33 (42)	
Size of liver disease (cm)			NS
1-3 cm	6 (21)	25 (32)	
4-6 cm	12 (50)	33 (42)	
> 7 cm	7 (29)	20 (26)	
Colon location			
Right colon	17 (67)	15 (18)	$P < 0.005$
Left colon	5 (21)	55 (71)	$P < 0.005$
Rectum	3 (12)	8 (11)	
Liver location			NS
Right lobe	20 (83)	61 (79)	
Left lobe	5 (17)	17 (21)	

NS: Not significant.

RESULTS

The age, gender and pathological features of the primary tumor did not differ between the two groups except that in the one-stage approach right-sided colon tumors dominated, 17 out of 25 vs 15 out of 78 ($P < 0.05$). In contrast, in the two-stage approach, left-sided colon tumors were more frequent, 63 out of 78 *vs* 8 out of 25 ($P < 0.05$) (Table 2). The size and location of liver metastases were equally distributed between the two groups (Table 1). The extent of liver resection and warm ischemia time were not different between the two groups. By contrast, operative time, blood loss and transfusion requirement to keep the hematocrit above 29% were significantly lower in the one-stage group compared to the two-stage group (Table 2). The rate of postoperative complications between the two groups was not different and no re-operation was needed to treat any of the complications. Subhepatic collections were treated with CT-guided aspiration (Table 3). The tumor-free margin was not different between the two groups (9 ± 1.4 mm in one-stage group *vs* 11 ± 1.2 mm in two-stage group). Hospital stay was shorter in the one-stage group compared to the two-stage group (12 ± 6 d *vs* 20 ± 8 d, $P < 0.05$). Overall survival was 90%, 40% and 28% at 1, 3 and 5 years, respectively after one-stage resections and 93%, 44% and 31% at 1, 3 and 5 years, respectively after two-stage resections.

DISCUSSION

Hepatic tumor resection constitutes the only therapeutic

Table 2 Intraoperative data of patients with synchronous colorectal metastases to the liver, operated on in one stage (Group A) and two stages (Group B) *n* (%)

Intraoperative data	Group A (*n* = 25)	Group B (*n* = 78)	*P*
Major liver resections (⩾ 3 segments)	7 (25)	23 (29)	NS
Minor liver resections (⩽ 2 segments)	18 (67)	55 (71)	NS
Warm ischemic time (min)	27 ± 9	32 ± 11	NS
Operative time (min)	260 ± 30	340 ± 60	$P < 0.05$
Transfusions (RBCs)	2 ± 1.8	4 ± 1.5	$P < 0.05$
Right hemicolectomies	67%	18%	$P < 0.05$
Left hemicolectomies	21%	71%	$P < 0.05$
Abdominoperineal resections	12%	11%	NS

NS: Not significant.

Table 3 Complications and hospital stay of patients with synchronous colorectal metastases to the liver, operated on in one stage (Group A) and two stage (Group B) *n* (%)

Postoperative data	One-stage group (*n* = 25)	Two-stage group (*n* = 78)	*P*
Hospital mortality	-	-	-
Wound infection	2 (8)	3 (4)	$P < 0.05$
Chest infection	4 (17)	20 (26)	$P < 0.05$
Pleural effusion	5 (21)	18 (24)	NS
Bile leak	2 (8)	7 (9)	NS
Subphrenic collections[1]	3 (12)	8 (11)	NS
Splenic rupture	-	1 (1)	NS
Anastomotic leak	-	1 (1)	NS
Rectovaginal fistula	1 (4)	-	NS
Hemorrhage	1 (4)	1 (1)	NS
Hospital stay (d)	12 ± 6	20 ± 8	$P < 0.05$

[1]Resolved with aspiration under CT guidance. NS: Not significant.

option with curative intent for patients with colorectal liver metastases[5,6,16]. All efforts should be made to eliminate the hepatic lesions after controlling the loco-regional disease and ruling out extrahepatic tumor spread. In such cases there are well documented reports demonstrating a 5-year survival of 20%-40%[1-6], and 20%-30% when a re-resection has been executed in highly selected individuals[6-9].

The indications and criteria of patient selection for liver surgery due to metachronous colorectal metastases have been clarified in numerous excellent papers[14-16]. In contrast, for synchronous metastases the prevailing issue is the timing of liver resection in relation to the treatment of the primary tumor[18,20,21]. The strategy of the two-stage surgical approach gained popularity over the years and has been established as the standard surgical practice[3-7]. However, the fact that two-stage surgery requires two separate operations and accumulating evidence of the negligible morbidity and mortality of modern liver surgery prompted some surgeons to attempt simultaneous resections of primary tumors and liver metastases[10,12,14,18,21]. This approach was awarded with a mortality of 0%-24%[10,12,14,18,24]. Nordlinger *et al*[15] reported a 7% mortality for one-stage surgery and 2% for two-stage. Bolton and Fuhrman showed a 12% mortality for synchronous liver resections, which increased to 25% when a major hepatectomy (resected segments ⩾ 3) was performed[24]. Martin *et al*[10] demonstrated a 4% mortality and comparable morbidity between the two surgical approaches[12]. Our study, with the inherent limitations of a retrospective analysis, indicates that one-stage approach is equally safe to the two-stage regarding the morbidity, mortality and long-term survival and is consistent with other studies[12-14,18].

The majority of studies addressing the issue of one-stage over two-stage surgical treatment of synchronous colorectal liver metastases are retrospective and thus some biases are unavoidable and should be taken into consideration[6,10,11,18,19]. However, helpful conclusions have been drawn concerning the criteria for patient selection for either strategy (one-stage and two-stage) and valuable lessons have been learned[2,10,11,16,17]. It has been shown that patients who underwent a single operation had invariably smaller and fewer hepatic metastases and were treated with less extensive liver resections[10,12,18,19]. The above mentioned variables are negatively associated with postoperative complications and should be taken into consideration when simultaneous liver resections are anticipated[6,7,16]. Bolton *et al*[24] proposed that complex hepatic resections should be delayed for at least 3 mo.

Expertise in liver resections is an important factor in determining patient outcome, since the majority of postoperative morbidity and mortality are mainly related to liver surgery, a point that has been established by many studies[4,10,18,24-26]. Bleeding during hepatectomy is a poor prognostic factor and all efforts should be centered at minimizing blood loss by meticulous techniques and liver vascular control[1-3,10,23]. It appears that application of the Pringle maneuver in an intermittent manner should be preferred because it causes less liver reperfusion injury and intestinal edema, which might compromise the safety of gut anastomoses[4,10,21]. Some bleeding from the area of gut resection can be easily controlled by careful ligation of the divided mesentery and is not a major problem as has been illustrated by Martin *et al*[10] and Weber *et al*[12] , who reported that intraoperative blood loss was less in the one-stage approach, a fact confirmed by our findings. However, in complex hepatectomies when protracted vascular occlusion is anticipated, the two-stage procedure seems more prudent.

In our series, complications related to sepsis around the liver appeared to be equally distributed in both groups, a finding possibly related to the precautions taken during surgery to eliminate spillage of intestinal contents (one-stage, 12%; two-stage, 11%). However, it is advisable to avoid one-stage procedure when bowel obstruction or a perforated tumor is found. Vascular occlusion of the liver does not jeopardize the safety of gut anastomoses and we think the protective ileostomy recommended by Elias *et al*[21] unnecessary. Nevertheless, we agree with these authors that gut resection should precede liver resection and intermittent vascular control should be applied. Cardio-respiratory status and complexity of liver surgery should be always taken into account when a combined

liver and colon resection is planned[10,12,25]. Biliary fistula, subphrenic abscess, liver failure and chest infection are cited as the leading causes of postoperative morbidity in the majority of studies[10-13]. Laurent *et al*[25] demonstrated a clear connection of postoperative morbidity with long-term survival. Therefore, in order to optimize the surgical outcome when dealing with colorectal liver metastases, the liver surgical technique should be prioritized over the colectomy, because as mentioned before, liver surgery is related to the majority of postoperative complications and long-term survival[5,10,24,26]. Adequate exposure of the liver should be the primary concern of the surgeon in order to achieve a safe hepatectomy fulfilling the oncological principles of liver resection with a sufficient tumor-free margin[13,16,21,24,26]. In that respect, our study did not show any difference in the oncological validity between the two techniques. Martin *et al*[10] observed increased positive margin rate in wedge excisions and advocate anatomic hepatectomies. This view is shared by Tanaka *et al*[26]. Bilateral subcostal incision provides excellent liver exposure and facilitates colon resection from the cecum up to the descending colon. In contrast, malignancies located in the sigmoid colon downward necessitate a midline incision and an extension to the right (Rio-Branco incision)[21].

In conclusion, simultaneous resections of the liver and primary colon malignancies are equally safe and efficient with the two-stage procedure. The overall complication, postoperative mortality and long-term survival rates are similar to those of two-stage procedures, but hospital stay was significantly shorter with the one-stage approach. Simultaneous liver and colon surgery should be preferred for most of the right colon lesions and for small liver lesions that can be approached from a midline incision, regardless of the colonic tumor location. It is advisable that complex liver resections should be postponed for a later stage, especially for patients having potential cardio-respiratory and liver impairment.

REFERENCES

1 **Scheele J**, Stangl R, Altendorf-Hofmann A, Gall FP. Indicators of prognosis after hepatic resection for colorectal secondaries. *Surgery* 1991; **110**: 13-29
2 **Penna C**, Nordlinger B. Surgery of liver metastases from colorectal cancer: new promises. *Br Med Bull* 2002; **64**: 127-140
3 **Nordlinger B**, Rougier P. Liver metastases from colorectal cancer: the turning point. *J Clin Oncol* 2002; **20**: 1442-1445
4 **Jaeck D**, Bachellier P, Guiguet M, Boudjema K, Vaillant JC, Balladur P, Nordlinger B. Long-term survival following resection of colorectal hepatic metastases. Association Française de Chirurgie. *Br J Surg* 1997; **84**: 977-980
5 **Scheele J**, Stang R, Altendorf-Hofmann A, Paul M. Resection of colorectal liver metastases. *World J Surg* 1995; **19**: 59-71
6 **Nordlinger B**, Quilichini MA, Parc R, Hannoun L, Delva E, Huguet C. Hepatic resection for colorectal liver metastases. Influence on survival of preoperative factors and surgery for recurrences in 80 patients. *Ann Surg* 1987; **205**: 256-263
7 **Takahashi S**, Inoue K, Konishi M, Nakagouri T, Kinoshita T. Prognostic factors for poor survival after repeat hepatectomy in patients with colorectal liver metastases. *Surgery* 2003; **133**: 627-634
8 **Tuttle TM**, Curley SA, Roh MS. Repeat hepatic resection as effective treatment of recurrent colorectal liver metastases. *Ann Surg Oncol* 1997; **4**: 125-130
9 **Adam R**, Bismuth H, Castaing D, Waechter F, Navarro F, Abascal A, Majno P, Engerran L. Repeat hepatectomy for colorectal liver metastases. *Ann Surg* 1997; **225**: 51-60; discussion 60-62
10 **Martin R**, Paty P, Fong Y, Grace A, Cohen A, DeMatteo R, Jarnagin W, Blumgart L. Simultaneous liver and colorectal resections are safe for synchronous colorectal liver metastasis. *J Am Coll Surg* 2003; **197**: 233-241; discussion 241-242
11 **Topal B**, Kaufman L, Aerts R, Penninckx F. Patterns of failure following curative resection of colorectal liver metastases. *Eur J Surg Oncol* 2003; **29**: 248-253
12 **Weber JC**, Bachellier P, Oussoultzoglou E, Jaeck D. Simultaneous resection of colorectal primary tumour and synchronous liver metastases. *Br J Surg* 2003; **90**: 956-962
13 **Liu LX**, Zhang WH, Jiang HC. Current treatment for liver metastases from colorectal cancer. *World J Gastroenterol* 2003; **9**: 193-200
14 **Jaeck D**, Bachellier P, Weber JC, Boudjema K, Mustun A, Pâris F, Schaal JC, Wolf P. Surgical strategy in the treatment of synchronous hepatic metastases of colorectal cancers. Analysis of a series of 59 operated on patients. *Chirurgie* 1999; **124**: 258-263
15 **Nordlinger B**, Guiguet M, Vaillant JC, Balladur P, Boudjema K, Bachellier P, Jaeck D. Surgical resection of colorectal carcinoma metastases to the liver. A prognostic scoring system to improve case selection, based on 1568 patients. Association Française de Chirurgie. *Cancer* 1996; **77**: 1254-1262
16 **Fong Y**, Fortner J, Sun RL, Brennan MF, Blumgart LH. Clinical score for predicting recurrence after hepatic resection for metastatic colorectal cancer: analysis of 1001 consecutive cases. *Ann Surg* 1999; **230**: 309-318; discussion 318-321
17 **Nordlinger B**, Peschaud F, Malafosse R. Resection of liver metastases from colorectal cancer--how can we improve results? *Colorectal Dis* 2003; **5**: 515-517
18 **Jaeck D**, Bachellier P, Weber JC, Mourad M, Walf P, Boudjema K. Surgical treatment of synchronous hepatic metastases of colorectal cancers. Simultaneous or delayed resection? *Ann Chir* 1996; **50**: 507-512; discussion 13-16
19 **Lambert LA**, Colacchio TA, Barth RJ. Interval hepatic resection of colorectal metastases improves patient selection. *Arch Surg* 2000; **135**: 473-479; discussion 479-480
20 **Bismuth H**, Castaing D, Traynor O. Surgery for synchronous hepatic metastases of colorectal cancer. *Scand J Gastroenterol Suppl* 1988; **149**: 144-149
21 **Elias D**, Detroz B, Lasser P, Plaud B, Jerbi G. Is simultaneous hepatectomy and intestinal anastomosis safe? *Am J Surg* 1995; **169**: 254-260
22 **Pringle JH**. V. Notes on the Arrest of Hepatic Hemorrhage Due to Trauma. *Ann Surg* 1908; **48**: 541-549
23 **Smyrniotis VE**, Kostopanagiotou GG, Contis JC, Farantos CI, Voros DC, Kannas DC, Koskinas JS. Selective hepatic vascular exclusion versus Pringle maneuver in major liver resections: prospective study. *World J Surg* 2003; **27**: 765-769
24 **Bolton JS**, Fuhrman GM. Survival after resection of multiple bilobar hepatic metastases from colorectal carcinoma. *Ann Surg* 2000; **231**: 743-751
25 **Laurent C**, Sa Cunha A, Couderc P, Rullier E, Saric J. Influence of postoperative morbidity on long-term survival following liver resection for colorectal metastases. *Br J Surg* 2003; **90**: 1131-1136
26 **Tanaka K**, Shimada H, Ohta M, Togo S, Saitou S, Yamaguchi S, Endo I, Sekido H. Procedures of choice for resection of primary and recurrent liver metastases from colorectal cancer. *World J Surg* 2004; **28**: 482-487
27 **Haskel CM**, Larey RS, Ramming KP. Colon and Rectum. In: Haskel CM, (Editor), Cancer treatment, 4th Ed, Philadelphia: WB. Saunders, 1996: 469-497

S- Editor Liu Y **L- Editor** Zhu LH **E- Editor** Ma WH

PO Box 2345, Beijing 100023, China
www.wjgnet.com
wjg@wjgnet.com

World J Gastroenterol 2007 March 7; 13(9): 1435-1437
World Journal of Gastroenterology ISSN 1007-9327

RAPID COMMUNICATION

Beneficial effect of an antibody against interleukin-2 receptor (daclizumab) in an experimental model of hepatocyte xenotransplantation

Dimitrios Papagoras, Apostolos Papalois, Alexandra Tsaroucha, Dimitrios Lytras, John Kyriazanos, Nikoletta Giannakou, Prodromos Laftsidis, Constantine Simopoulos

Dimitrios Papagoras, Apostolos Papalois, Alexandra Tsaroucha, Dimitrios Lytras, John Kyriazanos, Prodromos Laftsidis, Constantine Simopoulos, 2nd Department of Surgery, Medical School, "Democritus" University of Thrace, Alexandroupolis, Greece
Apostolos Papalois, Experimental-Research Department, Elpen Pharmaceuticals, Athens, Greece
Nikoletta Giannakou, Department of Pathology, "Aghia Olga" General Hospital, Athens, Greece
Correspondence to: Apostolos Papalois, PhD, Experimental-Research Department, Elpen Pharmaceuticals, 60 El. Venizelou st., 153 41 Aghia Paraskevi, Athens, Greece. apo@hol.gr
Telephone: +30-210-6537045 Fax: +30-210-6537045
Received: 2006-11-30 Accepted: 2007-01-18

Abstract

AIM: To investigate the use of Daclizumab (Dmab) as an immunosuppressive agent in an experimental model of hepatocyte xenotransplantation (XenoTx) in rats with fulminant hepatic failure (FHF).

METHODS: Two white male New Zealand rabbits were used as donors and 68 Wistar rats as recipients. FHF was induced by intravenous application of dimethylnitrosamine (DMNA). The isolated hepatocytes of the rabbits were xenotransplanted into the spleen of the rats 24 h after FHF induction. Group A (n = 13): no treatment; Group B (n = 14): FHF and XenoTx; Group C (n = 14): FHF and XenoTx and cyclosporin (CsA); Group D (n = 14): FHF and XenoTx and Dmab; Group E (n = 13): FHF and XenoTx and CsA and Dmab. The rats were followed for 15 d.

RESULTS: Statistical analysis showed better survival among groups D (92.86%) and E (76.92%) compared to group A (all rats died after 72 h), group B (28.57%) or group C (71.43%), although the differences were not statistically significant. Biochemical evaluation of the liver enzymes and histology confirmed satisfactory function and engraftment, respectively.

CONCLUSION: This experimental model has shown the safe, effective and beneficial use of Dmab in a xenotransplantation model of rabbit hepatocytes in rats.

Key words: Transplantation; Hepatocytes; Daclizumab; Cyclosporin

Papagoras D, Papalois A, Tsaroucha A, Lytras D, Kyriazanos J, Giannakou N, Laftsidis P, Simopoulos C. Beneficial effect of an antibody against interleukin-2 receptor (daclizumab) in an experimental model of hepatocyte xenotransplantation. *World J Gastroenterol* 2007; 13(9): 1435-1437

http://www.wjgnet.com/1007-9327/13/1435.asp

INTRODUCTION

The lack of a sufficient number of organ transplants constitutes the main problem in the field of organ transplantation. As far as the transplantation of hepatic cells is concerned, the same difficulty exists in collecting transplants. Other attractive alternatives as transgenetic xenotransplantion, xenotransplantation of hepatic cells and the artificial liver, are related to economic, technical or ethical issues that make their extensive clinical application very difficult[1].

Recent studies stress the important aspect of xenotransplantation as a possibility of a bridging therapy in patients with organ failure[2]. In the current experimental study we evaluate the safety and efficiency of Daclizumab, a monoclonal anti-CD25 antibody, and an IL-2 receptor antagonist, which selectively blocks IL-2 receptors on activated T helper cells in rats with acute liver failure and xenotransplantation of rabbit hepatocytes.

MATERIALS AND METHODS

Animals

Sixty-eight adult male Wistar rats weighing 200-400 g were obtained from the Pasteur Institute. Rats were acclimatized to our laboratory conditions for 1 wk prior to use in experiments. Rats ate commercial rat chow and had water ad libitum. Rabbits were obtained from the Pasteur Institute as well. All experimental procedures described below were approved by the Animal Care Committee of the Veterinary Directorate of the Local Prefecture, according to the European Union Act and the Greek Law 160, A-64, May 1991. Also all animals received proper

Table 1 Survival analysis and survival rate

	Median (95% CI)[1]	*n* (%)[2]
FHF	2 (1-2)	0/13 (0)
XenoTx	6 (3-9)[a]	4/14 (28.6)[e]
XenoTx + CsA	11 (8-14)[a,c]	10/14 (71.4)[e,f]
XenoTx + Dmab	15 (14-15)[a,c]	13/14 (92.9)[e,f]
XenoTx + Dmab + CsA	13 (12-15)[a,c]	10/13 (76.9)[e,f]

[1]Kaplan Meier-Log-rank test: [a]$P < 0.05$ *vs* FHF; [c]$P < 0.05$ *vs* XenoTx. [2]Chi-square, Fisher's exact test: [e]$P < 0.05$ *vs* FHF; [f]$P < 0.05$ *vs* XenoTx. FHF: fulminant hepatic failure.

Table 2 Histopathological analysis

	Median score (Min-Max)
FHF	2 (2-5)[a]
XenoTx	1 (0-3)
XenoTx + CsA	1 (1-5)[a]
XenoTx + Dmab	0 (0-3)
XenoTx + Dmab + CsA	3 (0-3)[a]

Kruskal-Wallis: $P = 0.001$; Mann-Whitney: [a]$P < 0.05$ *vs* Dmab. FHF: fulminant hepatic failure.

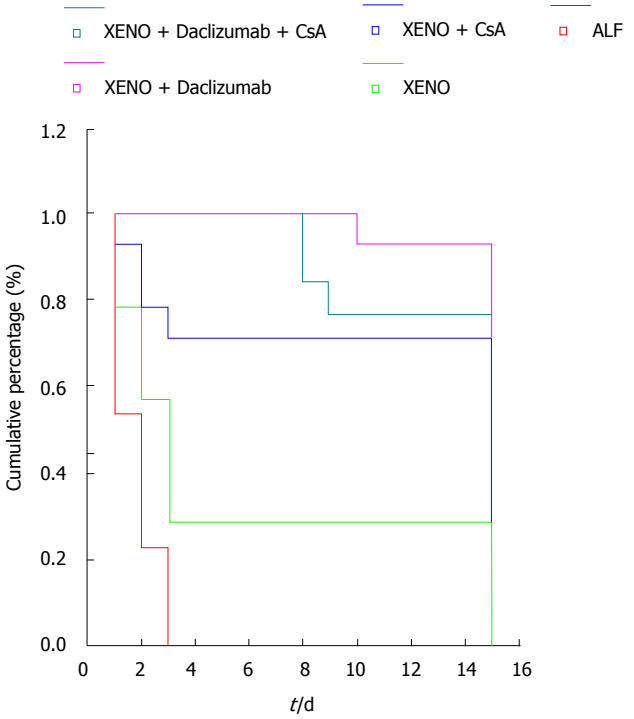

Figure 1 Survival rate 15 d after the induction of acute liver failure (ALF).

care in compliance with the "Principles of Laboratory Animal Care" and the Guide for the Care and Use of Laboratory Animals, prepared by the Academy of Science and published by the National Institute of Health.

Grouping

Fulminant hepatic failure (FHF) was induced in 68 wistar rats with intravenous application of N-dimethynitrosamine (N-DMNA) (Sigma, N-3632) in a dose of 18 mg/kg body weight. This dose has been shown to result in reproducible hepatic necrosis and high mortality rates. Twenty-four hours after the induction of toxic acute hepatic failure 55 rats received randomly approximately 10^8 viable rabbit hepatocytes injected intrasplenically. Two male white New Zealand rabbits weighing 2600 g were used for the isolation of hepatocytes according to the method described by Papalois *et al*[3]. Viability was 92% ± 6% by the trypan blue exclusion test (Serva 23 850) while contamination of non-parenchymal cell was less than 2%.

During the experimental period the animals had free access to water and regular diet. After fulminant hepatic failure (FHF) and intrasplenic xenotransplantation (XenoTx) of the rabbit hepatocytes, the rats were randomly assigned to 5 study groups: (1) Group A ($n = 13$): Toxic FHF with no treatment; (2) Group B ($n = 14$): FHF and XenoTx; (3) Group C ($n = 14$): FHF and XenoTx and cyclosporin (Cyclosporin-CsA); (4) Group D ($n = 14$): FHF and XenoTx and daclizumab (Daclizumab- Dmab); (5) Group E ($n = 13$): FHF and XenoTx and Dmab and CsA.

Dmab was administered in a dose of 0.05 mg/kg body weight immediately after the XenoTx and at the seventh day of the experiment (instructions of the manufacturer). CsA was administered immediately after the XenoTx in a dose of 20 mg/kg body weight per os/day. Fifteen days after the acute liver failure induction, the rats were sacrificed and blood was taken for biochemical evaluation (liver enzymes, bilirubin, cholestatic enzymes). The liver, spleen and kidney were resected for histopathology examination. Specimens were fixed in 10% neutral formalin and stained with hematoxylin-eosin. A histopathology grading score for the quantification of the liver damage was adopted from Ishak *et al*[4].

Statistical analysis

Quantitative data is presented as median (min-max) and qualitative data as frequencies (n) and percentages (%). All the results were computed with the SPSS version 12 package. To evaluate the differences in survival, the Kaplan-Meier survival analysis was performed and a log rank test was used for the evaluation of differences. Mann-Whitney and Kruskall-Wallis tests were used for the comparisons of histological and biochemical variables between groups. Statistical significance was set at a value of $P < 0.05$.

RESULTS

None of the rats with acute toxic hepatic failure and no further treatment survived beyond 48 h after the injection of N-DMNA. Rats treated with XenoTx and Dmab showed the best survival rate (Table 1 and Figure 1). In accordance to this survival rate, the Dmab group also had the best histopathology grading score (Table 2). The statistical analysis of the histopathological score also showed better results in the Dmab group. Values of hepatic enzymes, direct total bilirubin in the rats of the study groups are shown in Table 3. Statistical analysis

Table 3 Biochemical analysis

	SGOT[1] Median (Min-Max)	SGPT[2] Median (Min-Max)	Direct TBi[3] Median (Min-Max)
FHF	565.00 (3-1077)	257.00 (111-759)	0.03 (0.02-0.08)[e]
XenoTx	143.00 (83-154)[a]	60.00 (58-67)[c]	
XenoTx + CsA	58.00 (43-88)[a]	112.00 (85-183)[c]	0.03 (0.02-0.05)[e]
XenoTx + Dmab	246.00 (101-365)[a]	92.00 (50-339)[c]	0.02 (0.00-0.10)
XenoTx + Dmab + CsA	142.50 (98-247)[a]	58.50 (41-77)[c]	0.01 (0.00-0.03)

[1]Kruskal-Wallis $P < 0.0005$; Mann-Whitney: [a]$P < 0.05$ *vs* FHF; [2]Kruskal-Wallis: $P < 0.0005$; Mann-Whitney: [c]$P < 0.05$ *vs* FHF; [3]Kruskal-Wallis: $P = 0.044$; Mann-Whitney: [e]$P < 0.05$ *vs* XenoTx + Dmab + CsA. TBi: total bilirubin; FHF: fulminant hepatic failure; CsA: cyclosporin.

confirmed the improvement of liver function, especially in the Dmab group.

DISCUSSION

Despite the fact that XenoTx is far from a general use, most experts in the field of transplantation point out that a certain amount of research should be directed to this specific area of transplantation[5,6]. The main problem in organ transplantation, i.e. organ shortage, is also adherent to the collection, isolation and allotransplantation of human hepatocytes. XenoTx of hepatocytes could therefore represent an interesting form of "bridging therapy" in patients with fulminant hepatic failure[2,7].

We chose a xenotransplantation model in which rabbit hepatocytes were transplanted intrasplenically in rats with toxic acute liver failure. N-DMNA induced hepatic failure has the advantage of a non-invasive experimental model that mimics in certain degree the pathophysiology of acute liver failure in humans[8,9]. Daclizumab was used successfully in the clinical pancreatic islet transplantation program by Shapiro *et al*[10], and still is one of the most promising immunosuppressive agents[11,12]. Daclizumab has also been successfully used in an experimental model of allotransplantation of hepatocytes in rats with acute hepatic failure[13]. In the present experimental protocol, only 4 (28%) of the rats with acute liver failure survived by xenotransplantation without immunosuppressive treatment for 15 d. Regarding the survival rate of the study groups, the acute hepatic failure with no treatment group had the highest score in the liver injury grading system, whereas the Daclizumb group had the lowest score. As shown by the results, daclizumab was excellently tolerated, and so was the combination of cyclosporin and daclizumab. This monoclonal antibody has already been evaluated by clinical trials focusing on organ transplantation with excellent results[14]. The safety and effectiveness of cyclosporin was studied by Wen *et al*[15] in a xenograft model, whereas the safety and effectiveness of daclizumab was studied only in rats with acute liver failure and intrasplenic transplantation of rat hepatic cells[13]. To our knowledge, our data are the first about the safety and effectiveness of daclizumab in xenotransplantated rats with acute toxic liver failure.

REFERENCES

1 **Leckel K**, Blaheta RA, Markus BH. State of hepatocyte transplantation: a risk or a chance? *Zentralbl Chir* 2003; **128**: 283-290
2 **Horslen SP**, Fox IJ. Hepatocyte transplantation. *Transplantation* 2004; **77**: 1481-1486
3 **Papalois A**, Arkadopoulos N, Kostopanagiotou G, Theodorakis K, Peveretos P, Golematis B, Papadimitriou J. Experimental xenotransplantation of fresh isolated and cryopreserved pig hepatocytes: a biochemical and morphological study. *Transplant Proc* 1997; **29**: 2096-2098
4 **Ishak K**, Baptista A, Bianchi L, Callea F, De Groote J, Gudat F, Denk H, Desmet V, Korb G, MacSween RN. Histological grading and staging of chronic hepatitis. *J Hepatol* 1995; **22**: 696-699
5 **Auchincloss H**, Sachs DH. Xenogeneic transplantation. *Annu Rev Immunol* 1998; **16**: 433-470
6 **Inverardi L**, Pardi R. Early events in cell-mediated recognition of vascularized xenografts: cooperative interactions between selected lymphocyte subsets and natural antibodies. *Immunol Rev* 1994; **141**: 71-93
7 **Bloom ET**. Xenotransplantation--federal regulatory considerations. *Curr Top Microbiol Immunol* 2003; **278**: 239-251
8 **Arkadopoulos N**, Papalois A, Pataryas TH, Golematis B, Papadimitriou J. Experimental transplantation of hepatocytes in cases of toxic acute liver failure. An allograft model. *Transpl Int* 1994; **7** Suppl 1: S171-S174
9 **Contini S**, Pezzarossa A, Sansoni P, Mazzoni MP, Botta GC. Hepatocellular transplantation in rats with toxic induced liver failure: results of iso-, allo- and xenografts. *Ital J Surg Sci* 1983; **13**: 25-30
10 **Shapiro AM**, Lakey JR, Ryan EA, Korbutt GS, Toth E, Warnock GL, Kneteman NM, Rajotte RV. Islet transplantation in seven patients with type 1 diabetes mellitus using a glucocorticoid-free immunosuppressive regimen. *N Engl J Med* 2000; **343**: 230-238
11 **Sandrini S**. Use of IL-2 receptor antagonists to reduce delayed graft function following renal transplantation: a review. *Clin Transplant* 2005; **19**: 705-710
12 **Jorga A**, Johnston A. Novel therapies in transplantation. *Expert Opin Investig Drugs* 2005; **14**: 295-304
13 **Tsiolis I**, Papalois A, Loukopoulos I, Gravvanis A, Lykoudis E, Theodossopoulou E, Chairakakis A, Dimitroulopoulos D, Sfiniadakis I, Vassiliou I, Felekouras E, Dedeilias P, Kontogiorgi M, Papadimitriou L, Papadimitriou I. Experimental isolation and transplantation of hepatocytes with the use of antibody against interleukin-2 receptor (daclizumab) as immunosuppressive agent. *Transplant Proc* 2005; **37**: 1929-1930
14 **Vidhun JR**, Sarwal MM. Corticosteroid avoidance in pediatric renal transplantation: can it be achieved? *Paediatr Drugs* 2004; **6**: 273-287
15 **Wen L**, Grudé P, Conti F, Honiger J, Capeau J, Nordlinger B, Weill B, Calmus Y. Suppression of humoral immunization against encapsulated xenogeneic hepatocytes and prolongation of their function by 2-week cyclosporine treatment in the rat. *Surgery* 2000; **127**: 301-308

S- Editor Liu Y **L- Editor** Zhu LH **E- Editor** Zhou T

PO Box 2345, Beijing 100023, China
www.wjgnet.com
wjg@wjgnet.com

World J Gastroenterol 2007 March 7; 13(9): 1438-1444
World Journal of Gastroenterology ISSN 1007-9327

RAPID COMMUNICATION

Gene expression profile of esophageal cancer in North East India by cDNA microarray analysis

Indranil Chattopadhyay, Sujala Kapur, Joydeep Purkayastha, Rupkumar Phukan, Amal Kataki, Jagadish Mahanta, Sunita Saxena

Indranil Chattopadhyay, Sujala Kapur, Sunita Saxena, Institute of Pathology, Indian Council of Medical Research, Safdarjang Hospital Campus, Post Box No. 4909, New Delhi 110029, India
Joydeep Purkayastha, Amal Kataki, Dr.B.Borooah Cancer Institute, Guwahati-781016, Assam, India
Rupkumar Phukan, Jagadish Mahanta, Regional Medical Research Center, Dibrugarh-786001, Assam, India
Supported by Non Communicable Disease Division, Indian Council of Medical Research
Correspondence to: Dr. Sunita Saxena, Director, Institute of Pathology, Indian Council Of Medical Research, Safdarjang Hospital Campus, Post Box, No. 4909, New Delhi 110029, India. sunita_saxena@yahoo.com
Telephone: +91-11-26165797 Fax: +91-11-26198401
Received: 2006-11-17 Accepted: 2007-01-26

Abstract

AIM: To identify alterations in genes and molecular functional pathways in esophageal cancer in a high incidence region of India where there is a widespread use of tobacco and betel quid with fermented areca nuts.

METHODS: Total RNA was isolated from tumor and matched normal tissue of 16 patients with esophageal squamous cell carcinoma. Pooled tumor tissue RNA was labeled with Cy3-dUTP and pooled normal tissue RNA was labeled with Cy5-dUTP by direct labeling method. The labeled probes were hybridized with human 10K cDNA chip and expression profiles were analyzed by Genespring GX V 7.3 (Silicon Genetics).

RESULTS: Nine hundred twenty three genes were differentially expressed. Of these, 611 genes were upregulated and 312 genes were downregulated. Using stringent criteria ($P \leqslant 0.05$ and $\geqslant 1.5$ fold change), 127 differentially expressed genes (87 upregulated and 40 downregulated) were identified in tumor tissue. On the basis of Gene Ontology, four different molecular functional pathways (MAPK pathway, G-protein coupled receptor family, ion transport activity, and serine or threonine kinase activity) were most significantly upregulated and six different molecular functional pathways (structural constituent of ribosome, endopeptidase inhibitor activity, structural constituent of cytoskeleton, antioxidant activity, acyl group transferase activity, eukaryotic translation elongation factor activity) were most significantly downregulated.

CONCLUSION: Several genes that showed alterations in our study have also been reported from a high incidence area of esophageal cancer in China. This indicates that molecular profiles of esophageal cancer in these two different geographic locations are highly consistent.

Key words: Esophageal cancer; Gene expression profile; Tobacco consumption; Betel quid chewing; North East India

Chattopadhyay I, Kapur S, Purkayastha J, Phukan R, Kataki A, Mahanta J, Saxena S. Gene expression profile of esophageal cancer in North East India by cDNA microarray analysis. *World J Gastroenterol* 2007; 13(9): 1438-1444

http://www.wjgnet.com/1007-9327/13/1438.asp

INTRODUCTION

Environmental carcinogens have repeatedly been shown to affect the genetic material of host cells, leading to uncontrolled growth and ultimately malignant tumors[1]. The development of esophageal cancer is a leading example in which environmental carcinogens in addition to geographic and genetic factors appear to play major etiologic roles[2]. Esophageal cancer occurs at very high frequencies in certain parts of China, Iran, South Africa, Uruguay, France, Italy and in some regions of India[1]. The highest incidence of this cancer in India has been reported from Assam in the North-east region where it is the second leading cancer in men and third leading cancer in women[3].

Tobacco smoking, betel quid chewing, and alcohol consumption are the major known risk factors for esophageal cancer[4]. Tobacco smoke contains over 60 established carcinogens including polycyclic aromatic hydrocarbons and nitrosamines. Tobacco specific nitrosamines such as 4- (methyl nitrosamino)-1-butanone (NNK) and N'-nitrosonornicotine (NNN) that are carcinogens in smokeless tobacco, have been shown to enhance the risk of cancer development by forming adducts with DNA[5]. Betel quid chewing, a common habit

in Southeast Asia, has been found to increase the risk of developing esophageal cancer by 4.7-13.3 fold, although other exogenous risk factors may also be involved[4]. Betel quid usually comprises a piece of areca nut, which contains many polyphenols and several alkaloids, *Piper betle*, and lime with or without *Piper betle* leaves[6]. Arecoline, a major component of areca nut can produce 3-methyl nitrosamine propionitrile (MNPN), a potent carcinogen and safrole-like DNA adducts that have been shown to be genotoxic and mutagenic. Furthermore, contamination of areca nuts by fungi has been reported to produce carcinogenic aflatoxins. This assumes importance since using fermented areca nut with any form of tobacco is a common habit of people in Assam and has been reported to be a potential risk factor of esophageal cancer in this region[3].

The molecular mechanisms that may lead to the development of esophageal cancer in betel quid chewers and tobacco users are unknown. Recent studies are focusing on mechanisms that can explain the carcinogenic effects of tobacco and areca nut on epithelial cell lines. Incubation of areca nut extract or arecoline with primary oral keratinocytes has been reported to promote cell survival and an inflammatory response by induction of prostaglandin E_2, interleukin-6 (IL-6) and cyclooxygenase-2 (COX-2) production *via* activation of MEK1/ERK/c-Fos pathway[6]. Genotoxic stress as well as tissue inflammation and release of inflammatory mediators have been suggested to be key factors in carcinogenesis of gastrointestinal system. Genotoxic chemicals may induce the release of inflammatory mediators *via* mitogen activated protein kinase (MAPK) activation. Phosphorylated ERK1/2, JNK, p38 and ERK5 are reported to be significantly increased by exposure to tobacco smoke, indicating the activation of MAPK pathways[7]. NNK has recently been identified as a ligand of neuronal nicotinic acetylcholine receptors, which belong to G-protein-coupled receptors (GPCRs). GPCR induces proliferation through activation of members of the family of MAPKs[8,9].

The gene expression profile of esophageal cancer in a high incidence region of Assam where tobacco use and alcohol consumption are widespread and the users of these two substances are also betel quid chewers, has so far not been investigated. In the current study, cDNA microarray gene expression analysis was done to identify the genes differentially expressed in esophageal cancer associated with prevalent risk factors such as tobacco use and betel quid chewing in a high-risk Indian population.

MATERIALS AND METHODS

Collection of tumor samples

Endoscopic tissue biopsy specimens were taken from 16 patients at Dr. Bhubaneshwar Borooah Cancer Institute (BBCI), Guwahati, Assam. Routine histopathologic analysis was done to confirm the diagnosis. Tumor tissue and matched normal tissue distant to the tumor were collected during endoscopy in RNA later (Ambion, Austin, USA), snap-frozen in liquid nitrogen and stored at -70℃ until processed. Informed consent was obtained from all patients. Data of clinicopathologic parameters were obtained from patients' clinical records, operative notes and pathologic reports. Institutional Human Ethics Committee approved the study.

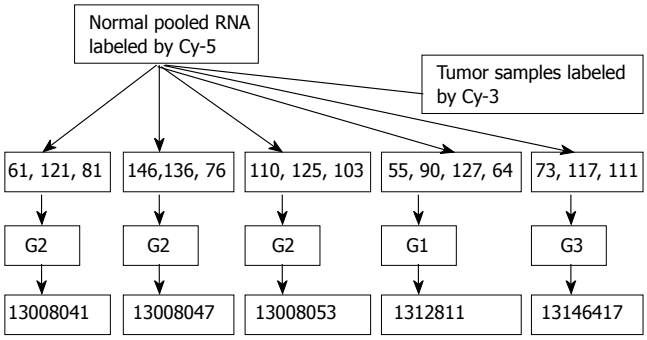

Figure1 Experimental design: G1, G2 and G3 indicate well-differentiated, moderately and poorly differentiated squamous cell carcinoma respectively. 13008041-53, 1312811 and 13146417 indicated barcode of microarray chips.

Sample preparation and chip hybridization

Total RNA isolation: Tissues were ground into powder in -196℃ liquid nitrogen and homogenized using Trizol reagent (Invitrogen Life Technologies, CA) for extraction of total RNA following the instruction of the manufacturer. The integrity of total RNA was checked by 1.2% formaldehyde agarose gel electrophoresis (visual presence of 28S and 18S bands). Total RNA with $OD_{260}/OD_{280} > 1.8$ was used for microarray experiments.

Experimental design: Total RNA was isolated from normal tissue of the esophagus from all the patients involved in this study and combined to make one common control. We pooled total RNA from biopsy samples of three to four patients in all five experiments on the basis of matching the histological grade to get sufficient amounts of total RNA for direct labeling. Pooled tumor RNAs were labeled with Cy-3 and hybridized against the Cy-5 labeled pooled samples of normal esophageal RNA, which generated a constant control to be used on chips analyzed. Figure 1 shows the study design. Sample pooling was done to rapidly identify tumor markers that were expressed by the majority of tumors in a population. Pooling of RNA samples isolated from tissue is a strategy that can be implemented in microarray experiments when the amount of sample RNA is limited or when variations across the samples must be reduced. The reason behind this approach is that the concentration of an mRNA molecule in a pooled sample is likely to be closer to the average concentration for the class than the concentration in a sample from a single individual. Pooled samples have been shown to accurately reflect gene expression in individual samples and yield reproducible data[10,11].

Labeling and hybridization: Twenty μg of total RNA from the tumor and matched normal tissue were labeled with cyanine 3-dUTP and cyanine 5-dUTP by direct labeling method (Perkin Elmer Life Sciences, USA: Micromax Direct labeling kit). The labeled probes were denatured at 95℃ for 5 min and hybridized with a human 10K cDNA chip (University Health Network, Microarray Centre, Toronto, Canada), which contains 9914 well-

characterized human clones, in a hybridization chamber (Corning Life Sciences, USA) at 65℃ water bath for 18 h. Before hybridization, slides were pre-hybridized in 5XSSC, 0.1% SDS and 1% BSA solution at 65℃ for 45 min to prevent nonspecific hybridization. After hybridization, the slides were washed in 2XSSC with 0.1% SDS, 0.1X SSC with 0.05% SDS and 0.1XSSC sequentially for 20 min each and then spin-dried.

Microarray image analysis: Hybridized arrays were scanned at 5 μm resolution on a Gene Pix 4200A scanner (Axon Instruments Inc. Foster City, CA) at various PMT voltage settings to obtain maximal signal intensities with < 0.1% probe saturation. The Cy5-labelled cDNAs were scanned at 635 nm and the Cy3-labeled cDNA samples were scanned at 532 nm. The resulting TIFF images were analyzed by Gene Pix Pro 6.0.1.27 software (Axon Instrument). Both digital images were overlaid to form a pseudo colored image and a detection method was then used to determine the actual target region based on the information from both red (Cy5) and green (Cy3) pixel values. The ratios of the sample intensity to the reference intensity (green: red) for all of the targets were determined and ratio normalization was performed to normalize the center of the ratio distribution to 1.0. Image processing analysis was used for estimation of spot quality by assigning a quality score to each ratio measurement[12].

Data analysis

Quality assurance: The data sets were imported into Microsoft Excel spreadsheets. Four parameters were used to assess quality of spots with the following features excluded: diameter < 50 μm; > 50% saturated pixels in both channels; < 54% of the pixels with an intensity greater than the median background intensity plus one standard deviation in either channel; flagged by Gene Pix as "not found" or "absent" or manually flagged as "bad" due to high background, misshapen features, scratches or debris on the slide undetected by Gene Pix[13].

Normalization: The results were normalized for labeling and detection efficiencies of the two fluorescence dyes, prior to determining differential gene expression between tumor and normal tissue samples. Intensities of selected spots were transformed into $\log_2$ (Cy3/Cy5) and data were normalized by locally weighted linear regression (LOWESS) method. Genespring software version GX7.3.1 (Silicon Genetics, Redwood, CA) was used to normalize values for each gene for data analysis.

Ranking of genes: Data analysis was performed using Genespring Software GXV 7.3 (Silicon Genetics, Redwood City, CA). Differentially regulated genes were ranked on the basis of signal intensity, normalized ratio, flag value and variance across replicate experiments. Top ranked genes had a higher intensity, high-normalized ratio for up and low for down, unflagged, very low variance or standard deviation. Filtered genes identified to be differentially expressed by 1.5 fold or greater in three of five chips were analyzed for functional gene clusters using GeneSpring software GXV 7.3. GeneSpring used data found publicly in genomic databases to build gene ontology based on annotation information. *t*-test was performed at the 0.05% significant level to find genes that vary significantly across samples. *P*-Value or probability value is the chance of set of genes involved in a particular function to be present in any given gene list with reference to the number of genes known to be involved in the function.

Hierarchical clustering: Average linkage hierarchical clustering was done using the Cluster Software version 3.0 written by Michael Eisen[14]. The Euclidean distance metric was used as a measure of similarity between the gene expression patterns for each pair of samples based on log-transformed ratios across all genes. The results were analyzed and visualized with the Tree View Program Version 1.50 also written by Michael Eisen. Those genes showing progressive fold increases or decreases in gene expression relative to normal mucosa were shown proportionally in red and green, respectively.

Pathway prediction analysis: We obtained annotations of the bioprocesses, molecular function and cellular localization using the freely available Gene Ontology and Source database[15]. The significant gene clusters were queried with known components of the biological pathways on the freely available KEGG database[16]. We also used the Biointerpreter software (http://www.genotypic.co.in/biointerpreter) for gene ontology.

Table 1 Demographic and clinical characteristics of esophageal squamous cell carcinoma cases

Patient ID	Age	Sex	Tobacco/ smoking habit	Alcohol use	Betel nut chewing	Pathological grade
EC-61	55	M	Yes	Yes	Yes	G2
EC-64	45	M	Yes	Yes	Yes	G1
EC-55	52	M	Yes	Yes	Yes	G1
EC-103	59	M	Yes	Yes	Yes	G2
EC-111	55	M	Yes	Yes	Yes	G3
EC-90	50	M	Yes	Yes	Yes	G1
EC-117	60	M	Yes	No	Yes	G3
EC-73	50	M	Yes	No	Yes	G3
EC-125	71	M	Yes	No	Yes	G2
EC-110	70	M	Yes	Yes	Yes	G2
EC-146	45	M	Yes	No	Yes	G2
EC-136	48	M	Yes	Yes	Yes	G2
EC-127	58	M	Yes	Yes	Yes	G1
EC-121	55	M	Yes	Yes	Yes	G2
EC-76	50	M	Yes	Yes	Yes	G2
EC-81	55	M	Yes	Yes	Yes	G1

G1 = Well differentiated squamous cell carcinoma; G2= Moderately differentiated squamous cell carcinoma; G3= Poorly differentiated squamous cell carcinoma.

RESULTS

Sixteen esophageal biopsy samples were compared with normal pooled esophageal tissue. All patients were male and gave a history of tobacco consumption and betel nut chewing (Table 1). Gene expression was measured using microarrays to detect changes in tumor samples compared to normal. Nine hundred and twenty three genes were differentially expressed at least 1 fold in 3 out of 5 experiments. Of these, 611 genes were upregulated and 312 genes were down regulated. The scaled data generated from Gene Pix Pro 6.0.1.27 software were imported into GeneSpring

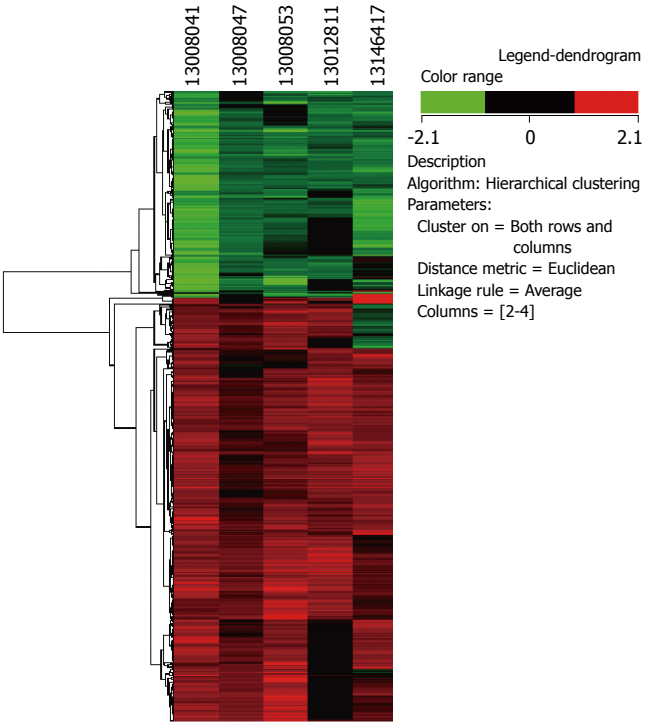

Figure 2 Hierarchical Clustering (Average Linkage Clustering) of the genes that were over or under expressed in tumor versus normal tissue in the 16 ESCC patients.

for fold change analysis, filtering, and cluster analysis. Hierarchical Clustering analysis of 923 genes selected from the 10 000-gene sets was performed (Figure 2). To identify highly reproducible changes, data were filtered based on select criteria. Transcripts modulated by a minimum 1.5 fold in at least three of five chips were used for further analyses. However, genes that had a $\geqslant$ 1.5 fold cutoff value or had a *P* value of $\leqslant$ 0.05 were also included for analysis to seek for subtle changes in gene expression. Using stringent criteria ($P \leqslant 0.05$ and $\geqslant$ 1.5 fold change), 127 differentially expressed genes (87 upregulated and 40 down regulated) were identified in tumor tissue. Using the Gene Ontology database, we categorized the 923 differentially expressed genes into known or probable functional categories. Genes involved in dimethylallyltransferase activity and farnesyltransferase activity (*CTLA4*), cation antiporter activity (*SLC9A2*) and cation transporter activity (*KCNN2*, *SLC30A4, KCNJ15, CACNA2D3*), G-protein coupled receptor (GPCR) activity (*GPR87, NPY*), MAPK signaling pathway (*FGF12*), and protein serine or threonine kinase activity (*GRK4*) were significantly upregulated (Table 2). Out of 87 upregulated genes, two genes were involved in GPCR group, five genes were involved in cation transporter activity, one gene each was involved in protein serine or threonine kinase activity and MAPK activity. Genes involved in anti-apoptosis activity (*BIRC1*), omega peptidase activity (*UCHL1*) and cellular proliferation (*EGR2*) were also significantly activated. Genes involved in structural constituent of the ribosome (*RPL32*, *RPS4X),* structural constituent of cytoskeleton (*KRT17*, *KRT8*, *PLA2G1B*), cysteine protease inhibitor activity (*CSTB*, *CSTA*), anti-oxidant activity (*PRDX6*), acyl groups transferase activity (*TGM3*), and

Table 2 List of significantly upregulated genes in esophageal cancer patients

Category	Genes in category	% Genes in category	Genes in list in category	% Genes in list category	*P*-value
GO: 4930: G-protein coupled receptor activity	150	2.148	23	3.433	0.0156
GO: 8324: cation transporter activity	307	4.396	39	5.821	0.0404
GO: 4674: protein serine/threonine kinase activity	285	4.081	38	5.672	0.022
GO: 4707: MAP kinase activity	20	0.286	5	0.746	0.0368
GO: 4161: dimethylallyltransferase activity	4	0.0573	3	0.448	0.00327

Table 3 List of significantly down-regulated genes in esophageal cancer patients

Category	Genes in category	% Genes in category	Genes in list in category	% Genes in list category	*P*-value
GO: 3735: structural constituent of ribosome	115	1.647	32	4.992	5.54E-09
GO: 4869: cysteine protease inhibitor activity	27	0.387	11	1.716	1.19E-05
GO: 5200: structural constituent of cytoskeleton	63	0.902	12	1.872	0.011
GO: 16746: transferase activity, transferring acyl groups	90	1.289	19	2.964	0.000422
GO: 16209: antioxidant activity	25	0.358	9	1.404	0.000232
GO: 3746: translation elongation factor activity	14	0.2	5	0.78	0.00636

translation elongation (*EEF1A1*) were significantly down-regulated (Table 3). Genes involved in humoral immune response (*CD24*) and base-excision repair (*MPG*) were significantly down regulated. Out of 40 down regulated genes, five genes were involved in structural constituent of the ribosome, four genes were involved in structural constituent of cytoskeleton, two genes were involved in cysteine protease inhibitor activity and one gene each was involved in anti-oxidant activity, acyl group transferase activity and translation elongation.

DISCUSSION

Several tobacco constituents, including nitrosamines, polycyclic aromatic hydrocarbons, aromatic amines, various aldehydes and phenols, may be causally related to esophageal cancer[1]. A previous report has shown that betel quid chewing with or without tobacco consumption

is associated with the development of esophageal cancer in Assam[3]. However, there are very few studies of gene expression profiles of tumors that may be associated with betel quid chewing as well as tobacco consumption. The current study was aimed to analyze genes and pathways that may be involved in tobacco and betel quid chewing related esophageal malignancies in this high incidence region of India.

Gene expression levels showed that there were four different molecular functional pathways that were most significantly upregulated and six different molecular functional pathways that were most significantly down regulated. Some of the significantly overexpressed molecular functional pathways like MAPK signaling pathway, G-protein coupled receptor and cation transporter activity have earlier been reported in esophageal and other cancers. However, genes such as *CTLA4* (involved in dimethylallyltransferase activity and farnesyltransferase activity) and *UCHL1, NPY*, *FGF12, KCNN2,* and *KCNJ15* were found to be significantly upregulated in our study and have not been reported earlier. Genes involved in structural constituent of ribosome (*RPL32, RPS4X, RPL7A)* and anti-oxidant activity (*PRDX6*) that were found to be significantly down regulated in our study, have also not been reported earlier. Some of the significantly down regulated molecular functional pathways like structural constituent of cytoskeleton (*KRT17*, *KRT8, KRT4),* acyl groups transferase activity (*TGM3)* and cysteine protease inhibitor activity (*CSTB*, *CSTA*), have already been reported previously in esophageal carcinoma. The data may be used for selection of a limited number of markers that can be screened in large populations by RT-PCR. All the genes identified here are of interest because of their potential roles in the natural history of esophageal squamous cell carcinoma.

The mitogen activated signaling cascade showed significant up-regulation in our study. Activated MAPK pathway has been detected in many human tumors including carcinomas of the breast, colon, kidney, and lung suggesting the possibility that MAPK may play a major role in tumor progression and metastasis. MAPK induces proteolytic enzymes that degrade the basement membrane, enhance cell migration, initiate several pro-survival genes and maintain growth[17]. Oxidants in cigarette smoke have previously been reported to activate MAPK signaling cascades in lung epithelial cells *in vitro* and *in vivo*. These signaling pathways lead to the enhanced ability of Jun and Fos family members to activate transcription of a number of AP-1 dependent target genes involved in cell proliferation, differentiation, and inflammation[18]. Phosphorylated ERK 1/2, JNK, p38 and ERK5 genes were significantly increased upon exposure to tobacco smoke, indicating the activation of MAPK pathways[7]. Benzo (a) pyrene quinines, which is the non-volatile component of cigarette smoke, have also been reported to increase cell proliferation, generate reactive oxygen species, and transactivate the epidermal growth factor receptor in breast epithelial cells[19].

TNF- alpha was found to be upregulated in our study. Cigarette smoke is known to enhance the induction of TNF-alpha by differentiated macrophage that is regulated primarily *via* the ERK ½ pathway[20]. TNF receptor super family member 17 has been shown to specifically bind to the TNF (ligand) super family member 13b (TNFSF13B/ TALL-1/BAFF) , which leads to activation of NF-kappaB and MAPK8/JNK.

Neuropeptide Y (NPY), which belongs to G-protein coupled receptor family, was found to be significantly upregulated in our study. Aberrant NPY expressions are early events in prostrate cancer development and are associated with a poor prognosis[21]. Activation of the Y1 receptor by NPY regulates the growth of prostate cancer cells. Estrogen upregulates NPY receptor expression in a human breast cancer cell line[22].

Ion channel regulating genes showed significant upregulation in our study. Several tumors such as prostrate, uterus, glial cells, stomach, pancreas, breast and colorectum are known to express Ca^{2+}activated K^+ channels. The complex process of carcinogenesis is triggered by oncogenic pathways *via* activation of K^+ channels. For example, p21 ras and the Raf kinase are known to induce oncogenic transformation *via* activation of Ca^{2+} dependent K^+ channels. Enhanced cell migration and tumor metastasis are associated with fluctuations in the activity of membrane transporters and ion channels that require K^+ channel activity[23]. Genes involved in calcium regulation and calcium signaling also seemed to be important in the progression of esophageal squamous dysplasia[24].

The deleted in colorectal cancer (DCC) gene, which was found to be upregulated in our study, is a candidate tumor suppressor gene which may be associated with differentiation and proliferation of normal cells. DCC protein expression seems to be a significant prognostic factor in high-risk resected gastric cancer. This gene may play a role in the metastatic potential of these tumors[15].

Transglutaminase-3 (TGase-3) that showed significant down regulation in our study has been reported in earlier studies. TGase-3 has been implicated in the formation and assembly of the cornified cell envelope of the epidermis, hair follicle and perhaps other stratified squamous epithelia. Alterated TGase-3 expression is a common event in human esophageal cancer[25]. The lowest levels of TGases 3 and 7 have been reported in patients with metastatic disease[26]. Tissue transglutaminase (tTG) is a high level phenotypic biomarker down regulated in prostate cancer[27].

Intermediate filaments form the cytoskeleton of cells and maintain the integrity of cells. Keratins (*KRT4* and *KRT8*) showed significant down regulation in our study. Overexpression of epithelial cell intermediate filaments and their isoforms (*KRT8)* have been reported earlier in colorectal polyp and cancer[28].

Reduced expression of cystatin B as found in our study, has earlier been reported to be associated with lymph node metastasis and may therefore prove to be a useful marker for predicting the biologic aggressiveness of esophageal cancer[29]. Overexpression of cystatin A has been shown to inhibit tumor cell growth, angiogenesis, invasion, and metastasis in esophageal cancer[30]. High levels of cystatin A and cystatin B have been reported to correlate with more favorable patient outcome in breast, lung and head and neck tumors.

A group of ribosomal proteins may function as cell cycle checkpoints and compose a new family of cell proliferation regulators. They play an important role in translational regulation and control of cellular transformation, tumor growth, aggressiveness and metastasis. Thus in addition to protein synthesis, they are involved in neoplastic transformation of cells. Ribosomal proteins were found to be significantly down regulated in our study. Expression of human ribosomal protein L13a has been shown to induce apoptosis, presumably by arresting cell growth in the G2/M phase of the cell cycle. In addition, a closely related ribosomal protein, L7, arrests cells in G1 and also induces apoptosis[15]. Mitochondrial ribosomal protein L41 suppresses cell growth in association with p53 and p27Kip1. *MRPL41* is reported to be either expressed at reduced levels or absent in most tumor types and cell lines[31]. Human apurinic apyrimidinic endonuclease (RPLP0) and its N terminal truncated form (AN34) are involved in DNA fragmentation during apoptosis. Down regulation of RPLP0 expression is associated with the induction of apoptosis in differentiating myeloid leukemia cells[32]. Simultaneously, three ribosomal proteins (RPL10, RPL32, and RPS16) also showed up-regulation in C81 cells. Overexpression of several ribosomal proteins including RPS16 has been reported in colon, breast, liver, and pancreatic tumors[33].

This is the first study to provide gene expression profiles of esophageal cancer in a high-risk region of Assam in India. The most salient finding was identification of down regulated genes involved in structural constituents of ribosome and upregulated genes involved in cation transporter activity. In a similar study of gene expression profiles in a high-risk area of China, Taylor *et al*[12] and Liu *et al*[35,36] have reported down regulation of *CSTB*, *CSTA*, *KRT4*, and *TGM3* and upregulation of G-coupled signaling, ion transport activity and MAPK activity[24]. In a recent study from a low risk area of India, deregulation of genes associated with zinc homeostasis in esophageal squamous cell carcinoma (ESCC) has been reported[34]. These data indicate the consistency of molecular profiles of esophageal cancer in two different geographic locations that have a high incidence of ESCC but different food habits and customs.

ACKNOWLEDGMENTS

The authors are thankful to Madavan Vasudevan, Dr. Sudha Rao and Dr. Raja Maugasimangalam of Genotypic Technology (P) Ltd. Bangalore, India for their valuable support in Microarray Data Analysis. The authors are thankful to Indian Council of Medical Research for their financial support. The authors are thankful to Jagannath Sharma of BBCI, Guwahati for histopathological analysis.

REFERENCES

1 **Stoner GD**, Gupta A. Etiology and chemoprevention of esophageal squamous cell carcinoma. *Carcinogenesis* 2001; **22**: 1737-1746

2 **Murtaza I**, Mushtaq D, Margoob MA, Dutt A, Wani NA, Ahmad I, Bhat ML. A study on p53 gene alterations in esophageal squamous cell carcinoma and their correlation to common dietary risk factors among population of the Kashmir valley. *World J Gastroenterol* 2006; **12**: 4033-4037

3 **Phukan RK**, Ali MS, Chetia CK, Mahanta J. Betel nut and tobacco chewing; potential risk factors of cancer of oesophagus in Assam, India. *Br J Cancer* 2001; **85**: 661-667

4 **Lee CH**, Lee JM, Wu DC, Hsu HK, Kao EL, Huang HL, Wang TN, Huang MC, Wu MT. Independent and combined effects of alcohol intake, tobacco smoking and betel quid chewing on the risk of esophageal cancer in Taiwan. *Int J Cancer* 2005; **113**: 475-482

5 **Rohatgi N**, Matta A, Kaur J, Srivastava A, Ralhan R. Novel molecular targets of smokeless tobacco (khaini) in cell culture from oral hyperplasia. *Toxicology* 2006; **224**: 1-13

6 **Chang MC**, Wu HL, Lee JJ, Lee PH, Chang HH, Hahn LJ, Lin BR, Chen YJ, Jeng JH. The induction of prostaglandin E2 production, interleukin-6 production, cell cycle arrest, and cytotoxicity in primary oral keratinocytes and KB cancer cells by areca nut ingredients is differentially regulated by MEK/ERK activation. *J Biol Chem* 2004; **279**: 50676-50683

7 **Zhong CY**, Zhou YM, Douglas GC, Witschi H, Pinkerton KE. MAPK/AP-1 signal pathway in tobacco smoke-induced cell proliferation and squamous metaplasia in the lungs of rats. *Carcinogenesis* 2005; **26**: 2187-2195

8 **Arredondo J**, Chernyavsky AI, Jolkovsky DL, Pinkerton KE, Grando SA. Receptor-mediated tobacco toxicity: cooperation of the Ras/Raf-1/MEK1/ERK and JAK-2/STAT-3 pathways downstream of alpha7 nicotinic receptor in oral keratinocytes. *FASEB J* 2006; **20**: 2093-2101

9 **Sud N**, Sharma R, Ray R, Chattopadhyay TK, Ralhan R. Differential expression of G-protein coupled receptor 56 in human esophageal squamous cell carcinoma. *Cancer Lett* 2006; **233**: 265-270

10 **Helm J**, Enkemann SA, Coppola D, Barthel JS, Kelley ST, Yeatman TJ. Dedifferentiation precedes invasion in the progression from Barrett's metaplasia to esophageal adenocarcinoma. *Clin Cancer Res* 2005; **11**: 2478-2485

11 **Agrawal D**, Chen T, Irby R, Quackenbush J, Chambers AF, Szabo M, Cantor A, Coppola D, Yeatman TJ. Osteopontin identified as lead marker of colon cancer progression, using pooled sample expression profiling. *J Natl Cancer Inst* 2002; **94**: 513-521

12 **Su H**, Hu N, Shih J, Hu Y, Wang QH, Chuang EY, Roth MJ, Wang C, Goldstein AM, Ding T, Dawsey SM, Giffen C, Emmert-Buck MR, Taylor PR. Gene expression analysis of esophageal squamous cell carcinoma reveals consistent molecular profiles related to a family history of upper gastrointestinal cancer. *Cancer Res* 2003; **63**: 3872-3876

13 **Samimi G**, Manorek G, Castel R, Breaux JK, Cheng TC, Berry CC, Los G, Howell SB. cDNA microarray-based identification of genes and pathways associated with oxaliplatin resistance. *Cancer Chemother Pharmacol* 2005; **55**: 1-11

14 **Eisen MB**, Spellman PT, Brown PO, Botstein D. Cluster analysis and display of genome-wide expression patterns. *Proc Natl Acad Sci USA* 1998; **95**: 14863-14868

15 **Diehn M**, Sherlock G, Binkley G, Jin H, Matese JC, Hernandez-Boussard T, Rees CA, Cherry JM, Botstein D, Brown PO, Alizadeh AA. SOURCE: a unified genomic resource of functional annotations, ontologies, and gene expression data. *Nucleic Acids Res* 2003; **31**: 219-223

16 **Altermann E**, Klaenhammer TR. PathwayVoyager: pathway mapping using the Kyoto Encyclopedia of Genes and Genomes (KEGG) database. *BMC Genomics* 2005; **6**: 60

17 **Reddy KB**, Nabha SM, Atanaskova N. Role of MAP kinase in tumor progression and invasion. *Cancer Metastasis Rev* 2003; **22**: 395-403

18 **Mossman BT**, Lounsbury KM, Reddy SP. Oxidants and signaling by mitogen-activated protein kinases in lung epithelium. *Am J Respir Cell Mol Biol* 2006; **34**: 666-669

19 **Burdick AD**, Davis JW, Liu KJ, Hudson LG, Shi H, Monske ML, Burchiel SW. Benzo(a)pyrene quinones increase cell proliferation, generate reactive oxygen species, and transactivate the epidermal growth factor receptor in breast epithelial cells. *Cancer Res* 2003; **63**: 7825-7833

20 **Demirjian L**, Abboud RT, Li H, Duronio V. Acute effect

of cigarette smoke on TNF-alpha release by macrophages mediated through the erk1/2 pathway. *Biochim Biophys Acta* 2006; **1762**: 592-597

21 **Rasiah KK**, Kench JG, Gardiner-Garden M, Biankin AV, Golovsky D, Brenner PC, Kooner R, O'neill GF, Turner JJ, Delprado W, Lee CS, Brown DA, Breit SN, Grygiel JJ, Horvath LG, Stricker PD, Sutherland RL, Henshall SM. Aberrant neuropeptide Y and macrophage inhibitory cytokine-1 expression are early events in prostate cancer development and are associated with poor prognosis. *Cancer Epidemiol Biomarkers Prev* 2006; **15**: 711-716

22 **Amlal H**, Faroqui S, Balasubramaniam A, Sheriff S. Estrogen up-regulates neuropeptide Y Y1 receptor expression in a human breast cancer cell line. *Cancer Res* 2006; **66**: 3706-3714

23 **Kunzelmann K**. Ion channels and cancer. *J Membr Biol* 2005; **205**: 159-173

24 **Joshi N**, Johnson LL, Wei WQ, Abnet CC, Dong ZW, Taylor PR, Limburg PJ, Dawsey SM, Hawk ET, Qiao YL, Kirsch IR. Gene expression differences in normal esophageal mucosa associated with regression and progression of mild and moderate squamous dysplasia in a high-risk Chinese population. *Cancer Res* 2006; **66**: 6851-6860

25 **Chen BS**, Wang MR, Xu X, Cai Y, Xu ZX, Han YL, Wu M. Transglutaminase-3, an esophageal cancer-related gene. *Int J Cancer* 2000; **88**: 862-865

26 **Jiang WG**, Ablin R, Douglas-Jones A, Mansel RE. Expression of transglutaminases in human breast cancer and their possible clinical significance. *Oncol Rep* 2003; **10**: 2039-2044

27 **Lewis TE**, Milam TD, Klingler DW, Rao PS, Jaggi M, Smith DJ, Hemstreet GP, Balaji KC. Tissue transglutaminase interacts with protein kinase A anchor protein 13 in prostate cancer. *Urol Oncol* 2005; **23**: 407-412

28 **Polley AC**, Mulholland F, Pin C, Williams EA, Bradburn DM, Mills SJ, Mathers JC, Johnson IT. Proteomic analysis reveals field-wide changes in protein expression in the morphologically normal mucosa of patients with colorectal neoplasia. *Cancer Res* 2006; **66**: 6553-6562

29 **Shiraishi T**, Mori M, Tanaka S, Sugimachi K, Akiyoshi T. Identification of cystatin B in human esophageal carcinoma, using differential displays in which the gene expression is related to lymph-node metastasis. *Int J Cancer* 1998; **79**: 175-178

30 **Li W**, Ding F, Zhang L, Liu Z, Wu Y, Luo A, Wu M, Wang M, Zhan Q, Liu Z. Overexpression of stefin A in human esophageal squamous cell carcinoma cells inhibits tumor cell growth, angiogenesis, invasion, and metastasis. *Clin Cancer Res* 2005; **11**: 8753-8762

31 **Yoo YA**, Kim MJ, Park JK, Chung YM, Lee JH, Chi SG, Kim JS, Yoo YD. Mitochondrial ribosomal protein L41 suppresses cell growth in association with p53 and p27Kip1. *Mol Cell Biol* 2005; **25**: 6603-6616

32 **Yoshida A**, Urasaki Y, Waltham M, Bergman AC, Pourquier P, Rothwell DG, Inuzuka M, Weinstein JN, Ueda T, Appella E, Hickson ID, Pommier Y. Human apurinic/apyrimidinic endonuclease (Ape1) and its N-terminal truncated form (AN34) are involved in DNA fragmentation during apoptosis. *J Biol Chem* 2003; **278**: 37768-37776

33 **Zhu Y**, Lin H, Li Z, Wang M, Luo J. Modulation of expression of ribosomal protein L7a (rpL7a) by ethanol in human breast cancer cells. *Breast Cancer Res Treat* 2001; **69**: 29-38

34 **Kumar A**, Chatopadhyay T, Raziuddin M, Ralhan R. Discovery of deregulation of zinc homeostasis and its associated genes in esophageal squamous cell carcinoma using cDNA microarray. *Int J Cancer* 2007; **120**: 230-242

35 **Luo A**, Kong J, Hu G, Liew CC, Xiong M, Wang X, Ji J, Wang T, Zhi H, Wu M, Liu Z. Discovery of Ca2+-relevant and differentiation-associated genes downregulated in esophageal squamous cell carcinoma using cDNA microarray. *Oncogene* 2004; **23**: 1291-1299

36 **Zhou J**, Zhao LQ, Xiong MM, Wang XQ, Yang GR, Qiu ZL, Wu M, Liu ZH. Gene expression profiles at different stages of human esophageal squamous cell carcinoma. *World J Gastroenterol* 2003; **9**: 9-15

S- Editor Liu Y **L- Editor** Zhu LH **E- Editor** Ma WH

PO Box 2345, Beijing 100023, China
www.wjgnet.com
wjg@wjgnet.com

World J Gastroenterol 2007 March 7; 13(9): 1445-1448
World Journal of Gastroenterology ISSN 1007-9327

RAPID COMMUNICATION

KN-93, a specific inhibitor of CaMKⅡ inhibits human hepatic stellate cell proliferation *in vitro*

Ping An, Jun-Yong Zhu, Yan Yang, Peng Lv, Yi-Hao Tian, Ming-Kai Chen, He-Sheng Luo

Ping An, Peng Lv, Ming-Kai Chen, He-Sheng Luo, Department of Gastroenterology, Renmin Hospital of Wuhan University, 238 Jiefang Road, Wuhan 430060, Hubei Province, China
Jun-Yong Zhu, Educational Administration Office, Renmin Hospital of Wuhan University, 238 Jiefang Road, Wuhan 430060, Hubei Province, China
Yan Yang, Department of Obstetrics and Gynecology, Hubei Xinhua Hospital, 5-6 Xin Tian Men Dun, Wuhan 430015, Hubei Province, China
Yi-Hao Tian, Faculty of Anatomy and Embryology, Wuhan University School of Medcine, Wuhan 430071, Hubei Province, China
Correspondence to: He-Sheng Luo, Professor, Department of Gastroenterology, Renmin Hospital of Wuhan University, 238 Jiefang Road, Wuhan 430060, Hubei Province, China. luohetang@yahoo.com
Telephone: +86-27-88041919-2134
Received: 2006-12-12 Accepted: 2007-03-07

Abstract

AIM: To investigate the effects of KN-93, a CaMKⅡ selective inhibitor on cell proliferation and the expression of p53 or p21 protein in human hepatic stellate cells.

METHODS: Human hepatic stellate cells (LX-2) were incubated with various concentrations (0-50 μmol/L) of KN-93 or its inactive derivative, KN-92. Cell proliferation was measured by CCK-8 assay, and the expression of two cell cycle regulators, p53 and p21, was determined by SDS-PAGE and Western blotting.

RESULTS: KN-93 (5-50 μmol/L) decreased the proliferation of human hepatic stellate cells in a dose-dependent manner from 81.76% (81.76% ± 2.58% *vs* 96.63% ± 2.69%, $P < 0.05$) to 27.15% (27.15% ± 2.86% *vs* 96.59% ± 2.44%, $P < 0.01$) after 24 h treatment. Incubation of 10 μmol/L KN-93 induced the cell growth reduction in a time-dependent manner from 78.27% at 8 h to 11.48% at 48 h. However, KN-92, an inactive derivative of KN-93, did not inhibit cell proliferation effectively. Moreover, analysis of cell cycle regulator expression revealed that KN-93 rather than KN-92 reduced the expression of p53 and p21.

CONCLUSION: KN-93 has potent inhibitory effect on proliferation of LX-2 cells by modulating the expression of two special cell cycle regulators, p53 and p21.

Key words: KN-93; Human hepatic stellate cells; LX-2; Cell proliferation

An P, Zhu JY, Yang Y, Lv P, Tian YH, Chen MK, Luo HS. KN-93, a specific inhibitor of CaMKⅡ inhibits human hepatic stellate cell proliferation *in vitro*. *World J Gastroenterol* 2007; 13(9): 1445-1448

http://www.wjgnet.com/1007-9327/13/1445.asp

INTRODUCTION

Many forms of acute and chronic liver injury, such as viral infection (especially hepatitis B and C), cholestasis, metabolic diseases, persistent alcohol abuse, and autoimmune liver diseases, result in hepatic fibrogenesis[1,2]. In the wound-healing process, retinoid-storing quiescent hepatic stellate cells (HSCs) are activated turning to myofibroblasts which are the major cell type responsible for producing excessive extracellular matrix, and play a pivotal role in the development of hepatic fibrosis[3-5]. For the outstanding importance in hepatic fibrosis, more and more researches focus on investigating the proliferation and apoptosis of HSC.

Among many signaling pathways of proliferation, intracellular calciumol/L has been extensively demonstrated to be very important[6]. In cytoplasm, calciumol/L binds to calmodulin, and then activates the Ca^{2+}/calmodulin (CaM) dependent kinases (CaMKs) which are a family of structurally related serine/threonine protein kinases including CaMKI-Ⅳ[7]. Recent studies have suggested that CaMKⅡ, a multi functional protein kinase, is ubiquitously involved in many physiological processes including control of cell cycle, apoptosis, gene expression, and neurotransmission[8,9]. Despite the important role of CaMKⅡ in cell cycle, no studies on CaMKⅡ and its inhibitors in HSC proliferation have been reported.

KN-93, as a membrane permeant compound of CaMKⅡ-selective inhibitor, can intensively prevent CaMK-Ⅱ activation by antagonizing CaM binding[10], and has been used in functional studies on living cells. In contrast to KN-93, KN-92 is a congener of KN-93 without CaM kinase inhibitory activity and has been used as an experimental control[11]. It was reported that KN-93 not only suppresses CaMKⅡ activity but is a strong inhibitor of cell proliferation[12].

This study was to explore the effects of KN-93 on proliferation of human HSC and its mechanism.

MATERIALS AND METHODS

Materials

KN-93 and KN-92 were provided by Calbiodhem (La Jolla, CA). Dimethyl sulfoxide (DMSO) trypsin, PMSF, aproptin and SDS were obtained from Sigma Chemical Company (St. Louis, MO, USA). Dulbecco's modified Eagle's medium (DMEM), glutamine, and penicillin-streptomycin were purchased from Gibco (Invitrogen, Carlsbad, CA). Fetal bovine serum (FBS) was from Hyclone. Primary antibody against β-actin, p53 and p21 were obtained from Santa Cruze Biotechnology (Santa Cruz, CA). WST-8 cell proliferation and cytotoxicity assay kit was from Beyotime Institute of Biotechnology (Jiangshu, China).

Cell line, culture conditions and KN-93 treatment

The human hepatic stellate cell line LX-2[13] was obtained from Institute of Liver Diseases, Shanghai University of Traditional Chinese Medicine. Cells were propagated in DMEM supplemented with 10% heat-inactivated fetal bovine serum, penicillin (100 U/mL) and streptomycin (100 g/L) under standard culture conditions (37℃, 950 mL/L humol/lidified air and 50 mL/L CO_2). A stock solution of 10 mmol/L KN-93 and 10 mmol/L KN-92 in DMSO was prepared, and final concentrations (1, 5, 10, 25, 50 μmol/L) in DMEM were prepared from stock solution immediately before use. DMEM with an equal volume of DMSO served as a negative control.

WST-8 assay

The proliferation of LX-2 cells was estimated by CCK-8 assay according to the manufacturer's guidelines. LX-2 cells treated with DMSO were used as a control. This assay is based on the cleavage of the tetrazolium salt WST-8 by mitochondrial dehydrogenase in viable cells. Briefly, LX-2 cells (2×10^3 cells/well) were incubated with 100 μL of culture medium in 96-multiwell plates. After incubated with KN-93 or KN-92 at indicated concentrations for 24 h or with 10 μmol/L of KN-93 or KN-92 for indicated periods of time, the media were removed and 100 μL of DMEM containing CCK-8 (10 μL) was added to each well. After a further 2 h incubation at 37℃, the absorbance at 450 nm of each well was measured with a Thermomax microplate reader. Each experiment was repeated three times, and the data represent the mean of all measurements.

Western blot analysis

A total of 5×10^5 LX-2 cells were plated in 6-well dishes. After attachment, KN-93 or KN-92 at indicated concentrations or vehicle control was added and incubated for 24 h. For Western blot analysis, the procedure was performed as described previously[14]. Briefly, an equal amount of protein lysates (40 μg) was electrophoresed on a 10% polyacrylamide gel and then electophoretically transferred to a polyvinylidene difluoride membrane. The membrane was blocked with 5% nonfat dry milk for 2 h at room temperature and incubated with the indicated primary antibody overnight at 4℃. After washing, the membrane was incubated with a horseradish peroxidase-conjugated secondary antibody (Amersham Biosciences, Piscataway, NJ). Subsequently, the blots were developed by using the ECL kit (Santa Cruz Biotechnology, Santa Cruz, CA) and exposed to X-ray film. Protein bands were quantified by densitometric scanning using a Bio-Rad GS-800-calibrated densitometer. Each experiment repeated three times.

Table 1 Effect of KN-93 and KN-92 on cell proliferation in human hepatic stellate cells (LX-2) after 24 incubation (n = 3, mean ± SD)

	Cell proliferation (% of control)	
Concentration	KN-93	KN-92
Control	100.00 ± 3.32	100.00 ± 3.32
5 μmol/L	81.76 ± 2.58[a]	96.63 ± 2.69
10 μmol/L	60.30 ± 2.59[b]	96.24 ± 3.14
25 μmol/L	33.42 ± 3.07[b]	95.61 ± 2.81
50 μmol/L	27.15 ± 2.86[b]	96.59 ± 2.44

[a]$P < 0.05$, [b]$P < 0.01$ *vs* control group.

Table 2 Effect of 10 μmol/L KN-93 and KN-92 on cell proliferation in human hepatic stellate cells (LX-2) after treatment for various periods of time (n = 3, mean ± SD)

	Cell proliferation (% of control)	
Time of treatment	KN-93	KN-92
Control	100.00 ± 2.86	100.00 ± 3.32
4 h	99.56 ± 3.53	97.12 ± 2.97
8 h	78.27 ± 2.92[b]	96.95 ± 2.56
16 h	52.26 ± 2.90[b]	98.34 ± 3.18
24 h	30.54 ± 2.82[b]	96.53 ± 2.67
48 h	11.48 ± 3.16[b]	97.12 ± 3.09

[b]$P < 0.01$ *vs* control group.

Statistical analysis

Data were expressed as mean ± SD. Statistical comparisons between groups were analyzed by the Student's t test. $P < 0.05$ was considered statistically significant.

RESULTS

KN-93 inhibited LX-2 cell growth

To assess the biological activity of KN-93 in LX-2 cell proliferation, KN-93 and its inactive derivative, KN-92 were chosen in CCK-8 assay. KN-93 significantly inhibited cell proliferation. After incubation of KN-93 at various concentrations for 24 h, the number of LX-2 cells reduced dramatically (Figure 1A) from 81.76% (5 μmol/L) to 27.15% (50 μmol/L) (Table 1). Exposure to 10 μmol/L KN-93 also significantly declined cell proliferation in a time-dependent manner (Figure 1B). The proliferation of LX-2 cells was reduced after KN-93 was incubated for 8 h ($P < 0.01$) and more obviously after further treatments (Table 2). Despite KN-93 had such a powerful influence on human hepatic stellate cells, KN-92 was ineffective

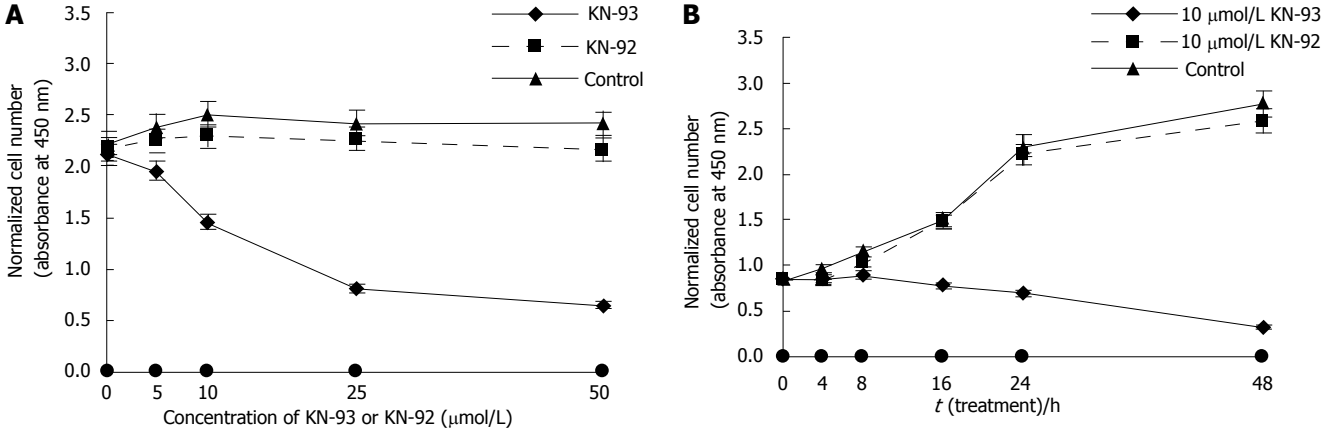

Figure 1 WST-8 assay showing the effect of KN-93 and KN-92 on the growth of LX-2 cells after incubation for 24 h (**A**) and at the indicated time (**B**). Data are expressed as mean ± SE of three experiments.

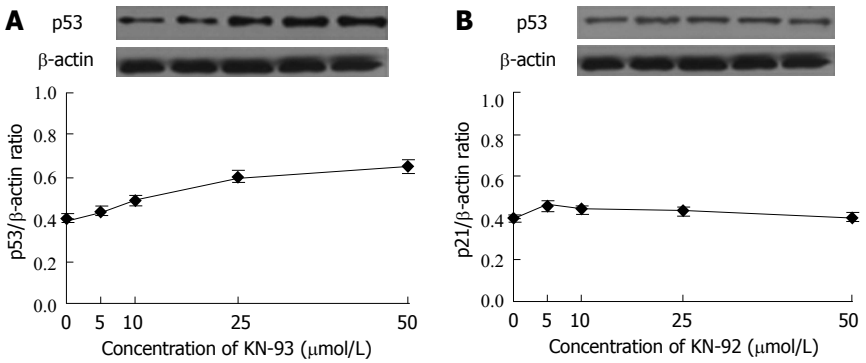

Figure 2 Effects of KN-93 (**A**) and KN-92 (**B**) on expression of p53 in LX-2 cells.

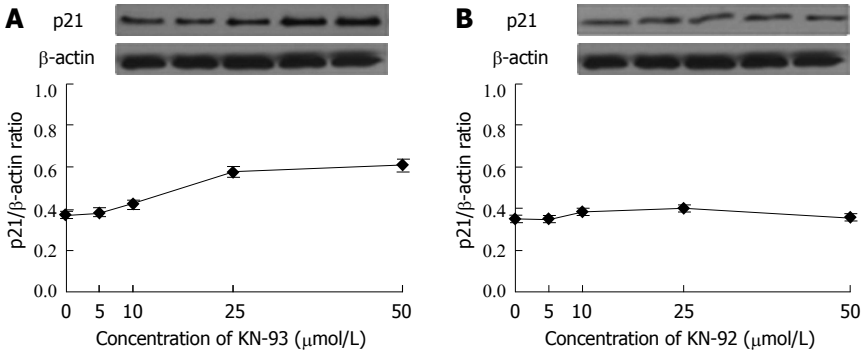

Figure 3 Effects of KN-93 (**A**) and KN-92 (**B**) on expression of p21 in LX-2 cells.

in blocking cell growth (Figure 1, Tables 1 and 2). These results implied that KN-93 inhibited proliferation of LX-2 cells in a dose- and time-dependent manner.

KN-93 increased the expression of p53

Next, we concentrated our studies on whether KN-93 influences the expression of cell cycle regulator, p53. The results from Western blotting and data analysis are exhibited in Figure 2. It was much clear that KN-93 at each concentration improved the expression of p53, especially at the concentration of 50 μmol/L (Figure 2A). As expected, KN-92 showed little impact on p53 expression (Figure 2B), demonstrating that it was KN-93 rather than KN-92 increased p53 expression in a dose-dependent manner.

KN-93 also increased expression of p21

Another important regulator involving cell cycle, p21, was examined. The level of p21 increased with the increase of KN-93 concentration (Figure 3A). Few changes in p21 expression were observed when KN-92 was added (Figure 3B).

DISCUSSION

During liver fibrosis, HSCs perform a phenotype change from vitamin A-rich cells to proliferative, contractile and fibrogenic myofibroblasts. The activated HSCs produce excess Ⅰ and Ⅲ collagens which deposit and lead to fibrotic tissue in liver[15,16].

KN-93, a specific inhibitor of CaMK Ⅱ is verified to

have a powerful capability of suppressing the activation of CaMK Ⅱ[17]. It was reported that KN-93 is involved in cell cycle arrest and proliferation[12], indicating that CaMK Ⅱ is necessary for cell cycle progression through G1 and is a key regulator in the transduction signals of cell growth. In Hela cells, KN-93 can also inhibit cell proliferation and elevate some cell cycle regulators such as CKD1[18]. These results indicate that CaMK Ⅱ is one of the most important factors for cell survival.

Our study suggested that KN-93 could significantly inhibit human hepatic stellate cell LX-2 proliferation in a dose-dependent manner. The inhibition increased with increase of incubation time. The effect of KN-92 on cell growth demonstrated the specificity of KN-93 in LX-2. These obvious results indicate that KN-93 might not only inhibit human HSC proliferation but also exert toxic effects on cells despite its negative effect on KN-92. In this study, 10 mmol/L KN-93 inhibited LX-2 cell proliferation in a time-depended manner, which is in agreement with the reported data showing the effect of KN-93 on apoptosis in NIH 3T3 cells[12], suggesting that HSCs and CaMKII can enhance cell proliferation.

Since KN-93 inhibits cell growth, we studied the regulators of cell cycle. P53, a suppressor protein, is a nuclear transcription factor controlling cell cycle progression[19,20]. Abriss *et al*[21] showed that constitutive expression of p53 is sufficient to induce cell arrest in HSCs. P53 can reduce proliferation of activated HSCs. In the present study, KN-93 significantly down-regulated the expression of p53 compared with KN-92 KN-92. Although KN-93 inhibited LX-2 proliferation, the exact mechanism by which KN-93 affects p53 is not clear and needs further study.

P21 is an inhibitor of cyclin-dependent kinases that control the cells to enter the S-phase[22]. P21 is regulated by the protein product of the gene p53, and is the downstream point. In this study, p21 expression was obviously decreased, suggesting that p21 is involved in KN-93-induced inhibition of HSC proliferation.

In conclusion, KN-93 has inhibitory effects on the proliferation of hepatic stellate cells. However, further studies are needed to explore the mechanism of KN-93 underlying the proliferation and apoptosis of hepatic stellate cells.

REFERENCES

1 **Friedman SL**, Schiff E, Sorrell M, Maddrey W. Diseases of the Liver. 8th ed. Philadelphia: Lippincott-Raven, 1998: 371–386
2 **Bissell DM**. Hepatic fibrosis as wound repair: a progress report. *J Gastroenterol* 1998; **33**: 295-302
3 **Friedman SL**. Seminars in medicine of the Beth Israel Hospital, Boston. The cellular basis of hepatic fibrosis. Mechanisms and treatment strategies. *N Engl J Med* 1993; **328**: 1828-1835
4 **Friedman SL**. Molecular regulation of hepatic fibrosis, an integrated cellular response to tissue injury. *J Biol Chem* 2000; **275**: 2247-2250
5 **Maher JJ**, Bissell DM, Friedman SL, Roll FJ. Collagen measured in primary cultures of normal rat hepatocytes derives from lipocytes within the monolayer. *J Clin Invest* 1988; **82**: 450-459
6 **Kahl CR**, Means AR. Regulation of cell cycle progression by calcium/calmodulin-dependent pathways. Endocr Rev 2003; **24**: 719-736
7 **Hook SS**, Means AR. Ca(2+)/CaM-dependent kinases: from activation to function. *Annu Rev Pharmacol Toxicol* 2001; **41**: 471-505
8 **Braun AP,** Schulman H. The multifunctional calcium/calmodulin-dependent protein kinase: from form to function. *Annu Rev Physiol* 1995; **57**: 417-445
9 **Heist EK**, Schulman H. The role of Ca2+/calmodulin-dependent protein kinases within the nucleus. *Cell Calcium* 1998; **23**: 103-114
10 **Mamiya N**, Goldenring JR, Tsunoda Y, Modlin IM, Yasui K, Usuda N, Ishikawa T, Natsume A, Hidaka H. Inhibition of acid secretion in gastric parietal cells by the Ca^{2+}/calmodulin-dependent protein kinase II inhibitor KN-93. *Biochem Biophys Res Commun* 1993; **195**: 608-615
11 **Rodriguez-Mora OG**, LaHair MM, McCubrey JA, Franklin RA. Calcium/calmodulin-dependent kinase I and calcium/calmodulin-dependent kinase kinase participate in the control of cell cycle progression in MCF-7 human breast cancer cells. *Cancer Res* 2005; **65**: 5408-5416
12 **Tombes RM**, Grant S, Westin EH, Krystal G. G1 cell cycle arrest and apoptosis are induced in NIH 3T3 cells by KN-93, an inhibitor of CaMK-II (the multifunctional Ca^{2+}/CaM kinase). *Cell Growth Differ* 1995; **6**: 1063-1070
13 **Xu L**, Hui AY, Albanis E, Arthur MJ, O'Byrne SM, Blaner WS, Mukherjee P, Friedman SL, Eng FJ. Human hepatic stellate cell lines, LX-1 and LX-2: new tools for analysis of hepatic fibrosis. *Gut* 2005; **54**: 142-151
14 **Han SW**, Lei ZM, Rao CV. Up-regulation of cyclooxygenase-2 gene expression by chorionic gonadotropin during the differentiation of human endometrial stromal cells into decidua. *Endocrinology* 1996; **137**: 1791-1797
15 **Reeves HL**, Friedman SL. Activation of hepatic stellate cells--a key issue in liver fibrosis. *Front Biosci* 2002; **7**: d808-d826
16 **Iredale JP**. Hepatic stellate cell behavior during resolution of liver injury. *Semin Liver Dis* 2001; **21**: 427-436
17 **Muthalif MM**, Karzoun NA, Benter IF, Gaber L, Ljuca F, Uddin MR, Khandekar Z, Estes A, Malik KU. Functional significance of activation of calcium/calmodulin-dependent protein kinase II in angiotensin II--induced vascular hyperplasia and hypertension. *Hypertension* 2002; **39**: 704-709
18 **Rasmussen G,** Rasmussen C. Calmodulin-dependent protein kinase II is required for G1/S progression in HeLa cells. *Biochem Cell Biol* 1995; **73**: 201-207
19 **Allred DC**, Harvey JM, Berardo M, Clark GM. Prognostic and predictive factors in breast cancer by immunohistochemical analysis. *Mod Pathol* 1998; **11**: 155-168
20 **Cox LS**, Lane DP. Tumour suppressors, kinases and clamps: how p53 regulates the cell cycle in response to DNA damage. *Bioessays* 1995; 17: 501-508
21 **Abriss B**, Hollweg G, Gressner AM, Weiskirchen R. Adenoviral-mediated transfer of p53 or retinoblastoma protein blocks cell proliferation and induces apoptosis in culture-activated hepatic stellate cells. *J Hepatol* 2003; **38**: 169-178
22 **Levine AJ**. p53, the cellular gatekeeper for growth and division. *Cell* 1997; **88**: 323-331

S- Editor Liu Y **L- Editor** Wang XL **E- Editor** Zhou T

PO Box 2345, Beijing 100023, China
www.wjgnet.com
wjg@wjgnet.com

World J Gastroenterol 2007 March 7; 13(9): 1449-1450
World Journal of Gastroenterology ISSN 1007-9327

CASE REPORT

Strangulated diaphragmatic hernia presenting clinically as pericarditis

Rohit Makhija, Jacob A Akoh

Rohit Makhija, Jacob A Akoh, Directorate of Surgery, Derriford Hospital, Plymouth PL6 8DH, United Kingdom
Correspondence to: Rohit Makhija, Directorate of Surgery, Derriford Hospital, 8 Winston Churchill Drive, King's Lynn, Norfolk, PE30 4YQ, United Kingdom. rohit100@doctors.net.uk
Telephone: +44-1553-771200
Received: 2006-08-15 Accepted: 2007-02-22

Abstract

A case of strangulation of the transverse colon in a traumatic left diaphragmatic hernia manifesting as pericarditis is reported. This is unusual because pericardial signs in traumatic diaphragmatic hernia have been previously described in association with direct pericardial injury. This is the only such case where electrocardiographic changes of pericarditis were seen without direct pericardial trauma. The possibility of internal herniation through a traumatic diaphragmatic hernia must be considered in patients with chest symptoms and a compatible history.

Key words: Strangulated colon; Diaphragmatic hernia; Pericarditis; Diaphragmatic injury

Makhija R, Akoh JA. Strangulated diaphragmatic hernia presenting clinically as pericarditis. *World J Gastroenterol* 2007; 13(9): 1449-1450

http://www.wjgnet.com/1007-9327/13/1449.asp

INTRODUCTION

We report an unusual case of strangulated diaphragmatic hernia presenting as pericarditis, which was not reported in English literature.

CASE REPORT

Mr CV, a 60-year old man presented to the casualty department with a history of vomiting and crampy abdominal pain. His previous medical history included a fall 4 years ago during which he sustained multiple rib fractures and a small left haemopneumothorax, which was treated conservatively at that time. Physical examination was unremarkable and he was empirically treated for gastroenteritis and discharged home. He returned the following day, with pleuritic left chest pain, dyspnoea, pyrexia of 38.5℃ and tachypnoea. Investigations revealed minimally elevated white cell count, left lower lobe consolidation on chest X-ray (CXR) (Figure 1) and normal electrocardiogram (ECG).

He was admitted to Medical Assessment Unit where he later complained of chest tightness. Repeat ECG revealed generalised ST elevation with upward concavity (Figure 2). A differential diagnosis of acute myocardial infarction and pericarditis was entertained and he was transferred to Coronary Care Unit (CCU) where he had a short episode of supraventricular tachycardia controlled with intravenous adenosine. Echocardiography revealed normal ventricular function with minor apical hypokinesis and no pericardial fluid. Twelve hours later he had signs of acute abdomen. Abdominal radiograph suggested large bowel obstruction, which was confirmed by GastrografinTM enema. The surgical team reviewed him and took him to the operating theatre with a diagnosis of peritonitis. However, its cause still remained unknown.

Laparotomy findings were faecal peritonitis with caecal perforation due to strangulated transverse colon in a left diaphragmatic hernia. Extended right hemicolectomy was performed with formation of ileostomy and a mucous fistula. The diaphragmatic opening was primarily repaired with non-absorbable sutures. Post-operative recovery was protracted with a long spell in the Intensive Care Unit. ECG changes reverted to normal shortly after surgery.

DISCUSSION

Traumatic diaphragmatic hernia is usually caused by blunt trauma and occurs more frequently on the left side as the liver often protects the right side[1,2]. As in this case, it is a diagnosis, which is often missed at the time of initial injury and only determined at laparotomy much later. This case is unusual because the presenting features so strongly simulated pericarditis that the patient was initially admitted to CCU after assessment by a cardiologist. This type of presentation has not been published in English literature previously. Whenever pericardial symptoms are associated with traumatic diaphragmatic hernia, there is a direct trauma to the pericardial sac[3,4]. However, in this patient, the pleuritic chest pain and ECG changes were presumably caused by pressure effects from the adjacent distended colon along with contaminated faecal fluid in the hernial sac.

In conclusion, all patients who have persistent basal

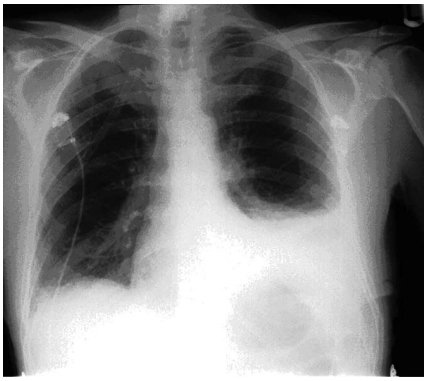

Figure 1 Chest X-ray showing stomach bubble in left hemi-thorax, above the left hemi-diaphragm.

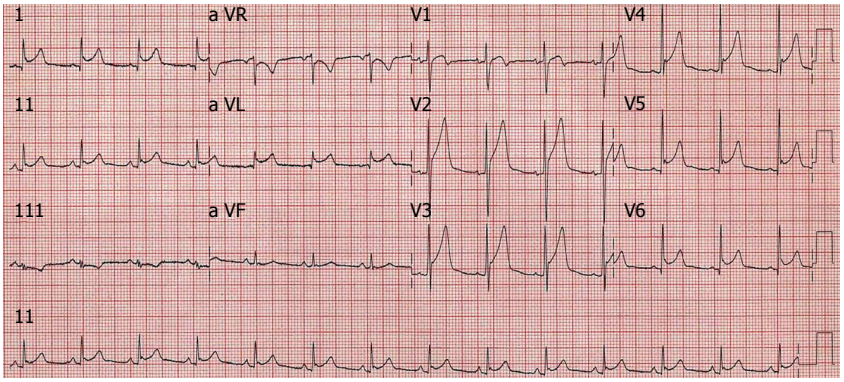

Figure 2 ECG with ST and T wave changes showing acute pericarditis.

abnormality on their chest X-ray after blunt thoraco-abdominal trauma should be radiologically evaluated to exclude the possibility of a ruptured diaphragm owing to the serious consequences of an undetected diaphragmatic hernia. The preferred radiological investigation is a contrast-enhanced computed tomography scan of the abdomen. In addition, the possibility of an incarceration should be kept in mind when assessing patients presenting with chest symptoms and a history suggestive of previously ruptured diaphragm.

REFERENCES

1 **Brown GL**, Richardson JD. Traumatic diaphragmatic hernia: a continuing challenge. *Ann Thorac Surg* 1985; **39**: 170-173
2 **Beauchamp G**, Khalfallah A, Girard R, Dube S, Laurendeau F, Legros G. Blunt diaphragmatic rupture. *Am J Surg* 1984; **148**: 292-295
3 **Aldhoheyan A**, Jain SK, Hamdy M, Alsebayel MJ. Traumatic intrapericardial diaphragmatic hernia. *Injury* 1992; **23**: 331-332
4 **Girzadas DV**, Fligner DJ. Delayed traumatic intrapericardial diaphragmatic hernia associated with cardiac tamponade. *Ann Emerg Med* 1991; **20**: 1246-1247

S- Editor Liu Y **L- Editor** Wang XL **E- Editor** Zho

PO Box 2345, Beijing 100023, China
www.wjgnet.com
wjg@wjgnet.com

World J Gastroenterol 2007 March 7; 13(9): 1451-1452
World Journal of Gastroenterology ISSN 1007-9327

CASE REPORT

Portal hypertensive duodenal polyp: A case report

Jean-David Zeitoun, Ariane Chryssostalis, Benoit Terris, Frederic Prat, Marianne Gaudric, Stanislas Chaussade

Jean-David Zeitoun, Ariane Chryssostalis, Frederic Prat, Marianne Gaudric, Stanislas Chaussade, Department of Gastroenterology, Cochin Hospital, Assistance Publique des Hôpitaux de Paris, Paris, France
Benoit Terris, Department of Pathology, Cochin Hospital, Assistance Publique des Hôpitaux de Paris, Paris, France
Correspondence to: Dr. Ariane Chryssostalis, Department of Gastroenterology, Cochin Hospital, 27 Rue du Faubourg Saint-Jacques, Paris 75014, France. ariane.chryssostalis@cch.aphp.fr
Telephone: +33-1-58411901 Fax: +33-1-58411930
Received: 2006-12-03 Accepted: 2007-01-25

Abstract

Abnormalities of gastric mucosa in patients with portal hypertension are well documented. Manifestations of portal hypertension in small bowel and colon are less common. Colonic polypoid lesions microscopically consisting of a normal mucosa, with dilatation of submucosal vessels, have been described. We here report the first case of portal hypertensive duodenal polyp, responsible for gastro-intestinal bleeding. Endoscopic treatment turned out to be successful.

Key words: Gastrointestinal bleeding; Cirrhosis; Portal hypertension; Small bowell; Endoscopy

Zeitoun JD, Chryssostalis A, Terris B, Prat F, Gaudric M, Chaussade S. Portal hypertensive dudoenal polyp: A case report. *World J Gastroenterol* 2007; 13(9): 1451-1452

http://www.wjgnet.com/1007-9327/13/1451.asp

INTRODUCTION

Esophagogastric varices are common manifestations of portal hypertension, but other lesions such as gastric mucosal changes, called portal hypertensive gastropathy[1], or colonic mucosal abnormalities[2,3] may occur. Duodenopathy has also been reported, with various forms[4-6] but never under the appearance of a polyp. We describe a patient who was found to have a portal hypertensive duodenal polyp, responsible for gastro-intestinal bleeding. Endoscopic treatment was performed with success.

CASE REPORT

A 70-year old man, with alcoholic cirrhosis, was hospitalized for a melena. Physical examination found superficial venous engorgement of the abdominal wall, with ascitis. Laboratory data revealed anemia and liver dysfunction. International normalized ratio (INR) value was 1.33.

An upper endoscopy showed large esophageal varices without red spots, and portal hypertensive gastropathy. In the descending portion of the duodenum, a 3-cm long, ulcerated and haemorrhagic polypoid lesion was seen (Figure 1).

We performed polypectomy using hemostatic clips on the pedicle, then a polypectomy snare. Anatomopathologic examination of the specimen showed a fibrous and inflammatory polyp, with numerous thick-walled capillaries in its subepithelial portion, and a few vascular ectasias were associated (Figure 2). This histological appearance was considered as portal hypertensive duodenopathy. There was no epithelial proliferation in favor of an inverted polyp or hamartomatous lesion.

No complication occurred, and control endoscopy was performed three days later. The duodenal mucosa appeared normal. Colonoscopy revealed an 8-mm polyp located in the left portion of the colon, which was removed with a polypectomy snare. Anemia resolved and the patient was still free of haemorrhagic recurrence six months later.

DISCUSSION

McCormack *et al*[1] first described portal hypertensive gastropathy, its appearance consists of mosaic pattern, cherry red spots and scarlatina rash. Other entities have then been documented, such as portal hypertensive enteropathy[4-10] and colonopathy[2,3].

Duodenum can thus be involved and with the exception of varices, lesions reported are erythema, scattered petechiae, friable mucosa, erosion, ulcer and edema.

In our patient, portal hypertensive duodenopathy took the unusual presentation of a polyp. Misra *et al*[11] and Ryushi Shudo *et al*[4] reported that the predominant pathological features of portal hypertension duodenopathy (PHD) are subepithelial edema, and increase of diameter and wall thickness of the capillaries. Now, numerous capillaries with a thickening wall were found in our specimen, suggesting that the polyp is due to portal hypertension duodenopathy. On the other hand, colonic polypoid lesions due to portal hypertensive colonopathy have already been described[12].

Moreover, many authors insist on the uncertain clinical significance of portal hypertensive enteropathy[13], in particular whether it can be responsible for gastro-

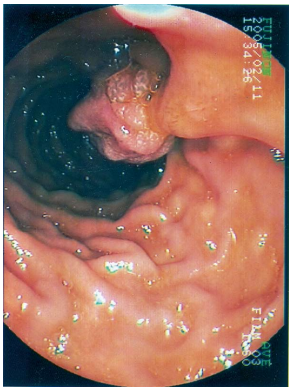

Figure 1 Endoscopic view of the duodenal polyp.

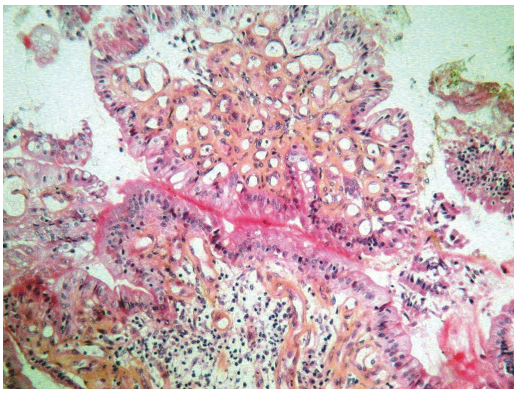

Figure 2 Polypoid lesion of the duodenum demonstrating the presence of multiples capillaries in the lamina propria, immediately beneath the surface epithelium.

intestinal bleeding.

In the reported case, the only haemorrhagic lesion was the duodenal polyp. Additionally, anemia resolved after polypectomy. This illustrates that portal hypertension duodenopathy is a potential aetiology of gastro-intestinal bleeding.

We removed the polyp using hemostatic clips before applying polypectomy snare, to avoid the potential risk of post polypectomy hemorrhage. Polypectomy appeared to be a safe procedure and allowed histological diagnosis.

In conclusion, we report the case of a cirrhotic patient who had upper gastro-intestinal haemorrhage due to a portal hypertensive duodenal polyp. To our knowledge, this is the first case of this form of portal hypertensive duodenopathy. Endoscopic treatment was performed successfully. Although the new data suggest that portal hypertensive enteropathy may present as a source of bleeding, its exact clinical significance has to be defined subsequently.

REFERENCES

1 **McCormack TT**, Sims J, Eyre-Brook I, Kennedy H, Goepel J, Johnson AG, Triger DR. Gastric lesions in portal hypertension: inflammatory gastritis or congestive gastropathy? *Gut* 1985; **26**: 1226-1232

2 **Kozarek RA**, Botoman VA, Bredfeldt JE, Roach JM, Patterson DJ, Ball TJ. Portal colopathy: prospective study of colonoscopy in patients with portal hypertension. *Gastroenterology* 1991; **101**: 1192-1197

3 **Bini EJ,** Lascarides CE, Micale PL, Weinshel EH. Mucosal abnormalities of the colon in patients with portal hypertension: an endoscopic study. *Gastrointest Endosc* 2000; **52**: 511-516

4 **Gupta R**, Saraswat VA, Kumar M, Naik SR, Pandey R. Frequency and factors influencing portal hypertensive gastropathy and duodenopathy in cirrhotic portal hypertension. *J Gastroenterol Hepatol* 1996; **11**: 728-733

5 **Vigneri S**, Termini R, Piraino A, Scialabba A, Bovero E, Pisciotta G, Fontana N. The duodenum in liver cirrhosis: endoscopic, morphological and clinical findings. *Endoscopy* 1991; **23**: 210-212

6 **Shudo R**, Yazaki Y, Sakurai S, Uenishi H, Yamada H, Sugawara K. Duodenal erosions, a common and distinctive feature of portal hypertensive duodenopathy. *Am J Gastroenterol* 2002; **97**: 867-873

7 **Nagral AS**, Joshi AS, Bhatia SJ, Abraham P, Mistry FP, Vora IM. Congestive jejunopathy in portal hypertension. *Gut* 1993; **34**: 694-697

8 **Viggiano TR**, Gostout CJ. Portal hypertensive intestinal vasculopathy: a review of the clinical, endoscopic, and histopathologic features. *Am J Gastroenterol* 1992; **87**: 944-954

9 **De Palma GD**, Rega M, Masone S, Persico F, Siciliano S, Patrone F, Matantuono L, Persico G. Mucosal abnormalities of the small bowel in patients with cirrhosis and portal hypertension: a capsule endoscopy study. *Gastrointest Endosc* 2005; **62**: 529-534

10 **Misra SP**, Dwivedi M, Misra V, Gupta M. Ileal varices and portal hypertensive ileopathy in patients with cirrhosis and portal hypertension. *Gastrointest Endosc* 2004; **60**: 778-783

11 **Misra V**, Misra SP, Dwivedi M, Gupta SC. Histomorphometric study of portal hypertensive enteropathy. *Am J Clin Pathol* 1997; **108**: 652-657

12 **Huang WH**, Hsu CT, Chao YC. Colonic polypoid lesions: an unusual endoscopic presentation of portal hypertensive colonopathy. *Gastrointest Endosc* 1999; **50**: 283-285

13 **Cheung RC**, Cooper S, Keeffe EB. Endoscopic gastrointestinal manifestations of liver disease. *Gastrointest Endosc Clin N Am* 2001; **11**: 15-44

S- Editor Liu Y **L- Editor** Wang XL **E- Editor** Zhou T

PO Box 2345, Beijing 100023, China
www.wjgnet.com
wjg@wjgnet.com

World J Gastroenterol 2007 March 7; 13(9): 1453-1457
World Journal of Gastroenterology ISSN 1007-9327

CASE REPORT

A case of mucosa-associated lymphoid tissue lymphoma forming multiple lymphomatous polyposis in the small intestine

Naoto Hirata, Kazunari Tominaga, Kensuke Ohta, Kaori Kadouchi, Hirotoshi Okazaki, Tetsuya Tanigawa, Masatsugu Shiba, Toshio Watanabe, Yasuhiro Fujiwara, Shiro Nakamura, Nobuhide Oshitani, Kazuhide Higuchi, Tetsuo Arakawa

Naoto Hirata, Kazunari Tominaga, Kensuke Ohta, Hirotoshi Okazaki, Tetsuya Tanigawa, Masatsugu Shiba, Toshio Watanabe, Yasuhiro Fujiwara, Shiro Nakamura, Kazuhide Higuchi, Tetsuo Arakawa, Department of Gastroenterology, Osaka City University Graduate School of Medicine, 1-4-3 Asahimachi, Abeno-ku, Osaka 545-8585, Japan
Kensuke Ohta, Department of Hematology, Osaka City University Graduate School of Medicine, 1-4-3 Asahimachi, Abeno-ku, Osaka 545-8585, Japan
Shiro Nakamura, Department of Gastroenterology, Rinku General Medical Center, 2-3 Rinkuouraikita, Izumisano, Osaka 598-0048, Japan
Supported in part by a Grant-in-Aid for Scientific Research (C) from the Ministry of Education, Science and Culture in Japan
Correspondence to: Kazunari Tominaga, Department of Gastroenterology, Osaka City University Graduate School of Medicine, 1-4-3 Asahimachi, Abeno-ku, Osaka 545-8585, Japan. tomy@med.osaka-cu.ac.jp
Telephone: +81-6-66453811 Fax: +81-6-66453813
Received: 2006-12-16 Accepted: 2007-03-03

Abstract

A 50-year old woman suffering from diabetes had a CT scan that revealed a diffuse thickening of small intestinal wall and swollen paraaortic lymph nodes. An esophago gastroduodenoscopy (EGD) confirmed multiple polypoid lesions in the duodenum and small intestine, and conventional histological testing revealed non-specific inflammatory changes. Further examinations including the immunohistochemical profiles of the biopsied specimens led us to diagnose the lesion as a marginal zone B-cell lymphoma of mucosa-associated lymphoid tissue type, forming multiple lymphomatous polyposis sequentially spreading from duodenal bulb to terminal ileum. According to Lugano's classification, its staging was clinically diagnosed as stage Ⅱ. Two courses of a standard CHOP (cyclophosphamide, doxorubicin hydrochloride, vincristine sulfate, and predonisolone) regimen with rituximab reduced the lesion and the patient had a almost complete response. A 5-year follow-up EGD and histological examinations detected no recurrence of the disease.

Key words: Intestinal lymphoma; Mucosa-associated lymphoid tissue lymphoma; Multiple lymphomatous polyposis

Hirata N, Tominaga K, Ohta K, Kadouchi K, Okazaki H, Tanigawa T, Shiba M, Watanabe T, Fujiwara Y, Nakamura S, Oshitani N, Higuchi K, Arakawa T. A case of mucosa-associated lymphoid tissue lymphoma forming multiple lymphomatous polyposis in the small intestine. *World J Gastroenterol* 2007; 13(9): 1453-1457

http://www.wjgnet.com/1007-9327/13/1453.asp

INTRODUCTION

Lymphomas in the gastrointestinal (GI) tract may be ulcerative, superficial, polypoid, or diffuse, and may also have other less common characteristics[1]. Multiple lymphomatous polyposis (MLP) is characterized by the formation of multiple mucosal polyps[2]. Polypoid lesions of MLP are usually widely spread to several regions of the GI tract including the esophagus, stomach, duodenum, and intestine. Histological findings tend to lead to the classification of most MLPs as mantle cell lymphomas[3-5]. Therefore, MLP may be one of the poor prognostic lymphomas in the GI tract, even though several regimens of systemic chemotherapy have been adapted for its treatment.

We report a rare and interesting case of MLP whose histology was a marginal zone B-cell mucosa-associated lymphoid tissue (MALT) lymphoma. A range of polypoid lesions was observed from duodenal bulb to the terminal ileum by various image examinations. The present case failed to respond to treatment to eradicate *H pylori*, but was successfully managed using a CHOP regimen combined with rituximab.

CASE REPORT

A 50-year old woman underwent an abdominal CT scan during an educational admission for diabetes mellitus at another hospital. CT scan revealed a diffuse thickening of small intestinal wall and swollen paraaortic lymph nodes, but no abnormal mass in her pancreas. Gallium citrate scintigraphy showed abnormal accumulation in the

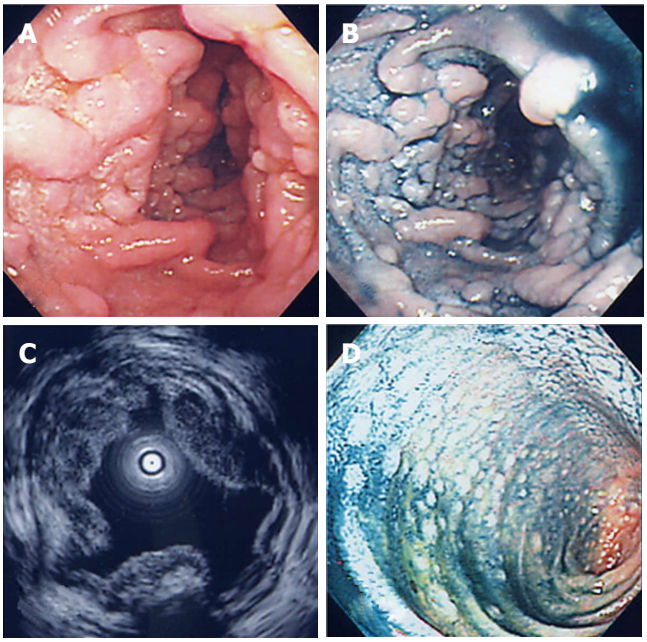

Figure 1 EGD (**A**), dye contrast EGD (**B**), EUS (**C**), and lower endoscopy (**D**) showing features of the lesions.

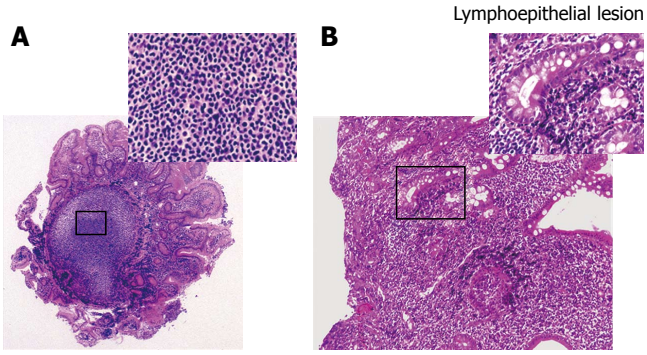

Figure 3 Follicular colonization (**A**) and many small lymphocytes and a few large lymphocytes in the duodenal tissues (**B**) in the biopsied specimens (HE, × 200)

small intestine. Esophagogastroduodenoscopy (EGD) showed multiple polypoid lesions in the duodenum, and histological finding revealed non-specific inflammatory changes including infiltration of lymphoid cells. All these findings indicated a lymphatic proliferative disease. To obtain a differential diagnosis, she underwent endoscopic partial mucosal resection to perform the Southern blot analysis for immunoglobulin (Ig) genes but results were negative for changes in Ig-heavy chain JH. Then the patient was admitted to our hospital for further examination and treatment.

On admission, she had no clinical symptoms. Physical examinations revealed no superficial lymphadenopathy and no abnormal abdominal mass. Laboratory findings showed only mild liver dysfunction, mild elevation of lactate dehydrogenase and total cholesterol. No atypical lymphocytes were seen in peripheral blood, and the serum soluble interleukin-2 level was within normal limits. EGD showed multiple yellowish granular polypoid lesions sequentially spreading from the bulb to the distal

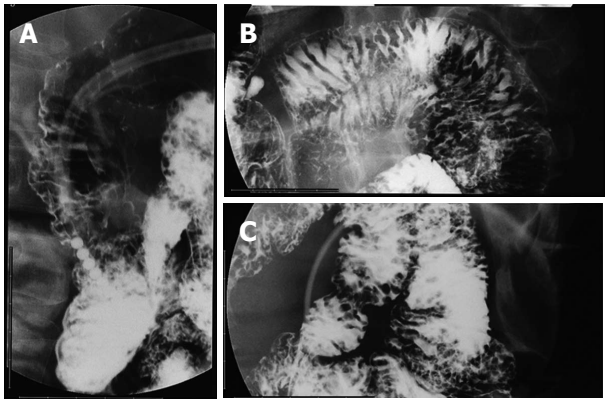

Figure 2 Fluoroscopic examinations showing many small round shaped defects in the second portion of the duodenum (**A**), jejunum (**B**), and ileum (**C**).

tract over descending portion of the duodenum (Figure 1A and B). On the other hand, such polypoid lesions were not detected in the stomach except for atrophic mucosa. Cultures were positive for *H pylori*. Endoscopic ultrasonography revealed hypoechoic thickening from the first to the second sonographic layer, indicating that it was almost confined to the mucosal layer (Figure 1C). Fluoroscopic examination of the small intestine aiming to estimate the extent of lesion showed many round defects from the duodenal bulb to the end of jejunum (Figure 2), suggesting that the lesion was extending from the duodenum to the jejunum and ileum. Lower endoscopic findings showed whitish small polypoid lesions in the terminal ileum, but no obvious lesion in the colon and rectum (Figure 1D). Abdominal CT scan showed thickening of the duodenal and small intestinal walls. Abdominal MRI images also showed swollen paraaortic lymph nodes (approximately 1 cm in diameter) and an abnormal mass at the left side of supra-mesenteric artery (7 cm × 3 cm) which was probably composed of swollen mesenteric lymph nodes.

Histological findings of the specimens obtained from the lesions of duodenum and ileum showed follicular colonization dominantly composed of many small lymphocytes and a few large lymphocytes (Figure 3A), as well as a lymphoepithelial lesion, one of the typical features of mucosa-associated lymphoid tissue (MALT) lymphoma (Figure 3B). Immunohistochemical examinations showed that a large number of lymphoma cells were positively stained for bcl-2 and CD20 (the B-cell marker), but negative for UCHL-1 (T-cell marker). On the other hand, the tumor cells were negatively stained for CD5, CD10, and Cyclin D1 (Figure 4). All these findings including the immunohistochemical profiles led us to diagnose this lesion as a marginal zone B-cell lymphoma of the MALT type according to the WHO classification[6] but not as a mantle cell lymphoma, forming MLP sequentially spreading from the duodenal bulb to the terminal ileum. According to Lugano's classification[7], its staging was clinically diagnosed as stage Ⅱ.

Eradication therapy was selected as the first treatment modality for *H pylori* infection (lansoprazole 60 mg/d, clarithromycin 800 mg/d, and amoxicillin 1500 mg/d,

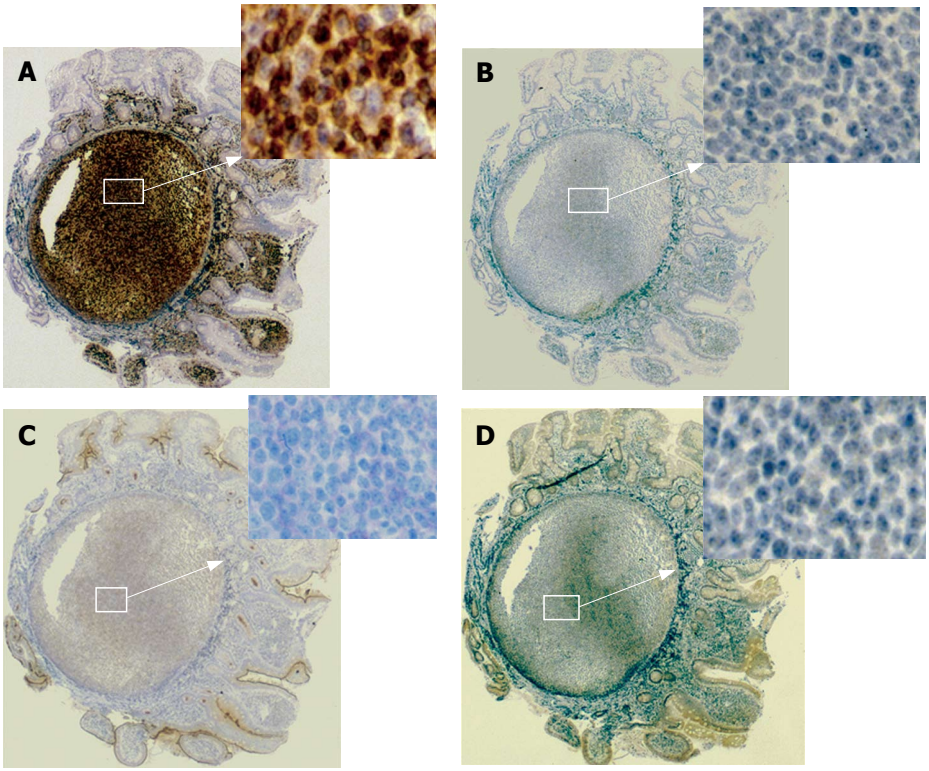

Figure 4 Immunohistological profiles of the lesions revealing positive staining for bcl-2 (**A**) and negative staining for CD5 (**B**), CD10 (**C**), and CyclinD1 (**D**).

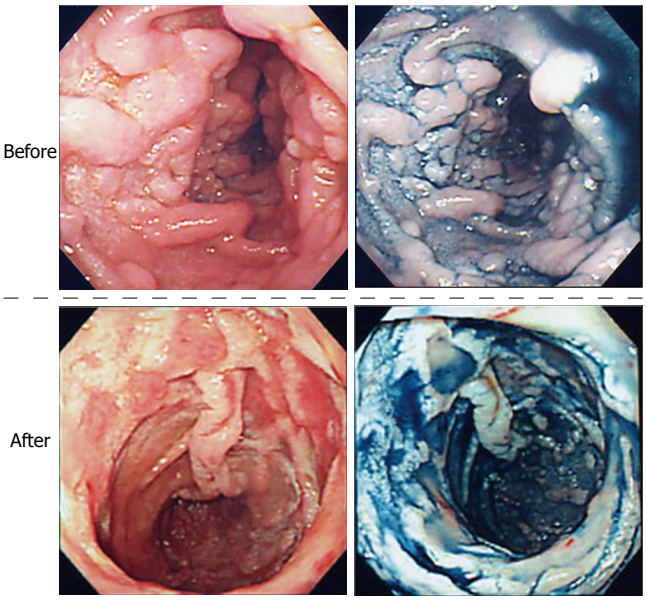

Figure 5 Endoscopic features of the lesions before and after the treatment.

for one week), since it was less invasive for the patient. Follow-up EGD findings after *H pylori* eradication showed no improvement of these lesions. We selected the systemic chemotherapy as the second treatment modality for *H pylori* infection because the lymphoma may spread to the duodenum and other areas, even though the histopathological findings did not reveal a high potential for it to become malignant. The patient then received a standard CHOP (cyclophosphamide: 750 mg/m^2, doxorubicin hydrochloride: 50 mg/m^2, vincristine sulfate: 1.4 mg/m^2, and predonisolone: 100 mg) regimen in combination with rituximab: 375 mg/m^2 regimen, followed by a further CHOP treatment at their half dose. Ten days after the first therapeutic course, EGD findings showed that each polypoid lesion of the duodenum became smaller, and their tops collapsed and showed evidence for erosion. Following 2 courses of CHOP plus rituximab regimen, the lesions and abdominal lymph nodes almost completely resolved (Figure 5). A 5-year follow-up with EGD and histological examination showed no recurrence of the disease.

DISCUSSION

The present case of lymphatic proliferative disease in the GI tract was diagnosed by endoscopy, radiographic imaging, and genetic profiling. The clinical features indicated a MLP type of lymphoma in the duodenum and small intestine. Actually, many reports have demonstrated the consensus that the majority of MLPs are histologically mantle cell type lymphomas, and a few cases of follicular lymphoma or T-cell lymphoma have been reported[8-12]. In the present case, however, histological examination showed characteristic findings such as lymphoepithelial lesions and immunohistological profiles (positive CD20 and bcl-2; negative UCHL-1, CD5, CD10, and CyclinD1). These findings motivated us to diagnose the case as a B-cell MALT lymphoma, which was discriminated from a mantle cell or follicular type lymphoma. On the other hand, the differential diagnosis was considered as an immunoproliferative small intestinal disease (IPSID), a subtype of MALT lymphoma[13]. However, this case was clinically different from the typical features of IPSID, because the dominant region for IPSID is duodenum and upper jejunum and it usually causes malabsorption

syndrome or protein-losing gastroenteropathy. Thus, the present case was more consistent with a MALT lymphoma forming MLP rather than IPSID. To our knowledge, only 4 cases of MALT lymphoma forming MLP have been reported[14-16], indicating that our present case is actually rare. In regard to the origin of this lymphoma, we could not completely deny the suspicion that a lymph node might be the origin of the disease because of the swollen mesenteric lymph nodes. However, the involvement of other lymph nodes was unremarkable although the polypoid lesions were widely distributed in the GI tract. Furthermore, no atypical lymphocytes were shown in peripheral blood, and this case was compatible with the definition about primary GI tract lymphoma described by Lewin and Herrmann[17,18]. Thus, it was more likely that the primary lesion of the present lymphoma was in the GI tract.

Recently, treatment to eradicate *H pylori* has become a standard management for primary gastric MALT lymphoma[19-21]. Certainly, there are various reports showing that eradication of *H pylori* is effective for duodenal MALT lymphoma[22,23]. Nakamura *et al*[24] reported that primary duodenal lymphoma might have different characteristics between locations at the bulb and descending portion. Lymphomas originating from duodenal bulb might have similar characteristics with gastric MALT lymphomas, suggesting that *H pylori* eradication therapy is often effective. Unfortunately, the lesions observed over the descending portion might be less associated with *H pylori* infection, indicating that *H pylori* eradication therapy cannot be expected to be totally effective. On the other hand, the efficacy of *H pylori* eradication therapy for the small intestine or colorectal lymphoma is not known, though a few responsive cases have been reported[25,26]. Since *H pylori* eradication therapy was ineffective in the present case, we used a more potent therapy due to the potential of the lymphoma to spread more extensively and its possible transformation of MALT lymphoma cells into diffuse large B cell lymphoma cells in the presence of a few large cells in the specimens. In general, surgical resection, systemic chemotherapy, and radiation therapy are performed in the treatment of malignant lymphoma in the GI tract[27]. Since curative surgical resection or radiation therapy was not suitable in our case because the lesion was already diffuse and widespread, we selected a systemic chemotherapy as a second line treatment. Combination therapy of a CHOP regimen, the most common regimen in combination with rituximab (a molecular targeting agent for this particular follicular type lymphoma), has been recently used in the treatment of GI tract lymphoma[28,29]. This combination therapy contributed to a significant improvement in the present case. We performed careful follow-up examinations such as laboratory analyses, EGD examination, and various abdominal images at every six months interval. EGD examination revealed no obvious recurrence of MLP and there was no evidence for recurrent lesions or clinical symptoms during the 5-year follow-up.

In conclusion, we reported a rare case of MALT lymphoma in the small intestine which was histologically diagnosed as a marginal zone B-cell MALT lymphoma. CHOP regimen in combination with rituximab is an effective therapy for MALT lymphomas in the GI tract.

REFERENCES

1 **Nakamura S**, Matsumoto T, Iida M, Yao T, Tsuneyoshi M. Primary gastrointestinal lymphoma in Japan: a clinicopathologic analysis of 455 patients with special reference to its time trends. *Cancer* 2003; **97**: 2462-2473

2 **Cornes JS**. Multiple lymphomatous polyposis of the gastrointestinal tract. *Cancer* 1961; **14**: 249-257

3 **Isaacson PG**, MacLennan KA, Subbuswamy SG. Multiple lymphomatous polyposis of the gastrointestinal tract. *Histopathology* 1984; **8**: 641-656

4 **Ruskoné-Fourmestraux A**, Delmer A, Lavergne A, Molina T, Brousse N, Audouin J, Rambaud JC. Multiple lymphomatous polyposis of the gastrointestinal tract: prospective clinicopathologic study of 31 cases. Groupe D'étude des Lymphomes Digestifs. *Gastroenterology* 1997; **112**: 7-16

5 **Lavergne A**, Brouland JP, Launay E, Nemeth J, Ruskone-Fourmestraux A, Galian A. Multiple lymphomatous polyposis of the gastrointestinal tract. An extensive histopathologic and immunohistochemical study of 12 cases. *Cancer* 1994; **74**: 3042-3050

6 **Harris NL**, Jaffe ES, Diebold J, Flandrin G, Muller-Hermelink HK, Vardiman J, Lister TA, Bloomfield CD. The World Health Organization classification of neoplasms of the hematopoietic and lymphoid tissues: report of the Clinical Advisory Committee meeting--Airlie House, Virginia, November, 1997. *Hematol J* 2000; **1**: 53-66

7 **Rohatiner A**, d'Amore F, Coiffier B, Crowther D, Gospodarowicz M, Isaacson P, Lister TA, Norton A, Salem P, Shipp M. Report on a workshop convened to discuss the pathological and staging classifications of gastrointestinal tract lymphoma. *Ann Oncol* 1994; **5**: 397-400

8 **Tomita S**, Kojima M, Imura J, Hori H, Ueda Y, Koitabashi A, Suzuki Y, Nakamura T, Nakamura Y, Mitani K, Terano A, Ohkura Y, Kawamata H, Fujimori T. Extranodal diffuse follicular center lymphoma mimicking mantle cell lymphoma of the intestine. *Am J Hematol* 2003; **74**: 287-289

9 **Sakata Y**, Iwakiri R, Sakata H, Fujisaki J, Mizuguchi M, Fukushima N, Fujimoto K. Primary gastrointestinal follicular center lymphoma resembling multiple lymphomatous polyposis. *Dig Dis Sci* 2001; **46**: 567-570

10 **Yoshino T**, Miyake K, Ichimura K, Mannami T, Ohara N, Hamazaki S, Akagi T. Increased incidence of follicular lymphoma in the duodenum. *Am J Surg Pathol* 2000; **24**: 688-693

11 **Isomoto H**, Maeda T, Akashi T, Tsuchiya T, Kawaguchi Y, Sawayama Y, Koida S, Ohnita K, Kohno S, Tomonaga M. Multiple lymphomatous polyposis of the colon originating from T-cells: a case report. *Dig Liver Dis* 2004; **36**: 218-221

12 **Hirakawa K**, Fuchigami T, Nakamura S, Daimaru Y, Ohshima K, Sakai Y, Ichimaru T. Primary gastrointestinal T-cell lymphoma resembling multiple lymphomatous polyposis. *Gastroenterology* 1996; **111**: 778-782

13 **Isaacson PG**, Norton AJ. Extranodal Lymphomas. Edinburgh: Churchill Livingstone, 1994: 1-65

14 **Saito T**, Toyoda H, Yamaguchi M, Nakamura T, Nakamura S, Mukai K, Fuke H, Wakita Y, Iwata M, Adachi Y, Shiku H. Ileocolonic lymphomas: a series of 16 cases. *Endoscopy* 2005; **37**: 466-469

15 **Breslin NP**, Urbanski SJ, Shaffer EA. Mucosa-associated lymphoid tissue (MALT) lymphoma manifesting as multiple lymphomatosis polyposis of the gastrointestinal tract. *Am J Gastroenterol* 1999; **94**: 2540-2545

16 **Yatabe Y**, Nakamura S, Nakamura T, Seto M, Ogura M, Kimura M, Kuhara H, Kobayashi T, Taniwaki M, Morishima Y, Koshikawa T, Suchi T. Multiple polypoid lesions of primary mucosa-associated lymphoid-tissue lymphoma of colon. *Histopathology* 1998; **32**: 116-125

17 **Herrmann R**, Panahon AM, Barcos MP, Walsh D, Stutzman L. Gastrointestinal involvement in non-Hodgkin's lymphoma. *Cancer* 1980; **46**: 215-222
18 **Lewin KJ**, Ranchod M, Dorfman RF. Lymphomas of the gastrointestinal tract: a study of 117 cases presenting with gastrointestinal disease. *Cancer* 1978; **42**: 693-707
19 **Boot H**, de Jong D. Gastric lymphoma: the revolution of the past decade. *Scand J Gastroenterol Suppl* 2002; (236): 27-36
20 **Ahmad A**, Govil Y, Frank BB. Gastric mucosa-associated lymphoid tissue lymphoma. *Am J Gastroenterol* 2003; **98**: 975-986
21 **Stolte M**, Bayerdörffer E, Morgner A, Alpen B, Wündisch T, Thiede C, Neubauer A. Helicobacter and gastric MALT lymphoma. *Gut* 2002; **50** Suppl 3: III19-III24
22 **Nagashima R,** Takeda H, Maeda K, Ohno S, Takahashi T. Regression of duodenal mucosa-associated lymphoid tissue lymphoma after eradication of Helicobacter pylori. *Gastroenterology* 1996; **111**: 1674-1678
23 **Toyoda H**, Yamaguchi M, Nakamura S, Nakamura T, Kimura M, Suzuki H, Mukai K, Sawa H, Kawamura K, Shiku H. Regression of primary lymphoma of the ampulla of Vater after eradication of Helicobacter pylori. *Gastrointest Endosc* 2001; **54**: 92-96
24 **Nakamura T**, Suzuki T, Matsuura A, Ohashi K, Yokoi T, Nakamura H. Clinocopathological features of MALT lymphoma and follicular lymphoma of the duodenum. *Stom & Intest* 2001; 36: 1529-1540
25 **Nakamura S**, Matsumoto T, Takeshita M, Kurahara K, Yao T, Tsuneyoshi M, Iida M, Fujishima M. A clinicopathologic study of primary small intestine lymphoma: prognostic significance of mucosa-associated lymphoid tissue-derived lymphoma. *Cancer* 2000; **88**: 286-294
26 **Raderer M**, Pfeffel F, Pohl G, Mannhalter C, Valencak J, Chott A. Regression of colonic low grade B cell lymphoma of the mucosa associated lymphoid tissue type after eradication of Helicobacter pylori. *Gut* 2000; **46**: 133-135
27 **Al-Shemmari SH**, Sajnani KP, Ameen RM, Ragheb AM. Primary gastrointestinal non-Hodgkin's lymphoma: treatment outcome. *Clin Lymphoma* 2003; **4**: 99-103
28 **Wöhrer S**, Püspök A, Drach J, Hejna M, Chott A, Raderer M. Rituximab, cyclophosphamide, doxorubicin, vincristine and prednisone (R-CHOP) for treatment of early-stage gastric diffuse large B-cell lymphoma. *Ann Oncol* 2004; **15**: 1086-1090
29 **Al-Salman J**, Salib H, Boonswang P. Successful treatment of gastrointestinal follicular lymphoma with rituxan and combination chemotherapy. *Med Oncol* 2001; **18**: 277-283

S- Editor Liu Y **L- Editor** Wang XL **E- Editor** Zhou T

PO Box 2345, Beijing 100023, China
www.wjgnet.com
wjg@wjgnet.com

World J Gastroenterol 2007 March 7; 13(9): 1458-1459
World Journal of Gastroenterology ISSN 1007-9327

CASE REPORT

Endoscopic transcystic stent placement for an intrahepatic abscess due to gallbladder perforation

Myung Soo Kang, Do Hyun Park, Ki Du Kwon, Jeong Hoon Park, Suck-Ho Lee, Hong-Soo Kim, Sang-Heum Park, Sun-Joo Kim

Myung Soo Kang, Do Hyun Park, Ki Du Kwon, Jeong Hoon Park, Suck-Ho Lee, Hong-Soo Kim, Sang-Heum Park, Sun-Joo Kim, Division of Gastroenterology, Department of Internal Medicine, Soon Chun Hyang University Cheonan Hospital, Cheonan, Korea
Correspondence to: Do Hyun Park, MD, PhD, Division of Gastroenterology, Department of Internal Medicine, Soon Chun Hyang University Cheonan Hospital, 23-20 Bongmyung-dong, Cheonan, Choongnam, 330-721, Korea. dhpark@schch.co.kr
Telephone: +82-41-5703675 Fax: +82-41-5745762
Received: 2006-12-17 Accepted: 2007-02-05

Abstract

Perforation of the gallbladder with cholecystohepatic communication is a rare cause of liver abscess. Because it is a rare entity, the treatment modality has not been fully established. We report for the first time a patient with an intrahepatic abscess due to gallbladder perforation successfully treated by endoscopic stent placement into the gallbladder who had a poor response to continuous percutaneous drainage.

Key words: Liver abscess; Gallbladder perforation; Endoscopic stent placement; Cholecystohepatic communication

Kang MS, Park DH, Kwon KD, Park JH, Lee SH, Kim HS, Park SH, Kim SJ. Endoscopic transcystic stent placement for an intrahepatic abscess due to gallbladder perforation. *World J Gastroenterol* 2007; 13(9): 1458-1459

http://www.wjgnet.com/1007-9327/13/1458.asp

INTRODUCTION

Perforation of the gallbladder with cholecystohepatic communication is a rare cause of liver abscess[1-3]. Percutaneous drainage with systemic antibiotics is the initial treatment for these conditions[2]. However, the presence of a biliary communication is associated with significantly longer periods of catheter drainage, because continuous bile flow into the abscess cavity through the communicating tract hindered the natural healing course, resulting in prolonged healing time[4]. Moreover, continuous catheter drainage has its drawbacks, including discomfort in the patient, the nuisance of catheter maintenance, and accidental catheter dislodgement[5,6].

To our knowledge, this is the first case of an intrahepatic abscess due to gallbladder perforation successfully treated by endoscopic transcystic stent placement to the gallbladder who had a poor response to continuous percutaneous drainage.

CASE REPORT

A 70-year-old man was hospitalized for fever, right upper quadrant pain, and general weakness due to a poor appetite.

Abdominal computed tomography (CT) was performed to clarify the origin of fever. A 5-cm hepatic abscess was found in the right lobe adjacent to the gallbladder (Figure 1A). An 8-Fr pigtail catheter was percutaneously inserted into the abscess pocket, and purulent pus was drained. Following catheter insertion, we discovered a communication between the abscess and the gallbladder with a large stone (Figure 2). Systemic antibiotics were administered. Although elective cholecystectomy was considered, his poor general condition which was associated with uncontrolled dementia and hemiparesis due to a previous stroke contraindicated surgery. Two weeks after percutaneous drainage, the patient unintentionally removed the inserted pigtail catheter. We decided to attempt internal drainage to prevent the patient from self-removing the percutaneous catheter repeatedly. There was no change in the size of the hepatic abscess on follow-up CT (Figure 1B). Therefore, endoscopic transcystic stent (a 7-Fr 10-cm-long double pigtail biliary stent, Zimmon; Wilson-Cook, Winston-Salem, N.C.) was placed into the gallbladder (Figure 3). There were no procedure-related complications such as bile leak, peroration, or bleeding.

Ten days after the insertion of the double pigtail biliary stent, the patient's general condition improved, and a follow-up abdominal CT showed that the size of abscess pocket decreased markedly measuring approximately 0.5 cm (Figure 1C). The patient was discharged after an uneventful recovery and has remained in good condition with the stent in place during the 7-mo follow-up.

DISCUSSION

Because liver abscesses associated with gallbladder perforation with cholecystohepatic communication is rare,

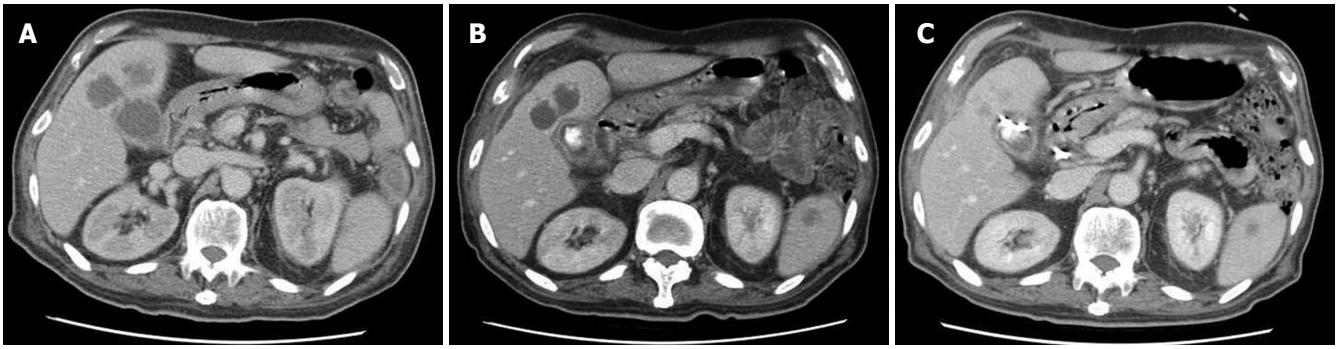

Figure 1 **A**: CT scan found an hepatic abscess in the right lobe adjacent to the gallbladder; **B**: Two weeks after the percutaneous drainage, the size of the hepatic abscess did not decrease much; **C**: Ten days after the insertion of a 7-Fr 10-cm-long double pigtail biliary stent, the size of the abscess pocket decreased markedly.

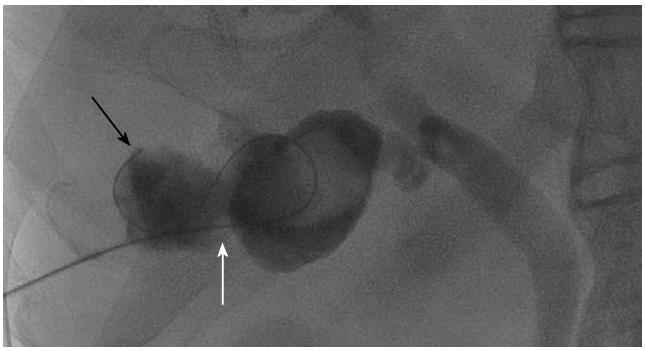

Figure 2 Percutaneous transhepatic cholangiography reveals a cholecystohepatic fistula (white arrow) between liver abscess (black arrow) and gallbladder with a large stone.

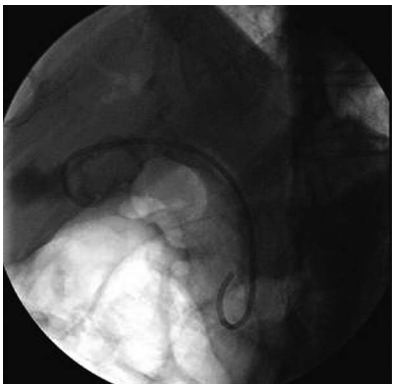

Figure 3 A 7-Fr 10-cm-long double pigtail biliary stent was placed into the gallbladder.

the treatment modality has not been fully established[1-3].

In this case, surgical management was not considered because of the patient's poor general condition. Although percutaneous drainage was maintained for the liver abscess, there was no clinical or radiological improvement. In addition, percutaneous drainage could not be kept for a long period, because the patient was demented. Some liver abscesses with biliary communication are refractory to percutaneous drainage alone. For such abscesses, endoscopic drainage including papillotomy, nasobiliary drainage, or biliary stenting may be an effective treatment[4,7]. We believe that a large gallstone may provoke bile flow of the gallbladder to the communicating tract, resulting in a poor response to percutaneous drainage for the intrahepatic abscess, and if the bile was diverted away from the communicating tract, the bile flow into the abscess cavity would cease, thereby enhancing the healing of both the tract and abscess[4]. Therefore, endoscopic transcystic biliary drainage of gallbladder was designed as an alternative management. To date, the stent has remained in situ without any complications for 7 mo of follow-up in this case. Because the patency results of the endoscopic gallbladder stent placement vary[8,9], regular evaluation of stent patency may be also required in this particular case.

In conclusion, the endoscopic transcystic placement of a biliary stent to the gallbladder may be effective as an alternative management for patients with hepatic abscesses caused by a perforated gallbladder with cholecystohepatic communication, who have poor responses to continuous percutaneous drainage.

REFERENCES

1 **Bakalakos EA**, Melvin WS, Kirkpatrick R. Liver abscess secondary to intrahepatic perforation of the gallbladder, presenting as a liver mass. *Am J Gastroenterol* 1996; **91**: 1644-1646
2 **Peer A**, Witz E, Manor H, Strauss S. Intrahepatic abscess due to gallbladder perforation. *Abdom Imaging* 1995; **20**: 452-455
3 **Chen JJ**, Lin HH, Chiu CT, Lin DY. Gallbladder perforation with intrahepatic abscess formation. *J Clin Ultrasound* 1990; **18**: 43-45
4 **Sharma BC**, Agarwal N, Garg S, Kumar R, Sarin SK. Endoscopic management of liver abscesses and cysts that communicate with intrahepatic bile ducts. *Endoscopy* 2006; **38**: 249-253
5 **Miller FJ**, Ahola DT, Bretzman PA, Fillmore DJ. Percutaneous management of hepatic abscess: a perspective by interventional radiologists. *J Vasc Interv Radiol* 1997; **8**: 241-247
6 **Yu SC**, Ho SS, Lau WY, Yeung DT, Yuen EH, Lee PS, Metreweli C. Treatment of pyogenic liver abscess: prospective randomized comparison of catheter drainage and needle aspiration. *Hepatology* 2004; **39**: 932-938
7 **Sugiyama M**, Atomi Y. Pyogenic hepatic abscess with biliary communication. *Am J Surg* 2002; **183**: 205-208
8 **Schlenker C**, Trotter JF, Shah RJ, Everson G, Chen YK, Antillon D, Antillon MR. Endoscopic gallbladder stent placement for treatment of symptomatic cholelithiasis in patients with end-stage liver disease. *Am J Gastroenterol* 2006; **101**: 278-283
9 **Conway JD**, Russo MW, Shrestha R. Endoscopic stent insertion into the gallbladder for symptomatic gallbladder disease in patients with end-stage liver disease. *Gastrointest Endosc* 2005; **61**: 32-36

S- Editor Liu Y **L- Editor** Ma JY **E- Editor** Ma WH

PO Box 2345, Beijing 100023, China
www.wjgnet.com
wjg@wjgnet.com

World J Gastroenterol 2007 March 7; 13(9): 1460-1465
World Journal of Gastroenterology ISSN 1007-9327

CASE REPORT

Rectal angiolipoma: A case report and review of literature

Sabite Kacar, Sedef Kuran, Tulay Temucin, Bulent Odemis, Nilufer Karadeniz, Nurgul Sasmaz

Sabite Kacar, Sedef Kuran, Bulent Odemis, Nurgul Sasmaz, Gastroenterology Department, Türkiye Yüksek Ihtisas Hospital, Ankara, Turkey
Tulay Temucin, Pathology Department, Türkiye Yüksek Ihtisas Hospital, Ankara, Turkey
Nilufer Karadeniz, Genetic Department, Zekai Tahir Burak Training and Research Hospital, Ankara, Turkey
Correspondence to: Sedef Kuran, MD, Gastroenterology Department, Türkiye Yüksek Ihtisas Hospital, Dikmen Cad., 220/A, No.17, Dikmen, Ankara, Turkey. sedefozdal@hotmail.com
Telephone: +90-533-3479969 Fax: +90-312-3124120
Received: 2006-12-14 Accepted: 2007-01-27

Abstract

Angiolipoma is a rare vascular variant of the benign lipomatous tumors and is generally seen in subcutaneous tissues. We report a 70-year-old female with abdominal distension not related to rectal small polypoid mass with peduncule described as angiolipoma by histologically, and review the literature.

Key words: Gastrointestinal tract angiolipoma; Gastrointestinal benign lipomatous tumors; Rectal angiolipoma

Kacar S, Kuran S, Temucin T, Odemis B, Karadeniz N, Sasmaz N. Rectal angiolipoma: A case report and review of literature. *World J Gastroenterol* 2007; 13(9): 1460-1465

http://www.wjgnet.com/1007-9327/13/1460.asp

INTRODUCTION

Lipomas, lipomatosis, lipoblastoma, lipoblastomatosis, angiolipomas, myolipomas, chondroid lipomas, spindle cell lipomas, and pleomorphic lipomas are the benign adipose tissue tumors[1]. Angiolipoma is one of the rare subcutaneous tissue tumors with its characteristic histology consisting of mature adipose tissue and interspersed proliferated vascular component[1-3]. It accounts for 5%-17% of lipomas[2,4,5], and is rarely seen in the gastrointestinal system (GIS). The locations of gastrointestinal angiolipoma according to the current literature are oropharyngeal region[4,6-8], esophagus[9], stomach[10-13], duodenum[14,15], small intestine[3,16-18], ileocecal valve[19-21], colon[14,22-24] and liver[25-28]. Angiolipomas localized in the gastrointestinal tract, characterized as submucosal solitary sessile[10,11,18,20] or endoluminal polypoid lesions[9,12,14,23,24], are diagnosed generally by postoperative histopathologic evaluation or after polypectomy. Radiologic techniques such as barium radiographs, enteroclysis, abdominal ultrasound, computed tomography (CT), and magnetic resonance imaging (MRI) can demonstrate the lesion in the gastrointestinal tract before histopathologic diagnosis[24].

CASE REPORT

A 70-year-old woman admitted to the hospital with complaints of abdominal distension and constipation. She had no abdominal pain, rectal bleeding or weight loss. Her total blood count, serum biochemistry, sedimentation rate and abdominal ultrasound were normal. A polyp (1 cm in diameter) with lobulated and degenerated hyperemic mucosa and normal peduncle was seen at proximal rectum. Polypectomy was performed by endoscopic polypectomy snare and no complication occurred. Angiolipoma was diagnosed after histopathologic evaluation in mature adipose tissue and proliferous blood vessels (Figure 1). There was no fibrin thrombus and no muscle structure in histologic examination with HMB45 (monoclonal mouse anti-human melanosome, Dako, USA) and anti-smooth muscle antibody (mouse anti-human primary alpha-smooth muscle actin, Dako, USA) tissue stainings. There were no other lesions in total colonoscopy and esophagogastroduodenoscopy. No photograph of the polyp was taken before resection because externally there was no special difference in adenomatous polyps with degenerated surface mucosa.

DISCUSSION

Angiolipomas are benign lipomatous lesions, which were first defined by Bowen[29] in 1912 and differentiated from lipomas histopathologically by Howard in 1960[30]. The lipomatous benign lesions are seen as musculoskeletal masses especially in soft tissues and bones[1,2]. They are generally subcutaneous and capsulated, about 50% patients feel painful on palpation, and seen in young adult males in their 2nd or 3rd decades of life[1,2,24]. They are also localized in neck[4,31], maxillofacial region[32-35] and non-subcutaneous tissues such as epidural[36], spinal[37-39], and suprasellar tissues[40]. Lipomas are seen more frequently, but angiolipomas are rare lesions[1,5]. Gastrointestinal angiolipoma is also a rare pathological condition[1,24]. The other uncommon localizations of angiolipomas are the renal tissue[41-44], adrenal tissue[45,46], breast[47], thyroid glands[48], parotid gland[49], mediastinum[50], orbits[51], myocardium[52] and scrotum[53].

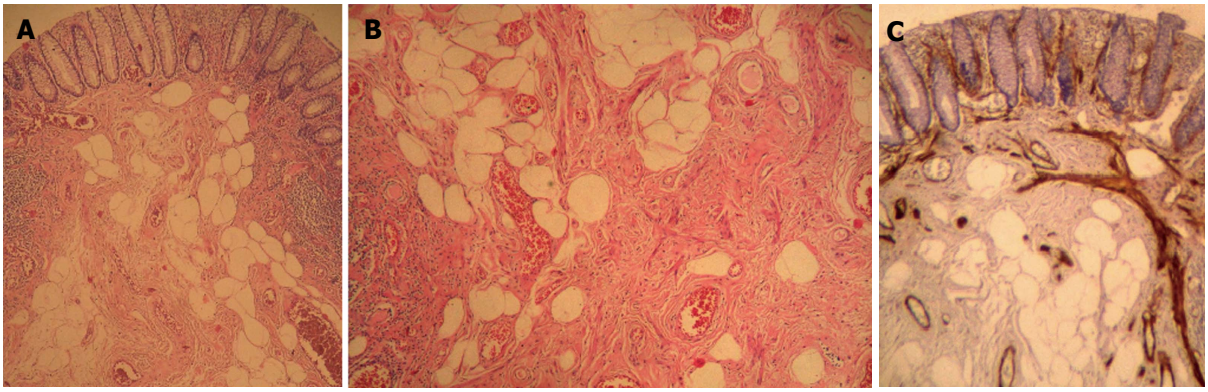

Figure 1 Histopathologic appearance of small rectal pedunculated angiolipoma (macroscopically 7 mm x 5 mm x 4 mm in diameter with normal mucosal appearence). **A**: Proliferated blood vessels and adipose cells in mature adipose tissue in submucosa of colon at small magnification (light microscope, HE); **B**: Proliferated vascular tissues and mature adipose tissue in submucosa. There was no fibrin trombus in blood vessels (light microscope, HE); **C**: SMA staining of angiolipoma.

Table 1 Gastrointestinal angiolipomas defined in literature

Literature	Localization	Case (age/sex)	Polyp size	Polyp peduncle	Symptom	Preoperative diagnostic imaging methods (except endoscopic procedure)	Therapy	Follow-up (F/U)/ recurrence
Jensen EH *et al*[9] 2006	Esophagus	85 yr/M	39 mm x 25 mm	Pedunculated large polyp	A 2-mo dysphagia to solids foods, complete esophageal obstruction; had prolapsed to the level of the GE junction	CT , EUS	Anterior esophagotomy, transsection of polyp using an endoscopic stapling device (open surgical excision)	No F/U
DeRidder Ph *et al*[10] (1989)	Stomach	59 yr/M	6 mm	Submucosal well demarcated mass	Chronic occult GI bleeding		Laparotomy-excision	12 mo/No recurrence
McGregor DH *et al*[11] (1993)	Stomach	69 yr/M	50 mm x 40 mm x 20 mm	Gastric submucosal mass on great curvature, without peduncle	Chronic hemorrhage and severe anemia		Exploratory laparotomy, mass resection	30 mo/No recurrence
Hunt J *et al*[12] (1996)	Stomach	27 yr/F	80 mm x 55 mm x 45 mm	Large polypoid mass with large peduncle	Suggestive of intussusception through the pylorus, acute GI hemorrhage		Exploratory laparotomy, distal partial gastrectomy, Billroth I gastric reconstruction, resection of polyp	not given/ No recurrence
Mohl W *et al*[14] (2004)[2]	Duodenum, Colon	The first was 66 yr/M, the second was 75 yr/F (2 pts with 1 duodenal and colonic A-L other duodenal A-Ls)	1st-10 mm located near papilla of Vater, and colon 2nd-23 mm at the upper duodenal knee	Both with peduncle	1st acute, 2nd chronic GI bleeding Upper GI bleeding due to duodenal A-L		Endoscopic snare polypectomy for 2 duodenal and for 1 colonic A-Ls	not given/ No recurrence
Jung IS *et al*[15] (2004)	Duodenum	60 yr/F	35 mm x 4 mm	With peduncle	Dyspepsia for 6 mo	EUS	Endoscopic polypectomy	No F/U
Kaneko T *et al*[16] (1996)[1]	Meckel's diverticulum accompanied A-L				Intussusception			
Ferrozzi F *et al*[3] (1998)	Ileal				With tuberous sclerosis	CT		

Manner M *et al*[17] (2001)	Proximal ileum	71 yr/F	38 mm	With peduncle	Occult bleeding, ileoileal intussusception	US, CT	Small bowel resection	
Kwak HS *et al*[18] (2003)	Small bowel/ proximal ileum	75 yr/M	30 mm	Intraluminal lobulated polypoid mass with peduncle	Epigastric discomfort, loss of appetite, weight loss	Enteroclysis, MRI	Surgery	No F/U
Aouad K *et al*[19] (2000)	(Bauhin valve) ileocecal valve				Gastrointestinal hemorrhage			
Kato K *et al*[20] (1999)[1]	Ileocecal valve	69 yr/M	52 mm x 50 mm x 40 mm	Without peduncle, a submucosal smooth surface mass A-L	3-d right lower quadrant abdominal pain	Contrast enhanced abdominal CT	Laparoscopy-assisted ileocecostomy, and a side-to-side anastomosis extracorporeally (a minimally invasive laparoscopic technique)	5 yr/No recurrence
Saroglia G *et al*[21] (1996)	Ileocecal valve	55 yr/M	55 mm	Submucousal mass	Invagination	Barium contrast graphy	Surgery	No F/U
Vandamme J *et al*[22] (1964)	Descending colon	43 yr/M	150 mm x 40 mm	With peduncle	GI bleeding and non painful sub-obstruction by invagination	Barium contrast graphy	Surgery, colon resection	not given/ No recurrence
Okuyama T *et al*[23] (2002)	Sigmoid colon	49 yr/M	65 mm x 23 mm	Pedunculated polyp with smooth surface	Asymptomatic, during routine exam positive fecal blood	Double contrast enema, enhanced CT	Hemostatic clip and endoscopic electro-surgical polypectomy	No F/U
Chen YY *et al*[24] (2005)	Transvers colon	70 yr/M	50 mm	With peduncle	Colonic obstruction	US, Abdominal CT, Colonic barium enema, colonoscopic examination	Surgical segmental resection	2 yr/No recurrence
Kacar S *et al*	Rectum	70 yr/F	10 mm	With peduncle	Asymptomatic	-	Polypectomy performed by endoscopic polypectomy snare	6 mo/No recurrence Under F/U

[1]Abstract of reference (full text not available); [2]Three lesions of angiolipoma in two patients, were defined. GE: Gastroesophageal; A-L: Angiolipoma.

In the musculoskeletal system, angiolipomas are 70% multiple and 10% familial[5]. It can have an autosomal dominant penetrance[1,22]. The mode of inheritence in GIS is still not clear[54].

Histologically, it is comprised of mature adipose tissue and proliferated vascular tissues. It can be classified as predominantly lipomatous or angiomatous type, based on the ratio of adipose tissue and vascular tissue composition[1,2,5]. Fibrin thrombus due to microtraumas is generally seen in angiomatous lesions[5,11,20,23,48]. Angiolipomas localized in muscle and cutaneous tissue can have two different behavior patterns: infiltrative or non-infiltrative[5]. But the gastrointestinal cases defined in the literature have been non-infiltrating and showed no recurrence during follow-up periods (Table 1).

Eight maxillofacial angiolipomas had been reported in the literature until 1989[7] and 17 head and neck angiolipomas until 1999[4]. There are also cases in the literature of oropharyngeal angiolipomas including tongue, cheek mucosa and palate[4,6-8].

Angiolipomas localized in the GIS or liver. Although hepatic localization of lipomatous tumors is seen more frequently than gastrointestinal tract, hepatic angiolipomas are also rare lesions in this group[27,28,55,56]. Most lipomatous lesions of the liver[55,56] and hepatic angiolipomas are associated with tuberous sclerosis complex[26].

Seven cases of angiolipoma hade been reported in the gastrointestinal tract in the literature up to 2005[24]. To the best of our knowledge, 17 cases of gastrointestinal angiolipoma have been reported to date (1 esophageal[9], 3 gastric[10-12], 2 duodenal[14,15], 4 small bowel[3,16-18], 3 ileocecal valve[19-21], and 4 colonic)[14,22-24]. Based on these reports, our case would be the first angiolipoma defined in the rectum.

There are syndromes accompanying angiolipomas, such as familial angiolipomatosis, which is rare and benign with mostly autosomal dominant inheritance and multiple angiolipomas of the extremities and trunk[57]. Birt-Hogg-Dube syndrome is an autosomal-dominant condition characterized by fibrofolliculomas, trichodiscomas, and acrochordons[58]. There is only one ileal angiolipoma-associated tuberous sclerosis in the literature[3]. Hunt *et al*[12] described a case with solitary gastric Peutz-Jeghers polyp and angiolipoma presenting as acute hemorrhage.

Angiolipamas are diagnosed generally as single lesions in the gastrointestinal tract, but Mohl *et al*[14] described a case of both colonic and duodenal angiolipoma. Angiolipomas in the gastrointestinal tract, as shown in Table 1, can be sessile[10,11,18,20] or pedunculated polypoid

Table 2 Histopathological findings of cases in literature

Literature	Histopathological findings under light microscope
Jensen EH *et al*[9]	A submucosal polypoid mass, consisting of benign lipomatous tissue mixed with vascular channels, consistent with benign angiolipoma
DeRidder *et al*[10]	Submucosa contained a well demarcated nodule composed of flat, extending from the under surface of the muscularis mucosa to the deep margin of biopsy. There were separate, well developed small arteries and veins
McGregor D *et al*[11]	A circumbscribed, lobular, pinkish-tan soft ovoid mass showing proliferation of mature adipose tissue and vascular tissue surrounded by a thin to focally thick fibrous capsule in the submucosa, no definite fibrin trombi
Hunt J *et al*[12]	A solitary Peutz-Jeghers-type polyp showing typical glandular epithelium, overriding a 5 cm gastric angiolipoma
Mohl W *et al*[14]	2 submucosal duodenal angiolipomas, one with large central vessel and one colonic angiolipoma
Yung IS *et al*[15]	A submucosal lesion composed of mature adipose tissue and small vessels with fibrin thrombi within the vascular channels
Manner M *et al*[17]	An angiolipoma with 20% vascular component and mucosal ulceration
Kwak HS *et al*[18]	Mature, higly vascular adipose tissue consistent with angiolipoma
Kato K *et al*[20]	A circumbscribed proliferation of mature adipose and vascular tissue surrounded by a thin to focally thick fibrous capsule in the submucosa, with fibrin thrombi in small capillaries
Saroglia G *et al*[21]	Mature adipose and vascular tissue
Vandamme J *et al*[22]	Angiolipoma with multiple small vessels and adipose tissue
Okuyama T *et al*[23]	Encapsulated by a thin layer of connective tissue, arising in the submucosa and composed of mature adipose tissue and proliferating capillaries, many fibrin thrombi in capillary lumen
Chen YY *et al*[24]	Encapsulated by a thin layer of connective tissue arising from the submucosa, histologically was comprised of mature adipose tissue and proliferative blood vessels
Kacar S *et al*	Proliferated submucosal blood vessels and mature adipose tissue. There was no fibrin thrombus

lesions[9,12,14,23,24], and the cases in the literature are generally diagnosed based on abdominal pain, obstruction, invagination, intussusception, and acute or chronic bleeding.

Diagnosis of GIS angiolipomas can be made radiologically via contrast barium enema, enteroclysis, abdominal ultrasound, endoscopic ultrasound, abdominal tomography, or MRI before the polypectomy or resection if the lesion is large[9,15,17,18,20,23,24]. Large lesion size and the symptom are the main factors in the radiologic diagnosis, but final diagnoses are done histologically. There is filling-defect in gastrointestinal lumen detected by barium enema[24] and enteroclysis[18], hyperechoic lesion in transabdominal ultrasonography[17,24], submucosal lesion in gastrointestinal wall in endosonography[9], hyperechoic lesion in CT[3,9,14,17,20,23], and central high signal intensity with peripheral iso-signal intensity on T1-weighted in-phase images in MRI[18].

Surgical resection is preferred to endoscopic resection in the case of broad-based or pedunculated large polyps due to risk of perforation and bleeding[9,10,11,12,17,18,20,24]. For pedunculated polyps, injection of epinephrine, or use nylon loop or metal hemostatic clip are suggested before polypectomy to decrease the risk of postoperative bleeding[14,23]. These patients can be treated by standard polypectomy. The level of urgency is also an important factor when choosing the most optimal treatment. In the case of intussusception[16,21], obstruction[9,24] or acute bleeding[12,19,22], emergent surgery is generally suggested. In some cases, minimally invasive laparoscopic techniques can be performed successfully. A cecal lesion was treated successfully with laparoscopy-assisted ileocecostomy and a five-year follow-up showed no recurrence in this patient[22].

Our patient was diagnosed by histopathologic evaluation after snare polypectomy of a single, small polyp with thin peduncle in the rectum. There was no complication after polypectomy. The peduncle was histologically normal. There were proliferated blood vessels and mature adipose tissue in the submucosa and no fibrin thrombus was found. Mature adipose tissue and proliferated blood vessels are the diagnostic components as defined in the literature. Fibrin thrombus in the vascular component is a common finding[5,11,20,23]. The histopathological findings of the cases in the literature are given in Table 2.

The polyp was not responsible for the dyspeptic symptoms and constipation in our patient. Although the polyp could have caused rectal bleeding, no bleeding occurred in our patient. The lesion was thus considered as asymptomatic. The sigmoid angiolipoma in literature[23] was asymptomatic, but 65 mm in diameter. Our case is the first rectal, small, asymptomatic angiolipoma diagnosed incidentally in the gastrointestinal tract.

Although angiolipomas are benign lesions among adipose tissue neoplasms, additional staining techniques are required to distinguish from malignant lipomatous forms like angioliposarcoma[27,28]. The resection material of our patient was stained by HMB45 and anti-smooth muscle antibody, and found negative for muscle fibers. The differential diagnosis was made between angiomyolipoma and angioliposarcoma.

In conclusion, it is important to remember that submucosal, sessile, or polypoid lesions in the gastrointestinal tract with or without symptoms can be an angiolipoma, a lipomatous tumor, although it is quite rare.

REFERENCES

1 **Murphey MD**, Carroll JF, Flemming DJ, Pope TL, Gannon FH, Kransdorf MJ. From the archives of the AFIP: benign musculoskeletal lipomatous lesions. *Radiographics* 2004; **24**: 1433-1466

2 **Punia RS**, Jain P, Amanjit H, Singh R. Subcutaneous angiolipomas: a clinicopathological study of 12 cases. *Indian J Pathol Microbiol* 2005; **48**: 197-198

3 **Ferrozzi F**, Rubino S, Uccelli M. Ileal angiolipoma in a patient with multisystemic manifestations of tuberous sclerosis: diagnosis with computerized tomography. *Radiol Med* 1998; **96**: 403-405

4 **Vigili MG**, Micozzi M, Moreschini G, Colacci AC, Masci P, Silvagni C. Oropharyngeal angiolipoma: a case study. *Acta Otorhinolaryngol Ital* 1999; **19**: 348-351

5 **Choong KK**. Sonographic appearance of subcutaneous angiolipomas. *J Ultrasound Med* 2004; **23**: 715-717
6 **Flaggert JJ**, Heldt LV, Keaton WM. Angiolipoma of the palate. Report of a case. *Oral Surg Oral Med Oral Pathol* 1986; **61**: 333-336
7 **Lin SC**, Wang TY, Hahn LJ. Angiolipoma of the tongue: report of a case. *Ann Dent* 1989; **48**: 37-38
8 **Brahney CP**, Aria AA, Koval MH, Najjar TA. Angiolipoma of the tongue: report of case and review of literature. *J Oral Surg* 1981; **39**: 451-453
9 **Jensen EH**, Klapman JB, Kelley ST. Angiolipoma of the esophagus: a rare clinical dilemma. *Dis Esophagus* 2006; **19**: 203-207
10 **DeRidder PH**, Levine AJ, Katta JJ, Catto JA. Angiolipoma of the stomach as a cause of chronic upper gastrointestinal bleeding. *Surg Endosc* 1989; **3**: 106-108
11 **McGregor DH**, Kerley SW, McGregor MS. Case report: gastric angiolipoma with chronic hemorrhage and severe anemia. *Am J Med Sci* 1993; **305**: 229-235
12 **Hunt J**, Tindal D. Solitary gastric Peutz-Jeghers polyp and angiolipoma presenting as acute haemorrhage. *Aust N Z J Surg* 1996; **66**: 713-715
13 **Ferrozzi F**, Tognini G, Bova D, Pavone P. Lipomatous tumors of the stomach: CT findings and differential diagnosis. *J Comput Assist Tomogr* 2000; **24**: 854-858
14 **Mohl W**, Fischinger J, Moser C, Remberger K, Zeuzem S, Stallmach A. Duodenal angiolipoma -- endoscopic diagnosis and therapy. *Z Gastroenterol* 2004; **42**: 1381-1383
15 **Jung IS**, Jang JY, Ryu CB, Hong SJ, Kim JO, Cho JY, Lee JS, Lee MS, Jin SY, Shim CS, Kim BS. Angiolipoma of the duodenum diagnosed after endoscopic resection. *Endoscopy* 2004; **36**: 375
16 **Kaneko T**, Karasawa Y, Inada H, Tamura Y, Yamamura N, Iijima Y, Nagata A, Oohata T, Shirota H, Nakamura T, Hara E. An adult case of intussusception due to inverted Meckel's diverticulum accompanied by angiolipoma. *Nihon Shokakibyo Gakkai Zasshi* 1996; **93**: 260-265
17 **Manner M**, Scholz E, Wehrmann M, Stickel W. Invagination caused by angiolipoma of the small intestine--a rare cause of occult gastrointestinal hemorrhage. *Chirurg* 2001; **72**: 305-307
18 **Kwak HS**, Kim CS, Lee JM. Small intestinal angiolipoma: MR imaging appearance. *Abdom Imaging* 2003; **28**: 515-517
19 **Aouad K**, Texier P, Bloch F, De Labriolle-Vaylet C, Bouillot JL. Benign angiolipoma of the Bauhin valve causing severe digestive tract bleeding. *Gastroenterol Clin Biol* 2000; **24**: 686-688
20 **Kato K**, Matsuda M, Onodera K, Sakata H, Kobayashi T, Kasai S. Angiolipoma of the colon with right lower quadrant abdominal pain. *Dig Surg* 1999; **16**: 441-444
21 **Saroglia G**, Coverlizza S, Roatta L, Leli R, Fontana D. Angiolipoma of the cecum. *Minerva Chir* 1996; **51**: 59-62
22 **Vandamme J**. Angiolipoma of the colon. *Acta Gastroenterol Belg* 1964; **27**: 750-757
23 **Okuyama T**, Yoshida M, Watanabe M, Kinoshita Y, Harada Y. Angiolipoma of the colon diagnosed after endoscopic resection. *Gastrointest Endosc* 2002; **55**: 748-750
24 **Chen YY**, Soon MS. Preoperative diagnosis of colonic angiolipoma: a case report. *World J Gastroenterol* 2005; **11**: 5087-5089
25 **Strotzer M**, Paetzel C, Feuerbach S. Multiple hepatic angiolipomas: a case report and review of literature. *Eur Radiol* 1999; **9**: 259-261
26 **Huber C**, Treutner KH, Steinau G, Schumpelick V. Ruptured hepatic angiolipoma in tuberous sclerosis complex. *Langenbecks Arch Chir* 1996; **381**: 7-9
27 **Zhang SH**, Cong WM, Xian ZH, Wu WQ, Dong H, Wu MC. Morphologic variants and immunohistochemical features of hepatic angiomyolipoma. *Zhonghua Binglixue Zazhi* 2004; **33**: 437-440
28 **Tsui WM**, Ng IO, Colombari R, Pea M. Hepatic angiomyolipomas. *Histopathology* 1993; **22**: 602-603
29 **Bowen JT**. Multiple subcutaneous hemangiomas, together with multiple lipomas, occurring in enormous numbers in an otherwise healthy, muscular subject. *Am J Med Sci* 1912; **144**: 189-192
30 **Howard WR**, Helwig EB. Angiolipoma. *Arch Dermatol* 1960; **82**: 924-931
31 **Saydam L**, Bozkurt MK, Ugur MB, Ozcelik T, Kutluay L. Angiolipoma of the neck: a case report. *Ear Nose Throat J* 2005; **84**: 375-377
32 **Hamakawa H**, Hino H, Sumida T, Tanioka H. Infiltrating angiolipoma of the cheek: a case report and a review of the literature. *J Oral Maxillofac Surg* 2000; **58**: 674-677
33 **Ali MH**, el-Zuebi F. Angiolipoma of the cheek: report of a case. *J Oral Maxillofac Surg* 1996; **54**: 213-215
34 **Shohet JA**, Simpson B, Coleman JR, Geiger XJ. Angiolipoma presenting as a nasal mass. *Otolaryngol Head Neck Surg* 1998; **118**: 848-849
35 **Pfannenstiel TJ**, Boseley M, Roach L. A case of paranasal sinus angiolipoma. *Laryngoscope* 2003; **113**: 1080-1081
36 **Hattori H**. Epidural angiolipoma is histologically distinct from its cutaneous counterpart in the calibre and density of its vascular component; a case report with review of the literature. *J Clin Pathol* 2005; **58**: 882-883
37 **Petrella G**, Tamburrini G, Lauriola L, Di Rocco C. Spinal epidural angiolipoma complicated by an intratumoral abscess. Case report. *J Neurosurg* 2005; **103**: 166-169
38 **Konya D**, Ozgen S, Kurtkaya O, Pamir NM. Lumbar spinal angiolipoma: case report and review of the literature. *Eur Spine J* 2006; **15**: 1025-1028
39 **White NJ**, Cochrane DD, Beauchamp R. Paraparesis caused by an angiolipomatous hamartoma in an adolescent with Proteus syndrome and scoliosis. *J Neurosurg* 2005; **103**: 282-284
40 **Shuangshoti S**, Wangsuphachart S. Angiolipoma of suprasellar region. *J Med Assoc Thai* 1995; **78**: 631-634
41 **Ewalt DH**, Diamond N, Rees C, Sparagana SP, Delgado M, Batchelor L, Roach ES. Long-term outcome of transcatheter embolization of renal angiomyolipomas due to tuberous sclerosis complex. *J Urol* 2005; **174**: 1764-1766
42 **de Perrot M**, Licker M, Robert J, Nicod L, Spiliopoulos A. Successful combined lung and kidney transplantation for pulmonary lymphangioleiomyomatosis and renal angiolipomas. *Eur Respir J* 1998; **12**: 1479-1481
43 **Verna C**, Mosso L, Moncelli G, Monaco A. Renal angiolipoma associated with bilateral double ureter. A clinical case. *Minerva Urol Nefrol* 1997; **49**: 39-44
44 **Alvo M**, Passalacqua W, Castro P, Wash A. Tuberous sclerosis with probable bilateral renal angiolipoma. *Rev Med Chil* 1988; **116**: 934-937
45 **Ramacciato G**, Lombardi M, Amodio PM, Mercantini P, Petrocca S, Stipa F, Di Giacomo G, Bellagamba R, Puce E, Ziparo V. Laparoscopic adrenalectomy: a worthwhile procedure performed in a general surgery department. *Am Surg* 2003; **69**: 427-433
46 **Maurea S**, Mainolfi C, Wang H, Varrella P, Panico MR, Klain M, Rossi R, Cremona F, Bazzicalupo L, Salvatore M. Positron emission tomography (PET) with fludeoxyglucose F 18 in the study of adrenal masses: comparison of benign and malignant lesions. *Radiol Med* 1996; **92**: 782-787
47 **Morakkabati-Spitz N**, Schild HH, Leutner CC, von Falkenhausen M, Lutterbey G, Kuhl CK. Dynamic contrast-enhanced breast MR imaging in men: preliminary results. *Radiology* 2006; **238**: 438-445
48 **Palazzo JP**, Coté SA. Primary angiolipoma of the thyroid gland: a case report. *Int J Surg Pathol* 2005; **13**: 305-307
49 **Reilly JS**, Kelly DR, Royal SA. Angiolipoma of the parotid: case report and review. *Laryngoscope* 1988; **98**: 818-821
50 **Gámez García P**, de Pablo Gafas A, Salas Antón C, Santolaya Cohen R, Madrigal Royo L, Varela de Ugarte A. Mediastinal dumbbell angiolipoma. *Arch Bronconeumol* 2002; **38**: 545-546
51 **Feinfield RE**, Hesse RJ, Scharfenberg JC. Orbital angiolipoma. *Arch Ophthalmol* 1988; **106**: 1093-1095
52 **Kiaer HW**. Myocardial angiolipoma. *Acta Pathol Microbiol Immunol Scand A* 1984; **92**: 291-292
53 **Rajagopalan S**. An unusual pediatric scrotal lump. *Indian J Pediatr* 2005; **72**: 801
54 **Sciot R**, Akerman M, Dal Cin P, De Wever I, Fletcher CD,

Mandahl N, Mertens F, Mitelman F, Rosai J, Rydholm A, Tallini G, Van den Berghe H, Vanni R, Willen H. Cytogenetic analysis of subcutaneous angiolipoma: further evidence supporting its difference from ordinary pure lipomas: a report of the CHAMP Study Group. *Am J Surg Pathol* 1997; **21**: 441-444

55 **Ji Y**, Zhu X, Xu J, Zhou J, Tan Y, Wang J, Fan J, Zhou Y. Hepatic angiomyolipoma: a clinicopathologic study of 10 cases. *Chin Med J (Engl)* 2001; **114**: 280-285

56 **Hirasaki S**, Koide N, Ogawa H, Ujike K, Shinji T, Tsuji T. Tuberous sclerosis associated with multiple hepatic lipomatous tumors and hemorrhagic renal angiomyolipoma. *Intern Med* 1999; **38**: 345-348

57 **Cina SJ**, Radentz SS, Smialek JE. A case of familial angiolipomatosis with Lisch nodules. *Arch Pathol Lab Med* 1999; *123*: 946-948

58 **Chung JY**, Ramos-Caro FA, Beers B, Ford MJ, Flowers F. Multiple lipomas, angiolipomas, and parathyroid adenomas in a patient with Birt-Hogg-Dube syndrome. *Int J Dermatol* 1996; **35**: 365-367

S- Editor Liu Y **L- Editor** Ma JY **E- Editor** Zhou T

PO Box 2345, Beijing 100023, China
www.wjgnet.com
wjg@wjgnet.com

World J Gastroenterol 2007 March 7; 13(9): 1466-1470
World Journal of Gastroenterology ISSN 1007-9327

CASE REPORT

Hepatic abscess induced by foreign body: Case report and literature review

Sofia A Santos, Sara CF Alberto, Elsa Cruz, Eduardo Pires, Tomás Figueira, Élia Coimbra, José Estevez, Mário Oliveira, Luís Novais, João R Deus

Sofia A Santos, Sara CF Alberto, Elsa Cruz, Eduardo Pires, João R Deus, Department of Gastroenterology, Fernando Fonseca Hospital, IC19, Amadora 2720-276, Portugal
Tomás Figueira, Élia Coimbra, Department of Radiology, Fernando Fonseca Hospital, IC19, Amadora 2720-276, Portugal
José Estevez, Department of Surgery, Fernando Fonseca Hospital, IC19, Amadora 2720-276, Portugal
Mário Oliveira, Department of Pathology, Fernando Fonseca Hospital, IC19, Amadora 2720-276, Portugal
Luís Novais, Center for the Study of Esophageal Diseases, Carnaxide, Portugal
Correspondence to: Dr. Sofia A Santos, Department of Gastroenterology, Fernando Fonseca Hospital, Estrada Serra da Mira, N22, 3ºDTO 2700-786, Amadora, Portugal. sofiasantos_md@sapo.pt
Telephone: +351-965-628190
Received: 2006-06-03 Accepted: 2007-02-07

Abstract

Hepatic abscess due to perforation of the gastrointestinal tract caused by ingested foreign bodies is uncommon. Pre-operative diagnosis is difficult as patients are often unaware of the foreign body ingestion and symptoms and imagiology are usually non-specific. The authors report a case of 62-year-old woman who was admitted with fever and abdominal pain. Further investigation revealed hepatic abscess, without resolution despite antibiotic therapy. A liver abscess resulting from perforation and intra-hepatic migration of a bone coming from the pilorum was diagnosed by surgery. The literature concerning foreign body-induced perforation of the gastrointestinal tract complicated by liver abscess is reviewed.

Key words: Liver abscess; Foreign body; Gastrointestinal perforation

Santos SA, Alberto SCF, Cruz E, Pires E, Figueira T, Coimbra E, Estevez J, Oliveira M, Novais L, Deus JR. Hepatic abscess induced by foreign body: Case report and literature review. *World J Gastroenterol* 2007; 13(9): 1466-1470

http://www.wjgnet.com/1007-9327/13/1466.asp

INTRODUCTION

Perforation of the gastrointestinal tract caused by ingested foreign bodies is uncommon and formation of posterior hepatic abscess is even more rare[1-5]. In the majority of cases an early diagnosis is difficult to make by laparotomy due to the variability of clinical presentation and non specificity of complementary examinations. The authors report a rare case of gastric perforation induced by a chicken bone with hepatic perforation and abscess formation. Despite computed tomography scan (CT) showed possible perforation, laparotomy established the diagnosis.

CASE REPORT

A 62-year old woman presented in March 2005 to our emergency room with abdominal pain, fever and asthenia. She had a history of hypertension, gastro-oesophageal disease and hemorrhoids and was treated with ramipril and lansoprazole.

She had a 6-wk history of intermittent epigastric pain that progressively worsened, asthenia, anorexia and more recently developed mild fever. There was no history of chills, nausea, vomiting, thoracic pain, jaundice, respiratory or urinary complaints.

Physical examination revealed stable vital signs. And lung examination was unremarkable. Her abdomen was soft and tender to palpation but the liver was mildly tender and enlarged.

Laboratory investigations revealed a haemoglobin level of 10 g/dL, leukocytosis with granulocytosis (16 600/mm^3 and 87%), C-reactive protein 24 mg/dL, elevated aspartate aminotransferase and alanine aminotransferase (43 and 35 IU/mL; normal < 31), γ-glutamil transferase 93 UI/L (N < 55), with normal bilirrubin and alkaline phosphatase. Plain radiographs of the chest and abdomen were normal. Abdomen ultrasound (US) revealed a hypoechoic lesion in the left lobe containing both gas and fluid. Contrast enhanced CT scan showed a large collection, measuring approximately 8.5 cm × 7.0 cm, consistent with left-sided intra-hepatic abscess extending up to the gastric antrum, that presented parietal thickening (Figure 1). An abdominal RM did not rule out a liver tumor, but failed to show continuity with the gastric antrum (Figure 2).

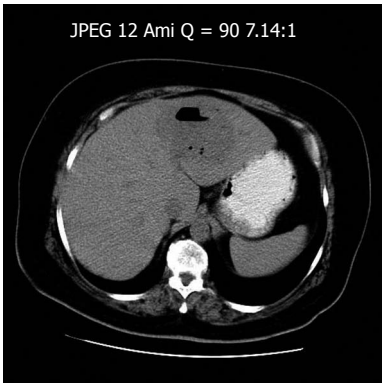

Figure 1 Contrast enhanced CT scan showing a low-density area with gas and fluid, measuring approximately 8.5 cm x 7.0 cm, consistent with left-sided intra-hepatic abscess.

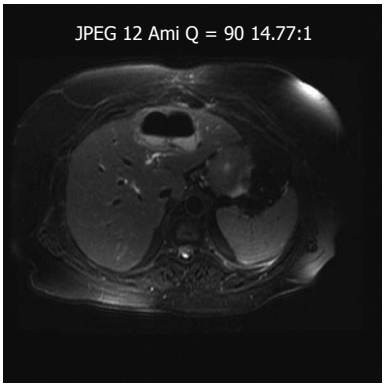

Figure 2 Abdominal RM demonstrating a large collection with gas and fluid.

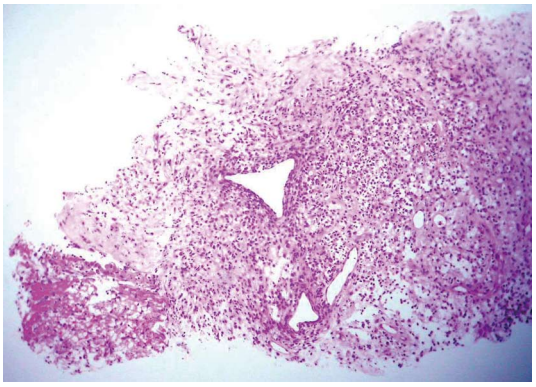

Figure 3 Biopsy of the liver abscess showing fibrosis, fibrin and acute inflammatory cells, consistent with abscess wall (HE).

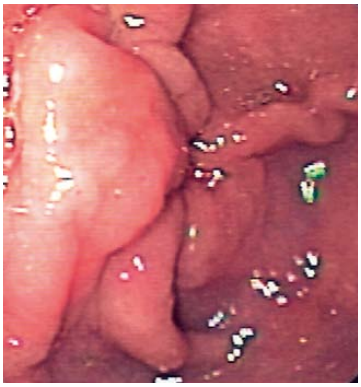

Figure 4 Upper GI endoscopy revealing a thickened gastric fold (pre-pyloric).

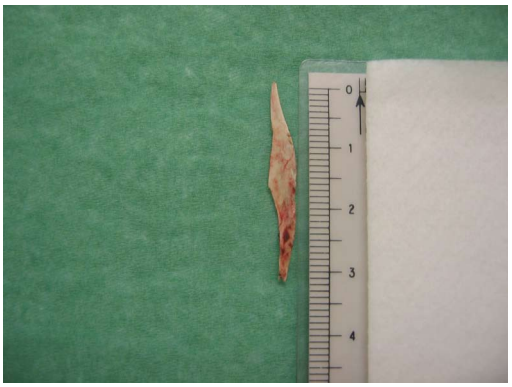

Figure 5 Removed foreign body (chicken bone, with 3.3 cm x 0.5 cm).

Using CT guidance, the hepatic abscess was drained percutaneously and pus and blood cultures were obtained. Microbiological examination of the drained fluid was negative and biopsies taken only revealed inflammatory process (Figure 3). Upper GI endoscopy revealed a pre-pyloric thickened fold (Figure 4), with normal histological evaluation. Entamoeba histolytica serology was negative.

The patient started on antibiotherapy (ampicilin, gentamicin and metronidazole) with clinical improvement. Four weeks later abdominal ultrasonography showed abscess size reduction (3 cm) and the patient was discharged and maintained antibiotic therapy.

Three weeks later the patient presented with fever, abdominal pain and elevated C-reactive protein. Abdominal ultrasonography and CT scan showed enlargement of the abscess cavity (8.4 cm × 5.3 cm), which extended to the gastric antrum. Laparotomy was then performed and a foreign body (bone) was found embedded in the left lobe of the liver, resulting in a gastric antrum perforation (Figure 5). The bone was removed, the abscess drained, the stomach defect closed and a drain placed. The post-operative course was uneventful.

DISCUSSION

About 80%-90% of ingested foreign bodies pass trough the gut without discovery within 1 wk[1,2,4]. When symptoms arise they are usually secondary to obstruction[1,2]. Gastrointestinal perforation has been reported in less than 1% of patients[3-5] and the most commonly affected areas are the ileocecal and rectosigmoidal regions[4,5] and duodenum[2]. Development of hepatic abscess due to penetration induced by a foreign body is even more rare, the first case was published in 1898[6]. Since then, the world literature has been increased, with 46 cases reported until now. The most common sites of perforation of the gut are stomach and duodenum[5] which can induced by sharp foreign bodies like fish bones, chicken bones, needles or toothpicks[2,4,5,6] although pens or dental plates have also been reported[6,7].

It is difficult to establish the time until the onset of symptoms as patients rarely recall the episode of ingestion[1,3,4] and the migrating foreign body may remain silent until an abscess formation[5].

Most patients have non specific symptoms such as

Table 1 World literature review of hepatic abscess induced by foreign bodies

Ref	Year	Author	Symptoms	Suffering period	Foreign body	Size (cm)	Penetration	Liver	Bacteria	Laparotomy	Treatment	Mortality
[1]	2003	Kanazana	Epigastralgia	1 mo	Toothpick	5.5	Stomach	Left lobe	Unknown	Yes	Abscess drained and removal of a small part of the liver	No
[2]	2000	Cheung	Epigastralgia, fever	3 mo	Toothpick	-	Stomach	Left lobe	Unknown	Yes	removal of the toothpick and a small part of the liver	No
[3]	2000	Broome	Epigastralgia, anorexia, fever	7 d	Chicken bone	4.0	Stomach	Left lobe	Unknown	Yes	Removal of the chicken bone and abscess drainage	No
[4]	1999	Horii	Fever, vomiting	2 wk	Fish bone	2.8	Unknown	Left lobe	Streptococcus constellatus	No	Percutaneous abscess drainage	No
[5]	2003	Chintamani	Fever, vomiting	1 yr	Needle	3.0	Unknown	Right lobe	Streptococcus pyogenes, E. coli	Yes	Removal of the needle and abscess drainage	No
[6]	2001	La Veja	Abdominal pain, vomiting	Unknown	Fish bone	2.5	Unknown	Right lobe	-	Autopsy		Yes
[7]	1999	Perkins	Fever, anaemia	2 wk	Pen	-	Duodenum	Right lobe	Streptococcus malleri (group C), Sreptococcus malleri	No	Removal of the pen and abscess drainage	No
[8]	1983	Shaw	Fever		Dental plate	-	Descending colon		Unknown			
[9]	1997	Tsui			Clothespin, Tooth pick	-	Duodenum Stomach		Unknown			
[10]	1993	Chen	Epigastralgia, fever, weight loss	3 mo	Chicken bone	4.0	Duodenum	Left lobe	Unknown	Yes	Removal of the chicken bone and abscess drainage	No
[11]	2003	Bilimoria	Right upper abdominal pain, fever	Unknown	Toothpick	-	Sigmoid colon	Right lobe	Estreptococcus	Yes	Removal of the toothpick and abscess drainage	No
[12]	2004	Tomimori	Epigastralgia	4 wk	Fish bone	1.0	Stomach	Left lobe	Sreptococcus constellatus	Yes	Removal of the fish bone and abscess drainage	No
[13]	2001	Kessler	Abdominal pain	4 wk	Fish bone	Unknown	Duodenum	Left lobe	Eikenella corrodens	Yes	Removal of the fish bone and abscess drainage	No
[14]	2000	Paraskeva	Abdominal pain	4 mo	Fish bone	3.7	Sigmoid colon	Right lobe	Sreptococcus malleri	No	Removal of the fish bone	No
[15]	1999	Drnovsek	Abdominal pain, vomiting	1 d	Toothpick	Unknown	Duodenum	Both	Streptococcus viridens	Yes	Removal of the toothpick	No
[16]	1999	Guglielminetti			Toothpick	-	Stomach	Left lobe	Unknown	No	Endoscopic toothpick removal and percutaneous abscess drainage	
[17]	2002	Theodoropoulou	Right upper abdominal pain, fever, jaundice	3 d	Fish bone	5.5	Stomach	Left lobe	Unknown	Autopsy		Yes
[18]	1981	Wood	Fever, diarrhea	9 mo	Needle	-	Retrocecal appendix	Right lobe	Streptococcus viridens	Yes	Removal of the needle and abscess drainage	
[19]	2005	Starakis	Right upper abdominal pain, fever	3 wk	Chicken bone	-	Duodenum	Left lobe	Sreptococcus viridans, Eikenella corrodens	Yes	Removal of the chiken bone and abscess drainage	No
[20]	2003	Houli	Right upper abdominal pain, fever	2 wk	Chicken bone	3.5	Transverse colon	Right lobe	Streptococcus angiosus and mixed anaerobic flora	Yes	Abscess drainage, removal of the chicken bone and a small part of the liver	No
[21]	2001	Byard	Abdominal pain, fever	Several years	Chicken bone	3.8	Duodenum	Both	*E. coli*, mixed anaerobes and Candida albicans	Autopsy		Yes
[22]	1999	Chan	Abdominal pain, fever	Unknown	Fish bone	-	Stomach		Unknown	Yes	Removal of the fish bone, abscess drainage and parcial gastrectomy	No
[23]	1999	Tsai	Abdominal pain, fever		Fish bone	3.7	Stomach	Left lobe	Unknown	No	Abscess drainage and simple closure of the perforated hole	No
[24]	1992	Shuldais			Fish bone	-	Stomach		Unknown			
[25]	1991	Masunaga	Abdominal pain, fever, vomiting	1wk	Fish bone	4.0	Stomach	Left lobe	Unknown	Yes	Percutaneous abscess drainage, parcial gastrectomy and lateral segmentectomy	
[26]	1990	Allimant	Fever, astenia	3 wk	Toothpick	-	Stomach	Left lobe	Unknown	Yes	Drainage and removal of the tooth pick and a small part of the liver	No
[27]	1986	Penderson	Abdominal pain, shock	Unknown	Toothpick	3.5	Stomach	Left lobe	Unknown	Yes	Removal of the toothpick and abscess drainage	No
[28]	1988	Gonzalez	Abdominal pain, fever, jaundice, nausea	1 mo	Fish bone	Unknown	Stomach	Left lobe	Unknown	Yes	Removal of the fish bone and abscess drainage	No
[29]	1981	Rafizadeth	Low-grade fever	10 d	Toothpick	4.2	Duodenum	Left lobe	Estreptococcus	Yes	Removal of the toothpick and abscess drainage	No

[30]	1966	Aron	Astenia, fever, jaundice	3 mo	Fish bone	2.2	Stomach	Right lobe	E. coli, Proteus	Yes	Removal of the toothpick, abscess drainage and piloroplasty	No
[31]	1971	Berk	Right upper abdominal pain	Several weeks	Chicken bone	4.0	Stomach	Left lobe	Unknown	Yes	Removal of the chicken bone, abscess drainage and parcial gastrectomy	
[32]	1996	Acosta			Needle	-	Appendix		Unknown			
[33]	1971	Abel	None	Unknown	Needle	2.5	Stomach	Left lobe	Unknown	Yes	Removal of the needle and segmentectomy	No
[34]	1981	Tsuboi	Epigastralgia, weight loss	1 mo	Fish bone	4.7	Stomach	Left lobe	Unknown	Yes	Removal of the fish bone and abscess drainage	No
[35]	1984	Bloch	Fever, myalgia	2 wk	toothpick	4.5	Stomach or Duodenum	Left lobe	Estreptococcus	Yes	Removal of the toothpick and abscess drainage	
[36]	1955	Griffiths	Septic shock	Unknown	Needle	4.0	Stomach	Right lobe	Unknown	Autopsy		Yes
	1955	Griffiths	Fever , vomiting	1 mo	Toothpick	6.0	Duodenum	Right lobe	Unknown	Autopsy		Yes
[37]	1990	Dugger	Fever, right upper abdominal pain	3 wk	Fish bone or Chicken bone	3.8	Stomach	Right lobe	E. coli, Proteus	Autopsy		
[38]	2005	Lee	Epigastralgia	5 d	Body piercing	5.0	Stomach	Left lobe	Klebsiella spp, Streptococcus milleri	Yes	Removal of the piercing, closure of the perforated hole and abscess drainage	No
	2005	Lee	Fever, epigastralgia, nausea, vomiting	1 wk	Fish bone	3.5	Stomach	Left lobe	Streptococcus milleri	Yes	Removal of the fish bone, closure of the perforated hole and abscess drainage	No
	2005	Lee	Epigastralgia	10 d	-	-	Stomach	Left lobe	Streptococcus milleri	Yes	Closure of the perforated hole	No
[39]	2005	Goh	Fever	5 d	Fish bone	3.0	Duodenum	Left lobe	Streptococcus milleri	Yes	Removal of the fish bone and abscess drainage	No
[40]	2006	Chiang	Right upper abdominal pain, fever	3 d	Toohpick	6.7	Duodenum	Right lobe	Staphylococcus aureus	No	Antibiotics (refused surgery)	No

abdominal pain, fever, vomiting, anorexia or weight loss[4,5,8] which are features of a systemic response against an infection or abscess formation[4]. Furthermore, the classical presentation of hepatic abscess (fever, abdominal pain and jaundice) is only present in a few cases[5].

The results of routine laboratory studies are also non specific and unless the foreign body is radio-opaque it will not be identified on plain radiography[3,4].

An abdominal US or CT scan is preferred techniques for the diagnosis, the latter is excellent in detection of foreign bodies due to its high resolution and accuracy[1,2,4]. Endoscopy may be helpful when performed early, before the foreign body migration and mucosal healing[2,9] (which happened in our patient). In addition, endoscopy does not allow examination of the mid-gut[2]. Therefore, pre-operative diagnosis is difficult and a high degree of suspicion is required[1,3].

We reviewed the world literature, and summarized it in Table 1. We found that fish bones were the most common foreign body and the stomach was the principal site of perforation. Abscess formation occurs more often on the left lobe. Microorganisms isolated on abscess or fluid cultures are usually part of the normal flora of human oropharynx[4,5,6,10-12]. Prognosis depends on a quick diagnosis, not only for morbidity but also for mortality[5,6].

Our clinical report is similar to the world literature and enhances the difficulty of diagnosing such an entity. Our patient who did not recall the ingestion, had non specific symptoms and laboratory results as well as US and CT showed a hepatic abscess on the left lobe and its fistulous track. The diagnosis was obtained after exploratory laparotomy. Considering all issues we suppose that the chicken bone perforated through the pylorus.

Hepatic abscess treatment includes aspiration and antibiotic therapy[4]. Nevertheless if we suspect perforation of the gut caused by a foreign body or it is detected by radiography, US or CT, surgery is the option[13], although there are some descriptions of endoscopic[4,12,15] or percutaneous[4,14] removal. In our case surgery not only allowed to make a diagnosis but also treated it.

In conclusion, hepatic abscess diagnosis based on perforation of the gastrointestinal tract caused by a foreign body is difficult due to a variety of non specific symptoms and because patients are often unaware of the ingestion. In a hepatic abscess that does not respond to aspiration and antibiotic therapy we should look for an aetiology. Despite its rarity we should consider a foreign body and surgical therapy. Surgery still has a major role in the diagnosis and treatment of hepatic abscess induced by a foreign body although US and CT may establish it in some cases.

REFERENCES

1 **Kanazawa S**, Ishigaki K, Miyake T, Ishida A, Tabuchi A, Tanemoto K, Tsunoda T. A granulomatous liver abscess which developed after a toothpick penetrated the gastrointestinal tract: report of a case. *Surg Today* 2003; **33**: 312-314

2 **Cheung YC**, Ng SH, Tan CF, Ng KK, Wan YL. Hepatic inflammatory mass secondary to toothpick perforation of the stomach: triphasic CT appearances. *Clin Imaging* 2000; **24**: 93-95

3 **Broome CJ**, Peck RJ. Hepatic abscess complicating foreign body perforation of the gastric antrum: an ultrasound diagnosis. *Clin Radiol* 2000; **55**: 242-243

4 **Horii K**, Yamazaki O, Matsuyama M, Higaki I, Kawai S, Sakaue Y. Successful treatment of a hepatic abscess that formed secondary to fish bone penetration by percutaneous transhepatic removal of the foreign body: report of a case. *Surg Today* 1999; **29**: 922-926

5 **Chintamani** V, Lubhana P, Durkhere R, Bhandari S. Liver abscess secondary to a broken needle migration--a case report. *BMC Surg* 2003; **3**: 8

6 **de la Vega M**, Rivero JC, Ruíz L, Suárez S. A fish bone in the liver. *Lancet* 2001; **358**: 982

7 **Shaw PJ**, Freeman JG. The antemortem diagnosis of pyogenic liver abscess due to perforation of the gut by a foreign body. *Postgrad Med J* 1983; **59**: 455-456

8 **Tsui BC**, Mossey J. Occult liver abscess following clinically unsuspected ingestion of foreign bodies. *Can J Gastroenterol* 1997; **11**: 445-448

9 **Bilimoria KY**, Eagan RK, Rex DK. Colonoscopic identification of a foreign body causing an hepatic abscess. *J Clin Gastroenterol* 2003; **37**: 82-85

10 **Tomimori K**, Nakasone H, Hokama A, Nakayoshi T, Sakugawa H, Kinjo F, Shiraishi M, Nishimaki T, Saito A. Liver abscess. *Gastrointest Endosc* 2004; **59**: 397-398

11 **Kessler AT**, Kourtis AP. Images in clinical medicine. Liver abscess due to Eikenella corrodens from a fishbone. *N Engl J Med* 2001; **345**: e5

12 **Paraskeva KD**, Bury RW, Isaacs P. Streptococcus milleri liver abscesses: an unusual complication after colonoscopic removal of an impacted fish bone. *Gastrointest Endosc* 2000; **51**: 357-358

13 **Drnovsek V**, Fontanez-Garcia D, Wakabayashi MN, Plavsic BM. Gastrointestinal case of the day. Pyogenic liver abscess caused by perforation by a swallowed wooden toothpick. *Radiographics* 1999; **19**: 820-822

14 **Guglielminetti D**, Poddie DB. Liver abscess secondary to ingestion of foreign body. A case report. *G Chir* 1999; **20**: 453-455

15 **Theodoropoulou A**, Roussomoustakaki M, Michalodimitrakis MN, Kanaki C, Kouroumalis EA. Fatal hepatic abscess caused by a fish bone. *Lancet* 2002; **359**: 977

16 **Wood MK**, Harrison MR. 'A-pin-dicitis' and liver abscess. *JAMA* 1981; **246**: 940

17 **Starakis I**, Karavias D, Marangos M, Psoni E, Bassaris H. A rooster's revenge: hepatic abscess caused by a chicken bone. *Eur J Emerg Med* 2005; **12**: 41-42

18 **Houli N**, MacGowan K, Hosking P. Hepatic abscess complicating foreign body perforation of the transverse colon. *ANZ J Surg* 2003; **73**: 255-259

19 **Byard RW**, Gilbert JD. Hepatic abscess formation and unexpected death: a delayed complication of occult intraabdominal foreign body. *Am J Forensic Med Pathol* 2001; **22**: 88-91

20 **Chan SC**, Chen HY, Ng SH, Lee CM, Tsai CH. Hepatic abscess due to gastric perforation by ingested fish bone demonstrated by computed tomography. *J Formos Med Assoc* 1999; **98**: 145-147

21 **Tsai JL**, Than MM, Wu CJ, Sue D, Keh CT, Wang CC. Liver abscess secondary to fish bone penetration of the gastric wall: a case report. *Zhonghua Yixue Zazhi* (Taipei) 1999; **62**: 51-54

22 **Shuldaĭs AK**, Sumin AV, Tkhorzhevskiĭ BB. Pyogenic hepatic abscess developing after perforation of the stomach by a fish bone. *Klin Khir* 1992; (11): 75-76

23 **Masunaga S**, Abe M, Imura T, Asano M, Minami S, Fujisawa I. Hepatic abscess secondary to a fishbone penetrating the gastric wall: CT demonstration. *Comput Med Imaging Graph* 1991; **15**: 113-116

24 **Allimant P**, Rosburger C, Zeyer B, Frey G, Morel E, Bietiger M, Dalcher G. An unusual cause of hepatic abscess. *Ann Gastroenterol Hepatol* (Paris) 1990; **26**: 5-6

25 **Pedersen VM**, Geerdsen JP, Bartholdy J, Kjaergaard H. Foreign body perforation of the gastrointestinal tract with formation of liver abscess. *Ann Chir Gynaecol* 1986; **75**: 245-246

26 **Gonzalez JG**, Gonzalez RR, Patiño JV, Garcia AT, Alvarez CP, Pedrosa CS. CT findings in gastrointestinal perforation by ingested fish bones. *J Comput Assist Tomogr* 1988; **12**: 88-90

27 **Rafizadeh F**, Silver H, Fieber S. Pyogenic liver abscess secondary to a toothpick penetrating the gastrointestinal tract. *J Med Soc N J* 1981; **78**: 377-378

28 **Aron E**, Roy B, Groussin P. Abscess of the liver caused by fish bone. *Presse Med* 1966; **74**: 1957-1958

29 **Berk RN**, Reit RJ. Intra-abdominal chicken-bone abscess. *Radiology* 1971; **101**: 311-313

30 **Acosta S**, Lantz L. A case report. A pin in the appendix caused hepatic abscess. *Lakartidningen* 1996; **93**: 4278

31 **Abel RM**, Fischer JE, Hendren WH. Penetration of the alimentary tract by a foreign body with migration to the liver. Arch Surg 1971; **102**: 227-228

32 **Tsuboi K**, Nakajima Y, Yamamoto S, Nagao M, Nishimura K, Yoshii M. A case of an intrahepatic fish bone penetration--possibility of the preoperative diagnosis by CT scan (author's transl). *Nihon Geka Hokan* 1981; **50**: 899-903

33 **Bloch DB**. Venturesome toothpick. A continuing source of pyogenic hepatic abscess. *JAMA* 1984; **252**: 797-798

34 **Griffiths FE**. Liver abscess due to foreign-body migration from the alimentary tract; a report of two cases. *Br J Surg* 1955; **42**: 667-668

35 **Dugger K**, Lebby T, Brus M, Sahgal S, Leikin JB. Hepatic abscess resulting from gastric perforation of a foreign object. *Am J Emerg Med* 1990; **8**: 323-325

36 **Lee KF**, Chu W, Wong SW, Lai PB. Hepatic abscess secondary to foreign body perforation of the stomach. *Asian J Surg* 2005; **28**: 297-300

37 **Goh BK**, Yong WS, Yeo AW. Pancreatic and hepatic abscess secondary to fish bone perforation of the duodenum. *Dig Dis Sci* 2005; **50**: 1103-1106

38 **Chiang TH**, Liu KL, Lee YC, Chiu HM, Lin JT, Wang HP. Sonographic diagnosis of a toothpick traversing the duodenum and penetrating into the liver. *J Clin Ultrasound* 2006; **34**: 237-240

S- Editor Liu Y **L- Editor** Wang XL **E- Editor** Zhou T

PO Box 2345, Beijing 100023, China
www.wjgnet.com
wjg@wjgnet.com

World J Gastroenterol 2007 March 7; 13(9): 1471
World Journal of Gastroenterology ISSN 1007-9327

AUTHORS FEEDBACK

The *World Journal of Gastroenterology* web site is loading much faster now

Jay Pravda

Jay Pravda, Inflammatory Disease Research Center, Gainesville, Florida 32614-2181, United States
Correspondence to: Jay Pravda, MD, Inflammatory Disease Research Center, Gainesville, Florida 32614-2181, United States. jaypravda@yahoo.com
Telephone: +1-352-5988866 Fax: +1-352-8547050
Received: 2007-01-27 Accepted: 2007-02-01

Pravda J. The *World Journal of Gastroenterology* web site is loading much faster now. *World J Gastroenterol* 2007; 13(9): 1471

http://www.wjgnet.com/1007-9327/13/1471.asp

Dear Xing-Xia Yang,

The *World Journal of Gastroenterology* (*WJG*) web site is loading much faster now. Thank you.

The *WJG* is unique in that it provides all its content free of charge for everyone to download. No other journal does this. This is the best way to disseminate information and ideas and is a critical factor that will make the *WJG* a very influential journal.

This goal can only be accomplished if everyone can download articles from the *WJG* easily and quickly. As such, the *WJG* depends much more on the internet than any other journal.

Feedback from the editorial board regarding the functionality of the *WJG* web site will enable the WJG to quickly correct internet connectivity problems in any part of the world and allow the *WJG* to maintain its position of preeminence as a leading world class journal.

S- Editor Liu Y **E- Editor** Ma WH

PO Box 2345, Beijing 100023, China
www.wjgnet.com
wjg@wjgnet.com

World J Gastroenterol 2007 March 7; 13(9): 1472
World Journal of Gastroenterology ISSN 1007-9327

ACKNOWLEDGMENTS

Acknowledgments to Reviewers of *World Journal of Gastroenterology*

Many reviewers have contributed their expertise and time to the peer review, a critical process to ensure the quality of *World Journal of Gastroenterology*. The editors and authors of the articles submitted to the journal are grateful to the following reviewers for evaluating the articles (including those were published and those were rejected in this issue) during the last editing period of time.

Fernando Azpiroz, MD
Digestive System Research Unit, University Hospital Vall d'Hebron, Paseo Vall d'Hebron, 119-129, Barcelona 08035, Spain

Jasmohan Singh Bajaj, Assistant Professor
Division of Gastroenterology and Hepatology, Medical College of Wisconsin, 9200 W Wisconsin Ave, Milwaukee WI 53212, United States

Gabrio Bassotti, MD
Department of Clinical and Experimental Medicine, University of Perugia, Via Enrico dal Pozzo, Padiglione W, Perugia 06100, Italy

Luigi Bonavina, Professor
Department of Surgery, Policlinico San Donato, University of Milano, via Morandi 30, Milano 20097, Italy

Markus W Büchler, MD
Department of General Surgery, University of Heidelberg, Im Neuenheimer Feld 110, Heidelberg D-69120, Germany

Ronan A Cahill
Department of General Surgery, Waterford Regional Hospital, Waterford, Cork, Ireland

Zong-Jie Cui, PhD, Professor
Institute of Cell Biology, Beijing Normal University, 19 XinJieKou-WaiDaJie, Beijing 100875, China

Giovanni D De Palma, Professor
Department of Surgery and Advanced Technologies, University of Naples Federico II, School of Medicine, Naples 80131, Italy

Olivier Detry, Dr
Department of Abdominal Surgery and Transplantation, University of Liège, CHU Sart Tilman B35, B-4000 Liège, Belgium

Fujimoto Kazuma Fujimoto, Professor
Department of Internal Medicine, Saga Medical School, Nabeshima, Saga, Saga 849-8501, Japan

Hirokazu Fukui, MD, PhD, Professor
Department of Surgical and Molecular Pathology, Dokkyo University School of Medicine 880, Kitakobayashi, Mibu, Shimotsuga, Tochigi 321-0293, Japan

Shannon S Glaser, Dr
Department of Internal Medicine, Scott & White Hospital, 702 SW HK Dodgen Loop, Medcial Research Building, Temple 76504, United States

Florian Graepler, Dr
Department of Gastroenterology, Hepatology and Infectious Diseases, University Hospital Tuebingen, Otfried-Mueller-Str. 10, D-72076 Tuebingen, Germany

Yik-Hong Ho, Professor
Department of Surgery, School of Medicine, James Cook University, Townsville 4811, Australia

Dusan M Jovanovic, Professor
Institute of Oncology, Institutski Put 4, Sremska Kamenica 21204, Serbia

Serdar Karakose, Dr, Professor
Department of Radiology, Meram Medical Faculty, Selcuk University, Konya 42080, Turkey

Serdar Karakose, Dr, Professor
Department of Radiology, Meram Medical Faculty, Selcuk University, Konya 42080, Turkey

Jutta Keller, Dr
Israelitic Hospital, University of Hamburg, Orchideenstieg 14, D-22297 Hamburg, Germany

Koniaris Leonidas G Koniaris, Professor
Alan Livingstone Chair in Surgical Oncology, 3550 Sylvester Comprehensive Cancer Center (310T), 1475 NW 12th Ave., Miami, FL 33136, United States

Howard Mertz, MD, Professor
Vanderbilt University, St Thomas Hospital, 4230 Harding Rd Ste 309 West, Nashville, TN 37205, United States

Masaki Nagaya, MD, PhD
Department of Emergency and Critical Care Medicine, St. Marianna University, School of Medicine, Kawasaki 261-8511, Japan

Yuji Naito, Professor
Kyoto Prefectural University of Medicine, Kamigyo-ku, Kyoto 602-8566, Japan

Massimo Raimondo, Dr
Division of Gastroenterology and Hepatology, Mayo Clinic, 4500 San Pablo Road, Jacksonville, FL 32224, United States

Nageshwar Duvvuru Reddy, Professor
Asian Institute of Gastroenterology, 6-3-652, Somajiguda, Hyderabad-500 082, India

Jean Rosenbaum, Dr
Inserm E362, Universite Victor Segalen Bordeaux 2, Bordeaux 33076, France

Spiros Sgouros, Dr
Naypaktias 5, Agia Paraskevi, Athens 15341, Greece

Michael Steer, Professor
Department of Surgery, Tufts-Nemc, 860 Washington St, Boston, Ma 02111, United States

Daniel Lindsay Worthley, Dr
Department of Gastroenterology and Hepatology, Flinders Medical Centre, Room 3D230, Bedford Park, SA 5042, Australia

PO Box 2345, Beijing 100023, China
www.wjgnet.com
wjg@wjgnet.com

World J Gastroenterol 2007 March 7; 13(9): 1473
World Journal of Gastroenterology ISSN 1007-9327

Meetings

MAJOR MEETINGS COMING UP

Meeting Falk Research Workshop: Morphogenesis and Cancerogenesis of the Liver
25-26 January 2007
Goettingen
symposia@falkfoundation.de

Meeting Canadian Digestive Diseases Week (CDDW)
16-20 February 2007
Banff-AB
cagoffice@cag-acg.org
www.cag-acg.org/cddw/cddw2007.htm

Meeting Falk Symposium 158: Intestinal Inflammation and Colorectal Cancer
23-24 March 2007
Sevilla
symposia@falkfoundation.de

Meeting BSG Annual Meeting
26-29 March 2007
Glasgow
www.bsg.org.uk/

NEXT 6 MONTHS

Meeting 42nd Annual Meeting of the European Association for the Study of the Liver
11-15 April 2007
Barcelona
easl2007@easl.ch
www.easl.ch/liver-meeting/

Meeting Falk Symposium 159: IBD 2007 - Achievements in Research and Clinical Practice
4-5 May 2007
Istanbul
symposia@falkfoundation.de

Meeting European Society for Paediatric Gastroenterology, Hepatology and Nutrition Congress 2007
9-12 May 2007
Barcelona
espghan2007@colloquium.fr

Digestive Disease Week
19-24 May 2007
Washington Convention Center, Washington DC

Meeting Gastrointestinal Endoscopy Best Practices: Today and Tomorrow, ASGE Annual Postgraduate Course at DDW
23-24 May 2007
Washington-DC
tkoral@asge.org

Meeting ESGAR 2007 18th Annual Meeting and Postgraduate Course
12-15 June 2007
Lisbon
fca@netvisao.pt

Meeting Falk Symposium 160: Pathogenesis and Clinical Practice in Gastroenterology
15-16 June 2007
Portoroz
symposia@falkfoundation.de

Meeting ILTS 13th Annual International Congress
20-23 June 2007
Rio De Janeiro
www.ilts.org

Meeting 9th World Congress on Gastrointestinal Cancer
27-30 June 2007
Barcelona
meetings@imedex.com

EVENTS AND MEETINGS IN 2007

Meeting Falk Research Workshop: Morphogenesis and Cancerogenesis of the Liver
25-26 January 2007
Goettingen
symposia@falkfoundation.de

Meeting Canadian Digestive Diseases Week (CDDW)
16-20 February 2007
Banff-AB
cagoffice@cag-acg.org
www.cag-acg.org/cddw/cddw2007.htm

Meeting Falk Symposium 158: Intestinal Inflammation and Colorectal Cancer
23-24 March 2007
Sevilla
symposia@falkfoundation.de

Meeting BSG Annual Meeting
26-29 March 2007
Glasgow
www.bsg.org.uk/

Meeting 42nd Annual Meeting of the European Association for the Study of the Liver
11-15 April 2007
Barcelona
easl2007@easl.ch
www.easl.ch/liver-meeting/

Meeting Falk Symposium 159: IBD 2007 - Achievements in Research and Clinical Practice
4-5 May 2007
Istanbul
symposia@falkfoundation.de

Meeting European Society for Paediatric Gastroenterology, Hepatology and Nutrition Congress 2007
9-12 May 2007
Barcelona
espghan2007@colloquium.fr

Meeting Gastrointestinal Endoscopy Best Practices: Today and Tomorrow, ASGE Annual Postgraduate Course at DDW
23-24 May 2007
Washington-DC
tkoral@asge.org

Meeting ESGAR 2007 18th Annual Meeting and Postgraduate Course
12-15 June 2007
Lisbon
fca@netvisao.pt

Meeting Falk Symposium 160: Pathogenesis and Clinical Practice in Gastroenterology
15-16 June 2007
Portoroz
symposia@falkfoundation.de

Meeting ILTS 13th Annual International Congress
20-23 June 2007
Rio De Janeiro
www.ilts.org

Meeting 9th World Congress on Gastrointestinal Cancer
27-30 June 2007
Barcelona
meetings@imedex.com

Meeting 15th International Congress of the European Association for Endoscopic Surgery
4-7 July 2007
Athens
info@eaes-eur.org
congresses.eaes-eur.org/

Meeting 39th Meeting of the European Pancreatic Club
4-7 July 2007
Newcastle
www.e-p-c2007.com

Meeting XXth International Workshop on Heliobacter and related bacteria in cronic degistive inflammation
20-22 September 2007
Istanbul
www.heliobacter.org

Meeting Falk Workshop: Mechanisms of Intestinal Inflammation
10 October 2007
Dresden
symposia@falkfoundation.de

Meeting Falk Symposium 161: Future Perspectives in Gastroenterology
11-12 October 2007
Dresden
symposia@falkfoundation.de

Meeting Falk Symposium 162: Liver Cirrhosis - From Pathophysiology to Disease Management
13-14 October 2007
Dresden
symposia@falkfoundation.de

American College of Gastroenterology Annual Scientific Meeting
12-17 October 2007
Pennsylvania Convention Center
Philadelphia, PA

Meeting APDW 2007 - Asian Pacific Digestive Disease Week 2007
15-18 October 2007
Kobe
apdw@convention.co.jp
www.apdw2007.org

15th United European Gastroenterology Week, UEGW
27-31 October 2007
Le Palais des Congrès de Paris, Paris, France

Meeting The Liver Meeting® 2007 - 57th Annual Meeting of the American Association for the Study of Liver Diseases
2-6 November 2007
Boston-MA
www.aasld.org

Gastro 2009, World Congress of Gastroenterology and Endoscopy London, United Kingdom 2009

PO Box 2345, Beijing 100023, China
www.wjgnet.com
wjg@wjgnet.com

World J Gastroenterol 2007 March 7; 13(9): 1474-1476
World Journal of Gastroenterology ISSN 1007-9327

Instructions to authors

GENERAL INFORMATION

World Journal of Gastroenterology (*WJG, World J Gastroenterol* ISSN 1007-9327 CN 14-1219/R) is a weekly journal of more than 48 000 circulation, published on the 7th, 14th, 21st and 28th of every month.

Original Research, Clinical Trials, Reviews, Comments, and Case Reports in esophageal cancer, gastric cancer, colon cancer, liver cancer, viral liver diseases, *etc.*, from all over the world are welcome on the condition that they have not been published previously and have not been submitted simultaneously elsewhere.

Indexed and abstracted in

Current Contents®/Clinical Medicine, Science Citation Index Expanded (also known as SciSearch®) and Journal Citation Reports/Science Edition, *Index Medicus*, MEDLINE and PubMed, Chemical Abstracts, EMBASE/Excerpta Medica, Abstracts Journals, *Nature Clinical Practice Gastroenterology and Hepatology*, CAB Abstracts and Global Health. ISI JCR 2003-2000 IF: 3.318, 2.532, 1.445 and 0.993.

Published by

The WJG Press

SUBMISSION OF MANUSCRIPTS

Manuscripts should be typed double-spaced on A4 (297 mm × 210 mm) white paper with outer margins of 2.5 cm. Number all pages consecutively, and start each of the following sections on a new page: Title Page , Abstract, Introduction, Materials and Methods, Results, Discussion, acknowledgements, References, Tables, Figures and Figure Legends. Neither the editors nor the Publisher is responsible for the opinions expressed by contributors. Manuscripts formally accepted for publication become the permanent property of The WJG Press, and may not be reproduced by any means, in whole or in part without the written permission of both the authors and the Publisher. We reserve the right to put onto our website and copy-edit accepted manuscripts. Authors should also follow the guidelines for the care and use of laboratory animals of their institution or national animal welfare committee.

Authors should retain one copy of the text, tables, photographs and illustrations, as rejected manuscripts will not be returned to the author(s) and the editors will not be responsible for the loss or damage to photographs and illustrations in mailing process.

Online submission

Online submission is strongly advised. Manuscripts should be submitted through the Online Submission System at: http://www.wjgnet.com/index.jsp. Authors are highly recommended to consult the ONLINE INSTRUCTIONS TO AUTHORS (http://www.wjgnet.com/wjg/help/instructions.jsp) before attempting to submit online. Authors encountering problems with the Online Submission System may send an email you describing the problem to wjg@wjgnet.com for assistance. If you submit your manuscript online, do not make a postal contribution. A repeated online submission for the same manuscript is strictly prohibited.

Postal submission

Send 3 duplicate hard copies of the full-text manuscript typed double-spaced on A4 (297 mm × 210 mm) white paper together with any original photographs or illustrations and a 3.5 inch computer diskette or CD-ROM containing an electronic copy of the manuscript including all the figures, graphs and tables in native Microsoft Word format or *.rtf format to:

Editorial Office

World Journal of Gastroenterology
Editorial Department: Apartment 1066, Yishou Garden,
58 North Langxinzhuang Road,
PO Box 2345, Beijing 100023, China
E-mail: wjg@wjgnet.com
http: //www.wjgnet.com
Telephone: +86-10-85381892
Fax: +86-10-85381893

MANUSCRIPT PREPARATION

All contributions should be written in English. All articles must be submitted using a word-processing software. All submissions must be typed in 1.5 line spacing and in word size 12 with ample margins. The letter font is Tahoma. For authors from China, one copy of the Chinese translation of the manuscript is also required (excluding references). Style should conform to our house format. Required information for each of the manuscript sections is as follows:

Title page

Full manuscript title, running title, all author(s) name(s), affiliations, institution(s) and/or department(s) where the work was accomplished, disclosure of any financial support for the research, and the name, full address, telephone and fax numbers and email address of the corresponding author should be included. Titles should be concise and informative (removing all unnecessary words), emphasize what is new, and avoid abbreviations. A short running title of less than 40 letters should be provided. List the author(s)' name(s) as follows: initial and/or first name, middle name or initial(s) and full family name.

Abstract

An informative, structured abstract of no more than 250 words should accompany each manuscript. Abstracts for original contributions should be structured into the following sections: AIM: Only the purpose should be included. METHODS: The materials, techniques, instruments and equipments, and the experimental procedures should be included. RESULTS: The observatory and experimental results, including data, effects, outcome, *etc.* should be included. Authors should present *P* value where necessary, and the significant data should accompany. CONCLUSION: Accurate view and the value of the results should be included.

The format of structured abstracts is at: http://www.wjgnet.com/wjg/help/11.doc

Key words

Please list 5-10 key words that could reflect content of the study mainly from *Index Medicus*.

Text

For most article types, the main text should be structured into the following sections: INTRODUCTION, MATERIALS AND METHODS, RESULTS and DISCUSSION, and should include in appropriate Figures and Tables. Data should be presented in the body text or in Figures and Tables, but not in both.

Illustrations

Figures should be numbered as 1, 2, 3 and so on, and mentioned clearly in the main text. Provide a brief title for each figure on a separate page. No detailed legend should be involved under the figures. This part should be added into the text where the figures are applicable. Digital images: black and white photographs should be scanned and saved in TIFF format at a resolution of 300 dpi; color images should be saved as CMYK (print files) but not as RGB (screen-viewing files). Place each photograph in a separate file. Print images: supply images of size no smaller than 126 mm × 85 mm printed on smooth surface paper; label the image by writing the Figure number and orientation using an arrow. Photomicrographs: indicate the original magnification and stain in the legend. Digital Drawings: supply files in EPS if created by freehand and illustrator, or TIFF from photoshops. EPS files must be accompanied by a version in native file format for editing purposes. Existing line drawings should be scanned at a resolution of 1200 dpi and as close as possible to the size where they will appear when printed. Please use uniform legends for the same subjects. For example: Figure 1 Pathological changes of atrophic gastritis after treatment. A: ...; B: ...; C: ...; D: ...; E: ...; F: ...; G: ...

Tables

Three-line tables should be numbered as 1, 2, 3 and so on, and mentioned clearly in the main text. Provide a brief title for each table. No detailed legend should be included under the tables. This part should be added into the text where the tables are applicable. The information should complement but not duplicate that contained in the text. Use one horizontal line under the title, a second under the column heads, and a third below the Table, above any footnotes. Vertical and italic lines should be omitted.

Notes in tables and illustrations

Data that are not statistically significant should not be noted. $^{a}P<0.05$, $^{b}P<0.01$ should be noted ($P>0.05$ should not be noted). If there are other series of *P* values, $^{c}P<0.05$ and $^{d}P<0.01$ are used. Third series of *P* values can be expressed as $^{e}P<0.05$ and $^{f}P<0.01$. Other notes in tables or under

illustrations should be expressed as ^1F, ^2F, ^3F; or some other symbols with a superscript (Arabic numerals) in the upper left corner. In a multi-curve illustration, each curve should be labeled with ●, ○, ■, □, ▲, △, *etc.* in a certain sequence.

Acknowledgments

Brief acknowledgments of persons who have made genuine contributions to the manuscripts and who endorse the data and conclusions are included. Authors are responsible for obtaining written permission to use any copyrighted text and/or illustrations.

REFERENCES

Coding system

The author should code the references according the citation order in text in Arabic numerals, put references codes in square brackets, superscript it at the end of citation content or the author name of the citation. For those citation content as the narrate part, the coding number and square brackets should be typeset normally. For example, Crohn's disease (CD) is associated with increased intestinal permeability[1,2]. If references are directly cited in the text, they would be put together with the text, for example, from references [19,22-24], we know that...

When the authors code the references, please ensure that the order in text is the same as in reference part and also insure the spelling accuracy of the first author's name. Do not code the same citation twice.

PMID requirement

PMID roots in the abstract serial number indexed by PubMed (http://www.ncbi.nlm.nih.gov/entrez/query.fcgi?db=PubMed). The author should supply the PMID for journal citation. For those references that have not been indexed by PubMed, a printed copy of the first page of the full reference should be submitted.

The accuracy of the information of the journal citations is very important. Through reference testing system, the authors and editor could check the authors name, title, journal title, publication date, volume number, start page, and end page. We will interlink all references with PubMed in ASP file so that the readers can read the abstract of the citations online immediately.

Style for journal references

Authors: the first author should be typed in bold-faced letter. The surname of all authors should be typed with the initial letter capitalized and followed by their name in abbreviation (For example, Lian-Sheng Ma is abbreviated as Ma LS, Bo-Rong Pan as Pan BR). Title of the cited article and italicized journal title (Journal title should be in its abbreviation form as shown in PubMed), publication date, volume number (in black), start page, and end page [PMID: 11819634]

Note: The author should test the references through reference testing system (http://www.wjgnet.com/cgi-bin/index.pl)

Style for book references

Authors: the first author should be typed in bold-faced letter. The surname of all authors should be typed with the initial letter capitalized and followed by their name in abbreviation (For example, Lian-Sheng Ma is abbreviated as Ma LS, Bo-Rong Pan as Pan BR) Book title. Publication number. Publication place: Publication press, Year: start page and end page.

Format

Journals

English journal article (list all authors and include the PMID where applicable)

1 **Grover VP**, Dresner MA, Forton DM, Counsell S, Larkman DJ, Patel N, Thomas HC, Taylor-Robinson SD. Current and future applications of magnetic resonance imaging and spectroscopy of the brain in hepatic encephalopathy. *World J Gastroenterol* 2006; **12**: 2969-2978 [PMID: 16718775]

Chinese journal article (list all authors and include the PMID where applicable)

2 **Lin GZ**, Wang XZ, Wang P, Lin J, Yang FD. Immunologic effect of Jianpi Yishen decoction in treatment of Pixu-diarrhoea. *Shijie Huaren Xiaohua Zazhi* 1999; **7**: 285-287

In press

3 **Tian D**, Araki H, Stahl E, Bergelson J, Kreitman M. Signature of balancing selection in Arabidopsis. *Proc Natl Acad Sci U S A* 2006; In press

Organization as author

4 **Diabetes Prevention Program Research Group**. Hypertension, insulin, and proinsulin in participants with impaired glucose tolerance. *Hypertension* 2002; **40**: 679-686 [PMID: 12411462]

Both personal authors and an organization as author

5 **Vallancien G**, Emberton M, Harving N, van Moorselaar RJ; Alf-One Study Group. Sexual dysfunction in 1, 274 European men suffering from lower urinary tract symptoms. *J Urol* 2003; **169**: 2257-2261 [PMID: 12771764]

No author given

6 21st century heart solution may have a sting in the tail. *BMJ* 2002; **325**: 184 [PMID: 12142303]

Volume with supplement

7 **Geraud G**, Spierings EL, Keywood C. Tolerability and safety of frovatriptan with short- and long-term use for treatment of migraine and in comparison with sumatriptan. *Headache* 2002; **42** Suppl 2: S93-99 [PMID: 12028325]

Issue with no volume

8 **Banit DM**, Kaufer H, Hartford JM. Intraoperative frozen section analysis in revision total joint arthroplasty. *Clin Orthop Relat Res* 2002; (**401**): 230-238 [PMID: 12151900]

No volume or issue

9 Outreach: bringing HIV-positive individuals into care. *HRSA Careaction* 2002; 1-6 [PMID: 12154804]

Books

Personal author(s)

10 **Sherlock S**, Dooley J. Diseases of the liver and billiary system. 9th ed. Oxford: Blackwell Sci Pub, 1993: 258-296

Chapter in a book (list all authors)

11 **Lam SK**. Academic investigator's perspectives of medical treatment for peptic ulcer. In: Swabb EA, Azabo S. Ulcer disease: investigation and basis for therapy. New York: Marcel Dekker, 1991: 431-450

Author(s) and editor(s)

12 **Breedlove GK**, Schorfheide AM. Adolescent pregnancy. 2nd ed. Wieczorek RR, editor. White Plains (NY): March of Dimes Education Services, 2001: 20-34

Conference proceedings

13 **Harnden P**, Joffe JK, Jones WG, editors. Germ cell tumours V. Proceedings of the 5th Germ Cell Tumour Conference; 2001 Sep 13-15; Leeds, UK. New York: Springer, 2002: 30-56

Conference paper

14 **Christensen S**, Oppacher F. An analysis of Koza's computational effort statistic for genetic programming. In: Foster JA, Lutton E, Miller J, Ryan C, Tettamanzi AG, editors. Genetic programming. EuroGP 2002: Proceedings of the 5th European Conference on Genetic Programming; 2002 Apr 3-5; Kinsdale, Ireland. Berlin: Springer, 2002: 182-191

Electronic journal (list all authors)

Morse SS. Factors in the emergence of infectious diseases. Emerg Infect Dis serial online, 1995-01-03, cited 1996-06-05; 1(1): 24 screens. Available from: URL: http//www.cdc.gov/ncidod/EID/eid.htm

Patent (list all authors)

16 **Pagedas AC**, inventor; Ancel Surgical R&D Inc., assignee. Flexible endoscopic grasping and cutting device and positioning tool assembly. United States patent US 20020103498. 2002 Aug 1

Inappropriate references

Authors should always cite references that are relevant to their article, and avoid any inappropriate references. Inappropriate references include those that are linked with a hyphen and the difference between the two numbers at two sides of the hyphen is more than 5. For example, [1-6], [2-14] and [1, 3, 4-10, 22] are all considered as inappropriate references. Authors should not cite their own unrelated published articles.

Statistical data

Present as mean ± SD or mean ± SE.

Statistical expression

Express t test as t (in italics), F test as F (in italics), chi square test as χ^2 (in Greek), related coefficient as r (in italics), degree of freedom as γ (in Greek), sample number as n (in italics), and probability as P (in italics).

Units

Use SI units. For example: body mass, m (B) = 78 kg; blood pressure, p(B) = 16.2/12.3 kPa; incubation time, t (incubation) = 96 h, blood glucose concentration, c (glucose) 6.4 ± 2.1 mmol/L; blood CEA mass concentration, p (CEA) = 8.6 24.5 μg/L; CO_2 volume fraction, 50 mL/L CO_2 not 5% CO_2; likewise for 40 g/L formaldehyde, not 10% formalin; and mass fraction, 8 ng/g, *etc.* Arabic numerals such as 23, 243, 641 should be read 23 243 641.

The format about how to accurately write common units and quantum is at: http://www.wjgnet.com/wjg/help/15.doc

Abbreviations
Standard abbreviations should be defined in the abstract and on first mention in the text. In general, terms should not be abbreviated unless they are used repeatedly and the abbreviation is helpful to the reader. Permissible abbreviations are listed in Units, Symbols and Abbreviations: A Guide for Biological and Medical Editors and Authors (Ed. Baron DN, 1988) published by The Royal Society of Medicine, London. Certain commonly used abbreviations, such as DNA, RNA, HIV, LD50, PCR, HBV, ECG, WBC, RBC, CT, ESR, CSF, IgG, ELISA, PBS, ATP, EDTA, mAb, can be used directly without further mention.

Italics
Quantities: *t* time or temperature, *c* concentration, *A* area, *l* length, *m* mass, *V* volume.
Genotypes: *gyr*A, *arg* 1, *c myc*, *c fos*, *etc.*
Restriction enzymes: *Eco*RI, *Hin*dI, *Bam*HI, *Kbo* I, *Kpn* I, *etc.*
Biology: *H pylori, E coli, etc.*

SUBMISSION OF THE REVISED MANUSCRIPTS AFTER ACCEPTED

Please revise your article according to the revision policies of *WJG*. The revised version including manuscript and high-resolution image figures (if any) should be copied on a floppy or compact disk. Author should send the revised manuscript, along with printed high-resolution color or black and white photos, copyright transfer letter, the final check list for authors, and responses to reviewers by a courier (such as EMS) (submission of revised manuscript by e-mail or on the *WJG* Editorial Office Online System is NOT available at present).

Language evaluation
The language of a manuscript will be graded before sending for revision. (1) Grade A: priority publishing; (2) Grade B: minor language polishing; (3) Grade C: a great deal of language polishing; (4) Grade D: rejected. The revised articles should be in grade B or grade A.

Copyright assignment form
Please downloaded CAF from http://www.wjgnet.com/wjg/help/9.doc.

We certify that the material contained in this manuscript:

Ms:

Title:

is original, except when appropriately referenced to other sources, and that written permission has been granted by any existing copyright holders. We agree to transfer to WJG all rights of our manuscript, including: (1) all copyright ownership in all print and electronic formats; (2) the right to grant permission to republish or reprint the stated material in whole or in part, with or without a fee; (3) the right to print copies for free distribution or sale; (4) the right to republish the stated material in a collection of articles or in any other format. We also agree that our article be put on the Internet.

Criteria for authorship: The WJG requests and publishes information about contributions of each author named to the submitted study. Authorship credit should be based on (1)direct participation in the study, including substantial contributions to conception and design of study, or acquisition of data, or analysis and interpretation of data; (2) manuscript writing, including drafting the article, or revising it critically for important intellectual content; (3)supportive work, including statistical analysis of data, or acquisition of funding, or administration, technology and materials support, or supervision, or supportive contributions. Authors should meet at least one of the three conditions. The WJG does not publish co-first authors and co-corresponding authors.

We hereby assign copyright transfer to WJG if this paper is accepted.

Author Name in full (Full names should be provided, with first name first, followed by middle names and family name at the last, eg, Eamonn MM Quigley). Handwritten names are not accepted.

Author Name in abbreviation (Family name is put first in full, followed by middle names and first name in abbreviation with first letter in capital, eg, Quigley EMM). Handwritten names are not accepted.

1 Full Name: _____
Abbreviation Name: _____
Signed: _____
Date: _____

2 Full Name: _____
Abbreviation Name: _____
Signed: _____
Date: _____

3 Full Name: _____
Abbreviation Name: _____
Signed: _____
Date: _____

4 Full Name: _____
Abbreviation Name: _____
Signed: _____
Date: _____

5 Full Name: _____
Abbreviation Name: _____
Signed: _____
Date: _____

6 Full Name: _____
Abbreviation Name: _____
Signed: _____
Date: _____

7 Full Name: _____
Abbreviation Name: _____
Signed: _____
Date: _____

8 Full Name: _____
Abbreviation Name: _____
Signed: _____
Date: _____

9 Full Name: _____
Abbreviation Name: _____
Signed: _____
Date: _____

10 Full Name: _____
Abbreviation Name: _____
Signed: _____
Date: _____

Final check list for authors
The format is at: http://www.wjgnet.com/wjg/help/13.doc

Responses to reviewers
Please revise your article according to the comments/suggestions of reviewers. The format for responses to the reviewers' comments is at: http://www.wjgnet.com/wjg/help/10.doc

Proof of financial support
For paper supported by a foundation, authors should provide a copy of the document and serial number of the foundation.

Publication fee
Authors of accepted articles must pay publication fee.
EDITORIAL and LETTERS TO THE EDITOR are free of change.